

University of Groningen

Evolutionary game dynamics for two interacting populations under environmental feedback

Gong, Lulu; Cao, Ming

IMPORTANT NOTE: You are advised to consult the publisher's version (publisher's PDF) if you wish to cite from it. Please check the document version below.

Document Version

Publisher's PDF, also known as Version of record

Publication date:

2018

[Link to publication in University of Groningen/UMCG research database](#)

Citation for published version (APA):

Gong, L., & Cao, M. (2018). *Evolutionary game dynamics for two interacting populations under environmental feedback*. 136-136. Abstract from 37th Benelux meeting on Systems and Control, Soesterberg, Netherlands.

Copyright

Other than for strictly personal use, it is not permitted to download or to forward/distribute the text or part of it without the consent of the author(s) and/or copyright holder(s), unless the work is under an open content license (like Creative Commons).

The publication may also be distributed here under the terms of Article 25fa of the Dutch Copyright Act, indicated by the "Taverne" license. More information can be found on the University of Groningen website: <https://www.rug.nl/library/open-access/self-archiving-pure/taverne-amendment>.

Take-down policy

If you believe that this document breaches copyright please contact us providing details, and we will remove access to the work immediately and investigate your claim.

Downloaded from the University of Groningen/UMCG research database (Pure): <http://www.rug.nl/research/portal>. For technical reasons the number of authors shown on this cover page is limited to 10 maximum.

37th Benelux Meeting
on
Systems and Control

March 27 – 29, 2018

Soesterberg, The Netherlands

Book of Abstracts

The 37th Benelux Meeting on Systems and Control is sponsored by



Raffaella Carloni, Bayu Jayawardhana, and Mircea Lazar (Eds.)
Book of Abstracts - 37th Benelux Meeting on Systems and Control

University of Groningen
PO Box 72
9700 AB Groningen
The Netherlands

All rights reserved. No part of the publication may be reproduced in any form by print, photo print, microfilm or by any other means without prior permission in writing from the publisher.

ISBN: 978-94-034-0551-3

Part 1

Programmatic Table of Contents

Tuesday, March 27, 2018

Plenary: P0 Steyl
Welcome and Opening

Chair: Raffaella Carloni 11.25–11.30

Mini Course: P1 Steyl
Networks of Dissipative Systems - Part I
Murat Arcak

Chair: Bayu Jayawardhana 11.30–12.30

Networks of Dissipative Systems - Part I 189
M. Arcak

Mini Course: P2 Steyl
Networks of Dissipative Systems - Part II
Murat Arcak

Chair: Bayu Jayawardhanar 13.40–14.40

Networks of Dissipative Systems - Part II 189
M. Arcak

TuA01 Steyl
System Identification A

Chair: Tom Oomen 15.10-17.40

TuA01-1 15.10-15.35
Subspace identification for linear parameter-varying systems 19

P. Cox Eindhoven University of Technology
R. Toth Eindhoven University of Technology
P. Van den Hof Eindhoven University of Technology

TuA01-2 15.35-16.00
Identification of LTI models from concatenated data sets 20

S. Vasquez Université Libre de Bruxelles
M. Kinnaert Université Libre de Bruxelles
R. Pintelon Vrije Universiteit Brussel

TuA01-3 16.00-16.25
Local rational method with prior system knowledge: with application to mechanical and thermal systems 21

E. Evers Eindhoven University of Technology
B. de Jager Eindhoven University of Technology
T. Oomen Eindhoven University of Technology

TuA01-4 16.25-16.50
Order estimation of multidimensional transfer function by calculating Hankel intersections 22

B. Vergauwen Katholieke Universiteit Leuven
O.M. Agudelo Katholieke Universiteit Leuven
B. De Moor Katholieke Universiteit Leuven

TuA01-5 16.50-17.15
Prior knowledge and the least costly identification experiment 23

G. Birpoutsoukis Université Catholique de Louvain
X. Bombois Ecole Centrale de Lyon

TuA01-6 17.15-17.40

Closed-loop identification without external excitation 24

W. Yan Eindhoven University of Technology
P. Van den Hof Eindhoven University of Technology

TuA02 Angola

Optimal Control A

Chair: Dimitri Jeltsema 15.10-17.40

TuA02-1 15.10-15.35

A suboptimality approach to distributed linear quadratic optimal control 25

J. Jiao University of Groningen
H. Trentelman University of Groningen
M. Camlibel University of Groningen

TuA02-2 15.35-16.00

Vehicle energy management with ecodriving: A sequential quadratic programming approach with dual decomposition 26

Z. Khalik Eindhoven University of Technology
G. Padilla Eindhoven University of Technology
T. Romijn Eindhoven University of Technology
M. Donkers

TuA02-3 16.00-16.25

Power quality: A new challenge in systems and control 27

D. Jeltsema HAN University of Applied Science

TuA02-4 16.25-16.50

Spline-based trajectory generation for CNC-machines 28

T. Mercy Katholieke Universiteit Leuven
G. Pipeleers Katholieke Universiteit Leuven

TuA02-5 16.50-17.15

Optimized thermal-aware workload scheduling and control of data centers 29

T. Van Damme University of Groningen
C. De Persis University of Groningen
P. Tesi University of Groningen

TuA02-6 17.15-17.40

On convexity of the eco-driving problem 30

G. Padilla Eindhoven University of Technology
S. Weiland Eindhoven University of Technology
M. Donkers Eindhoven University of Technology

TuA03 Argentinië

Aerospace and Automotive Applications A

Chair: Bram de Jager 15.10-17.40

TuA03-1 15.10-15.35

Attitude control of a UAV in presence of motor asymmetry 31

B. Njinwoua Mons University
A. Vande Wouwer Mons University

TuA03-2 15.35-16.00

Longitudinal stability augmentation system for a highly unstable forward swept wing UAV by employing a neutral canard angle 32

M. Creyf Katholieke Universiteit Leuven
F. Debrouwere Katholieke Universiteit Leuven
M. Versteijne Katholieke Universiteit Leuven
S. Debruyne

TuA03-3 16.00-16.25

Control of tethered quadrotors through geodesics 33

T. Nguyen Université Libre de Bruxelles
E. Garone Université Libre de Bruxelles

TuA03-4 16.25-16.50

Constrained attitude control of rigid bodies via explicit reference governor 34

S. Nakano Université Libre de Bruxelles
T. Nguyen Université Libre de Bruxelles
E. Garone Université Libre de Bruxelles

TuA03-5 16.50-17.15

Design, modeling, and geometric control on $SE(3)$ of a fully-actuated hexarotor for aerial interaction 35

R. Rashad University of Twente
P. Kuipers University of Twente
J. Engelen University of Twente
S. Stramigioli

TuA03-6 17.15-17.40

Heat release analysis of advanced combustion concepts 36

M. Oom Eindhoven University of Technology
B. de Jager Eindhoven University of Technology
F. Willems Eindhoven University of Technology

TuA04 Bolivia**Distributed Control and Estimation A**

Chair: Tamas Keviczky 15.10-17.15

TuA04-1 15.10-15.35

Divertor detachment control in nuclear fusion devices 37

T. Ravensbergen Eindhoven University of Technology
M. van Berkel Eindhoven University of Technology

TuA04-2 15.35-16.00

Unified passivity-based distributed control of mechanical systems 38

L. Valk Delft University of Technology
T. Keviczky Delft University of Technology

TuA04-3 16.00-16.25

Consensus on the unit sphere, the Stiefel manifold and $SO(d)$: The hunt for almost global convergence 39

J. Thunberg University of Luxembourg
J. Markdahl University of Luxembourg
J. Goncalves University of Luxembourg

TuA04-4 16.25-16.50

A robust consensus algorithm for DC microgrids 40

M. Cucuzzella University of Groningen
S. Trip University of Groningen
C. De Persis University of Groningen
X.Cheng, A. Ferrara, A. van der Schaft

TuA04-5 16.50-17.15

Fractional order PI autotuning method applied to multi-agent system 41

R. Cajo Ghent University
R. De Keyser Ghent University
D. Plaza Escuela Superior Politecnica del Litoral
C. Ionescu

TuA04-6 17.15-17.40

The normal form: A systematic approach to transform non-convex sets into convex sets 42

A. Cotorruelo Jiménez Université Libre de Bruxelles
D. Limón Marruedo Universidad de Sevilla
E. Garone Université Libre de Bruxelles

TuA05 Botswana**Model Reduction**

Chair: Siep Weiland 15.10-17.40

TuA05-1 15.10-15.35

Model order reduction for drilling automation . . . 43

H. Bansal Eindhoven University of Technology
L. Iapichino Eindhoven University of Technology
W. Schilders Eindhoven University of Technology
N. van de Wouw

TuA05-2 15.35-16.00

Model reduction of coherent clusters in dynamic power system models 44

J. Leung Université Libre de Bruxelles
M. Kinnaert Université Libre de Bruxelles
J. Maun Université Libre de Bruxelles
F. Villella

TuA05-3 16.00-16.25

Model order reduction for an electrochemistry-based Li-ion battery model 45

L. Xia Eindhoven University of Technology
E. Najafi Eindhoven University of Technology
H. Bergveld Eindhoven University of Technology
M. Donkers

TuA05-4 16.25-16.50

Synchronization persevering model reduction of Lure networks 46

X. Cheng University of Groningen
J. Scherpen University of Groningen

TuA05-5 16.50-17.15

Reduced order controller design for disturbance decoupling problems 47

R. Merks Eindhoven University of Technology
S. Weiland Eindhoven University of Technology
R. Merks Eindhoven University of Technology

TuA05-6 17.15-17.40

Error analysis for parametric model order reduction using Krylov subspace method 48

D. Lou Eindhoven University of Technology
S. Weiland Eindhoven University of Technology

TuA06 Congo**Nonlinear Control A**

Chair: Bayu Jayawardhana 15.10-17.40

TuA06-1	15.10-15.35	TuA07-4	16.25-16.50
<i>Robust stability of feedback linearizable nonlinear systems</i>	49	<i>Modeling and control of thermo-fluidic processes in spatially interconnected structure</i>	58
S. Azizi	Université Libre de Bruxelles	A. Das	Eindhoven University of Technology
E. Garone	Université Libre de Bruxelles	S. Weiland	Eindhoven University of Technology
TuA06-2	15.35-16.00	TuA07-5	16.50-17.15
<i>Power-controlled Hamiltonian systems</i>	50	<i>Dynamic density estimation from cell population snapshot data</i>	59
P. Monshizadeh	University of Groningen	A. Küper	Katholieke Universiteit Leuven
J. Machado	SUPELEC	R. Dürr	Katholieke Universiteit Leuven
R. Ortega	SUPELEC	S. Waldherr	Katholieke Universiteit Leuven
A. van der Schaft		TuA07-6	17.15-17.40
TuA06-3	16.00-16.25	<i>Stability and passivity of multi-physic systems with irreversible entropy production</i>	60
<i>A port-Hamiltonian approach to secondary control of microgrids</i>	51	V. Benjamin	Université Catholique de Louvain
M. Adibi	Delft University of Technology	D. Denis	Université Catholique de Louvain
J. van der Woude	Delft University of Technology	N. Hudon	Queen's University
TuA06-4	16.25-16.50	L. Lefevre	
<i>Frequency-driven market mechanisms for optimal power dispatch</i>	52	TuA08	Kenia
T. Stegink	University of Groningen	System Theory	
A. Cherukuri	ETH Zurich	Chair: Eric Steur	15.10-17.40
C. De Persis	University of Groningen	TuA08-1	15.10-15.35
A. van der Schaft, J. Cortés		<i>On representations of linear dynamic networks</i>	61
TuA06-5	16.50-17.15	E. Kivits	Eindhoven University of Technology
<i>Hybrid integrator-gain based elements for nonlinear motion control</i>	53	P. Van den Hof	Eindhoven University of Technology
S. van den Eijnden	Eindhoven Univ. of Technology	TuA08-2	15.35-16.00
M. Heertjes	Eindhoven Univ. of Technology	<i>Partitioning and stability for linear time-varying large-scale systems</i>	62
H. Nijmeijer	Eindhoven Univ. of Technology	T. Pippia	Delft University of Technology
Y. Knops		J. Sijs	Delft University of Technology
TuA06-6	17.15-17.40	B. De Schutter	Delft University of Technology
<i>Formal controller synthesis using genetic programming</i>	54	TuA08-3	16.00-16.25
C. Verdier	Delft University of Technology	<i>Strong structural controllability of systems on colored graphs</i>	63
M. Mazo	Delft University of Technology	J. Jia	University of Groningen
TuA07	Mozambique	H. Trentelman	University of Groningen
Distributed Parameter Systems		M. Camlibel	University of Groningen
Chair: Steffen Waldherr	15.10-17.40	W. Baar	
TuA07-1	15.10-15.35	TuA08-4	16.25-16.50
<i>On LQG control of infinite-dimensional stochastic port-Hamiltonian systems</i>	55	<i>Numerical analysis of oscillations in nonlinear networks</i>	64
F. Lamoline	University of Namur	K. Rogov	Eindhoven University of Technology
J. Winkin	University of Namur	A. Pogromsky	Eindhoven University of Technology
TuA07-2	15.35-16.00	E. Steur	Eindhoven University of Technology
<i>Nonlinear stabilization of infinite-dimensional port-Hamiltonian systems applied to repetitive control</i>	56	H. Nijmeijer	
F. Califano	University of Bologna	TuA08-5	16.50-17.15
A. Macchelli	University of Bologna	<i>Approximate controllability of an axially vibrating nanorod embedded in an elastic medium</i>	65
TuA07-3	16.00-16.25	H. Heidari	Damghan University
<i>Port-Hamiltonian formulation of vibrations in a nanorod</i>	57	TuA08-6	17.15-17.40
H. Zwart	University of Twente	<i>Multiple input multiple output Cepstrum coefficients</i>	66
H. Heidari	Damghan University	O. Lauwers	Katholieke Universiteit Leuven
		B. De Moor	Katholieke Universiteit Leuven

Wednesday, March 28, 2018

Mini Course: P3 Steyl
Networks of Dissipative Systems - Part III
 Murat Arcak
Chair: Mircea Lazar 9.15–10.15

Networks of Dissipative Systems - Part III . . . 189
 M. Arcak

Plenary: P4 Steyl
Distributed stochastic MPC
 Tamas Keviczky
Chair: Mircea Lazar 10:40–11.40

Distributed stochastic MPC 204
 T. Keviczky

WeM01 Steyl
System Identification B
Chair: Johan Schoukens 13.10-15.40

WeM01-1 13.10-13.35

A nonlinear state-space model of the transverse fluid force on an oscillating cylinder in a fluid flow 67
 J. Decuyper Vrije Universiteit Brussel
 T. De Troyer Vrije Universiteit Brussel
 M. Runacres Vrije Universiteit Brussel
 J. Schoukens

WeM01-2 13.35-14.00

From nonlinear identification to linear parameter varying models: Benchmark examples 68
 M. Schoukens Eindhoven University of Technology
 R. Toth Eindhoven University of Technology

WeM01-3 14.00-14.25

Grammar-based encoding of well-posed model structures for data-driven modeling 69
 D. Khandelwal Eindhoven University of Technology
 R. Toth Eindhoven University of Technology
 P. Van den Hof Eindhoven University of Technology

WeM01-4 14.25-14.50

Nonparametric regularization for time-varying operational modal analysis 70
 P. Csurcsia Vrije Universiteit Brussel
 J. Schoukens Vrije Universiteit Brussel
 B. Peeter Siemens Industry Software NV.

WeM01-5 14.50-15.15

A recursive least squares approach to distributed MISO system identification 71
 T. Steentjes Eindhoven University of Technology
 M. Lazar Eindhoven University of Technology
 P. Van den Hof Eindhoven University of Technology

WeM01-6 15.15-15.40

Identification of heat flux components in fusion plasmas 72
 M. van Berkel DIFFER
 T. Kobayashi National Institute for Fusion Science

WeM02 Angola
Optimal Control B
Chair: Mircea Lazar 13.10-15.40

WeM02-1 13.10-13.35

A penalty method algorithm for obstacle avoidance using nonlinear model predictive control 73
 B. Hermans Katholieke Universiteit Leuven
 G. Pipeleers Katholieke Universiteit Leuven
 P. Patrinos Katholieke Universiteit Leuven

WeM02-2 13.35-14.00

Real-time proximal gradient method for linear MPC 74
 R. Van Parys Katholieke Universiteit Leuven
 G. Pipeleers Katholieke Universiteit Leuven

WeM02-3 14.00-14.25

Combining optimal sensor and actuator selection with H-inf control design 75
 T. Singh Katholieke Universiteit Leuven
 M. De Mauri Katholieke Universiteit Leuven
 J. Swevers Katholieke Universiteit Leuven
 G. Pipeleers

WeM02-4 14.25-14.50

Optimal sensor configurations for collision avoidance: A minimax optimization approach 76
 R. Mohan Eindhoven University of Technology
 R. Gielen Philips Healthcare
 B. de Jager Eindhoven University of Technology

WeM02-5 14.50-15.15

Risk-averse risk-constrained optimal control 77
 D. Herceg IMT Lucca
 P. Sopasakis Katholieke Universiteit Leuven
 A. Bemporad IMT Lucca
 P. Patrinos

WeM02-6 15.15-15.40

Optimal control for a class of differential inclusions 78
 J. Eising University of Groningen
 M. Camlibel University of Groningen

WeM03 Argentinië
Aerospace and Automotive Applications B
Chair: Jan Swevers 13.10-15.40

WeM03-1 13.10-13.35

Driver intervention detection based on vehicle reference dynamics 79
 W. Schinkel Eindhoven University of Technology
 T. van der Sande Eindhoven University of Technology
 J. Loof Eindhoven University of Technology
 H. Nijmeijer

WeM03-2 13.35-14.00

Motion planning for automated connected vehicles 80
 R. van Hoek Eindhoven University of Technology
 J. Ploeg TNO
 H. Nijmeijer Eindhoven University of Technology

WeM03-3 **14.00-14.25**
String stability analysis of MPC-based heterogeneous platooning 81
 J. Reinders Eindhoven University of Technology
 E. van Nunen TNO
 E. Semsar-Kazerooni TNO
 N. van de Wouw

WeM03-4 **14.25-14.50**
Co-design of active controlled systems: Application to state-of-the-art CVT systems 82
 C. Fahdzyana Eindhoven University of Technology
 T. Hofman Eindhoven University of Technology

WeM03-5 **14.50-15.15**
Powertrain design sensitivity study of a heavy-duty hybrid electric truck 83
 F. Verbruggen Eindhoven University of Technology
 T. Hofman Eindhoven University of Technology

WeM03-6 **15.15-15.40**
Feed-forward ALINEA: A ramp metering control algorithm for nearby and distant bottlenecks . . . 84
 J. Frejo Delft University of Technology
 B. De Schutter Delft University of Technology

WeM04 **Bolivia**
Distributed Control and Estimation B
Chair: Tamas Keviczky **13.10-15.40**

WeM04-1 **13.10-13.35**
A robust PID autotuning method for steam/water loop in large scale ships 85
 S. Zhao Ghent University
 R. De Keyser Ghent University
 S. Liu Harbin Engineering University
 C. Ionescu

WeM04-2 **13.35-14.00**
Controlling triangular formations using angle information 86
 L. Chen University of Groningen
 M. Cao University of Groningen
 C. Li Harbin Institute of Technology

WeM04-3 **14.00-14.25**
Safe formation-motion control of mobile robots . 87
 N. Chan University of Groningen
 B. Jayawardhana University of Groningen
 J. Scherpen University of Groningen

WeM04-4 **14.25-14.50**
Distributed constraint optimization for mobile sensor coordination 88
 J. Fransman Delft University of Technology
 B. De Schutter Delft University of Technology
 J. Sijts Delft University of Technology

WeM04-5 **14.50-15.15**
Coping with collisions in decentralized event-triggered control 89
 M. Balaghiinaloo Eindhoven University of Technology
 D. Antunes Eindhoven University of Technology

WeM04-6 **15.15-15.40**
Distributed fault and malicious behaviour detection in multi vehicle systems 90
 N. Jahanshahi Delft University of Technology
 R. Ferrari Delft University of Technology

WeM05 **Botswana**
Mechanical Engineering A
Chair: Bayu Jayawardhana **13.10-15.40**

WeM05-1 **13.10-13.35**
Extending Cummins' equation to floater arrays: A port-Hamiltonian approach 91
 M. Almuzakki University of Groningen
 J. Barradas-Berglind University of Groningen
 Y. Wei University of Groningen
 M. Arias, A. Vakis, B. Jayawardhana

WeM05-2 **13.35-14.00**
Constrained multivariable extremum-seeking applied to optimization of Diesel engine fuel-efficiency 92
 R. van der Weijst Eindhoven University of Technology
 T. van Keulen Eindhoven University of Technology
 F. Willems Eindhoven University of Technology

WeM05-3 **14.00-14.25**
Reset control for transient performance improvement of systems with friction 93
 R. Beerens Eindhoven University of Technology
 N. van de Wouw Eindhoven University of Technology
 M. Heemels Eindhoven University of Technology
 H. Nijmeijer

WeM05-4 **14.25-14.50**
Symbolic equation extraction from SimScape . . . 94
 J. Gillis MECO Research Team
 E. Kikken Flanders Make

WeM05-5 **14.50-15.15**
Nonlinear modeling for analysis of directional drilling processes 95
 F. Shakib Eindhoven University of Technology
 E. Detournay University of Minnesota
 N. van de Wouw Eindhoven University of Technology

WeM05-6 **15.15-15.40**
Clamping strategies for belt-type CVT systems: An overview 96
 S. Prakash Eindhoven University of Technology
 T. Hofman Eindhoven University of Technology
 B. de Jager Eindhoven University of Technology

WeM06 **Congo**
Nonlinear Control B
Chair: Luis Pablo Borja Rosales **13.10-15.40**

WeM06-1 **13.10-13.35**
Capabilities of nonlinear iterative learning control with RoFaLT 97
 A. Steinhauser Katholieke Universiteit Leuven
 J. Swevers Katholieke Universiteit Leuven

WeM06-2 **13.35-14.00**
Learning control in practice: Novel paradigms for industrial applications 98
 J. Willems Flanders Make
 E. Hostens Flanders Make
 B. Depraetere Flanders Make
 A. Steinhauser, J. Swevers

WeM06-3 **14.00-14.25**
Passivity-based control of gradient systems. 99
 L. Borja-Rosales University of Groningen
 J. Scherpen University of Groningen
 A. van der Schaft University of Groningen

WeM06-4 **14.25-14.50**
Virtual differential passivity based control of mechanical systems in the port-Hamiltonian framework 100
 R. Baez University of Groningen
 A. van der Schaft University of Groningen
 B. Jayawardhana University of Groningen

WeM06-5 **14.50-15.15**
Projective contraction of switching systems 101
 G. Berger Université Catholique de Louvain
 F. Forni University of Cambridge
 R. Jungers Université Catholique de Louvain
 R. Sepulchre

WeM06-6 **15.15-15.40**
Nonlinear trajectory tracking via incremental passivity 102
 C. Wu Zhejiang University
 A. van der Schaft University of Groningen
 J. Chen Zhejiang University

WeM07 **Mozambique**
Model-based Control A
Chair: Leyla Ozkan **13.10-15.40**

WeM07-1 **13.10-13.35**
Modeling and localized feedforward control of thermal deformations induced by a moving heat load 103
 D. van den Hurk Eindhoven University of Technology
 S. Weiland Eindhoven University of Technology
 K. van Berkel ASML Netherlands B.V.

WeM07-2 **13.35-14.00**
Ten years of control for nuclear fusion in the Netherlands 104
 M. de Baar DIFFER

WeM07-3 **14.00-14.25**
Model-based control of reactive systems using extent-based LPV models 105
 C. Mendez-Blanco Eindhoven University of Technology
 A. Marquez-Ruiz Eindhoven University of Technology
 L. Ozkan Eindhoven University of Technology

WeM07-4 **14.25-14.50**
Tube-based linear parameter-varying MPC for a thermal system 106
 J. Hanema Eindhoven University of Technology
 R. Toth Eindhoven University of Technology
 M. Lazar Eindhoven University of Technology

WeM07-5 **14.50-15.15**
Design of distributed thermal actuators for a one-dimensional thermomechanical model 107
 D. Veldman Eindhoven University of Technology
 R. Fey Eindhoven University of Technology
 H. Zwart University of Twente
 M. van de Wal, J. van den Boom, H. Nijmeijer

WeM07-6 **15.15-15.40**
Design and modeling for controllable UHVCVD . 108
 M. Dresscher University of Groningen
 B. Kooi University of Groningen
 J. Scherpen University of Groningen
 B. Jayawardhana

WeM08 **Kenia**
Systems Biology
Chair: Steffen Waldherr **13.10-15.15**

WeM08-1 **13.10-13.35**
Partial synchronization in networks of Kuramoto-oscillator networks 109
 Y. Qin University of Groningen
 Y. Kawano University of Groningen
 M. Cao University of Groningen

WeM08-2 **13.35-14.00**
Integration of protein dynamics in batch bioprocess optimization 110
 G. Jeanne SUPELEC
 S. Tebbani SUPELEC
 D. Dumur SUPELEC
 A. Goelzer, V. Fromion

WeM08-3 **14.00-14.25**
Variable selection in linear dynamical systems . . 111
 A. Aalto University of Luxembourg
 J. Goncalves University of Luxembourg

WeM08-4 **14.25-14.50**
Nonlinear model predictive control of Escherichia coli culture 112
 A. Merouane University of Mons
 S. Tebbani SUPELEC
 D. Dumur SUPELEC
 A. Vande Wouwer, L. Dewasme

WeM08-5 **14.50-15.15**
Dynamic constraint-based modelling of bioprocesses: a dynamic flux balance analysis model for recombinant Streptomyces lividans 113
 K. De Becker Katholieke Universiteit Leuven
 K. Bernaerts Katholieke Universiteit Leuven
 W. Daniels Katholieke Universiteit Leuven
 K. Simoens

WeA01 **Steyl**
System Identification C
Chair: Julien Hendrickx **16.00-18.30**

- WeA01-1** **16.00-16.25**
Topology identification in dynamic Bayesian networks 114
 S. Shi Eindhoven University of Technology
 G. Bottegal Eindhoven University of Technology
 P. Van den Hof Eindhoven University of Technology
- WeA01-2** **16.25-16.50**
Topology reconstruction of dynamical networks via constrained Lyapunov equations 115
 H. van Waarde University of Groningen
 P. Tesi University of Groningen
 M. Camlibel University of Groningen
- WeA01-3** **16.50-17.15**
Local transfer functions recovery in networked system identification 116
 J. Hendrickx Université Catholique de Louvain
 M. Gevers Université Catholique de Louvain
 A. Bazanella Univ. Federal do Rio Grande do Sul
- WeA01-4** **17.15-17.40**
A sequential least squares algorithm for ARMAX model identification in a closed-loop with sensor noise 117
 H. Weerts Eindhoven University of Technology
 G. Bottegal Eindhoven University of Technology
 P. Van den Hof Eindhoven University of Technology
- WeA01-5** **17.40-18.05**
Sparse identification of linear parameter-varying systems using B-splines 118
 D. Turk Katholieke Universiteit Leuven
 G. Pipeleers Katholieke Universiteit Leuven
 J. Swevers Katholieke Universiteit Leuven
- WeA01-6** **18.05-18.30**
Local module identification in dynamic networks using regularized kernel-based methods 119
 K. Ramaswamy Eindhoven University of Technology
 G. Bottegal Eindhoven University of Technology
 P. Van den Hof Eindhoven University of Technology
- WeA02** **Angola**
Optimization
Chair: Jan Swevers **16.00-18.30**
- WeA02-1** **16.00-16.25**
Computing controlled invariant sets using semidefinite programming 120
 B. Legat Université Catholique de Louvain
 R. Jungers Université Catholique de Louvain
 P. Tabuada UCLA
- WeA02-2** **16.25-16.50**
Decoupling multivariate functions: exploring multiple derivative information 121
 J. De Geeter Vrije Universiteit Brussel
 P. Dreesen Vrije Universiteit Brussel
 M. Ishteva Vrije Universiteit Brussel
- WeA02-3** **16.50-17.15**
Solving multivariate polynomial optimization problems via numerical linear algebra 122
 C. Vermeersch Katholieke Universiteit Leuven
 O. Mauricio-Agudelo Katholieke Universiteit Leuven
 B. De Moor Katholieke Universiteit Leuven
- WeA02-4** **17.15-17.40**
Lookup tables in optimization with CasADi and OptiSpline 123
 J. Gillis Katholieke Universiteit Leuven
- WeA02-5** **17.40-18.05**
Proximal outer approximation 124
 M. De Mauri Katholieke Universiteit Leuven
 G. Pipeleers Katholieke Universiteit Leuven
 J. Swevers Katholieke Universiteit Leuven
- WeA02-6** **18.05-18.30**
Parametric and robust optimization with OptiSpline 125
 J. Gillis Katholieke Universiteit Leuven
 E. Lambrechts Katholieke Universiteit Leuven
 G. Pipeleers Katholieke Universiteit Leuven
- WeA03** **Robotics A** **Argentinië**
Chair: Mircea Lazar **16.00-18.30**
- WeA03-1** **16.00-16.25**
Semantic world modeling for autonomous cars . 126
 M. Dolatabadi Eindhoven Univ. of Technology
 M. van de Molengraft Eindhoven Univ. of Technology
 M. Steinbuch Eindhoven Univ. of Technology
- WeA03-2** **16.25-16.50**
Gearbox design for a flapping twin-wing robot . . 127
 H. Altartouri Université Libre de Bruxelles
 E. Garone Université Libre de Bruxelles
 A. Preumont Université Libre de Bruxelles
- WeA03-3** **16.50-17.15**
Implementation aspects of time-optimal predictive path following for robot arms 128
 N. van Duijkeren Katholieke Universiteit Leuven
 G. Pipeleers Katholieke Universiteit Leuven
 M. Diehl University of Freiburg
 J. Swevers
- WeA03-4** **17.15-17.40**
In-eye forbidden-region virtual fixtures based on optical-coherence-tomography-probe proximity measurements 129
 Y. Douven Eindhoven Univ. of Technology
 M. van de Molengraft Eindhoven Univ. of Technology
 M. Steinbuch Eindhoven Univ. of Technology
- WeA03-5** **17.40-18.05**
3D path-following using a guiding vector field . . 130
 W. Yao University of Groningen
 Y. Kapitanyuk University of Groningen
 M. Cao University of Groningen

WeA03-6 **18.05-18.30**
Identification of the time-varying joint impedances for the application to bionic devices 131
 G. Cavallo Vrije Universiteit Brussel
 M. van de Ruit Delft University of Technology
 A. Schoutens Delft University of Technology
 J. Lataire

WeA04 **Bolivia**
Games and Agent-Based Models A
Chair: Riccardo Ferrari **16.00-18.30**

WeA04-1 **16.00-16.25**
Resilience against misbehaving nodes in asynchronous networks 132
 D. Senejohnny University of Groningen
 S. Sundaram Purdue University
 C. De Persis University of Groningen
 P. Tesi

WeA04-2 **16.25-16.50**
The synchronizing probability function for primitive sets of matrices 133
 C. Catalano Gran Sasso Science Institute
 R. Jungers Université Catholique de Louvain

WeA04-3 **16.50-17.15**
Asynchronous proximal dynamics in multi-agent network games 134
 C. Cenedese University of Groningen
 S. Grammatico Delft University of Technology
 M. Cao University of Groningen

WeA04-4 **17.15-17.40**
Smart detection and real-time learning in water distribution 135
 C. Geelen Wageningen University

WeA04-5 **17.40-18.05**
Evolutionary game dynamics for two interacting populations under environmental feedback 136
 L. Gong University of Groningen
 M. Cao University of Groningen

WeA04-6 **18.05-18.30**
The indefinite soft-constrained differential game revisited 137
 J. Engwerda Tilburg University

WeA05 **Botswana**
Mechanical Engineering B
Chair: Karel J. Keesman **16.00-18.30**

WeA05-1 **16.00-16.25**
Inferential control of a wafer stage using disturbance observers 138
 N. Mooren Eindhoven University of Technology
 N. Dirks ASML Netherlands B.V.
 R. Voorhoeve Eindhoven University of Technology
 T. Oomen

WeA05-2 **16.25-16.50**
Dynamic simulation of ventilated potatoes in large-scale bulk storage facilities 139
 N. Grubben Wageningen University
 K. Keesman Wageningen University

WeA05-3 **16.50-17.15**
Modelling & control of a photopolymerization-based ceramic additive manufacturing process 140
 T. Hafkamp Eindhoven University of Technology
 B. de Jager Eindhoven University of Technology
 G. van Baars TNO
 P. Etman

WeA05-4 **17.15-17.40**
Modeling non-equilibrium multiphase systems 141
 A. Romo-Hernandez Université Catholique de Louvain
 D. Dochain Université Catholique de Louvain
 N. Hudon Queen's University
 E. Ydsite

WeA05-5 **17.40-18.05**
Data-driven inverse-model feedforward control using non-causal rational basis functions 142
 L. Blanken Eindhoven University of Technology
 S. Koekebakker OcÅI Technologies B.V.
 T. Oomen Eindhoven University of Technology

WeA05-6 **18.05-18.30**
A linear single degree of freedom model for acoustophoresis 143
 M. Hakan Kandemir Wageningen Univ. & Research
 R. Wagterveld Wetsus
 D. Yntema Wetsus
 K. Keesman

WeA06 **Congo**
Nonlinear Control C
Chair: Arjan van der Schaft **16.00-18.30**

WeA06-1 **16.00-16.25**
Lyapunov stability: Why uniform results are important, and how to obtain them 144
 E. Lefeber Eindhoven University of Technology

WeA06-2 **16.25-16.50**
Robust automatic generation control in power systems 145
 M. Cucuzzella University of Groningen
 S. Trip University of Groningen
 J. Scherpen University of Groningen
 C. De Persis, A. Ferrara

WeA06-3 **16.50-17.15**
On guaranteeing tracking performance and stability with LPV control for nonlinear systems 146
 G. Sales Mazzocante Eindhoven Univ. of Technology
 R. Toth Eindhoven Univ. of Technology
 S. Weiland Eindhoven Univ. of Technology

WeA06-4	17.15-17.40
<i>Performance tuning in extremum seeking control via Lie bracket approximations</i>	
C. Labar	Université Libre de Bruxelles
J. Feiling	University of Stuttgart
C. Ebenbauer	University of Stuttgart
WeA06-5	17.40-18.05
<i>Nonlinear model order reduction for MPD systems</i> 148	
S. Naderilordejani	Eindhoven Univ. of Technology
B. Besseblink	University of Groningen
N. van de Wouw	Eindhoven Univ. of Technology
W. Schilders	
WeA06-6	18.05-18.30
<i>Construction of PID passivity-based controllers for port-Hamiltonian systems</i>	
L. Borja-Rosales	University of Groningen
R. Ortega	SUPELEC
J. Scherpen	University of Groningen
WeA07	Mozambique
Model-based Control B	
Chair: Simon van Mourik	16.00-18.30
WeA07-1	16.00-16.25
<i>Robust greenhouse climate control</i>	
W. Kuijpers	Eindhoven Univ. of Technology
D. Katzin	Wageningen Univ. & Research
R. van de Molengraft	Eindhoven Univ. of Technology
S. van Mourik, E. van Henten	
WeA07-2	16.25-16.50
<i>Flexible bio-hydrogen supply based on model predictive control for balancing an urban hybrid renewable energy system</i>	
Y. Jiang	Wageningen University & Research
WeA07-3	16.50-17.15
<i>Model learning predictive control with applications to batch processes</i>	
M. Loonen	Eindhoven Univ. of Technology
A. Marquez-Ruiz	Eindhoven Univ. of Technology
M. Bahadir Saltik	Eindhoven Univ. of Technology
L. Azkan	
WeA07-4	17.15-17.40
<i>A model based scenario study for balanced crop irrigation</i>	
F. Mondaca-Duarte	Wageningen University
S. van Mourik	Wageningen University
E. van Henten	Wageningen University
WeA07-5	17.40-18.05
<i>Supervisory control synthesis for a lock-bridge combination</i>	
F. Reijnen	Eindhoven Univ. of Tech.
J. van de Mortel-Fronczak	Eindhoven Univ. of Tech.
J. Rooda	Eindhoven Univ. of Tech.
WeA07-6	18.05-18.30
<i>Prediction-based delay compensation for staged crystallization</i>	
M. Porru	Eindhoven University of Technology
L. Ozkan	Eindhoven University of Technology

WeA08	Kenia
State Observer and Estimation	
Chair: Bayu Jayawardhana	16.00-18.30
WeA08-1	16.00-16.25
<i>State estimation for nonlinear systems with communication constraints</i>	
Q. Voortman	Eindhoven University of Technology
A. Pogromsky	Eindhoven University of Technology
H. Nijmeijer	Eindhoven University of Technology
WeA08-2	16.25-16.50
<i>Cooperative adaptive cruise control: an observer-based approach to increase robustness over unreliable networks</i>	
F. Acciani	University of Twente
A. Stoorvogel	University of Twente
P. Frasca	University Grenoble Alpes
G. Hejjenk	
WeA08-3	16.50-17.15
<i>Real-time plasma state monitoring and supervisory control on the TCV Tokamak</i>	
T. Blanken	Eindhoven University of Technology
F. Felici	Eindhoven University of Technology
C. Galperti	EPFL
T. Vu, M. Kong, O. Sauter	
WeA08-4	17.15-17.40
<i>On experiment design for parameter estimation of equivalent-circuit battery models</i>	
H. Beelen	Eindhoven University of Technology
H. Bergveld	Eindhoven University of Technology
M. Donkers	Eindhoven University of Technology
WeA08-5	17.40-18.05
<i>A study on recurrent deep learning methods for state of charge estimation in Lithium-Ion batteries</i> 160	
E. Najafi	Eindhoven University of Technology
F. Zanjani	Eindhoven University of Technology
H. Bergveld	Eindhoven University of Technology
M. Donkers	
WeA08-6	18.05-18.30
<i>Similarity-based adaptive complementary filter for IMU fusion</i>	
A. Andrian	Eindhoven Univ. of Technology
D. Antunes	Eindhoven Univ. of Technology
R. van de Molengraft	Eindhoven Univ. of Technology
M. Heemels	

Thursday, March 29, 2018

Pleanary: P5 **Steyl**
Robot learning
Dongheui Lee
Chair: Raffaella Carloni **8.30–9.30**

Robot learning **231**
 D. Lee

Pleanary: P6 **Steyl**
Robot learning
Dongheui Lee
Chair: Raffaella Carloni **9.45–10.45**

Robot learning **244**
 D. Lee

ThM01 **Angola**
Medical Applications
Chair: Julien Hendrickx **10.45–12.50**

ThM05-1 **10.45–11.10**
Modeling and control of pharmacokinetic models **162**
 P. Themans University of Namur
 F. Musuamba University of Limoges
 J. Winkin University of Namur

ThM05-2 **11.10–11.35**
Control and state estimation for MR-guided HIFU hyperthermia **163**
 D. Deenen Eindhoven University of Technology
 B. Maljaars Eindhoven University of Technology
 B. de Jager Eindhoven University of Technology
 M. Heemels, L. Sebeke, E. Heijman

ThM05-3 **11.35–12.00**
Application of digital technologies in proton therapy treatment: Fast calibration **164**
 Z. Wang Université Catholique de Louvain
 Q. Flandroy IBA Group
 B. Herregods IBA Group
 R. Jungers

ThM05-4 **12.00–12.25**
EEG classification based on inductive means . . . **165**
 E. Massart Université Catholique de Louvain
 S. Chevallier Université de Versailles
 J. Hendrickx Université Catholique de Louvain
 P. Absil

ThM05-5 **12.25–12.50**
Quench detection for the cooling system of a particle accelerator for proton therapy **166**
 B. Dehem Université Catholique de Louvain
 N. Tran IBA Group
 F. Glineur Université Catholique de Louvain

ThM02 **Argentinië**
Robotics B
Chair: Raffaella Carloni **10.45–12.50**

ThM01-1 **10.45–11.10**
Composable skill programming framework for complex sensor-based robot tasks **167**
 Y. Pane Katholieke Universiteit Leuven
 W. Decre Katholieke Universiteit Leuven
 J. De Schutter Katholieke Universiteit Leuven

ThM01-2 **11.10–11.35**
Modelling and control of soft robot manipulators **168**
 B. Caasenbrood Eindhoven University of Technology
 H. Nijmeijer Eindhoven University of Technology
 A. Pogromsky Eindhoven University of Technology

ThM01-3 **11.35–12.00**
Development and implementation of a reconfigurable assembly cell **169**
 M. Verbandt Katholieke Universiteit Leuven
 R. Van Parys Katholieke Universiteit Leuven
 M. Kotzé Katholieke Universiteit Leuven
 J. Swevers, J. Philips, G. Pipeleers

ThM01-4 **12.00–12.25**
A variable stiffness joint with variable stiffness springs **170**
 R. Carloni University of Groningen
 V. Lapp University of Twente
 A. Cremonese University of Twente
 J. Belcari, A. Zucchelli

ThM01-5 **12.25–12.50**
A supervisory control and data acquisition (SCADA) system in agriculture and related path planning problems **171**
 N. Bono Rossello Université Libre de Bruxelles
 E. Garone Université Libre de Bruxelles
 A. Gasparri University of Roma Tre
 R. Carpio

ThM03 **Bolivia**
Games and Agent-Based Models B
Chair: Bart Besselink **10.45–12.50**

ThM02-1 **10.45–11.10**
Projected-gradient methods for generalized equilibrium seeking in aggregative games are preconditioned forward-backward splitting **172**
 G. Belgioioso Eindhoven University of Technology
 S. Grammatico Delft University of Technology

ThM02-2 **11.10–11.35**
Performance comparison of routing strategies for automated guided vehicles **173**
 V. Mazulina Eindhoven University of Technology
 A. Pogromsky Eindhoven University of Technology
 H. Nijmeijer Eindhoven University of Technology

ThM02-3 **11.35–12.00**
Exact potential of nonlinear public good games on networks **174**
 A. Govaert Eindhoven University of Technology
 M. Cao Eindhoven University of Technology

ThM02-4 **12.00-12.25**
Sets of stochastic matrices with converging products: Bounds and complexity 175
 P. Chevalier Université Catholique de Louvain
 V. Gusev Université Catholique de Louvain
 J. Hendrickx Université Catholique de Louvain

ThM02-5 **12.25-12.50**
Bursty walkers backtrack 176
 M. Gueuning University of Namur
 R. Lambiotte University of Namur
 J. Delvenne Université Catholique de Louvain

ThM04 **Botswana**
Electro-Mechanical Engineering
Chair: Bram de Jager **10.45-12.50**

ThM03-1 **10.45-11.10**
Torsional vibration- and backlash- compensation in drive-lines using non-linear feedforward control 177
 C. Vaseur Flanders Make
 A. Rosich Flanders Make
 M. Witters Flanders Make
 B. de Jager

ThM03-2 **11.10-11.35**
Identification of the drive train of an electric vehicle 178
 A. De Preter Octinion
 L. Jacobs MECO Research Team
 J. Anthonis Octinion
 G. Pipeleers, J. Swevers

ThM03-3 **11.35-12.00**
Constrained charging of Li-ion batteries 179
 A. Goldar Université Libre de Bruxelles
 R. Romagnoli Université Libre de Bruxelles
 L. Daniel Couto Université Libre de Bruxelles
 E. Garone, M. Kinnaert

ThM03-4 **12.00-12.25**
On power grids with grounded capacitors 180
 M. Jeeninga University of Groningen

ThM03-5 **12.25-12.50**
Modelling and control of a nanometer-accurate motion system 181
 I. Proimadis Eindhoven University of Technology
 T. Bloemers Eindhoven University of Technology
 R. Toth Eindhoven University of Technology
 H. Butler

ThM05 **Congo**
Model-based Control C
Chair: Leyla Ozkan **10.45-12.50**

ThM04-1 **10.45-11.10**
Structuring multilevel discrete-event systems modeled with extended finite state automata 182
 M. Goorden Eindhoven Univ. of Tech.
 M. Reniers Eindhoven Univ. of Tech.
 J. van de Mortel-Fronczak Eindhoven Univ. of Tech.
 J. Rooda

ThM04-2 **11.10-11.35**
L2-gain analysis of periodic event-triggered systems with varying delays using lifting techniques 183
 N. Srijbosch Eindhoven University of Technology
 G. Dullerud University of Illinois
 A. Teel UCSB
 M. Heemels

ThM04-3 **11.35-12.00**
Systems and control in precision farming: Prospects and challenges 184
 S. van Mourik Wageningen University
 P. Koerkamp Wageningen University
 E. van Henten Wageningen University

ThM04-4 **12.00-12.25**
LCToolbox - A MATLAB toolbox for robust control design 185
 L. Jacobs Katholieke Universiteit Leuven
 M. Verbandt Katholieke Universiteit Leuven
 J. Swevers Katholieke Universiteit Leuven
 G. Pipeleers

ThM04-5 **12.25-12.50**
Effortless NLP modeling with CasADi Opti stack 186
 J. Gillis MECO Research Team

Event: E1 **Steyl**
DISC Certificates & Best Thesis Award
Chair: Henk Nijmeijer **12.50-13.10**

Event: E2 **Steyl**
Best Junior Presentation Award
Chair: Award Committee **13.10-13.25**

Pleanary: P7 **Steyl**
Closure
Chair: Organizing Committee **13.25-13.30**

Part 1: Programmatic Table of Contents 3
 Overview of scientific program

Part 2: Contributed Lectures 17
 Abstracts

Part 3: Plenary Lectures 187
 Presentation slides

Part 4: List of Participants 255
 Alphabetical list

Part 5: Organizational Comments 265
 Comments, overview program, map

Part 2

Contributed Lectures

Subspace Identification for Linear Parameter-Varying Systems^{*}

P. B. Cox, R. Tóth, and P. M. J. Van den Hof

Control Systems Group

Eindhoven University of Technology

P.O. Box 513, 5600 MB Eindhoven, The Netherlands

p.b.cox@tue.nl

1 Introduction

In recent years, the *linear parameter-varying* (LPV) modelling paradigm has been applied to many practical applications to synthesise controllers with performance guarantees even under nonlinear or temporal variations of the underlying system [1]. In the majority of these methods, an LPV *state-space* (SS) model of the system at hand is required, particularly with static and affine dependence on the scheduling signal. However, identification of such a representation based on observations of the plant is not straightforward and converting other representation based models – that might be easier to identify – into an SS form suffer from several disadvantages. Popular *subspace identification* (SID) schemes used for SS model estimation start by identifying a specific *input-output* (IO) structure using convex optimisation, wherefrom an SS model is constructed by matrix decomposition techniques. Current LPV subspace schemes depend on over-restrictive assumptions and/or the number of the to-be-estimated variables grows exponentially, leading to ill-conditioned IO estimation problems with high computational demand. Therefore, it is currently infeasible to identify moderate to large scale systems with LPV SID schemes. To lower the computational load and ease certain assumptions, we analyse state-of-the-art SID schemes combined with an in-depth examination of LPV IO to SS realisation theory to be able to formulate a unified LPV subspace identification framework and tackle the bottlenecks.

2 Deriving the data-equations

Subspace schemes are based on various forms of so-called *data-equations*, surrogate IO models to represent the underlying system. We will derive such open-loop and closed-loop data-equations given that the data-generating system is in the following innovation form (similar to, e.g., [2, 3]):

$$\check{x}_{t+1} = \mathcal{A}(p_t)\check{x}_t + \mathcal{B}(p_t)u_t + \mathcal{K}(p_t)\xi_t, \quad (1a)$$

$$y_t = \mathcal{C}(p_t)\check{x}_t + \mathcal{D}(p_t)u_t + \xi_t, \quad (1b)$$

where subscript t is the discrete time, x is the state variable, y is the measured output signal, u denotes the input signal, ξ is a zero-mean white noise process satisfying $\xi_t \sim \mathcal{N}(0, \mathcal{Q})$ with covariance matrix \mathcal{Q} , and $\mathcal{A}, \dots, \mathcal{K}$ are affine functions

in the scheduling signal, i.e., $\mathcal{A}(p_t) = A_0 + \sum_{i=1}^{n_p} A_i p_t^{[i]}$ with $p_t^{[i]}$ the i -th element in p_t . The to-be-estimated coefficients are $\{A_i, \dots, K_i\}_{i=1}^{n_p}$. The innovation representation (1) can arbitrarily well approximate a representation with independent parameter-varying noise sources on both the state and output equations. The difficulty in applying subspace identification on the derived open-loop and closed-loop data-equations using (1) is that the realization is need to be accomplished under a time-varying observability matrix.

3 Parametric subspace identification

To obtain an SS realisation from either the open-loop or closed-loop data-equation, we derive a uniform projection based formulation for the LPV realisation problem established on a maximum-likelihood and stochastic realisation based argument; therefore, extending various well-known linear time-invariant SID schemes to the LPV setting. Furthermore, we show that applying the *moving average with exogenous inputs* (MAX) IO model set in the LPV open-loop identification setting can significantly decrease the complexity of the IO estimation problem for SIDs. In addition, we introduce a basis reduced formulation that can lower the computational complexity significantly in the IO to SS model realisation step. These two new developments lead to better scalable SID schemes. Concluding, we will discuss a unified understanding of LPV subspace identification including LPV IO to SS realisation theory with computationally efficient methods leading to competitive schemes to estimate LPV-SS models.

References

- [1] J. Mohammadpour and C. Scherer, editors. *Control of Linear Parameter Varying Systems with Applications*. Springer, 2012.
- [2] P. Lopes dos Santos, J. A. Ramos, and J. L. Martins de Carvalho. Subspace identification of linear parameter-varying systems with innovation-type noise models driven by general inputs and a measurable white noise time-varying parameter vector. *Int. J. of Systems Science*, 39(9):897–911, 2008.
- [3] J. W. van Wingerden and M. Verhaegen. Subspace identification of bilinear and LPV systems for open- and closed-loop data. *Automatica*, 45(2):372–381, 2009.

^{*} This work has received funding from the European Research Council (ERC) under the European Union's Horizon 2020 research and innovation programme (grant agreement No 714663).

Identification of LTI models from concatenated data sets

Sandra Vásquez^{1,2}, Michel Kinnaert¹ and Rik Pintelon²

¹Department SAAS (ULB), ²Department ELEC (VUB)

Email: savasque@ulb.ac.be

1 Introduction

For some industrial applications, experimental data is available in the form of several data sets corresponding to the operation of the plant under the same conditions. An example of such an application is the condition monitoring of a wind turbine based on SCADA data. Here, one is interested in the identification of a turbine's subsystem for a specific wind condition. However, long records of a given operating condition might be difficult to obtain. Hence, one needs to select multiple short data-records from the operational data to identify the system. In this case, identification approaches where missing data are treated as unknown parameters [1, 2] are not feasible due to the large amount of lost data. Then, the best option is to concatenate the data sets, and introduce additional parameters to handle the transient effects [3]. Our aim is to verify the consistency of the estimates when considering this last approach. To this end, we performed a Montecarlo simulation to prove consistency when dealing with AR and ARX model structures.

2 Results

The concatenation of M data sets is done as follows

$$x^c(tT_s) = \begin{cases} x_1(tT_s) & t = 0, \dots, N_1 - 1 \\ x_2(tT_s) & t = N_1, \dots, N_1 + N_2 - 1 \\ \vdots & \vdots \\ x_M(tT_s) & t = (N_1 + \dots + N_{M-1}), \dots, N \end{cases}$$

Then, the input/output DFT spectra (U^c, Y^c) satisfy

$$Y^c(z_k^{-1}) = G(z_k^{-1}, \theta) U^c(k) + H(z_k^{-1}, \theta) E(k) + T_1(z_k^{-1}, \theta) + z_k^{-N_1} T_2(z_k^{-1}, \theta) + \dots + z_k^{-(N_1 + \dots + N_{M-1})} T_M(\Omega_k, \theta)$$

with $G(z_k^{-1}, \theta) = B(z_k^{-1}, \theta)/A(z_k^{-1}, \theta)$ and $H(z_k^{-1}, \theta) = C(z_k^{-1}, \theta)/D(z_k^{-1}, \theta)$ the plant and noise rational transfer function models, and $T_l(z_k^{-1}, \theta)$ the transient terms. For the AR and ARX model structures, $C = 1$, $D = A$, and $T_l(z_k^{-1}, \theta) = I_l(z_k^{-1}, \theta)/A(z_k^{-1}, \theta)$. In addition, $B = 0$ for the AR case.

To verify the consistency on the parameter estimation for both AR and ARX cases, a Montecarlo simulation is performed to compare two situations: the concatenation of data from M experiments (with record length of N_m), and one single experiment (with $N = N_m M$ samples). A first order system and transient term are considered ($A = 1 + a_1 z_k^{-1}$, $B = 0$ or $B = 1$, $I_l = i_l$), and the excitation [$e(t)$ or $u(t)$] is

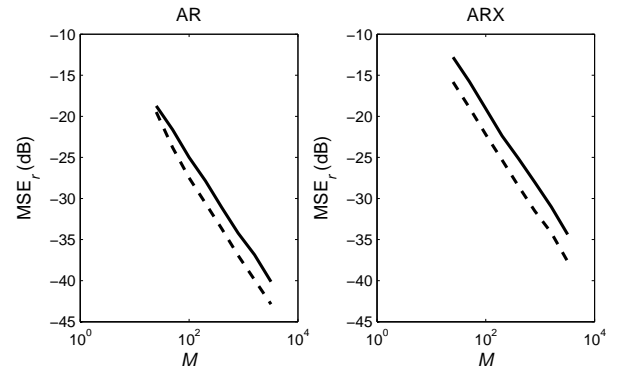


Figure 1: Normalized Mean Square Error MSE_r for AR and ARX: concatenated data sets (—), one data record (---)

white noise with zero mean and unit variance. We tested $N_m = 2$, which corresponds to the extreme case where the data records are just large enough to estimate the parameters.

Figure 1 presents the mean square error (MSE) on the estimation of a_1 for different values of M . These results show that for both AR and ARX, the parameter estimation departing from concatenated data is consistent, since the MSE decreases with M at the same rate as the case of one data record. The observed difference on the MSE corresponds to the information loss for the concatenated case. Indeed, for this case one sample out N_m is used to estimate the transient coefficient (i_l). Hence, the theoretical difference is $\text{db}(MSE_{conc}/MSE_{one\ rec}) = \text{db}(\sqrt{N_m/(N_m - 1)})$. The results for the simulation of both AR and ARX follow well this theoretical difference (3 db, see Fig. 1).

Acknowledgment

This work is supported by the Fonds de la Recherche Scientifique FNRS (research fellow grant), and is partially supported by the Flemish government (Methusalem grant METH1) and the Belgian federal government (IAP network DYSCO).

References

- [1] A. J. Isaksson, Identification of ARX-Models Subject to Missing Data. IEEE Transactions on automatic control, Vol. 38, no. 5, May 1993.
- [2] R. J. A. Little and D. B. Rubin, Statistical Analysis with Missing Data. New York: Wiley, 1987.
- [3] R. Pintelon and J. Schoukens, System identification: A frequency domain approach. IEEE Press, 2012.

Local Rational Method with prior system knowledge: with application to mechanical and thermal systems

Enzo Evers¹, Bram de Jager¹, Tom Oomen¹

¹ Eindhoven University of Technology, Department of Mechanical Engineering, Control Systems Technology group

PO Box 513, 5600MB Eindhoven, The Netherlands, e-mail: e.evers@tue.nl

1 Background

Frequency Response Function (FRF) identification is fast, inexpensive and accurate, and often used in applications. These FRFs are used either directly, e.g., for controller tuning or stability analysis, or as a basis for parametric identification. Identification of FRFs has been substantially advanced over recent years, particularly by explicitly addressing transient errors. The Local Polynomial Method (LPM) [1] exploits the assumed smoothness of the transient response and approximates locally the transfer function by a polynomial such that the transient can be removed.

2 Problem

Consider the output of a LTI system in the frequency domain

$$Y(k) = G(e^{i\omega_k})U(k) + T(e^{i\omega_k}) + V(k) \quad (1)$$

where $G(e^{i\omega_k})$ is the frequency response function of the dynamic system, $Y(k), U(k), V(k)$ are the output, input and noise terms and k denotes the k -th frequency bin. Where $T(e^{i\omega_k})$ accounts for the transients of both the system response and the noise. An extension of the LPM, the Local Rational Method (LRM) [2, 3] approximates the terms $G(e^{i\omega_k})$ and $T(e^{i\omega_k})$ in (1) such that in the local window

$$Y(k+r) = \frac{N_{k+r}}{D_{k+r}}U(k+r) + \frac{M_{k+r}}{D_{k+r}} + V(k+r) \quad (2)$$

As a consequence of the rational parameterization, the local estimation problem is no longer linear in the parameters which poses additional challenges. The aim of the present paper is to investigate alternative parametrizations, which are also recovered as a special case of the LRM, yet are linear in the parameters while exploiting the advantages of rationally parametrized model structures.

3 Approach

Enabling a convex optimization while maintaining the rational parameterization is done by pre-specifying the system poles based on prior knowledge. Consider again a local window around a DFT bin k such that locally

$$G(e^{i\omega_{k+r}}) = \sum_{b=1}^{Nb} \theta_{G_b} B_b(e^{i\omega_{k+r}}), \quad T(e^{i\omega_{k+r}}) = \sum_{b=1}^{Nb} \theta_{T_b} B_b(e^{i\omega_{k+r}}) \quad (3)$$

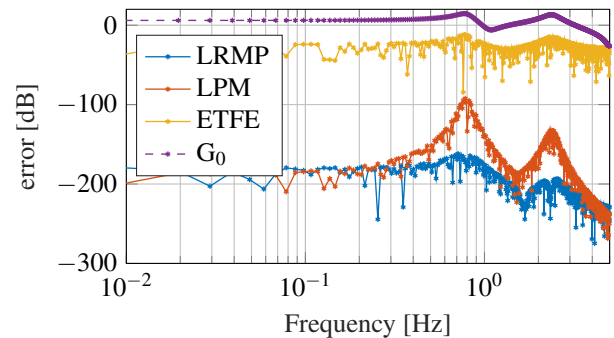


Figure 1: Estimation error of the Local Rational Method with Prior knowledge (LRMP) versus the LPM and classical method (ETFE). G_0 denotes the true system.

with basis functions $B_b(e^{i\omega_{k+r}})$ and parameters $\theta_{G_b}, \theta_{T_b}$. If the basis functions B_b contain the true system dynamics of $G(w_{k+r})$ and $T(e^{i\omega_{k+r}})$, then the basis in (3) can approximate the system in the local window arbitrarily well.

4 Result

A resonant system with two resonance modes is used for simulation. The discrete system has two sets of complex conjugated poles at $z_1 = 0.8359 \pm 0.4540i, z_2 = 0.0673 \pm 0.8581i$. An orthonormal basis is composed of single complex poles, e.g., $\zeta = [0.8359 + 0.4540i, 0.0673 + 0.8581i]$ where ζ are a subset of the poles of the true system. The result in Fig. 1 shows an improved estimation accuracy for both resonance modes. Extensive simulations reveal that the method is robust for inaccurate ζ and for real poles occurring in thermal systems.

Acknowledgments

Supported by the ATC and NWO-VIDI nr 15698.

References

- [1] R. Pintelon and J. Schoukens, System identification: a frequency domain approach, 2nd ed. 2012.
- [2] D. Verbeke and J. Schoukens, Local parametric modeling based on rational approximation, in 36th Benelux Meeting on Systems and Control, Spa, Belgium, 2017.
- [3] R. Voorhoeve, A. van der Maas, and T. Oomen, Non-parametric identification of multivariable systems: A local rational modeling approach with application to a vibration isolation benchmark, Mechanical Systems and Signal Processing, vol. 105, pp. 129152, May 2018.

Order estimation of multidimensional transfer function by calculating Hankel intersections

Bob Vergauwen Oscar Mauricio Agudelo Bart De Moor

KU Leuven, Department of Electrical Engineering (ESAT), Stadius Center for Dynamical Systems, Signal Processing and Data Analytics.

bob.vergauwen@esat.kuleuven.be; mauricio.agudelo@esat.kuleuven.be; bart.demoor@esat.kuleuven.be

1 Introduction

This presentation introduces a data-driven method for determining the order of the transfer function representation of a multidimensional (nD) linear system. A Hankel matrix (referred to as recursive Hankel matrix) is constructed from the available multidimensional data in a recursive way. This work extends the concept of past and future data to nD systems and introduces the concept of mode- k left and right data. The intersection between two mode- k left and right matrices reveals the order of the system in dimension k .

2 Problem statement

In this work the class of nD models is restricted to linear difference equations [1], referred to as PdEs. All equations are defined on a rectangular domain in n -dimensions. For a two-dimensional model, the class of linear PdEs is given by,

$$\sum_{i=0}^{N_1} \sum_{j=0}^{N_2} \beta_{i,j} y[k_1 + i, k_2 + j] = \sum_{i=0}^{N_1} \sum_{j=0}^{N_2} \alpha_{i,j} u[k_1 + i, k_2 + j], \quad (1)$$

where k_1 and k_2 are two independent variables. $u[\cdot, \cdot]$ and $y[\cdot, \cdot]$ are the input and output variables respectively, $\beta_{i,j}$ and $\alpha_{i,j}$ are the coefficients of the PdE and N_1 and N_2 determine the order of the PdE. Note that the order of the PdE is a tuple: for every dimension the order of the PdE is equal to the highest order of the shift operator.

At the basis of the identification algorithm presented in this work lies the concept of the recursive Hankel matrix. This matrix is a block Hankel matrix where all the blocks are Hankel themselves.

3 Intersections between past, future, left and right.

The intersection algorithm presented in [2] calculates the intersection between past and future Hankel matrices. For a two-dimensional dataset, past and future is extended with left and right. Graphically the concept of past and future, left and right is shown in Fig. 1. The data matrix is first Hankelized, and afterwards split up in four matrices, past, future, left and right. The intersections between these matrices reveals the order of the PdE.

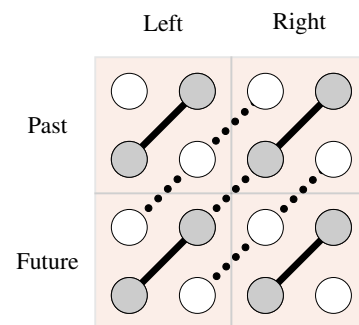


Fig. 1: Multidimensional transfer functions can graphically be represented by stencils. The dots in this figure represent data points distributed in two dimensions. The solid and dashed lines connecting two points represent linear relations between adjacent data points. By splitting up the data in left-right, past-future some relations are removed, these linear relations are denoted by the dashed lines.

4 Results

The main result of this presentation is an algorithm to estimate the order of a PdE on a rectangular grid with a uniform sampling time/distance. The data is Hankelized and split up in different Hankel matrices. Based on the rank of these matrices the order of the PdE is estimated. The presented method for estimating the order of a PdE is demonstrated on a numerical simulation example.

Acknowledgements

This research receives support from FWO under EOS project GOF6718N (SeLMA) and from KU Leuven Internal Funds: C16/15/059 and C32/16/013.

References

- [1] Richard Courant, Kurt Friedrichs, and Hans Lewy. On the partial difference equations of mathematical physics. *IBM journal*, 11(2):215–234, 1967.
- [2] Marc Moonen, Bart De Moor, Lieven Vandenberghe, and Joos Vandewalle. On-and off-line identification of linear state-space models. *International Journal of Control*, 49(1):219–232, 1989.

Prior Knowledge and the Least Costly Identification Experiment

Georgios Birpoutsoukis

ICTEAM, Université Catholique de Louvain, B1348 Louvain la Neuve, Belgium

georgios.birpoutsoukis@uclouvain.be

Xavier Bombois

Laboratoire Ampère UMR CNRS 5005, Ecole Centrale de Lyon, 69134 Ecully, France

e-mail: xavier.bombois@ec-lyon.fr

1 Introduction

Optimal input design (OID) is one of the most challenging problems in the field of system identification. In this work, OID for linear systems in the presence of prior knowledge is studied. Information related to exponential decay and smoothness is incorporated in the OID problem by making use of the Bayes rule of information. Three different cases of modeling the linear dynamics are considered, namely Finite Impulse Response (FIR) model with and without prior knowledge, as well as the rational transfer function case. It is shown that the prior information affects the spectrum of the minimum power optimal input. The input with the least power is obtained for the transfer function model case.

2 The OID problem

A stable linear time-invariant system S_0 is considered in an output error framework such that $y = G_0 u + e$ where y is the measured output, u denotes the input to the system, G_0 is a rational transfer function and e is i.i.d. noise ($e \sim \mathcal{N}(0, \sigma_e^2)$). The OID problem is defined as:

$$\begin{aligned} \Phi_{u,opt}(\omega_n) &= \arg \min_{\Phi_u(\omega_n)} p_u(\Phi_u(\omega_n)) \\ \text{s.t. } M_{\text{total}} &> R_{\text{adm}}(\omega), \forall \omega \\ \Phi_u(\omega_n) &\geq 0 \forall \omega_n \end{aligned} \quad (1)$$

where the power spectrum Φ_u of the multisine input u is the design variable of the OID problem which is affine in $\Phi_u(\omega_n)$. The first constraint sets a bound on the information matrix M_{total} . It is shown in [1] that accuracy constraints on the identified model can be transformed into a constraint in the form $M_{\text{total}} > R_{\text{adm}}$ where R_{adm} is in this case a frequency-dependent constraint on the model error achieved at transfer function level of the identified model. In case of prior information available, the total information matrix is given by $M_{\text{total}} = M + P^{-1}$ where M denotes the Fisher matrix representing the information linked to the new experiment and P^{-1} represents prior information about the identified model. The second constraint is necessary for the signal to be realizable. The optimal design problem (1) is convex in the design variables, therefore there is no risk of resulting in a local minimum.

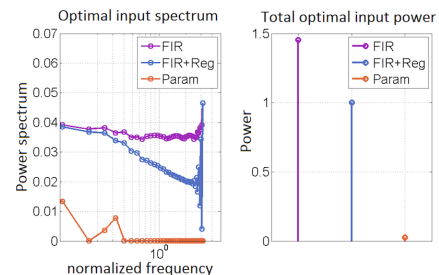


Figure 1: The optimal input for a linear system in three different cases of model structures. Left: Optimized input spectra for the different model structures. Right: Total power of the optimal input signals.

3 Results

The result of the OID problem (1) is depicted in Fig. 1. The optimal input spectrum in case of FIR modeling approaches the one of a white noise signal, as expected. However, when prior knowledge about smoothness of the impulse response is considered, it will suppress the power of the estimated transfer function in the high frequency region. Under this condition, the more relaxed the constraint on the modulus of the transfer function, the more is the prior information able to deliver a model inside the allowable model error bounds. Therefore, the power of the optimal input signal decreases in the high frequency region as the constraint on the transfer function modulus relaxes.

4 Acknowledgments

This work was supported in part by the Fund for Scientific Research (FWO-Vlaanderen), by the Flemish Government (Methusalem), the Belgian Government through the Inter university Poles of Attraction (IAP VII) Program, and by the ERC advanced grant SNLSID, under contract 320378.

References

- [1] Bombois, X., & Scorletti, G. Design of least costly identification experiments: The main philosophy accompanied by illustrative examples. *Journal Européen des Systèmes Automatisés (JESA)*, 46(6-7):587-610, 2012.

Closed-loop identification without using external excitation.

Wengang Yan, Paul M.J. Van den Hof

Control Systems Group, Department of Electrical Engineering, Eindhoven University of Technology,
5600 MB Eindhoven, The Netherlands

Email: w.yan@tue.nl; p.m.j.vandenhof@tue.nl

1 Introduction

System identification is a fundamental step in model-based control. Most identification based controller tuning methods use test signals during the identification test. However, test signals disturb process operation, which is a cost in production unit. To reduce the cost of identification, it would be ideal to use no test signal during the identification test. For closed-loop identification, when there is no external excitation, the informative condition must be fulfilled to ensure that the identification criterion has a unique minimum and the parameter estimation is consistent. In this work, the informative conditions are firstly introduced and developed. Then, a method of closed-loop test without using test signals is proposed to achieve the informative condition. Finally, a model error bound is adopted to do the model validation.

2 Informative condition

Informativity is a concept that central in identification problems. Loosely speaking, the problem is whether the dataset $z(t)$ allows us to distinguish between different models in model set $M(\theta)$. The necessary and sufficient conditions for single-input single-output (SISO) closed-loop systems to produce informative data are discussed by Gevers et al. [1]. In this work, we extend their results to multi-input single-output (MISO) closed-loop systems. Note that the multi-input multi-output (MIMO) systems are typically identified as a series of MISO systems. Here, we briefly introduce one main result. Consider the ARMAX model structure,

$$A(q^{-1})y(t) = \sum_{i=1}^m B_i(q^{-1})u_i(t) + C(q^{-1})e(t) \quad (1)$$

with n_a , n_b and n_c are the degrees of corresponding polynomials, and the controller $K(q^{-1}) = \left[\frac{S_1(q^{-1})}{R(q^{-1})} \dots \frac{S_m(q^{-1})}{R(q^{-1})} \right]^T$, with n_s and n_r are the degrees of the controller. Then, under some reasonable assumptions, the informative condition for data set $z(t)$ generated by the MISO closed-loop system without external excitation is as follows:

$$\max(n_s - n_a, n_r - n_b) \geq (m - 1)n_b \quad (2)$$

In summary, for linear time-invariant controller, the informative conditions indicate that the orders of the regulator must be high enough to make the data set generated by the closed-loop system informative.

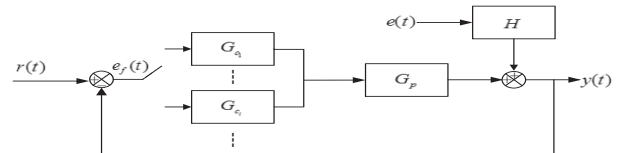


Figure 1: Closed-loop system under shifting controller

3 Method to achieve informativity

According to Ljung[2], using nonlinear controllers can make closed-loop systems produce informative data. In this work, the nonlinearity of controller is obtained by using a linear regulator that shifts between different settings, which is shown in Fig. 1. For identification-based control, this method is very useful. Additionally, by developing some proper shifting rules, the control performance of closed-loop system could be improved during identification test.

4 Model validation

For a model based control method, model validation is required to check whether the identified model is suitable for control. In [3], a stochastic model error bound is derived based on the asymptotic properties. The model error bound $\Delta(\omega)$ is given as:

$$|G^0(e^{j\omega}) - \hat{G}(e^{j\omega})| \leq \Delta(\omega) \triangleq 3 \sqrt{\frac{n_h}{N} \frac{\Phi_v(\omega)\sigma_e^2}{\Phi_u(\omega)\sigma_e^2 - |\Phi_{ue}(\omega)|^2}} \quad (3)$$

To use the error bound, an engineering solution is adopted. This is done by comparing the relative size of the bound with the model over the low and middle frequencies. When the size of bound is smaller than half that of the model, the model can be accepted as a "good" model.

References

- [1] M. Gevers, A. Bazanella and L. Mišković, Identification and the Information Matrix: How to Get Just Sufficiently Rich?, *IEEE Transactions on Automatic Control* 54(12) (2010), 2828-2840.
- [2] L. Ljung, System identification: Theory for the User, Second Edition, Prentice-Hall, Englewood, Cliffs, NJ, 1999.
- [3] Y. Zhu, Multivariable process identification for MPC: the asymptotic method and its applications, *Journal of Process Control* 8(2) (1998),

A Suboptimality Approach to Distributed Linear Quadratic Optimal Control

Junjie Jiao, Harry L. Trentelman, and M. Kanat Camlibel

Johann Bernoulli Institute for Mathematics and Computer Science,

University of Groningen, The Netherlands

j.jiao@rug.nl, h.l.trentelman@rug.nl, m.k.camlibel@rug.nl

1 Introduction

In this work, we consider the distributed linear quadratic optimal control problem for multi-agent networks [1], [2]. In this problem, we are given a number of identical agents represented by a finite dimensional linear input-state system, and an undirected graph representing the communication between these agents. Given is also a quadratic cost functional that penalizes the differences between the states of neighbouring agents and the size of the local control inputs. The distributed linear quadratic problem is then to find a distributed diffusive control law that, for given initial states of the agents, minimizes the cost functional, while achieving consensus for the controlled network. This problem is non-convex and difficult to solve, and it is unclear whether in general a solution exists. Therefore, in this work, instead of addressing the version formulated above, we will study a suboptimal version of the distributed optimal control problem. Our aim is to design suboptimal distributed diffusive control laws that guarantee the controlled network to reach consensus and the associated cost to be smaller than an a priori given upper bound.

2 Problem Formulation

In this work, we consider a multi-agent system consisting of N identical agents. The underlying graph is assumed to be undirected and connected, and the corresponding Laplacian matrix is denoted by L . The dynamics of the identical agents is given by

$$\dot{x}_i(t) = Ax_i(t) + Bu_i(t), \quad x_i(0) = x_{i0}, \quad i = 1, 2, \dots, N \quad (1)$$

where $A \in \mathbb{R}^{n \times n}$, $B \in \mathbb{R}^{n \times m}$, and $x_i \in \mathbb{R}^n$, $u_i \in \mathbb{R}^m$ are the state and input of the i -th agent, respectively. We assume that the pair (A, B) is stabilizable. Furthermore, we can rewrite multi-agent system (1) in compact form as

$$\dot{x} = (I_N \otimes A)x + (I_N \otimes B)u, \quad x(0) = x_0 \quad (2)$$

with $x = (x_1^\top, \dots, x_N^\top)^\top$, $u = (u_1^\top, \dots, u_N^\top)^\top$, where $x \in \mathbb{R}^{nN}$, $u \in \mathbb{R}^{mN}$ contain the states and inputs of all agents, respectively. Moreover, we consider the cost functional that integrates the weighted quadratic difference of states between every agent and its neighbors, and also penalizes the inputs

in a quadratic form, which is given by

$$J(u) = \int_0^\infty x^\top (L \otimes Q)x + u^\top (I_N \otimes R)u dt, \quad (3)$$

where $Q \geq 0$ and $R > 0$ are given real weighting matrices.

Our aim is to design a class of suboptimal distributed diffusive control law of the form $u = (L \otimes K)x$, where $K \in \mathbb{R}^{m \times n}$ is an identical feedback gain for all agents, such that the overall network dynamics

$$\dot{x} = (I_N \otimes A + L \otimes BK)x \quad (4)$$

reaches consensus and the associated cost

$$J(K) = \int_0^\infty x^\top (L \otimes Q + L^2 \otimes K^\top RK) x dt. \quad (5)$$

is smaller than an a priori given upper bound. More concretely, we consider the following problem:

Problem 1. Consider multi-agent system (2) with associated cost functional (3). Assume the network graph is a connected undirected graph with Laplacian L . Let $\gamma > 0$ be an a priori given upper bound for the cost to be achieved. The problem is to find a distributed controller $L \otimes K$ so that the controlled network (4) reaches consensus and the cost (5) associated with this controller is smaller than the given upper bound, i.e., $J(K) < \gamma$.

3 Main Results

We present two design methods for computing suboptimal distributed diffusive control laws, both based on computing a positive semi-definite solution of a single Riccati inequality of dimension equal to the dimension of single agent dynamics. Furthermore, we relax the requirement of exact knowledge of the smallest nonzero and largest eigenvalue of the graph Laplacian by using only lower and upper bounds on these eigenvalues.

References

- [1] F. Borrelli and T. Keviczky, "Distributed LQR Design for Identical Dynamically Decoupled Systems," *IEEE Transactions on Automatic Control*, vol. 53, no. 8, pp. 1901 - 1912, Sept 2008.
- [2] D. H. Nguyen, "A sub-optimal consensus design for multi-agent systems based on hierarchical LQR," *Automatica*, vol. 55, pp. 88 - 94, 2015.

Vehicle Energy Management with Ecodriving: A Sequential Quadratic Programming Approach with Dual Decomposition

Z. Khalik G.P. Padilla T.C.J. Romijn M.C.F. Donkers

department of Electrical Engineering, Eindhoven University of Technology

{z.khalik, g.p.padilla.cazar, t.c.j.romijn, m.c.f.donkers}@tue.nl

1 Introduction

Energy consumption of the vehicle is optimized by controlling the power flow between energy storage (e.g. fuel tank and battery), the consumers (e.g. wheels, HVAC, etc) and converters (e.g. internal combustion engine and electric motor). However, in these Vehicle Energy Management (VEM) problems, the vehicle speed is assumed to be given, while most of the power generated by the powertrain is used for propelling the vehicle. Therefore, optimizing the speed of a vehicle over a certain trajectory, thereby allowing for an optimal conversion of potential energy from the road profile into kinetic energy of the vehicle, can lead to a considerable energy consumption reduction. We refer to this latter problem as the ecodriving problem.

2 Energy Management with Ecodriving

The ecodriving problem is defined as minimizing traction power P_{trac} over a certain trajectory, subject to the longitudinal vehicle dynamics and some bounds on the speed v and input u , i.e.,

$$\min_{v(t), s(t), u(t)} \int_{t_0}^{t_f} P_{\text{trac}}(v(t), u(t)) dt, \quad (1a)$$

$$\begin{cases} \dot{v}(t) = \sigma_u u(t) - \sigma_v v(t)^2 - \sigma_r - g \sin(\alpha(s(t))), \\ \dot{s}(t) = v(t), \end{cases} \quad (1b)$$

$$\underline{v}(t) \leq v(t) \leq \bar{v}(t), \quad \underline{u}(t) \leq u(t) \leq \bar{u}(t), \quad (1c)$$

with $v(0)$, $s(0)$, $v(t_f)$, $s(t_f)$ known, and where σ_r , σ_u , σ_v , g are some vehicle dynamics related parameters, s is the distance traveled and α is the road slope. To arrive at a finite dimensional optimization problem, we can discretize (1) using a forward Euler discretization, and arrive discrete-time nonlinear optimal control problem. With the problem in this form, it can be solved using Sequential Quadratic Programming (SQP), in which we form a convex SQP subproblem by using linearizing the objective function of the discrete-time problem and adding Tikhonov regularization, as well as linearizing the state dynamics. The ecodriving problem can be integrated into the VEM problem, of which an SQP formulation can be made and be decentralized using dual decomposition [1]. This distributed approach is presented in [2] to solve a Complete Vehicle Energy Management (CVEM) problem, in which auxiliary components (e.g. a refrigerated semi-trailer) are added to the energy management

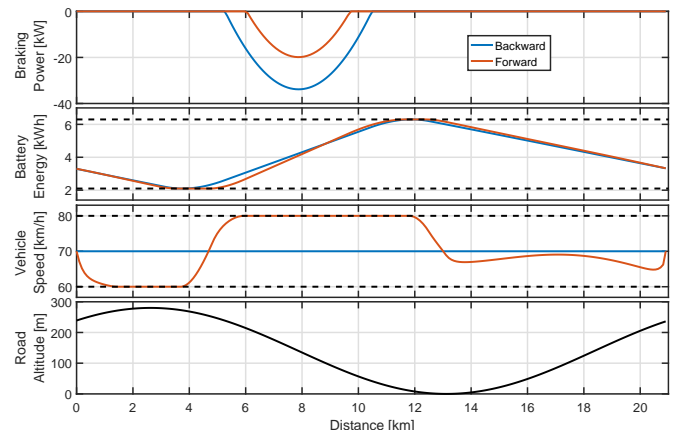


Figure 1: Backward vs forward optimization. The dotted lines represent minimum and maximum state constraints.

problem [2]. Hence, the SQP and dual decomposition approach presented here lay a foundation to solve the CVEM with ecodriving problem.

3 Results

A simulation study for the energy management with ecodriving problem for a series-hybrid electric vehicle is done, and the results are shown in Fig. 1. Here, 'backward' and 'forward' refer to solving the energy management problem with and without ecodriving respectively. We can observe that the amount of braking power is reduced significantly overall, and furthermore, the vehicle speed is now used as a buffer (along side the battery), e.g., the speed is on the lower bound at 4 km, so that the potential energy that is available from 4 km on, is maximally converted to kinetic energy. This allows the fuel consumption to be reduced from 23.41 l/100 km to 22.31 l/100 km, which is a decrease of 4.7%, by including the ecodriving into the VEM problem.

References

- [1] Khalik, Z., et al. "Vehicle Energy Management with Ecodriving: A Sequential Quadratic Programming Approach with Dual Decomposition.", Submitted to American Control Conference, 2017.
- [2] Romijn, T. C. J., et al. "A distributed optimization approach for complete vehicle energy management.", IEEE Transactions on Control Systems Technology, 2018.

Spline-based trajectory generation for CNC-machines

Tim Mercy and Goele Pipeleers
 MECO Research Team, KU Leuven, Leuven, Belgium
 DMMS lab, Flanders Make, Leuven, Belgium
 Tim.Mercy@kuleuven.be

1 Introduction

In the modern manufacturing industry, Computerized Numerical Control (CNC) machines are commonly used for the production of workpieces. Generally, the workpiece geometry is described as a connection of GCode segments, building its contour. In order to create the workpiece, the machine tool needs to track this contour, requiring a set of trajectories for its axes. Various strategies exist to compute trajectories that let the tool center point trace the contour within the desired accuracy. A popular strategy is to first re-shape the contour, by e.g. rounding sharp corners. Afterwards, the feed rate of the tool along the re-shaped contour is planned, where the rounded shape allows for a higher average velocity [1]. However, this so-called decoupled approach leads to suboptimal results, since the complete problem is not solved in a single step.

This abstract presents a novel spline-based trajectory generation method for CNC machines that simultaneously optimizes the workpiece geometry and the tool feed rate. This coupled approach uses an optimal control problem (OCP) formulation to immediately take into account the machine limits like velocity, acceleration and jerk bounds and process limits like the maximum feed rate. In addition, the method directly includes the provided workpiece tolerance by converting it into a tube inside which the machine tool has to stay. Since a lower tolerance inevitably leads to a higher machining time, the method allows making a trade-off between accuracy and productivity, while returning near-optimal trajectories.

2 Methodology

The proposed approach computes machine tool trajectories by assigning a separate spline to each GCode segment. This leads to easy contouring constraints that keep the tool inside the tolerance tube. However, when optimizing only one trajectory in each OCP, the tool must come to standstill at the end of each segment, in order to connect any subsequent segment in a smooth way. These decoupled trajectories are suboptimal, except for the case of exact contour tracking (tolerance zero). To avoid decoupling, the proposed method simultaneously optimizes a sequence of N segments by solving a single OCP. Connection constraints impose continuity up to acceleration level at the spline interconnections. In combination with the tolerance tube around

each segment, which creates an overlap region between subsequent segments, this allows connecting subsequent segments smoothly (see Figure 1). In addition, the trajectories can exploit the tolerance band, increasing productivity.

In order to limit the amount of splines that are optimized simultaneously (N), which reduces the complexity of the OCP, the proposed trajectory generator uses a moving horizon approach. From the computed trajectories for the first N segments, only the one for the first segment is saved. Afterwards, the horizon is shifted, removing segment one from the OCP and adding segment $N + 1$.

The receding horizon approach allows making a good initial guess for all segments. In addition, the presented method exploits spline properties to obtain an efficient problem formulation [2]. Together, this leads to OCP's that require a low solving time.

3 Results

Figure 1 shows the computed machine tool trajectories for an anchor-shaped workpiece with a tolerance of 0.5mm.

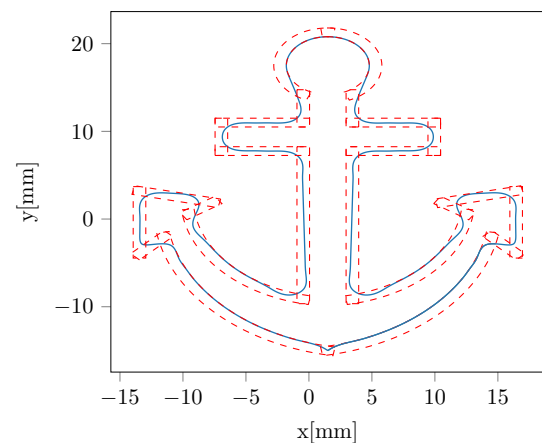


Figure 1: Anchor-shaped workpiece - machine tool trajectories

Acknowledgement This work benefits from KU Leuven-BOF PFV/10/002 Centre of Excellence: Optimization in Engineering (OPTEC), from the project G0C4515N of the Research Foundation-Flanders (FWO-Flanders), from Flanders Make ICON project: Avoidance of collisions and obstacles in narrow lanes, and from the KU Leuven Research project C14/15/067: B-spline based certificates of positivity with applications in engineering.

References

- [1] F. Sellmann, *Exploitation of tolerances and quasi-redundancy for set point generation*. PhD thesis, ETH Zürich, 2014.
- [2] T. Mercy, W. Van Loock, and G. Pipeleers, "Real-time motion planning in the presence of moving obstacles," in *European Control Conference (ECC)*, pp. 1586–1591, 2016.

Optimized thermal-aware workload scheduling and control of data centers

Tobias Van Damme, Claudio De Persis, Pietro Tesi
 ENTEG - Smart Manufacturing Systems
 University of Groningen
 Nijenborgh 4, 9747AG Groningen
 The Netherlands

Email: {t.van.damme, c.de.persis, p.tesi}@rug.nl

1 Abstract

Recent years have seen a huge increase in online data traffic. Nowadays everything is computed and stored in the cloud. Web giants as Google and Facebook process huge amounts of data on a daily basis. All this processing and storing is done in data centers, halls with thousands of servers. The size of these data centers have increased to the point where they consume megawatts of energy on a yearly basis. With this increase of energy consumption has come a corresponding drive to optimize the control and cooling of a data center such that the operational costs can be kept as low as possible.

Major challenges in controlling data centers lie in providing adequate cooling and preventing thermal hot spots from occurring, and optimizing the number of servers which are on at any given time [1, 2, 3]. In an attempt to reduce power consumption, thermal-aware control strategies have been studied and analyzed. The main control objective for a thermal-aware workload scheduler is to keep the temperature of all data processing units below a certain threshold while at the same time maximizing energy efficiency of the system.

2 Thermodynamical Model

To address this problem a thermodynamical model of the data center is derived[4]. Following this model, the change of temperature of a part of the data center can then be given by:

$$mc_p \dot{T}(t) = Q_{in}(t) - Q_{out}(t) + P(t)$$

where m is the mass of the air, c_p is the heat capacity, $Q_{in}(t)$ is the heat entering the unit, $Q_{out}(t)$ is the heat exiting the unit, and $P(t)$ is the power consumed by the unit. The thermal model directly links the power consumption of the server infrastructure to the temperature changes of the individual components. In the previous work, this model was used to solve an optimization problem that minimizes the energy consumption of the cooling equipment in the data center. Furthermore controllers were designed which steer the data center to this optimal operating point.

3 Project goals

1. A key part in the thermodynamical model are the air flows in the data center. These air flows are chaotic and data-center-dependent, and furthermore difficult to determine. In order to provide a method for finding these parameters, the field of system identification is explored to find proper algorithms to tackle this challenge.
2. The current controllers only work in the interior of the constraint set of the optimization problem. Efforts to extend the controller to operate on the constraint boundaries are done.
3. The theoretical models are integrated into an extensive simulation framework, where the interaction with more heuristic approaches is studied. This is an important stepping stone towards understanding the interaction between different control algorithms and studying the theory behind the combination of these algorithms.

References

- [1] N. Vasic, T. Scherer, and W. Schott, *Thermal-Aware Workload Scheduling for Energy Efficient Data Centers*, Proc. 7th int. conf. on Autonomic computing, 2010, pp.169-174.
- [2] Parolini, L. and Krogh, B., *A cyber-physical systems approach to data center modeling and control for energy efficiency*, Proceedings of the IEEE, 1(2012), 100, pp.254-268.
- [3] S. Li, H. Le, N. Pham, J. Heo and T. Abdelzaher, *Joint Optimization of Computing and Cooling Energy: Analytic Model and A Machine Room Case Study*, 32nd Int. Conf. on Distributed Computing Systems, 2012, pp. 396-405.
- [4] T. Van Damme, C. De Persis and P. Tesi, *Optimized Thermal-Aware Job Scheduling and Control of Data Centers*, 20th IFAC World Congress, 2017, Vol. 50, No. 1, pp. 8244-8249.

On Convexity of the Eco-driving Problem

G.P. Padilla, S. Weiland, M.C.F. Donkers

Control Systems Group, Dep. of Electrical Engineering, Eindhoven University of Technology

{g.p.padilla.cazar, s.weiland, m.c.f.donkers}@tue.nl

1 Introduction

Improving energy efficiency of vehicles is an important topic of research for the automotive industries. The problem of reducing the energy consumption of a vehicle over a certain drive cycle can be formulated as an optimal control problem and its solution is often referred to as an energy management strategy. These strategies are traditionally focused on controlling the power split between the energy buffers and consumers in the vehicle. However, a recent trend is to extend this energy management system to incorporate the vehicle velocity (and thereby the power needed to propel the vehicle) in the optimal control problem; this approach is known as the eco-driving problem.

2 Eco-driving Problem

Eco-driving is a driving strategy that aims to increase the energy efficiency of a vehicle. This strategy is the solution to an optimal control problem that aims at obtaining an optimal traction force $u(t)$ and velocity profile $v(t)$ that minimizes the total power $P(v, u)$ consumed by a vehicle while travelling during a given time interval $[t_o, t_f]$ over a given trajectory $s(t) \in [s_o, s_f]$ with known geographical characteristics; while being subject to longitudinal vehicle dynamics (1b), non-negative velocity bounds $v(t) \in [\underline{v}, \bar{v}]$, and boundary conditions on position and velocity. This can be stated in the form of the following optimal control problem:

$$\min_{s(t), v(t), u(t)} \int_{t_o}^{t_f} P(v(t), u(t)) dt \quad (1a)$$

$$\text{subject to } m \frac{dv}{dt} = u - f(v, s), \quad (1b)$$

$$\frac{ds}{dt} = v, \quad (1c)$$

$$s(t_o) = s_o, s(t_f) = s_f \quad (1d)$$

$$v(t_o) = v_o, v(t_f) = v_f \quad (1e)$$

$$\underline{v} \leq v \leq \bar{v}, \quad (1f)$$

The consumed power $P(v, u)$ can be obtained from different modeling approaches that capture the energy consumption in the powertrain.

In general, (1) is a non-linear optimal control problem that might be nonconvex due to specific features of the vehicle model and road profile. This implies that direct optimization methods or methods based on PMP only provide candidate minima, which might not correspond to the global solution to problem (1).

3 Convexity of the Eco-driving Problem

Several methods have been already proposed to solve (1), see, e.g., [1]. However, the literature related to the convexity of the eco-driving problem is scarce. For this reason the work presented in [2] aims to expose a detailed view of the convexity issues of the eco-driving optimal control problem. These results are used to warrant the global optimality of the solution for equivalent convex optimization problems. The main contributions of this research are three fold: First, a method to reformulate and discretize the problem preserving its convexity is presented; second, a set of physically realistic conditions that guarantee a convex (discretized) eco-driving problem are given (see Fig 1; and finally, a sequential quadratic programming method with a convex quadratic programming sub-problem is proposed in order to efficiently solve the eco-driving problem (see Fig. 2).

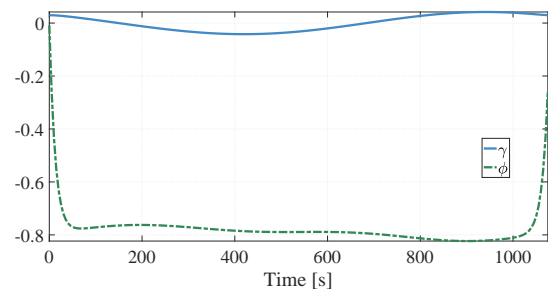


Figure 1: Certification of convexity ($\gamma \geq \phi$).

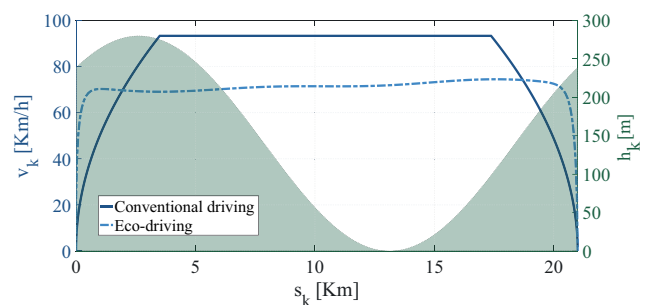


Figure 2: Conventional vs. eco-driving profiles.

References

- [1] A. Sciarretta, G. D. Nunzio, and L. L. Ojeda, "Optimal Eco-driving Control: Energy-Efficient Driving of Road Vehicles as an Optimal Control Problem," *IEEE Control Systems*, vol. 35, no. 5, pp. 71–90, Oct. 2015.
- [2] G. P. Padilla, Siep Weiland and M. C. F. Donkers, "On Convexity of the Eco-driving Problem," Submitted to ACC, 2018.

Attitude control of a UAV in presence of motor asymmetry

Njinwoua Brice
Control Department
Mons University
Boulevard Dolez 31, Mons
Belgium

Email: Brice.Njinwoua@umons.ac.be

Alain Vande Wouwer
Control Department
Mons University
Boulevard Dolez 31, Mons
Belgium

Email: Alain.Vandewouwer@umons.ac.be

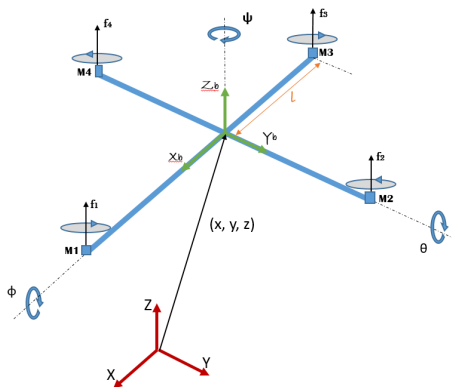


Figure 1: Quadcopter coordinate system.

1 Abstract

Quadcopter (Fig. 1), is one of the most used UAVs in both military and commercial in and out-door applications. The stabilisation and the guidance of the quadcopter have been widely study by researchers as they represent a complex problem because of the non linearity of the model and the four control inputs used to control the 6 degrees of freedom of the copter.

In this study, a cascade control strategy with PD and PI loop is presented (Fig. 2) to achieve a multirotor stabilization when the electrical actuators have discrepancies in their characteristics. The external disturbance created by the actuator asymmetry is compensated by the PI loop, while the PD loop ensures closed-loop stabilization. The robustness of the control strategy is tested in simulation (Fig. 3) as well as in real-life experiments.

References

- [1] Modelling, Simulation and Altitude-Range-Analysis of Quad-copter UAV, Barve et al., 2014
- [2] Aerodynamics and control of autonomous quadrotor helicopters in aggressive maneuvering, Huang et al., 2009
- [3] Attitude control of a quadrotor, Dikmen et al., 2009

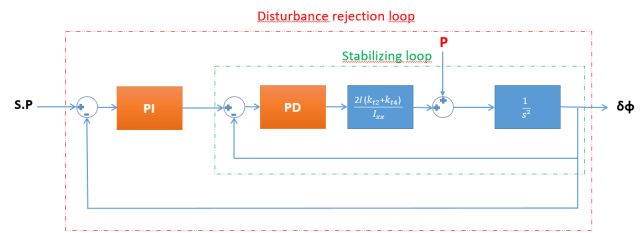


Figure 2: Cascade control.

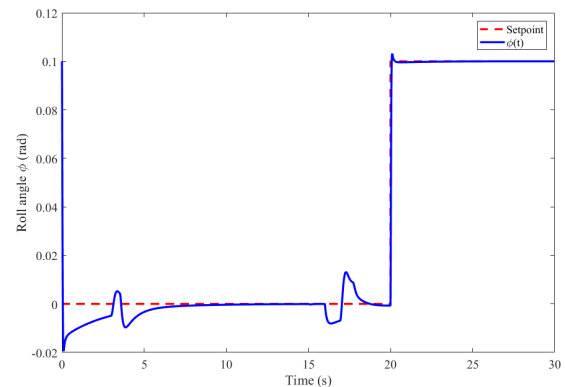


Figure 3: Roll angle : disturbances rejection (10% discrepancy and coupling effects of the Yaw angle).

- [4] Pitch and Roll control of a Quadcopter using Cascade Iterative Feedback Tuning, Douglas et al., 2016
- [5] Different approaches of PID control UAV type quadrotor, Szafranski et al., 2011
- [6] The true role of accelerometer feedback in quadrotor control, Martin et al., 2010
- [7] Quadcopter physical parameter identification and altitude system analysis, Mustapha et al., 2014

Longitudinal Stability Augmentation System for a highly unstable forward swept wing UAV by employing a neutral canard angle.

Mathias Creyf Frederik Debrouwere Mark Versteyhe Stijn Debruyne
Department of Mechanical Engineering, M-Group, KU Leuven Campus Bruges, Belgium

Introduction

Unmanned Aerial Vehicles (UAV) are typically designed to be statically stable, resulting in systems that are easy to fly remotely. Inherent aircraft stability however significantly reduces the maneuverability. In order to cope with this, the authors are designing a Forward Swept Wing (FSW) UAV which shows great maneuverability but is inherently highly unstable around the pitch axis. In order to facilitate the remote piloting of this aircraft, a Stability Augmentation System (SAS) in pitch is hence required. This paper presents the design of the longitudinal SAS, based on the linearized state space model. It will be shown that it is required to incorporate a neutral canard angle in the model in order to meet the targeted response requirements.

Setup Description

The conceptual design of the forward swept wing UAV is presented in Figure 1. Sweeping the wing forward leads to a span wise lift distribution with more lift closer to the wing root, which reduces the wing bending moment, resulting in a lowered structural weight of the wing. Also, a FSW inherently starts to stall at the wing root. This enhances the low speed handling capabilities of the UAV since the ailerons are not stalled, greatly reducing the risk of entering a spin when the UAV starts to stall.



Figure 1: (left) Conceptual design of the FSW UAV. The canard is indicated in orange. (right) Neutral canard angle

Since the UAV will be used for high angle of attack flight, the canard offers some advantages. Since it is in front the wing, the canard always experiences ‘clean’ air and so the UAV does not have the risk of pitch-up tendencies from the blanketing of a conventional tail. Also the canard vortex interacts with the wing, potentially leading to a delay in wing stall and higher lift at and beyond stall.

Approach

The presented research first focuses on the stabilization of the UAV in the longitudinal direction (pitch); (later adding roll and yaw and the coupling). The goal of the SAS is to stabilize the pitch rate of the FSW UAV while a desired pitch rate can be commanded through the pilot stick.

Stabilization is taken care of by a full state feedback controller, which will receive its input from a state observer, since natural responses of an inherent stable UAV are typically specified in open loop pole locations. These open loop pole locations are then considered as the target pole locations of the closed loop stabilized SAS. Tracking of the desired pitch rate will be taken care of by a PI controller. The longitudinal system dynamics are linearized around trim conditions and aerodynamic parameters are estimated from the initial UAV geometry. The state is composed of forward speed, angle of attack, pitch rate and pitch angle, while the input is the canard deflection angle.

It was observed that stabilization of the longitudinal dynamics is infeasible with a full state feedback controller for the targeted pole locations obtained for the short period and phugoid modes. Since the UAV is designed to be neutrally stable with the canard removed, the canard should always be more or less parallel to the airflow in order to be able to stabilize the longitudinal dynamics (see Figure 1 (right)). This is referred to as the neutral canard angle. The canard control signal is hence the neutral angle added with the control signal for stabilization and tracking. The authors proposed to embed this neutral canard angle in the system state space equations. The system remains highly unstable but it is now feasible to derive a full state feedback controller which meets the targeted requirements.

Results and future work

Flight tests were performed with the full non-linear model in Matlab and Simulink. Future work will include identified aerodynamic parameters from wind tunnel tests. Furthermore, since the system is highly nonlinear in the angle of attack a gain scheduling controller will be implemented. Special care will be taken beyond the stall area since then it is possible to exploit the full capabilities of the FSW UAV manoeuvrability. Actuator dynamics will also be considered since now it is assumed that the canard actuator can track the neutral angle and control angle infinitely fast.

Control of Tethered Quadrotors through Geodesics

Tam Nguyen
SAAS department
Université libre de Bruxelles
Av. F. Roosevelt 50, CP 165/55, 1050 Brussels
Belgium
Email: tanguyen@ulb.ac.be

Emanuele Garone
SAAS department
Université libre de Bruxelles
Av. F. Roosevelt 50, CP 165/55, 1050 Brussels
Belgium
Email: egarone@ulb.ac.be

1 Abstract

This abstract addresses the control problem of quadrotors physically connected to the ground by means of tether cables. The control problem is to stabilize the UAV to a desired position while ensuring that the cable remains taut at all times (see Figure 1). Under the assumption of a massless

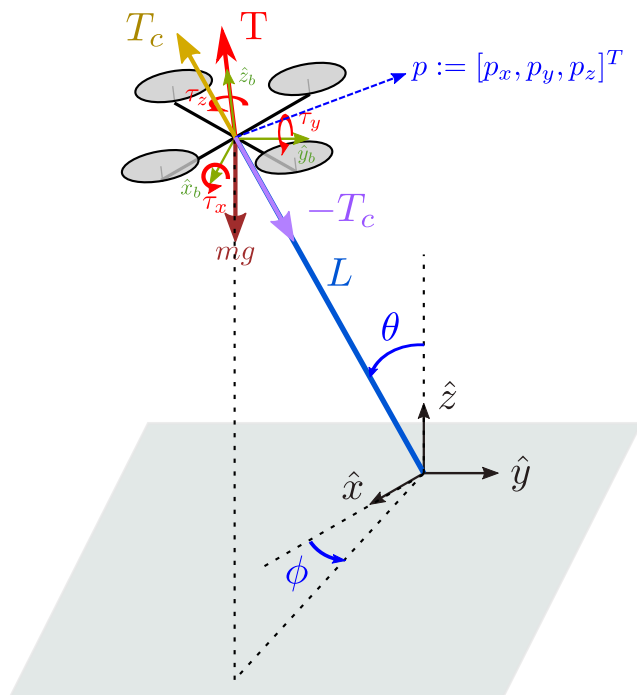


Figure 1: Quadrotor tethered to the ground.

and inextensible cable and assuming that the cable can be kept taut at all times, the dynamics of the system is the usual model of a UAV [1] subject to a holonomic constraint

$$\begin{cases} m\dot{p} = TR\hat{z} - mg\hat{z} & (1) \\ \mathcal{J}\dot{\omega} = -\omega^\wedge \mathcal{J}\omega + \tau, & (2) \\ \dot{q} = \frac{1}{2}E(q)\omega, & (3) \\ \text{subject to:} & \\ \|p\| = L, & (4) \end{cases}$$

where $m \in \mathbb{R}_0^+$ is the mass of the UAV, $p \in \mathbb{R}^3$ the position of the UAV, $T \in \mathbb{R}^+$ the UAV thrust, $R \in SO(3)$ the UAV attitude, $\hat{z} := [0, 0, 1]^T$ the vertical component of the inertial frame, $g \in \mathbb{R}_0^+$ the gravity acceleration, $\mathcal{J} \in \mathbb{R}_0^{+, 3 \times 3}$ the moment of inertia of the UAV, $\omega := [\omega_x, \omega_y, \omega_z]^T \in \mathbb{R}^3$ the angular velocity of the UAV, $\tau \in \mathbb{R}$ the resultant torque of the UAV, $L \in \mathbb{R}_0^+$ the length of the cable, and $q \in \mathbb{H}$ the quaternion associated to R . We also consider the saturations of the actuators

$$0 \leq T \leq T_{max}, \quad T_{max} \in \mathbb{R}_0^+. \quad (5)$$

The strategy is to use a cascade control approach where the inner loop controls the attitude of the UAV, whereas the outer loop controls its position. More specifically, the outer loop is designed so that the control law:

- compensates the natural gravity force of the system;
- ensures that the cable is taut at all times;
- uses the path of the great-circle navigation called the "geodesic path".

In order to prove asymptotic stability of the overall control scheme, Small Gain arguments are used. The control scheme is augmented with a nonlinear Reference Governor to enforce constraints satisfaction.

References

- [1] Mayhew, Christopher G., Ricardo G. Sanfelice, and Andrew R. Teel. "Robust global asymptotic attitude stabilization of a rigid body by quaternion-based hybrid feedback." Decision and Control, 2009 held jointly with the 2009 28th Chinese Control Conference. CDC/CCC 2009. Proceedings of the 48th IEEE Conference on. IEEE, 2009.
- [2] Nicotra, Marco M., Roberto Naldi, and Emanuele Garone. "Nonlinear control of a tethered UAV: The taut cable case." Automatica 78 (2017): 174-184.
- [3] Nguyen, Tam, and Emanuele Garone. "Control of a UAV and a UGV Cooperating to Manipulate an Object." American Control Conference (ACC), 2016. IEEE, 2016.

Constrained Attitude Control of Rigid Bodies via Explicit Reference Governor

Satoshi Nakano, Tam Nguyen, Emanuele Garone
 Service d'Automatique et d'Analyses des Systèmes
 Université libre de Bruxelles
 Avenue Franklin Roosevelt 50, Brussels 1050
 Belgium

Email: snakano@ulb.ac.be, tanguyen@ulb.ac.be, egarone@ulb.ac.be

This paper focuses on the constrained attitude control of a fully actuated rigid body. The dynamics considered is the second order system [1]

$$\dot{R} = R\hat{\omega}, \quad (1)$$

$$J\dot{\omega} = (J\omega)^\wedge \omega + \tau, \quad (2)$$

where $R \in SO(3)$ is the rotation matrix, $\omega \in \mathbb{R}^3$ the angular velocity, $J \in \mathbb{R}^{3 \times 3}$ the inertia matrix and $\tau \in \mathbb{R}^3$ the control torque. Furthermore we define the operator $\wedge : \mathbb{R}^3 \rightarrow so(3)$ such that $x^\wedge y = x \times y, x, y \in \mathbb{R}^3$ and the inverse operator of \wedge as \vee such that $(x^\wedge)^\vee = x$, where $so(3)$ is the set of $\mathbb{R}^{3 \times 3}$ skew-symmetric matrices. We assume that conic constraints are considered [2, 3]

$$a_{ci}^T R a_{bi} \leq \cos \theta_{ci}, a_{ci}, a_{bi} \in \mathbb{S}^2, 0 < \theta_{ci} < \pi, i = \{1, \dots, n_c\} \quad (3)$$

where \mathbb{S}^2 is the set of the unit sphere on \mathbb{R}^3 i.e. $\mathbb{S}^2 \subset \mathbb{R}^3 = \{a \in \mathbb{R}^3 \mid \|a\| = 1\}$, a_{ci} the center of the constraint and $R a_{bi} \in \mathbb{S}^2$ the direction attached to the body frame Σ_b whose configuration is R (see Fig. 1). These constraints represent the restrictions of the pointing directions attached to the rigid body. One of the applications is to avoid damaging sensitive devices e.g. pointing exclusion of cameras towards the sun.

The control objective is to design τ in Eq. (2) such that: (i) $\lim_{t \rightarrow \infty} \text{sk}(R^T R_d)^\vee = 0, \text{sk}(A) = \frac{1}{2}(A - A^T)$; (ii) for any reference attitude $R_d(t) \in SO(3)$, constraints (3) are satisfied.

The proposed control scheme (see Fig. 2) consists of the cascade of two control laws, the first which is tasked with the stabilization of the system (Attitude Control) and the second which takes care of modifying the reference to the attitude control to take into account the constraints. The stabilization control is based on a $SO(3)$ Lyapunov approach based on geodesic arguments. For the constraints satisfaction, we design an Explicit Reference Governor [4] to suitably modify the reference such that constraints are enforced during the transient. All the proposed control laws are defined in terms of rotation matrices in $SO(3)$ and do not make use of any parameterization.

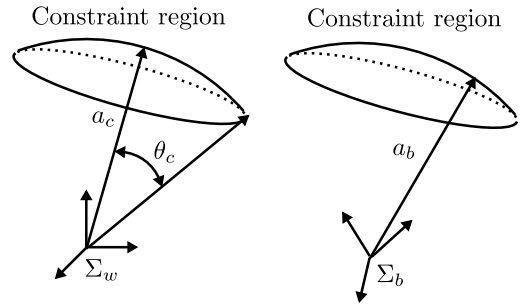


Figure 1: Coordinate Frames

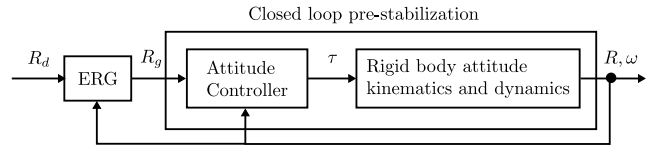


Figure 2: Control scheme

Acknowledgement

This work is supported by WBI, FRIA Ref. F-3-5-5/FRIA/FC-12687 and FNRS MIS Ref. F.4526.17.

References

- [1] R. M. Murray, Z. Li, and S. S. Sastry, *A Mathematical Introduction to Robotic Manipulation*, 1994.
- [2] U. Kalabic, R. Gupta, S. Di Cairano, A. Bloch, and I. Kolmanovsky, "Constrained Spacecraft Attitude Control on $SO(3)$ Using Reference Governors and Nonlinear Model Predictive Control," in *Proceedings of the 2014 American Control Conference*, 2014, pp. 5586–5593.
- [3] S. Kulumani and T. Lee, "Constrained Geometric Attitude Control on $SO(3)$," *International Journal of Control, Automation and Systems*, vol. 15, no. 6, pp. 2796–2809, 2017.
- [4] E. Garone and M. M. Nicotra, "Explicit Reference Governor for Constrained Nonlinear Systems," *IEEE Transactions on Automatic Control*, vol. 61, no. 5, pp. 1379–1384, 2016.

Design, Modeling, and Geometric Control on $SE(3)$ of a Fully-Actuated Hexarotor for Aerial Interaction

Ramy Rashad, Petra Kuipers, Johan Engelen and Stefano Stramigioli
 Faculty of Electrical Engineering, Mathematics and Computer Science, University of Twente,
 Enschede, The Netherlands. Email: r.a.m.rashadhashem@utwente.nl
 Faculty of Engineering Technology. University of Twente, Enschede, The Netherlands.

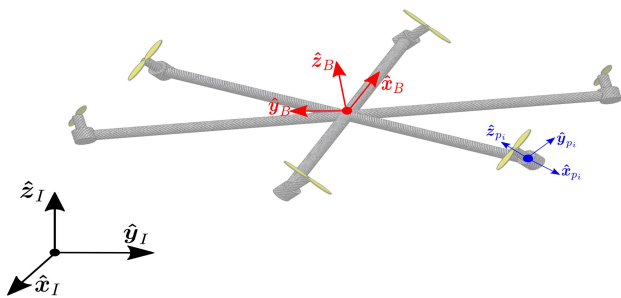


Figure 1: The fully actuated hexarotor with the reference frames defined.

1 Introduction

Most multi-rotor UAVs currently used, such as quadrotors or hexarotors, are designed and optimized for flying without physical interaction with the environment. This limits the ability to perform complex physical interaction tasks with the environment as it cannot reject arbitrary reaction wrenches from the environment. In this paper, we introduce the design, modeling and control of a fully-actuated omnidirectional hexarotor. The proposed hexarotor has propellers pointing in dissimilar directions optimized by maximizing the generated wrench of the UAV. In addition to the optimization-based design, we also approach the modeling and control design of the proposed UAV in a geometric approach by exploiting the configuration space $SE(3)$ of the UAV.

2 UAV Design

In this work, each rotor's orientation is fixed and parametrized by two fixed angles designed to maximize the static generated wrench of the propellers on the UAV's body. Consequently, this maximizes the UAV's agility, payload, and interaction wrench with the environment. Another requirement for an omnidirectional vehicle with fixedly-oriented propellers, is the ability of the rotors to produce thrust bi-directionally. In practice, this can be achieved by variable pitch propellers as in [1] or reversible electronic speed controllers as in [2]. The optimization problem formulation is based on the framework introduced in [3].

3 Geometric Tracking Controller Design

The control problem for the class of UAVs under study is to design a control law for the propellers' thrusts that enables the tracking of arbitrary trajectories for the UAV's configuration. In order for the controller design methodology to be generic, it will be assumed that the desired control wrench on the vehicle's body results from the control law. Then, in a model-based manner, the desired propellers' thrust are computed by the inverse of the mapping between the propellers' thrusts and the wrench. This mapping is ensured to be always invertible by the design of the hexarotor.

The methodology used in this work for the control system design is based on the framework introduced by Bullo and Murray [4] for geometric tracking on $SE(3)$. A measure of the configuration error between the UAV's configuration and the desired configuration is by an error function, which denotes a positive definite map on the Lie group $\phi : SE(3) \rightarrow \mathbb{R}$. The choice for the error function made in this paper yields a coordinate-free controller that is invariant under a change of inertial frame [4]. The designed geometric controller has been simulated on the fully actuated UAV to track a desired position and orientation trajectory from a non-hovering initial configuration.

References

- [1] M. Cutler, N. K. Ure, B. Michini, and J. P. How, "Comparison of fixed and variable pitch actuators for agile quadrotors," in *AIAA Guidance, Navigation, and Control Conference (GNC)*, vol. 2, 2011.
- [2] D. Brescianini and R. D'Andrea, "Design, modeling and control of an omni-directional aerial vehicle," in *2016 IEEE Int. Conf. Robot. Autom.* IEEE, may 2016, pp. 3261–3266.
- [3] S. Park, J. Her, J. Kim, and D. Lee, "Design, modeling and control of omni-directional aerial robot," in *2016 IEEE/RSJ Int. Conf. Intell. Robot. Syst.* IEEE, oct 2016, pp. 1570–1575.
- [4] F. Bullo and R. M. Murray, "Tracking for fully actuated mechanical systems: a geometric framework," *Automatica*, vol. 35, no. 1, pp. 17–34, 1999.

Heat Release Characterization for Advanced Combustion Concepts

Michiel Oom, Bram de Jager, Frank Willems
 Eindhoven University of Technology
 PO Box 513, 5600 MB Eindhoven, The Netherlands
 Email: m.e.e.oom@tue.nl

1 Introduction

The worldwide demand for diesel in the transportation sector is projected to continue to grow until 2040 [1]. Furthermore, the energy usage of freight trucks is projected to increase with 50% in 2040 compared to 2012. It is therefore important to keep on improving the fuel consumption and emissions of internal combustion engines.

Whilst in conventional Diesel engines there exists a trade-off between fuel economy and emissions, advanced combustion concepts allow for a simultaneous improvement of these two aspects. These concepts rely on the spontaneous auto-ignition of a relative homogeneous air-fuel mixture.

The control objective is to condition the mixture such that the ignition is well timed. Figure 1 shows a widely used combustion control scheme. Using the first law of thermodynamics for closed systems, the combustion heat release is inferred from an in-cylinder pressure measurement. Combustion metrics are extracted from the heat release profile and controlled using the fueling strategy.

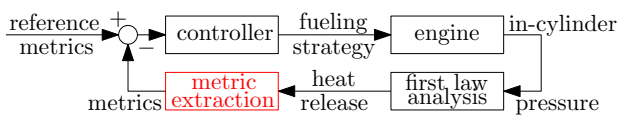


Figure 1: Advanced combustion concept control scheme.

2 Current Combustion Metrics

Figure 2 (top) shows commonly used combustion metrics. These metrics, θ_{10} , θ_{50} and θ_{90} , point out the crankshaft angles at which 10%, 50% and 90% of the total heat is released. These comply closely with the start, the weight and the end of combustion. However, they do not fully define the actual shape of the heat release, which varies greatly in advanced combustion concepts. Shaping this heat release is crucial in optimizing the thermal efficiency of the engine.

The current understanding, originating from fundamental combustion research, divides the combustion process in a premixed, rate-controlled and late combustion phase. Different emission formation and reduction mechanisms are assigned to these three phases.

3 Proposed Characterization

In this study, a new characterization for the heat release profile is proposed. This characterization consists of a superposition of three Gaussian curves, complying with the three combustion phases, given by:

$$\dot{Q}_{combustion}(\theta) = \sum_{i=1}^3 a_i e^{-(\theta-b_i)^2/c_i^2}, \quad (1)$$

where $\theta \in [-360, 360]$ [°] is the crankshaft angle and $a_i, b_i, c_i \in \mathbb{R}$, $i = 1, 2, 3$, the proposed combustion metrics. Figure 2 (bottom) shows this characterization (red) for a measured heat release signal (blue) and the remaining signals are the components of the fit.

In the accompanying presentation, a wide range of operating conditions are analyzed using the proposed metrics. Furthermore, the role of these metrics in control oriented models is examined. Finally, an outlook is given to the design of the controller.

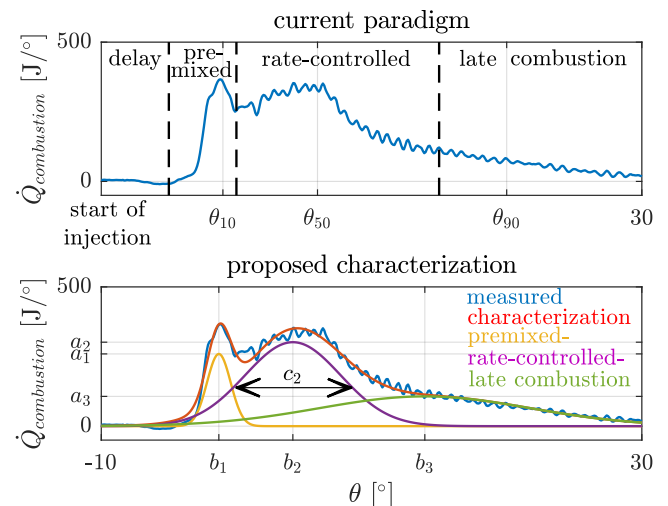


Figure 2: Current and proposed combustion metrics.

References

- [1] U.S Energy Information Administration (2016), International Energy Outlook 2016 with Projections to 2040.

Divertor detachment control in nuclear fusion devices

T. Ravensbergen
T.Ravensbergen@differ.nl

M. van Berkel
M.vanBerkel@differ.nl

Dutch Institute for Fundamental Energy Research, De Zaale 20, 5612 AJ Eindhoven, The Netherlands

1 Particle exhaust in tokamaks

One of the open issues on the road to viable and clean energy production via nuclear fusion is the heat and particle load on the inner wall of the device. In a tokamak, magnetic fields are used to confine the hot plasma in which hydrogen atoms are fusing to form helium and great amounts of energy. The bottom part of the reactor, called the divertor, acts as a helium exhaust. Plasma from the hot core drifts radially outwards, entering a thin region called the *scrape-off-layer* (SOL). Here, the plasma rapidly flows towards the divertor target plates. Without precaution, the resulting heat load can be up to 150 MWm^{-3} , greatly exceeding the engineering limit of 10 MWm^{-3} [1]. A promising but challenging solution is to increase the plasma density in the divertor via neutral (impurity) gas puffing. This leads to stagnation of the plasma flow, and high power and momentum losses, causing the temperature to drop significantly along the field line. As such, the plasma extinguishes near the divertor target, leading to so-called *divertor detachment*. Even though the precise physics of detachment are not yet fully understood, different loss mechanisms such as impurity radiation, ionization, and recombination dominate at different temperatures, causing various fronts to arise. These fronts are indicated by different colors in Figure 1).

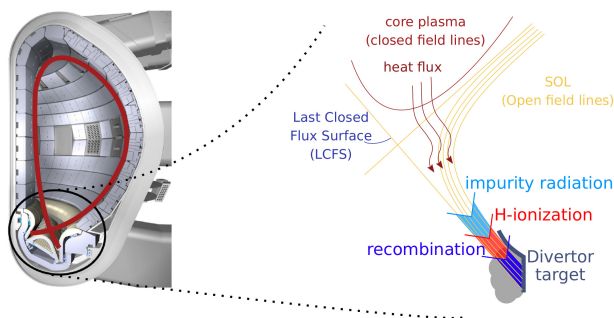


Figure 1: Schematic view of the divertor plasma, including detachment fronts.

2 Controlling plasma detachment

While plasma detachment evidently leads to significantly lower target temperatures and particle fluxes, experiments on machines existing today show that it is difficult to con-

trol the location of the detachment front [2]. Depending on the divertor geometry and other machine characteristics, the front is often observed to move inside the confined plasma region, affecting the plasma stability and fusion performance. Hence, the challenge is to measure the front location and control the uncertain dynamics of detached plasmas using slow actuators (gas puffing). In this work, we focus on a carbon machine in operation today called MAST-U.

3 Diagnostic development for MAST-U

A promising solution to locate the detachment front is multispectral imaging, where multiple cameras equipped with spectral filters observe the same portion of the divertor plasma [3]. Carbon will be the prominent radiating species in a carbon machine, such that a high intensity region in a CIII-filtered image is likely to be an excellent estimate of the radiation front. At the same time, other spectral lines provide information on recombination and ionization [4].

In this work, we apply standard multiscale edge detection based on wavelets [5] to first detect the plasma edge in real-time. Then, along this edge, another wavelet-based detector is employed to locate the radiation front. Finally, using a coordinate transform [6], we can map this front location to the poloidal plane, yielding our to-be controlled variable. The next step involves a set of dedicated system identification experiments on the MAST-U tokamak in the UK. This data will provide a basis for simple controller design, and possible benchmark of control-oriented models.

References

- [1] Wenninger, R.P. *et al.* 2014 *Nuclear Fusion* **54**
- [2] Potzel, S. *et al.* 2013 *Journal of Nuclear Materials* **438** S285
- [3] Vijvers, W.A.J. *et al.* 2017 *Journal of instrumentation* **12** C12058
- [4] Verhaegh, K. *et al.* 2017 *Nuclear Materials and Energy* **12** 1112
- [5] Van Berkel, M. *et al.* 2011 *Fusion Engineering and Design* **86** 2908
- [6] Hommen, G. 2014 *Optical boundary reconstruction for shape control of tokamak plasmas* Ph.D. thesis Eindhoven University of Technology

Unified Passivity-Based Distributed Control of Mechanical Systems

Laurens Valk and Tamás Keviczky

Delft Center for Systems and Control, Delft University of Technology

Email: l.r.valk@student.tudelft.nl, t.keviczky@tudelft.nl

Introduction

Passivity-based control is a well-established method for controlling fully-actuated mechanical systems such as robotic manipulators. Relying on concepts such as energy storage, routing, and dissipation, many design procedures exist to achieve a control goal with guaranteed stability properties. Using similar passivity arguments, several distributed control strategies have been developed to cooperatively control networks of such systems, in order to achieve control goals such as state synchronization or formation forming [1–4].

While these distributed control methods are derived from similar passivity principles, the control laws differ depending on the desired group behaviors (synchronization or formation), the information exchange (positions and/or velocities), the method of energy dissipation (by the network, the agents, or both), and the presence of a group reference.

We present a unified control scheme that encompasses the methods [1–4] for fully-actuated mechanical systems in a connected, undirected network without time delays (Fig. 1).

Unified Control Scheme

As common in robotics literature, a fully-actuated agent i with coordinates $q_i \in \mathbb{R}^n$ is assumed to have the dynamics

$$M_i(q_i)\ddot{q}_i + C_i(q_i, \dot{q}_i)\dot{q}_i + G_i(q_i) = \tau_i \quad (1)$$

with a control input $\tau_i \in \mathbb{R}^m$ and an output $y_i \in \mathbb{R}^m$ given by

$$y_i = \dot{x}_i - v \quad \text{with} \quad \dot{x}_i = \dot{q}_i + \Lambda q_i, \quad v = \dot{q}_d(t) + \Lambda q_d(t) \quad (2)$$

where $\Lambda \geq 0$. The reference signals q_d and \dot{q}_d are either given as functions of time or set to zero, depending on the group objective. Each agent uses a control law of the form

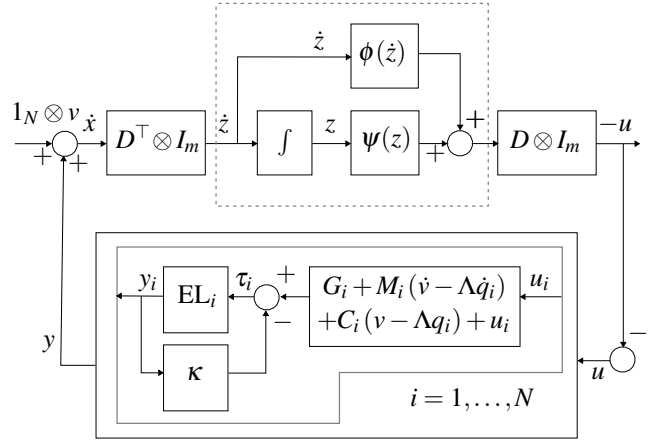
$$\tau_i = G_i + M_i(\dot{v} - \Lambda \dot{q}_i) + C_i(v - \Lambda q_i) - \kappa y_i + u_i \quad (3)$$

to render the system passive from the new input u_i to output y_i . It is lossless if $\kappa = 0$ or strictly output passive if $\kappa > 0$.

The difference variable $z_k = x_i - x_j$ associated with the bidirectional edge k is a measure of distance between agent i and j . The distributed control goal is to ensure that either all z_k converge to specified target sets, or that all y_i converge to one another. This is accomplished by using the control law

$$u = -(D \otimes I_m)(\psi(z) + \phi(\dot{z})) \quad (4)$$

where D is the incidence matrix of the network. The functions $\psi(\cdot)$ and $\phi(\cdot)$ are cf. [1] and [2], and can be conceptualized as virtual spring and damper forces, respectively.



	κ	Λ	q_d	\dot{q}_d	ϕ	ψ	Storage	Dissip.	Exch.
[1]	> 0	$= 0$	n/a	\dot{q}_d	$= 0$	$\neq 0$	both	agents	q_i
[2]	$= 0$	> 0	0	0	$\neq 0$	$= 0$	agents	network	q_i, \dot{q}_i
[3]	> 0	> 0	q_d	\dot{q}_d	$\neq 0$	$= 0$	agents	both	q_i, \dot{q}_i
[4]	> 0	$= 0$	0	0	$\neq 0$	$\neq 0$	both	both	q_i, \dot{q}_i

Fig. 1: Unified control scheme extended from [1], and the specializations to obtain the control laws u_i of [1–4].

Energy Storage and Dissipation

The unified scheme facilitates a comparison of the methods, as done here for energy storage and dissipation. In [1, 4], coupling between the coordinates q_i and q_j is achieved by virtual spring forces $\psi_k(z_k)$ generated as gradients of the energy stored in the network, whereas in [2, 3] it is accomplished due to $\Lambda > 0$, which implies synchronization of all q_i if all y_i synchronize. Likewise, energy can be dissipated by the agents when choosing $\kappa > 0$ as in [1, 3, 4] or by the network when choosing $\dot{z}_k^T \phi_k(\dot{z}_k) \geq 0$ as in [2, 3, 4].

References

- [1] M. Arcak, “Passivity as a design tool for group coordination,” IEEE Transactions on Automatic Control, vol. 52, no. 8, pp. 1380–1390, 2007
- [2] M. W. Spong and N. Chopra, “Synchronization of networked Lagrangian systems,” Lagrangian and Hamiltonian Methods for Nonlinear Control. LNCIS, vol. 366, 2007
- [3] S. J. Chung and J. J. E. Slotine, “Cooperative robot control and concurrent synchronization of Lagrangian systems,” IEEE Tr. Robotics, vol. 25, no. 3, pp. 686–700, 2009
- [4] W. Ren, “Distributed leaderless consensus algorithms for networked EulerLagrange systems,” International Journal of Control, vol. 82, no. 11, pp. 2137–2149, 2009

Consensus on the unit sphere, the Stiefel manifold and $SO(d)$: the hunt for almost global convergence

Johan Thunberg, Johan Markdahl, and Jorge Gonçalves
Luxembourg Centre for Systems Biomedicine
University of Luxembourg
6, avenue du Swing, L-4367 Belvaux, Belvaux
Luxembourg

Email: {johan.thunberg, johan.markdahl, jorge.goncalves}@uni.lu

1 Introduction

For the Euclidean space well-established convergence results are available for consensus systems dating back more than a decade. There is a collection of such results stating that if individual agents in the system are moving into the convex hulls of their neighbors' positions, the states will aggregate over time and finally all converge to a fixed point, i.e., the consensus point or the synchronization point. Those results hold under weak connectivity assumptions for possible time-varying interaction network.

For multi-agent systems evolving in other spaces than the Euclidean, the equivalent convergence result does not hold in general. Examples of such non-Euclidean spaces are the unit sphere, the Stiefel, and the special orthogonal group. Those are all interesting from application perspectives. Consensus on the unit sphere can be seen as equivalent to heading-alignment of multi-robot systems as well as systems in nature. Also the problem of synchronization of phase oscillators is closely related to that of consensus on the unit circle. Consensus of orthogonal matrices is an active research topic, also referred to as attitude synchronization within the application of rigid bodies in space. Consensus on the Stiefel manifold can be seen as a problem residing between the other two, i.e., with the unit sphere and the special orthogonal group as extremes.

2 New convergence results

We aim to bring two recent papers to the forefront [1, 2] as well as discuss possible generalizations thereof. They provide new controllers and convergence results to the aforementioned consensus control problems.

It used to be a held belief that a globally convergent consensus controller on the unit sphere could not be based on purely relative and local (and intrinsic) information. Previous works have shown that classical geodesic control laws on the unit circle fail to achieve almost global convergence. Various approaches have been suggested to overcome this. Examples of such include so-called shaping functions or the introduction of estimation variables.

However, as shown in [1], the unit circle comprises an odd exception to the rule. In fact for all unit spheres of dimensions larger than or equal to 2, classical geodesic control laws using only relative and local information achieves consensus almost globally for undirected graph topologies and symmetric weights. Furthermore, these weights do not need to be constant, but can be chosen as a non-negative nonlinear functions of the relative distance between agents. The result in [1] are perhaps non-intuitive based on what was previously known about the convergence on the circle.

In [2] we provide a collection of synchronization controllers for all the three manifolds mentioned in the introduction. The interaction graph of the multi-agent system is assumed to be quasi-strongly connected. We show that the closed loop systems under the controllers achieve almost global convergence to the consensus set. However, the convergence results come at price. Even though only relative information is used in terms of the states, we introduce additional estimation variables that are communicated between neighboring agents. This approach is all but new, however here we do it in a way that makes the same approach applicable for the unit sphere and the special orthogonal group as well as all the Stiefel manifolds in between; we use the *QR*-decomposition of a matrix. This allows to obtain a closed loop dynamics that is on strict feedback form, where the dynamics of the k first columns are decoupled from the remaining ones.

With these results as a starting point, we also aim to investigate further generalizations such as extensions of the results in [1] to the Stiefel manifold.

References

- [1] Johan Markdahl, Johan Thunberg, and Jorge Gonçalves. Almost global consensus on the n -sphere. *IEEE Transactions on Automatic Control*, 2017.
- [2] Johan Thunberg, Johan Markdahl, and Jorge Gonçalves. Dynamic controllers for column synchronization of rotation matrices: a QR-factorization approach. *To appear in Elsevier's Automatica*.

A robust consensus algorithm for DC microgrids

M. Cucuzzella*, S. Trip*, C. De Persis*, X. Cheng*, A. Ferrara**, A. van der Schaft***

* University of Groningen, Nijenborgh 4, 9747 AG Groningen, The Netherlands

** University of Pavia, via Ferrata 5, 27100 Pavia, Italy

*** University of Groningen, Nijenborgh 9, 9747 AG Groningen, The Netherlands

Email: m.cucuzzella@rug.nl

Abstract

In the last decades, due to economic, technological and environmental aspects, the main trends in power systems focused on the modification of the traditional power generation and transmission systems towards incorporating smaller Distributed Generation units (DGUs). Moreover, the ever-increasing energy demand and the concern about the climate change have encouraged the wide diffusion of Renewable Energy Sources (RES). The so-called microgrids have been proposed as conceptual solutions to integrate different types of RES and to electrify remote areas. Two main control objectives in DC microgrids are voltage regulation and current sharing (or, equivalently, load sharing) [1].

This work proposes a novel robust control algorithm to obtain simultaneously proportional current sharing among the DGUs and a form of voltage regulation in a resistive-inductive DC power network, independently of the initial voltage conditions, facilitating Plug-and-Play capabilities. In order to achieve current sharing, a communication network is exploited where each DGu communicates in real-time the value of its generated current to its neighbouring DGUs. The overall network is represented by a connected and undirected graph $\mathcal{G} = (\mathcal{V}, \mathcal{E})$, where the nodes, $\mathcal{V} = \{1, \dots, n\}$, represent the DGUs and the edges, $\mathcal{E} = \{1, \dots, m\}$, represent the distribution lines interconnecting the DGUs. The network topology is represented by its corresponding incidence matrix $\mathcal{B} \in \mathbb{R}^{n \times m}$. Consequently, the DC microgrid system can be written compactly for all nodes $i \in \mathcal{V}$ as

$$\begin{aligned} L_t \dot{I}_t &= -R_t I_t - V + u \\ C_t \dot{V} &= I_t + \mathcal{B}I - I_L \\ L \dot{I} &= -\mathcal{B}^T V - RI, \end{aligned} \quad (1)$$

where $I_t, V, I_L, u \in \mathbb{R}^n$, $I \in \mathbb{R}^m$, while $C_t, L_t, R_t \in \mathbb{R}^{n \times n}$ and $R, L \in \mathbb{R}^{m \times m}$ are positive definite diagonal matrices. The meaning of the symbols used in (1) follows straightforwardly from Fig. 1. Now, we make the considered control objectives explicit:

Objective 1 (Proportional Current sharing)

$$\lim_{t \rightarrow \infty} I_t(t) = \bar{I}_t = W^{-1} \mathbf{1}_n i_t^*, \quad (2)$$

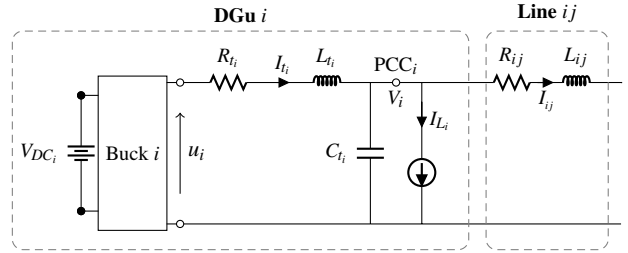


Figure 1: The considered DC microgrid electrical scheme.

where $i_t^* = \mathbf{1}_n^T I_L / (\mathbf{1}_n^T W^{-1} \mathbf{1}_n) \in \mathbb{R}$, $W = \text{diag}\{w_1, \dots, w_n\}$, $w_i > 0$, for all $i \in \mathcal{V}$, and $\mathbf{1}_n \in \mathbb{R}^n$ is the vector consisting of all ones.

Objective 2 (Voltage balancing)

$$\lim_{t \rightarrow \infty} \mathbf{1}_n^T W^{-1} V(t) = \mathbf{1}_n^T W^{-1} \bar{V} = \mathbf{1}_n^T W^{-1} V^*, \quad (3)$$

where $V^* \in \mathbb{R}^n$ is the voltage reference. In order to achieve Objectives 1 and 2 simultaneously, we constrain the state of system (1) on the following desired manifold:

$$\{(I, V, I, \theta) : W^{-1}(V - V^*) - \theta = \mathbf{0}\}, \quad (4)$$

where $\theta \in \mathbb{R}^n$ is an additional state variable (distributed integrators), with dynamics given by

$$\dot{\theta} = -\mathcal{L}_c W I, \quad \mathbf{1}_n^T \theta(0) = 0 \quad (5)$$

\mathcal{L}_c denoting the weighted Laplacian matrix associated with the (undirected and connected) communication graph, which can be different from the topology of the microgrid.

To constrain the state of the system (1) to the designed manifold (4) in a finite time, we propose robust controllers of Sliding Mode type [2].

References

- [1] C. De Persis, E. R. A. Weitenberg, F. Dörfler, “A power consensus algorithm for DC microgrids,” *Automatica*, 2018.
- [2] V. I. Utkin, “Sliding Modes in Control and Optimization,” Springer-Verlag, 1992.

Fractional Order PI Autotuning Method Applied to Multi-Agent System

Ricardo Cajo^{1,2}, Robin De Keyser¹, Douglas Plaza² and Clara M. Ionescu¹

¹Research group on Dynamical Systems and Control, Ghent University, Belgium

²Facultad de Ingeniería en Electricidad y Computación, Escuela Superior Politécnica del Litoral
Campus Gustavo Galindo Km 30.5 Vía Perimetral, P.O. Box 09-01-5863, Guayaquil, Ecuador

RicardoAlfredo.CajoDiaz@UGent.be

1 Introduction

In order to significantly improve operational efficiency, reduce costs and increase the degree of operational redundancy. Hence, multi-agent systems (MAS) are widely used in the construction of complex systems. Therefore, they are being widely recognized as new technologies for the next generation of distributed and intelligent industrial automation systems [1]. The distributed control systems approach is preferable for the development of applications that involve multiple autonomous units, which have to communicate with each other to achieve the common goal through their coordinated actions.

2 Control Strategies

A novel fractional order PI autotuner based on KC method [2] is applied to the multi-agent systems. This method consists in defining a forbidden region in the Nyquist plane based on user-defined specs, which will guarantee the system margin requirements. Its performance is compared with two other fractional order controllers based on PI gain-crossover autotuning method [3] and Internal Model Control (IMC) present in [4]. A numerical example considered is described by the following transfer function $G(s)$ mimicking a part of a multi-agent flock:

$$G(s) = \begin{bmatrix} \frac{1.64}{50s+1} & \frac{2.49}{250s+1} \\ \frac{2.56}{75s+1} & \frac{1.28}{275s+1} \end{bmatrix}; \Lambda = \begin{bmatrix} -0.49 & 1.49 \\ 1.49 & -0.49 \end{bmatrix} \quad (1)$$

Checking input-output pairings, with a RGA (Relative Gain Array) analysis of the multivariable process. Its matrix Λ suggest that the pairing 1-2/2-1 is suitable, since the main diagonal has negative values

3 Results and Conclusions

According to results shown in Figure 1 and Figure 2, the KC method produces fractional order PI controllers that achieve excellent load disturbance rejection, while maintaining a good reference tracking performance. It is important to note

that the proposed method does not use the full knowledge of the system model. However, this shows that the KC method could obtain similar or better results than other controllers, which use the full knowledge of the system.

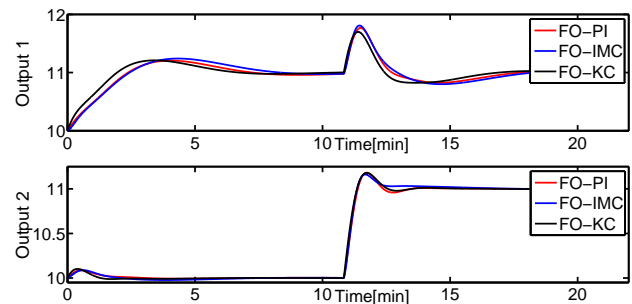


Figure 1: Comparative setpoint tracking test

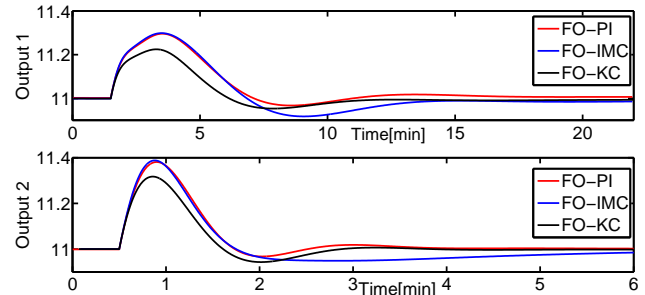


Figure 2: Comparative disturbance rejection test

References

- [1] P. Kadera, "Methods for Development of Industrial Multi-Agent Systems," Czech Technical University in Prague, Doctoral Thesis, 2015.
- [2] De Keyser R, Ionescu CM. and Muresan CI, "Comparative Evaluation of a Novel Principle for PID Autotuning," 11th Asian Control Conference (ASCC), pp. 1164-1169, 2017
- [3] De Keyser R, Muresan CI. and Ionescu CM, "A novel auto-tuning method for fractional order PI/PD controllers," ISA Transactions, vol. 62, pp. 268-275, 2016.
- [4] Muresan CI, Dutta A, Dulf E, Pinar Z, Maxim A. and Ionescu CM, "Tuning algorithms for fractional order internal model controllers for time delay processes," International Journal of Control, vol. 89, pp. 579-593, 2016.

The normal form: a systematic approach to transform non-convex sets into convex sets

Andrés Cotorruelo Jiménez, Emanuele Garone
 Université Libre de Bruxelles, Belgium
 {acotorru, egarone}@ulb.ac.be

Daniel Limón Marruedo
 Universidad de Sevilla, Spain
 dlm@us.es

1 Introduction

The need to find a mapping that transforms non-convex sets into convex ones appears in a wide variety of settings: from the path planning for robotic systems, to the calculation of the desired steady-state trajectory of a system subject to non-convex constraints. In this talk we present an approach to this problem. To this end, we define the normal form as a way of defining a set. Every time that a set can be expressed in this form, it can be easily morphed into a convex set by means of a normalization.

2 Results

Our objective is to find a continuous, preferably bijective mapping between an original non-convex set into a convex one. The main result we will present is the definition of a form that may be used to represent a wide class of common non-convex sets. We have called this the normal form, and defined it as follows:

Definition 1. Let $\mathbf{x} \in \mathbb{R}^n$ be a set of coordinates describing an n -dimensional non-convex set Ω . We say that \mathbf{x} is in normal form if the first $n - 1$ coordinates, \mathbf{x}_c , belong to a convex set Ω_C and the last variable x_n is lower and upper bounded by two, possibly nonlinear, functions of \mathbf{x}_c :

$$\mathbf{x} = \begin{bmatrix} x_1 \\ x_2 \\ \vdots \\ x_n \end{bmatrix} \in \Omega, \quad \mathbf{x}_c = \begin{bmatrix} x_1 \\ x_2 \\ \vdots \\ x_{n-1} \end{bmatrix} \in \Omega_C$$

$$\underline{f}(x_1, \dots, x_{n-1}) \leq x_n \leq \bar{f}(x_1, \dots, x_{n-1})$$

By expressing a domain in this way, we isolate the non-convexities in x_n . If we then normalize x_n in the following way:

$$\tilde{x}_n = \frac{x_n - \underline{f}(x_1, \dots, x_{n-1})}{\bar{f}(x_1, \dots, x_{n-1}) - \underline{f}(x_1, \dots, x_{n-1})}$$

$$\tilde{x}_n \in [0, 1]$$

We map the lower and upper bound of x_n to 0 and 1, respectively. This way, we *stretch* the set in the direction of x_n , turning it into a convex set.

A few classes of sets that can be expressed in this way such as, for example, star-shaped sets and projectable sets (i.e: sets whose boundary can be described as viewed from a segment within it). Below, we show an example and an application: tracing a path between two points of a non-convex polygon.

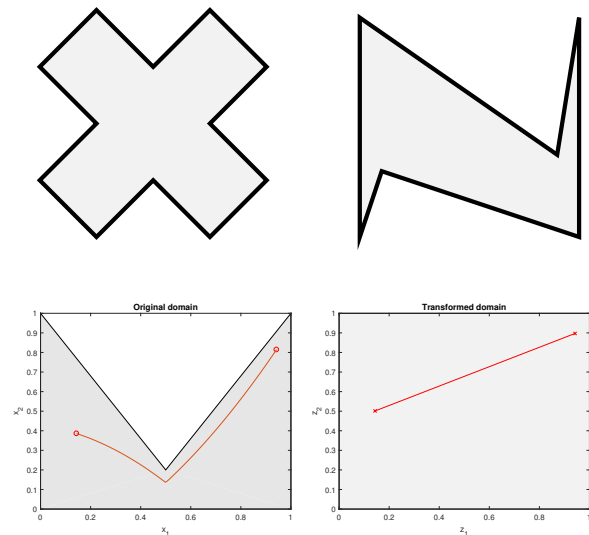


Figure 1: Star-shaped set (top left), projectable set (top right), path in a non-convex domain (bottom left) and path in the transformed domain (bottom right)

Acknowledgements

This research has been funded by the FNRS MIS “Optimization-free Control of Nonlinear Systems subject to Constraints”, Ref. F.4526.17.

Model Order Reduction for Drilling Automation

Harshit Bansal, Laura Iapichino, Wil Schilders

Department of Mathematics and Computer Science
Eindhoven University of Technology
Eindhoven, The Netherlands
Email: {h.bansal,l.iapichino,w.h.a.schilders}@tue.nl

Nathan van de Wouw

Mechanical Engineering, Eindhoven Univ of Technology
Civil, Environmental and Geo-Engineering, Univ of Minnesota
Delft Center for Systems and Control, Delft Univ of Technology
Email: n.v.d.wouw@tue.nl

1 Abstract

Model Order Reduction (MOR) of systems of non-linear parameterized Hyperbolic Partial Differential Equations (PDEs) is a challenging research topic. Poor regularity of the solution map is a major hindrance to obtain a reduced-order model representation. This work focuses on developing a framework for multi-phase hydraulic modelling and model complexity reduction for Managed Pressure Drilling (MPD) operations to explore oil, gas, minerals and geo-thermal energy. Considering the safety critical aspect of MPD, the primary focus is to enable an accurate and precise control of the down-hole pressure while performing various transient operational scenarios. We aim to develop models that uniquely combine high predictive capacity and low complexity, and thus enable their usage in virtual drilling scenario testing and in drilling automation strategies for down-hole pressure management.

In view of virtual drilling scenario testing for MPD operations, current hydraulic models have significantly reduced accuracy in obtaining an accurate prediction and maintaining a real-time and robust control of transient down-hole effects in case of gas-influx into the well. The Drift Flux Model (DFM) [1], a system of multiscale non-linear Hyperbolic PDEs, is hydraulic model typically used to capture wave propagation phenomena. Classical numerical discretization techniques are not suitable for real-time estimation and control or multi-query simulations due to the high computational time and data storage required. Moreover, the high fidelity model is highly non-linear due to the model based and discretization based non-local non-linearities. The development of non-linear MOR techniques is hence an indispensable step.

Both Proper Orthogonal Decomposition (POD) and Reduced Basis Method (RBM), in conjunction with (Discrete) Empirical Interpolation Method ((D)EIM) are well known reduced order modelling techniques to deal with non-linear and non-affine nature of the problem [2]. This work begins with the application of POD and RBM in conjunction with (D)EIM to obtain a reduced-order representation of the DFM for a representative multi-phase shock tube test case. We observe that POD/RBM-(D)EIM capture the dynamics dictated by the DFM in an essentially non-oscillatory manner and help to reduce the dimension-

ality of the problem. However, the reduced-order model still does not fit our requirements for real-time estimation and control or multi-query simulations. This occurs as the solutions of convection dominated problems show a diagonal structure in space-time diagram and demonstrate high variability during time evolution. Hence, a very large number of basis functions is required to construct a reduced subspace. This observation motivates us to investigate and propose efficient and automated reduction approaches.

Stationary or moving discontinuous features are representative characteristics of wave propagation phenomena. These localized discontinuous features affect the performance of global approximations. Moreover, the location of discontinuous fronts and the speed of propagation varies for different parameters of interest. The inherent travelling dynamics need to be factored out before making an effort to obtain reduced-order model representations. We use the Method of Freezing/ Symmetry Reduction [3] to pre-process a solution manifold and separate the dynamics in the group direction from the dynamics in the remaining directions of the phase space. This approach is envisioned to deal with wavefront movement, wave interaction induced topological changes and provide transformed variables, which possess better regularity characteristics. We use [4] to implement this Method of Freezing in conjunction with standard model reduction approaches and then demonstrate the efficacy of such strategy in dealing with the challenges faced in the model reduction of the DFM.

References

- [1] S. Evje and K. K. Fjelde. "Hybrid Flux-Splitting Schemes for a Two-Phase Flow Model." *Journal of Computational Physics* 175, no. 2 (January 2002): 674-701.
- [2] A. Quarteroni and G. Rozza, eds. "Reduced Order Methods for Modeling and Computational Reduction." Cham: Springer International Publishing, 2014.
- [3] C. Rowley, I. G. Kevrekidis, J. E. Marsden, and K. Lust. "Reduction and Reconstruction for Self-Similar Dynamical Systems." *Nonlinearity* 16, no. 4 (2003): 1257.
- [4] M. Ohlberger and S. Rave. "Nonlinear Reduced Basis Approximation of Parameterized Evolution Equations via the Method of Freezing." *Comptes Rendus Mathematique* 351, no. 2324 (December 2013): 901-906.

Model Reduction of Coherent Clusters in Dynamic Power System Models

Johnny Leung¹, Michel Kinnaert¹, Jean-Claude Maun², and Fortunato Villella³

¹Department of Control Engineering and System Analysis, Université libre de Bruxelles (ULB), Belgium

²Department of Bio-, Electro- And Mechanical Systems, Université libre de Bruxelles (ULB), Belgium

³Elia Grid International (EGI), Belgium

Email: {johnny.leung, michel.kinnaert, jcmaun}@ulb.ac.be,
fortunato.villella@eliagrid-int.com

1 Introduction

For dynamic stability studies, a transmission system operator¹ (TSO) relies on a dynamic power system model that includes its own network (*study area*), the influential neighboring networks (*buffer area*), and the remaining remote networks (*external area*) [1]. By simulating disturbances within the study area, a TSO is able to evaluate the stability of its network. The latter two areas are modeled to take account of their reaction on the study area.

As modern power systems grow in size and in complexity, running stability analyses is becoming problematic on a fully detailed model. The construction of the model requires the collective effort of many utilities, and the resultant simulations are computationally demanding. To ease the burden, one solution is to derive a linear reduced-order model for the less significant external area [2]. The goal of this contribution is to develop a new reduction method, which is suitable for large-scale power systems.

2 Problem Statement

Let $B(s)$ and $G(s)$ denote the linearized buffer and external area systems respectively. They are interconnected as in Fig. 1. The stated objective is to reduce $G(s)$ while preserving the input-output behavior (u_1^B, y_1^B) of the interconnected system at the interface with the study area.

This type of problem is typically solved with a structured model reduction approach such as the interconnected system balanced truncation (ISBT) method [2]. However, the ISBT method requires $\mathcal{O}(n^3)$ operations for an interconnected system of order n and is impractical on a real power system model. The new proposal consists in partitioning the interconnected system into a set of coherent clusters denoted $G_\bullet(s)$ and reducing the clusters $G_\bullet(s)$ individually.

Similarly to the initial problem, the reduction of the clusters $G_\bullet(s)$ must be performed while accounting for the rest of the

¹A TSO is an actor in the electricity market which is responsible for operating, ensuring the maintenance of and, if necessary, developing the transmission system in a given area.

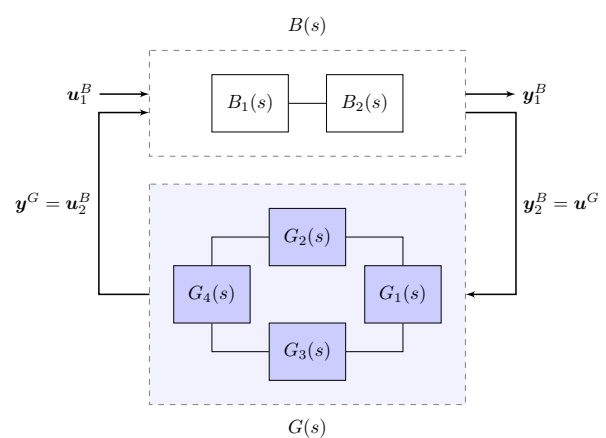


Figure 1: Partitioning of the linearized buffer $B(s)$ and external $G(s)$ area systems into coherent clusters.

interconnected system. The efficiency of the new proposal depends on the ability to reproduce the remaining system in an inexpensive way. Such a feat is namely achieved by building equivalent systems that contain the adjacent clusters, consider the coherent nature of the neglected clusters, and recognize the prominent role of voltage phase angle inputs after an electrical fault.

This work is supported by the Brussels-Capital Region (Innoviris) through the project **More Grids - Model Reduction and Simplification for Dynamic Grid Security Studies**

References

- [1] K. Morison and L. Wang, "Reduction of large power system models: A case study," in *Power System Coherency and Model Reduction*, J.H. Chow, Ed. New York, NY: Springer New York, 2013, pp. 143–158.
- [2] C. Sturk, L. Vanfretti, Y. Chompoobutgool, and H. Sandberg, "Coherency-independent structured model reduction of power systems," *IEEE Transactions on Power Systems*, vol. 29, no. 5, pp. 2418–2426, Sept 2014.

Model Order Reduction for an Electrochemistry-based Li-ion Battery Model

L.Xia E. Najafi H.J. Bergveld M.C.F. Donkers

Eindhoven University of Technology, P.O. Box 513, 5600 MB Eindhoven, the Netherlands

Emails: {l.xia1, e.najafi, h.j.bergveld, m.c.f.donkers}@tue.nl

1 Introduction

Featured by high energy density, lithium-ion (Li-ion) batteries are used in various applications. In order to efficiently analyse and control the batteries, models of Li-ion batteries are essential. The Doyle-Fuller-Newman (DFN) model is a popular electrochemistry-based Li-ion model, which allows high-rate discharge and describes the inherent phenomena of the lithium cells during charging, discharging or relaxation using a set of nonlinear partial differential equations. However, implementation of the full DFN model requires significant computation time.

2 Model implementation

In this paper, we propose to apply model order reduction (MOR) technique to simplify the full DFN model, combining with our previously proposed numerical scheme [1]. Instead of applying MOR to the whole DFN model, MOR has been independently applied to each governing equation, using the combination of the discrete empirical implementation method (DEIM) and proper orthogonal decomposition (POD) method [1]. POD is a data-based MOR technique used to find a low-dimensional approximation of large-scale systems. However, it usually causes large computational complexities while dealing with nonlinear models. DEIM is an effective way to solve this problem. It approximates the nonlinear parts of the POD-based reduced-order model (P-ROM) by projecting the nonlinearities onto a subspace spanned by a basis determined by some selected interpolation indices. As such, the order of P-ROM becomes proportional to the small selected number of interpolation indices.

3 Simulation Result

Computational performance and accuracy of the POD-DEIM-based reduced-order model (PD-ROM) have been studied using a simulation study of a 6 (Ah) Li-ion Hybrid Electric Vehicle cell [1].

Fig. 1 illustrates a comparison of the full order model (FOM) and the PD-ROMs with snapshots constructed at different numbers of reduced basis in terms of the battery voltage and their absolute errors. It can be observed that changing the number of reduced basis of c_e , ϕ_e and ϕ_s does not make a remarkable influence on accuracy, while changing the number of basis of c_s does play a significant role in accuracy. One

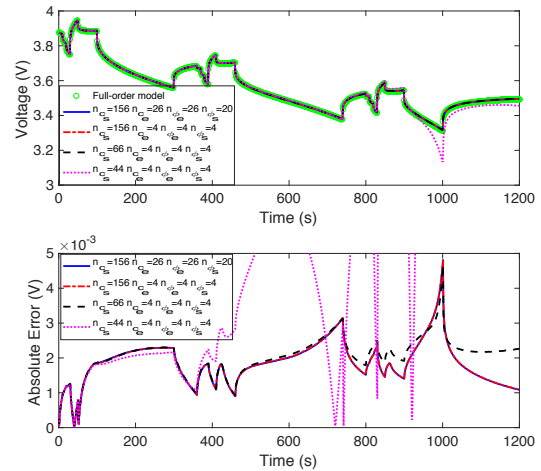


Figure 1: Comparison of the FOM and the PD-ROMs with snapshots constructed at different numbers of reduced basis in terms of battery voltage and absolute errors between the FOM and the PD-ROMs.

Table 1: Computation time of the FOM and the PD-ROM

Drive cycle	FOM	PD-ROM
5C-rate discharge for 600 (s)	168 (s)	138 (s)
Hybrid (dis)charge for 1200 (s)	279 (s)	157 (s)
Pulse (dis)charge for 3000 (s)	1805 (s)	85 (s)

can easily choose the number of reduced basis by striking a balance between accuracy and computation time, e.g., setting the accuracy criterion, where the absolute errors are less than 5×10^{-3} (V).

Table 1 states the computation time of the FOM (1832nd) and the PD-ROM (100th) during a constant discharge, dynamic (dis)charge and pulse (dis)charge profile. In fact, the PD-ROM implementation can achieve a computation time that is 4-35 times faster than real-time while maintaining the same accuracy as the FOM implementation. In addition, the model order has been significantly reduced by a factor 18.

References

- [1] L. Xia, E. Najafi, L. Zhi, H.J. Bergveld, M.C.F. Donkers, "A computationally efficient implementation of a full and reduced-order electrochemistry-based model for Li-ion batteries," *Applied Energy*, 208,1285-1296, 2017.

Synchronization Persevering Model Reduction of Lure Networks

Xiaodong Cheng, Jacquelin M.A. Scherpen

Faculty of Science and Engineering

University of Groningen

Nijenborgh 4, 9747 AG Groningen

The Netherlands

Email: {x.cheng, j.m.a.scherpen}@rug.nl

This paper considers a model order reduction problem that reduces the complexity of interconnected Lur'e-type subsystems while simultaneously preserving the synchronization property of the network, relevant results can be found in e.g., [1, 2, 3]. The system consists of multiple identical Lur'e systems that evolve on a connected undirected graph. The dynamics of nodes are described by identical nonlinear dynamical systems as follows.

$$\Sigma_i : \begin{cases} \dot{x}_i = Ax_i + Bu_i + Ez_i \\ y_i = Cx_i \\ z_i = -\phi(y_i, t) \end{cases}, i = 1, 2, \dots, N, \quad (1)$$

where $x_i \in \mathbb{R}^n$, $u_i, y_i, z_i \in \mathbb{R}$. We assume that the uncertain feedback nonlinearity $\phi(\cdot)$ in (1) is **slope-restricted** as

$$0 \leq \frac{\phi(y_a) - \phi(y_b)}{y_a - y_b} \leq \mu, \quad (2)$$

for all $y_a, y_b \in \mathbb{R}$ and $y_a \neq y_b$, where $\mu > 0$ and $\phi(0) = 0$. Furthermore, the Lur'e dynamics Σ_i is assumed to be **absolutely stable**.

All the subsystems on the network are interconnected according to the following static output-feedback protocol.

$$u_i = \sum_{j=1}^N w_{ij}(y_i - y_j), \quad i = 1, 2, \dots, N, \quad (3)$$

where $w_{ij} \in \mathbb{R} \geq 0$ is the (i, j) -th entry of weighted adjacency matrix of the underlying graph and stands for the intensity of the coupling between subsystem i and j . Then, combining (3) and (1) leads to a compact form of the Lur'e dynamical network as

$$\Sigma : \begin{cases} \dot{x} = (I_N \otimes A - L \otimes BC)x - (I_N \otimes E)\Phi(y), \\ y = (I_N \otimes C)x, \end{cases} \quad (4)$$

where $\Phi(y) := [\phi(y_1), \phi(y_2), \dots, \phi(y_N)]^T$, and $x := [x_1^T, x_2^T, \dots, x_N^T]^T$, $y := [y_1, y_2, \dots, y_N]^T$ are the collections of the states and outputs of the N subsystems. The vector $d := [d_1, d_2, \dots, d_N]^T$ are external disturbances, and the matrix L is the graph Laplacian of underlying network.

The following lemma relates the synchronization of Σ with the largest eigenvalue of L .

Lemma 1 *If there exists a positive definite matrix \mathcal{Q} such that*

$$\begin{bmatrix} A^T \mathcal{Q} + \mathcal{Q}A + C^T C & \lambda_N \mathcal{Q}B & \mathcal{Q}E - C^T \\ \lambda_N B^T \mathcal{Q} & -I & 0 \\ E^T \mathcal{Q} - C & 0 & 0 \end{bmatrix} \prec 0, \quad (5)$$

with λ_N is the largest eigenvalue of L in (4), then the Lur'e network Σ robustly synchronizes.

Using the maximum and minimal solutions of (5), we can do balanced truncation and obtain the reduced-order agent model

$$\hat{\Sigma}_i : \begin{cases} \dot{\hat{x}}_i = \hat{A}\hat{x}_i + \hat{B}u_i + \hat{E}\hat{z}_i \\ \hat{y}_i = \hat{C}\hat{x}_i \\ \hat{z}_i = -\phi(\hat{y}_i) \end{cases}, i = 1, 2, \dots, N, \quad (6)$$

with $\hat{x}_i \in \mathbb{R}^k$, and $\hat{z}_i, \hat{y}_i \in \mathbb{R}$. Consequently, it leads to reduced-order Lur'e network dynamics as

$$\hat{\Sigma} : \begin{cases} \dot{\hat{x}} = (I_N \otimes \hat{A} - L \otimes \hat{B}\hat{C})\hat{x} - (I_N \otimes \hat{E})\Phi(\hat{y}), \\ \hat{y} = (I_N \otimes \hat{C})\hat{x}, \end{cases} \quad (7)$$

comparing to (4).

The following theorem shows that the synchronization property is preserved after the reduction.

Theorem 1 *Consider the full-order Lur'e network Σ in (4) and its reduced-order model $\hat{\Sigma}$ in (7). If Σ robustly synchronizes due to Lemma 1, then $\hat{\Sigma}$ also robustly synchronizes.*

References

- [1] X. Cheng, J. M.A. Scherpen. Robust Synchronization Preserving Model Reduction of Lure Networks *Submitted*.
- [2] F. Zhang, H. L. Trentelman, and J. M. A. Scherpen, Fully distributed robust synchronization of networked Lure systems with incremental nonlinearities, *Automatica*, vol. 50, no. 10, pp. 2515–2526, 2014.
- [3] B. Besselink, N. van de Wouw, and H. Nijmeijer, An error bound for model reduction of Lure-type systems in *Proceedings of the 48th IEEE Conference on Decision and Control*, held jointly with the 28th Chinese Control Conference. IEEE, 2009, pp. 3264–3269.

Reduced Order Controller Design for Disturbance Decoupling Problems

R.W.H. Merks¹
r.w.h.merks@tue.nl

S. Weiland¹
s.weiland@tue.nl

¹Department of Electrical Engineering, Eindhoven University of Technology
P.O. Box 513, 5600 MB Eindhoven, The Netherlands

1 Abstract

Over the past 50 years, many techniques for model based control have been developed. These techniques are typically applied to small-scale systems with up to ~ 10 states. From industry there is an increasing interest in applying model based control techniques to large-scale models that contain over 1,000 states. These models typically show up for systems that are described by partial differential equations, which are spatially discretized using finite elements or finite volume methods.

Due to computational limitations, it is in practice required to determine a controller that contains at most ~ 100 states. Therefore the problem of designing of a reduced order controller for a full order system is of great interest. For the design of a reduced order controller, typically 3 approaches as depicted in fig. 1 are considered:

1. First the full order system Σ is reduced in state dimension, which leads to a reduced order system $\hat{\Sigma}$. For $\hat{\Sigma}$ an optimal controller $\hat{\Sigma}_C$ is created.
2. First an optimal full order controller Σ_C is created for system Σ . Σ_C is then reduced in state dimension, which leads to a reduced order controller $\hat{\Sigma}_C$.
3. The reduced order controller $\hat{\Sigma}_C$ is created directly for the full order system Σ .

Approaches 1 and 2 could be applied in practice, while approach 3 is viewed as an open problem. As a model order reduction procedure for approaches 1 and 2, standard model order reduction techniques like balanced truncation and moment matching are considered. There exist control relevant model order reduction techniques as described in [1][2][3][4][5], where typically standard state-space systems are considered and optimality of $\hat{\Sigma}_C$ is not always guaranteed for Σ . Therefore, the design of an optimal reduced order controller $\hat{\Sigma}_C$ for a full order system Σ that is described by a generalized plant model is, to the knowledge of the authors, an open problem.

In this presentation we consider the problem to directly derive (if it exists) a low complexity controller that achieves exact decoupling of disturbances for a given dynamical system from its to-be-controlled outputs. Disturbance decoupling problems and the conditions that determine whether these problems can be solved, are well understood in terms of concepts from geometric control theory. It will be shown how this understanding leads to novel insights into the synthesis of a reduced order controller, which will achieve exact disturbance decoupling on a full order system.

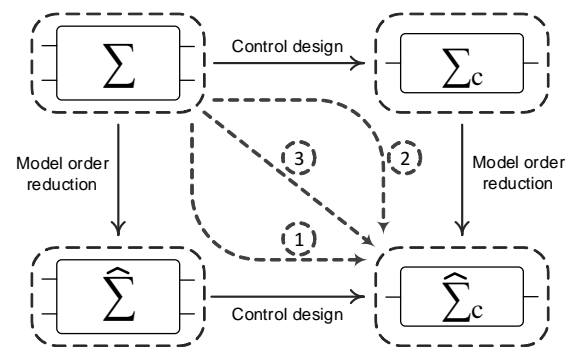


Figure 1: Reduced order controller design approaches.

References

- [1] E. Jonckheere and L. Silverman, "A new set of invariants for linear systems – Application to reduced order compensator design", *IEEE Transactions on Automatic Control*, vol. 28, no. 10, pp. 953-964, 1983.
- [2] P. Wortelboer, "Frequency-weighted balanced reduction of closed-loop mechanical servo-systems: Theory and tools", Ph.D. thesis, Eindhoven University of Technology, 1994.
- [3] P. Goddard, "Performance-Preserving Controller Approximation", Ph.D. thesis, Trinity College, Cambridge, 1995.
- [4] G. Obinata and B. Anderson, *Model reduction for control system design*. London: Springer London, 2013.
- [5] A. Varga and B. Anderson, "Accuracy-enhancing methods for balancing-related frequency-weighted model and controller reduction", *Automatica*, vol. 39, no. 5, pp. 919-927, 2003.

Error analysis for parametric model order reduction using Krylov subspace method

Daming Lou, Siep Weiland

Department of Electrical Engineering, Eindhoven University of Technology

Email: {d.lou, s.weiland}@tue.nl

I. INTRODUCTION

Parametric model order reduction (pMOR) aims to reduce the computational complexity while preserving the parameter-dependency. When the task is to optimize the design or to estimate crucial parameters of complex systems, pMOR techniques become an indispensable tool, because the finite element method (FEM) commonly yields large-scale models for such systems. Since creating a new reduced model for every new design or every parameter value is inefficient and computationally costly. In our previous work, the proposed method[1] does not require to repeat the reduction procedure for any change in parameters, but simply the evaluation of the parametric model. The simulation results showed good match between the reduced model and original model at expansion points, it leads to a challenging topic which has been left without attention, how to choose the optimal expansion points with or without prior knowledge.

Unfortunately, an effective error estimation for Krylov-subspace methods is still an open research open. Single-frequency error estimations were proposed in [2]. A posteriori error estimation was presented in [3] that evaluates the error after the reduction procedure, however, the computation of the original model is inevitable.

In this work, we present an upper bound of the approximation error between the reduced model and the original model, which allows prior estimating the misfit without calculating the exact reduced model. In particular, we derive an explicit prior error bound in frequency domain for Krylov-subspace method.

II. PROBLEM STATEMENT

In this presentation we shall consider a linear parameter-varying model with $p(t) = [p_1(t), \dots, p_\ell(t)]^T \in \mathbb{R}^\ell$

$$\Sigma(p) := \begin{cases} E(p)\dot{x}(t) = A(p)x(t) + B(p)u(t) \\ y(t) = C(p)x(t) \end{cases} \quad (1)$$

where $x(t) \in \mathbb{R}^n$, $u(t) \in \mathbb{R}^m$ and $y(t) \in \mathbb{R}^q$ denote, respectively, the state vector, the input and the output. Here n is the cardinality of the mesh of a spatially distributed configuration space Ω (usually of dimension 3). The state-space matrices are functions $A : \mathbb{R}^\ell \rightarrow \mathbb{R}^{n \times n}$, $E : \mathbb{R}^\ell \rightarrow \mathbb{R}^{n \times n}$ etc. With the time-invariant p , the general transfer function of (1) is meaningful.

Multi-parameter and multi-frequency moment-matching was introduced in [1] to provide an approximation to the

LPV systems in a form that the Taylor series of the general transfer function expands at desired expansion points with finite derivative. This yields a reduced order model whose transfer function

$$G_r(s, p) = C_r(p)[sE_{(r,0)} + \sum_{i=1}^{\ell} sE_{(r,i)}p_i - A_r(p)]^{-1}B_r(p)$$

coincides in as many coefficients of the Taylor series of the original model about (s, p) as possible for a given order of the reduced model.

III. ERROR ESTIMATION

In this section we will present an error estimate between $G(s, p)$ and $G_n(s, p)$ which provides local accuracy at points $(s_0, p_0) \in \mathcal{S} \times \mathcal{P}$ and their neighbourhood. That is, the error estimate of $G(s, p) - G_n(s, p)$ will have local validity in (s_0, p_0) and is based on the truncation order of the Taylor series.

We define $\forall (s_0, p_0) \in I_{(s,p)}$ and there exists

$$\|G(s, p) - G_n(s, p)\| \leq \mathcal{M} \underbrace{\left[\begin{array}{c} s - s_0 \\ p - p_0 \end{array} \right] \otimes \dots \otimes \left[\begin{array}{c} s - s_0 \\ p - p_0 \end{array} \right]}_{n+1};$$

where

$$\mathcal{M} := \sup_{(\xi_s, \xi_p) \in I_{(s,p)}} \left\| \frac{D^{(n+1)}H(\xi_s, \xi_p)}{(n+1)!} \right\| \quad (2)$$

is the suprema induced norm of the tensor $[D^{|n+1|}H]$ over $I_{(s,p)}$. $[D^{|k|}f]_k$ can be interpreted as the coefficients of a order $|k|$ tensor (i.e. multi-linear functional)

$$[D^{|k|}f] : \underbrace{\mathbb{C}^\ell \times \mathbb{C}^\ell \times \dots \times \mathbb{C}^\ell}_{|k| \text{ copies}} \rightarrow \mathbb{C} \quad (3)$$

Here $k = (k_1, \dots, k_\ell)$ is defined as a multi-index with k_i positive integers, and let $|k| = \sum_i k_i$ be its cardinality.

A prior upper bound on the reduction error using multi-parameter and multi-frequency moment matching method is derived. Furthermore, this error bound allows for finding the optimal expansion points and truncated order.

REFERENCES

- [1] D.Lou, S.Weiland, "Parametric model order reduction for large-scale and complex thermal systems." IEEE ECC, Limassol, Cyprus, 2018.
- [2] Grimme, Eric James. Krylov projection methods for model reduction. Diss. University of Illinois at Urbana-Champaign, 1997.
- [3] Haasdonk, Bernard, and Mario Ohlberger. "Efficient reduced models and a posteriori error estimation for parametrized dynamical systems by offline/online decomposition." Mathematical and Computer Modelling of Dynamical Systems 17.2 (2011): 145-161.

Robust Stability of Feedback Linearizable Nonlinear Systems

Sajad Azizi, Emanuele Garone

Service d'Automatique ed d'Analyse des Systemès, Université Libre de Bruxelles

50 F.D. Roosevelt Av, CP 165/55, 1050 Brussels, Belgium

Emails: {Sajad.Azizi, egarone}@ulb.ac.be

1 Introduction

In this note a systematic approach to the robust stabilization of a class of feedback linearizable systems is proposed. As an example, the longitudinal dynamics of a general aviation aircraft, having parametric uncertainties, is investigated. The Lyapunov redesign methodology together with the proposition of sufficient LMI conditions for the system in new coordinates is suggested to tackle zero steady-state robust stability.

2 Preliminaries and System Definition

Consider the class of non-minimum phase feedback linearized rational system in the quasi-canonical form [1]:

$$\dot{z}(t) = A_c z(t) + b_c v(t) + W(z, \zeta, u, \delta p), \quad (1)$$

where $\zeta \in \mathbb{R}^{n-r}$ is the vector of internal dynamics states, $z(t) \in \mathbb{Z} \subset \mathbb{R}^r$, in which $\mathbb{Z} = \{z \mid a_k z \leq 1, k = 1, \dots, n_e\}$, $\delta p \in \Delta$ is the vector of parametric uncertainties belonging to the polytope Δ , $v(t) \in \mathbb{R}^m$ is the new input control vector and $W = W_1(z, \zeta, v, \delta p) + W_2(\zeta, \delta p)$ is the vector of remaining nonlinearities after approximate linearization attempt such that the above system with W_1 can be recast as [2]:

$$\begin{aligned} \dot{z}(t) &= A_1(z, \zeta, \delta p)z + A_2(z, \zeta, \delta p)\pi + A_3(z, \zeta, \delta p)v, \\ 0 &= \Pi_1(z, \zeta, \delta p)z + \Pi_2(z, \zeta, \delta p)\pi + \Pi_3(z, \zeta, \delta p)v, \end{aligned} \quad (2)$$

with π the vector of dumped nonlinearities, A_1 - A_3 and Π_1 - Π_3 being affine matrix functions and Π_2 a full rank matrix.

3 Stability Analysis

For subsystem (2) the following theorem is recalled from [1].

Theorem 1 For system (2) with $v = Kz$. Let Δ be a set of admissible uncertainties and suppose there exist matrices $Q = Q^T > 0$, $Y \in \mathbb{R}^{m \times r}$, and $\eta > 0$ such that LMIs

$$\begin{bmatrix} QA_1^T + A_1Q + Y^T A_3^T + A_3Y & A_2 & Q\Pi_1^T + Y^T \Pi_3^T \\ A_2^T & -\eta I & (\Pi_2 + I)^T \\ \Pi_1 Q + \Pi_3 Y & \Pi_2 + I & -I \end{bmatrix} < 0,$$

$$\begin{bmatrix} v_{\max}^2 I & Y \\ Y^T & Q \end{bmatrix} \geq 0, \begin{bmatrix} 1 & -a_k^T Q \\ -Q a_k & Q \end{bmatrix} \geq 0, k = 1, \dots, n_e,$$

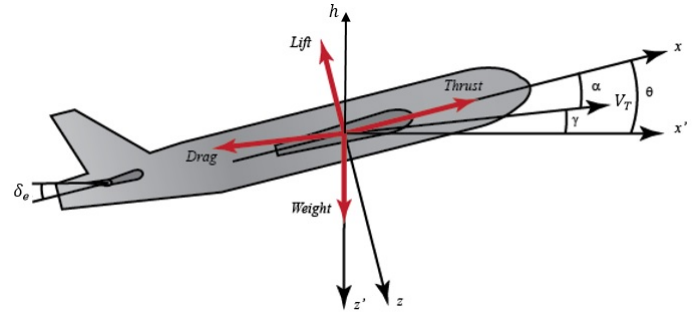


Figure 1: Schematic of the longitudinal dynamics of an aircraft.

are feasible in all vertices of $\Delta \times \mathbb{Z}$. Then there exists the Lyapunov function $V = z^T P z$, $P > 0$, in \mathbb{Z} , and the control gain $K = YQ^{-1}$ such that for all $\delta p \in \Delta$ the trajectory of $z(t)$ is locally asymptotically stable.

In order to tackle the zero steady-state stability one has to incorporate the effect of W_2 in the analysis. Therefore, the designed controller $v = Kz$ is replaced by $v + \nu$ such that

$$\nu = \begin{cases} -\lambda \frac{A_3^T \beta}{\|\beta^T A_3\|_2} & \text{if } \lambda \|\beta^T A_3\|_2 \geq \varepsilon, \\ -\lambda^2 \frac{A_3^T \beta}{\varepsilon} & \text{if } \lambda \|\beta^T A_3\|_2 < \varepsilon. \end{cases} \quad (3)$$

where $\beta = Pz$ and λ, ε are properly chosen positive scalars.

4 Results and Conclusion

The proposed approach has been implemented on the longitudinal dynamics of a general aviation aircraft. Schematic of the system's dynamics is depicted in Figure 1. The simulations showed that the velocity and altitude tracking problem is well addressed. More details on the simulation results can be found in [1].

References

- [1] S. Azizi, "Sufficient LMI Conditions and Lyapunov Redesign for the Robust Stability of a Class of Feedback Linearized Dynamical Systems, ISA transactions 68 (2017): 90-98
- [2] D.F. Coutinho, et al. " \mathcal{L}_2 gain analysis and control of uncertain nonlinear systems with bounded disturbance inputs," International Journal of Robust and Nonlinear Control 18.1 (2008): 88-110

Power-Controlled Hamiltonian Systems

Pooya Monshizadeh

University of Groningen
9712 CP Groningen
The Netherlands

Juan E. Machado

CNRS-SUPELEC
91192, Gif-sur-Yvette
France

Romeo Ortega

CNRS-SUPELEC
91192, Gif-sur-Yvette
France

Arjan van der Schaft

University of Groningen
9712 CP Groningen
The Netherlands

p.monshizadeh@rug.nl, {juan.machado, ortega}@lss.supelec.fr, a.j.van.der.schaft@rug.nl

1 Introduction

In recent years, port-Hamiltonian (pH) modeling of physical systems has gained extensive attention. pH systems theory provides a systematic framework for modeling and analysis of physical systems and processes. Conventionally, the external inputs (controls or disturbances) in pH systems act on the flow variables—that is on the derivative of the energy storing coordinates. However, in some cases of practical interest, these external inputs act on the systems *power*, either as the control variable, or as a power that is extracted from (or injected to) the system. We refer to this kind of systems as *Power-controlled Hamiltonian* (P_wH) systems. Since P_wH systems cannot be modeled with constant control input matrices, showing passivity or stability of the system is nontrivial.

An example of P_wH systems is electrical systems with instantaneous constant-power loads (CPLs), which model the behavior of some point-of-load converters that are widely used in modern electrical systems. It is well-known that CPLs introduce a destabilizing effect that gives rise to significant oscillations or to network collapse, and hence they are the most challenging component of the standard load model—referred to as ZIP model. Therefore, the study of *stability* of the equilibria of the systems with CPL is a topic of utmost importance.

Notation— For a given vector $a \in \mathbb{R}^n$, the diagonal matrix $\text{diag}\{a_1, a_2, \dots, a_n\}$ is denoted in short by $\langle a \rangle$.

2 Problem Formulation

The dynamics of the pH system investigated here is given by

$$\dot{x} = (J - R)\nabla\mathcal{H}(x) + G(x)u, \quad x \in \Omega^+, \quad (1)$$

with $\Omega^+ := \{x \in \mathbb{R}^n : \langle \nabla\mathcal{H}(x) \rangle > 0\}$, where x is the system state, $u \in \mathbb{R}^n$ is an external signal that represents, either a control input or a constant disturbance, \mathcal{H} is the systems Hamiltonian (energy) function, $G \in \mathbb{R}^{n \times n}$ is the input matrix, while $J = -J^\top \in \mathbb{R}^{n \times n}$ and $R \geq 0 \in \mathbb{R}^{n \times n}$, both being *constant*, are the structure and the dissipation matrices respectively. The rate of change of the Hamiltonian of the system (1) reads as

$$\dot{\mathcal{H}} = -\nabla\mathcal{H}^\top(x)R\nabla\mathcal{H}(x) + \nabla\mathcal{H}^\top(x)G(x)u.$$

Note that the control input is not *directly* applied to the power of the system. We assume that G may be written in the form

$$G(x) = \langle \nabla\mathcal{H}(x) \rangle^{-1}. \quad (2)$$

Now, we have

$$\dot{\mathcal{H}} = -\nabla\mathcal{H}^\top(x)R\nabla\mathcal{H}(x) + \mathbb{1}^\top u,$$

implying that, in the proposed model, the external input acts directly on the power (rate of change of the Hamiltonian) of the system. Here, we aim at deriving conditions for shifted passivity and stability of the system (1), (2).

3 Main Result

Define the steady-state relation

$$\mathcal{E} := \{(x, u) \in \mathbb{R}^n \times \mathbb{R}^m \mid (J - R)G(x)u = 0\}.$$

Fix $(\bar{x}, \bar{u}) \in \mathcal{E}$, and let $Z(x) := G(\bar{x})\langle \bar{u} \rangle G(x)$. The main result is formalized as the following theorem.

Theorem 1 For all trajectories $x \in \Omega_p$ of the system (1), (2), with

$$\Omega_p := \{x \in \Omega^+ : R + Z(x) \geq 0\},$$

we have that

$$\dot{\mathcal{S}} \leq (y - \bar{y})^\top (u - \bar{u}),$$

where \mathcal{S} is the shifted Hamiltonian [1]

$$\mathcal{S}(x) := \mathcal{H}(x) - (x - \bar{x})^\top \nabla\mathcal{H}(\bar{x}) - \mathcal{H}(\bar{x}),$$

and

$$y = G^\top(x)\nabla\mathcal{S}(x).$$

Moreover, if the Hamiltonian \mathcal{H} is convex, this implies that the mapping $(u - \bar{u}) \mapsto (y - \bar{y})$ is passive.

Using Theorem 1, conditions for asymptotic stability of equilibria can also be derived. Furthermore, we show that under the condition that the Hamiltonian is quadratic, a precise estimate of the region of attraction can be provided. For the proof and more details see [2].

References

- [1] B. Jayawardhana, R. Ortega, E. García-Canseco, and F. Castaños, “Passivity of nonlinear incremental systems: Application to PI stabilization of nonlinear RLC circuits,” *Systems & Control Letters*, vol. 56, no. 9, pp. 618–622, 2007.
- [2] P. Monshizadeh, J. E. Machado, R. Ortega, and A. van der Schaft, “Power-controlled hamiltonian systems: Application to electrical systems with constant power loads,” *arXiv preprint arXiv:1802.02483*, 2018.

A Port-Hamiltonian Approach to Secondary Control of Microgrids

Mahya Adibi and Jacob van der Woude
 Delft Institute of Applied Mathematics, TUDelft
 2628 XE Delft, The Netherlands
 Email: {m.adibi, j.w.vanderwoude}@tudelft.nl

1 Introduction

Due to rapid penetration of renewable energy sources in microgrids, new modeling and control techniques are needed to guarantee reliable operation of electrical power systems. Based on a generic mathematical model of a microgrid, primary droop controllers are employed to stabilize the system and achieve power sharing [1]. However, droop control results in the deviations of the voltage and frequency from their nominal values according to the load demand.

We approach the problem of regulating the voltages in a microgrid to a desired value by developing a secondary controller from a port-Hamiltonian perspective. The port-Hamiltonian approach provides a systematic and structured framework for modeling and stability analysis of a wide range of multi-physical systems and it also provides a natural starting point for control design [2].

The basis of our design is the well-known energy shaping methodology, which is the essence of passivity-based control (PBC). The idea is to design the control input which results in a closed-loop system that is again a port-Hamiltonian system with the total energy being the sum of the plant and the controller's energy functions. Thereafter, we end up obtaining the closed-loop plant dynamics with a modified (shaped) Hamiltonian. The energy shaping approach modifies the potential energy of the system such that the new potential energy function has a strict local minimum in the desired equilibrium point. Furthermore, we analysis the stability of the overall system considering the Hamiltonian as the candidate Lyapunov function.

2 Methodology

The microgrid system dynamics can be represented in the port-Hamiltonian form

$$\dot{x} = (J - R(x))\nabla_x H(x) + gu(x), \quad (1)$$

where $x \in \mathbb{R}^n$ is the state vector, $J \in \mathbb{R}^{n \times n}$ and $R(x) \in \mathbb{R}^{n \times n}$ are interconnection and dissipation matrices respectively, $\nabla_x H(x) \in \mathbb{R}^n$ is the vector of partial derivatives of the Hamiltonian $H(x)$ with respect to the state x , $g \in \mathbb{R}^{n \times n}$ is the coefficient vector and $u(x) \in \mathbb{R}^n$ is the (secondary) control input.

We propose a new energy function $H_c(x)$ supplied by the controller and an energy shaping control input $u(x)$ such that the port-Hamiltonian closed-loop system

$$\dot{x} = (J - R(x))\nabla_x H_d(x), \quad (2)$$

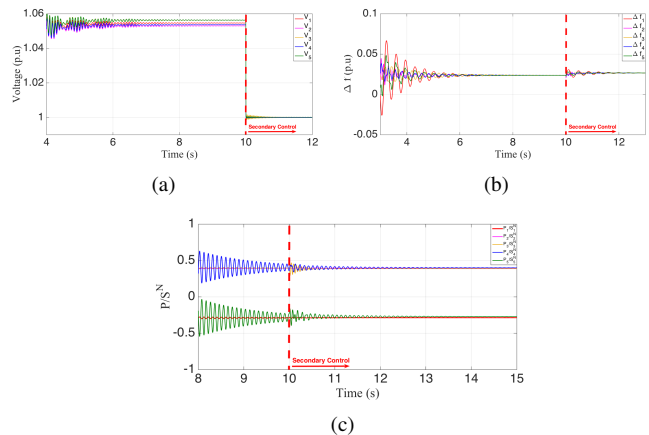


Figure 1: The secondary controller is switched on at $t = 10$ s, (a) Distributed generation units output voltage amplitudes: $V^d = 1$ p.u., (b) Relative frequencies: $\Delta f_i = (\omega_i - \omega^d)/(2\pi)$, (c) Active power outputs normalized by the source ratings: P_i/S_i^N .

with $H_d(x) = H(x) + H_c(x)$ is stabilized at the desired equilibrium point. Moreover, we derive a condition on the gains of the proposed controller $u(x)$. Satisfying this condition, the stability of the system is guaranteed.

3 Results and Conclusions

Fig. 1 shows the effectiveness of the proposed secondary voltage controller for part of a benchmark microgrid that consists of 2 loads ($i = 1, 5$) and 3 generation sources ($i = 2, 3, 4$). V^d and ω^d are the nominal values for the voltage and frequency respectively. As seen in Fig. 1 (a), while the primary control keeps the voltage amplitudes in a stable range but with a steady state offset ($t < 10$), the secondary control returns all terminal voltage amplitudes to the pre-specified reference value $V^d = 1$ p.u. ($t > 10$). Furthermore, the secondary voltage controller does not cause instability in the operating frequency of the microgrid Fig. 1 (b). Moreover, the active power is shared by the generating sources proportional to their ratings in the steady state, while the batteries are charged in proportion to their ratings (Fig. 1 (c)).

References

- [1] J. Schiffer, R. Ortega, A. Astolfi, J. Raisch and T. Sezi, "Conditions for Stability of droop-controlled inverter-based microgrids," *Automatica*, 50(10): 2457-2469, 2014.
- [2] A. van der Schaft and D. Jeltsema, "Port-Hamiltonian Systems Theory: An Introductory Overview," Now Publishers Incorporated, 2014.

Frequency-driven market mechanisms for optimal power dispatch

T.W. Stegink¹ A. Cherukuri² C. De Persis¹ A.J. van der Schaft¹ J. Cortés³

1 Motivation

Generation planning has been traditionally done hierarchically. Broadly, at the top layer cost efficiency is ensured via market clearing and at the bottom layer, frequency control and regulation is ensured via primary and secondary controllers. For the most part, research on improving the performance of these two layers has developed independently. The reasons for this include the difference in time-scales at which they operate (market clearing happens at the order of minutes/hours/days and frequency control at the order of seconds/milliseconds) and the objectives they intend to meet (minimizing cost versus achieving stability). With the goal of integrating renewable generation and other distributed energy resources into the grid, there is an increasing body of research that seeks to merge the operation of these layers, see e.g., [2], and synthesize procedures that simultaneously tackle market clearing and frequency stabilization, see e.g., [3]. This merging is envisioned to provide better flexibility, reliability, and cost efficiency when faced with the uncertain behavior of distributed energy resources. Our work is motivated by these considerations. We study the stability of the interconnection of the market and the frequency dynamics. While previous work studying this interconnection assumes generators to be price-takers, we consider a more realistic scenario where they bid in the market (and hence are price-setters).

2 Problem statement

We consider an electrical power network consisting of the independent system operator (ISO) and a group of generators. Given a power demand, the ISO runs a market where generators can bid to provide power. The ISO's goal is to ensure that the generation meets the load with minimum possible cost and frequency is regulated to the nominal value. Each generator is strategic, aims to maximize its individual profit and does not share its true cost with the ISO. Instead, it submits a bid consisting of the price per unit of electricity at which it is willing to provide power. In our previous work [1], we have exclusively considered the market dynamics, we have shown that iterative bidding with appropriate bid adjustment schemes for the generators leads to bids that are at a Nash equilibrium (that is, generators are not willing

to deviate from their bid) and generation levels that minimize the total cost. Given the motivation outlined above, our goal is to investigate the stability properties of the interconnection of an iterative bidding dynamics as in [1] with the frequency dynamics modeled by the second-order swing equations.

3 Main results

Our overall algorithm design couples the market and the frequency evolution. On the market side, we consider an iterative bidding scheme that converges to the efficient Nash equilibrium (the point where the generation levels minimize the total cost and each generator does not want to deviate from its bid). The rationale behind the bid adjustment by the generators in this iterative bidding strategy is simple: at any instance, if the ISO demands more generation than what the generator is willing to produce, then the generator increases its bid; similarly, if the demand is less than the desired generation, then the generator decreases its bid. Having established the convergence of the bidding dynamics, we interconnect it with the frequency dynamics as follows: the generators inject into the grid the setpoints that the iterative bidding dynamics provide and change their bid in with the rationale explained above; the ISO tries to find the optimal generation given the bids to minimize the cost but also uses the frequency as a feedback signal in the negotiation process. Hence, the frequency from the physics is injected into the bidding dynamics and the power generation from the bidding dynamics is injected into the physics. By exploiting the ISS property of the system, we prove that under suitable triggering conditions the resulting closed-loop system converges to the efficient Nash equilibrium and a state of frequency regulation, showing that the proposed market mechanism results in stable grid operation.

References

- [1] A. Cherukuri and J. Cortés. Iterative bidding in electricity markets: rationality and robustness. *arXiv preprint arXiv:1702.06505*, 2017. submitted to *IEEE Transactions on Control of Network Systems*.
- [2] F. Dörfler, J. W. Simpson-Porco, and F. Bullo. Breaking the hierarchy: Distributed control & economic optimality in microgrids. *IEEE Transactions on Control of Network Systems*, 3(3):241–253, 2016.
- [3] D. J. Shiltz, M. Cvetković, and A. M. Annaswamy. An integrated dynamic market mechanism for real-time markets and frequency regulation. *IEEE Transactions on Sustainable Energy*, 7(2):875–885, 2016.

¹T. W. Stegink and C. De Persis and A. J. van der Schaft are affiliated with the Jan C. Willems Center for Systems and Control, University of Groningen, the Netherlands. {t.w.stegink, c.de.persis, a.j.van.der.schaft}@rug.nl

²A. Cherukuri is with the Automatic Control Laboratory, ETH Zürich. cashish@control.ee.ethz.ch

³J. Cortés is with the Department of Mechanical and Aerospace Engineering, University of California, San Diego. cortes@ucsd.edu

Hybrid integrator-gain based elements for nonlinear motion control

S.J.A.M. van den Eijnden*, Y. Knops**, M.F. Heertjes*^{*,**,\dagger}, and H. Nijmeijer*

*Dynamics & Control and **Control Systems Technology Groups, Eindhoven University of Technology, The Netherlands

\dagger ASML, Mechatronics System Development, The Netherlands

s.j.a.m.v.d.eijnden@tue.nl

1 Introduction

To meet future performance specifications, the product roadmap of high-precision mechatronic systems is typically translated toward servo-control in the direction of increased controller bandwidths. However, using linear control elements, the associated bandwidth is often limited by Bode's gain-phase relationship. In order to possibly surpass this fundamental limitation, recently in [1] a hybrid integrator-gain element (HIGS) has been introduced. Depending on specific switching conditions, this element switches between an integrator and gain mode in such a manner that the output is continuous, confined to a sector, and always of equal sign to the input. As such, the corresponding describing function $\mathcal{D}(j\omega)$ demonstrates first-order low-pass characteristics with a phase lag of only 38.15 degrees. Driven by the apparent phase advantage, in this abstract the idea of HIGS-based controller elements for bandwidth improvements of essentially linear systems is discussed.

2 HIGS-Based Controller Elements

A HIGS-based controller element is proposed as the series interconnection of the HIGS and a linear filter $\mathcal{N}(s)$. Through specific design of this filter, the element's describing function

$$\mathcal{D}_{NL}(j\omega) = \mathcal{D}(j\omega)\mathcal{N}(j\omega), \quad (1)$$

can be shaped in such a manner that it has desirable magnitude characteristics with reduced phase lag. For the purpose of example, consider the HIGS in series with a filter $\mathcal{N}(s)$, given in frequency domain by:

$$\mathcal{N}(s) = \frac{\omega_{lp}^2}{\omega_2} \cdot \frac{1}{s + \omega_1} \cdot \frac{(s + \omega_1)(s + \omega_2)}{s^2 + 2\beta\omega_{lp}s + \omega_{lp}^2}, \quad (2)$$

with corner frequencies ω_i , $i \in \{1, 2\}$, ω_{lp} , and dimensionless damping coefficient β . It follows from the first-order low-pass characteristics of the HIGS, that by appropriate tuning of ω_2 in (2), the describing function (1) has similar magnitude characteristics as a classical linear second-order low-pass filter with complex poles, however, with significantly reduced phase lag. From a linear point-of-view, elements with such apparent properties could potentially aid the loopshaping design, and give rise to increased bandwidths.

3 Wafer Stage Measurement Results

To illustrate the potential of a HIGS-based controller, the nonlinear second-order low-pass filter is experimentally em-

bedded in the motion control context of Fig. 1. Here, \mathcal{C} is some base-linear controller (e.g. PID and notch filters) and \mathcal{P} represents a scanning stage of an industrial wafer scanner. Using a quasi-linear loopshaping procedure, eval-

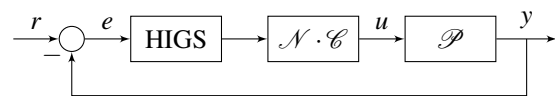


Figure 1: Feedback control structure.

uated through describing functions, the controller is structurally tuned and shows a bandwidth improvement of around 11% compared to an optimal linear controller design. Time-domain measurement results of several experiments are presented in Fig.2 in terms of the moving average \mathcal{M}_A and the moving standard deviation \mathcal{M}_{SD} . These performance measures reflect the low- and high-frequency content of the measured data-sampled error $e(t)$, respectively. The results of the nonlinear controller (red) are compared to those of an optimally tuned linear controller (black). A substantial im-

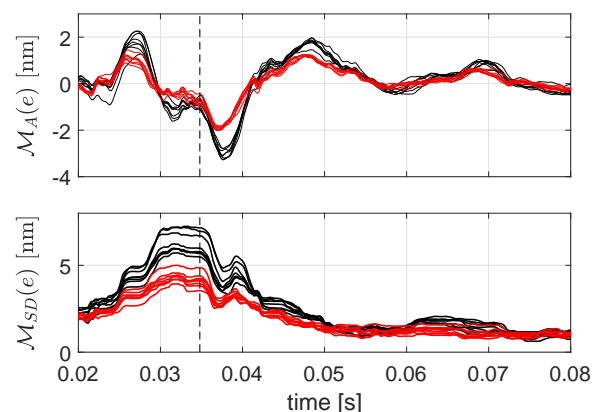


Figure 2: Moving average $\mathcal{M}_A(e)$ and moving standard deviation $\mathcal{M}_{SD}(e)$ for the linear (black) and nonlinear (red) closed-loop system.

provement in low-frequency disturbance suppression can be observed, without deterioration of the \mathcal{M}_{SD} . Although no rigorous stability criteria for the true nonlinear system are specified, this real-world closed-loop example shows convincingly robustly stable behavior.

References

- [1] D.A. Deenen, M.F. Heertjes, W.P.M.H. Heemels and H. Nijmeijer, Hybrid integrator design for enhanced tracking in motion control, *American Control Conference*, (2017).

Formal controller synthesis using genetic programming

Cees F. Verdier and Manuel Mazo Jr.

Delft Center for Systems and Control, Delft University of Technology

Mekelweg 2, 2628 CD Delft, The Netherlands

Email: {c.f.verdier, m.mazo}@tudelft.nl

1 Introduction

Correct-by-design controller synthesis for safety and reachability specifications traditionally involves abstraction through discretization or synthesis of (control) Lyapunov Barrier functions (LBFs) using sum of squares approaches, restricting the class of systems and solutions to polynomials. We propose a framework that is capable of automatic synthesis of both analytic controllers and LBFs, without the need for discretization or limiting to polynomial systems and solutions.

Consider the class of nonlinear dynamical systems described by

$$\begin{cases} \dot{x}(t) = f(x(t), u(t)) \\ x(0) \in I \end{cases} \quad (1)$$

where the variables $x(t) \in \mathbb{R}^n$ and $u(t) \in \mathbb{R}^m$ denote the state and input respectively and I is an initial set. The desired closed loop specification involves reaching a goal set G (reachability) and/or staying in a safety set S (safety). These conditions can be implicitly proven by means of a Lyapunov and/or barrier function.

2 The Framework

We propose a framework which uses genetic programming (GP) in combination with a Satisfiability Modulo Theories (SMT) solver to synthesize and verify a controller and LBF. GP is an evolutionary algorithm which evolves encoded representations of candidate solutions to improve their performance over multiple iterations [1]. As opposed to other optimization methods, it is capable of synthesizing analytic expressions, rather than optimizing over parameters, and thus does not impose a fixed structure on the solution. An SMT solver is a tool which determines whether a first-order logic formula can be satisfied [2]. This framework allows to search and verify controllers and Lyapunov-like functions that include non-polynomial functions. The proposed methodology sets itself apart from previous work using GP-based controller synthesis in that it can provide formal guarantees on the behavior of the system, as opposed to test-based approaches using samples or simulations.

The framework is illustrated in Figure 2. GP is used to simultaneously propose and evolve a population of pairs of candidate controllers and LBFs. In the fitness assessment, reachability and safety specifications are verified by means

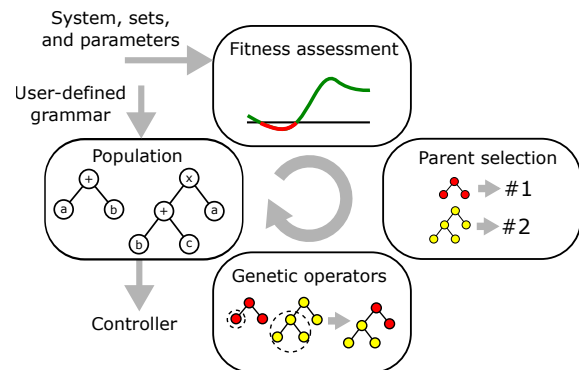


Figure 1: Schematic overview of the framework

of checking if the proposed controller and Lyapunov-like function satisfies a number of nonlinear inequalities w.r.t. the closed-loop system. An initial verification check is done by checking the inequalities over a finite number of states and ultimately the inequalities are formally verified using an SMT solver. Based on this, solutions are scored, which dictates their chance to be selected and modified using genetic operators in order to create a new population. This cycle of proposing and verifying solutions is repeated until a solution is found or a maximum number of generations in met.

3 Results

Given a specification to reach a goal set, while always staying in a safe set, the framework has been proven effective for synthesizing controllers for nonlinear systems with up to 3 states.

4 Acknowledgements

This work is supported by NWO Domain TTW, the Netherlands, under the project CADUSY- TTW#13852.

References

- [1] J. R. Koza, *Genetic Programming: On the Programming of Computers by Means of Natural Selection*. Cambridge, MA, USA: MIT Press, 1992.
- [2] C. W. Barrett, R. Sebastiani, S. A. Seshia, and C. Tinelli, "Satisfiability modulo theories." *Handbook of satisfiability*, vol. 185, pp. 825–885, 2009.

On LQG Control of Infinite-dimensional Stochastic port-Hamiltonian Systems

François Lamoline and Joseph J. Winkin

Namur Institute for Complex Systems (naXys) and Department of Mathematics,
University of Namur, Rempart de la vierge 8, B-5000 Namur, Belgium

Email: francois.lamoline@unamur.be, joseph.winkin@unamur.be

1 Abstract

The class of stochastic port-Hamiltonian systems (SPHSs) was introduced in [3] on finite-dimensional spaces and recently generalized by the authors on infinite-dimensional spaces with boundary control and observation in [1]. This class is the stochastic extension of deterministic first order port-Hamiltonian systems, see [2]. From a practical perspective, it represents mechanical, electrical and electromechanical systems subject to uncertainties such as modeling inaccuracies, external environment disturbances and measurement noises depending on the quality of the sensors. The stochastic modeling helps to improve the quality of the model by considering these neglected effects.

Let us consider a Hilbert space Z and let us denote by $\mathcal{L}(Z)$ the space of all bounded linear operators from Z into Z , equipped with the usual operator norm. Here, we consider this class of infinite-dimensional SPHSs with bounded control and observation operators governed by the following stochastic partial differential equation (SPDE):

$$\frac{\partial X}{\partial t}(\zeta, t) = P_1 \frac{\partial}{\partial \zeta} (\mathcal{H}(\zeta)X(\zeta, t)) + P_0 \mathcal{H}(\zeta)X(\zeta, t) + Bu(t) + (H\eta(t))(\zeta), \quad (1)$$

where $P_1 = P_1^T$ is invertible, $P_0 = -P_0^T$ and $\mathcal{H}(\zeta) \in L^\infty([a, b]; \mathbb{R}^{n \times n})$ is symmetric and $mI \leq \mathcal{H}(\zeta) \leq MI$ for a.e. $\zeta \in [a, b]$ for some constants $m, M > 0$. $\eta(t)$ stands for a Z -valued Gaussian white noise process defined on a complete probability space $(\Omega, \mathcal{F}, \mathbb{F}, \mathbb{P})$, wherein $\mathbb{F} := (\mathcal{F}_t)_{t \geq 0}$ is a filtration. The operators $B \in \mathcal{L}(\mathbb{R}^m, L^2([a, b]; \mathbb{R}^n))$ and $H \in \mathcal{L}(Z, L^2([a, b]; \mathbb{R}^n))$ represent the control and the noise ports.

To the best of our knowledge, no attempt has already been made to develop an adapted approach in order to study and solve the Linear Quadratic Gaussian (LQG for short) control problem for this class of stochastic port-Hamiltonian systems on infinite-dimensional spaces.

The LQG control problem is to minimize the functional

$$J(u) = \lim_{T \rightarrow \infty} \mathbb{E} \int_0^T \|B^* \mathcal{H}X(t)\|_{\mathbb{R}^m}^2 + \|\tilde{R}^{1/2}u(t)\|_{\mathbb{R}^m}^2 dt, \quad (2)$$

over the admissible class of mean-square integrable controls u and subject to (1) and the observation model given by

$$dZ(t) = B^* \mathcal{H}X(t)dt + Fdv(t), \quad (3)$$

where $v(t)$ is a \mathbb{R}^m -valued Wiener process with invertible incremental covariance matrix V and intensity $F \in \mathbb{R}^{m \times m}$. The weight matrix \tilde{R} is assumed to be symmetric and positive definite and $\mathcal{H}BB^*\mathcal{H}$ is assumed to be positive definite.

In this study the class of stochastic port-Hamiltonian systems is presented as in [1] except for the fact that the control and observation operators are bounded. The LQG control problem is addressed for this specific class of systems and solved by using the separation principle. Furthermore, conditions are derived to keep the stochastic port-Hamiltonian structure of the LQG controller and thus the closed-loop dynamic can be interpreted as the interconnection of infinite-dimensional stochastic port-Hamiltonian systems. Eventually, the theory is illustrated by an example of an inhomogeneous vibrating string subject to a space and time dependent Gaussian white noise process. This study is meant to be a first attempt to address the LQG control problem for infinite-dimensional SPHSs in a stochastic context.

Acknowledgement

This research was conducted with the financial support of F.R.S-FNRS. François Lamoline is a FRIA Research Fellow under the grant F 3/5/5-MCF/BC. This abstract presents research results of the Belgian Programme on Interuniversity Poles of Attraction, initiated by the Belgian State, the Prime Minister's Office for Science, Technology and Culture. The scientific responsibility rests with its authors.

References

- [1] F. Lamoline and J.J. Winkin. On Stochastic Port-Hamiltonian Systems with Boundary Control and Observation. In proceedings of the 56th IEEE Conference on Decision and Control, pages 2492–2497, December 2017.
- [2] Y. Le Gorrec, H.J. Zwart, and B. Maschke. Dirac Structures and Boundary Control Systems associated with Skew-Symmetric Differential Operators. *SIAM J. Control and Optimization*, 44(5):1864–1892, December 2005.
- [3] S. Satoh and K. Fujimoto. Passivity Based Control of Stochastic Port-Hamiltonian Systems. *IEEE Transactions on Automatic Control*, 58(5):1139–1153, May 2013.

Nonlinear Stabilization of Infinite-Dimensional port-Hamiltonian Systems applied to Repetitive Control

Federico Califano and Alessandro Macchelli

Department of Electrical, Electronic, and Information Engineering (DEI) “Guglielmo Marconi,”
University of Bologna

federico.califano2@unibo.it

alessandro.macchelli@unibo.it

1 Introduction

Repetitive controllers are applied to reject periodic disturbances with a known time period and their effectiveness relies on the Internal Model Principle so the main issue is to prove stability of the overall scheme. A port-Hamiltonian approach proposed in the linear case [1] is non trivially extended to the nonlinear case by exploiting novel results dealing with stability of closed-loop systems merging from the interconnection of boundary control systems and particular classes of nonlinear systems [2]. The obtained results are used to present a new class of nonlinear control systems for which a RC scheme is first well-posed, and then asymptotically/exponentially stable.

2 Repetitive Control and port-Hamiltonian Systems

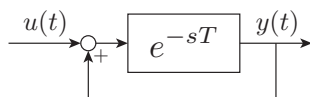


Figure 1: The repetitive compensator

From a system theoretical point of view, the dynamics associated to the internal model based controller present in RC schemes and shown in Fig. 1 can be described by means of the PDE representing a pure time delay of T seconds

$$\frac{\partial x}{\partial t}(t, z) = -\frac{\partial x}{\partial z}(t, z)$$

where the spatial domain is $[0, T]$. By choosing properly the input and the output as combinations of the state variables on the boundary of the spatial domain it turns out that the controller can be described by an infinite-dimensional boundary control system in port-Hamiltonian form. With this new perspective a new set of tools developed in this framework for well-posedness and stabilization of distributed parameter systems can be exploited to study stability of RC schemes.

3 Nonlinear Interconnection

The feedback interconnection of the port-Hamiltonian system in Fig.1 and a finite-dimensional system is an equivalent way to look at classical RC scheme. The case of the system being a linear time-invariant system has been studied in [1] leading to stability conditions for the closed-loop system which are expressed in state-space form and are consistent with classical results. Very recently [2] tools for handling the nonlinear case have been developed. It is possible to non trivially reformulate them in this framework to introduce a class of nonlinear systems which result in a stable closed-loop system. In this way a characterization of nonlinear systems for which repetitive control laws can be successfully applied is determined.

4 Conclusion

A characterization of a class of nonlinear control systems that results first in a well-posed and then in an asymptotically/exponentially RC scheme is presented. The problem has been tackled by decomposing the closed-loop system in the interconnection of a port-Hamiltonian boundary control system and of a finite-dimensional nonlinear system. Future activities are devoted to extend the class of nonlinear systems that result in a stable RC scheme.

References

- [1] F. Califano, A. Macchelli, and C. Melchiorri, “Stability analysis of repetitive control: The port-hamiltonian approach,” in *2017 IEEE 56th Annual Conference on Decision and Control (CDC)*, pp. 1894–1899, Dec 2017.
- [2] H. Ramirez, H. Zwart, and Y. L. Gorrec, “Stabilization of infinite dimensional port-hamiltonian systems by nonlinear dynamic boundary control,” *Automatica*, vol. 85, pp. 61 – 69, 2017.

Port-Hamiltonian formulation of vibrations in a nanorod

Hans Zwart

Department of Applied Mathematics
University of Twente
P.O. Box 217, 7500 AE Enschede
and

Department of Mechanical Engineering
Eindhoven University of Technology
P.O. Box 513, 5600 MB Eindhoven
The Netherlands.

h.j.zwart@utwente.nl, H.J.Zwart@tue.nl

Hanif Heidari

Department of Applied Mathematics,
Damghan University
P.O. Box 36715-364,
Damghan, Iran.

heidari@du.ac.ir, hanif.heidari@gmail.com

1 Abstract

The physics at micro- and nano-scale is fundamentally different from that at macro-scale. Whereas on a macro scale it is normally assumed that there is a local stress strain relation, in nanorods this is no longer the case, and we find nonlocal models like, [3],

$$\sigma_{xx} - \mu \frac{d^2 \sigma_{xx}}{dx^2} = E \varepsilon_{xx}$$

with $\mu \geq 0$. Using this, the model for a one-dimensional nanorod with distributed axial force $F = a^2 w$ becomes

$$a^2 w + \rho \frac{\partial^2 w}{\partial t^2} - \mu \frac{\partial^2}{\partial x^2} \left(a^2 w + \rho \frac{\partial^2 w}{\partial t^2} \right) = E \frac{\partial^2 w}{\partial x^2},$$

where w is the displacement in the x -direction, ρ the mass density, and E the elastic modulus. For $\mu = 0$ this is a standard wave equation. Like the standard wave equation, the above partial differential equation can be written as a port-Hamiltonian system. However, the standard formulation cannot be used for this. We show that for $z^T = (w \ \rho \frac{\partial w}{\partial t} \ Qw)$ the above partial differential equation can be written as

$$\dot{z}(t) = P_{1,Q} \mathcal{H} z(t) + P_0 \mathcal{H} z(t),$$

with

$$P_{1,Q} = \begin{pmatrix} 0 & 0 & 0 \\ 0 & 0 & -Q' \\ 0 & Q & 0 \end{pmatrix}, \quad P_0 = \begin{pmatrix} 0 & 1 & 0 \\ -1 & 0 & 0 \\ 0 & 0 & 0 \end{pmatrix}$$

and

$$\mathcal{H} = \begin{pmatrix} a^2 & 0 & 0 \\ 0 & \rho^{-1} & 0 \\ 0 & 0 & E \end{pmatrix}.$$

Here Q, Q' are the formal operators

$$Q = \frac{\frac{d}{dx}}{1 - \sqrt{\mu} \frac{d}{dx}}, \quad Q' = \frac{-\frac{d}{dx}}{1 + \sqrt{\mu} \frac{d}{dx}}.$$

Here the formulation resembles that of standard Hamiltonian systems as can be found in [1] and [2], but is different, since it does not use the standard derivative. Nevertheless, similarly as in the above mentioned papers we can also characterise all boundary conditions such the semigroup associated to the above partial differential equation is a contraction semigroup. We remark that for $\mu > 0$ the infinitesimal generator is bounded, which in particular implies that the eigenvalues/poles lie in a bounded region.

References

- [1] Y. Le Gorrec, H. Zwart, B. Maschke, Dirac structures and boundary control systems associated with skew-symmetric differential operators, *SIAM journal on control and optimization*, (2005), 1864–1892.
- [2] B. Jacob, H.J. Zwart, *Linear port-Hamiltonian Systems on Infinite-Dimensional Spaces*, Series: Operator Theory: Advances and Applications, Vol. 223, Subseries: Linear Operators and Linear Systems, Birkhäuser, Basel, 2012.
- [3] T. Murmu, S. Adhikari, Nonlocal effects in the longitudinal vibration of double-nanorod systems, *Physica E*, (2010), 43: 415–422.

Modeling and Control of Thermo-Fluidic Processes in Spatially Interconnected Structure

Amritam Das, Siep Weiland

Control Systems Group, Department of Electrical Engineering
Eindhoven University of Technology, P.O. Box 513, 5600 MB Eindhoven

Email: am.das@tue.nl, s.weiland@tue.nl

1 Introduction

In many multi-physics phenomenon, the mutual effects of thermal energy on fluids and vice-versa play a key role when their physical interaction is allowed. Such coupled phenomena are typically called thermo-fluidic processes. These thermo-fluidic processes can be observed in numerous engineering applications. For example, in the commercial printing and packaging industries, the drying of paper, cardboard, wood, etc. typically involve heat and moisture diffusion through composite materials [1]. There are two salient features in all these applications, namely, a) coupled interaction of multiple quantities and b) simultaneous interaction of various components in a spatially distributed structure. In order to predict, optimize and control these the thermo-fluidic processes, in this presentation, we develop a generic mathematical framework which can describe such infinite dimensional continuum dynamics with mathematical models of lower complexity. Moreover, we propose an open loop control strategy to steer such thermo-fluidic processes from arbitrary state to a desired state within a finite time.

2 Modeling Framework

We consider the spatial interconnection of multiple thermo-fluidic processes as a network of systems under a topological structure. A finite graph \mathcal{G} describes such network with a set of nodes \mathcal{N} and edges \mathcal{E}

$$\mathcal{G} = (\mathcal{N}, \mathcal{E}). \quad (1)$$

Each element in $\mathcal{N} = \{\mathcal{N}_1, \dots, \mathcal{N}_M\}$ describes a specific thermo-fluidic processes. The elements in $\mathcal{E} = \{\mathcal{E}_{i,j}\}$ describes the interconnection between two adjacent nodes (\mathcal{N}_i and \mathcal{N}_j) defined on the their common boundary. Figure 1 illustrates an example topology of a set of thermo-fluidic processes in spatially interconnected structure. At each node \mathcal{N}_i we describe the continuum processes in terms of spatio-temporal variable $z_i(s,t)$ using the following infinite dimensional setting:

$$E_i \frac{\partial z_i}{\partial t} = A_i z_i + B_i^{\text{int}} q_i^{\text{int}}. \quad (2)$$

The interaction with the external environment is modeled by mixed non-homogeneous boundary conditions with external boundary input q_i^{ext} :

$$H_i^{\text{ext}} z_i = B_i^{\text{ext}} q_i^{\text{ext}}. \quad (3)$$

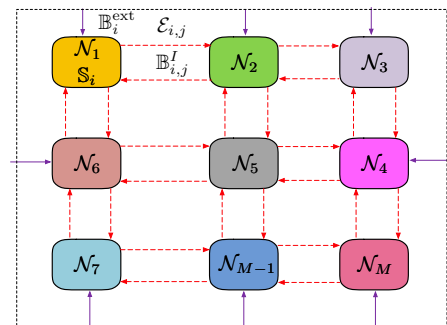


Figure 1: Topological schematic of thermo-fluidic processes in cascade structure.

We artificially impose boundary conditions to preserve the net flux among interconnected nodes as

$$P_{i,j}^I \begin{bmatrix} z_i \\ z_j \end{bmatrix} = 0. \quad (4)$$

3 Model Order Reduction

The approximated solution of z_i in the above network can be given as a partial sum $z_i(s,t) \approx \sum_{m=1}^R \Phi_{i,m}(s) \Theta_{i,m}(t)$ for a particular truncated order R . In this presentation, we compare and demonstrate the approximation results of such low order models that are inferred from different choices of basis functions $\{\Phi_{i,m}(s)\}$ and $\{\Theta_{i,m}(t)\}$.

4 Open-loop Trajectory Planning

Apart from computationally fast model, the problem of trajectory planning, i.e., the design of an open-loop control in order to realize a finite time transition between an initial and a final state along a prescribed trajectory is crucial for numerous application. In this presentation we also provide a systematic parametrization of input that explicitly provides regular open-loop controls achieving these desired trajectories[2].

References

- [1] W. J. Auhorn, "Handbook of Paper and Board". Wiley-VCH Verlag GmbH & Co. K.Ga.A, 2006, pp. 62-149.
- [2] T. Meurer, "Control of Higher-Dimensional PDEs." Berlin, Heidelberg: Springer, 2013, pp. 3-20.

Dynamic density estimation from cell population snapshot data

Armin Küper, Robert Dürr, and Steffen Waldherr

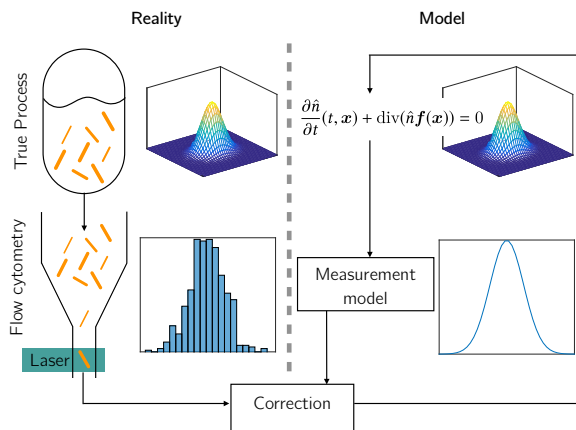
Department of Chemical Engineering

KU Leuven

3001 Leuven, Belgium

Email: {armin.kueper, robert.duerr, steffen.waldherr}@kuleuven.be

Populations of living cells commonly display phenotypic cell-to-cell variability. This heterogeneity is presumed to cause reduced product yields and process instabilities in biomanufacturing [1]. Monitoring and controlling the heterogeneity is therefore crucial.



Experimental data of heterogeneous cell populations is available through high-throughput single cell measurements (e.g. flow cytometry) in the form of population snapshot data [2]. This experimental setup does not provide single cell time series data but information on a representative sample from the population at discrete time points, which can be represented by density distributions with respect to the measured cellular properties. Moreover, technical and financial restrictions prevent the measurement of all intracellular states. For example, the cell size might be available through measurements, while the growth rate is not. To reconstruct the full heterogeneity, model-based online state estimation methods are required. These methods continuously combine measurements and model predictions (see Figure).

Population balance modeling [4] describes cell heterogeneity through a time-dependent cell number density function $n(t, \mathbf{x})$ (NDF) over the internal cell states \mathbf{x} . In basic cases the population balance equation (PBE) is of the form

$$\frac{\partial n}{\partial t}(t, \mathbf{x}) + \text{div}(n(t, \mathbf{x})\mathbf{f}(\mathbf{x})) = 0.$$

Here, the single cell model $\mathbf{f}(\mathbf{x})$ is a vector field describing the dynamics of the individual cellular properties. In this work we only consider short time horizons and therefore neglect population dynamics such as cell division and death.

Taking these phenomena into account results in a non-zero right hand side.

In past studies, the implementation of state estimation techniques like Kalman or particle filters [5] for population balance models has been done with large dimensional systems of ordinary differential equations resulting from the discretization of the PBEs [3]. In that approach, the computational load increases exponentially with the model dimension, rendering it infeasible for high-dimensional PBEs, which often result from cell population modeling. Motivated by this, we introduce a so-called *characteristics-based observer* that uses sample-based approximations of the NDF, compared to the finite-dimensional approximations used in the discretization-based designs. Sample cells are propagated with the easy to handle single cell model $\mathbf{f}(\mathbf{x})$. To give an estimate for the NDF, we employ a Gaussian mixture distribution to approximate the sample distribution. Measured and estimated distribution are combined through regularized resampling of a new set of samples.

For a one and two-dimensional benchmark problem, we compared a discretization-based particle filter and our proposed *characteristics-based observer*. We were able to show that our approach is more accurate in reconstructing the NDF and less computational demanding, especially for the two-dimensional PBE. For a three-dimensional PBE describing gene expression, we demonstrated that our approach is able to reconstruct the full three-dimensional NDF from two-dimensional measurements.

References

- [1] D. Binder, T. Drepper, K.-E. Jaeger, F. Delvigne, W. Wiechert, D. Kohlheyer, A. Grünberger (2017) Homogenizing bacterial cell factories: Analysis and engineering of phenotypic heterogeneity, *Metabolic Engineering* 42, 145–156.
- [2] J. Hasenauer, S. Waldherr, M. Doszczak, N. Radde, P. Scheurich, F. Allgöwer (2011) Identification of models of heterogeneous cell populations from population snapshot data, *BMC Bioinformatics* 12(1):125.
- [3] M. Mangold (2012) Use of a Kalman filter to reconstruct particle size distributions from FBRM measurements *Chemical Engineering Science* 70, 99–108.
- [4] D. Ramkrishna (2000), *Population Balances* Academic Press.
- [5] D. Simon (2006), *Optimal State Estimation* John Wiley & Sons.

Stability and passivity of multi-physic systems with irreversible entropy production

Benjamin Vincent and Denis Dochain
ICTEAM, INMA

Université Catholique de Louvain
B-1348 Louvain-la-Neuve, Belgium

{benjamin.vincent, denis.dochain}@uclouvain.be

Nicolas Hudon
Department of Chemical Engineering,
Queen's University,
Kingston, ON Canada K7L 3N6
nicolas.hudon@queensu.ca

Laurent Lefèvre
Univ. Grenoble Alpes, LCIS
F-26902, France
laurent.lefevre@lcis.grenoble-inp.fr

We consider multi-physics systems, a class of systems described by conservation laws where the state depends on both time and space [1]. Modeling for this class of distributed parameter systems is based on classical irreversible thermodynamics [2]. Recent developments extended classical modeling formulation of multi-physics to non-equilibrium thermodynamic systems, using geometric representations aiming at improving modeling, analysis, and (feedback) control design methods for multi-physics systems [1, 3]. Conservative phenomena dynamics are generated by the gradient of an energy functional, through Poisson brackets or Stokes–Dirac structures. Dissipative phenomena dynamics are generated by the gradient of a potential, typically the entropy functional for non-equilibrium thermodynamic systems, through dissipative structures. As the representation for a given multi-physics system is not unique, an entropy functional can be formulated by characterizing a measure of dissipation along the system evolution with respect to time. An entropy balance equation can be derived for multi-physics systems within the above framework using the Gibbs relation [2]. The second law of thermodynamics constrains the irreversible entropy production to be positive along the evolution of the system. The entropy production term is usually used to define the phenomenological relations characterizing transport phenomena within the system. This is achieved, classically, using Onsager’s linear transport theory, where the transport matrix, relating forces and fluxes, is positive semi-definite. The irreversible entropy source term coupled with Onsager linear transport theory can be used as a Lyapunov functional candidate to prove stability of closed non-equilibrium systems [2]. This approach is investigated in this contribution.

In this presentation, we study stability and passivity conditions for closed and open multi-physics systems. Following the application of classical results on stability of irreversible thermodynamics applied to multi-physics

closed systems, the approach is extended to passivity of multi-physics open systems by introducing time-varying boundary variables. The stability and passivity proofs are constructed by considering geometric properties of both the model and Onsager linear transport theory [4].

The proposed method is successfully applied to burning plasmas in Tokamak in a recent contribution [5]. For clarity of this presentation, heat diffusion in 1D is first considered. Then, a system of coupled conservation laws is investigated: the Saint-Venant equations describing the propagation of water in open channels.

Acknowledgement

This research is supported by the Belgian Network DYSCO (Dynamical Systems, Control, and Optimization), funded by the Interuniversity Attraction Poles Program, initiated by the Belgian Science Policy Office. Benjamin Vincent is a FRIA fellow (F.R.S.-FNRS).

References

- [1] V. Duindam, A. Macchelli, S. Stramigioli, and H. Bruyninckx (2009). *Modeling and Control of Complex Physical Systems: The Port-Hamiltonian Approach*. Springer, Berlin Heidelberg.
- [2] S. R. de Groot and P. Mazur (1984). *Non-equilibrium Thermodynamics* Dover Books on Physics, New York.
- [3] H. C. Öttinger (2005). *Beyond Equilibrium Thermodynamics*. Wiley, NJ.
- [4] J. E. Marsden, T. Ratiu, R. Abraham (2001). *Manifolds, Tensor Analysis, and Applications*. 2nd edition. Springer-Verlag, New York.
- [5] B. Vincent, N. Hudon, L. Lefèvre, and D. Dochain *Passivity and stability properties of multi-physics systems using the entropy production*. Proceedings of the 6th IFAC Workshop LHMNC. Valparaíso, Chile. (2018) Paper number 16.

On Representations of Linear Dynamic Networks¹

E.M.M. Kivits
Control Systems Group
Department of Electrical Engineering
Eindhoven University of Technology
P.O. Box 513, 5600 MB Eindhoven
The Netherlands
Email: e.m.m.kivits@tue.nl

P.M.J. Van den Hof
Control Systems Group
Department of Electrical Engineering
Eindhoven University of Technology
P.O. Box 513, 5600 MB Eindhoven
The Netherlands
Email: p.m.j.vandenhof@tue.nl

1 Introduction

Linear dynamic networks are typically described in either a state-space form or a module representation. The question arises under which conditions these representations are equivalent and can be transformed into one another. To be able to appropriately compare the network representations, both descriptions are reformulated in the same framework: the module dynamic network.

2 Module dynamic network

A module dynamic network is a network consisting of interconnections of nodes and excitations through transfer function matrices (or modules). Module dynamic networks allow for self-loops and MIMO modules and hence, they are a generalisation of the module representation in [1]. State-space forms can be formulated as special module dynamic networks, referred to as state-space dynamic networks, where every state variable is a node signal and every module is of the form $q^{-1}A(j,i)$ or $q^{-1}B(j,k)$.

3 Zooming out

Module dynamic networks allow to zoom out on the network to exclude more detailed structural information. Zooming out takes place via immersion [1], where node signals are removed from the network by lifting the paths through the nodes. This process can be performed in two ways: in single-path immersion each path is lifted individually resulting in a new module for each path, while in multi-path immersion all paths are lifted together and combined to create a single (multi-variate) module.

As a result, a state-space dynamic network with minimal state-space dimension n can be transformed by immersion into a general module dynamic network with generic McMillan degree² $\geq n$. Equality holds if and only if the modules in the resulting network have no shared states.

¹This project has received funding from the European Research Council (ERC), Advanced Research Grant SYSDYNET, under the European Union's Horizon 2020 research and innovation programme (grant agreement No 694504).

Zooming out is equivalent to viewing the network as the interconnection of sub-networks, where each sub-network consists of several modules. A network can be partitioned into sub-networks by removing all nodes in a certain (boxed) area from the network. Figure 1 shows a module dynamic network with sub-networks G_{132} and G_{45} . To represent the network in terms of these sub-networks, the red nodes are removed from the network by immersion.

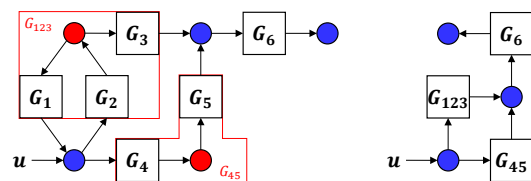


Figure 1: Left: a module dynamic network with modules (blocks) and nodes (circles). Right: the resulting network after removing the red nodes by immersion (of either type).

4 Zooming in

Module dynamic networks allow to zoom in on the network to include more detailed structural information. Zooming in takes place via realisation, where nodes (measured states) are added to the network by finding state-space realisations of the modules. Due to the freedom in creating (minimal) realisations of single modules, the resulting module dynamic network is not unique. However, the already existing node signals remain invariant.

As a result, a module dynamic network with generic McMillan degree² n can be transformed by realisation into a state-space dynamic network with state-space dimension n .

References

- [1] A. Dankers, P.M.J. Van den Hof, X. Bombois, and P.S.C. Heuberger, "Identification of dynamic models in complex networks with prediction error methods: Predictor input selection," *IEEE Transactions on Automatic Control*, 61(4), 937-952, 2016.

²The generic McMillan degree of a system is the McMillan degree of the system when all parameters take numerical values that preserve the network structure and avoid special situations, such as pole-zero cancellations.

Partitioning and stability for linear time-varying large-scale systems

Tomas Pippia, Joris Sijs, and Bart De Schutter

Delft Center for Systems and Control

Delft University of Technology

Delft, The Netherlands

t.m.pippia@tudelft.nl

1 Introduction

Large-scale systems (LSSs) have received an increasing amount of attention in the recent years. Examples of LSSs are water networks, traffic networks, and power networks. Due to the number of elements in LSSs and to their size, LSSs are usually difficult to control. Centralized control strategies are either computationally inefficient or even impossible to implement. Therefore, a common approach is to partition LSSs into several, smaller subsystems, such that a non-centralized control approach can be applied. Partitions are usually aimed at reducing coupling and at balancing the number of elements per subsystem. However, no attention has been devoted to partitioning of time-varying systems, whose structure can change in time. An example of this kind of systems is a power network with electric vehicles, which are elements that move around in the network from one point to another. Because of these changes in the system, it might be necessary to repartition the system when it is subject to a change in its structure. We propose a new partitioning approach for partitioning a specific class of time-varying LSSs. Once the partitioning approach has been applied, a stability analysis is required to guarantee that the system will be stable even when the system and the partition will change in time. We propose a stability analysis based on results from switching systems [1].

2 Partitioning approach

We consider linear time-varying systems of the kind $x(k+1) = A(k)x(k) + B(k)u(k)$, where x represents the state vector, u the input vector, and A and B are the state matrix and the input matrix, respectively. Note that these two matrices depend on k because they are time-varying. Indeed, we consider a system in which the matrices A and B can change in time, but they take values from a set of already known matrices. For each (A, B) pair we propose a different partition, so that to each configuration of the system we associate a different partition.

Our partitioning approach is inspired by [2, 3], which present two graph-based multi-step partitioning algorithms. Such a method consists in performing first a global partitioning, which results in an initial partition that is then refined in the second step, called refining step. Differently from [3], we predefine the number of subsystems and like in [2] we implement a negotiation-based iterative refining step.

3 Decentralized control scheme and stability

Once each (A, B) pair has been partitioned, we apply to each subsystem a decentralized state feedback control law of the form $u(k) = -Kx(k)$, where K is a gain matrix. Our goal is that each subsystem and the centralized system are asymptotically stable, for each possible (A, B) pair and thus each partition. We achieve this by solving an LMI problem and we obtain a block-diagonal centralized K matrix, i.e. a local controller is implemented in each subsystem. We then obtain the closed-loop equation for the centralized system $x(k+1) = (A(k) - B(k)K(k))x(k)$, where $A(k) - B(k)K(k)$ is the asymptotically stable time-varying closed-loop matrix. After we have found a K matrix that stabilizes each possible (A, B) pair of the system, we consider an average dwell-time stability scheme [1]. Indeed, due to the time-varying nature of the system under control, guaranteeing stability of each single centralized system is not enough for guaranteeing stability of the overall system. By modeling the centralized system as a switching system and adapting the proof provided in [1], we are able to guarantee exponential stability both of the centralized system and of each single subsystem. We obtain this result under the condition that the average dwell time is higher than a certain lower bound.

Acknowledgement

Research supported by the European Union's Horizon 2020 research and innovation programme under Marie Skłodowska-Curie grant agreement No 675318 (INCITE).

References

- [1] G. Zhai, B. Hu, K. Yasuda, and A. N. Michel. Stability and \mathcal{L}_2 gain analysis of discrete-time switched systems. *Transactions of the Institute of Systems, Control and Information Engineers*, 15(3):117–125, 2002.
- [2] C. Ocampo-Martinez, S. Bovo, and V. Puig. Partitioning approach oriented to the decentralised predictive control of large-scale systems. *Journal of Process Control*, 21(5):775–786, 2011.
- [3] S. Kamelian and K. Salahshoor. A novel graph-based partitioning algorithm for large-scale dynamical systems. *International Journal of Systems Science*, 46(2):227–245, 2015.

Strong Structural Controllability of Systems on Colored Graphs

Jiajia Jia, Harry L. Trentelman, Wouter Baar, M. Kanat Camlibel

Johann Bernoulli Institute for Mathematics and Computer Science, University of Groningen

{j.jia, h.l.trentelman, m.k.camlibel}@rug.nl, w.baar.1@student.rug.nl

1 Introduction

The study of controllability of networked systems has attracted a lot of attentions in recent years. Most of the research has focused on weak structural controllability and strong structural controllability. A basic assumption in the study of (strong) structural controllability is the independence of the nonzero parameters in the patterned matrices in the qualitative class, i.e., the choice of the interconnection weights is completely free. However, in many real-world networks, this assumption is not satisfied, and some links may have identical weights (for example, in undirected graph), or some interconnection weights may be already fixed.

In this presentation, we consider linear time-invariant dynamical networked systems where the interconnections can have identical weights. We consider leader-follower networks, where a subset of the node set is chosen as the set of leaders to which external inputs are applied, and the remaining nodes are called followers. To describe the property that arcs are allowed to have identical weights, we develop a definition of ‘colored graph’. Then the system is called ‘colored strongly structurally controllable’ if the system is controllable for every choice of arc weights in the colored graph. Our aim is to provide graph-theoretic conditions under which the networked system is ‘colored strongly structurally controllable’.

2 Problem Formulation

Let $\mathcal{G} = (V, E)$ be a digraph in which each arc has a color. Arcs having the same color means that their weights are identical. More concretely, we have a partition $\pi_E = \{E_1, E_2, \dots, E_k\}$ of the edge set E and all arcs in E_i are assumed to have the same color. We then denote the corresponding ‘colored digraph’ as $\mathcal{G}_\pi = (V(\mathcal{G}), E(\mathcal{G}), \pi_E)$. To describe the family of system matrices associated with \mathcal{G}_π , we define the ‘colored qualitative class’ as the set of all $A \in \mathbb{C}^{n \times n}$ with the properties that for all $i \neq j$ we have $A_{ij} \neq 0$ if and only if $(j, i) \in E$ and $A_{ij} = A_{kl}$ if there exists r such that $(j, i), (l, k) \in E_r$. Associated with the colored digraph \mathcal{G}_π and leader set $V_L \subset V$, we then consider the class of systems

$$\dot{x} = Ax + Bu, \quad (1)$$

where $A \in \mathcal{Q}_\pi(\mathcal{G})$ is the system matrix, and B encodes the leader vertices V_L . The networked system is called ‘colored strongly structurally controllable’ if (A, B) is controllable for

all $A \in \mathcal{Q}_\pi(\mathcal{G})$. For example, the system with graph in Figure 1 is ‘colored strongly structurally controllable’. The goal of this work is to establish graph-theoretic conditions under which (\mathcal{G}_π, V_L) is ‘colored strongly structurally controllable’.

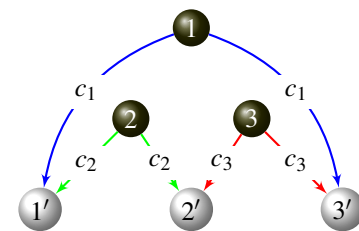


Figure 1: A colored digraph with leader set $\{1, 2, 3\}$.

3 Results and Current Work

In this presentation we will present two main results. On the one hand, we will provide a sufficient graph-theoretic condition in terms of the concept ‘colored zero forcing set’. More specifically, we first develop a ‘colored color change rule’, and then define the notion of colored zero forcing set based on that rule. In order to obtain this colored color change rule, we study ‘colored bipartite graphs’. In fact, for colored bipartite graphs, we establish a necessary and sufficient graph-theoretic condition for the nonsingularity of its associated pattern class. On the other hand, we establish an algebraic condition in terms of ‘generalized balancing set’. We show that every colored zero forcing set is also a generalized balancing set, which means that latter condition is more general.

As our final goal is to establish graph-theoretic conditions, we are currently seeking for a graph-theoretic representation of the latter sufficient condition. Besides, we are also working on developing a necessary and sufficient graph-theoretic condition under which a networked system is colored strongly structurally controllable.

References

- [1] N. Monshizadeh, S. Zhang, and M. K. Camlibel (2014). Zero Forcing Sets and Controllability of Dynamical Systems Defined on Graphs. *IEEE Transactions on Automatic Control*, 59(9):2562-2567.
- [2] Shima Sadat Mousaviy, Mohammad Haeriy, and Mehran Mesbahi(2017). On the Structural and Strong Structural Controllability of Undirected Networks. *IEEE Transactions on Automatic Control*, DOI 10.1109/TAC.2017.2762620.

Numerical analysis of oscillations in nonlinear networks

K.Rogov¹, A.Pogromsky¹, E.Steur^{1,2} and H.Nijmeijer¹

¹Dynamics and Control, Dept. of Mechanical Engineering, Eindhoven University of Technology

²Delft Center for Systems and Control, Dept. 3mE, Delft University of Technology

Email:k.rogov@tue.nl

1 Introduction

The study of large oscillatory networks of identical nonlinear systems is challenging due to the large number of systems and the many possible network structures. Coupling several even globally asymptotically stable systems into a network can result in emergent behavior among which co-existing oscillatory patterns that may be multi-stable. It makes the application of common methods such as the direct Lyapunov method to analyze these phenomena nontrivial. Our goal is to develop a numerically efficient method to analyze the oscillatory behavior occurring in networks. The oscillations appear via a Hopf bifurcation and show sinusoidal-like behavior around a bifurcation point. That allows us to use the describing function method to replace nonlinearities by their linear approximation and then to analyze the system of linear equations by means of the multivariable harmonic balance (MHB) method. The MHB method for networks of specific structure was described by Iwasaki in [1] and here we present an extension of the MHB method to networks with a more general structure and dynamic.

2 Problem statement

The idea is to turn the problem of determining an oscillation profile (frequency ω , amplitudes α_i , phases ϕ_i) into an easily solvable eigenvalue problem rather than doing a dynamical analysis. The network of identical interconnected (sub)system can be described by a dynamical mapping from the input u to the output of interest q :

$$q_i = f_i(j\omega)u_i, \quad u_i = \sum_{m=1}^n \mu_{im}(j\omega)v_m, \quad v_i = \psi_i(q_i),$$

where $i = 1, \dots, n$ is a number of subsystems, j is the imaginary unit, $f(j\omega) \in \mathbb{C}^1$ is a frequency response which represents the linear time-invariant part of each subsystem, $\psi(q_i)$ is the static nonlinear function, $q \in \mathbb{C}^n$ is the output and $\mu_{im}(j\omega)$ is a frequency response of connection from m^{th} system to i^{th} system. In a vector form, the dynamic can be written

$$q = \mathcal{M}(j\omega)v, \quad \mathcal{M}(j\omega) = F(j\omega)M(j\omega), \quad v = \Psi(q), \\ F(j\omega) := f(j\omega)I_n, \quad \Psi := \psi(q_i)I_n,$$

where $M(j\omega)$ is the frequency response matrix of the coupling whose (i, m) entry is $\mu_{im}(j\omega)$. We use the describing function method to replace the nonlinearities by their linear

approximations. With these approximations, the dynamical equations reduce to the MHB equations

$$(\mathcal{M}(j\omega)\mathcal{K}(\alpha) - I_n)g = 0, \quad g_i := \alpha_i e^{j\phi_i}, \quad g \in \mathbb{C}^n, \quad (1)$$

where $\mathcal{K}(\alpha) := k(\alpha_i)I_n$ is a diagonal matrix of the describing functions. We consider the uniform amplitude case and we are thus looking for $\alpha_i = \alpha_0 \forall i$.

3 Oscillation profile

As an example we studied a ring network of diffusively coupled identical systems whose dynamic is described in [2]. After some transformations, we arrive at the condition that some matrix of a relatively low order only has imaginary eigenvalues for $\pm j\omega$, where ω stands for frequency of the oscillations. In other words, $k(\alpha_0)$, and consequently the amplitude α_0 and ω can be derived from the Hopf bifurcation condition. The last component of the oscillation profile can be determined from some matrix which represents the topology of the network. The phases ϕ_i are encoded in an eigenvector that corresponds to a maximal eigenvalue of the topology matrix. The maximal eigenvalue is defined to be the eigenvalue with the largest real part. We now have all components of the oscillation profile and can construct the approximation of the output of the network using

$$q_i(t) \cong \alpha_0 \sin(\omega t + \phi_i). \quad (2)$$

The uniform amplitude case is fully investigated and the oscillation profile is determined. The MHB method provides a very good approximation of the oscillations around the bifurcation point.

Acknowledgements

The UCoCoS program has received funding from the European Union's EU Framework Program for Research and Innovation Horizon 2020 under Grant Agreement No 675080.

References

- [1] T. Iwasaki, "Multivariable harmonic balance for central pattern generators", *Automatica*, 44(12):3061-3069, 2008.
- [2] A. Pogromsky, N. Kuznetsov and G. Leonov, "Pattern generation in diffusive networks: How do those brainless centipedes walk?", *Proceedings of the IEEE Conference on Decision and Control*, 7849-7854, 2011.

Approximate controllability of an axially vibrating nanorod embedded in an elastic medium

Hanif Heidari

Department of Applied Mathematics

Damghan University

P.O. Box 36715-364 Damghan

Iran

Email: heidari@du.ac.ir, hanif.heidari@gmail.com

1 Introduction

In recent years, vibration analysis of nanorod has been considered by many researchers since its wide applications in nano-electro mechanical system (NEMS) [1]. In this paper, stability and controllability of vibration of a nanorod embedded in an elastic medium are investigated using semi-group theory.

2 Problem Formulation

Consider a nanorod in the physical domain determined by thin elastic rod with length ℓ . Let $\Omega = (0, \ell)$ be a bounded open set in \mathbb{R} , $T > 0$ and $D = \Omega \times (0, T)$. The PDE describing the longitudinal vibration of a nanorod which embedded in an elastic medium over domain D can be expressed as follows [2]:

$$-\mathbb{E}\mathbb{A} \frac{\partial^2}{\partial x^2} u + Ku - (e_0 a)^2 K \frac{\partial^2}{\partial x^2} u + (1 - (e_0 a)^2 \frac{\partial^2}{\partial x^2}) m \frac{\partial^2}{\partial t^2} u = b(x)f(x, t), \quad (x, t) \in D \quad (1)$$

where $u(x, t)$ is axial displacements, \mathbb{E} is the modulus of elasticity, \mathbb{A} is the cross-sectional area of the nanorods, K is stiffness of elastic medium, m is the mass per unit length, a is an internal characteristic length, e_0 is a constant, $b(x)$ represents the shaping function around the control point x_0 and $f(t)$ axially distributed external control force. The clamped-clamped boundary conditions are considered as follows

$$u(0, t) = u(\ell, t) = 0. \quad (2)$$

As the state space we choose

$$z = \begin{pmatrix} z_1 \\ z_2 \end{pmatrix} = \begin{pmatrix} u \\ \dot{u} \end{pmatrix} \in H^2(\Omega) \cap H_0^1(\Omega), \quad (3)$$

with the following inner product

$$\left\langle \begin{pmatrix} z_1 \\ z_2 \end{pmatrix}, \begin{pmatrix} w_1 \\ w_2 \end{pmatrix} \right\rangle = \int_{\Omega} z_1 w_1 + J(z_2)J(w_2) dx, \quad (4)$$

where $J = 1 - (e_0 a)^2 \frac{\partial^2}{\partial x^2}$.

It can be proved that the operator J is invertible in the space $\mathcal{H} = H^2(\Omega) \cap H_0^1(\Omega)$. Therefore, the abstract form of Eq. (1) is as follows

$$\dot{z} = Az + Bf = \begin{pmatrix} 0 & 1 \\ \frac{J^{-1}}{m} \left[(\mathbb{E}\mathbb{A} + (e_0 a)^2 K) \frac{\partial^2}{\partial x^2} - K \right] & 0 \end{pmatrix} z + \begin{pmatrix} 0 \\ b(x)f(t) \end{pmatrix} \quad (5)$$

Lemma 2.1. *The set of eigenvalues of matrix A and its correspond eigenfunctions are as follows respectively:*

$$\lambda = \{ \lambda_{\pm n} = \pm \frac{[(\mathbb{E}\mathbb{A} + (e_0 a)^2 K) (\frac{n\pi}{\ell})^2 + K]}{m(1 + (e_0 a)^2 (\frac{n\pi}{\ell})^2)} i \mid n \in \mathbb{N} \} \quad (6)$$

$$\phi = \{ \phi_{\pm n} = \begin{pmatrix} \sin(\frac{n\pi x}{\ell}) \\ \lambda_{\pm n} \sin(\frac{n\pi x}{\ell}) \end{pmatrix} \mid n \in \mathbb{N} \} \quad (7)$$

Theorem 2.2. *The normalize eigenfunctions of operator A form Riesz basis in \mathcal{H} .*

Theorem 2.3. *The operator A is infinitesimal generator of a C_0 -semigroup.*

Theorem 2.4. *Assume that the function $b(x)$ is defined as Ref. [1]. Consider the system (1) with given initial and boundary conditions defined in (2). The system is approximate controllable if and only if the following condition is satisfied*

$$\sin\left(\frac{n\pi x_0}{\ell}\right) \sin\left(\frac{n\pi \varepsilon}{\ell}\right) \neq 0, \quad \forall n \in \mathbb{N}. \quad (8)$$

A comparison between this presentation and [1] concludes that the controllability condition of an axially vibrating nanorod which is embedded in an elastic medium is as same as a nanorod that is not embedded in an elastic medium. Therefore, this physical change of system does not affect the controllability property.

References

- [1] H. Heidari, International Journal of Applied Mathematics 29(2016) 263–270.
- [2] M. Aydogdu, Mechanics Research Communications 43(2012) 34–40.

Multiple Input Multiple Output Cepstrum Coefficients

Oliver Lauwers Bart De Moor

KU Leuven, Department of Electrical Engineering (ESAT), Stadius Center for Dynamical Systems,
Signal Processing and Data Analytics.

oliver.lauwers@kuleuven.be; bart.demoor@kuleuven.be

1 Introduction

The (power) cepstrum of a signal is a technique stemming from the field of *homomorphic signal processing* [2]. It has several applications, most notably in human speech recognition. The power cepstrum was defined for univariate signals coming from stochastic systems. In this presentation, we will discuss a method to extend the notion of scalar power cepstrum coefficients to signals coming from Multiple Input Multiple Output (MIMO) systems.

2 SISO cepstrum

The *power cepstrum coefficients* of a univariate signal $y(k)$, with k denoting time, are defined as [2]

$$c_y(k) = \mathcal{F}^{-1}(\log \Phi_y(e^{i\omega})), \quad (1)$$

with $\Phi_y(e^{i\omega}) = |Y(e^{i\omega})|^2$ the *power spectrum* of the signal (and $Y(e^{i\omega})$ the *Fourier transform* of the signal), and \mathcal{F}^{-1} denoting the *inverse Fourier transform* operator.

A signal from a stochastic system, given in z -domain as

$$Y(z) = \frac{b(z)}{a(z)}U(z), \quad (2)$$

with $U(z)$ describing white noise, $a(z)$ the pole polynomial with the poles α_i as roots and $b(z)$ the pole polynomial with the poles β_j as roots, has cepstrum coefficients

$$c_y(k) = \sum_{j=1}^p \frac{\alpha_j^{|k|}}{|k|} - \sum_{j=1}^q \frac{\beta_j^{|k|}}{|k|}, \quad \forall k \neq 0. \quad (3)$$

In this sense, the cepstrum is as much a characteristic of the system generating the signal as of the signal itself. Any extension of the cepstrum to MIMO-systems should thus retain this property: it should be interpretable in terms of poles and zeros of the underlying MIMO system.

3 MIMO cepstrum

Traditionally, for MIMO systems, a cepstrum coefficient matrix is constructed, naively following Equation (1). In this presentation, we will follow an alternative route, and construct scalar cepstrum coefficients, which we will show to be interpretable in terms of poles and *transmission zeros* of the system.

Writing the transfer function of the MIMO system (assumed square to keep notation simple, but an extension to rectangular systems is possible) in its Smith-McMillanform,

$$U(z)T(z)V(z) = U(z) \begin{pmatrix} \frac{b_1(z)}{a_1(z)} & 0 & \dots & 0 \\ 0 & \frac{b_2(z)}{a_2(z)} & \dots & 0 \\ \vdots & \vdots & \ddots & \vdots \\ 0 & 0 & \dots & \frac{b_r(z)}{a_r(z)} \end{pmatrix} V(z), \quad (4)$$

with $U(z)$ and $V(z)$ unimodular matrices, we can derive an expression that resembles the pole/zero-structure of the SISO cepstrum coefficients. Here the $a_i(z)$ and $b_i(z)$ are polynomials with poles and zeros as roots respectively, with $\{b_i(z), a_i(z)\}$ coprime, $b_i(z)|b_{i+1}(z)$ and $a_{i+1}(z)|a_i(z)$.

The determinant of this matrix gives the full zero/pole polynomials, allowing us to construct scalar cepstrum coefficients, interpretable in terms of poles and zeros.

4 Applications

We look at different applications, and investigate for which applications our generalization of the cepstrum works. We will focus on cepstrum-based distance measures [1], but will briefly discuss traditional signal processing applications, stemming from homomorphic signal processing [2].

Acknowledgements

O.L. is a FWO SB fellow. This research receives support from FWO under EOS project G0F6718N (SeLMA) and from KU Leuven Internal Funds: C16/15/059 and C32/16/013.

References

- [1] Lauwers O., De Moor B., "Applicability and interpretation of the deterministic weighted cepstral distance", Internal Report 18-12, ESAT-STADIUS, KU Leuven (Leuven, Belgium), 2018.
- [2] Oppenheim, A., Schaffer, R., *Digital Signal Processing* (1st Edition), 1975, Pearson, New jersey

A nonlinear state-space model of the transverse fluid force on an oscillating cylinder in a fluid flow

Jan Decuyper, Tim De Troyer, Mark C Runacres, Johan Schoukens
Vrije Universiteit Brussel, INDI
Pleinlaan 2, 1050 Brussels
Belgium

Email: jan.decuyper@vub.be, tim.de.troyer@vub.be,

Email: mark.runacres@vub.be, johan.schoukens@vub.be

1 Introduction

A well known problem of many civil engineering applications are the forces which arise when fluids and structures interact. Of particular interest are the forces related to vortex shedding on bluff bodies. Modelling the displacement-force relationship has proven to be challenging, mainly due to the highly nonlinear nature of the system. In this work the problem is tackled using the polynomial nonlinear state-space model (PNLSS) class. As a result, an accurate simulation model is obtained.

2 Approach

PNLSS (Eq. (1)) is a data driven modelling approach that identifies a parametric nonlinear state-space model [1]:

$$x(t+1) = \mathbf{A}x(t) + \mathbf{B}y(t) + \mathbf{E}\zeta(x(t), y(t)) \quad (1a)$$

$$c_y(t) = \mathbf{C}x(t) + \mathbf{D}y(t) + \mathbf{F}\eta(x(t), y(t)), \quad (1b)$$

with ζ and η containing monomial cross products between the states and the input raised to user defined powers. The input corresponds to the displacement $y(t)$ while the output is the transverse force coefficient $c_y(t)$. The procedure can be summarised in the following four steps.

1. **Acquiring data:** The necessary data were obtained using CFD simulations of a 2-dimensional cylinder at $Re = 100$. An imposed motion, transverse to the oncoming flow was applied as input.
2. **Initialise the model:** As initialisation the best linear approximation of the system is used [2].
3. **Tuning of the model:** The model is tuned to the data using the Levenberg-Marquardt algorithm, minimising the least-squares cost function,

$$V = \sum_{t=1}^N \|c_y(t) - \hat{c}_y(t)\|^2 \quad (2)$$

4. Validate the model.

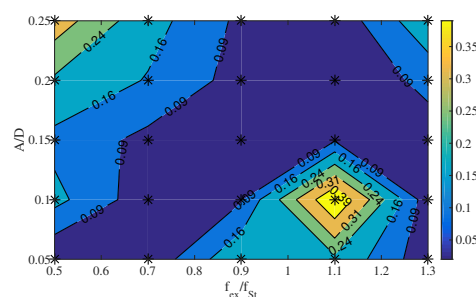


Figure 1: Single sine validation for various frequencies and amplitudes of imposed motion (root-mean-square error).

3 Results

The first results were already published in [3]. Using the FAST nonparametric distortion analysis method [2], the nonlinear behaviour was characterised as being odd-nonlinear. This insight was translated in using only odd monomial basis functions of order 3 and 5. As training data a concatenation of swept sine signals, of various amplitude levels, were used. A good fit to the training data is obtained (root-mean-square error of 4%). Validation results are shown in Fig. 1. A mean rms error of 12% was obtained.

4 Conclusion

Using the PNLSS model class we constructed a nonlinear model, able to accurately simulate the forces on an oscillating cylinder in a fluid flow. The model covers a wide range of frequency and amplitude of oscillation.

References

- [1] J. Paduart, L. Lauwers, J. Swevers, K. Smolders, J. Schoukens, R. Pintelon, "Identification of nonlinear systems using Polynomial Nonlinear State Space models," *Automatica* 46, 647-656, 2010.
- [2] R. Pintelon, J. Schoukens, "System Identification: A Frequency Domain Approach," IEEE Press, 2001.
- [3] J. Decuyper, T. De Troyer, M.C. Runacres, K. Tiels, J. Schoukens, "Nonlinear state-space modelling of the kinematics of an oscillation circular cylinder in a fluid flow", *Mechanical Systems and Signal Processing* 98, 209-230, 2018.

From Nonlinear Identification to Linear Parameter Varying Models: Benchmark Examples

Maarten Schoukens and Roland Tóth
Control Systems Group, Eindhoven University of Technology
Eindhoven, The Netherlands
Email: m.schoukens@tue.nl, r.toth@tue.nl

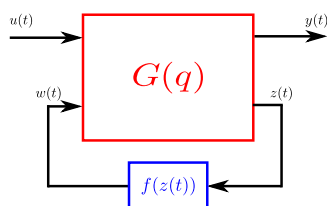


Figure 1: The nonlinear LFR structure: a two-input two-output LTI block $G(q)$ and a static nonlinear block $f(z(t))$.

Introduction: Linear parameter-varying (LPV) models form a powerful model class to analyze and control nonlinear systems [3]. Identifying an LPV model of a nonlinear system can be challenging due to the difficulty of selecting the scheduling variable(s) a priori, especially in case a first principles based understanding of the system is unavailable.

This abstract presents a systematic LPV embedding approach based on SISO nonlinear fractional representation models [2]. The proposed approach is illustrated on two well-established nonlinear modeling benchmark examples: the Silverbox [4] and the Wiener-Hammerstein [1] benchmark, available through www.nonlinearbenchmark.org.

Approach: A nonlinear system is identified first using a nonlinear block-oriented linear fractional representation (LFR) model [2], see Figure 1. This nonlinear LFR model class is embedded into the LPV model class by a specific factorization approach of the static nonlinear block present in the model. As a result of the factorization an LPV-LFR or an LPV state-space model with an affine dependency results. This approach also facilitates the selection of the scheduling variable from a data-driven perspective. The estimation is not affected by measurement noise on the scheduling variables, which is often left untreated by LPV model identification methods.

Results: The result obtained on the two considered benchmark cases are shown in Figures 2 and 3. A large improvement can be observed by using the embedded LPV model compared to an LTI model, for both cases.

Acknowledgments: This work has received funding from the European Research Council (ERC) under the European Union's Horizon 2020 research and innovation programme (grant agreement nr. 714663).

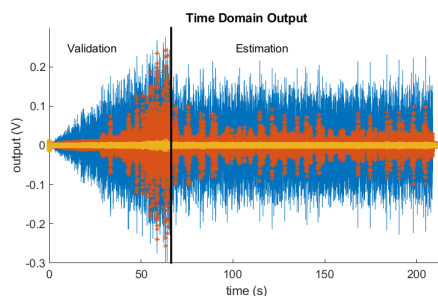


Figure 2: Output response of the Silverbox data-generating system validation and estimation dataset (blue). The simulation error obtained using the LTI approximation (red), and the LPV model (orange).

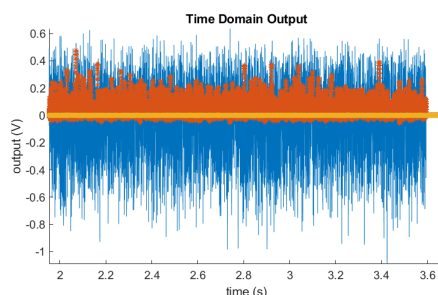


Figure 3: Output response of the Wiener-Hammerstein data-generating system validation dataset (blue). The simulation error obtained using the LTI approximation (red), and the LPV model (orange).

References

- [1] J. Schoukens, J.A.K. Suykens, and L. Ljung. Wiener-Hammerstein benchmark. In *15th IFAC Symposium on System Identification (SYSID)*, Saint-Malo, France, July 2009.
- [2] M. Schoukens and K. Tiels. Identification of block-oriented nonlinear systems starting from linear approximations: A survey. *Automatica*, 85:272–292, 2017.
- [3] R. Tóth. Modeling and Identification of Linear Parameter-Varying Systems, volume 403 of *Lecture Notes in Control and Information Sciences*. Springer-Verlag Berlin Heidelberg, 2010.
- [4] T. Wigren and J. Schoukens. Three free data sets for development and benchmarking in nonlinear system identification. In *European Control Conference (ECC)*, pages 2933–2938, July 2013.

Grammar-based Encoding of Well-posed Model Structures for Data-Driven Modeling

D. Khandelwal, R. Tóth, P.M.J. Van den Hof
 Control Systems Group
 Department of Electrical Engineering
 Eindhoven University of Technology
 P.O. Box 513, 5600 MB, Eindhoven, The Netherlands
 Email: D.Khandelwal@tue.nl

1 Introduction

In the field of systems and control, a large number of data-driven modelling tools have been proposed. These tools differ not only in the numerical methods used, but also in the structure they impose on the underlying physical phenomena. In fact, very often, the choice of dynamical structure imposed on the physical process governs the numerical methods that can be applied within these tools. Due to the inter-dependence of the dynamical structure of the model to-be-estimate and the numerical methods that are viable in that setting, the idea of a unified framework for dynamical system identification has proved to be elusive. In this submission, a method for encoding well-posed model structures in a tree-based format is proposed. The tree-based encoding method is intended to represent models belonging to a broad range of model classes. It must be stressed that the present submission discusses only the method for encoding model-structures and not the optimization tools can be applied on the tree-based encodings. The latter remains a subject of future research.

2 Tree Adjoining Grammar (TAG)

TAG is tree generating system that was developed for linguistic applications [1]. Although developed for modelling of natural languages, TAG has also been used to express static mathematical models, for example in [2]. Already in the case of static models, one can observe that several classes of mathematical models conform to an underlying syntax. TAGs can be used to capture such a syntax using simple tree structures.

TAGs use two sets of trees - *initial trees* (I) and *auxiliary trees* (A) that capture the basic syntax of a well-posed model structure. The trees in sets I and A can be combined using two operations - *substitution* and *adjunction*. As an example, consider the case of encoding the structure of Output Error (OE) model class, described by the equation

$$y(k) = G(q^{-1})u(k) + e(k). \quad (1)$$

Figure 1 shows the sets of initial trees (I) and auxiliary trees (A) that can be used to construct process model $G(q^{-1})$ for

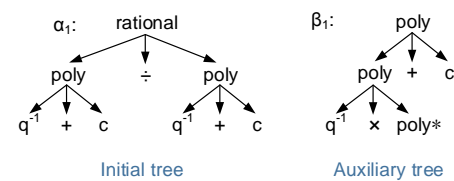


Figure 1: Examples of Initial and auxiliary trees.

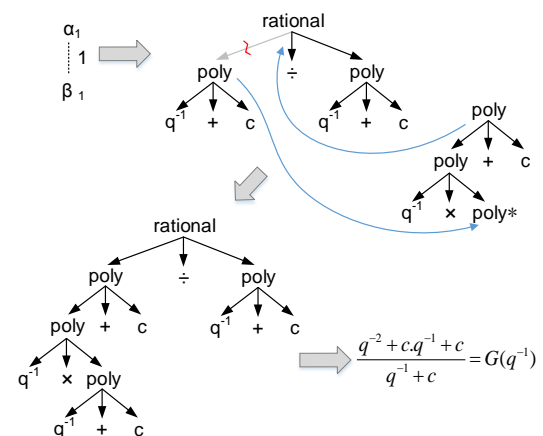


Figure 2: Illustration of the adjunction operation.

any OE model. Figure 2 illustrates the use of the adjunction operator in order to construct OE models in an equivalent tree representation.

3 Remarks

It can be shown that a wide range of functional classes, ranging from FIRs to NARMAX models, can be expressed using TAG, making it a powerful tool to express dynamical models. Future research will be focused on developing numerical tools that can optimize in the space of TAG based trees.

References

- [1] Joshi, A. K., Schabes, Y., *Tree-adjoining grammars*, Handbook of formal languages, 3, 69-124., 1997.
- [2] Hoai, N. X. et. al., *Solving the symbolic regression problem with tree-adjunct grammar guided genetic programming: The comparative results*, CEC 2002, Vol. 2, pp. 1326-1331.

Nonparametric Regularization for Time-Varying Operational Modal Analysis

Péter Zoltán Csurcsia^{1,2}, Johan Schoukens¹, Bart Peeters²

1) Vrije Universiteit Brussel, Pleinlaan 2, 1050 Elsene, Belgium

2) Siemens Industry Software NV., Interleuvenlaan 68, 3001 Leuven, Belgium

Email: peter.zoltan.csurcsia@vub.ac.be

1 Introduction

The paper deals with the time variations of mechanical and civil structures described by the nonparametric Operational Modal Analysis (OMA) framework. OMA is a special identification technique for estimating the modal properties (e.g. resonance frequencies, damping, mode shapes) of structures based on vibration data collected when the structures are under real operating conditions without having access to the excitation signals. Modelling time-varying (TV) behaviour is important because the unmodelled time variations might lead to instability and structural failures. Contrary to the classical identification frameworks, a further challenge with the OMA framework is that the excitation signal is not known exactly, but it is assumed to be white noise. In this work a nonparametric regularization method [1] is provided to estimate the time-varying output autocorrelation function of vibrating structures and applied to a measurement of wind tunnel testing of an airplane [2].

2 An example

This section presents an industrial example of the in-line flutter assessment of the wind tunnel testing of a scaled airplane model. The measurement time is 424 sec, the sampling frequency is 500 Hz, the number of data samples is 212000. The segmented window size is 500 samples (which corresponds to 1 sec, 1 Hz resolution). The Mach number is varying between 0.07 and 0.79. An illustration of the measurement setup is given in Fig 1. In this paper, wind tunnel data at various flow conditions are used to validate the approach for tracking the evolution of the resonance frequencies, damping ratios.

The results for the classical Short-time Fourier transform (SFT) and the proposed approach are shown in Fig 2. Observe that the proposed method gives a smooth estimate with better SNR. Further details on the measurement procedure can be found in [2]. Exact specifications on the airplane are omitted due to the confidentiality of the industrial project.

3 Summary

In this work a powerful time domain estimation method is developed for LTV systems in OMA setup. This technique is illustrative, flexible, user friendly.

With respect to the system dynamics using the proposed method, it is possible 1) to decrease the effect of the disturbing noise 2) eliminate the transient.

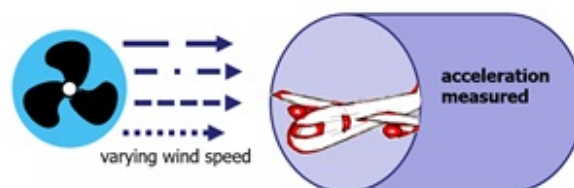


Figure 1: The measurement setup is shown. The airflow (wind speed) is varying while the airplane's acceleration is measured in the wind tunnel.

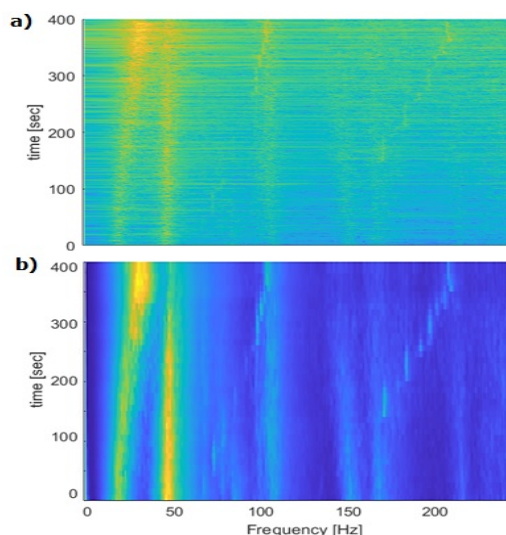


Figure 2: The time-varying output power spectrum estimate of the observed system is shown when a) the classical SFT method is considered b) the proposed method is considered.

References

- [1] P. Z. Csurcsia and J. Lataire, Nonparametric Estimation of Time-varying Systems Using 2D Regularization, IEEE TIM, 2016
- [2] B. Peeters, P. Karkle, M. Pronin and R. Van der Vorst R, Operational Modal Analysis for in-line flutter assessment during wind tunnel testing, 15th International Forum on Aeroelasticity and Structural Dynamic, 2011

A recursive least squares approach to distributed MISO system identification¹

Tom R.V. Steentjes, Mircea Lazar and Paul M.J. Van den Hof
Eindhoven University of Technology
The Netherlands

E-mails: t.r.v.steentjes@tue.nl, m.lazar@tue.nl, p.m.j.vandenhof@tue.nl

1 Introduction

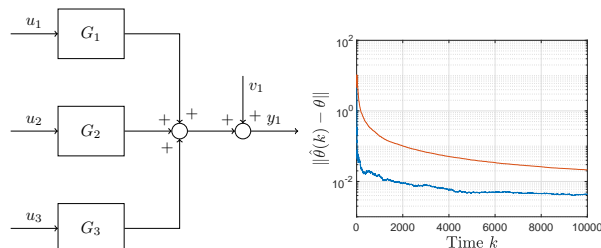
Prediction-error identification methods provide a powerful tool for obtaining consistent system parameter estimates [1]. However, when dealing with large scale interconnected systems, such as the ones arising from biology or power grids, the identification problem becomes more challenging. Given a structure of a network of linear dynamical systems, various prediction error methods are readily operational for identifying these systems, while imposing certain conditions on the network [2].

Among the prediction error methods for computing consistent network modules, we single out the direct and two-stage method for a general network topology [2]. Utilizing one of these methods for the identification of a local transfer function module in the network, typically yields a multiple-input-single-output (MISO) identification problem. More precisely, the singled-out prediction error methods rely on the identification of a MISO network building block, on the basis of measurements of multiple inputs and one, possibly disturbed, output. An example of such a MISO building block with three inputs is shown in Figure 1(a).

Although the prediction error methods for dynamical networks can consistently identify network modules, they require the output signal and all input signals of a MISO identification problem to be available centrally. Central data collection and computation of the network module estimates may not always be desirable due to computational constraints or desired flexibility, analogously to the control of interconnected systems, where distributed or decentralized controllers can be preferable over centralized ones.

Therefore, in this work, we develop a distributed solution for the MISO prediction error identification problem. Due to the simplifying property of yielding output predictors that are linear in the parameters, ARX and FIR model structures serve as a basis for the developed distributed identification method. We distinguish two features in the considered distributed identification method. First, we utilize a so-called recursive least squares (RLS) estimator for the system parameters, i.e., we process the data recursively in time rather

¹This project has received funding from the European Research Council (ERC), Advanced Research Grant SYSDYNET, under the European Unions Horizon 2020 research and innovation programme (Grant Agreement No. 694504).



(a) Example of a MISO structure with three subsystems. (b) Evolution of the estimator error $\|\hat{\theta}(k) - \theta\|$ for the distributed-red and central-blue method.

Figure 1: MISO system structure and simulation results.

than collecting all data and subsequently computing a batch estimator. Second, we distribute the computation of the RLS estimator among the individual systems within the MISO system. Each subsystem computes an estimate of the local parameter vector, which is an appropriate subvector of the full parameter vector, in contrast to the consensus-based distributed RLS estimator [3], wherein one common parameter vector is estimated in each subsystem. Computation of the local RLS estimator is performed via local input and output signal measurements, while communication with other estimators is maintained via scalar-valued signals. The communication yields limited information exchange and a degree of flexibility in case of subsystem dropout.

Simulation results for the system in Figure 1(a), with three third-order FIR subsystems, reveal convergence of the distributed RLS estimator to the same value as its central counterpart, but at a slower rate. Figure 1(b) shows the estimation error of the parameter vector for both the distributed and central RLS method.

References

- [1] L. Ljung, *System Identification: Theory for the User*. Upper Saddle River, NJ, USA: Prentice Hall PTR, 1999.
- [2] P. M. J. Van den Hof, A. G. Dankers, P. S. C. Heuberger, and X. Bombois, "Identification of dynamic models in complex networks with prediction error methods – Basic methods for consistent module estimates," *Automatica*, vol. 49, no. 10, pp. 2994 – 3006, 2013.
- [3] G. Mateos and G. B. Giannakis, "Distributed recursive least-squares: Stability and performance analysis," *IEEE Transactions on Signal Processing*, vol. 60, no. 7, pp. 3740–3754, 2012.

Identification of heat flux components in fusion plasmas

Matthijs van Berkel

Integrated Modelling and Transport group, Dutch Institute for Fundamental Energy Research
Mech. Eng. - Control Systems Technology group, Eindhoven University of Technology
Dept. of Fundamental Electricity and Instrumentation, Vrije Universiteit Brussel
DIFFER, PO Box 6336, 5600 HH, Eindhoven, NL
m.vanberkel@diffier.nl

Tatsuya Kobayashi

High-Temperature Plasma Physics Research Division
National Institute for Fusion Science
322-6 Oroshi-cho, Toki-city, Gifu, 509-5292, Japan

1 Introduction

How well we can confine the heat in a nuclear fusion reactor largely determines its efficiency. Hence, it is important to identify the different transport mechanisms that determine the heat transport including how local heating affects the heat transport.

2 Problem of estimating the heat flux

The (electron) heat transport in fusion devices is generally described by the heat equation in one-dimensional

$$\frac{\partial}{\partial t} (n_e T_e(\rho, t)) = \nabla_\rho (-q_e(\rho, t)) + p(\rho, t), \quad (1)$$

where $T_e(\rho, t)$ is the electron temperature, ρ the normalized radius, n_e the electron density, and $p(\rho, t)$ the heating power density.

The heat flux is crucial in understanding what drives transport. However, as the heat flux cannot be directly measured and it is a time and space dependent quantity, we have to identify it implicitly. The standard approach in identification, inverse problems, and fusion is to pre-define the heat flux dependencies [1]. The two standard forms are

$$q_e = -n_e \chi_e \nabla_\rho T_e, \quad (2)$$

where χ_e is the diffusion coefficient. This law is known as Fourier's law. Alternatively, we can also include convection V_e (flow) as an additional transport mechanism

$$q_e = -n_e \chi_e \nabla_\rho T_e - n_e V_e T_e. \quad (3)$$

Casting the heat flux in a specific dependence allows the estimation of the time invariant quantities χ_e and V_e . However, it also poses a danger as we made an assumption of the heat flux structure in (2) and (3).

3 Heat flux reconstruction

We propose an alternative approach by combining the heat flux reconstruction in [2] and advanced frequency domain signal processing techniques used in system identification to directly estimate the heat flux q_e [3]. The experimental result is shown in Fig. 1.

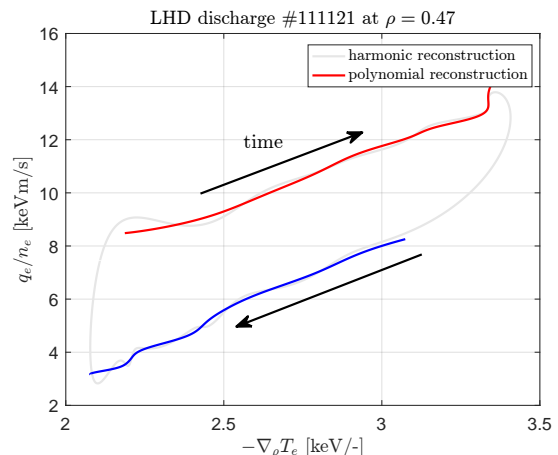


Fig. 1: Experimentally determined relative heat flux q_e as a consequence of a symmetric block-wave power modulation.

Based on Fig. 1 we can identify different transport properties, e.g., the slope can represent the diffusion coefficient χ_e , see (2) [3].

References

- [1] M. van Berkel, et al. Frequency domain sample maximum likelihood estimation for spatially dependent parameter estimation in PDEs, *Automatica*, pp. 2113 - 2119, 2014.
- [2] S. Inagaki, et al. How is turbulence intensity determined by macroscopic variables in a toroidal plasma?, *Nucl. Fusion*, pp. 113006, 2013.
- [3] M. van Berkel, T. Kobayashi, et al. Heat flux reconstruction and effective diffusion estimation from perturbative experiments using advanced filtering and confidence analysis, (submitted to) *Plasma Phys. Control. Fusion*, 2018.

A penalty method algorithm for obstacle avoidance using nonlinear model predictive control

Ben Hermans and Goele Pipeleers
 MECO Research Team, KU Leuven, Leuven, Belgium
 DMMS lab, Flanders Make, Leuven, Belgium
 Email: ben.hermans2@kuleuven.be

Panagiotis Patrinos
 KU Leuven, Leuven, Belgium
 Department of Electrical Engineering,
 Division ESAT-STADIUS

1 Introduction

Applications of autonomous motion systems are arising more and more in industry. Examples are driverless cars, fruit-picking robots and automated guided vehicles in an automated warehouse. Computation of a collision free trajectory is essential in such applications. Various techniques to compute motion trajectories that satisfy collision-avoidance constraints have been proposed, including graph-search methods, virtual potential field methods and methods using the concept of velocity obstacles. Recently, optimization-based strategies are becoming more popular. In such strategies, the search for a time, energy... optimal trajectory is formulated as an optimization problem. In order to take into account disturbances and uncertainty in the environment, this optimization problem needs to be solved in real time.

This abstract presents a penalty method algorithm to calculate a trajectory while satisfying collision-avoidance constraints. Through the introduction of penalty parameters, a trade-off is possible between the optimality of the trajectory and the extent to which the obstacle constraints are violated. The resulting optimization problems are solved using a proximal averaged Newton-type method for optimal control (PANOC), as proposed in [1]. In addition, some heuristics are developed for dealing with local optima when the obstacles are non-convex.

2 Methodology

The trajectory computation is formulated as an optimal control problem. Nonlinear vehicle dynamics can be accounted for, and the problem is transformed into a small-scale nonlinear program using single shooting. Box constraints on the inputs can directly be accounted for by PANOC, whereas state constraints can only be included through a penalty. Hence, for our application, the objective of the control problem comprises two parts: a least squares objective in terms of the states and inputs, and a penalty that represents the violation of the obstacle boundaries. This second term is directly related to our formulation of an obstacle as the intersection of a finite number of m strict nonlinear inequalities:

$$O = \{z \in \mathbb{R}^n : h_i(z) > 0, i \in \mathbb{N}_{[1,m]}\}.$$

The obstacle avoidance constraint can then be written as:

$$\psi_O(z) := \frac{1}{2} \prod_{i=1}^m [h_i(z)]_+^2 = 0.$$

This equality constraint is relaxed into a penalty term in the objective function for every obstacle, $\mu_O \psi_O(z)$, where μ_O is the penalty factor. The penalty method consists of solving the problem with higher and higher penalties, until the obstacles are avoided.

3 Results

The effectiveness of this algorithm has been tested for various obstacle configurations and multiple vehicle models using numerical simulations, benchmarking it against state-of-the-art interior point and SQP solvers. Figure 1 shows for example a vehicle with a trailer moving from different starting points to a destination while avoiding a crescent-shaped obstacle.

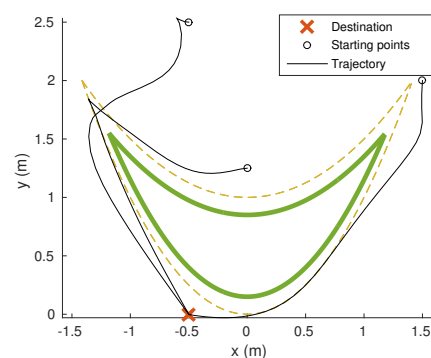


Figure 1: Obstacle avoidance of a non-convex obstacle, depicted by the thick green line. The enlarged obstacle (in dotted line) is defined by $O = \{(x, y) : y - x^2 > 0, 1 + 0.5 \cdot x^2 - y > 0\}$.

References

- [1] L. Stella, A. Themelis, P. Sopasakis, and P. Patrinos, "A simple and efficient algorithm for nonlinear model predictive control," *arXiv preprint arXiv:1709.06487*, 2017.

Acknowledgement This work benefits from KU Leuven-BOF PFV/10/002 Centre of Excellence: Optimization in Engineering (OPTeC), from the project G0C4515N of the Research Foundation-Flanders (FWO-Flanders), from Flanders Make ICON project: Avoidance of collisions and obstacles in narrow lanes, and from the KU Leuven Research project C14/15/067: B-spline based certificates of positivity with applications in engineering.

Real-time proximal gradient method for linear MPC

Ruben Van Parys and Goele Pipeleers

MECO Research Team, Department Mechanical Engineering, KU Leuven

DMMS lab, Flanders Make, Leuven, Belgium

ruben.vanparys@kuleuven.be

1 Introduction

Since the past few years, there has been an increased interest in using first-order methods for model predictive control (MPC). In contrast to active-set or interior-point schemes, first-order methods do not require the solution of a linear system at every iteration which makes them the ultimate choice to obtain fast MPC on resource-constrained embedded computing hardware [1]. This work focuses on the proximal gradient method (PGM) and proposes a PGM-based real-time iteration scheme for linear MPC.

2 Linear model predictive control

This work addresses the control of a discrete-time linear time-invariant (LTI) system of the form $x_{k+1} = Ax_k + Bu_k$. Given an estimate of the current state x_k , a linear MPC controller will compute an input trajectory $q = \{q(0), \dots, q(N-1)\}$ over a time horizon of N samples by solving an optimal control problem of the form

$$\min_{q \in \mathcal{Q}(x_k)} V_N(x_k, q) = \frac{1}{2} q^T F q + \frac{1}{2} x_k^T G x_k + q^T H x_k, \quad (1)$$

where $\mathcal{Q}(x_k)$ represents the set of feasible trajectories, including input limitations. An optimal MPC approach would then apply the first sample of the optimal solution $q^*(x_k)$ to the system, i.e. $u_k = q^*(x_k, 0)$.

3 Real-time proximal gradient method

The proximal gradient method (PGM) is an extension of the (projected) gradient method and a popular first-order method for linear MPC with simple input constraints. Applied to the OCP (1), the PGM iteratively updates the estimate for q as

$$q_k^+ = \Pi_{\mathcal{Q}(x_k)}(q_k - \gamma \nabla_q V_N(x_k, q_k)), \quad (2)$$

with γ the step size and $\Pi_{\mathcal{Q}(x_k)}(\cdot)$ the projection on $\mathcal{Q}(x_k)$.

This work proposes an MPC scheme that implements a real-time version of the PGM to solve OCP (1) in receding horizon. This means that only one PGM step (2) is performed per control update in stead of solving (1) to the desired accuracy. The first sample of the resulting input trajectory is applied to the system, i.e. $u_k = q_k^+(0)$, and a warm-start for the next update is computed using the current solution q_k^+ .

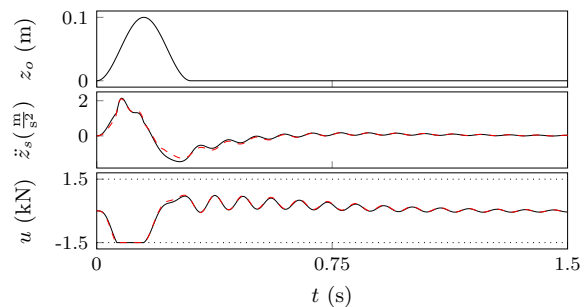


Figure 1: Bump response on a controlled quarter-car system. The black lines indicate the response using the real-time PGM while the dash red lines indicate the response using an optimal MPC approach.

When applying the real-time PGM scheme to LTI systems with simple input constraints, the resulting control law consists of simple steps involving matrix-vector multiplication, addition and saturation and offers possibilities to obtain fast control rates even on resource-constrained hardware such as PLCs or FPGAs. Closed-loop stability is proven for both the system's state and the input trajectory, i.e. over the control updates the system's state is attracted to a stable equilibrium while the suboptimal input trajectory is converging towards its optimal value.

4 Numerical example

The closed-loop performance of the real-time PGM is validated on a simulation example considering the control of an active vehicle suspension system based on a 2-DOF quarter-car model. The control objective is chosen to minimize the RMS acceleration of the car body. The resulting body acceleration \ddot{z}_s and constrained control signal u are represented in Figure 1 when a bump road disturbance z_o is applied to the quarter-car system. The red dashed lines indicate the response using an optimal MPC approach. While the optimal MPC executes on average 100 PGM iterations during a control cycle, the real-time PGM only executes one iteration while the relative deviation in RMS body acceleration is limited to 0.04. One could thus conclude that the real-time PGM forms a computational cheap alternative for an optimal MPC approach with little loss in performance.

References

- [1] J. L. Jerez, P. J. Goulart, S. Richter, G. A. Constantinides, E. C. Kerrigan, and M. Morari, "Embedded online optimization for model predictive control at megahertz rates," *IEEE Transactions on Automatic Control*, vol. 59, no. 12, pp. 3238–3251, 2014.

Acknowledgement This work benefits from KU Leuven-BOF PFV/10/002 Centre of Excellence Optimization in Engineering (OPTEC); from the project G0C4515N of the Research Foundation-Flanders (FWO-Flanders); and from the KU Leuven Research project C14/15/067. Ruben Van Parys is a PhD fellow of FWO-Flanders. Flanders Make is the Flemish strategic research centre for the manufacturing industry.

Combining optimal sensor and actuator selection with \mathcal{H}_∞ control design

Taranjitsingh Singh, Massimo De Mauri, Jan Swevers and Goele Pipeleers
 MECO Research Team, Department of Mechanical Engineering, KU Leuven
 DMMS Lab, Flanders Make, Leuven, Belgium
 Email: taranjtsingh.singh@kuleuven.be

1 Introduction

There are many industries that have to deal with multivariable systems that show complex dynamic behaviour. \mathcal{H}_∞ control design is able to deal with such systems, but there is often a need to determine the optimal set of sensors and actuators. It is clear that the best closed-loop performance is achieved by using all the possible available sensors and actuators. However, economically, it may be beneficial to install only a subset of sensors and actuators provided that the reduction of performance is acceptable.

The optimal selection of sensors and actuators is a combinatorial problem that requires a broad search which becomes complex if the problem is combined with \mathcal{H}_∞ control design. In this work, we present a branch and bound (BNB) approach to solve this optimization problem.

2 Problem Formulation

Here, we want to select k sensors out of the available n_s sensors and l actuators out of the available n_a actuators. In order to define whether the respective sensor or actuator is selected or not, boolean decision variables $s_i, a_i \in \{0, 1\}$ are assigned to each possible sensor and actuator respectively, with $i = \{1 \dots n_s\}$ and $j = \{1 \dots n_a\}$. With these decision variables, the \mathcal{H}_∞ control design problem combined with the optimal selection of k sensors and l actuators can be transformed into the following Mixed Boolean Semi-Definite Programming (MBSDP) problem

$$\begin{aligned} & \text{minimize: } \gamma \\ & \text{subject to: } \text{LMIs} < 0, \mathbf{1}^T s = k, \mathbf{1}^T a = l, \end{aligned} \quad (1)$$

where $\|\mathcal{T}\|_\infty < \gamma$, \mathcal{T} is the closed-loop transfer function in the \mathcal{H}_∞ control design, LMIs represents the Linear Matrix Inequalities (LMI) of this control design and $\mathbf{1}$ is the vector with all entries one.

Optimizing the column sparsity of the controller input matrix optimizes the number of sensors while optimizing the row sparsity of the controller output matrix optimizes the number of actuators. The sparsity of a matrix can be imposed by using Big-M reformulations of these matrices with suitable bounds [1] and introducing them in the MBSDP

problem. The algorithm used to solve this problem is the BNB algorithm from YALMIP [2] for MATLAB.

3 Case Study

The case study that is considered here to validate this approach is a linearized 8th order model with 4 actuators and 7 sensors of a multi-purpose helicopter from [3]. Here, we focus on optimal selection of sensors 5 to 7, that is, the first 4 sensors and the 4 actuators are considered in all control designs. The first 4 sensors are used to track given references. Table 1 summarizes the achieved results.

Sensors	Actuators	γ	γ_0
all	all	-	2.421877
{5, 6}	all	2.435514	2.435487
{6}	all	2.454425	2.454632

Table 1: Achieved performance with the desired optimal number of sensors for the helicopter model

With $k = 2$, the approach suggests to select the 5th and 6th sensors with $\gamma = 2.435514$ as seen in Table 1. Here, γ_0 represents the closed-loop performance if the \mathcal{H}_∞ control design is solved without the last sensor. It is observed that the developed approach provides the global solution. Similarly, with $k = 1$, the approach suggests to select the 6th sensor. A full search confirms that these optimal selections provide the minimum performance.

References

- [1] D. G. Luenberger, Y. Ye *et al.*, *Linear and nonlinear programming*. Springer, 1984, vol. 2.
- [2] J. Lofberg, "YALMIP: A toolbox for modeling and optimization in MATLAB," in *Computer Aided Control Systems Design, 2004 IEEE International Symposium on*. IEEE, 2004, pp. 284–289.
- [3] S. Skogestad and I. Postlethwaite, *Multivariable feedback control: analysis and design*. Wiley New York, 2007, vol. 2.

Acknowledgement: This work is supported by Flanders Make: SBO ROC-SIS: Robust and Optimal Control of Systems of Interacting Subsystems. This work also benefits from KU Leuven Research project C14/15/067: B-spline based certificates of positivity with applications in engineering, KU Leuven-BOF PFV/10/002 Centre of Excellence: Optimization in Engineering (OPTEC) and the Belgian Programme on Interuniversity Attraction Poles, initiated by the Belgian Federal Science Policy (DYSCO).

Optimal Sensor Configurations for Collision Avoidance: A Minimax Optimization Approach

Rishi Mohan¹, Rob Gielen² and Bram de Jager¹

¹Eindhoven University of Technology, Department of Mechanical Engineering, Eindhoven, The Netherlands

²Philips Healthcare, Best, The Netherlands

Email: R.Mohan@tue.nl

1 Introduction

The optimal location and orientation of different sensors in a target environment is an important design problem as it impacts the performance and cost of the network. For collision avoidance in dynamic environments, sensor planning needs to account for uncertain, dynamic occlusions to efficiently detect potential collision scenarios. Dynamic occlusions, caused by mobile objects such as humans or other robots, cause random loss of object capture and are problematic since their inherent nature is unpredictable [1].

The majority of existing research employs a probabilistic framework to deal with dynamic occlusions [2], where the probability distribution function (PDF) of positions of dynamic occluders around the workspace becomes the defining factor in sensor placement. Previous works either assume that PDF is known *a priori* or is approximated from measured historical data. These assumptions prove to be highly detrimental in critical applications like collision avoidance.

2 Proposed Solution

The present work proposes a worst-case optimization approach (Minimax) for determining optimal sensor configurations. Minimax optimization presents the advantage of being independent of a PDF [3]. Moreover, a bound on the performance of the sensor configuration is obtained. The optimal configuration guarantees a certain visibility of the robotic workspace regardless of occluder locations.

Given a robotic workspace \mathcal{W} , an optimal sensor configuration ($\mathcal{S}_{minimax}^*$) is determined by considering occluder positions (\mathcal{O}) that potentially try to maximize the occluded robotic workspace (NV), i.e., worst-case occluder scenarios.

$$\mathcal{S}_{minimax}^* = \arg \min_{\mathcal{S}} \max_{\mathcal{O}} NV(\mathcal{O}, \mathcal{S}) \quad (1)$$

Table 1: Optimal Sensor Configuration ($\hat{\mathcal{S}}^*$)

Sensor	x [m]	y [m]	z [m]	θ [°]
\mathcal{S}_1	0	2.729	2.983	0
\mathcal{S}_2	3.408	0	0.241	0
\mathcal{S}_3	8	1.502	1.269	0
\mathcal{S}_4	7	5	2	0

3 Evaluation and Results

The optimization problem (1) is evaluated for $n_s = 4$ sensors by considering a robotic manipulator (green) and $n_o = 2$

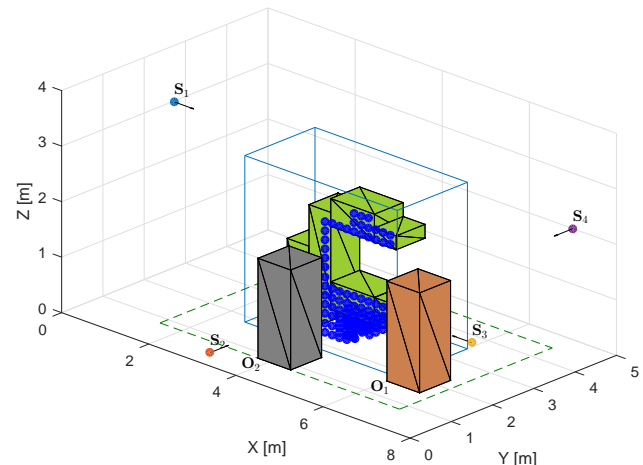


Figure 1: Worst Case Optimal Placement

dynamic occluders (Figure 1). The occluders \mathcal{O}_1 and \mathcal{O}_2 form different occluder configurations \mathcal{O} depending on their locations. The non-visible volume (NV) related to the optimal solution $\hat{\mathcal{S}}^*$ (Table 1) is 5.1245% (blue) of the total workspace and is associated with the occluder locations presented in the figure. The occluded volume for any other configuration is guaranteed to be less than 5.1245%.

4 Conclusions

A worst case optimization (Minimax) approach is proposed which generates sensor configurations based on occluder scenarios that cause maximum obstruction of the robotic workspace. The optimal solution is deterministic and provides a guaranteed level of workspace visibility for the sensor configuration. Evaluation of the approach shows the solution to be robust to the impact of dynamic occlusions while providing a guarantee on workspace visibility. Additionally, the results also provides insights to the user on the impact of the worst case situation on workspace visibility.

References

- [1] A. Mavrincac and X. Chen, "Modeling coverage in camera networks: A survey," *International Journal of Computer Vision*, vol. 101, no. 1, pp. 205–226, 2013.
- [2] F. Flacco and A. De Luca, "Multiple depth/presence sensors: Integration and optimal placement for human/robot coexistence," in *2010 IEEE International Conference on Robotics and Automation (ICRA)*. IEEE, 2010, pp. 3916–3923.
- [3] A. Shapiro and A. Kleywegt, "Minimax analysis of stochastic problems," *Optimization Methods and Software*, vol. 17, no. 3, pp. 523–542, 2002.

Risk-averse risk-constrained optimal control¹

Domagoj Herceg*, Pantelis Sopasakis**, Alberto Bemporad* and Panagiotis Patrinos**

* IMT School for Advanced Studies Lucca
Piazza S. Francesco, 19, 55100 Lucca, Italy

{domagoj.herceg, alberto.bemporad}@imtlucca.it

** KU Leuven, Department of Electrical Engineering (ESAT),
STADIUS Center for Dynamical Systems, Signal Processing and Data Analytics,
Kasteelpark Arenberg 10, 3001 Leuven, Belgium

{pantelis.sopasakis, panos.patrinis}@kuleuven.be.

1 Abstract

The theory of risk measures, branching out primarily from the field of stochastic finance and operations research, has gained a lot of attention in the last decade [1]. Roughly speaking, risk measures quantify the right tail of a distribution of a cost, accounting for *high effect* events that happen with *low probability*. The average value-at-risk (AV@R) is perhaps the most popular risk measure because of its intuitive interpretation and because of the fact that it is a tight convex approximation of the quantile function.

There exist two widely known approaches to deal with multistage decision making under uncertainty. In the *stochastic* approach we minimize the *expectation* of the uncertain cost with respect to a reference probability measure, whereas, in the *worst-case* approach we minimize the maximum (worst-case) cost. The first approach is naive in assuming a perfect knowledge of the underlying distribution, while the second one is pessimistic and disregards any probabilistic information which is typically available. The risk-averse approach seeks to remedy the shortcomings of the two conventional approaches by using risk measures. These allow to interpolate between these two optimal control paradigms. The resulting optimal control problems are termed “risk averse” because they lead to decisions which are less sensitive to high-effect low-probability events. Additional constraints on the risk of a random function may also be imposed, often as surrogates of intractable probabilistic constraints. Overall, in multistage risk-averse formulations, the cost function is the composition of several (typically nonsmooth) mappings, yielding numerically challenging optimization problems.

In our previous work [2] we showed how to decompose problems involving nested risk mappings of the AV@R type by exploiting their special structure. However, this approach

does not extend directly to other risk measures. Here we propose appropriate decompositions for multistage risk-averse risk-constrained optimal control problems with general risk measures (such as general polytopic risk measures, the entropic value-at-risk and more).

In this work we formulate the risk constraints as feasibility problems by means of the epigraph of the underlying risk measure. The same idea naturally extends to the decomposition of nested conditional risk mappings. We demonstrate that this approach is computationally tractable and the resulting problems can be solved efficiently in the convex case, typically leading to well-structured conic optimization problems. The proposed scheme allows the efficient solution of large-scale risk-averse risk-constrained optimal problems.

Moreover, we discuss different types of risk constraints. The most straightforward one is to have stage-wise constraints on the risk of a random function at each time instant. Another very interesting possibility is to have nested risk constraints, which take into the account the temporal dimension of the problem, i.e., how the probability distribution at a certain time instant is produced and how uncertainty propagates in time. This new approach is more conservative, yet more suitable for multistage optimal control problems as we demonstrate with a few examples. The above reformulations apply in all these cases deeming risk-averse problems suitable for control applications.

References

- [1] A. Shapiro, D. Dentcheva, and Ruszczycki, *Lectures on stochastic programming: modeling and theory*. SIAM, 2nd ed., 2014.
- [2] D. Herceg, P. Sopasakis, A. Bemporad and P. Patrinos, *Risk-averse model predictive control*, arXiv: 1704.00342, 2017.

¹The work of D. Herceg and A. Bemporad was supported by the EU-funded H2020 research project DISIRE, grant agreement no. 636834. The work of P. Patrinos was supported by the KU Leuven Research Council under BOF/STG-15-043.

Optimal control for a class of differential inclusions

J. Eising

JBI - University of Groningen

Email: j.eising@rug.nl

M. K. Camlibel

JBI - University of Groningen

Email: m.k.camlibel@rug.nl

Introduction

The study of optimal control of constrained linear systems is one with a large number of differing approaches and methods. Most of these are either specific to a given application or use iterative methods to solve the problem. This allows computers to solve the problems, but usually gives little insight onto the mathematical structures involved. Similar to the differences between geometric control theory and the (sometimes) ad-hoc or situational feedback design, the aim is to construct theory for solving optimal control problems over classes of differential inclusions. These can be specified to solve constrained linear problems.

The problem

We consider the primal problem of minimizing:

$$\frac{1}{2} \int_0^T \begin{pmatrix} x(t) \\ \dot{x}(t) \end{pmatrix}^T Q \begin{pmatrix} x(t) \\ \dot{x}(t) \end{pmatrix} dt, \quad (1)$$

where Q is positive definite, making the integrand strictly convex, and where $x(t)$ is an absolutely continuous arc, with $\dot{x} \in L_2$, subject to:

$$x(0) = x_0, \quad \dot{x}(t) \in H(x(t)) \text{ for almost all } t. \quad (2)$$

Where H is some set-valued map: A map between \mathbb{R}^n and its power set. Informally, G maps a point to a set of possible derivatives. We will assume that the graph of H , the set $\{(x, y) \mid y \in H(x)\}$, is closed and convex.

In fact, this forms a direct generalization of constrained optimal control, the problem of minimizing 1 subject to dynamics given by:

$$x(0) = x_0, \quad \dot{x} = Ax + Bu, \quad y = Cx + Du \in \mathcal{Y}.$$

Where \mathcal{Y} is a closed convex set. This framework admits input, output and state constraints, and can be shown to take the form of our considered problem by taking:

$$H(x) = \{Ax + Bu \mid Cx + Du \in \mathcal{Y}\}$$

which is closed and convex but not necessarily non-empty for each x . Therefore our problem generalizes this more familiar problem.

Methods

We use the framework of *generalized problems of Bolza*, introduced by R.T. Rockafellar [1], to give a duality result connecting the optimality of this problem to that of a dual problem. This dual problem is not necessarily a simpler problem, but is given in terms of convex conjugates. This allows us to use Fenchel's inequality to prove that the optimal values of the primal and dual problems sum to 0. Furthermore this gives generalized Euler-Lagrange and Hamiltonian conditions to prove optimality of a pair of primal-dual arcs.

In addition, Rockafellar's extension [2] of the theory allows us to prove existence of optimal solutions in the case that H is strict, where strictness is the property that $H(x) \neq \emptyset$ for all $x \in \mathbb{R}^n$. However this still only proves existence of optimal arcs: These do not necessarily have finite cost. If however the dynamics (2) admit *any* trajectory for which the minimand (1) is finite, this found optimal value is as well. The strictness assumption helps for these proofs, but in practise this is very restrictive. For example, it stops state constraints from being considered, and thus we are interested in non-strict dynamics.

Using the *Moreau-Yosida* approximation [3] (or most books on differential inclusions, e.g. [4]) we can approximate, or regularize, our problem to one that does satisfy the conditions of [2]. This means that the regularized problems attain their respective optimal values. Furthermore, the differentiability of the approximations simplifies the generalized Euler-Lagrange conditions.

What rests is proving that the limit of the solutions of the regularized problems exists, is absolutely continuous and is the optimal value for the primal problem.

References

- [1] R. T. Rockafellar, "Conjugate convex functions in optimal control and the calculus of variations," *Journal of Mathematical Analysis and applications*, no. 32, 1970.
- [2] R. T. Rockafellar, "Existence and duality theorems for convex problems of Bolza," *Transactions of the American Mathematical Society*, vol. 159, Sep. 1971.
- [3] J.J. Moreau, "Proximité et dualité dans un espace Hilbertien". *Bull. Soc. Math. Fr.* 93, 1965
- [4] J.P. Aubin and H. Frankowska, "Set-valued Analysis", ser. Systems & Control: Foundations & Applications. Boston, MA: Birkhuser Boston Inc., 1990, vol. 2.

Driver intervention detection based on vehicle reference dynamics

Wouter Schinkel, Tom van der Sande, Jan Loof, Henk Nijmeijer

Section Dynamics and Control

Department of Mechanical Engineering

Eindhoven University of Technology

P.O. Box 513, 5600 MB Eindhoven, The Netherlands

Email corresponding author: W.S.Schinkel@tue.nl

1 Introduction

The current trend in autonomous driving makes driver intervention detection of significant importance. With driving automation level 3 (in agreement with the SAE J3036 standard [1]), projected to be realized in 2018, the driver is considered as a fall-back for the vehicle control systems, making driver intervention detection a relevant research topic. Numerous studies investigate driver take-over [2, 5]. However, most of these studies only consider emergency/hazardous situations or vehicle initiated take-over requests. Moreover, the majority of the proposed solutions require additional hardware, e. g. cameras, capacitive sensors on the steering wheel or wearable devices. In this presentation we focus on the detection of driver initiated take-over requests by comparing the plant dynamics with reference dynamics. A driver intervention detection method is presented which does not require additional hardware. Here it is assumed that the vehicle is equipped with both electric power steering and a steering column angle sensor. The detection logic is considered to be the main contribution of this work. The study is limited to autonomous driving, where initially the vehicle is not controlled by the driver.

2 Vehicle model

For this study a single-track vehicle model is used, which is extended with a lumped mass 2-degree of freedom steering system model as used in [3]. The model is parametrized with frequency response measurements covering a frequency range from 1 to 30 Hz. A relevant aspect of the steering system model is that it accounts for driver hands-on/off. More details on the vehicle model, including the differences for driver hands-on/off, are included in the presentation.

3 Detection logic

The detection logic is primarily based on the effect of driver hands-on/off on the steering system dynamics. Such methods are gaining more interest in recent years, e. g. [4]. The main difference between a driver (not) holding the steering wheel is a shift in the anti-resonance frequency (considering the transfer function from the electric power steering motor to the steering column angle). By comparing the steering column dynamics at this anti-resonance frequency with

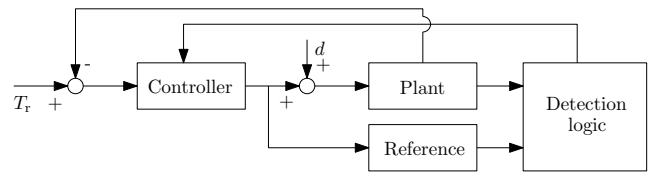


Figure 1: Schematic overview of detection logic

a reference model, driver hands-on/off can be detected. A schematic representation of such a method is shown in Fig. 1, where d is a disturbance and T_r the reference torque of the electric power steering unit. Information from the detection logic is sent to the controller, such that in the event of a take-over the control over the vehicle can be shifted back to the driver. Specific details regarding the detection logic are included in the presentation.

Acknowledgements

This work is part of the research program i-CAVE with project number 14893, which is partly financed by the Netherlands Organisation for Scientific Research (NWO).

References

- [1] J3016: Taxonomy and Definitions for Terms Related to Driving Automation Systems for On-Road Motor Vehicles. Technical report, SAE International, Sept. 2016.
- [2] B. Mok, M. Johns, K. J. Lee, D. Miller, D. Sirkin, P. Ive, and W. Ju. Emergency, Automation Off: Unstructured Transition Timing for Distracted Drivers of Automated Vehicles. pages 2458–2464. ITSC 2015, Sept. 2015.
- [3] A. Pick and D. Cole. Neuromuscular dynamics and the vehicle steering task. *The Dynamics of Vehicles on Roads and on Tracks*, 41:182–191, 2003.
- [4] J. A. Urhahne. Hands-on-off steering wheel detection for motor vehicle. *US9096262 B2*, aug 2015.
- [5] A. P. van den Beukel, M. C. van der Voort, and A. O. Eger. Supporting the changing driver's task: Exploration of interface designs for supervision and intervention in automated driving. *Transportation Research Part F: Traffic Psychology and Behaviour*, 43:279–301, Nov. 2016.

Including communication in generating longitudinal trajectories for automated vehicles

Robbin van Hoek¹, Jeroen Ploeg², Henk Nijmeijer¹

Eindhoven University of Technology¹, TNO Integrated Vehicle Safety²
P.O. Box 513, 5612 AP Eindhoven¹, P.O. Box 756, 5700 AT Helmond²

Email corresponding author: r.b.a.v.hoek@tue.nl

1 Introduction

Research in vehicle automation aims to solve road congestion issues and mitigate the risk of accidents. Generally speaking we can make the distinction between two classes of automated vehicles. The first being cooperative vehicles, which aim to improve traffic flow by means of communication, and the second being fully autonomous vehicles. These autonomous vehicles typically make use of a trajectory planner, which provides a reference for the vehicle's trajectory control system. In this work we attempt to include communication of cooperative vehicles into the framework of the trajectory planner of the autonomous vehicle.

2 Path Planner

We adopt the planner framework presented in [1], in which in frenet frame, \vec{z}^2 , (Figure 1) is defined along a reference spatial path. The planning problem then reduces to finding trajectories $\{s(t), d(s(t))\}$ with respect to a reference trajectory, where s is the curvilinear distance along the reference path, and d , the lateral offset. To minimize jerk, a set of fifth order polynomials, trajectories is generated with discretized terminal conditions at terminal time, τ , for both coordinates, which are tested for feasibility and collisions. A cost function is then used to select the trajectory that will be executed.

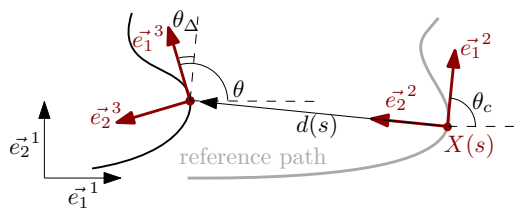


Figure 1: Reference path described by $X(s)$, and trajectory coordinates $s(t)$ and $d(s(t))$.

3 Communication

We focus on generating the path progression trajectory $s(t)$. In cooperative vehicles, typically a constant time gap spacing policy is used for the purpose of string stability [2]. This can be used to formulate a terminal constraint for the planned trajectory of $s(t)$,

$$s_i(\tau) = s_{i-1}(\tau) - c - h\dot{s}_i(\tau), \quad (1)$$

where $s_{i-1}(\tau)$ and $s_i(\tau)$ denote the curvilinear position of the predecessor and host vehicle, c a standstill distance in-

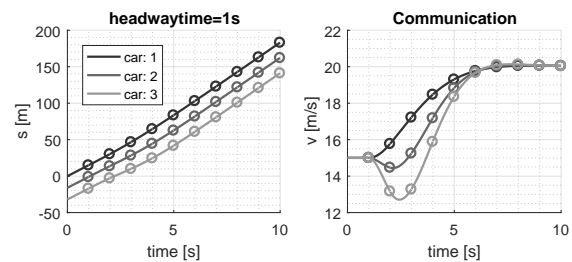


Figure 2: Trajectories $s(t)$, markers indicate planner update

cluding vehicle length and h the time gap. Including V2V communication allows access to the planned trajectories of preceding vehicle $s_{i-1}(\tau)$. Minimum jerk trajectories for $s(t), t \in [0, \tau]$ are then generated such that $s(\tau) = s_i(\tau)$, $\dot{s}(\tau) = \dot{s}_i(\tau) = \dot{s}_{i-1}(\tau)$

This algorithm is implemented in a simulation environment in which the planner runs online at a frequency of 1Hz. The results for $s(t)$ are shown in Figure 2. The leading vehicle makes a change in forward velocity using a minimum jerk maneuver. The follower vehicles use spacing policy (1) with the described planning algorithm to generate trajectories. The minimum jerk nature of the trajectories results in an initial deceleration, which amplifies rearward in the string. This result demonstrates that the minimum jerk trajectories cannot be applied directly in the trajectory planner framework of the autonomous vehicle. Instead, the criteria for string stability should be explicitly included in formulating the functions for the longitudinal trajectory $s(t)$.

Acknowledgements

This work is part of the research program i-CAVE with project number 14893, which is partly financed by the Netherlands Organisation for Scientific Research (NWO).

References

- [1] M. Werling et al., "Optimal trajectories for time-critical street scenarios using discretized terminal manifolds", The International Journal of Robotics Research, 2012.
- [2] J. Ploeg et al., "Design and experimental evaluation of cooperative adaptive cruise control", International IEEE Conference on Intelligent Transportation Systems, 2011.

String stability analysis of MPC-based heterogeneous platooning

Joey Reinders¹, Ellen van Nunen², Elham Semsar-Kazerooni² and Nathan van de Wouw^{1,3,4}

¹ Department of Mechanical Engineering, Eindhoven University of Technology, Eindhoven

² Integrated Vehicle Safety, TNO, Helmond

³ Department of Civil, Environmental & Geo-Engineering, University of Minnesota, U.S.A.

⁴ Delft Center for Systems and Control, Delft University of Technology, Delft

Email: j.m.f.reinders@tue.nl

Background

Cooperative Adaptive Cruise Control (CACC) aims to longitudinally control a following vehicle to obtain a certain desired inter-vehicle distance. CACC is known as a possible solution to problems such as increasing pollution and traffic congestion. To enable small inter-vehicle distances, vehicle-to-vehicle communication (V2V) is used. Moreover, string stability is a property which ensures no amplification of disturbances in upstream direction, which is essential for guaranteeing safety. However, V2V is subject to packet losses, which might degrade the string stability properties of a CACC system. To increase robustness against limited packet loss, Model Predictive Control (MPC) is considered as a promising solution, since an obtained prediction can be applied in case a package is lost [1]. However, vehicle platoons are typically heterogeneous, with vehicles having different dynamic properties, which makes employing a model-based control approach, such as MPC, challenging. This work presents an MPC-based control strategy for heterogeneous platoons, that guarantees string stability and warrants confidentiality of the vehicle characteristics.

MPC control approach

Since the states of a vehicle (e.g., distance error) depend on the predecessor's behavior (e.g., acceleration), the predicted behavior of the predecessor is included in the linear prediction model of the MPC controller. This information is obtained through V2V between successive vehicles. A cost function with the goals of vehicle following, minimizing fuel consumption and ensuring string stability is designed. Furthermore, state constraints are added to this optimization to ensure vehicle constraints and to ensure safety.

Discrete-time string stability

String stability has been studied for continuous-time models of platooning systems [2]. When using MPC control, one typically has a discrete-time controller and plant/prediction model. Therefore, discrete-time string stability properties for the CACC-MPC system have been proposed. Using the assumption that the obtained prediction vector of the predecessor is the same as the actual future behavior of the predecessor, a string stability analysis is conducted. An advantage of this analysis is that it is independent of the predecessor

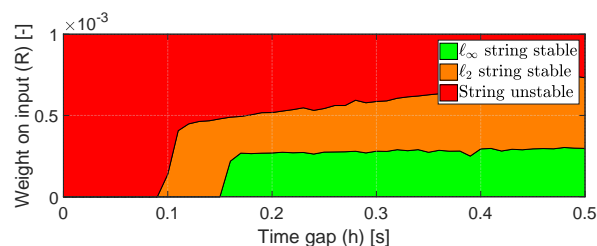


Figure 1: String stability properties for different weighting of the input (R) and time gaps (h).

sors (often unknown) system parameters. Therefore, this approach is particularly suitable for heterogeneous platooning. Figure 1 visualizes the string stability properties of a certain vehicle for different time gaps h and weighting on the control input in the objective function. This figure shows that the minimal time gap to ensure string stability is strongly decreased compared to traditional linear control [2], which ensures \mathcal{L}_∞ string stability at a minimal time gap of 0.5 s.

Simulation and experimental results

Simulations and experiments are performed to examine the properties of the obtained controller in practice. In simulation, the newly proposed MPC approach showed significant improvements over existing controllers, in terms of vehicle following and string stability properties. In experiments, it was found that the developed MPC approach improves string stability. However, the existing controllers show better performance in terms of error rejection, comfort and fuel efficiency. As such, further research is needed to obtain an optimal balance between these performance criteria for platooning.

References

- [1] E. van Nunen, J. Verhaegh, E. Silvas, E. Semsar-Kazerooni, and N. Van de Wouw, "Robust model predictive cooperative adaptive cruise control subject to V2V impairments," in *Intelligent Transportation Systems - (ITSC), 20th International IEEE Conference*, pp. 2013-2020, 2017.
- [2] J. Ploeg, N. van de Wouw, and H. Nijmeijer, " \mathcal{L}_p string stability of cascaded systems: Application to vehicle platooning," *IEEE Trans. Control Syst. Technol.*, vol. 22, no. 2, pp. 786-793, 2014.

Co-design of Active Controlled Systems: Application to State-of-the-art CVT Systems

Chyannie Amarillio Fahdzyana
 Mechanical Engineering
 Eindhoven University of Technology
 Den Dolech 2, 5600 MB Eindhoven
 The Netherlands
 Email: c.a.fahdzyana@tue.nl

Dr. Ir. Theo Hofman
 Mechanical Engineering
 Eindhoven University of Technology
 Den Dolech 2, 5600 MB Eindhoven
 The Netherlands
 Email: t.hofman@tue.nl

1 Introduction

A Continuously Variable Transmission (CVT) is a type of transmission system that provides smooth shifting and continuous gear ratio values within a certain range. Besides the better driving comfort that it provides, a CVT is also able to operate the engine at its Optimal Operation Line (OOL), therefore increasing the overall energy efficiency of a conventional vehicle [1]. However, there is a tradeoff between tracking the desired gear ratio values and the actuation system losses. Therefore, in the design of a CVT system, both plant and control design parameters must be considered in order to obtain the optimal value between minimizing the losses and maximizing the tracking performance. This research proposed plant and control parameters design strategy of a CVT based on co-design method.

2 Co-design of a CVT System

Co-design is a term that describes a multi-objective optimization method to eventually obtain the optimal design of a system where the control and plant parameters are coupled. A co-design optimization can be formulated mathematically as

$$\min_{\mathbf{x}_p, \mathbf{x}_c} J = f(\mathbf{x}_p, \mathbf{x}_c, t) \quad (1)$$

$$\text{s.t. } \mathbf{g}(\mathbf{x}_p) \leq 0 \quad (2)$$

$$\mathbf{h}(\mathbf{x}_p) = 0 \quad (3)$$

where \mathbf{x}_p and \mathbf{x}_c are the plant and control parameters. J is the cost function to be minimized throughout the process subject to a set of design constraints \mathbf{g} and \mathbf{h} . The general scheme of a Co-design process is depicted in Figure 1.

The goal of this research project is to implement a co-design method in order to achieve the optimal design of CVT system. However, a CVT is a non-linear and dynamic system, which can lead to large computation time during the process of design optimization. One of the methods to reduce the computation time in many optimization problem is by using a surrogate model, which can be created using input and output datasets from simulation.

A surrogate model can be used in place of the mathematical model as a function of only the relevant parameters, therefore reducing the complexity of the optimization and the computation time significantly [3]. To build a surro-

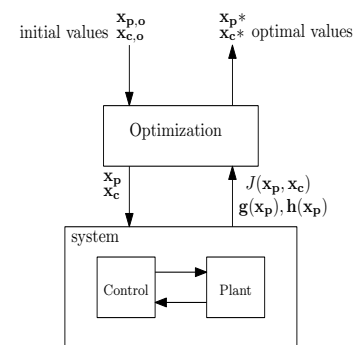


Figure 1: Proposed scheme of Co-design of CVT System

gate model, first the relevant design parameters of the plant for the complete co-design formulation must be determined. Using an appropriate input-output mapping function, a generalized function of the design parameters can be obtained. Finally, a suitable optimization framework is performed on the system, which now consists of a controller and a surrogate model that replaces the complex plant mathematical formulation. The main challenge of this approach in co-design formulation is the accuracy of the surrogate model used throughout the optimization process, as it can have an impact on how the final design results are achieved.

References

- [1] I. Aladağlı, "Advanced CVT Modeling and Control," *PhD Thesis*, 2014.
- [2] G. Carbone, L. Mangialardi, and G. Mantriota, "The influence of pulley deformations on the shifting mechanism of metal belt cvt," *Journal of Mechanical Design*, vol. 127, no. 1, p. 103, 2005.
- [3] Anand P. Deshmukh and James T. Allison "Design of Nonlinear Dynamic Systems Using Surrogate Models of Derivative Functions," *Journal of Mechanical Design*, vol. 139, 2017.

Powertrain design sensitivity study of a heavy-duty hybrid electric truck

F.J.R. Verbruggen, T. Hofman

Control Systems Technology, Eindhoven University of Technology, Den Dolech 2, 5600 MB Eindhoven, The Netherlands

Email: f.j.r.verbruggen@tue.nl, t.hofman@tue.nl

1 Introduction

Most of the research related to powertrain design focuses on finding the optimal design under given conditions. However, only limited research is focused on the design space around this optimum, which would be interesting in order to determine the robustness of the optimum found. This creates insight into the sensitivity of the optimal performance to variations in the design and/or conditions of the vehicle. This is crucial for research into the design of 'modular' powertrain components, components designed for multiple vehicle segments.

2 Sensitivity studies

Multiple types of sensitivity studies are available, ranging from one-factor-at-a-time (OAT) to variance based methods. Since the purpose of the use of sensitivity studies here is in the first phase of vehicle design, high computational expenses should be avoided. Therefore, computational inexpensive, but still accurate enough, sensitivity studies are preferred. In this work, discussed in more detail in [1], a sensitivity study based on a two-level factorial design is performed on a hybrid electric heavy-duty truck.

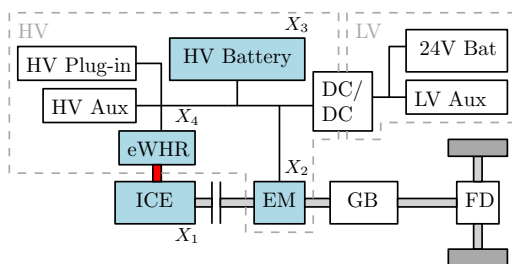


Figure 1: Topology of the vehicle studied [1].

3 Two-level factorial design

The vehicle studied is a parallel hybrid plug-in heavy-duty truck. The vehicle's topology is shown in Figure 1. The factors studied are indicated in blue, which are: sizing of the internal combustion engine (X_1), electric machine (X_2), and battery (X_3), and the presence of a WHR system (X_4). The objectives studied are: (f_1) the fuel savings, (f_2) powertrain efficiency, (f_3) energy generated by the WHR system, (f_4) reduction in total cost of ownership, and (f_5) the average torque split.

The research leading to these results has received funding from the European Community's Horizon 2020 Programme under grant agreement No. 653468 (ECOCHAMPS).

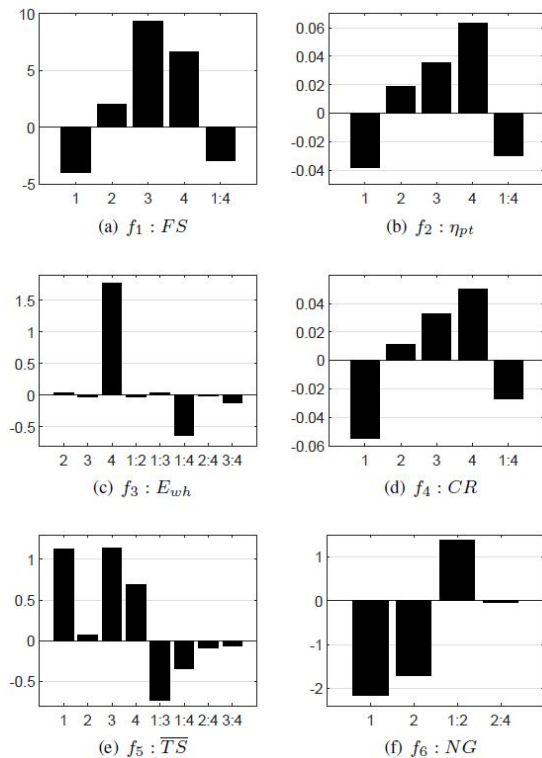


Figure 2: Plots of significant regression model parameters for each of the six objectives studied [1].

The method is based on a two-level factorial design, where for each factor studied two levels are simulated. For each of the objectives a linear regression model is fitted w.r.t. to the four factors. A more detailed description of the method can be found in [1]. The significant regression model parameters are plotted in Figure 2.

4 Conclusions

The main conclusions that could be drawn for the vehicle studied using this method, and visible in Figure 2, are:

- Non-optimal vehicle design w.r.t. cost and fuel
- Cost effective WHR system
- Significant coupling between ICE and WHR

References

- [1] F.J.R. Verbruggen and T. Hofman, "Design sensitivity analysis for heavy-duty hybrid electric trucks with a waste heat recovery system," in Proceedings of *Vehicle Propulsion and Powertrain Conference*, Belfort, France, 2017

Feed-Forward ALINEA: A ramp metering control algorithm for nearby and distant bottlenecks

José Ramón D. Frejo

Delft Center for Systems and Control

Delft University of Technology

Mekelweg 2, 2628 CD, Delft, The Netherlands

Email: J.R.DominguezFrejo@tudelft.nl

Bart De Schutter

Delft Center for Systems and Control

Delft University of Technology

Mekelweg 2, 2628 CD, Delft, The Netherlands

Email: B.DeSchutter@tudelft.nl

1 Introduction

Traffic congestion on freeways causes many social and economic problems like waste of time and fuel, a greater accident risk, and an increase in pollution. In many cases, the use of dynamic control signals such as ramp metering may be an economical and effective solution.

This paper proposes a new ramp metering control algorithm, Feed-Foward ALINEA (FF-ALINEA), for bottlenecks located both nearby on an on-ramp and further away from it (i.e. more than just a few hundred meters). The formulation of the controller is based on a feed-forward modification of the well-known control algorithm for ramp metering, ALINEA [1]. The feed-forward structure allows to anticipate the future evolution of the bottleneck density in order to avoid or reduce traffic breakdowns.

2 FF-ALINEA

For a given on-ramp, the control law for the implementation of FF-ALINEA is:

$$r(k+1) = r(k) + K_{FF}(\hat{\rho}(k) - \rho_b(k)) \quad (1)$$

where $r(k)$ is the ramp metering rate, $\rho_b(k)$ is the density measurement collected at a bottleneck downstream of the controlled on-ramp and K_{FF} is a positive parameter. Unlike ALINEA, the computation of the density set-point $\hat{\rho}(k)$ is time-varying:

$$\hat{\rho}(k) = \rho_{b,c} - \max\left(\frac{L_A}{\lambda_b L_b \hat{v}_A(k)}(Q_{ib}(k) - C_b), 0\right) \quad (2)$$

where L_b , L_A , and λ_b are parameters that are based on the network topology, $\rho_{b,c}$ and C_b are the critical density and the capacity of the bottleneck, and $Q_{ib}(k)$ and $\hat{v}_A(k)$ are the flow entering the bottleneck and the mean speed upstream of the bottleneck during a considered period T_A . Note that $Q_{ib}(k)$ and $\hat{v}_A(k)$ have to be estimated on-line using measurements available from detectors located upstream of the bottleneck.

The main advantage of FF-ALINEA, compared with previously proposed controllers such as ALINEA and PI-ALINEA [2], is that the proposed controller is able to activate ramp metering before the bottleneck is congested in

case the flow arriving to the bottleneck is higher than its capacity.

3 Case study

The proposed controller is tested, for a simple network that includes one on-ramp located upstream (7 kms) of a bottleneck and using the macroscopic traffic flow model METANET [3], for 9 scenarios and the results are compared with the ones obtained with ALINEA, PI-ALINEA, and with an optimal controller. The simulations show that FF-ALINEA is able to approach the optimal behavior, thereby outperforming ALINEA and PI-ALINEA. Moreover, the results indicate that FF-ALINEA is quite robust in cases where different demands are considered, there is a limited number of available detectors, or there are errors in the estimation of the capacity and/or the critical density of the bottleneck.

Table 1: Average Total Time Spent (TTS) reduction for the 9 simulated scenarios

Uncontrolled	Optimal	ALINEA	PI-ALINEA	FF-ALINEA
0%	-31.8 %	-10.3 %	-19.4 %	-30.6 %

4 Acknowledgments

This research was supported by the European Union's Horizon 2020 research and innovation programme under the Marie Skłodowska-Curie grant agreement No 702579.

References

- [1] M. Papageorgiou, H. Hadj-Salem and J. M. Blosseville, "ALINEA: A local feedback control law for on-ramp metering," *Transportation Research Record: Journal of the Transportation Research Board*, vol. 1320, pp 58-67, 2001.
- [2] Y. Wang and M. Papageorgiou, "Local ramp metering in the case of distant downstream bottlenecks," *IEEE Conference on Intelligent Transportation Systems*, pp. 426-431, Toronto, Canada, 2006.
- [3] M. Papageorgiou, I. Papamichail, A. Messmer and Y. Wang, "Traffic simulation with METANET," *Fundamentals of Traffic Simulation*, Springer, 2010.

A Robust PID Autotuning Method for Steam/Water Loop in Large Scale Ships

Shiquan Zhao^{1,2}, Robin De Keyser¹, Sheng Liu² and Clara M. Ionescu¹

¹Research group on Dynamical Systems and Control, Ghent University, Belgium

²College of Automation, Harbin Engineering University

Shiquan.Zhao@UGent.be

1 Introduction

During the voyage of the ship, disturbance from the sea is changeable and frequent, and the ship operation mode is also changeable. So it is needed to have good control for steam/water loop in large scale ships [1]. Due to the strong interaction and complexity existing in the steam/water loop in large scale ships, there is few study about the control for whole system, and most study is about the control for single sub-loop in this system. In this paper, a robust proportional-integral-derivative (PID) autotuning method [2] is presented and applied to the system. Based on single sine tests for every sub-loop in the steam/water loop, the controller is obtained during which the user-defined robustness margins guaranteed. Its performance is compared against to other PID autotuners, and results show its superiority.

2 System Description and Methodology

The steam/water loop works as follows. Firstly, the feed water is supplied into the boiler after heated in the economizer. Secondly, due to the higher density of the feed water, it will flow into the mud drum. Then, after heated in risers under the burning of the fuel, the feed water turn into saturated mixture of water and steam. Thirdly, the steam is separated from the mixture and used in steam turbine. Finally, the used steam will be condensed, deoxygenated and pumped to the boiler once again [3]. The main control problems existing in this system include the following aspects, i) drum water level control; ii) condensate and deaerator water level control loop; iii) deaerator and exhaust pipe pressure control.

The purpose of KC autotuner is to move a point B on the Nyquist curve of process $P(j\omega)$ to another point A on the Nyquist curve of the loop $L(j\omega)=P(j\omega)C(j\omega)$ through the PID controller indicated by $C(j\omega)$. Hence, the system can have a good dynamic characteristic. The tuning procedure is summarized as follows. i) Select a frequency ω ; ii) Perform sine tests at frequency on the steam/water sub-loops; iii) Define a forbidden region for robustness in the Nyquist plane according to the loop modulus margin; iv) For each point on the region border, calculate PID controller; v) Find the point where the loop $L(j\omega)$ is tangent to the forbidden region; vi) The PID controller from step v) are final.

3 Results and Conclusions

In order to validate the performance of the proposed method, other PID autotuners such as Åström-Hägglund (AH), Phase Margin (PM) and Kaiser-Rajka (KR) are designed. According to the results shown in Figure 1, the steam/water loop obtained an ideal performance in tracking of system commands, and the proposed autotuning method obtains better results in all sub-loops.

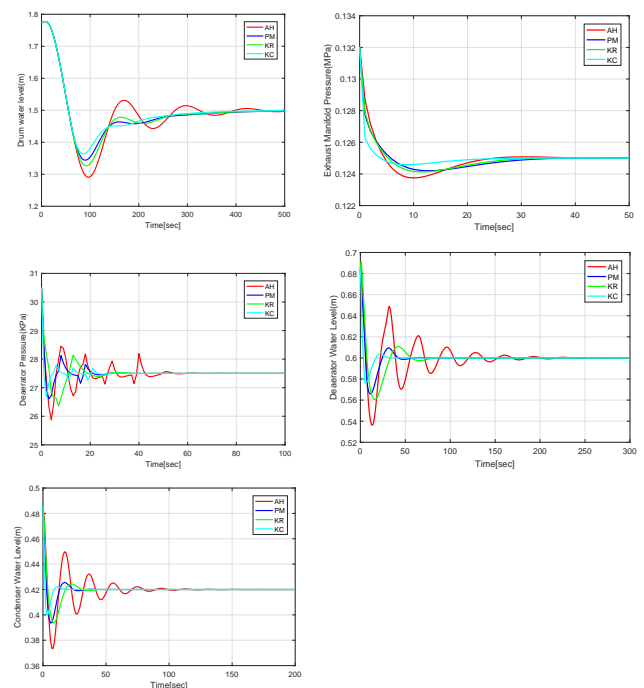


Figure 1: System outputs with different PID controllers

References

- [1] S. Liu, S. Zhao, Y. Wang, "Smooth Sliding Mode Control and Its Application in Ship Boiler Drum Water Level," *Mathematical Problems in Engineering*, 2016.
- [2] R. De Keyser, C.M. Ionescu, C.I. Muresan, "Comparative Evaluation of a Novel Principle for PID Autotuning," In *11th Asian Control Conference (ASCC)*, 2017, pp. 1164-1169.
- [3] L. Drbal, K. Westra, P. Boston, "Power plant engineering," Springer Science & Business Media, 2012.

Controlling triangular formations using angle information

Liangming Chen^{1,2}, Ming Cao¹, Chuanjiang Li²

1. Faculty of Science and Engineering, University of Groningen, The Netherlands
 2. Department of Control Science and Engineering, Harbin Institute of Technology, China
- Email: l.m.chen@rug.nl, m.cao@rug.nl, lichuan@hit.edu.cn

1 Introduction

Distance-based formation control problems have been investigated in the past decade under the setup where the target formation is specified by inter-agent distances, and each agent can measure relative positions or pure distances with respect to its neighbors. Instead of distances, this study investigates the angle-based formation control problem which is motivated by the fact that angle measurements are usually cheaper, more reliable and accessible than relative position or distance measurements. Angle information can be easily obtained by the full-range radar or vision-based camera. In this study, for triangular formations, the formation control algorithm using only angle information is designed to achieve the desired triangle shape.

2 Problem formulation

For a triangular formation in the plane consisting of agent 1, 2 and 3, the motion dynamics of an agent i are governed by

$$\dot{p}_i = v_i \begin{bmatrix} \cos \beta_i \\ \sin \beta_i \end{bmatrix}, i = 1, \dots, 3 \quad (1)$$

where $p_i = [x_i, y_i]^T \in \mathbb{R}^2$, and both v_i and β_i are the control inputs to be determined. The heading β_i is defined counter-clockwise from agent i 's local x_i -direction and always takes a value from $(-\pi, \pi]$.

Agent i measures only the bearing $\phi_{ij} \in (-\pi, \pi], \forall j \in \mathcal{N}_i$ counter-clockwise from its local x_i -direction to agent j , in which \mathcal{N}_i denotes the set of the neighbors of agent i . α_i is subtended at agent i by two lines passing through respectively the positions of the two agents in \mathcal{N}_i . Then, one can get

$$\alpha_i = \begin{cases} \theta_i, & \text{if } \theta_i \leq \pi \\ 2\pi - \theta_i, & \text{otherwise} \end{cases} \quad (2)$$

with $\alpha_i \in [0, \pi]$, and $\theta_i = |\phi_{i(i+1)} - \phi_{i(i-1)}| \in [0, 2\pi)$ is the angle measured counter-clockwise from the $\min(\phi_{i(i+1)}, \phi_{i(i-1)})$ to $\max(\phi_{i(i+1)}, \phi_{i(i-1)})$ in agent i 's local coordinate frame.

In this study, we aim to achieve the triangular formation control, i.e.,

$$\lim_{t \rightarrow \infty} (\alpha_i - \alpha_i^*) = 0, \forall i = 1, 2, 3 \quad (3)$$

where α_i^* is the desired angle of agent i .

3 Main result

Note that for each agent i , the angle becomes larger when it moves towards the inside of the triangle and smaller when it moves towards the outside of the triangle along the bisection of $\angle(i-1)i(i+1)$. Thus, we can design the formation control algorithm using only angle information

$$v_i = -k_i \frac{\alpha_i - \alpha_i^*}{\sin(\alpha_i/2)}, i = 1, 2, 3 \quad (4)$$

$$\beta_i = \begin{cases} \alpha_i/2 + \min(\phi_{i(i+1)}, \phi_{i(i-1)}), & \text{if } \theta_i \leq \pi \\ \alpha_i/2 + \max(\phi_{i(i+1)}, \phi_{i(i-1)}), & \text{if } \theta_i > \pi \end{cases} \quad (5)$$

where k_i is a positive constant.

4 Simulation example

To illustrate the effectiveness of the proposed formation control algorithm, we use Matlab/Simulink software to simulate the formation system.

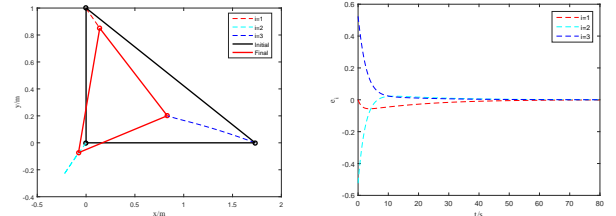


Figure 1: The moving trajectories of three agents. Figure 2: The relative angle errors of three agents

5 Conclusion

In this study, we use the inside-increasing and outside-decreasing moving strategy for each agent to realize the triangular formation control using only angle information.

References

- [1] Basiri, Meysam and Bishop, Adrian N and Jensfelt, Patric, "Distributed control of triangular formations with angle-only constraints," Systems & Control Letters, 2010, 59(2): 147-154.

Safe Formation-Motion Control of Mobile Robots

Nelson P.K. Chan, Bayu Jayawardhana, and Jacquelinen M.A. Scherpen
DTPA, ENTEG, University of Groningen, The Netherlands

Email: {n.p.k.chan, b.jayawardhana, j.m.a.scherpen}@rug.nl

1 Introduction

In the present work, we consider the problem of moving a group of 2-D mobile robots towards a desired position while maintaining a 2-D formation and avoiding obstacles during the transition period. The problem is motivated by the possible application of mobile robots in smart manufacturing or logistic systems where low-cost mobile robots can be deployed to collaboratively carrying out tasks as a group while guaranteeing safety of the whole group. In literature, the problem of formation control and obstacle avoidance has been studied, among many others, in [1, 2] where a decentralized controller is designed based on the use of a navigation function. In this work, we propose a new decentralized controller for solving reaching formation and avoiding obstacles where we have used a separation principle, i.e., the formation control and the obstacle avoidance control are designed independent of each other and they are linearly combined. The group motion control is still centralized and based on the centroid of the formation.

2 Systems description and problem formulation

We consider a group of mobile agents in \mathbb{R}^2 where each agent is modeled as a single integrator, $p_i = u_i$, $i = 1, \dots, N$, with p_i and u_i denoting respectively the position and the controlled velocity of agent i . A global coordinator is present which, based on the positions of the individual agents, can calculate the formation centroid and as such provide to the agents instructions on how to move towards a desired position for the centroid. Without loss of generality, we take the origin as the formation centroid's desired position. The agent's interaction is modeled as a connected undirected graph. The neighbors of agent i are the agents j with whom agent i has a direct link with. We consider static circular obstacles with center p_{obs} and radius R_{obs} . The obstacles are fixed regions in the plane.

3 The safe formation-motion control design

For each of the subtasks for the group and agents (maintaining formation, obstacle avoidance and group motion control), the control law for each agent i will be of the following form $u_i = u_{i_{\text{form}}} + u_{i_{\text{group}}} + u_{i_{\text{obs}}}$, where $u_{i_{\text{form}}}$ is the standard relative-position based formation control law given by $u_{i_{\text{form}}} = k_f \sum_{j \in \mathcal{N}_i} w_{ij} \left(p_j - p_i - \begin{pmatrix} z_{ij}^* \\ \end{pmatrix} \right)$, where k_f is the formation gain, w_{ij} the weight of the interaction and $\begin{pmatrix} z_{ij}^* \\ \end{pmatrix}$ is the desired relative displacement between agent i and its neighbor j . The centralized motion controller is a proportional-integral controller given by

$$u_{\text{group}} = -k_{\text{group}p} p_{\text{cen}} - k_{\text{group}\gamma} \dot{\gamma}, \quad \dot{\gamma} = p_{\text{cen}} \quad (1)$$

where $k_{\text{group}p} > 0$ and $k_{\text{group}\gamma} > 0$ are the proportional and integral gain, respectively, p_{cen} is the formation centroid and γ is the integrator state. For the obstacle avoidance control, we introduce a virtual state ζ_i for each agent which satisfies

$$u_{i_{\text{obs}}} = \dot{\zeta}_i, \quad \dot{\zeta}_i = -k_{\zeta} \sum_{j \in \mathcal{N}_i} w_{ij} (z_j - z_i) + u_{i_{\text{vir}}}$$

where

$$u_{i_{\text{vir}}} = \begin{cases} 0 & \text{if } \|p_i - p^*\| > R_{\text{safe}} + \varepsilon \\ -k_{\text{vir}} \zeta_i & \text{if } R_{\text{safe}} < \|p_i - p^*\| < R_{\text{safe}} + \varepsilon \\ -k_{\text{vir}} \frac{p_i - p^*}{\|p_i - p^*\|^4} & \text{if } \|p_i - p^*\| < R_{\text{safe}} \end{cases} \quad (2)$$

The idea for the state variable ζ_i is to allow the diffusion of the obstacle control action from the agent i , which is in close vicinity to the obstacle boundary (given by the term $\|p_i - p^*\|$), to the other agents. The constants R_{safe} and ε are distances added to the boundary of the circular obstacle.

4 Simulation results

Figure 1 shows the simulation results of a group of three agents whose centroid has to go to the origin while the group has to maintain a formation and avoid obstacle that is given by a circle.

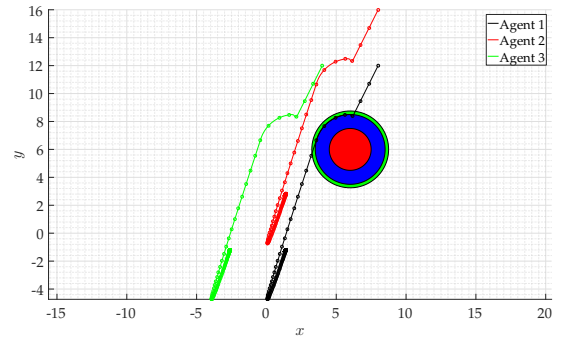


Figure 1: Simulation result of 3 agent formation transitioning from initial position to the final desired position.

References

- [1] M. D. Gennaro and A. Jadbabaie, "Formation control for a cooperative multi-agent system using decentralized navigation functions," in *2006 American Control Conference*. IEEE, 2006.
- [2] Z. Kan, A. P. Dani, J. M. Shea, and W. E. Dixon, "Network connectivity preserving formation stabilization and obstacle avoidance via a decentralized controller," *IEEE Transactions on Automatic Control*, vol. 57, no. 7, pp. 1827–1832, jul 2012.

Distributed constraint optimization for mobile sensor coordination

Jeroen Fransman, Bart De Schutter, and Joris Sijs
Delft Center for Systems and Control
Delft University of Technology
Delft, The Netherlands
Email: J.E.Fransman@tudelft.nl

1 Introduction

A wide range of real world problems can be modeled as Multi Agent Systems (MAS): scheduling problems [1], mobile sensor team cooperation [2], coordination of emergency responders and robots such as RoboCup Rescue. The main challenge of MAS is to coordinate their actions by a distributed process, since centralized coordination would become intractable for large number of agents or variables. In this paper a Distributed Constraint Optimization Problem (DCOP) framework is proposed to represent variables with continuous domains. Additionally, an iterative any-time algorithm based on Distributed Pseudo tree Optimization Procedure (DPOP) is presented.

2 Distributed Constraint Optimization Problems for continuous domains

A DCOP is typically represented as a constraint graph, where nodes represent the variables of the problem, and edges represent a constraint or utility relation between the variables. The agents coordinate their actions by exchanging utility messages between neighbors. Neighbors are defined as agents connected by edges. The utility values represent the difference in cost and benefits of the actions for the individual agents. DCOP defines control variables with finite discrete domains, which limits the use for problems with continuous variables. The continuous domains can be transformed into discrete domains by sampling the domains of the continuous variables with a desired resolution. However, this would result in a rapid growth in the computational complexity to solve the DCOP. The complexity growth is due to the exponentially growth of the *size* of the search space with respect to the size of the domains and induced width the graph (number of edges of the nodes). Complexity reduction is done by three predominant methods: *reducing the induced width* of the graph, *restricting the number of variables* in the messages, *limit the growth of the messages* by pruning. In this paper a fourth option is explored that *restricts the number of samples of the continuous domains*. An iterative algorithm (C-DPOP) is developed to sample the search space effectively based on local optima. After every iteration all agents have determined their actions, which results in an any-time property. The proposed restriction strategy is based on the annealing schedule of simulated annealing. By this, the sampling of the continuous domain is fo-

cused around the optimal value (an area with high utility), while the compression of the domain iteratively reduces the exploration (of the area around the found optimum). The compression of the domain is a key part of the algorithm, since it refines the solution after every compression step.

3 Sensor coordination problem

A mobile sensor coordination problem is used to explore the performance and computational requirements of the C-DPOP algorithm in comparison with DPOP. The problem is adapted from [2] where a team of mobile sensors with limited sensing range need to coordinate their positions (starting from random initial positions) in order to minimize the number of unobserved targets in an area. The problem is extended for resource constraint (limited memory and limited computation time) agents that are able to select positions over continuous domains within a two-dimensional plane. Here it was found that C-DPOP achieves a higher utility compared to DPOP with uniform domain sampling. Equal utility could be achieved while using less resources (time, memory) by sampling the parts of the domains more thoroughly in areas of higher utility.

References

- [1] R. Maheswaran, M. Tambe, E. Bowring, J. Pearce, and P. Varakantham, "Taking DCOP to the real world: efficient complete solutions for distributed multi-event scheduling," *Proceedings of the Third International Joint Conference on Autonomous Agents and Multiagent Systems, 2004. AAMAS 2004.*, 2004.
- [2] R. Zivan, H. Yedidsion, S. Okamoto, R. Grinton, and K. Sycara, "Distributed constraint optimization for teams of mobile sensing agents," *Autonomous Agents and Multi-Agent Systems*, vol. 29, no. 3, pp. 495–536, 2015.

Coping with collisions in decentralized event-triggered control

M. Hadi Balaghi I.
Control System Technology
Eindhoven University of Technology
P.O. Box 513, NL-5600 MB Eindhoven
The Netherlands
Email: m.balaghiinaloo@tue.nl

Duarte J. Antunes
Control System Technology
Eindhoven University of Technology
P.O. Box 513, NL-5600 MB Eindhoven
The Netherlands
Email: d.antunes@tue.nl

I. Introduction

In many applications of cyber-physical systems (CPS), control loops are closed over shared communication networks. Designing the controller and the communication protocol separately typically results in a conservative design in terms of closed-loop specifications and in an inefficiency use of communication resources. However, the performance of the control loop is highly affected by the communication quality and the transmission rate of the feedback data. Therefore, a resource-aware design approach should be pursued in order to maximize control performance with respect to the communication resource constraints. Moreover, bandwidth limitations and network deficiencies, such as data drop-out and collision, are some of the main constraints in the existing communication channels. Therefore, designing control and scheduling strategies by taking these constraints into account can highly enhance the control performance.

One of the promising directions to tackle the bandwidth limitation is to replace the time-triggered transmission paradigm with the event-triggered transmission paradigm. In the event-triggering strategy, every network user transmits only when there is a significant change in the value of its data. Moreover, it is fairly well-known that there are some event-triggered strategies which can outperform time-triggered strategies. On the other hand, when applied in the context of shared networks, event-triggered control is more prone to data collisions, as opposed to time-triggered (periodic) strategies, associated with protocols such as time division multiplexing (TDMA). Motivated by this, in this work we consider the effects of data collision on the stability and the performance of the event-triggered controllers. In particular we are interested in understanding if in this setting these can still outperform periodic control.

II. Problem definition

We consider several LTI systems which are physically decoupled. They utilize a shared communication channel to have a sensor-controller communication. This structure is shown in Fig. 1 for illustration. The arbitration mechanism of the communication channel is assumed to be random and based on the slotted ALOHA protocol in which every transmission duration is equal to one slot size. In case two or

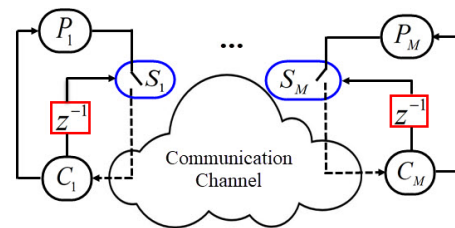


Figure 1: Decentralized Event-triggering control loops with the shared communication channel

more schedulers try to transmit in one transmission slot, a collision will occur and none of the colliding data is received successfully which will degrade the performance of the control loops. In this work the goal is to compare the control performance of the decentralized stochastic based triggering policies. More specifically, we want to compare the control performance of the purely stochastic and the state-based stochastic triggering policies as we take into account the effect of the data collision.

Our analysis shows the better control performance of the state-based stochastic triggering policy compared with the one for the purely stochastic triggering policy with the same transmission rate. However, for running the state-based stochastic triggering policy, the scheduler is in need of an acknowledgment from the controller when the data is received successfully. This condition is necessary for keeping the separation property of the controller and the estimator which will result in an optimal LQG controller to be a linear function of the estimated state [1]. Moreover, we come up with the stability criteria for the stochastic based triggering policies when they are sharing a common communication channel operating based on the slotted ALOHA protocol.

References

- [1] Schenato, Luca, Bruno Sinopoli, Massimo Franceschetti, Kameshwar Poolla, and S. Shankar Sastry. "Foundations of control and estimation over lossy networks." Proceedings of the IEEE 95, no. 1 (2007): 163-187.

Distributed Fault and Malicious Behaviour Detection in Multi Vehicle Systems

Niloofar Jahanshahi
 Delft Centre for Systems and Control
 Delft University
 The Netherlands
 N.Jahanshahi@tudelft.nl

Riccardo Ferrari
 Delft Centre for Systems and Control
 Delft University
 The Netherlands
 R.Ferrari@tudelft.nl

I. ABSTRACT

The issue of formation control for mobile vehicles/robots has become a popular topic in the control community due its wide applications. There are many tasks that a vehicle can not accomplish alone due to limitations in sensors, actuators, costs, etc, thus cooperating as a team enhances the system's performance. One of the basic missions assigned to mobile vehicles is following a given trajectory [1], [2]. Inspired from the nature, other cooperative activities such as rendezvous and formation can be assigned for multi vehicle systems, MVSs. One of the common activities done by groups in nature is swarming, which is the gathering/traveling of animals in large numbers such as flocking birds or schooling fishes. Swarming can be defined as the coordination of MVSs where interaction between the robots and environment takes place in order to obtain a desired collective behaviour [3], and a specific type of swarming named as formation is defined when the vehicles endeavour to keep a geometric pattern, which is usually defined in advanced. In order for the vehicles to be able to keep the pattern, each agent should have access to its neighbours information. Since MVSs are physical entities with communication and computation capabilities, they are considered as a class of cyber physical systems, hence the possibility of cyber attacks should be considered, which is the issue addressed here.

In this work a group of vehicles with identical dynamics are considered. The vehicles are assumed to have a second order model and the framework is carried out in two dimensions. The

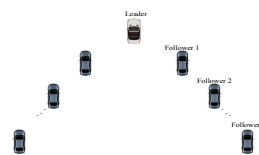


Fig. 1: Leader- follower structure

vehicles are required to accomplish a given mission, such as following a trajectory, while keeping a desired inter-vehicle formation pattern. A leader follower formation structure is an example for this where one of the vehicles is the leader and the rest are followers and the vehicles are required to keep a V formation where the leader is considered to be the front vehicle at the peak of the V and each follower can only communicate with its front vehicle, as shown in Figure.1. The MVS considered in this work is subjected to communication attacks and the aim is to design a detection scheme in such way that the system is able to keep the desired formation despite the occurrence of the attacks.

REFERENCES

- [1] A. De Luca, G. Oriolo, and C. Samson, *Feedback control of a -0.5 -nonholonomic car-like robot*, in Robot Motion Planning and Control, J.- P.Laumond, Ed.London,U.K.: Springer-Verlag,198,vol.29,Lecture Notes in Computer and Information Sciences, pp. 171-253.
- [2] C.Canudas de Wit, H. Khennouf, C. Samson, and O. J. Sordalen, *Nonlinear control design for mobile robots*, in Recent Trends in Mobile Robots,Y. F. Zheng, Ed.Singapore: WorldScientific,1993,vol.1,pp. 121-156.
- [3] Tan Y, Zheng ZY. *Research advance in swarm robotics*. Defence Technology. 2013 Mar 31;9(1):18-39.

Extending Cummins' Equation to Floater Arrays: a port-Hamiltonian Approach

M.Z. Almuzakki^{1,*}, J.J. Barradas-Berglind¹, Y. Wei¹, M. Muñoz-Arias², A.I. Vakis¹, & B. Jayawardhana¹

¹Engineering and Technology Institute Groningen, University of Groningen, Groningen 9747AG, the Netherlands.

²Zernike Institute for Advanced Materials, University of Groningen, Groningen 9747AG, the Netherlands.

*Corresponding author e-mail: m.z.almuzakki@rug.nl.

1 Abstract

A wave energy converter (WEC) is a device that converts (oceanic) wave energy into other types of energy, such as, electrical energy as in most WEC systems or potential energy as in the Ocean Grazer (OG) WEC. This particular WEC consists of an array of floating elements attached to individual pumping systems that in turn circulate fluid from a lower to an upper reservoir. In our previous work in [Barradas, et.al.(2017)], the OG-WEC was described as a single floater-piston-pump in the port-Hamiltonian (pH) framework [Maschke & van der Schaft(1992)] by considering a mechanical system representing the wave-structure, coupled to a hydraulic system representing the reservoirs. However, the hydrodynamic couplings were not included, which are important elements when considering an array of floater-piston-pump systems as in the OG-WEC.

This work casts the well-known Cummins' equation [Cummins(1962)] for the single floater case in the pH framework together with a simplified pumping force, i.e., corresponding to a linear power take off (PTO) system. Subsequently, the pH Cummins' equation is extended to the multi-floater case, providing some insights on the passivity and radiation energy properties of the system. Accordingly, the Cummins' equation for a single floating element with a simple geometry and displacement $q(t)$ is given by

$$m\ddot{q}(t) + m_\infty \ddot{q}(t) + \int_0^t \underbrace{\varphi(t-\tau)}_{f_r} \dot{q}(\tau) d\tau + f_{\text{pto}}(t) + f_b(t) = f_{\text{ex}}(t), \quad (1)$$

where m is the mass of the floating body, $f_{\text{ex}}(t)$ is the excitation force, f_b is the restoring (or buoyancy) force, $f_{\text{pto}} = k_{\text{pto}}q(t) + b_{\text{pto}}\dot{q}(t)$ corresponds to the (linear) PTO force, and the radiation terms (in the radiation force f_r) are characterized by the added mass m_∞ and the convolution kernel φ .

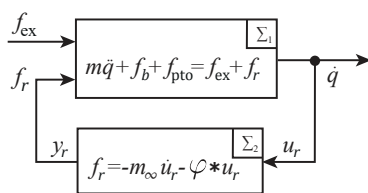


Figure 1: Single floater interconnection with the radiation force.

The system in (1) can be regarded as the negative interconnection of a passive mechanical system Σ_1 and a radiation system Σ_2 as shown in Figure 1 with $u_r = \dot{q}$ and $y_r = f_r$. One can show that Σ_2 is also passive and thus, the whole wave-structure system for a single floater is passive with respect to the supply rate $\dot{q}f_{\text{ex}}$.

In order to extend (1) to the multi-floater case, the radiation interactions between floaters need to be considered (in the heaving direction here); this is sketched in Figure 2. More concisely, we show the passivity of each individual radiation system does not guarantee passivity of the complete system, i.e., the passivity of each radiation system does not guarantee passivity of the complete system. In this work we provide: i) the formulation of a WEC array in the pH framework for the heaving direction, ii) the energy interpretation of the body-to-body radiation terms, and iii) the validation against the open-source code simulator WEC-Sim.

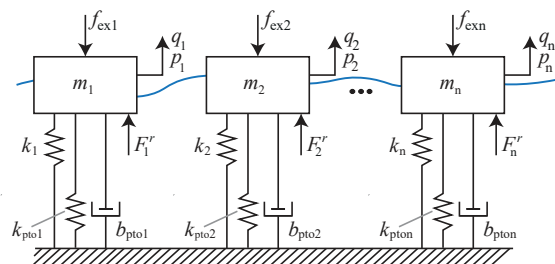


Figure 2: Multi-floater system diagram (the aggregated radiation forces on each floater are given by F_i^r for $i = 1, \dots, n$).

References

- [Barradas, et.al.(2017)] J.J. Barradas-Berglind, M. Munoz-Arias, Y. Wei, W.A. Prins, A.I. Vakis, and B. Jayawardhana, *Towards Ocean Grazer's Modular Power Take-Off System Modeling: a Port-Hamiltonian Approach*. In Proc. of the IFAC 2017 World Congress, p.16233–16239, 2017.
- [Cummins(1962)] W.E.. Cummins, *The impulse response function and ship motions*. David Taylor Model Basin Washington DC, 1962.
- [Maschke & van der Schaft(1992)] B. Maschke, and A. van der Schaft, *Port-controlled Hamiltonian systems: modeling origins and system-theoretic properties*. In Proc. IFAC Symp. on Nonlinear Control Sys., p.282–288, 1992.

Constrained multivariable extremum-seeking applied to optimization of Diesel engine fuel-efficiency

Robert van der Weijst* (r.v.d.weijst@tue.nl), Thijs van Keulen**, Frank Willems*,***

* Control Systems Technology Group, Eindhoven University of Technology, Eindhoven, the Netherlands

** DAF Trucks N.V., Eindhoven, the Netherlands, *** TNO Automotive, Helmond, the Netherlands

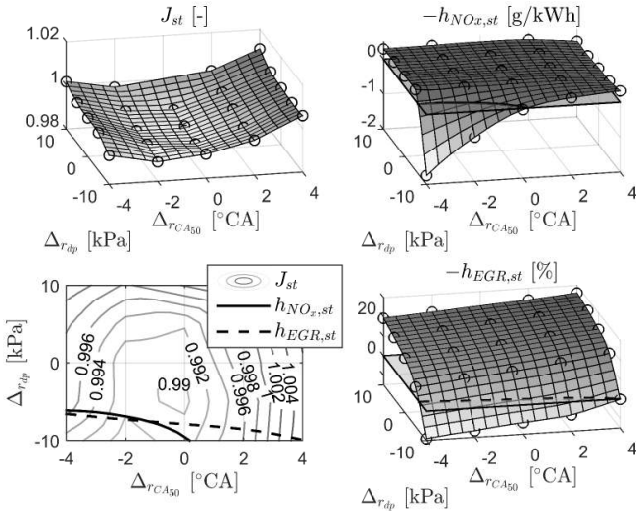


Figure 1: Measured steady-state input-output maps of the system Σ in Figure 2, for constant engine speed and load.

The objective in control of Diesel engines is to deliver power, while satisfying emission (in particular NO_x) constraints set by legislation, with a minimal brake specific fuel consumption (BSFC). However, there exists a NO_x -BSFC trade-off. The considered engine has a control system which enables tracking of four reference signals: r_{IMEP_n} and r_{NO_x} , related to power and NO_x emission, respectively, and $r_{CA_{50}}$ and r_{dp} , which influence the NO_x -BSFC trade-off. CA_{50} is a combustion phasing parameter and dp is the pressure difference between the engine intake and exhaust manifolds.

Approach

Due to production tolerances, fouling, aging or changing ambient conditions, the optimal values of $r_{CA_{50}}$ and r_{dp} are unknown. Therefore, we apply extremum-seeking (ES) (adaptive optimization) to optimize BSFC, by adjusting $r_{CA_{50}}$ and r_{dp} with a delta: $\Delta = [\Delta_{r_{CA_{50}}} \Delta_{r_{dp}}]^T$. In Figure 1, measured steady-state maps are depicted of an online implementable BSFC-equivalent cost function output J , NO_x tracking constraint $h_{\text{NO}_x} \leq 0$, and exhaust gas recirculation (EGR) actuator constraint $h_{EGR} \leq 0$, as a function of Δ . The optimization input Δ is perturbed with a (sinusoidal) dither signal $d \in \mathbb{R}^{2 \times 1}$, see Figure 2, such that the gradients of J , h_{EGR} , and h_{NO_x} can be estimated. Gradient \tilde{g} is a weighted combination of the gradient estimates \tilde{g}_J , $\tilde{g}_{h_{EGR}}$, and $\tilde{g}_{h_{\text{NO}_x}}$, obtained as a function of h_{EGR} and h_{NO_x} . Subsequently, \tilde{g} is used in gradient descent optimization. This constraint handling approach is adopted from [1].

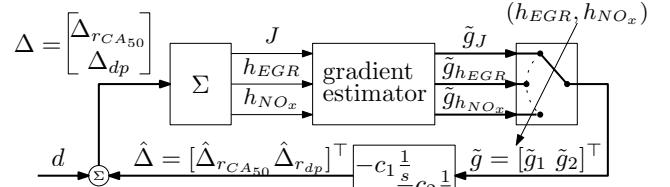


Figure 2: Extremum-seeking (ES) schematics. Signals in $\mathbb{R}^{2 \times 1}$ indicated by thick arrows, scalar signals by thin arrows. $c_1, c_2 > 0$ are gradient descent optimizer gains.

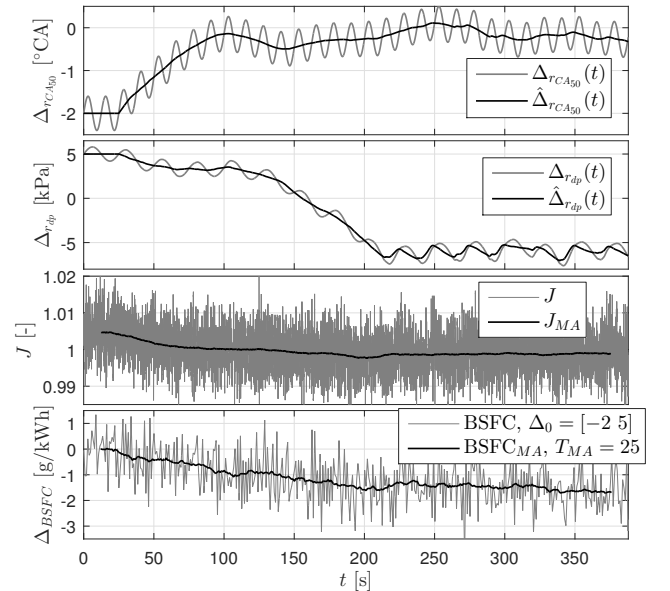


Figure 3: ES inputs $\Delta_{r_{CA_{50}}}$, $\Delta_{r_{dp}}$, cost J and BSFC saving Δ_{BSFC} , and their moving averages J_{MA} , $\Delta_{BSFC_{MA}}$.

Results

Figure 3 depicts measurement results obtained on an Euro VI engine, operating at the same constant speed and load as for the results in Figure 1. To emphasize the functionality of the ES method, an offset initial condition is used: $\Delta_0 = \Delta(0) = [-2 \ 5]$. For this measurement, the optimum is constrained in the $\Delta_{r_{dp}}$ direction. Clearly the decrease of J corresponds to a decrease of the BSFC. In [2], the ES controller is presented in more detail, and additional measurement results are provided.

References

- [1] M. Ramos, C. Manzie, and R. Shekhar, "Online optimisation of fuel consumption subject to NO_x constraints", *Preprints of the 20th IFAC World Congress, Toulouse, France, 9-14 July 2017*, pages 9231–9236, 2017.
- [2] Robert van der Weijst, Thijs van Keulen, Frank Willems, "On-line fuel-efficiency optimization of Diesel engines using constrained multivariable extremum-seeking", *European Control Conference*, 2018.

Reset control for transient performance improvement of systems with friction

Ruud Beerens, Nathan van de Wouw, Maurice Heemels, Henk Nijmeijer

Eindhoven University of Technology, dept. of Mechanical Engineering,

PO Box 513, 5600MB Eindhoven, the Netherlands

{r.beerens, n.v.d.wouw, w.p.m.h.heemels, h.nijmeijer} @tue.nl

1 Introduction

The use of cost-effective hardware components in high-precision positioning systems yield economic benefits, but induces nonlinearities such as backlash, hysteresis and friction. It is therefore essential to develop control strategies that are able to deal with these effects. In this work, a reset integral control technique is proposed to improve settling of systems with friction.

A PID-controlled motion system subject to Coulomb and viscous friction may suffer from long settling times due to the depletion and refilling of the integrator buffer upon overshoot, see the top and middle plot in Fig. 1 (grey, dashed line). We propose a particular reset of the integrator to circumvent a large part of this process to significantly decrease settling times.

2 Reset integrator

Consider the following (mass normalized) dynamics of a PID-controlled inertia:

$$\begin{bmatrix} \dot{z}_1 \\ \dot{z}_2 \\ \dot{z}_3 \end{bmatrix} \in \begin{bmatrix} z_2 \\ -F_s \text{Sign}(z_2) - k_p(z_1 - r) - k_d z_2 - k_i z_3 \\ z_1 - r \end{bmatrix}, \quad (1)$$

with z_1 the position, z_2 the velocity, and z_3 the state of the integrator, respectively. The constant setpoint is denoted by r , and Sign denotes the *set-valued* signum function. We apply the following useful coordinate transformation:

$$\xi = \begin{bmatrix} \sigma \\ \phi \\ v \end{bmatrix} := \begin{bmatrix} -k_i(z_1 - r) \\ -k_p(z_1 - r) - k_i z_3 \\ z_2 \end{bmatrix}, \quad (2)$$

such that the closed-loop dynamics in (1) can be written as

$$\begin{bmatrix} \dot{\sigma} \\ \dot{\phi} \\ \dot{v} \end{bmatrix} \in \begin{bmatrix} -k_i v \\ \sigma - k_p v \\ \phi - F_s \text{Sign}(v) - k_d v \end{bmatrix}. \quad (3)$$

Note that σ is a generalized position, and ϕ is the controller state which contains both the proportional and the integral control action. To reduce the length of the stick periods, see Fig. 1, and decrease settling times accordingly, the controller state ϕ is reset when the system 1) overshoots the setpoint, and 2) enters a stick phase, i.e.,

$$\phi^+ = -\phi, \quad \text{when } \xi \in \{\xi \in \mathbb{R}^3 \mid \phi \sigma \leq 0, \phi v \leq 0\}. \quad (4)$$

This particular reset of the controller state ϕ coincides with a (practically implementable) reset of the integrator state z_3 in (1) as follows:

$$z_3^+ = -z_3 - \frac{k_p}{k_i}(z_1 - r) \quad (5)$$

A formal stability analysis using a recently developed discontinuous Lyapunov function (see [1]) is performed and it is proven that the position z_1 asymptotically converges to the setpoint r , see [2].

3 Illustrative example

A numerical time-stepping simulation on system (1), including reset law (4),(5), is performed to correctly deal with the set-valued nature of the dynamics. The position response and control effort for simulations with a *classical* PID controller, and the proposed reset controller are presented in Fig. 1. The reset controlled system achieves a significant reduction in settling time by circumventing the depletion and refilling process of the integral buffer.

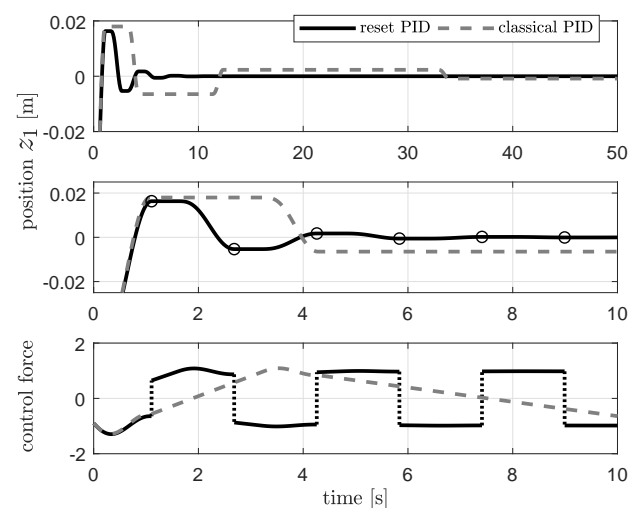


Fig. 1: Position response (top), zoomed view (middle), and corresponding control force (bottom).

References

- [1] A. Bisoffi et al. “Global asymptotic stability of a PID control system with Coulomb friction”, to appear in IEEE-TAC, 2018.
- [2] R. Beerens et al. “Reset integral control for improved settling of motion systems with friction”, submitted to Automatica, 2018.

Symbolic equation extraction from SimScape

Joris Gillis[†], Edward J.G.J. Kikken[‡]

[†] MECO Research Team, Department Mechanical Engineering, KU Leuven

[†] DMMS lab, Flanders Make, Leuven, Belgium

[‡] Flanders Make, Leuven, Belgium

joris.gillis@kuleuven.be, edward.kikken@flandersmake.be

1 Introduction

MATLAB SimScape is a popular equation-based modeling tool, embedded in MATLAB Simulink. While the model and its first order sensitivities can be evaluated numerically within MATLAB or externally via an API, there is no automated way to export the resulting equations themselves.

This abstract presents an open-source tool¹, that extracts equations from SimScape models. The tool supports parametric, time-dependent, time-delayed, nonlinear models, even with if-tests, but not models with a finite state-machine involved (such as the clutch component).

The output is a set of differential algebraic equations (DAE):

$$\begin{cases} \dot{x}(t) &= f(t, x(t), z(t), u(t), p, w(t)) \\ 0 &= g(t, x(t), z(t), u(t), p, w(t)) \end{cases} \quad (1)$$

with t time, x the state vector, z the algebraic variables, u the inputs, p parameters, and w representing a dependence on a time-delayed signal:

$$w(t) = \begin{cases} W(t-T, x(t-T), u(t-T), p) & t \geq T \\ 0 & t < T \end{cases} \quad (2)$$

Besides symbolic descriptions of f, g , and W , the tool provides meta-data for the variables (names).

2 Design

The tool, still in *alpha* stage, involves four steps:

1. C-code generation is performed on the Simulink model.
2. The SimScape part of the C code is parsed.
3. A MATLAB class that implements f, g , and W using CasADi [1] symbols is created.
4. The index of the DAE is optionally reduced with the help of the MATLAB's Symbolic Toolbox.

3 Example

Figure 1 provides a SimScape model view on a driveline consisting of linear and nonlinear parametrized components

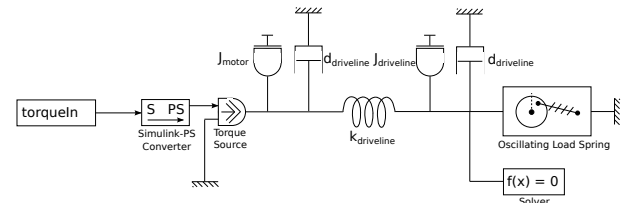


Figure 1: SimScape model

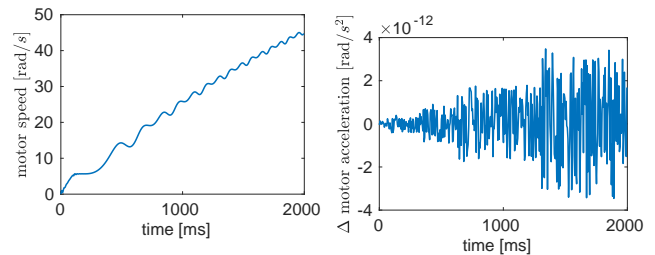


Figure 2: SimScape simulation

Figure 3: Model error

performing motions induced by a torque source.

A numerical validity check was performed. Figure 2 shows a forward simulation of the original SimScape model, integrated with implicit Euler steps by Simulink. Figure 3 shows the error between an evaluation of the extracted model ODE right-hand side f on the simulation trajectory and finite differences on the SimScape model trajectory.

Using the extracted model, dynamic optimization can readily be performed efficiently using algorithmic differentiation, and without the need for Simulink/SimScape.

References

- [1] Joel Andersson. *A General-Purpose Software Framework for Dynamic Optimization*. PhD thesis, Arenberg Doctoral School, KU Leuven, Department of Electrical Engineering (ESAT/SCD) and Optimization in Engineering Center, Kasteelpark Arenberg 10, 3001-Heverlee, Belgium, October 2013.

Acknowledgement. This work has been carried out within the framework of projects Flanders Make ICON: Physical and control co-design of electromechanical drivetrains for machines and vehicles, and KU Leuven-BOF PFV/10/002 Centre of Excellence: Optimization in Engineering (OPTEC).

¹Obtainable from <https://github.com/jgillis/simscape2casadi>

Nonlinear Modeling for Analysis of Directional Drilling Processes

Fahim Shakib¹, Emmanuel Detournay², Nathan van de Wouw^{1,2,3}

¹ Dept. of Mechanical Engineering, Eindhoven, Univ. of Tech., The Netherlands

² Dept. of Civil, Environmental, and Geo- Engineering, Univ. of Minnesota, USA

³ Dept. of Mechanical, Maritime and Materials Engineering, Delft, Univ. of Tech., The Netherlands

Email: m.f.shakib@tue.nl

1 Introduction

Directional drilling allows for the drilling of boreholes with complex shapes, which are needed to reach unconventional reservoirs of oil, gas and mineral resources. Figure 1 shows a sketch of a directional drilling system. The drillstring is a hollow slender pipe with most of it is in tension under its own weight, except for the bottom hole assembly (BHA), which is in compression. The BHA contains several stabilizers ensuring centering of the BHA inside the borehole, a bit penetrating the rock formation and a rotary steerable system (RSS), being a robotic actuator, steering the BHA. In practice, directional drilling often results in spiraled boreholes, see Figure 2 for an illustration. These are unwanted self-excited oscillations in the borehole geometry which negatively influence the drilling process and the borehole quality.

2 Problem Setting & Approach

The previously developed borehole propagation model (BPM) in [1] describes the onset of borehole spiraling through a local stability analysis. However, it is insufficient to predict steady-state borehole spiraling (non-local limit-cycling). In this work, we aim to capture and understand the borehole spiraling phenomenon by extending the current BPM with two essential nonlinearities and analyzing the resulting global dynamics. The first nonlinearity deals with stabilizers that are smaller in diameter than the borehole, and therefore experience unilateral contact with the borehole walls. The second nonlinearity involves a saturation on the bit tilt, where the bit tilt is defined as the orientation difference between the bit and the borehole at the bit.

3 Results

A BPM, incorporating the two aforementioned nonlinearities, is derived for planar (two-dimensional) directional drilling processes [2]. The model can be classified as a delay complementarity system [3]. The delay nature of the resulting model stems from the delayed influence of the borehole geometry on the deformation of the BHA. Complementarity relations are used to describe the unilateral contact of non-ideal stabilizers with the borehole walls and to encompass the saturation on the bit tilt.

Analysis on this model reveals that a particular parameter group controls both the directional capabilities as well as the stability of the responses of directional drilling systems. This group consists of properties of the BHA, the bit and the rock formation. Numerical simulations show the emergence of limit cycles under certain conditions. These limit cycles

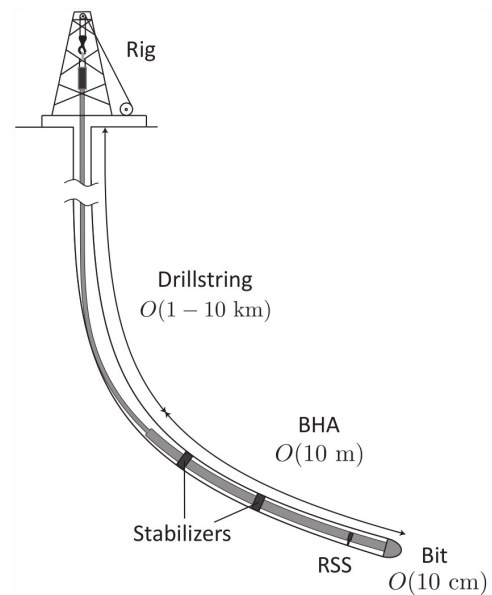


Figure 1: Overview of a directional drilling system.

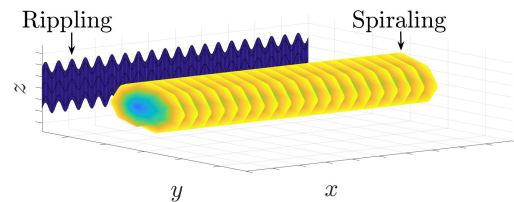


Figure 2: Illustration of borehole spiraling and borehole rippling.

represent borehole rippling, which is a planar equivalent of borehole spiraling. The resulting model thus provides valuable insights in the effects causing borehole rippling.

References

- [1] L. Perneder, J. Marck, E. Detournay, *A Model of Planar Borehole Propagation*, SIAM J. Appl. Math., Vol. 77, Issue 4, pp. 1089–1114, 2017.
- [2] M.F. Shakib, *Nonlinear Modeling for Dynamic Analysis of Directional Drilling Processes*, M.Sc. dissertation, Eindhoven University of Technology, The Netherlands, November 2017.
- [3] J.J.B. Biemond, W. Michiels, N. van de Wouw, *Stability analysis of equilibria of linear delay complementarity systems*, IEEE Control Systems Letters, Vol. 1, Issue 1, pp. 158–163, July 2017.

Clamping Strategies for Belt-Type CVT systems: An Overview

Suraj Prakash, Theo Hofman and Bram de Jager
Eindhoven University of Technology, The Netherlands.

1 Introduction

Continuously Variable Transmissions (CVTs) are devices that are able to provide a continuous range of gear ratios for transmission of power in mechanical systems. Using such a device in a vehicular driveline would enable the engine to be operated at its optimal efficiency points at all times, reducing fuel consumption. Among several ways of realizing a CVT, the pushbelt and chain type CVTs have been prominently used in vehicular applications due to their torque capacity.

Since pushbelt and chain type CVTs are friction-based systems, their actuation entails a trade-off: while sufficient actuation (clamping) forces are required to ensure safe operation, excess clamping forces would result in inefficient operation. Early works on CVT control employed conservative strategies for clamping. In later works, the clamping strategies have received increased attention. This paper presents an overview of the works addressing the clamping force control objective of belt-type CVTs.

2 Clamping force control objective

The ability of a CVT to transmit torque at a certain gear ratio is quantified using the traction coefficient μ . The dependence of μ on the slip ν is illustrated by the traction curve (Fig. 1) where, the slip is defined as,

$$\nu = 1 - \frac{r_s}{r_g} \quad (1)$$

where r_s and r_g are the speed ratio and the geometric ratio. In the macroslip region, the CVT shows unstable be-

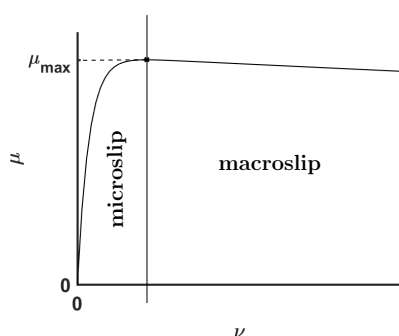


Figure 1: Traction curve

havior and moreover, damage could be caused due to gross-slip. Hence, the microslip region is preferred for safe operation. However, this is maintained by applying relatively high clamping forces which would in-turn result in higher energy losses. The clamping force control objective is to minimize these losses while still ensuring safe functioning of the CVT.

3 Overview of proposed strategies

The minimum clamping force required at either of the pulleys for safe operation is obtained using,

$$F_{min} = \frac{|T| \cos \beta}{2\mu_{max}R} \quad (2)$$

where T is the torque transmitted by the pulley, β and R are the half-wedge angle and running radius of the pulley, respectively. Conventionally, the set points for applied clamping forces are generated by adding safety-margins to F_{min} . However, this strategy is conservative since the safety-margins were deduced accounting for worst-case situations. To enhance efficiency, advanced clamping strategies are pro-

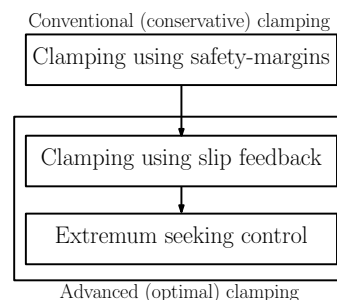


Figure 2: Development of methods for clamping force control

posed for more optimal operation: works such as [1] propose using feedback of slip for clamping force control. This enabled more confidence (more robustness) for operation of the CVT at the optimum (i.e. around the boundary of the micro and macroslip region). Although such a method showed good results, it required the use of an additional sensor (to those present in a conventional CVT) for the measurement of slip. This could be an infeasible in automotive applications due to cost considerations. To overcome this limitation, a strategy is proposed such as in [2] which uses the extremum seeking control (ESC) method. An inherent quality of this method allows for "sensor-free" optimization. These developments are presented in Fig. 2.

4 Conclusion and future work

In this paper, a broad overview of the works on the clamping force control objective was presented.

The present ESC designs in [2] are evaluated only over the NEDC driving cycle. For future work, performance of the designs over more dynamic driving cycles can be analyzed. Furthermore, advancements made in control theory on the ESC method can be applied to improve the convergence times of the present designs.

References

- [1] B. Bensen, "Efficiency optimization of the push-belt CVT by variator slip control." Ph.D. dissertation, Eindhoven University of Technology, 2006.
- [2] S. van der Meulen, "High-performance control of continuously variable transmissions," Ph.D. dissertation, Eindhoven University of Technology, 2010.

Capabilities of Nonlinear Iterative Learning Control with ROFALT

Armin Steinhauser and Jan Swevers

MECO Research Team, Department Mechanical Engineering, KU Leuven

DMMS lab, Flanders Make

Celestijnenlaan 300B, 3001 Heverlee, Belgium

Email: `firstname.lastname@kuleuven.be`

1 Introduction

While iterative learning control (ILC) was intensely researched for linear systems, the available approaches will yield suboptimal performance for nonlinear systems. Crucial knowledge of nonlinear effects is disregarded and nonlinearities might only be captured by an unnecessarily large uncertainty bound, resulting in a conservative controller design. A fully generic approach for nonlinear systems was first presented in [1], where it is shown that norm-optimal ILC can be interpreted as a two-step procedure: At first computing an explicit model correction and subsequently inverting the corrected system dynamics as shown in Fig. 1. Within this framework, no restrictions are imposed on the system structure or its complexity and both steps are formulated as optimization problems, which additionally allows to consider actuator limits or dynamic constraints.

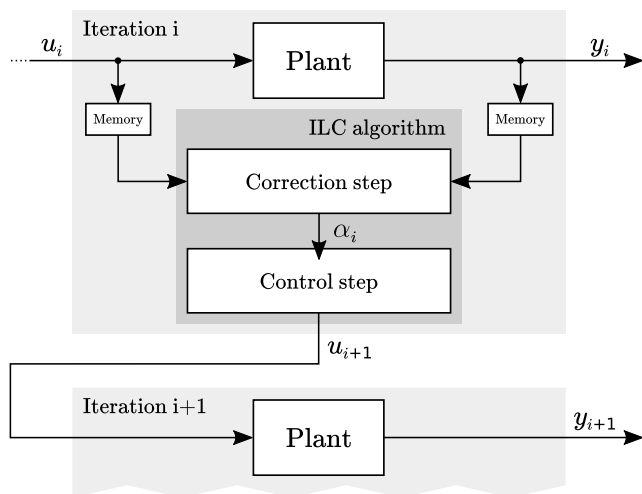


Figure 1: Illustration of the optimization-based two-step iterative learning control algorithm

2 ROFALT Software

Following the approach of a model-based two-step algorithm, a novel MATLAB tool called ROFALT was recently introduced [2]. It implements the optimization-based approach to nonlinear ILC and represents a universal nonlinear ILC package that is freely available¹ and open-source. The

¹<https://gitlab.mech.kuleuven.be/meco-software/rofalt/>

main purpose of its development is to enable a controller design with just a handful of simple commands, where the trade-off between convergence speed and robustness can easily be adjusted. ROFALT accepts arbitrary nonlinear models and allows profound adaptations, such that specific objectives and constraints can be taken into account.

3 Application

To explore the capabilities of nonlinear ILC and the ease of use of ROFALT we consider a simulation case of an overhead crane. Besides a classical tracking problem with a predefined trajectory we also investigate the iterative learning of an energy-optimal point-to-point motion. Both parametric and nonparametric model correction methods are compared. While parametric corrections seem appealing due to their physical interpretation and independence of the task, it is shown that they typically result in inferior performance compared to nonparametric corrections. These in turn represent a more generic approach and yield low converged errors at the expense of convergence speed and validity only for the considered task. Furthermore, different strategies to increase convergence speed and robustness—e.g. unequal weighting of objective terms, penalizing or constraining correction updates, etc.—are analysed.

Acknowledgements

This work has been carried out within the framework of Flanders Make's ICON project 'RoFaLC' (Robust and Fast Learning Control, IWT.150531) funded by the agency Flanders Innovation & Entrepreneurship (VLAIO) and Flanders Make. This work also benefits from the project G0A6917N of the Research Foundation - Flanders (FWO - Flanders), the project G.0915.14 of the Research Foundation - Flanders (FWO - Flanders) and KU Leuven-BOF PFV/10/002 Centre of Excellence: Optimization in Engineering (OPTEC).

References

- [1] M. Volckaert, J. Swevers, and M. Diehl, "A two step optimization based iterative learning control algorithm," in *Proc. ASME 2010 Dynamic Systems and Control Conf.*, Cambridge, MA, 2010.
- [2] A. Steinhauser, T. D. Son, E. Hostens, and J. Swevers, "RoFaLT: An Optimization-based Learning Control Tool for Nonlinear Systems," *15th IEEE International Workshop on Advanced Motion Control (AMC)*, Tokyo, Japan, 9–11 March 2018.

Learning Control in Practice: Novel Paradigms for Industrial Applications

Jeroen Willems[†], Erik Hostens[†], Bruno Depraetere[†], Armin Steinhauser* and Jan Swevers*

[†] Flanders Make, Oude Diestersebaan 133, 3920 Lommel, Belgium

* MECO Research Team, Department of Mechanical Engineering, KU Leuven, Belgium

* DMMS lab, Flanders Make, Leuven, Belgium

jeroen.willems@flandersmake.be

1 Introduction

Iterative learning control (ILC) for linear systems is well elaborated by both theoretical proofs and experimental validations [1]. In case of nonlinear system dynamics, however, the restriction to linear systems often yields a suboptimal control performance. The expansion of the idea of ILC to nonlinear systems was presented in [2]. Following this idea, [3] introduces a MATLAB toolbox called ROFALT, which stands for *robust and fast learning tool*. The main purpose of this tool is to close the gap between the theory of nonlinear ILC and its application. Although the internal working of ROFALT meets the requirement of optimality also for nonlinear systems, a number of issues are still an obstruction for using it in practice.

1. *Safety*: The behaviour of learning control can be unpredictable because of model-plant mismatch and nonlinearity of the system. Most applications in industry need guarantees for not crossing boundaries, to avoid unsafe situations or damage. The lack hereof is a major cause of distrust in learning control.
2. *Learning similar tasks*: A machine, even if its operation is repetitive, is mostly intended for customized use for different configurations or tasks. In order to minimize the calibration time, fast re-learning or re-using of information for similar tasks is required.
3. *Computational effort*: ROFALT solves non-linear optimization problems, for which the required computational effort might be too high for basic embedded hardware.

2 Paradigms for learning control in practice

Three paradigms to deal with the application of ILC in practice are developed. The algorithms are illustrated on an experimental setup: a non-linear electromechanical slider-crank system. The control goal is to perform one revolution of the crank while minimizing the energy consumption. The problem is subject to a set of constraints on the timing of the slider displacement.

1. **Safe learning** offers a robust solution by starting the control actions with conservative margins, which are gradually decreased as more information about the variation of the system is learned over the iterations. The application of safe learning leads to a balanced tradeoff between safety (constraint satisfaction) and performance (minimal

energy consumption), when the system is subject to exogenous disturbances.

2. **Shared learning** can be applied to simultaneously learn optimal control actions for a wide range of configurations, thereby speeding up the calibration process significantly. The key idea is to employ a multidimensional interpolation algorithm. In Figure 1, it can be seen that the use of shared learning drastically reduces the amount of iterations required to converge by re-using data from previous tasks. Every ten iterations, a new task is considered.

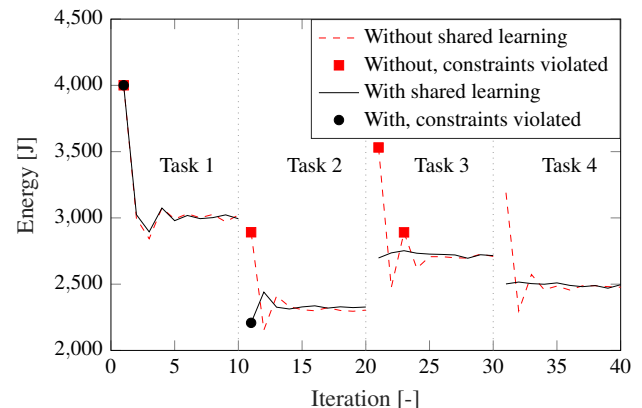


Figure 1: Energy consumption with and without shared learning.

3. **Simple learning** is the translation of the original full optimization problem into a simplified relation between input and output parameters, which can be used in an on-line, rule-based strategy. As such, learning control is possible, even on lower-level controllers, and is also more in line with control strategies that are widely used in industry. Additionally, the use of simple learning can improve the predictability of the online behaviour.

References

- [1] D. A. Bristow, M. Tharayil, and A. G. Alleyne, 'A survey of iterative learning control', IEEE Control Systems 26.3, 2006.
- [2] M. Volckaert, M. Diehl, and J. Swevers, 'A two step optimization based iterative learning control algorithm.' Dynamic Systems and Control Conference. 2010.
- [3] A. Steinhauser, T. Son, E. Hostens, J. Swevers, 'RoFaLT: An Optimization-based Learning Control Tool for Nonlinear Systems', Proceedings of the 15th International Workshop on Advanced Motion Control, Tokyo, 2018. This work has been carried out within the framework of Flanders Make's ICON project 'RoFaLC' (Robust and Fast Learning Control, IWT.150531) funded by the agency Flanders Innovation & Entrepreneurship (VLAIO) and Flanders Make. This work also benefits from the projects G0A6917N and G.0915.14 of the Research Foundation - Flanders (FWO) and KU Leuven-BOF PFV/10/002 Centre of Excellence: Optimization in Engineering (OPTEC). Flanders Make is the Flemish strategic research centre for the manufacturing industry.

Passivity-based control of gradient systems.

L.P. Borja*, J.M.A. Scherpen* and A.J. van der Schaft**.

*Nijenborgh 4, **Nijenborgh 9, 9747 AG Groningen, The Netherlands.

e-mail: l.p.borja.rosales [j.m.a.scherpen] [a.j.van.der.schaft]@rug.nl

1 Abstract

Since its origin more than two decades ago, Passivity-based control (PBC) has attracted the attention of many researchers and currently, it is one of the most popular controller design techniques for nonlinear systems. The basic idea of PBC is to design a controller that accomplishes the control task by rendering the system *passive* with respect to a desired *energy function* and by injecting damping into the closed-loop system [1]. In general, PBC techniques can be classified in two main groups, namely,

- The techniques that select the structure of the closed-loop energy function *a priori*, and subsequently design a controller that renders this function non-increasing with respect to the equilibrium point.
- The techniques that select a desired closed-loop, where the family of possible energy functions is characterized by a partial differential equation (PDE).

This work is devoted to the stabilization of a particular class of systems, *i.e.*, the so-called *gradient systems*, by means of PBC techniques. These systems are not necessarily passive, therefore, a first step towards our goal is to establish the conditions under which a gradient system has the aforementioned property, and thus explore the applicability of different PBC techniques.

In local coordinates x for some n -dimensional state space manifold \mathcal{X} , the dynamics of a gradient system is given by¹ [2]

$$G(x)\dot{x} = -\nabla P(x) + \nabla h(x)u, \quad (1)$$

where $u \in \mathbb{R}^m$ is the input vector, the matrix $G(x) = G^\top(x)$ is invertible and $h : \mathcal{X} \rightarrow \mathbb{R}^m$, $P : \mathcal{X} \rightarrow \mathbb{R}$ are the *potential functions*. Accordingly, in order to design a PBC that stabilizes² system (1), we adopt two different approaches:

- We identify under which conditions system (1) defines a passive mapping from u to a *passive output* $y \in \mathbb{R}^m$. Moreover, when this passivity condition is fulfilled, there exists a storage function $S : \mathcal{X} \rightarrow \mathbb{R}$ satisfying the so-called *passive inequality* given by

$$\dot{S} \leq u^\top y.$$

¹where $\nabla P(x) = [\frac{\partial P(x)}{\partial x_1}, \dots, \frac{\partial P(x)}{\partial x_n}]^\top$ and $\nabla h(x)$ denotes the Jacobian matrix.

²at a desired equilibrium point.

Therefore, we propose a control law such that the closed-loop storage function takes the form

$$S_d(x) = S(x) + \frac{1}{2}\|\gamma(x) + \kappa\|_{K_I}^2 + \frac{1}{2}\|y\|_{K_D}^2,$$

where the gains K_I, K_D are constant, symmetric and positive definite matrices of appropriate dimension, $\kappa \in \mathbb{R}^m$ is a *free* constant vector and $\gamma : \mathcal{X} \rightarrow \mathbb{R}^m$ satisfies $\dot{\gamma} = y$. In this case, if the desired equilibrium is an isolated minimum of $S_d(x)$, then we can claim stability of the equilibrium point [3].

- We obviate the passivity condition over system (1), but alternatively we impose a desired structure to the closed-loop system of the form

$$G_d(x)\dot{x} = -\nabla P_d(x)$$

such that $G_d(x) = G_d^\top(x)$ is invertible, $P_d : \mathcal{X} \rightarrow \mathbb{R}$ is the desired potential function and there exists a closed-loop storage function $S_d : \mathcal{X} \rightarrow \mathbb{R}$ satisfying

$$\dot{S}_d \leq 0, \quad \arg \min\{S_d\} = x_*,$$

where $x_* \in \mathcal{X}$ denotes the desired equilibrium.

In both cases, the closed-loop storage function $S_d(x)$ qualifies as a Lyapunov function and a further analysis is carried out to determine *asymptotic stability* of the equilibrium point.

References

- [1] Ortega, R., Van Der Schaft, A. J., Mareels, I., and Maschke, B. (2001). Putting energy back in control. *IEEE Control Systems*, 21(2), 18-33.
- [2] van der Schaft, A. J. (2011). On the relation between port-Hamiltonian and gradient systems. *IFAC Proceedings Volumes*, 44(1), 3321-3326.
- [3] Zhang, M., Borja, P., Ortega, R., Liu, Z., and Su, H. (2017). PID Passivity-Based Control of Port-Hamiltonian Systems. *IEEE Transactions on Automatic Control*.

Virtual differential passivity based control of mechanical systems in the port-Hamiltonian framework

Rodolfo Reyes-Báez, Arjan van der Schaft, Bayu Jayawardhana

Jan C. Willems Center for Systems and Control, Faculty of Science and Engineering, University of Groningen
 {r.reyes-baez, a.j.van.der.schaft, b.jayawardhana}@rug.nl

1 Introduction

Based on recent advances in contraction methods in systems and control, we propose the virtual differential passivity based control (v-dPBC) technique. This is a constructive method that combines the concept of virtual systems and of differential passivity. The method is used to solve the tracking problem in mechanical port-Hamiltonian systems.

2 Differential passivity and virtual systems

Let Σ be a control system with state space \mathcal{X} of dimension N and affine in the input $u \in \mathcal{U}$,

$$\Sigma_u : \begin{cases} \dot{x} = f(x) + \sum_{i=1}^n g_i(x)u_i, \\ y = h(x), \end{cases} \quad y \in \mathcal{Y}. \quad (1)$$

Definition 1 A prolonged system of (1) corresponds to the system $\Sigma_u^{\delta\Sigma_u}$ formed by Σ_u and is variational system

$$\delta\Sigma_u : \begin{cases} \delta\dot{x} = \frac{\partial f}{\partial x}(x)\delta x + \sum_{i=1}^n u_i \frac{\partial g_i}{\partial x}(x)\delta x_i + \sum_{i=1}^n g_i(x)\delta u_i, \\ \delta y = \frac{\partial h}{\partial x}(x)\delta x, \end{cases} \quad (2)$$

with $(u, \delta u) \in T\mathcal{U}$, $(x, \delta x) \in T\mathcal{X}$, and $(y, \delta y) \in T\mathcal{Y}$.

The standard definition of passivity of system (1) is naturally extended to the context of differential Lyapunov framework for contraction analysis ([2]) in the following definition.

Definition 2 ([1]) Consider system $\Sigma_u^{\delta\Sigma_u}$. If there exist a differential storage function $W : T\mathcal{X} \rightarrow \mathbb{R}_{\geq 0}$ satisfying

$$\frac{dW}{dt}(x, \delta x) \leq \delta y^\top \delta u, \quad (3)$$

for all $x, \delta x, u, \delta u$. Then, system Σ_u is differentially passive.

By means of the so-called virtual control systems, the concept of differential passivity can be generalized. To this end, consider the following definitions.

Definition 3 ([3]) A virtual control system for system (1), in the state $x_v \in \mathcal{X}$ and output $y_v \in \mathcal{Y}$, is defined as the system

$$\begin{cases} \dot{x}_v = \Gamma_v(x_v, x, u), \\ y_v = h_v(x_v, x), \end{cases} \quad (4)$$

parametrized by $x \in \mathcal{X}$, with $h_v : \mathcal{X} \times \mathcal{X} \times \mathbb{R}_{\geq 0} \rightarrow \mathcal{Y}$ and $\Gamma : \mathcal{X} \times \mathcal{X} \times \mathcal{U} \times \mathbb{R}_{\geq 0} \rightarrow T\mathcal{X}$ satisfying

$$\begin{cases} \Gamma(x, x, u)_v = f(x) + G(x)u, \\ h_v(x, x) = h(x), \end{cases} \quad \forall u, \forall t \geq t_0. \quad (5)$$

It follows that any solution $x(t)$ of (1), for a certain input $u \in \mathcal{U}$, generates a solution $x_v(t)$ to system (4). However, *not* every solution $x_v(t)$, corresponds to a solution of the actual system (2). Thus, for any curve $x(t)$, we may consider the time-varying system with state x_v .

Definition 4 ([4]) If system (4) is differentially passive. Then, system (1) is said to be virtually differentially passive.

3 Virtual differential passivity based control

We can now introduce the v-dPBC technique. The design method is divided in three main steps:

1. Design the virtual control system (4) for system (1).
2. Design the feedback $u = \eta(x_v, x, t) + \omega$ for (4) such that the closed-loop virtual system is differentially passive for the input-output pair $(\delta y_v, \delta \omega)$ and has a desired trajectory $x_d(t)$ as steady-state solution.
3. Define the controller for system (1) as $u = \eta(x, x, t)$. Then all closed-loop system trajectories will converge to $x_d(t)$, when the external input $\omega = 0$.

4 Tracking in mechanical pH systems

With above methodology, the trajectory tracking problem is solved as in [4] using a virtual mechanical system.

References

- [1] A.J van der Schaft. "On differential passivity" IFAC Proceedings Volumes 46.23 (2013): 21-25.
- [2] F. Forni and R. Sepulchre, "A differential Lyapunov framework for contraction analysis", IEEE Transaction on Automatic Control 59.3 (2014): 614-628.
- [3] W. Wang and J.J. Jacques Slotine, "On partial contraction analysis for coupled nonlinear oscillators", Biological Cybernetics, 92.1 (2005): 38-53.
- [4] R. Reyes-Báez, A.J. van der Schaft and B. Jayawardhana, "Virtual Differential Passivity based Control for Tracking of Flexible-joints Robots", Accepted in Workshop on Lagrangian and Hamiltonian Methods for Nonlinear Control - LHMNC, 2018.

Projective Contraction of Switching Systems

Guillaume Berger

Université Catholique de Louvain, Belgium
Email: guillaume.berger@uclouvain.be

Raphaël M. Jungers

Université Catholique de Louvain, Belgium
Email: raphael.jungers@uclouvain.be

Fulvio Forni

University of Cambridge, United Kingdom
Email: f.forni@eng.cam.ac.uk

Rodolphe Sepulchre

University of Cambridge, United Kingdom
Email: r.sepulchre@eng.cam.ac.uk

1 Introduction

An important feature of dynamical systems is the contraction of the trajectories *in the projective space*: given a discrete-time dynamical system $x(t+1) = f(x(t))$, under what conditions do two trajectories $x(t) \in \mathbb{R}^n$ and $y(t) \in \mathbb{R}^n$ satisfy $\lim_{t \rightarrow \infty} \|\hat{x}(t) - \hat{y}(t)\| = 0$, where $\hat{v} = v/\|v\|$ (projection on the unit ball)? The question of *projective contraction* of the trajectories is important for applications where one is more interested in the *orientation* of $x(t)$ along the trajectories of the systems than by the value (or the norm) of $x(t)$ itself: e.g., cooperative and competitive systems, attitude control systems, and modeling and control of chemistry and biological systems (see [1], [2] and references therein).

For LTI systems $x(t+1) = Ax(t)$, projective contraction is well understood. Geometrically speaking, projective contraction is a synonym of cone invariance, and conditions are known to go from cone invariance to projective contraction. This is the essence of Perron-Frobenius theory.

This work is a continuation of [3], where the notion of path-complete positivity for switching systems is introduced. In a nutshell, a switching linear system¹ $x(t+1) = A_\sigma x(t)$ is path-complete positive with respect to the set of cones $\{\mathcal{K}_1, \dots, \mathcal{K}_M\}$ if for every finite word $\sigma_1 \sigma_2 \dots \sigma_\ell \in \Sigma^*$, there exists a sequence $i_1 i_2 \dots i_\ell i_{\ell+1}$ such that $A_{\sigma_k}(\mathcal{K}_{i_k} \setminus \{0\}) \subseteq \text{int } \mathcal{K}_{i_{k+1}}$ for every $1 \leq k \leq \ell$ (see Figure 1 for an illustration). It is also proved that path-complete positivity is a sufficient condition for the switching system to be contracting in the projective space.

Next to this, the authors propose an algorithm to compute a *common contracting cone* \mathcal{K} for the family $\{A_\sigma\}$ (i.e., $\{A_\sigma\}$ is path-complete positive for $\{\mathcal{K}\}$) or conclude that no such cone exists. The algorithm relies on two assumptions: the set $\{A_\sigma\}$ must be *irreducible*, meaning that there exists no non-trivial linear subspace that is invariant for each A_σ ; and each A_σ must be *invertible*.

2 Our contribution

In the present work, we show how to relax the second assumption (invertibility) in the algorithm of [3]. Therefore,

¹A switching system is defined by a finite set of matrices $\{A_\sigma : \mathbb{R}^n \rightarrow \mathbb{R}^n\}$ where the index σ belongs to the finite set Σ . At each discrete time $t \geq 0$, $x(t+1)$ is the image of $x(t)$ by A_σ where σ can take any value in Σ .

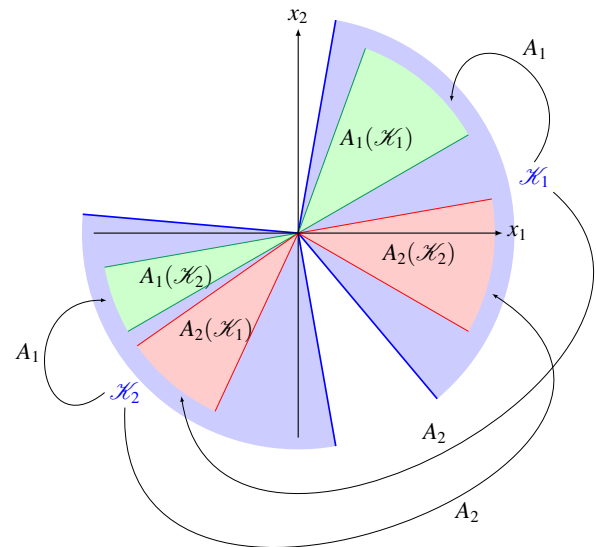


Figure 1: If A_1 and A_2 are linear operators that map the cones \mathcal{K}_1 and \mathcal{K}_2 as shown on the figure above, then the switching linear system defined by $\{A_1, A_2\}$ is path-complete positive w.r.t. the set of cones $\{\mathcal{K}_1, \mathcal{K}_2\}$.

we introduce a relaxation of the contractiveness property of a cone: a cone is *pseudocontracting* for the family $\{A_\sigma\}$ if $A_\sigma(\mathcal{K} \setminus \{0\}) \subseteq \text{ri}(\mathcal{K} \cap \mathcal{H}_\sigma)$ (*relative interior* of $\mathcal{K} \cap \mathcal{H}_\sigma$) where $\mathcal{H}_\sigma = \text{Im}(A_\sigma)$. We show that the existence of a pseudocontracting cone or a path-complete pseudocontracting set of cones is sufficient to guarantee the projective contraction of the trajectories of the switching system. We show how the algorithm of [3] can be modified to compute pseudocontracting cones (or conclude that no such cone exists), dropping the assumption that $\{A_\sigma\}$ contains only invertible matrices, and thus allowing to deal with more general switching linear systems.

References

- [1] B. K. Ghosh, C. F. Martin, “Homogeneous dynamical systems theory.” *IEEE Transactions on Automatic Control*, 47(3), 462–472, 2002.
- [2] D. Angeli, E. D. Sontag, “Monotone control systems.” *IEEE Transactions on Automatic Control*, 48(10), 1684–1698, 2003.
- [3] F. Forni, R. M. Jungers, R. Sepulchre, “Path-complete positivity of switching systems.” *IFAC-PapersOnLine*, 50(1), 4558–4563, 2017.

Nonlinear trajectory tracking via incremental passivity

Chengshuai Wu ^{a,b}, Arjan van der Schaft ^a, and Jian Chen ^b

^a Johann Bernoulli Institute for Mathematics and Computer Science, University of Groningen
P.O. Box 407, 9700 AK Groningen, the Netherlands

^b Institute of Cyber-Systems & Control, Zhejiang University
Hangzhou, 310027, China

Email: cwu@zju.edu.cn, a.j.van.der.schaft@rug.nl, jchen@zju.edu.cn

1 Introduction

Trajectory tracking for nonlinear systems is one of the most important research topics in control and system theory. Previous results mainly focus on nonlinear systems of particular form, for example, chains of integrators, or strict-feedback systems. In order to enrich the existing results on nonlinear trajectory tracking, we study a class of nonlinear systems that are not required to be in certain form, but instead, we assume that they possess the property of incremental passivity [1]. This is an extension of the conventional passivity concept and it describes the incremental stability of systems with respect to its input-output relation.

In this work, the incremental passivity of the studied system is specified by a condition given in [2]. It is shown that for this class of nonlinear systems, the error dynamics with respect to a desired trajectory can be obtained formulated in port-Hamiltonian form, which facilitates the tracking control design. A tracking controller is first developed in the case that both the desired trajectory and its velocity are known. Next, the robust tracking problem is studied when the velocity of the desired trajectory is unknown. An appealing feature of both methods is that they do not rely on nonlinearity cancellation, or on high-gain feedback.

2 Problem Formulation

Consider the following nonautonomous nonlinear system

$$\dot{x} = f(x, t) + Gu \quad (1)$$

where $x \in \mathbb{R}^n$, $u \in \mathbb{R}^m$, and $n > m$. The mapping $f: \mathbb{R}^n \times \mathbb{R}_+ \rightarrow \mathbb{R}^n$ is continuous in t and C^1 in x , and $G \in \mathbb{R}^{n \times m}$ is a constant matrix of full rank.

Assume that $x_d(t) \in \mathbb{R}^n$ is a desired trajectory for (1). As a necessary condition, $x_d(t)$ should be a solution of (1), which means that there exists $u_d(t)$ such that

$$\dot{x}_d = f(x_d, t) + Gu_d(t). \quad (2)$$

The incremental passivity of (1) is ensured by the following assumption.

Assumption 1: For system (1), there exists a constant symmetric positive definite matrix $P \in \mathbb{R}^{n \times n}$, such that the following condition holds

$$\frac{\partial f}{\partial x}(x, t)P + P \frac{\partial^T f}{\partial x}(x, t) \leq 0. \quad (3)$$

Throughout the work, it is assumed that G and P are known. The control objective is to design a state-feedback law for system (1) to asymptotically track the desired trajectory $x_d(t)$ with/without the information of $u_d(t)$. Note from (2) that the unknown $u_d(t)$ results in the fact that \dot{x}_d is unknown, which is usually the case in applications.

3 Main results

We present two state feedback tracking controllers (a continuous and a discontinuous one) for (1) such that a desired trajectory x_d with unknown velocity, i.e., \dot{x}_d , can be asymptotically tracked. The continuous controller requires extra information of $f(x, t)$ and utilizes a dynamic state-feedback method which is related to an online estimation for \dot{x}_d . As a static state-feedback law, the discontinuous controller is based on the sliding mode method. In both cases, some mild assumptions are made regarding the boundedness of the desired trajectory. The asymptotic tracking result is guaranteed by a zero-state detectability condition [3]. Furthermore, the proposed methods are validated on a nonlinear spring-mass-damper system.

References

- [1] A. van der Schaft, “ L_2 -Gain and Passivity Techniques in Nonlinear Control,” Springer, 2017.
- [2] A. Pavlov, and L. Marconi, “Incremental passivity and output regulation,” *Systems & Control Letters*, 57(5), 400-409, 2008.
- [3] K. Fujimoto, K. Sakurama, and T. Sugie, (2003). “Trajectory tracking control of port-controlled Hamiltonian systems via generalized canonical transformations”, *Automatica*, 39(12), 2059-2069, 2003.

Modeling and Localized Feedforward Control of Thermal Deformations Induced by a Moving Heat Load

D.P.M. van den Hurk¹
d.p.m.v.d.hurk@tue.nl

S. Weiland¹
s.weiland@tue.nl

K. van Berkel²
koos.van.berkel@asml.com

¹Department of Electrical Engineering, Eindhoven University of Technology
P.O. Box 513, 5600 MB Eindhoven, The Netherlands

² ASML Netherlands B.V., Veldhoven, The Netherlands

1 Background

In high-tech machinery, changes in thermoelasticity of materials and components are often an undesirable side effect which is due to the operation of the machine. This is especially important for optical lithography equipment, where accuracies in the order of nanometers are required to meet customer demands. In the optical lithography process, a wafer is exposed by a light-source that images a chip pattern onto it. The light used for the exposure adds a significant thermal load to the wafer which causes it to heat up. This effect, called wafer heating, ultimately results in deformations of the wafer which reduce performance of the lithography tool in terms of properties as overlay and focus [1][2]. With increasing source powers and performance requirements for next generation lithography tools, this effect is becoming ever more important.

2 Problem description

In this presentation we consider the modeling and control of the thermal induced deformations of a cross-section of the wafer, which is modeled as a beam. The control inputs are forces, in- and out-of-plane, supplied by a high number of actuators which are located below the beam. The complexity of this problem mainly lies in the spatio-temporal nature of the heat load and area of interest (AOI), which in this case are equal. In the lithography process, only a small section of the wafer is exposed at any given time and only deformations in this AOI need to be minimal. Additionally, the high number of control inputs further increases complexity.

3 Wafer Heating Model

For prediction of the induced deformations, quasi-stationary thermoelasticity is considered. This is a valid simplification, as the difference in time scales of both processes, thermal diffusion τ_d and mechanical elasticity τ_e , is so large, e.g.

$$\frac{\tau_d}{\tau_e} = \frac{\rho c_p \sqrt{\frac{\rho}{2\mu + \lambda}}}{\kappa} L > 10^8. \quad (1)$$

This model is then solved using the finite element method

(FEM) to give accurate temperature and deformation profiles.

4 Localized Feedforward Control

The control objective is to compute the optimal actuator forces $F_{act}(x, t)$, which minimize the worst case deformations of the wafer in the AOI, as a result of thermal induced deformations $d_{th}(x, t)$. This is achieved by the proposed controller using indicator functions to localize the problem to the AOI and relevant actuators. The effect each actuator has on the deformations of the beam is stored in $S(x, t)$. Relevant actuators are then those which have an effect in the AOI. This way a distributed controller is created which reduces the computational complexity of the problem significantly. Finally, the controller solves the constrained optimization problem,

$$\begin{aligned} \min_{F_{act}(x,t)} & \|\beta(t)(d_{th}(x,t) + S(x,t)F_{act}(x,t))\|_{\infty} \\ \text{s.t.} & F_{min} \leq F_{act}(x,t) \leq F_{max}, \end{aligned}$$

pointwise in time, to determine optimal actuator forces in x- and y-direction which are then applied in feedforward. Solving this problem over the length of the beam, gives the results shown in Figure 1.

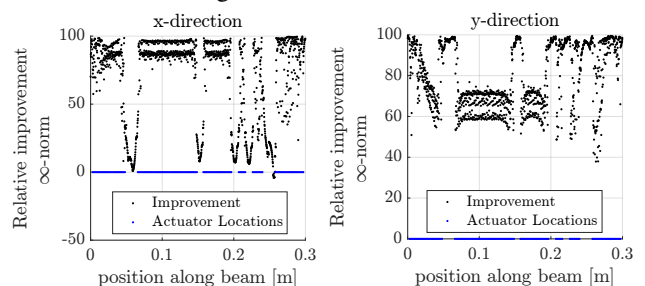


Figure 1: Relative improvement of the ∞ -norm when optimizing deformations in x- and y-direction simultaneously.

References

- [1] L. Subramany et al., Analysis of wafer heating in 14nm duv layers, pp. 9778 9778 7, 2016.
- [2] P. Kochersperger, Overlay correction by reducing wafer slipping after alignment, Patent US 20 070 165 357 A1.

Ten years of control for nuclear fusion in the Netherlands

Marco de Baar

Fusion energy, Dutch Institute For Fundamental Energy Research
 Mechanical Engineering - Control Systems Technology group, Eindhoven University of Technology
 DIFFER, PO Box 6336, 5600 HH, Eindhoven, NL
 M.R.deBaar@diffier.nl

1 Introduction

Last year August marked the 10 year anniversary of the birth of the control for nuclear fusion programme in the Netherlands. The control program was set-up as a collaboration between the Control Systems Technology group at the Eindhoven University of Technology and the FOM institute for plasma physics (now DIFFER). This presentation gives an overview of the results achieved in the past 10 years and a vision on the control programme for the coming years.

2 What is nuclear fusion?

In a nuclear fusion reactor (see Fig. 1) hydrogen isotopes are fused to produce helium and a neutron. This reaction runs at temperatures in excess of 150 million Kelvin as a consequence of which the hydrogen atoms are ionised. The ionised fuel is confined using magnetic fields. The magnetically confined fuel (a.k.a. the plasma) is unstable due to magnetohydrodynamic instabilities and underperforming due to turbulent transport of heat and particles.

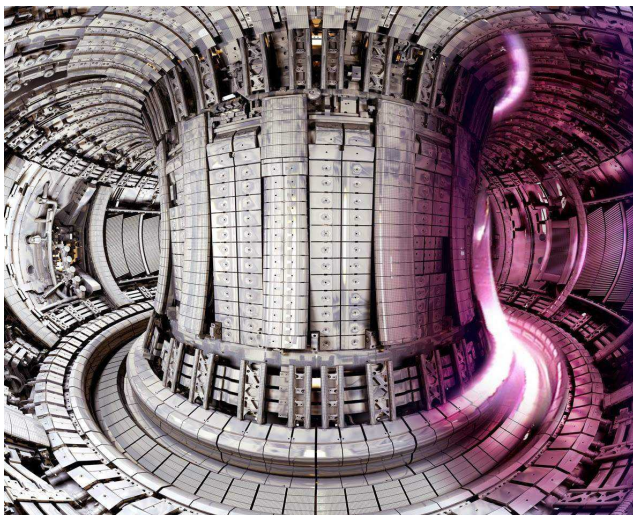


Fig. 1: Interior of the Joint European Tokamak (JET) currently the largest fusion device operated in the world (source: EUROfusion)

3 Control challenges

Active control is used to shape and position the plasma column, to improve the performance of the plasma (that is to

suppress the turbulent transport), and the stability of the plasma (that is to actively reject the magnetohydrodynamic instabilities). For this purpose a novel control system is developed known as the in-line electron cyclotron emission system, which allows simultaneously measuring and actuation of magnetohydrodynamic instabilities. This system is shown in Fig. 2. In addition, the exhaust of heat and particles must be controlled to a level that is tolerable for the first wall of the reactor. In this presentation, I will first introduce nuclear fusion and discuss the main device for the confinement of nuclear fusion plasmas, the tokamak. Then I will introduce the MHD stability and turbulent transport of heat and particles. Finally, I will show in some detail the design of novel sensors, models, and actuators for these control tasks.

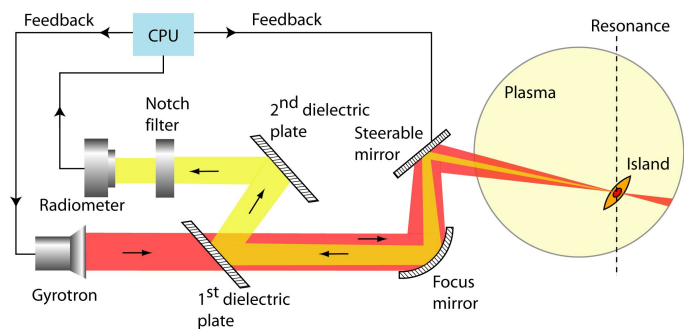


Fig. 2: Schematic overview of the in-line electron cyclotron emission - electron cyclotron resonance heating control system. The yellow beam gives the measurement signal of a few nanowatts, whereas the red beam is the microwave heating of one megawatt. The 'Notch filter' blocks the stray radiation such that both the actuation and the measurement can be performed using the same path. In other words, microwave radiation is deposited at the same location as it is being measured.

4 Acknowledgements

This work was only possible because of my excellent staff Federico Felici and my (former) PhD students in chronological order: Bart Hennen, Gert Witvoet, Gillis Hommen, Menno Lauret, Morten Lennholm, Matthijs van Berkel, Bert Maljaars, Thomas Blanken, Timo Ravensbergen.

Model-based control of reactive systems using extent-based LPV models

C.S. Méndez-Blanco, A. Márquez-Ruiz, L. Özkan
Control Systems Group, Eindhoven University
email: {c.s.mendez.blanco, a.marquez.ruiz, l.ozkan}@tue.nl

1 Introduction

The use of rigorous process models for process design and optimization in an offline way has been well established [2]. The use of such models for online model-based operation is still very limited. Most industrial chemical processes are operated at steady-state using a linear time-invariant (LTI) model, linearizing it around a particular operating point. However, this particular implementation is not flexible if a set point change is required during the operation, and it cannot handle changes in the chemical kinetics nonlinear behavior. This paper addresses the transformation of the general nonlinear model of a continuous stirred-tank reactor (CSTR) to a linear parameter-varying (LPV) representation, and presents a brief example using a linear quadratic regulator (LQR) to control concentrations of the species and process temperature.

2 Approach

Consider the mole and energy balance equations for a homogeneous reactive system with S species, R independent reactions, ι independent inlet flows and one outlet flow, given by:

$$\begin{bmatrix} \dot{n}(t) \\ \dot{T}(t) \end{bmatrix} = \begin{bmatrix} V(t)N^T r(t) + X_{in}F_{in}(t) - \theta(t)n(t) \\ F_{in}(t)\alpha(t) - \theta(t)T(t) - \beta(t)V(t)r(t) + \gamma(t)Q_{in} \end{bmatrix} \quad (1)$$

with $\theta = \frac{F_{out}(t)}{m(t)}$, $\alpha = \frac{C_{pin}T_{in}}{m(t)C_{pmix}(t)}$, $\beta = \frac{\Delta H_f^\circ N^T}{m(t)C_{pmix}(t)}$, $\gamma = \frac{1}{m(t)C_{pmix}(t)}$ and initial conditions $n(0) = n_0$ and $T(0) = T_0$

where T_{in} and T are the inlet and mixture temperature, ΔH_f° is the vector of standard heat of formation; Q_{in} is the heat duty, C_{pin} and C_{pmix} are the inlet and mixture heat capacity, respectively; n is the vector of moles, V is the reaction mixture volume; r is the reaction kinetics vector; F_{in} and F_{out} are the inlet and outlet mass flows; m is the reacting mixture mass; N is the stoichiometric coefficient matrix and X_{in} is the inlet composition matrix.

We can apply a linear diffeomorphism \mathcal{T} (see [1] for details)

$$\begin{bmatrix} x_r \\ x_{in} \\ \lambda \end{bmatrix} = \mathcal{T}n \Rightarrow \begin{cases} \dot{x}_r(t) = Vr(t) - \theta(t)x_r(t), & x_r(0) = 0 \\ \dot{x}_{in}(t) = F_{in}(t) - \theta(t)x_{in}(t), & x_{in}(0) = 0 \\ \dot{\lambda}(t) = -\theta(t)\lambda(t), & \lambda(0) = 1 \end{cases} \quad (2)$$

The research leading to these results has been done in a cooperation with the Institute for Sustainable Process Technology (ISPT) within the scope of the INSPEC project.

where x_r is the extent of reaction, x_{in} is the extent of inlet and inlet invariants and λ is the initial conditions discounting factor.

Let us define a new variable x_T and its \dot{x}_T ¹ as:

$$x_T(t) = \beta x_r + T \quad (3a)$$

$$\dot{x}_T(t) = \beta \dot{x}_r + \dot{T} \quad (3b)$$

Substituting the expressions of \dot{x}_r , \dot{T} and x_T in (3b)

$$\dot{x}_T(t) = -\theta(t)x_T + \alpha(t)F_{in}(t) + \gamma(t)Q_{in}, \quad x_T(0) = x_{T_0} \quad (4)$$

Using (2) and (4) a linear parameter varying model can be developed

$$\begin{aligned} \dot{\xi} &= \mathcal{A}(\theta)\xi + \mathcal{B}(\alpha, \gamma)u \\ y &= \mathcal{C}\xi \end{aligned} \quad (5)$$

where $\xi^\top = [x_{in}^\top \ \lambda^\top \ x_T^\top]$, and $u^\top = [F_{in}^\top \ Q_{in}^\top]$

3 Linear Quadratic Regulator

Assuming the reaction $A+B \rightleftharpoons C+D$, and for fixed initial conditions n_0 and T_0 , we want to steer the concentrations of reactants A and B to different set points and regulate the reactor temperature. Selecting appropriate weighting matrices $\mathbf{Q} = \text{diag}(10^2 \cdot I_{\iota+2}, 2 \times 10^3 \cdot I_\iota, 7.5 \times 10^2)$ and $\mathbf{R} = \text{diag}(15, 15, 1.95 \times 10^{-3})$

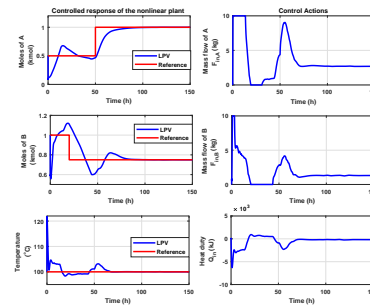


Figure 1: Controlled variables and control actions

References

- [1] M. Armhein, N. Bhatt, B. Srinivasan and D. Bonvin. "Extent of reaction and flow for homogeneous reaction systems with inlet and outlet streams." *AIChE Journal*, vol. 56, no. 11, pp. 2873–2886, 2010.
- [2] C. Pantelides and J.G. Renfo. "The online use of first-principles models in process operations: Review, current status and future needs." *Computers & Chemical Engineering*, vol. 51, pp. 136–148, 2013.

¹ Under the assumption that $m(t)C_{pmix}(t)$ remains approximately constant during the process operation

Tube-based linear parameter-varying MPC for a thermal system

J. Hanema, R. Tóth, M. Lazar

Control Systems Group, Dept. of Electrical Engineering

Eindhoven University of Technology

j.hanema@tue.nl

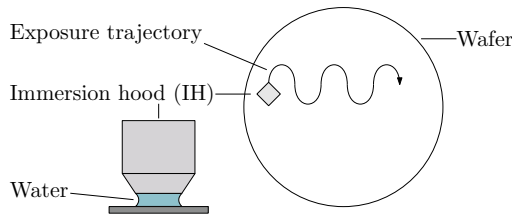


Figure 1: Immersion lithography.

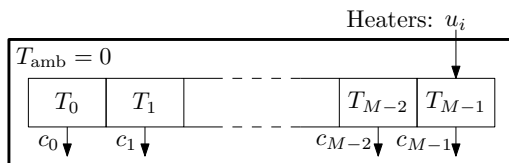


Figure 2: The simplified thermal system, a 1-D slice of wafer.

1 Introduction

In immersion lithography, a thin layer of water is held in between the wafer being illuminated and the so-called *immersion hood* (IH) (Figure 1). During the exposure cycle the IH moves over the wafer according to a pattern, and a local cooling effect occurs leading to a non-uniform temperature distribution in the wafer. To minimize unwanted mechanical deformations at the wafer surface, it is desired to keep the temperature as uniform as possible by using heaters.

To study how these heaters should be controlled, the following simplified model is considered. A “slice” of the wafer is modeled as a one-dimensional beam. The beam is split into M identical elements (Figure 2), and the temperature within each element is assumed to be uniform. Each element obeys a differential equation of the form

$$C\dot{T}_i = c_e(T_{i+1} + T_{i-1} - 2T_i) - c_i T_i + u_i, \quad (1)$$

except for the first and last element, where there is no T_{i-1} (resp., T_{i+1}) and $c_e T_i$ appears only once. In Equation (1), C [J/K] is the heat capacity of a single element, c_e [W/K] is the thermal conductance between two elements, c_i [W/K] is the thermal conductance between the i -th element and the environment, and u_i [W] is an external heat flow produced by a heater located at element i . It is assumed that the water layer is of the ambient temperature. The movement of the IH over the wafer is modeled by choosing the conductances c_i

time-varying: when the IH is in contact with element i , the conductance c_i is much higher than when there is no contact.

2 LPV modeling and MPC

After temporal discretization of (1), the thermal system can be modeled by the LPV representation

$$x(k+1) = A(\theta(k))x(k) + Bu(k) \quad (2)$$

where the M -dimensional state variable x corresponds to the temperatures T_i and the M -dimensional scheduling variable θ corresponds to the thermal conductances c_i , which are varying as a function of the IH position. To control (2), it is proposed to use an “anticipative” tube-based LPV MPC approach [1]. The system is highly constrained because the actuators can heat up, but not actively cool down, motivating the use of MPC. Further, in the considered application, the IH (and hence, the scheduling variables) follow a trajectory that is approximately known in advance. An “anticipative” controller can exploit this future information to possibly improve performance.

3 Outlook

The purpose of this work is to discover if [1] is a viable control approach for the considered thermal system.

Although the model (1) looks simple, applying LPV MPC appears to be challenging. A central issue is that [1] requires an invariant set for the system (2). The state dimension is equal to M , which must be large in order to obtain an accurate model. Based on physics, it can be deduced that the M -dimensional hypercube is an invariant set, however its representation complexity in terms of vertices scales exponentially as 2^M . Another challenge arises from the dimension of the scheduling variable, which also equals M .

Important questions to be answered are (i) what is the maximal M that can be handled by the proposed control approach, and (ii) if and how use of the “anticipative” feature can lead to increased control performance. Obtained results will be discussed in the presentation.

References

- [1] J. Hanema, M. Lazar, and R. Tóth, “Stabilizing Tube-Based Model Predictive Control: Terminal Set and Cost Construction for LPV Systems,” in *Automatica* 85, 2017.

Design of distributed thermal actuators for a one-dimensional thermomechanical model

Daniël Veldman¹, Rob Fey¹, Hans Zwart^{1,2}, Marc van de Wal³, Joris van den Boom³, Henk Nijmeijer¹

¹ Department of Mechanical Engineering, Eindhoven University of Technology, The Netherlands

² Department of Applied Mathematics, University of Twente, The Netherlands

³ ASML, Veldhoven, The Netherlands

1 Introduction

ASML's photolithography machines project a pattern of electronic connections onto a silicon wafer. The light used to project the pattern causes the wafer to heat up and expand, which leads to a degraded image quality. This thermal expansion can be reduced by thermal actuators in the supporting structure below the wafer. Since the location where the pattern is projected moves over the surface of the wafer and actuators are fixed in the supporting structure (see Figure 1), designing the most effective actuator shapes to reject the effect of the moving disturbance is not trivial.

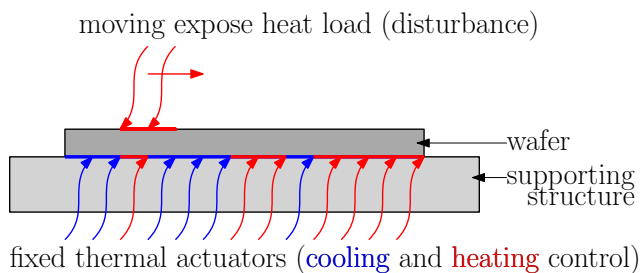


Figure 1: Fixed thermal actuators in the supporting structure are used to reduce the effect of the moving expose heat load

2 Thermomechanical model

A Finite Element (FE) model for the temperature field in the wafer is of the form

$$E\dot{x}(t) = Ax(t) + B_d(t)\bar{d} + Bu(t), \quad (1)$$

where $x(t) \in \mathbb{R}^n$ is the vector of nodal temperatures, E is the heat capacity matrix, A is the heat conduction matrix, $B_d(t)$ describes the moving location of the expose light with constant intensity $\bar{d} \in \mathbb{R}$, the columns of B describe the location of the (fixed) thermal actuators, and $u(t) \in \mathbb{R}^m$ is the vector of heat loads applied by each actuator. The displacements resulting from this temperature field are computed by solving

$$Kq(t) = Lx(t), \quad (2)$$

where $q(t)$ is the vector of nodal displacements, K is the stiffness matrix, and L is the thermal load matrix. The quality of the projected image is only determined by the deformation in the exposed area. The performance variable $z(t)$

is therefore defined as

$$z(t) = S(t)q(t), \quad (3)$$

where $S(t)$ selects the entries of $q(t)$ corresponding to nodes in the (moving) exposed area.

3 Actuator layout design

Note that the actuator shapes are described by the columns of the input matrix B . Actuator placement strategies typically use a binary formulation ($B_{ij} \in \{0, 1\}$) that leads to a combinatorial growth in the number of possible configurations [1], making these approaches computationally intractable for the large FE models considered in this application. We therefore propose an actuator placement strategy without this binary requirement ($B_{ij} \in \mathbb{R}$). Instead, we require that the columns of B are orthogonal, i.e.

$$B^T B = I_m. \quad (4)$$

We determine the optimal columns of B , i.e. the optimal actuator shapes, and the corresponding optimal actuator heat loads $u(t)$ to reject the effect of the (known) disturbance $B_d(t)\bar{d}$ by minimizing

$$\min_{B, u(t)} \int_0^T z(t)^T Q z(t) dt + \int_0^T u(t)^T R u(t) dt, \quad (5)$$

subject to (1)–(4), where $Q \geq 0$ and $R > 0$ are weights. In the considered non-binary formulation, both the optimal control input $u(t)$ as well as the input matrix B can be efficiently computed by a gradient-based method, see e.g. [2]. The method can therefore be applied to large FE models.

For proof of principle, the proposed method is applied to a representative one-dimensional thermomechanical system of the form (1)–(3). The optimized B reduces the cost function by 30% compared to the minimal cost achieved for a uniform actuator shape. The designed actuator shapes, as well as the corresponding $u(t)$, have a clear physical interpretation.

References

- [1] S. Skogestad and I. Postlethwaite, “Multivariable feedback control: analysis and design”, Wiley, 2005.
- [2] D. E. Kirk, “Optimal control theory: an introduction”, Dover, 1998.

Design and modeling for controllable UHVCVD

M. Dresscher
Nijenborgh 4
9747 AG Groningen
m.dresscher@rug.nl

B.J. Kooi
b.j.kooi@rug.nl

J. M. A. Scherpen
j.m.a.scherpen@rug.nl

B. Jayawardhana
b.jayawardhana@rug.nl

Abstract

One of the major techniques for depositing thin films is vacuum evaporation. This is mainly due to its simplicity and its potential to deposit films of extremely high purity. Vacuum deposition is typically referred to as a physical vapor deposition (PVD) technique, as the evaporated vapors will have a strong tendency to bind to the first available surface through physisorption. Accordingly, such a process typically evaporates the precursor materials in line-of-sight of the deposition target (the substrate). The process is furthermore typically cold-wall processes, meaning that the surfaces in the reactor are not heated. This causes vapor pressures to become very small and fluxes to the substrate are then almost fully determined by the evaporation process. In a related process, namely ultra-high vacuum chemical vapor deposition (UHVCVD), migration is promoted by heating the reactor surfaces (e.g. it is a hot-wall process). This allows for building sufficient background pressures in the reactor for depositions, and therefore allows evaporation sources to be placed out of the line-of-sight of the substrate. When the physisorptions no longer facilitate binding to the surfaces (which includes the substrate), an additional binding mechanism becomes necessary. This then occurs through chemisorption, which can either cause the precursors to chemically bind to the substrate or cause the precursors to form new molecules that have a lower vapor pressure. Hence, UHVCVD is a chemical vapor deposition process. The indirect migration in a UHVCVD process offers three advantages: (i) evaporated contaminants with lower vapor pressures than the precursors become trapped on reactor surfaces other than the substrate, (ii) the precursor partial pressures can be stabilized with time, while direct fluxes deposit instantaneously and (iii) the indirect migration causes incident angles to the substrate to be more uniform than for line-of-sight evaporation, in turn allowing for more uniform depositions.

Let us shortly discuss some of the challenges associated with UHVCVD. Desirably, the process allows for deposition of thin films with arbitrary material properties like composition and crystal structure. The occurring reactions are principally a result of reactant availability and temperature, in accordance with the law of mass action. Accordingly, for any specific reaction to occur, desired amounts of reactants and reaction temperatures can be attained such that (epitaxial) growth of the desired compound is maximized. How-

ever, desired amounts of reactants and reaction temperatures are often unknown because the vacuum conditions and high operating temperatures restrict placement of *in-situ* sensors. Furthermore, knowledge on the fundamental processing dynamics is often lacking, causing operating recipes to be determined empirically with the limited data available. This is further complicated by run-to-run variations of the substrate surface geometry, precursor material purity and reactor conditions, in turn causing major variations in the chemistry occurring at nanoscale. These effects result in fluctuations in end-product quality between runs while applying the same operation recipe. Reproducibility and process optimization are therefore difficult. Such observations are in line with a more general evaluation of semiconductor and thin film processes by [1]. As emphasized by [1], a way to deal with these challenges is by implementation of both real-time and run-to-run controllers. To develop these controllers, a starting point has to be made with enabling real-time measurements of relevant reactor states. The relevant reactor states for a UHVCVD process are accordingly the background pressures (or magnitude of the fluxes directed at the substrate), the substrate temperature and the layer characteristics. These measurements subsequently need to be connected to the reactor inputs or actuators through models suitable for controller design.

With this research, we contribute to the development of a the controlled UHVCVD process by providing a UHVCVD reactor design that implements atomic absorption spectroscopy (AAS) [2] measurements. We furthermore connect the measured outputs (precursor partial pressures and relevant temperatures) to the input through dynamic mathematical models suitable for controller design. Lastly, we compare obtained measurements with simulated results.

References

- [1] T. F. Edgar, S. W. Butler, W. Campbell, C. Pfeiffer, C. Bode, S. B. Hwang, K. Balakrishnan, and J. Hahn, "Automatic control in microelectronics manufacturing: Practices, challenges, and possibilities," *Automatica*, vol. 36, no. 11, pp. 1567 – 1603, 2000.
- [2] M. Klausmeier-Brown, J. Eckstein, I. Bozovic, and G. Virshup, "Accurate measurement of atomic beam flux by pseudo-double-beam atomic absorption spectroscopy for growth of thin-film oxide superconductors," *Applied physics letters*, vol. 60, no. 5, pp. 657–659, 1992.

Partial Synchronization in Networks of Networks of Kuramoto Oscillators

Yuzhen Qin, Yu Kawano and Ming Cao
 Faculty of Science and Engineering,
 ENTEG, University of Groningen,
 Groningen, 9747 AG, the Netherlands
 Email: {y.z.qin, y.kawano, m.cao}@rug.nl

1 Introduction

It has been found that neuronal ensembles in the human brain have the intrinsic property to behave as oscillators, which are also connected by chemical and electrical couplings [1]. The pattern of synchronization (or phase cohesiveness), which has been seen across regions of human brain, is believed to facilitate communication among neuronal ensembles [2]. However, abnormal patterns of synchronization can trigger neurological disorder, which is regarded as the cause of some serious diseases. It suggests that a non-pathological brain has powerful regulation mechanisms not only to render synchronization, but also to prevent unnecessary synchronization among the neuronal ensembles that do not need communication. Motivated by these phenomena observed in the human brain, we study community-driven partial phase cohesiveness in networks of community-tinized Kuramoto oscillators, where each community consists of all-to-all coupled oscillators.

2 Problem Formulation and Results

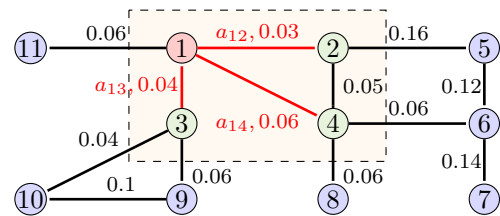
To the best of our knowledge, all the results for modeling dynamics in the human brain rely on the simplifying treatment that the dynamics of the neuronal ensemble in an anatomical region of the brain is modeled as a single oscillator. In fact, anatomical regions of the brain often exhibit a network-of-networks topology. Each anatomical region can consist of heterogeneous neuronal ensembles, which can interact not only within a region but also with neurons from other regions. This motivates us to analyze a more challenging and perhaps more precise model described by

$$\dot{\theta}_i^p = \omega_i^p + \frac{K_p}{N} \sum_{n=1}^N \sin(\theta_n^p - \theta_i^p) + \sum_{l=1}^M \frac{a_{pl}}{N} \sum_{n=1}^N \sin(\theta_n^l - \theta_i^p),$$

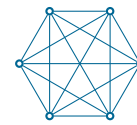
$$i = 1, 2, \dots, N; p = 1, 2, \dots, M,$$

where $\theta_i^p \in \mathbb{S}^1$ and $\omega_i^p \geq 0$ denote the phase and natural frequency of the i th oscillator in the p th community (anatomical region). The second term on the right-hand side represents the interconnection within community p , which is all-to-all. The interconnection-

s among communities are described by an undirected, and weighted graph $\mathcal{G}(\mathcal{V}, \mathcal{E}, \mathcal{A})$ with adjacency matrix $A = [a_{ij}] \in \mathbb{R}^{M \times M}$. An example is given in Fig.1.



(a) The inter-community network: driving community 1 (red) and target communities 2, 3, 4 (green).



(b) The well mixed graph within each community

Figure 1: A network of networks.

The problem of interest is to seek conditions such that target communities (see the green ones in Fig.1) can reach phase cohesiveness caused by the driven community (see the red one in Fig.1). The result we obtained is as follows.

Result 1 Assume that the algebraic connectivity $\lambda_2(L)$ of $\mathcal{G}_{\mathcal{R}}$ is larger than a critical value (\mathcal{R} is the target communities), the oscillators in \mathcal{R} can reach partial phase cohesiveness.

References

- [1] N. Kopell, et. al “Gamma rhythms and beta rhythms have different synchronization properties,” Proceedings of the National Academy of Sciences, vol. 97, no. 4, pp. 18671872, 2000.
- [2] T. Womelsdorf, et. al, “Modulation of neuronal interactions through neuronal synchronization,” Science, vol. 316, no. 5831, pp. 16091612, 2007.

Integration of protein dynamics in batch bioprocess optimization

Guillaume Jeanne^{1,2}, Sihem Tebbani¹, Didier Dumur¹, Anne Goelzer², Vincent Fromion²

1 Introduction

The production of products of interest in batch bioreactors is becoming a real opportunity for more and more industries. In batch operating mode, the culture medium is defined at the beginning of the experiment and cannot be changed over time. As a consequence, in order to optimize the process, it is necessary to focus on cell modification and strain design. To do so, it is important to develop a model with more information than Monod model or other macroscopic models.

Constraint based models are good candidates for modelling intracellular processes. Actually, the predictability of these methods relies on mass conservation and optimal resource allocation principle in cell in general. As an example, Resource Balance Analysis (RBA) method developed in [1] is an intracellular process description relying on: (i) mass conservation, (ii) ribosome capacity limitation to produce proteins, (iii) constant total protein concentration, (iv) maximization of growth rate. The constraints are centred on proteins as it is known to be the main cell's resources allocation. Coupling constraint-based models to production optimization has already been done, notably in [2]. The optimal strategy is divided into two steps. In the first phase, the goal is that the cells grow as much as possible without producing. In a second stage, growth is minimal and production is at its maximum. The main contribution of our work compared to [2] is the consideration of protein dynamics in the calculation of the optimum. As it is the largest spending pole of the cell, it is relevant to take it into account.

2 Approach

In this work, an aggregated model is developed: the bioreactor dynamics (substrate concentration, product of interest quantity and biomass dynamics) is coupled to the intracellular species dynamics which are gathered in representative pools of components. The intracellular processes are described with the same approach as in [1]. As an example, in this model, the growth rate formulation results from a compromise between constraints (i), (ii), (iii) and (iv), not from empirical observations. The model is the same as in [3].

The problem at stake is to maximize the product quantity by time, that is to say the yield of the process: $P(t_f)/t_f$.

The nonlinear optimization problem is discretized and solved by the collocation approach [4].

¹L2S, CentraleSupélec - CNRS - Univ. Paris-Sud, Université Paris-Saclay, Control Department, Plateau du Moulon, 91190 Gif-sur-Yvette, France (e-mail: firstname.name@centralesupelec.fr)

²MaIAGE, INRA, UR1404, Université Paris-Saclay, 78350 Jouy-en-Josas, France (e-mail: firstname.name@inra.fr).

3 Results & Interpretation

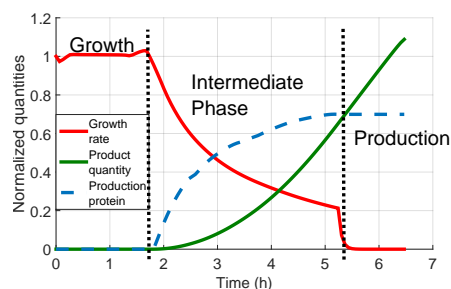


Figure 1: Optimal time evolution of three main variables

Optimal strategy is presented in Figure 1.

As in [2] and fed-batch classical strategies, the optimization result is first to grow and then to produce the product of interest. But, the great difference is the intermediate phase during which the growth rate gradually decreases while the concentration of production proteins increases as well as product quantity produced in the bioreactor. In fact, there is a need for this intermittent phase during which the behaviour of the cells changes: the proteins catalyzing the production flux have to be produced and it takes time.

4 Perspectives

As an ongoing work, the methodology could be extended to fedbatch bioreactors. In fact, the impact of protein dynamics on the global control strategy must be taken into account and would certainly change the optimal feeding profile.

References

- [1] A. Goelzer, V. Fromion, and G. Scorletti, "Cell design in bacteria as a convex optimization problem," *Automatica*, vol. 47, no. 6, pp. 1210–1218, 2011.
- [2] B. Jabarivelisdeh and S. Waldherr, "Improving bioprocess productivity using constraint-based models in a dynamic optimization scheme," *IFAC-PapersOnLine*, vol. 49, no. 26, pp. 245–251, 2016.
- [3] G. Jeanne, S. Tebbani, A. Goelzer, V. Fromion, and D. Dumur, "Modelling and optimization of metabolic pathways in bacteria," in *2016 20th ICSTC Conference*, pp. 312–317, IEEE, 2016.
- [4] L. T. Biegler, "An overview of simultaneous strategies for dynamic optimization," *Chemical Engineering and Processing: Process Intensification*, vol. 46, no. 11, pp. 1043–1053, 2007.

Variable selection in linear dynamical systems

Atte Aalto and Jorge Gonçaves

Luxembourg Centre for Systems Biomedicine, University of Luxembourg
6 avenue du Swing; 4367 Belvaux; Luxembourg
atte.aalto@uni.lu, jorge.goncalves@uni.lu

1 Introduction

We address the problem of variable selection in linear dynamical systems. More precisely, we wish to reconstruct the zero-structure of the matrix A in the system $\dot{x} = Ax + u$ from sampled measurements $y_j = x(t_j) + v_j$. Here u is an unknown noise process modelled as white noise, and v_j 's are measurement errors. The problem is motivated by the gene regulatory network reconstruction problem, which is characterized by low sampling frequency and small number of data points in the time series data. The identification problem is underdetermined, and therefore we impose a sparsity requirement on A , as per general knowledge on the gene expression process. However, the sparsity requirement is imposed on the continuous time system, and due to the low sampling frequency, sparse matrix A does not correspond to a sparse discrete time matrix $e^{A\Delta t}$. Therefore the continuous time nature of the system needs to be taken into account.

The more or less classical approach to variable selection problems is the so-called Lasso algorithm, that is, a least squares solution with a penalty on the 1-norm of A . In the context of dynamical systems, the Lasso has been combined with the EM method in [2]. We will introduce a fully Bayesian method for the task, based on Markov Chain Monte Carlo sampling of the sparsity pattern of A as well as the trajectory x which is considered as a latent variable.

2 The method

A more detailed presentation can be found in [1]. Denote by $Y = [y_0, \dots, y_N]$ the collection of the time series data. Let us split A into an indicator variable S controlling the sparsity pattern of A , and a magnitude variable H , so that $[A]_{i,j} = [S]_{i,j}[H]_{i,j}$ where $[S]_{i,j} \in \{0, 1\}$. In the Bayesian spirit, we are interested in the posterior probability distribution for the indicator variable S for given data Y , for which we have

$$\begin{aligned} p(S|Y) &= \iint p(S, H, dx|Y) dH \\ &\propto \iint p(Y|x) p(dx|S, H) p(S) p(H) dH \\ &= p(S) \int p(Y|x) \left(\int p(dx|S, H) p(H) dH \right). \end{aligned}$$

where the first equality is the marginalization integral and the second is the Bayes' law. The distributions on the

last line are the prior for the zero structure $p(S)$ (preferring sparse A), the measurement noise model $p(y_j|x) = N(x(t_j), R)$, the process noise model obtained from the Wiener measure using the Cameron–Martin theorem, and independent normal priors for the rows of H . With this prior for H , the latter integral above can be computed analytically.

Denote by $S^{(l)}$ and $x^{(l)}$ the current MCMC sample. The sampling algorithm then proceeds as follows:

Algorithm 1

- 1) Sample \hat{S} from $S^{(l)}$ by randomly picking one element and changing it from one to zero or zero to one.
- 2) Sample \hat{x} from $x^{(l)}$ by Crank–Nicolson sampling [3].
- 3) Compute the Metropolis–Hastings acceptance probability and with that probability, set $S^{(l+1)} = \hat{S}$ and $x^{(l+1)} = \hat{x}$. Otherwise, set $S^{(l+1)} = S^{(l)}$ and $x^{(l+1)} = x^{(l)}$.

After collecting k samples, the matrix $\frac{1}{k} \sum_{l=1}^k S^{(l)}$ approximates the probabilities of the corresponding elements of A being nonzero. Some results on a test problem are shown in Figure 1, where the presented method outperforms the EM-Lasso.

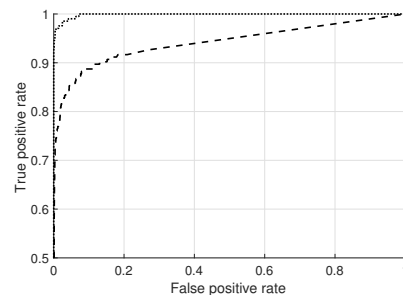


Figure 1: ROC curves for a 100-dimensional test problem. The dotted line shows the results of the presented method and the dashed line shows results of the EM-Lasso.

References

- [1] A. Aalto and J. Goncalves. Bayesian variable selection in linear dynamical systems. *ArXiv:1802.05753*, 2018.
- [2] K. Kojima *et al.* A state space representation of VAR models with sparse learning for dynamic gene networks. *Intl. Conference on Genome Informatics*, 22:56–68, 2010.
- [3] S.L. Cotter, G.O. Roberts, A.M. Stuart, and D. White. MCMC methods for functions: modifying old algorithms to make them faster. *Statistical Science*, 28(3):424–446, 2013.

Nonlinear model predictive control of *Escherichia coli* culture

M. Abadli^{a, b}, S. Tebbani^a, D. Dumur^a, L. Dewasme^b, A. Vande Wouwer^b

^aLaboratoire des Signaux et Systèmes, CentraleSupélec, CNRS, Univ. Paris Sud,

Univ. Paris-Saclay, Control Department, 3 rue Joliot-Curie, 91192 Gif sur Yvette, France

merouane.abadli@centralesupelec.fr, sihem.tebbani@centralesupelec.fr, didier.dumur@centralesupelec.fr

^bAutomatic Control Laboratory, University of Mons, 31, Boulevard Dolez, 7000 Mons, Belgium

alain.vandewouwer@umons.ac.be laurent.dewasme@umons.ac.be

1 Introduction

Escherichia coli is a popular microorganism in biotechnology applications, and the most commonly used host cell for the production of recombinant proteins and many other bio-pharmaceutical products. This production is mainly achieved through fed-batch cultures.

In order to maximize the biomass production and reach high cell densities, a substrate feeding strategy must be considered.

Feeding the culture with a rich medium containing a high glucose concentration might seem the ideal approach. However, it has been shown that exceeding a critical level of concentration of glucose can lead into acetate production, a cell growth inhibiting byproduct.

To avoid this undesired behavior, and maintain the culture in optimal operating conditions, an optimal closed-loop regulation and feeding strategy is needed. This feeding strategy requires the development of an optimal closed-loop control algorithm based on the known measured outputs, and the estimated states.

2 Modeling

A mechanistic model of *E. coli* growth is considered. This model is based on Sonnleitner's bottleneck assumption (figure 2):

During a culture, the cells metabolism changes due to their limited oxidative capacity represented by a bottleneck.

When the substrate (glucose) is in excess, its concentration (denoted S) exceeds a critical value ($S > S_{crit}$), acetate is produced by the cells, and the regime is called respiro-fermentative regime.

Otherwise, when the substrate is low (*i.e.* $S < S_{crit}$), the available glucose and/or acetate are oxidized. The regime is called respirative regime [1–3].

3 Control strategy

An efficient control strategy of *E. coli* culture in fed-batch mode aims to maximize biomass production while maintaining acetate concentration at a low level.

In order to achieve this objective, as a first step, an exponential feeding rate and its corresponding biomass

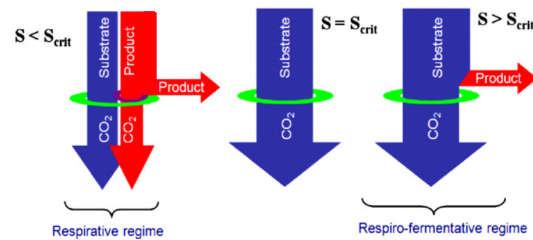


Figure 1: Sonnleitner's bottleneck assumption [3]

concentration profile are considered as a reference trajectory to track by the controller. The goal is to force cells growth to a desired regime and to maintain the culture in optimal conditions, starting from a different initial conditions and thus different regime.

The developed controller is a nonlinear model predictive controller (NMPC), minimizing a cost function that includes the tracking error on biomass concentration, and the difference between the reference and applied control inputs.

The NMPC controller performance is then compared to a PID controller, in order to highlight the higher performance of the NMPC in comparison to classical control strategies [2].

This optimizing controller depends on the knowledge of the real time values of the different variables. However, reliable probes for online measurements with the desired accuracy are not always available.

To tackle the issue, in future work the NMPC controller will be coupled with an estimation algorithm to reconstruct unmeasured variables. An Unscented Kalman Filter (UKF) will be investigated.

References

- [1] I. Rocha, *Model-based strategies for computer-aided operation of recombinant E. coli fermentation*. PhD Thesis, Universidade do Minho, 2003
- [2] S. Tebbani, D. Dumur, G. Hafidi, A. Vande Wouwer *Nonlinear predictive control of fed-batch cultures of E. coli*. Chem Eng & Tech, 2010,
- [3] L. Dewasme, G. Goffaux, A.-L. Hantson, A. Vande Wouwer, *Experimental validation of an Extended Kalman Filter estimating acetate concentration in E.coli cultures*. J. of Process Control 23, 2013

Dynamic constraint-based modelling of bioprocesses: a dynamic flux balance analysis model for recombinant *Streptomyces lividans*

Kobe De Becker, Wouter Daniels, Kenneth Simoens, Kristel Bernaerts
Bio- & chemical systems engineering, reactor engineering and safety (CREaS)
KU Leuven, Celestijnenlaan 200f, 3001 Heverlee, Belgium

Email: kobe.debecker@kuleuven.be, kristel.bernaerts@kuleuven.be

In recent years, progress in systems biology allowed to model biological systems with more complex formalisms. These models serve as in silico alternatives for costly and time-consuming experiments or help to improve observer and controller performance on an industrial scale. In this contribution, dynamic modelling using constraint-based optimization network models (CBM) will be discussed by means of a case study: the implementation of a dynamic flux balance analysis (DFBA) model for recombinant *Streptomyces lividans*.

In CBM models, biomass is considered to consist of multiple metabolites which are converted into each other by biochemical reactions. The stoichiometry of these reactions is given by a metabolic network. To each of the reactions a flux is attributed. The flux distribution inside a cell is determined by maximizing a predefined criterion, mostly (but not exclusively) biomass growth. The flux distribution should satisfy multiple biological and thermodynamic constraints, e.g., reaction irreversibility. DFBA uses this approach to predict concentration profiles of extracellular metabolites (substrates and products). It has first been introduced by Mahadevan et al. (2002) in [1].

Starting from the already known reaction stoichiometry, a DFBA model for *S. lividans* is constructed. The implementation method is in accordance with the static-optimization approach (SOA) in which three steps are iteratively executed. First the uptake fluxes of glucose and amino acids and the production fluxes of cellulase and organic acids are determined based on kinetic expressions. Parameter identification happens by least-squares fitting of kinetic expressions onto experimental data. The uptake and production fluxes are used as constraints in the second step to solve an LP-problem in order to determine the flux distribution inside the cells. In a third step, this flux distribution is used to update the extracellular metabolite concentrations - glucose, amino acids, organic acids and dissolved oxygen - by a forward Euler discretization. The procedure is described by the following equations:

$$\max c^T v \quad (1)$$

$$\text{s.t. } Sv = 0 \quad (2)$$

$$v_{min} \leq v \leq v_{max} \quad (3)$$

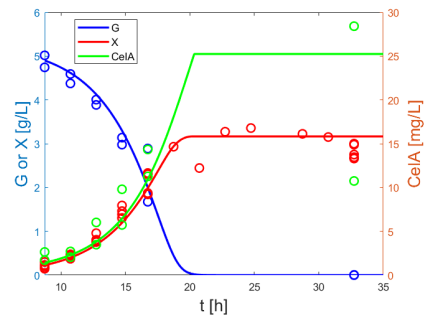


Figure 1: Glucose (G), biomass (X) and cellulase (CelA) concentration estimates (full lines) and measurements (circles)

$$z(t_{i+1}) = z(t_i) + S_{exc}v(t_i)z_n(t_i)\Delta t \quad (4)$$

$$z(t) \geq 0, \forall t \in [t_0; t_f] \quad (5)$$

c is a weighting vector and v is the vector of fluxes [$mmol/g_{DW}h$]. S is the stoichiometric matrix, taking into account the stoichiometry of the reaction network which is assumed to be in steady-state (2). v_{min} and v_{max} impose boundaries on the fluxes. These can be fixed values or kinetic expressions. z is the vector of extracellular metabolite concentrations [mol/L] and z_n is the biomass concentration [g_{DW}/L], which is the n -th element in z . Equation (4) describes the update of the concentrations with Δt the length of the time interval [h]. S_{exc} is a matrix describing the stoichiometry of the exchange reactions.

The implemented DFBA model correctly predicts the grand dynamics. However, the experimental results show a deviation from exponential growth at the end of the growth phase. This is not predicted by the model due to an overestimation of the glucose uptake rate. A general conclusion is that the presented DFBA model forms a good preliminary model framework which can be extended in future studies. Figure 1 shows the glucose, biomass and cellulase predictions and compares them to experimental measurements. Current research of the author focuses on the use of CBM models for bioprocess estimation and control.

References

- [1] R. Mahadevan et al., *Biophys J.*, 2002 Sep, 83(3):1331-40.

Topology identification in dynamic Bayesian networks¹

S. Shi, G. Bottegal, P. M. J. Van den Hof

Control Systems Group, Department of Electrical Engineering,
Eindhoven University of Technology,
The Netherlands

Email: {s.shi, g.bottegal, p.m.j.vandenhof}@tue.nl

1 Introduction

System identification methods for complex networks commonly rely on the assumption that the topology of the network is known [1]. Given a dataset collected from a dynamic network, we formulate the problem of topology identification as a structure learning problem in the context of dynamic Bayesian networks [2]. The advantage of this approach is that the reconstruction of the topology does not require the identification of the parameters of the modules composing the network.

2 Dynamic Bayesian networks (DBN)

A static Bayesian network is defined by a pair (S, P) , where S is a directed acyclic graph and P is the joint distribution over the random variables $\mathbf{w}_1, \dots, \mathbf{w}_n$, which constitute the measured variables of the network. The joint distribution factorizes over the graph S , i.e. it satisfies the chain rule

$$P(\mathbf{w}_1, \dots, \mathbf{w}_n) = \prod_{i=1}^n P(\mathbf{w}_i | Pa(\mathbf{w}_i)),$$

where $Pa(\mathbf{w}_i)$ denotes the set of parents of the node \mathbf{w}_i . The DBN extends the static model to temporal data, where one variable at one time instant is modeled as one random variable. Thus, the factorization of the new joint distribution based on the new structure over time is

$$P(\{\mathbf{w}_1(t)\}_{t=0}^T, \dots, \{\mathbf{w}_n(t)\}_{t=0}^T) = P(\mathbf{w}_{1:n}(0)) \prod_{t=1}^T \prod_{i=1}^n P(\mathbf{w}_i(t) | Pa(\mathbf{w}_i(t))),$$

where $Pa(\mathbf{w}_i(t))$ is defined by the graph structure. An example of DBN is given in Figure 1.

3 Structure learning of DBN

There are several approaches available for structure learning and the one used in this work is usually referred to as score-based. In this approach, the structure learning problem is formulated as a discrete optimization problem

$$\max_{S \in \mathbb{S}} \text{Score}(S),$$

¹This project has received funding from the European Research Council (ERC), Advanced Research Grant SYSDYNET, under the European Union's Horizon 2020 research and innovation programme (grant agreement No 694504).

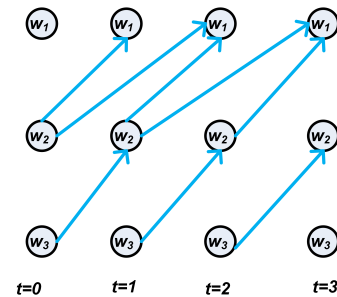


Figure 1: Example of DBN.

where \mathbb{S} contains all possible structures and the number of elements in it grows exponentially as a function of the number of variables. The score corresponds to the logarithm of the marginal likelihood which is calculated as

$$\text{Score}(S) = \log P(D|S) = \log \left[\int P(D|S, \theta) P(\theta|S) d\theta \right],$$

where D denotes the data and θ denotes the parameters describing the module dynamics. It can be seen the parameters are integrated out and thus parameter estimation is not needed for structure learning. To solve this optimization problem, we apply a heuristic-based greedy search algorithm.

4 Current and Future work

Some simple simulations have been conducted to show the possibility to solve the topology identification problem using DBN model. The future extension would be to incorporate structure priors $P(S)$ and kernel-based methods, which are used to formulate the prior distribution $P(\theta|S)$ in order to account for the stability of the network.

References

- [1] P. M. J. Van den Hof, A. Dankers, P. S. C. Heuberger, and X. Bombois. Identification of dynamic models in complex networks with prediction error methods/basic methods for consistent module estimates. *Automatica*, 49(10):2994–3006, 2013.
- [2] D. Koller and N. Friedman. *Probabilistic graphical models: principles and techniques*. 2009.

Topology reconstruction of dynamical networks via constrained Lyapunov equations

Henk J. van Waarde
University of Groningen
h.j.van.waarde@rug.nl

Pietro Tesi
University of Groningen
p.tesi@rug.nl

M. Kanat Camlibel
University of Groningen
m.k.camlibel@rug.nl

1 Introduction

Networks of dynamical systems appear in many contexts, including power networks, water distribution networks, and biological networks. The interconnection structure of such networks is often represented by a graph, where each vertex (or node) of the graph corresponds with a dynamical system, and edges represent interaction between systems. Unfortunately, the interconnection structure of dynamical networks is often unavailable. For instance, in the case of wireless sensor networks the locations of sensors, and hence, communication links between sensors is not always known. Other examples of dynamical networks with unknown network topologies are encountered in biology, for instance in neural networks. Consequently, the problem of *network reconstruction* is studied in the literature (see, e.g., [1], [2], and the references therein). The aim of network reconstruction (also called topology identification) is to find the network structure of a dynamical network, using measurements obtained from the network. In this abstract, we consider network reconstruction for *deterministic* networks of linear dynamical systems. In contrast to papers studying network reconstruction for specific network dynamics such as consensus dynamics or adjacency dynamics, we consider network reconstruction for *general* linear network dynamics. It is our aim to infer the unknown network topology of such dynamical networks, from *state measurements* obtained from the network.

2 Problem formulation

Consider an undirected graph $G = (V, E)$, where $V = \{1, 2, \dots, n\}$ is the vertex set, and E is the set of edges. Associated with G , we consider the network system

$$\begin{aligned} \dot{x}(t) &= Xx(t) \text{ for } t \in \mathbb{R}_{\geq 0} \\ x(0) &= x_0, \end{aligned} \quad (1)$$

where $x \in \mathbb{R}^n$ is the *state* of the network, and the interconnection matrix X is contained in the so-called *qualitative class* $\mathcal{Q}(G)$ of matrices carrying the structure of the graph G . Examples of members of the qualitative class are the *Laplacian* and *adjacency* matrices associated with the graph G . We denote the state trajectory of (1) by $x_{x_0}(\cdot)$. In this work, we assume that the interconnection matrix X (and graph G) is *unknown*, but the state of the network $x_{x_0}(t)$ can be *measured* for $t \in [0, T]$, where $T \in \mathbb{R}_{>0}$. It is our goal to re-

construct X (and hence, G) using these measurements. Of course, it is possible that multiple *different* network systems of the form (1) generate the *same* measurements $x_{x_0}(t)$ for $t \in [0, T]$. If, on the other hand, the measurements $x_{x_0}(t)$ for $t \in [0, T]$ correspond to a *unique* network system (1), we say the network reconstruction problem is *solvable* (for a more formal definition we refer to Definition 1 of [1]).

The first problem of this abstract is to find conditions under which the network reconstruction problem is solvable. Secondly, we want to find a method to reconstruct the matrix X using the measurements $x_{x_0}(t)$ for $t \in [0, T]$.

3 Results and discussion

As our first main result, we give necessary and sufficient conditions under which the network reconstruction problem is solvable. These conditions are stated in terms of certain *unobservable subspaces* associated with (1). Subsequently, we show that the network reconstruction problem is solvable if and only if there exists a unique solution (equal to the matrix X) to a certain constrained *Lyapunov equation*. This provides a general methodology to reconstruct the state matrix X . Lyapunov equations can be solved efficiently, e.g., using techniques from [3].

Nonetheless, the approach has some limitations. Specifically, system (1) does not take into account possible noise in the system dynamics and in the measurements. Future work should hence focus on extending the results to stochastic dynamical systems. Moreover, it is of interest to consider nonlinear dynamics instead of the linear dynamics (1).

References

- [1] H.J. van Waarde, P. Tesi, and M.K. Camlibel, "Topology Reconstruction of Dynamical Networks via Constrained Lyapunov Equations", *Submitted to IEEE Transactions on Automatic Control*, 2017 (available at <https://arxiv.org/pdf/1706.09709>).
- [2] S. Shahrampour, and V. M. Preciado, "Topology Identification of Directed Dynamical Networks via Power Spectral Analysis", *IEEE Transactions on Automatic Control*, 60(8):2260–2265, 2015.
- [3] V. Simoncini, "A New Iterative Method for Solving Large-Scale Lyapunov Matrix Equations", *SIAM Journal on Scientific Computing*, 29(3):1268–1288, 2007.

Local transfer functions recovery in networked system identification

Julien M. Hendrickx

ICTEAM, Université catholique de Louvain
Louvain la Neuve, Belgium
julien.hendrickx@uclouvain.be

Michel Gevers

ICTEAM, Université catholique de Louvain
Louvain la Neuve, Belgium
michel.gevers@uclouvain.be

Alexandre S. Bazanella
Department of Automation and Energy
Universidade Federal do Rio Grande do Sul
Porto Alegre, Brazil
bazanella@ufrgs.br

1 Introduction

We consider the problem of identifying a networked LTI dynamical system where (i) a subset of nodes are measured, and (ii) all nodes are excited. Assuming that the closed-loop transfer functions from excited to measured nodes have been identified, we determine which local transfer functions can be recovered. We show that this essentially depends on the structure of the networked system, and derive a graph-theoretical condition to separate the transfer functions that can be recovered from those that cannot. An important outcome of our research is that, under those assumptions, a network can often be identified using only a small subset of node measurements. Detailed results are available in [1, 2].

2 Problem Statement

We consider that the network is made up of L nodes, with node signals denoted by $\{w_1(t), \dots, w_L(t)\}$, evolving according to the following network equations, in which the matrix $G^0(q)$ is called the **network matrix**:

$$w(t) = G^0(q)w(t) + r(t) + v(t). \quad (1)$$

In (1) q^{-1} is the delay operator, $w(t)$ is the vector of node signals, $r(t)$ is a vector of known external excitation signals and $v(t)$ is a vector of stochastic noise. We suppose that we measure a subset \mathcal{C} of the nodes. Letting C be the matrix selecting these nodes, i.e. a matrix where each row contains one element 1 corresponding to a distinct measured node, and zeros everywhere else, the input-output dynamics of the network can be rewritten as

$$w(t) = CT^0(q)r(t) + \bar{v}(t) := C(I - G^0(q))^{-1}r(t) + v(t)$$

where we assume $(I - G^0(q))^{-1}$ to be proper and stable. We suppose that the closed-loop transfer function CT^0 has been identified. Our goal is then to determine which local transfer functions $G_{ij}(q)$ can be uniquely recovered from CT^0 .

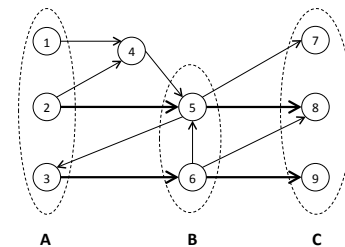


Figure 1: The paths $(2, 5, 8)$ and $(3, 6, 9)$ are vertex-disjoint paths from $\mathcal{A} = \{1, 2, 3\}$ to $\mathcal{C} = \{7, 8, 9\}$. An alternative set of such paths is $(1, 4, 5, 7)$ and $(3, 6, 9)$. The maximal number of vertex-disjoint paths is equal to the smallest set disconnecting \mathcal{A} from \mathcal{C} . Here, $\mathcal{B} = \{5, 6\}$ is such a set because every path starting from \mathcal{A} and arriving in \mathcal{C} goes through it.

3 Graph Representation

We associate to G^0 a graph \tilde{G} , connecting the edge (j, i) if $G_{ij}^0 \neq 0$. Similarly, we say that a network matrix G^0 is *consistent* with \tilde{G} if $G_{ji}^0 \neq 0$ implies the presence of an edge (i, j) in \tilde{G} . It turns out that the possibility of recovering G_{ji}^0 uniquely from CT^0 is a generic property: for a given graph and set of measured nodes, either G_{ji}^0 can be recovered uniquely from CT^0 for almost all network matrices G^0 consistent with \tilde{G} , or it can never be recovered. We prove a necessary and sufficient condition for this generic recovery, related to the maximal number of vertex-disjoint paths between the out-neighbors of i and the set of measured nodes \mathcal{C} , a notion illustrated in Figure 1.

References

- [1] J. M. Hendrickx, M. Gevers and A. S. Bazanella, "Identifiability of dynamical networks with partial node measurements," preprint available on J. H.'s website.
- [2] A. S. Bazanella, M. Gevers, J. M. Hendrickx and A. Parraga, "Identifiability of dynamical networks: which nodes need be measured?" Proceedings of CDC 2017

A Sequential Least Squares algorithm for ARMAX model identification in a closed-loop with sensor noise¹

H.H.M. Weerts², G. Bottegal, P.M.J. Van den Hof,
Eindhoven University of Technology,
Department of Electrical Engineering

1 Introduction

Modern engineering systems such as the smart electricity grid can be operated more efficiently and safely when accurate models of it are available. One challenge is obtaining such a model, for example by measuring and then taking a data-driven way to identify the model. Many large-scale systems can be modeled as a dynamic network, where dynamics of the system as well as the internal structure are modeled.

Sensor or measurement noise is a classical problem in system identification. Projection methods such as the instrumental variable (IV) method are able to provide consistent estimates of a single module, even when there is sensor noise in the network. However the excitation provided by process noise is not used to reduce variance of the estimated module in the IV method. It can be shown that sensor noise can be rewritten as a correlated process noise. Recently it was shown that the joint-direct method can provide consistent estimates of a module when process noises are correlated [2]. This means that the joint-direct method can be used to deal with sensor noise. When using an ARMAX model structure, an estimate with the same asymptotic properties as the joint-direct method can be obtained by a sequential least squares (SLS) algorithm [1]. When combining these new techniques, a natural question is whether the SLS algorithm can outperform the instrumental variable method on an example closed-loop system with sensor noise.

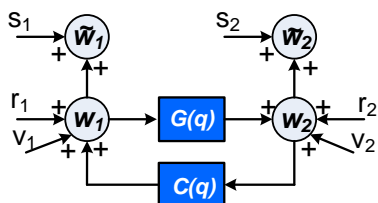


Figure 1: Closed-loop influenced by sensor noise.

¹This project has received funding from the European Research Council (ERC), Advanced Research Grant SYSDYNET, under the European Union's Horizon 2020 research and innovation programme (grant agreement No 694504).

²Contact details: h.h.m.weerts@tue.nl or P.O. Box 513, 5600 MB Eindhoven, The Netherlands.

2 Identification setup

The system under study is the closed-loop depicted in Figure 1, where the r_i are known excitation signals, the nodes w_i are unknown but measured as \tilde{w}_i .

In the joint-direct method this system is modeled by a prediction error which models correlated noise

$$\begin{bmatrix} \varepsilon_1 \\ \varepsilon_2 \end{bmatrix} = \begin{bmatrix} H_{11} & H_{12} \\ H_{21} & H_{22} \end{bmatrix}^{-1} \left(\begin{bmatrix} 1 & -C \\ -G & 1 \end{bmatrix} \begin{bmatrix} \tilde{w}_1 \\ \tilde{w}_2 \end{bmatrix} - \begin{bmatrix} r_1 \\ r_2 \end{bmatrix} \right). \quad (1)$$

Minimizing $\varepsilon_1^2(t, \theta) + \varepsilon_2^2(t, \theta)$ over θ leads to consistent estimates of $G(q)$ and $C(q)$ [3].

The SLS algorithm [1] operates in 3 steps. First a MIMO ARX model is estimated in order to obtain an estimate of the innovation sequence. This innovation is used as a known input in an ARMAX model, making it linear in the parameters. Then in the second step the ARMAX model is consistently estimated. Finally in the third step the noise model is refined, and the estimate is improved.

Simulations on the system in Figure 1 show that the proposed algorithm is competitive with IV.

3 Acknowledgements

We acknowledge the contributions of A. Dankers, M. Galrinho and H. Hjalmarsson.

References

- [1] H.H.M. Weerts, M. Galrinho, G. Bottegal, H. Hjalmarsson and P.M.J. Van den Hof, "A sequential least squares algorithm for ARMAX dynamic network identification," 18th IFAC Symposium on System Identification (SYSID), *submitted*.
- [2] H.H.M. Weerts, P.M.J. Van den Hof and A. Dankers "Prediction error identification of linear dynamic networks with rank-reduced noise," *Automatica, submitted, arXiv:1711.06369 [cs.SY]*.
- [3] P.M.J. Van den Hof, A. Dankers and H.H.M. Weerts "From closed-loop identification to dynamic networks: generalization of the direct method," , 56th IEEE Conference on Decision and Control (CDC), 2017, page 5845-5850.

Sparse identification of linear parameter-varying systems using B-splines

Dora Turk, Goele Pipeleers and Jan Swevers
 MECO Research Team, Department of Mechanical Engineering, KU Leuven
 DMMS lab, Flanders Make, Belgium
 Email: dora.turk@kuleuven.be

1 Introduction

Linear parameter-varying (LPV) systems are nonlinear systems described by a linear model with coefficients varying as a function of one or more scheduling parameters. Determining the dependency of the linear model on the scheduling parameter(s), generally described through a set of basis functions, is often challenging, especially if little or no prior information of the nonlinear system dynamics is available. This abstract proposes an LPV identification method that models the scheduling parameter dependency through B-spline basis functions. B-splines are known to have better interpolating properties than polynomials. Furthermore, B-spline-based LPV models are the core of the recently developed LPV controller design method [1] we want to comply with. This LPV identification approach combines a quadratic fitting criterion with a basis pursuit approach to determine the optimal B-spline knot locations.

2 B-spline-based state-space model

We consider the following discrete-time LPV model:

$$\begin{cases} x(t+1) = A(\alpha(t))x(t) + B(\alpha(t))u(t) \\ y(t) = C(\alpha(t))x(t) + D(\alpha(t))u(t), \end{cases} \quad (1)$$

where $x(t) \in \mathbb{R}^n$, $u(t) \in \mathbb{R}^r$, $y(t) \in \mathbb{R}^l$, and $\alpha(t) \in \mathbb{R}$, are respectively the state vector, the input vector, the output vector, and the scheduling parameter, at time instance t . For simplicity is here assumed that α is a scalar on a closed and bounded interval $[\underline{\alpha}, \bar{\alpha}] \subset \mathbb{R}$. The extension to multiple scheduling parameters is trivial though.

Let $\xi = (\xi_0, \dots, \xi_{l+1})$ be a sequence of points satisfying

$$\underline{\alpha} = \xi_0 < \xi_1 < \dots < \xi_l < \xi_{l+1} = \bar{\alpha}. \quad (2)$$

The state-space matrices of the model (1) have a piecewise polynomial dependency on α and can all be expressed as:

$$S(\alpha) = \sum_{i=1}^{n_\lambda - g - 1} C_i B_{i,g,\lambda}(\alpha), \quad (3)$$

where $B_{i,g,\lambda}(\alpha)$ is the i^{th} normalized B-spline basis function of degree g for the knot sequence $\lambda \in \mathbb{R}^{n_\lambda}$

$$\underbrace{(\xi_0, \dots, \xi_0)}_{g+1}, \underbrace{(\xi_1, \dots, \xi_1)}_{g+1-v}, \dots, \underbrace{(\xi_l, \dots, \xi_l)}_{g+1-v}, \underbrace{(\xi_{l+1}, \dots, \xi_{l+1})}_{g+1}, \quad (4)$$

and C_i , $i = 1, \dots, n_\lambda - g - 1$ are matrix-valued coefficients [1]. The B-splines $B_{i,g,\lambda}(\alpha)$, $\alpha \in [\underline{\alpha}, \bar{\alpha}]$, are computed using the Cox-de Boor recursive formula [2].

3 Identification strategy

The procedure we propose starts with obtaining an initial model estimate using the SMILE technique [3], with B-spline basis functions of a desired degree and the knots placed at the scheduling points of the local measurements. After the initial estimate is determined, additional knots are inserted into the knot sequence, which elevates the model's degree of freedom without changing the shape of its splines. With this knot elevation, we augment the fitting capabilities of the model, aiming to obtain an as simple as possible scheduling parameter dependency while preserving or improving the LPV model accuracy. This dual goal is pursued by combining the classical weighted squared difference between the model response and corresponding measured system response focusing on the model accuracy, with a weighted $\ell_{2,1}$ -norm regularization in charge of removing redundant knots.

For a polynomial spline matrix $S(\alpha)$ of degree g with internal break points ξ_1, \dots, ξ_l and continuity condition v it holds that in a breakpoint ξ_i , $i \in \{1, \dots, l\}$, $S(\alpha)$ and its derivatives up to the order v are continuous [1]. The differentiation between the significant and redundant knots is based on the differences between adjacent elements of the v^{th} derivative and it involves specific grouping of the model coefficients followed by the $\ell_{2,1}$ -norm regularization.

4 Acknowledgement

This work has been carried out within the framework of Flanders Make SBO ROCSIS project (Robust and Optimal Control of Systems of Interacting Subsystems), FWO G.0915.14 project of the Research Foundation - Flanders (FWO - Flanders), and KU Leuven-BOF PFV/10/002 Centre of Excellence: Optimization in Engineering (OPTEC).

References

- [1] G. Hilhorst, E. Lambrechts, and G. Pipeleers, "Control of Linear Parameter-Varying Systems using B-Splines", 2016 IEEE 55th Conference on Decision and Control (CDC), pages 3246–3251.
- [2] C. De Boor, "A Practical Guide to Splines", ser. Applied Mathematical Sciences. Springer-Verlag, 2001, vol. 27.
- [3] J. De Caigny, J. F. Camino, and J. Swevers, Interpolating model identification for SISO linear parameter-varying systems, Mechanical Systems

Local module identification in dynamic networks using regularized kernel-based methods¹

Karthik R. Ramaswamy, Giulio Bottegal, and Paul M.J. Van den Hof
 Department of Electrical Engineering, Eindhoven University of Technology
 Email: {k.r.ramaswamy, g.bottegal, p.m.j.vandenhof}@tue.nl

1 Introduction and problem setting

In recent years increasing attention has been devoted to the identification of dynamic networks by the system identification community. One interesting problem, first tackled in [1], deals with the identification of one particular component –or module– of the network.

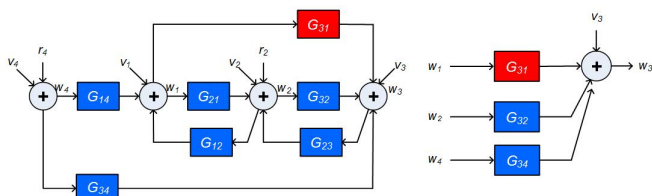


Figure 1: Left: An example of dynamic network, where the module of interest is G_{31} (in red). Right: MISO system describing the dynamics of the output of G_{31} .

It was shown in [1] that, in order to identify a given module of interest, one has to set up a MISO identification problem where the modules entering the MISO structure correspond to the modules of the network sharing the same output with the module of interest (see Fig. 1 for an example). This implies that it is required to 1) identify all such modules, a task that increases the variance of the estimates, and 2) determine the model order of all the modules, a task that may give inaccurate results.

2 Approach and results

In order to avoid the aforementioned problems, we suggest to use regularized nonparametric kernel-based methods [2]. Considering known topology, we keep a parametric model for the module of interest. The remaining modules contributing to the output are modeled as Gaussian vectors with covariance matrix (kernel) given by the first-order stable spline kernel [2].

Using this approach, one obtains a Gaussian probabilistic description of the problems that depends on a vector of parameters η containing the unknown module parameters and the hyperparameters characterizing the stable spline kernel.

¹This project has received funding from the European Research Council (ERC), Advanced Research Grant SYSDYNET, under the European Unions Horizon 2020 research and innovation programme (Grant Agreement No. 694504).

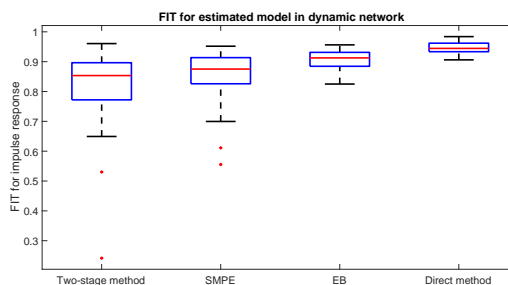


Figure 2: Box plot of the fit of the impulse response of a module obtained by the Direct method [1], the Two-stage method [1], the Simultaneous Minimization of Prediction Error (SMPE) [3], and the proposed method. Number of data samples ($N = 2000$).

Therefore, by estimating η we can retrieve the parameters of interest. To accomplish this task, we use an Empirical Bayes (EB) approach, where η is estimated by maximizing the marginal likelihood of the module output. The solution of the problem is carried out with an iterative Expectation-Maximization (EM) scheme.

Numerical experiments performed with a dynamic network example illustrate the potentials of the proposed method on comparison with the already available methods. Fig. 2 shows that a reduced variance is observed in the identified model due to the integration of regularization approach in the proposed method.

References

- [1] Van den Hof, P. M. J., Dankers, A. G., Heuberger, P. S. C., and Bombois, X., "Identification of dynamic models in complex networks with prediction error methods Basic methods for consistent module estimates", *Automatica*, 4(10):2994-3006, 2013.
- [2] Pillonetto, G., Dinuzzo, F., Chen, T., De Nicolao, G. and Ljung, L., 2014. "Kernel methods in system identification, machine learning and function estimation: A survey". *Automatica*, 50(3), pp.657-682.
- [3] Gunes, B., Dankers, A. G., and Van den Hof, P. M. J., "A variance reduction technique for identification in dynamic networks", *IFAC Proceedings Volumes*, 47(3):2842-2847, 2014.

Computing controlled invariant sets using semidefinite programming

Benoît Legat, Raphaël M. Jungers
 Université catholique de Louvain
 Avenue Georges Lemaitre, 4
 B-1348 Louvain-la-Neuve
 Belgium

Email: benoit.legat@uclouvain.be,
 raphael.jungers@uclouvain.be

Paulo Tabuada

Department of Electrical and Computer Engineering
 UCLA

Email: tabuada@ee.ucla.edu

The problem of computing a controlled invariant set is a paradigmatic challenge in the broad field of systems and control. Indeed, it is for instance crucial in safety-critical applications, such as the control of a platoon of vehicles or air traffic management; see for instance [5], where firm guarantees are needed on our ability to maintain the state in a safe region (e.g., with a certain minimal distance between vehicles). In other situations, the dynamical system might be too complicated to analyze exactly in every point of the state space, but yet it can be possible to confine the state within a guaranteed set.

A set is *controlled invariant* (sometimes also referred to as *viable*) if, any trajectory whose initial point is in the set can be kept inside it by means of a proper control action. Given a system with constraint specifications on the states and/or input, the controlled invariant set can be used to determine initial states such that trajectories with these initial conditions are guaranteed to meet the specifications. Moreover, in some situations, a state feedback control law can be derived from the knowledge of the controlled invariant set; see [1] for a survey.

The computation of invariant sets is usually achieved using either polyhedral computations or semidefinite programming. If the system contains a control input, the computational complexity of the problem becomes even more challenging. Indeed, this requires the computation of projections of polytopes (see e.g., the procedure p. 201 in [2]) or the parametrization of a family of polytopes [4] when using polyhedral computations and semidefinite programming techniques are not directly applicable. The problem of polyhedral projection is well known to severely suffer from the curse of dimensionality.

We give a method based on semidefinite programming to compute ellipsoidal invariant sets in [3]. A key ingredient in our technique is that we work in the dual space of the geometric problem. Given a discrete-time control system

$$x_{k+1} = Ax_k + Bu_k, \quad x_k \in \mathcal{X}$$

we show that an ellipsoid

$$\mathcal{E}_{p-1} = \{x \in \mathbb{R}^n \mid x^\top P^{-1} x \leq 1\}$$

is controlled invariant if and only if $\mathcal{E}_{p-1} \subseteq \mathcal{X}$ and

$$EAPA^\top E^\top \preceq EPE^\top$$

where E is a projection on $\text{Im}(B)^\perp$.

For a system with constraints on the input:

$$x_{k+1} = Ax_k + Bu_k, \quad x_k \in \mathcal{X}, \quad u_k \in \mathcal{U}$$

we show that \mathcal{E}_{p-1} is controlled invariant if and only if there exists a set

$$\mathcal{E}_{Q-1} = \{y \in \mathbb{R}^n \mid y^\top Q^{-1} y \leq 1\}$$

such that $\mathcal{E}_{p-1} \subseteq \mathcal{X}$, $\mathcal{E}_{Q-1} \subseteq \mathcal{X} \times \mathcal{U}$ and

$$(A \ B)Q(A \ B)^\top \preceq P \preceq (I \ 0)Q(I \ 0)^\top.$$

All these constraints are LMI-representable, and this allows us to introduce a new efficient procedure for the computation of controlled invariant sets. Our general method is presented in [3] and can be applied to affine hybrid control system, we only present here the particular case of linear control systems.

References

- [1] F. Blanchini. Set invariance in control. *Automatica*, 35(11):1747–1767, 1999.
- [2] F. Blanchini and S. Miani. *Set-theoretic methods in control*. Springer, second edition, 2015.
- [3] B. Legat, P. Tabuada, and R. M. Jungers. Computing controlled invariant sets for hybrid systems with applications to model-predictive control. *ArXiv e-prints*, Feb. 2018.
- [4] S. V. Rakovic and M. Baric. Parameterized robust control invariant sets for linear systems: Theoretical advances and computational remarks. *IEEE Transactions on Automatic Control*, 55(7):1599–1614, 2010.
- [5] C. Tomlin, G. J. Pappas, and S. Sastry. Conflict resolution for air traffic management: A study in multiagent hybrid systems. *IEEE Transactions on automatic control*, 43(4):509–521, 1998.

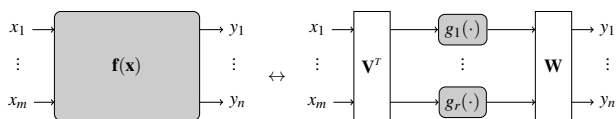
Decoupling multivariate functions: exploring multiple derivative information

Jeroen De Geeter Philippe Dreesen Mariya Ishteva
Vrije Universiteit Brussel (VUB), Dept. ELEC, Pleinlaan 2, B-1050 Brussels, Belgium
Jeroen.De.Geeter@vub.be

1 Introduction

Descriptions of nonlinear systems often involve a set of multivariate real functions. While very flexible, this has the downside of having a large number of parameters which makes gaining insight based on such models very difficult. When decoupling a set of multivariate real functions, these functions are expressed as a linear combination of univariate functions - removing cross terms. Such a decoupled representation may give more insight into the problem, reduce the number of variables or may be useful to simplify a complex system.

Formally, this decomposition can be written as $\mathbf{f}(\mathbf{x}) = \mathbf{W}\mathbf{g}(\mathbf{V}^T\mathbf{x})$ with \mathbf{V} and \mathbf{W} being linear transformation matrices and \mathbf{g} the set of univariate functions.



In order to compute this decomposition, [1] looks at the first-order information of the function, i.e. the Jacobian which can be written as $\mathbf{J}(\mathbf{x}) = \mathbf{W}\text{diag}(g'_i(\mathbf{v}_i^T\mathbf{x}))\mathbf{V}^T$. Stacking these matrices for sampling points $\mathbf{x}^{(k)}$, $k = 1, \dots, N$, results in a third order tensor \mathcal{J} . The canonical polyadic decomposition (CPD) [2, 3]

$$\mathcal{J} = \llbracket \mathbf{W}, \mathbf{V}, \mathbf{G}' \rrbracket = \sum_{i=1}^r \mathbf{w}_i \circ \mathbf{v}_i \circ \mathbf{g}'_i$$

gives us the different elements of the decoupled function with \circ denoting the outer product and \mathbf{g}'_i containing the evaluations of $g'_i(\mathbf{v}_i^T\mathbf{x}^{(k)})$ in the N sampling points.

In the exact case, we can integrate this result to retrieve the decomposition of the function up to a constant. However, this no longer holds in the presence of noise. Secondly, systems described by a single multivariate polynomial - related to the Waring problem - are also no candidate for the method in [1].

2 Methodology

In this contribution, we will directly look at the decomposition of the function as well as the decomposition of the second-order information, by looking at the Hessian.

	$\xrightarrow{N \text{ samples}}$	$\xrightarrow{\text{CPD}}$	
$\frac{\partial}{\partial \mathbf{x}} \downarrow$	$\mathbf{f}(\mathbf{x})$ $n \times 1$	$\mathbf{f}(\mathbf{x}^{(k)})$ $n \times N$	$\mathbf{F} = \llbracket \mathbf{W}, \mathbf{G}' \rrbracket$ $n \times R \quad N \times R$
$\frac{\partial}{\partial \mathbf{x}} \downarrow$	$\mathbf{J}(\mathbf{x})$ $n \times m$	$\mathbf{J}(\mathbf{x}^{(k)})$ $n \times m \times N$	$\mathcal{J} = \llbracket \mathbf{W}, \mathbf{V}, \mathbf{G}' \rrbracket$ $n \times R \quad m \times R \quad N \times R$
	$\mathcal{H}(\mathbf{x})$ $n \times m \times m$	$\mathcal{H}(\mathbf{x}^{(k)})$ $n \times m \times m \times N$	$\mathcal{H} = \llbracket \mathbf{W}, \mathbf{V}, \mathbf{V}, \mathbf{G}'' \rrbracket$ $n \times R \quad m \times R \quad N \times R$

Next to the linear transformation matrices \mathbf{W} (and \mathbf{V}) being the same for each of the three (two) decompositions there is partial symmetry with \mathbf{V} occurring twice in the CPD of the Hessians. These constraints can be imposed using Tensorlab's [4] structured data fusion functionality [5].

By leveraging the relationship between the decompositions we hope to improve the decoupling method for noisy data.

3 Acknowledgements

This work was supported in part by the Fund for Scientific Research (FWO-Vlaanderen) - projects G.0280.15N and G.0901.17N, by the Flemish Government (Methusalem), the Belgian Government through the FWO-FNRS Excellence of Science (EOS) program - project number 30468160 - SeLMA, and by the ERC Advanced Grant SNLSID under contract 320378.

References

- [1] P. Dreesen, M. Ishteva, J. Schoukens. Decoupling multivariate polynomials using first-order information and tensor decompositions. *SIAM J. Matrix Anal. Appl.*, 36(2):864–879, 2015.
- [2] R. A. Harshman. Foundations of the PARAFAC procedure: Models and conditions for an “explanatory” multimodal factor analysis. *UCLA Working Papers in Phonetics*, 16:1–84, 1970.
- [3] J. Carroll, J. Chang. Analysis of individual differences in multidimensional scaling via an N-way generalization of “Eckart-Young” decomposition. *Psychometrika*, 35(3):283–319, 1970.
- [4] N. Vervliet, O. Debals, L. Sorber, M. Van Barel, L. De Lathauwer. Tensorlab 3.0, 2016. Available online.
- [5] L. Sorber, M. Van Barel, L. De Lathauwer. Structured data fusion. *IEEE Journal of Selected Topics in Signal Processing*, 9(4):586–600, 2015.

Solving Multivariate Polynomial Optimization Problems via Numerical Linear Algebra

Christof Vermeersch Oscar Mauricio Agudelo Bart De Moor

KU Leuven, Department of Electrical Engineering (ESAT),

STADIUS Center for Dynamical Systems, Signal Processing, and Data Analytics

{christof.vermeersch, mauricio.agudelo, bart.demoor}@esat.kuleuven.be

1 Introduction

Within system identification and model reduction, multivariate polynomial optimization problems emerge frequently, e.g., when determining the model parameters from input-output data or minimizing the error of a reduced model. In this research, we explore a new approach to solve these optimization problems, using numerical linear algebra techniques. Although many heuristic approaches exist, state-of-the-art algorithms, mostly based on non-linear optimization, are not guaranteed to converge to the global optimal solution. Therefore, the main goal of our research is to solve these optimization problems exactly, i.e., to find the global optimal solution. Some work has been done by Dreesen et al. [2] and during this research we continue their efforts.

2 Research methodology

Polynomial optimization problems, as in Equation (1), are optimization problems for which the objective function $J(\mathbf{x}) \in \mathcal{P}(\mathbb{R})$ and constraints $g_i(\mathbf{x}) \in \mathcal{P}(\mathbb{R})$ are multivariate polynomials with real coefficients in the unknown optimization variable $\mathbf{x} \in \mathbb{C}^n$. Although the restrictions, these problems arise in numerous engineering applications, e.g., system identification, control theory, computer vision, robotics, computational biology, and many more [2].

$$\begin{aligned} & \inf_{\mathbf{x}} J(\mathbf{x}) \\ \text{s.t. } & \begin{cases} g_1(\mathbf{x}) = 0 \\ \vdots \\ g_s(\mathbf{x}) = 0 \end{cases} \end{aligned} \quad (1)$$

We tackle these optimization problems by embedding the objective function and the constraints, using Lagrange multipliers $\mu_i \in \mathbb{R}$, into a Lagrangian, of which the partial derivatives with respect to the components of \mathbf{x} and μ lead to a (potentially large) system of multivariate polynomials [2]. This system corresponds to a set of difference equations (see Dreesen et al. [1]). Consequently, the kernel of the Macaulay matrix (constructed from the coefficients of the multivariate polynomials), which is spanned by Vandermonde-like vectors constructed from the roots, is a multidimensional observability matrix. Thus, we find these roots via the construction of an autonomous multi-

dimensional (nD) linear state space model (realization theory), followed by a large eigenvalue calculation.

We do not need to find all the roots (which might be many, including at infinity), but only the optimal one. Therefore, we use a little trick. We define $M = \frac{1}{J(\mathbf{x})} \in \mathbb{R}$ and then add one extra equation to the system, namely $MJ(\mathbf{x}) = 1$. We can reformulate now, after some technical steps, the eigenvalue problem as to find the maximal eigenvalue M . This implies that the power method (or more advanced iterative eigenvalue solvers, e.g., Arnoldi, Lanczos, etc. (see [3])) can be used to find, in an iterative way, the optimizing root of our original polynomial optimization problem.

3 Presentation outline

In our presentation, we will elaborate on how one can set up, from the Macaulay matrix, an eigenvalue problem, of which one of the eigenvalues is the optimal value of the objective function. Furthermore, we will develop two algorithms to find this optimal solution. The first one starts from the kernel of the Macaulay matrix, the second one (or dual approach) works directly on the columns of the Macaulay matrix.

4 Acknowledgments

This research receives support from FWO under EOS project G0F6718N (SeLMA) and from KU Leuven Internal Funds: C16/15/059 and C32/16/013.

References

- [1] Philippe Dreesen, Kim Batselier, and Bart De Moor. Multidimensional realization theory and polynomial system solving. Internal report 15-145, ESAT-STADIUS, KU Leuven (Leuven, Belgium), 2015. *International Journal of Control.*, Lirias number: 593599.
- [2] Philippe Dreesen and Bart De Moor. Polynomial optimization problems are eigenvalue problems. In Paul M.J. Hof, Carsten Scherer, and Peter S.C. Heuberger, editors, *Model-Based Control: Bridging Rigorous Theory and Advanced Technology*. Springer, 2009.
- [3] Gene H. Golub and Charles F. Van Loan. *Matrix Computations*. Johns Hopkins University Press, 4th edition, 2013.

Lookup tables in optimization with CasADi and OptiSpline

Joris Gillis

MECO Research Team, Department Mechanical Engineering, KU Leuven
DMMS lab, Flanders Make, Leuven, Belgium
Yacoda BVBA, Belgium
joris.gillis@kuleuven.be

1 Introduction

The use of look-up tables is ubiquitous in industrial modeling practice. Common occurrences of look-up tables are efficiency maps of motors, and maps of aerodynamic properties. For the parties that set up the laborious measurement campaigns to generate them, they are the prized and protected possessions that allow for accurate simulation of the modeled process.

For engineers working on gradient-based (dynamic) optimization, on the other hand, models containing look-up tables can be a nuisance because of (a) lack of support for optimization modeling languages, and (b) lack of smoothness or introduction of oscillations when smoothness is enforced.

To handle problem (a), this abstract presents the addition of a fully differentiable B-spline node into the open-source CasADi [1] framework for algorithmic differentiation and numerical optimization. To handle problem (b), this abstract proposes the use of the OptiSpline¹ toolbox to design B-splines with desirable properties out of measured data.

2 B-splines in CasADi

The new look-up table node, packaged as `Function.bspline`, evaluates a B-spline function $\Pi: \mathbb{R}^n \mapsto \mathbb{R}^m$, and possesses the following properties:

- defined on a tensor-product grid of n dimensions,
- restricted to numerical knot locations and coefficients.

CasADi computational graphs containing the node support:

- algorithmic differentiation up to the degree of the spline,
- code-generation,
- an evaluation time independent on grid resolution².

In addition, we provide an exact interpolation with knot-to-knot end conditions, mirroring MATLAB's `interp`:

```
[X,Y] = ndgrid(xgrid,ygrid)
V = sqrt(5*X.^2+Y.^2)+1;
lut = interpolant('LUT','bspline',
    {xgrid,ygrid},V(:))
lut([0.5 1])
interp(X,Y,V,0.5,1,'spline')
```

¹Obtainable from github.com/meco-group/optispline

²Only for uniform grids at the moment

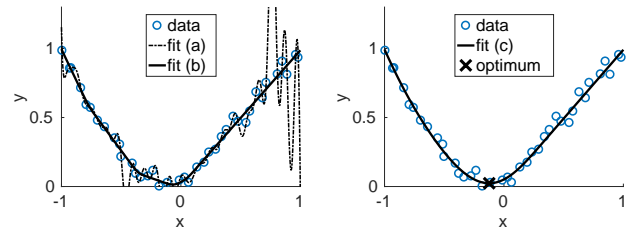


Fig. 1. Three fitting strategies for given data

3 Fitting B-splines with OptiSpline

Consider noisy data vectors $x, y \in \mathbb{R}^n$ and a 1D B-spline with coefficients C to be optimized. Fit (a) from Figure 1, smooth but oscillatory, is given by a least-squares formulation with $\|\Pi(C; x_i) - y_i\|_2$:

```
opti = OptiSpline()
basis = BSplineBasis([-1,1],4,N)
F = opti.Function(basis)
e = F.list_eval(x)-y
opti.minimize(e'*e)
```

Fit (b) is made convex by the addition of a positive definiteness constraint $\frac{\partial^2 \Pi}{\partial x^2} \geq 0$:

```
H = F.hessian_matrix()
opti.subject_to(H>=0)
```

Fit (c) is most desirable since its local quadratic optimization is more constant by regularizing its variation:

```
reg = integral(H.jacobian_matrix^2)
opti.minimize(e'*e+1e-4*reg)
```

The resulting spline can be optimized over in pure CasADi:

```
X = opti.variable()
Fsol = to_casadi(sol.value(F))
opti.minimize(Fsol(X))
```

References

- [1] Joel Andersson. *A General-Purpose Software Framework for Dynamic Optimization*. PhD thesis, Arenberg Doctoral School, KU Leuven, Department of Electrical Engineering (ESAT/SCD) and Optimization in Engineering Center, Kasteelpark Arenberg 10, 3001-Heverlee, Belgium, October 2013.

Acknowledgement. This work has been carried out within the framework of projects Flanders Make ICON: Physical and control co-design of electromechanical drivetrains for machines and vehicles, and KU Leuven-BOF PFV/10/002 Centre of Excellence: Optimization in Engineering (OPTeC). This work also benefits from KUL-C1: KU Leuven Research project C14/15/067: B-spline based certificates of positivity with applications in engineering.

Proximal Outer Approximation

Massimo De Mauri, Goele Pipeleers and Jan Swevers

KU Leuven/LRD, Dept. Mechanical Engineering

Flanders Make ICON project: Concept Design

Email: massimo.demauro@kuleuven.be

Many engineering and scientific applications require the solution of Mixed-integer Non-Linear Problems (MINLPs). However, efficiently solving medium-large MINLPs remains a challenge.

MINLPs are harder to solve than Non-Linear Problems (NLPs) and Mixed-Integer Linear Problems (MILPs). Consequently, Duran and Grossmann in 1986 [1] proposed an algorithm, called Outer Approximation (OA), that finds an optimal point for a given convex MINLP via the solution of an alternating sequence of MILPs and NLPs. After more than thirty years, the algorithmic ideas of the original OA method are still at the core of the most competitive MINLP solution approaches.

1 Outer Approximation

OA is a multi-step iterative procedure that starts from an initial set L of linearizations of the non-linear constraints of the MINLP, and then, at each iteration:

1. L and the original objective function (that, w.l.o.g., can be assumed linear) are used to define a MILP whose solution \bar{x} yields a lower-bound on the optimal objective value of the MINLP.
2. The value of the discrete components of \bar{x} is fixed in the original MINLP, whereby, it reduces to a NLP. If the NLP is feasible, it is solved obtaining \hat{x} which is a feasible solution for the original MINLP and yields an upper-bound on the optimal objective value of the MINLP. If the NLP is infeasible, \hat{x} is set as the minimizer of a certain infeasibility measure.
3. If the current best upper-bound and lower-bound found coincide, the algorithm stops. Otherwise, new linearizations around \hat{x} of the non-linear constraints are added to L and the procedure restarted from step 1.

If the discrete components of x are bounded, then, OA is guaranteed to converge to an optimal solution for the MINLP in a finite (although often large) number of steps.

2 Our Contribution

The main criticalities regarding the OA algorithm consist of:

- Often, and especially during the earliest iterations, the set of linearizations poorly approximates the non-linear constraints leading to scarcely meaningful MILP optimal points.

- In case of infeasible discrete assignments in the second step, setting \bar{x} as the minimizer of an infeasibility measure leads to linear approximations which aren't necessarily optimally tight.

Partially inspired by the recent developments on Feasibility Pump like heuristics for MINLPs (ref. [2] for an overview) we will present a new adaptive OA scheme: the Proximal Outer Approximation (POA), where:

- The MILP objective is set as a convex combination of the original objective and the $L1$ distance between the MILP solution and the most recent NLP solution in order to increase the odds of finding a feasible solution at each iteration. The parameters of such combination are adapted depending on the estimated quality of the current linear approximations set.
- The second step detects infeasibility by finding the closest point \hat{x} to \bar{x} along the discrete components of x which is feasible w.r.t. the non-linear constraints. Then, depending on the distance between \hat{x} and \bar{x} either feasibility or infeasibility is declared. In case of feasibility, the algorithm proceeds as OA, while, in case of infeasibility, \hat{x} is used to obtain tighter linearizations w.r.t OA
- At each iteration, special linear cuts are added to L to speed-up the convergence.

POA has the same optimality guarantees of OA but exhibit better runtime performances.

3 Results

The performances of the POA algorithm are compared with the ones of the classical OA algorithm implemented in Bonmin [3]. The results show that the former consistently outperforms the latter over the Bonmin test Library, despite its not optimized python implementation. Moreover, the proposed scheme finds good solutions earlier during the iterations making it more suitable for real time optimization tasks.

References

- [1] M. A. Duran, I. E. Grossmann. An outer-approximation algorithm for a class of mixed-integer nonlinear programs, 1986.
- [2] T. Berthold, A. Lodi, D. Salvagnin. Ten years of Feasibility Pump and counting, 2017.
- [3] Bonmin, <https://www.coin-or.org/Bonmin>.

Parametric and robust optimization with OptiSpline

Joris Gillis, Erik Lambrechts, and Goele Pipeleers
 MECO Research Team, Department Mechanical Engineering, KU Leuven
 DMMS lab, Flanders Make, Leuven, Belgium
 {erik.lambrechts,joris.gillis,goele.pipeleers}@kuleuven.be

1 Introduction

B-Splines relaxations have been successfully applied to solve semi-infinite optimal control problem for flat systems [3] with guarantees for constraint satisfaction, and to compose robust controllers [2] for linear parameter varying systems (LPV). This abstract introduces a fresh open-source project, OptiSpline¹, that consolidates the various research codes that have supported the above-cited research into a general-purpose toolbox.

2 Design

The toolbox introduces the following concepts:

Basis A set of basis functions on a domain.

BSplineBasis A concrete instance of `Basis`, this concept represents a set of B-Spline basis function on a 1D domain, defined by knot locations. This set forms a partition of unity, enjoys local support, and any linear combination of members is guaranteed to lie inside the control polygon.

TensorBasis The outer product of arbitrary `Basis` objects.

Function A linear combination of all basis functions of a `TensorBasis`, with the weights collectively referred to as *coefficient tensor*.

These concepts give rise to (immutable) objects, with a range of methods to derive from them or compose with them (e.g. taking the integral, degree elevation, addition). The code-base has been developed in C++², with Python and MATLAB interfaces. Some unique properties of the proposed toolbox are:

1. Support for parametric knot locations, symbolic coefficients, symbolic evaluation points (CasADi [1] is used as back-end).
2. Integrated support with optimization tools for nonlinear (NLP) and convex programming.
3. Support for labels to refer to particular dimensions of a higher-dimensional spline.

3 Examples

Figure 1 shows a B-Spline approximation to a solution manifold $F(p) = \operatorname{argmin}(p-x)^2 + 5(y-x^2)^2$ solved with

¹Obtainable from github.com/meco-group/optispline

²The choice for C++ is motivated by portability, not speed.

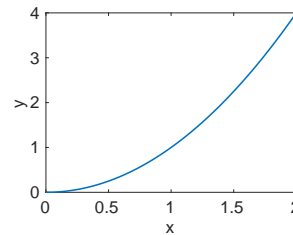


Fig. 1. Parametric solution

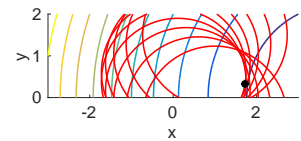


Fig. 2. Robust solution

the following MATLAB code:

```
import splines.*
S = OptiSpline();
b = BSplineBasis([0,2],2,3)
x = S.Function(b)
y = S.Function(b)
p = Function.linear([0,2],[0,2])
obj = (p-x)^2+5*(y-x^2)^2
S.minimize(obj.integral())
```

Figure 2 shows the robust solution to an NLP with a disturbance $d \in [-1, 1]$ in its constraint, solved with:

```
d = Function.linear([-1,1],[-1,1])
d = d.degree_elevation(2)
d = d.midpoint_refinement(4)
x = S.variable()
y = S.variable()
S.minimize((x-4)^2+y^2)
S.subject_to((d^2-x)^2+(y-d-0.5)^2 <= 3)
```

References

- [1] Joel Andersson. *A General-Purpose Software Framework for Dynamic Optimization*. PhD thesis, Arenberg Doctoral School, KU Leuven, Department of Electrical Engineering (ESAT/SCD) and Optimization in Engineering Center, Kasteelpark Arenberg 10, 3001-Heverlee, Belgium, October 2013.
- [2] G. Hilhorst, E. Lambrechts, and G. Pipeleers. Control of linear parameter-varying systems using b-splines. In *2016 IEEE 55th Conference on Decision and Control (CDC)*, pages 3246–3251, Dec 2016.
- [3] T. Mercy, W. Van Loock, and G. Pipeleers. Real-time motion planning in the presence of moving obstacles. In *2016 European Control Conference (ECC)*, pages 1586–1591, June 2016.

Acknowledgement. This work has been carried out within the framework of projects Flanders Make ICON: Physical and control co-design of electromechanical drivetrains for machines and vehicles, and KU Leuven-BOF PFV/10/002 Centre of Excellence: Optimization in Engineering (OPTEC). This work also benefits from KUL-C1: KU Leuven Research project C14/15/067: B-spline based certificates of positivity with applications in engineering.

Semantic world modeling for autonomous cars

Marzieh Dolatabadi Rene van de Molengraft Maarten Steinbuch
 Control Systems Technology Group
 Eindhoven University of Technology
 P.O. Box 513, 5600MB Eindhoven
 The Netherlands
 Email: m.dolatabadi.farahani@tue.nl

1 Introduction

The possibility to drive autonomously (driverless) through an urban environment has been a vision for many years. One of the many serious challenges of an autonomous car is driving safely through urban traffic, sharing the roads with other traffic participants, such as other cars, pedestrians and bicycles [1]. Having an accurate description of the environment is an important requirement to deal with these challenges. In this research/project, the problem of a semantic environmental description (world model) for autonomous cars in a campus environment is investigated. We achieve this world model for an autonomous car by using a probabilistic multiple hypothesis tree that combines with Bayesian sensor fusion techniques.

2 Approach

To estimate features and track objects depending on the task and the objects that are involved (cars, pedestrians, cyclists, etc.), an autonomous car should overcome various challenges. In the following part some of these problems, which are solved during the current work, are mentioned.

1. In urban environment, tracking object attributes and associating measurements are non-trivial tasks due to the uncertainty in their states. The combination of these two problems is called multiple target tracking (MTT) [2]. The Multiple Hypothesis Tracker (MHT) is a popular method to solve MTT.
2. Linking measured attributes to semantical objects is another challenge to solve in order to have a meaningful description of the environment. Creating and maintaining this link is called anchoring [3].

Incorporation of MHT in an anchoring strategy is a solution which is applied in this world model. Applying this algorithm, it is possible to combine different forms of evidence into a common and updated world representation dynamically. Objects attributes, classification and prior knowledge are associated in the hypotheses tree. Figure 1 gives a schematic overview of the complete algorithm. In this Figure every hypothesis contains a list of anchors and has a

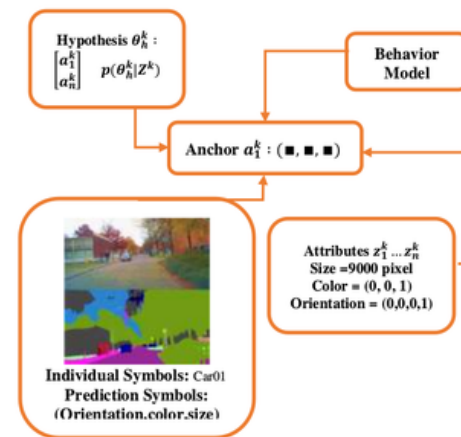


Figure 1: Schematic overview of algorithm [3].

probability of being correct. Each anchor on its turn contains an individual symbol, a set of measurements and a probabilistic signature that consists out of a mixture of probability density functions (pdfs) generated by a set of behavior models. The predicate attribute space represents predicate grounding relations that link attribute values and predicate symbols [3]. As a first proof of concept for a world model for autonomous cars, the algorithm is applied on a stream of images taken from TU/e campus. After cars, cyclists and pedestrians detection, input data is fed to the world model. A constant velocity Kalman filter and a uniform distribution of objects movement are used as initial conditions. The results have so far shown that our world model has the ability to perform correctly in tracking multiple attributes. This is the same as it is being done in anchoring algorithms and using prior knowledge to prediction.

References

- [1] F. Andrei, L. Vlacic. "An object-oriented design of a world model for autonomous city vehicles." Intelligent Vehicles Symposium (IV), 2010 IEEE. IEEE, 2010.T.
- [2] D. Laet, R. Bayesian. "multitarget tracking and localization", Ph.D. Thesis, May 2010.
- [3] J. Elfring, et al. "Semantic world modeling using probabilistic multiple hypothesis anchoring." Robotics and Autonomous Systems 1.2 (2013): 95-105.

Gearbox design for a Flapping Twin-Wing Robot

Hussein Altartouri

Email: haltarto@ulb.ac.be

Emanuele Garone

Email: egarone@ulb.ac.be

André Preumont

Email: apreumon@ulb.ac.be

Active Structures Laboratory, Department of Control Engineering and System Analysis
Université Libre de Bruxelles

1 Introduction

The amazing agility of insects and hummingbirds has always fascinated the humans and, over the past 40 years, biologists have gradually uncovered the complex unsteady aerodynamic mechanisms leading to extraordinary aerodynamic forces generated by their flapping wings. Simultaneously, the extreme miniaturization of avionics has made possible to consider building robots mimicking the behavior of insects and birds.

The project at Active Structures Laboratory (ASL) aims at designing and controlling a MAV capable of hovering with flight autonomy of several minutes. The weight and wingspan are restricted to the hummingbird size. Figure 1 shows a general view of the being developed robot 'Colibri Robot' [1].

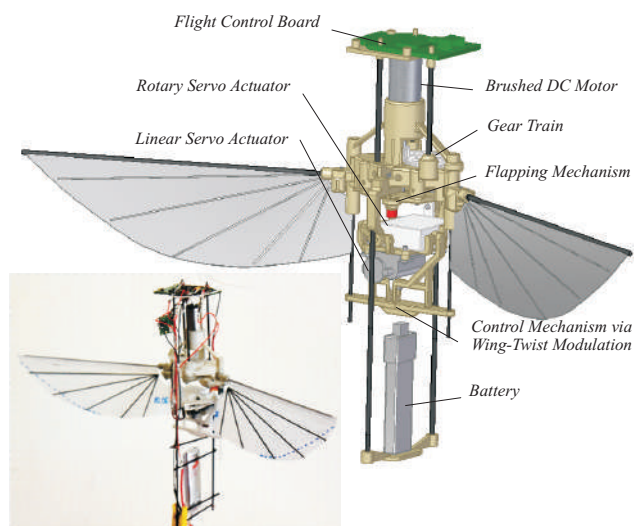


Figure 1: General view of the Colibri robot.

2 Gearbox design

The flapping mechanism is the mechanism responsible for flapping the wings. The input of the mechanism is connected to the motor by a gearbox with a gear ratio of G . Figure 2 shows the characteristics of the motor (torque versus rotation speed) for various voltages and the (measured) torque

requirements versus rotation speed (flapping frequency \times gear ratio) of the flapping mechanism [2]. In order to characterize the flapping mechanism load, the armature current and the flapping frequency are monitored and recorded for various motor voltages. Then the required torque is computed using the motor torque constant; a high speed camera is used to evaluate the flapping frequency. The crossing of the two curves is the operating point of the mechanism, provided that the corresponding current is below the thermal limit allowed for the motor.

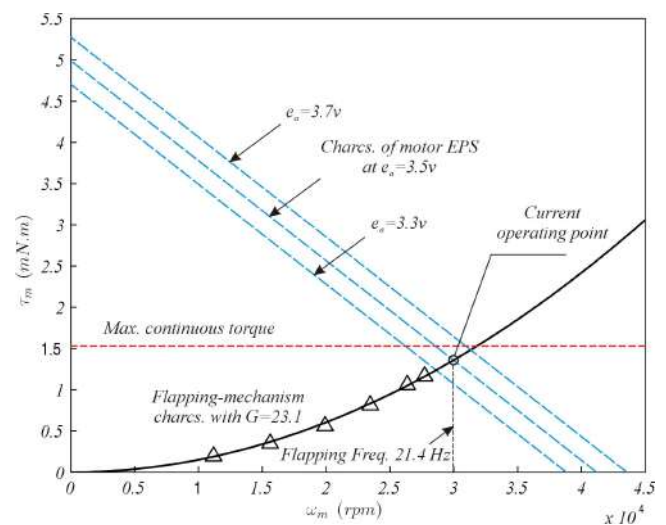


Figure 2: Torque versus rotation speed of the motor, for various voltages, and measured torque requirements of the mechanism for a gear ratio of $G = 23.1 : 1$. The crossing of the two curves is the operating point of the mechanism.

References

- [1] H. Altartouri, A. Roshanbin, G. Andreolli, L. Fazzi, M. Karásek, M. Lalami, and A. Preumont, "Passive Stability Enhancement with Sails of a Hovering Flapping Twin-Wing Robot," *International Journal of Micro Air Vehicles*, recently accepted 'to appear'.
- [2] A. Roshanbin, H. Altartouri, and A. Preumont, "COLIBRI: A hovering flapping twin-wing robot," *International Journal of Micro Air Vehicles*, volume: 9, issue: 4, pp: 270-282, 2017.

Implementation aspects of time-optimal predictive path following for robot arms

Niels van Duijkeren, Goele Pipeleers, and Jan Swevers

MECO Research Team, Department Mechanical Engineering, KU Leuven & DMMS lab, Flanders Make

Email: Niels.vanDuijkeren@kuleuven.be

Moritz Diehl

IMTEK, University of Freiburg

1 Introduction

Planning of time-optimal trajectories for robots is an old problem that is still relevant today. In many applications, among which manufacturing, the robot is operating most cost effectively when tasks are completed in minimum time. Let us consider the class of tasks that can be described by tracking a geometric curve as fast as possible, given a set of bounds on states and inputs. The works of [1, 2], and more recently [3], presented constructive methods to find trajectories that exactly track a path in the configuration space of a robot manipulator time optimally. In an offline optimization phase reference trajectories are generated, which are subsequently fed to the online tracking controllers for the joint positions and velocities; traditionally cascaded PID controllers.

The advantage of separating the optimization from reference tracking is that the burden of computing optimal trajectories is entirely offline. This greatly relaxes the performance requirements on the computational hardware on the robot itself. However, it also implies that trajectories cannot be updated during the execution of the reference tracking phase. With current computational hardware and available embedded optimization algorithms, the reference tracking controllers can in principle be replaced with or augmented by online optimization algorithms. If such optimizations are executed periodically in a receding horizon manner one obtains a so-called Economic Nonlinear Model Predictive Control (E-NMPC) scheme [4]. The application of E-NMPC increases the flexibility of the control task: during operation, it can deal with temporary changes in the environment and modifications in parts of the reference path yet to traverse. Also, due to the online optimization, the economic performance objective can be taken into account while attenuating disturbances and to, for instance, exploit tolerance bounds for increased performance [5].

2 Main result

In line with recent developments in fast embedded optimization software, this talk presents results from the application of minimum-time predictive path following to an experimental setup. Considered is an ABB IRB120, a six degree

of freedom robot arm, controlled at 250Hz using a Linux workstation on a real-time kernel. The problem formulation is based on [6] and takes two ingredients: a geometric curve defined in the workspace of the robot manipulator, and a tolerance bound with respect to the path. A finite horizon optimal control problem (OCP) results, in which we wish to optimize for minimum motion time along the curve, while staying inside the tolerance bound, and respecting bounds on states and inputs. This OCP is discretized using a direct multiple shooting method to obtain a nonlinear program (NLP), which is to be solved in every sampling interval.

Due to the economic nature of the objective, the implemented sequential quadratic programming approach requires second order sensitivities to obtain a good local quadratic model of the NLP. This is essential to obtain fast convergence behavior, but it also greatly increases the computational complexity. Approaches to mitigate the added computational burden in application to the case study, such as employing inexact sensitivities [7], are investigated. The results demonstrate that economic NMPC is a viable approach for the control of fast mechatronic systems.

References

- [1] J. Bobrow, S. Dubowsky, and J. Gibson, "Time-optimal control of robotic manipulators along specified paths," *The International Journal of Robotics Research*, vol. 4, pp. 3–17, Sept. 1985.
- [2] K. G. Shin and N. D. McKay, "Minimum-time control of robotic manipulators with geometric path constraints," *IEEE Transactions on Automatic Control*, vol. 30, pp. 531–541, June 1985.
- [3] D. Verscheure, B. Demeulenaere, J. Swevers, J. De Schutter, and M. Diehl, "Time-optimal path tracking for robots: A convex optimization approach," *IEEE Transactions on Automatic Control*, vol. 54, no. 10, pp. 2318–2327, 2009.
- [4] M. Ellis, J. Liu, and P. Christofides, *Economic Model Predictive Control*. Springer-Verlag GmbH, 2016.
- [5] N. van Duijkeren, T. Faulwasser, and G. Pipeleers, "NMPC with economic objectives on target manifolds," in *Proceedings of the 56th IEEE Conference on Decision and Control (CDC)*, (Melbourne, Australia), Dec. 2017.
- [6] T. Faulwasser and R. Findeisen, "Nonlinear model predictive control for constrained output path following," *IEEE Transactions on Automatic Control*, vol. 61, no. 4, pp. 1026–1039, 2016.
- [7] N. van Duijkeren, G. Pipeleers, J. Swevers, and M. Diehl, "Towards dynamic optimization with partially updated sensitivities," in *Proceedings of the 20th IFAC World Congress*, (Toulouse, France), pp. 8680–8685, July 2017.

Acknowledgements This work is supported by the EU via FP7-ITN-TEMPO (607 957), with Niels van Duijkeren being a fellow of the TEMPO Initial Training Network. This work also benefits from support from projects G0C4515N and G0A6917N of the Research Foundation - Flanders (FWO - Flanders), from Flanders Make, and from KU Leuven-BOF PFV/10/002 Centre of Excellence: Optimization in Engineering (OPTEC).

In-eye Forbidden-Region Virtual Fixtures based on Optical-Coherence-Tomography-probe proximity measurements

Y.G.M. Douven, M.J.G. van de Molengraft, M. Steinbuch

Control Systems Technology Group, Eindhoven University of Technology

P.O. Box 513, 5600MB Eindhoven, the Netherlands. E-mail: y.g.m.douven@tue.nl

1 Introduction

Vitreoretinal surgery addresses sight-threatening conditions on the back of the eye. Since structures on the back of the eye are often only a few micrometers, the technical demands placed on the surgeon by these procedures are very high. Robotic systems can provide a distinct and positive alteration in patient outcome when they can show to really enhance the surgeon's capability by providing both physical and mental assistance. Although the use of a stereomicroscope provides a three dimensional image to the physician, determining the distance between instrument-tip and retina proves to be very hard.

2 Proximity sensing

The surgical instrument, which is connected to a robotic setup that is controlled by the surgeon, is equipped with an Optical Coherence Tomography (OCT) probe. OCT [1] is a sensor solution based on interference between two light paths and can be used to measure a one-dimensional depth image (A-scan). Figure 1 shows an A-scan measured from an OCT-probe inside a porcine eye.

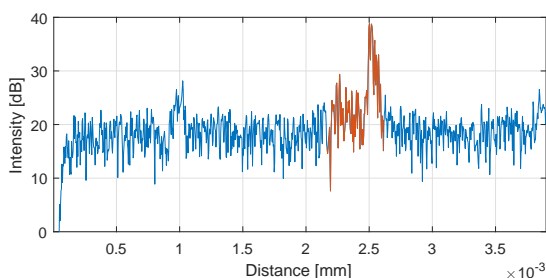


Figure 1: A-scan measured in an in-vivo porcine eye. The x-axis shows the depth in mm. The retina and choroid can be seen around 2.2 mm.

3 Retina detection and tracking

The measured A-scans are processed using template matching to create a discrete probability distribution of where the retina might be in the A-scan. Combined with the measured robot position, a discrete Bayesian filter is then used to track the retina in one dimension (along the axis of the measurement). The robot position is here essentially used as an initial guess to where the retina might be in the A-scan. When

the robot moves towards the retina, the retina is expected to move left in the A-scan.

This filter now provides one dimensional distance information towards the retina. However, when moving sideways above a curved retina, no prediction can be made on the distance, since the exact shape of the eye is unknown. Therefore, the retinal surface is mapped by fitting a polynomial plane through the measured distances. For this, an Extended Kalman Filter is used, with the measured distance and the robot encoders as input. Now, when moving sideways, the relative displacement of the polynomial plane w.r.t. the robot is used as input to the Bayesian filter.

4 Retina proximity feedback

The robotic system is a telemanipulation setup developed by PRECEYES [2], consisting of a motion controller (master) and an instrument manipulator (slave). The surgeon controls the motion controller and the measured position of the motion controller is used as a reference to the instrument manipulator. The calculated distance to the retina is now used to limit the reference to the instrument manipulator, thereby decoupling the master and slave in one direction. This provides forbidden-region virtual fixtures to the surgeon.

When moving sideways, the virtual fixture not only consists of a limit to the reference in axial direction, but also contains a gradient. This gradient is based on the polynomial plane that represents the retina and functions as feed-forward to increase precision.

Next to decoupling the telemanipulation setup at a virtual fixture, the measured distance is fed back to the surgeon using auditory cues. This greatly increases depth perception, which, combined with the virtual fixtures, decreases stress to the surgeon and increases safety.

References

- [1] Yaqoob, Z., Wu, J., & Yang, C. (2005). Spectral domain optical coherence tomography: a better OCT imaging strategy. *BioTechniques*, 39
- [2] Preceyes. (2018, Jan.) Website. [Online]. Available: <http://www.preceyes.nl/>

3D Path-following Using a Guiding Vector Field

Weijia Yao, Yuri A. Kapitanyuk, Ming Cao
 ENTEG, University of Groningen

Email: {w.yao, i.kapitaniuk, m.cao}@rug.nl

When solving a path-following problem using the guiding vector field (GVF), a vector field is designed so that its integral curves approach the desired path, and thus guides a robot to follow the path asymptotically. In [1], a 2D GVF is designed for a non-holonomic wheeled robot to follow a smooth desired path in general forms. This paper presents some preliminary results on the extension of [1], where a 3D desired path is considered and a corresponding 3D GVF is designed.

1 Problem Formulation

A desired 3D path \mathcal{P} can be described by the intersection of two surfaces in their implicit forms:

$$\mathcal{P} \triangleq \{(x, y, z) : \phi_1(x, y, z) = 0, \phi_2(x, y, z) = 0\} \subset \mathbb{R}^3, \quad (1)$$

where $\phi_i \in C^2 : \mathbb{R}^3 \rightarrow \mathbb{R}$, $i = 1, 2$. We only consider the case where the intersection is composed of **one** smooth curve. Given any vector $r \in \mathbb{R}^n$, a *bounded operator* on r is defined as $\bar{r} = \frac{r}{1+|r|^2}$ such that the norm of \bar{r} is bounded. The corresponding guiding vector field is designed as

$$v(\xi) = \overline{n_1(\xi)} \times \overline{n_2(\xi)} - \overline{k_1 e_1(\xi) n_1(\xi)} - \overline{k_2 e_2(\xi) n_2(\xi)}, \quad (2)$$

on \mathbb{R}^3 , where $n_i(\xi) = \nabla \phi_i(\xi)$, $e_i(\xi) = \phi_i(\xi)$ and $k_i > 0$ are constants, for $i = 1, 2$. Therefore, $\mathcal{P} = \{\xi \in \mathbb{R}^3 : e(\xi) = 0\}$, where $e(\xi) = [e_1(\xi) \ e_2(\xi)]^T$.

We denote the distance between a point $p_0 \in \mathbb{R}^3$ and a set $S \subset \mathbb{R}^3$ by $\text{dist}(p, S) = \inf\{\|p - p_0\| : p \in S\}$. In addition, the distance between two sets $A, B \subset \mathbb{R}^3$ is defined as $\text{dist}(A, B) = \inf\{\|p_1 - p_2\| : p_1 \in A, p_2 \in B\}$. Next, we define a set $\mathcal{M} \triangleq \{\xi \in \mathbb{R}^3 : N(\xi)Ke(\xi) = 0\}$. This set contains the desired path \mathcal{P} . Furthermore, a **critical set** is defined as $\mathcal{C} = \{\xi \in \mathcal{M} : \text{rank}(N(\xi)) \leq 1\}$. Since the set $\mathcal{T} \triangleq \{\xi \in \mathcal{M} : \text{rank}(N(\xi)) = 2\} \subset \mathcal{P}$, it follows that $\mathcal{P} \cup \mathcal{C} = \mathcal{M}$. Let $N(\xi) = [n_1(\xi) \ n_2(\xi)]_{3 \times 2}$ and $K = \begin{bmatrix} k_1 & 0 \\ 0 & k_2 \end{bmatrix}$. The following assumptions are made.

Assumption 1: For any given constant $\kappa > 0$ and $p \in \mathbb{R}^3$, it follows that $\inf\{\|e(p)\| : \text{dist}(p, \mathcal{P}) \geq \kappa\} > 0$.

Assumption 2: $\text{dist}(\mathcal{C}, \mathcal{P}) > 0$.

Assumption 3: For any given constant $\kappa > 0$ and $p \in \mathbb{R}^3$, it follows that $\inf\{\|N(p)Ke(p)\| : \text{dist}(p, \mathcal{M}) \geq \kappa\} > 0$.

2 Main Results

The integral curves of (2) correspond to the trajectories of the following autonomous ordinary differential equation:

$$\frac{d}{dt} \xi(t) = v(\xi(t)), \quad t \geq 0, \quad (3)$$

where $\xi(t) : t \mapsto (x, y, z) \in \mathbb{R}^3$. Now we present the following theorem stating that the integral curves of (3) converge to either the desired path or the critical set.

Theorem 1 *Let $\xi(t)$ be a solution to (3). Then it will converge to the set $\mathcal{M} = \{\xi \in \mathbb{R}^3 : N(\xi)Ke(\xi) = 0\}$. Particularly, two outcomes are possible: (1) $\lim_{t \rightarrow \infty} \text{dist}(\xi(t), \mathcal{P}) = 0$, that is, the solution converges to the desired path. (2) $\lim_{t \rightarrow \infty} \text{dist}(\xi(t), \mathcal{C}) = 0$, that is, the solution converges to the critical set.*

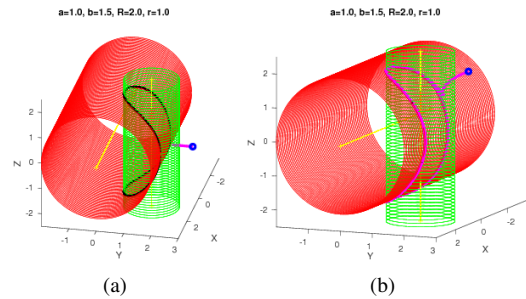


Figure 1: An example. Trajectory (pink) converges to the critical set (a) and to the path (b) respectively.

3 Example

Consider two surfaces in their explicit forms $\phi_1(x, y, z) = 0$ and $\phi_2(x, y, z) = 0$, where $\phi_1(x, y, z) = (x - a)^2 + (y - b)^2 - r^2$, $\phi_2(x, y, z) = y^2 + z^2 - R^2$. Note that $a, b, R, r \in \mathbb{R}$ and $R > r > 0$. When $b \in (-R - r, -R + r) \cup (R - r, R + r)$, the curve and the simulation results are shown in Fig. 1.

References

- [1] Y. A. Kapitanyuk, A. V. Proskurnikov and M. Cao, "A Guiding Vector-Field Algorithm for Path-Following Control of Nonholonomic Mobile Robots," IEEE Transactions on Control Systems Technology, vol. PP, no. 99, pp. 1-14.

Identification of the Time-Varying Human Joint Impedance for the Application to Bionic Devices

Gaia Cavallo* gaia.cavallo@vub.be, Mark van de Ruit⁺, Alfred C. Schouten⁺, John Lataire*

* Vrije Universiteit Brussel, Dpt. ELEC, Pleinlaan 2, B-1050 Brussels, Belgium

⁺ Dpt. of Biomech. Eng., Delft University of Technology, Mekelweg 2, 2628CD, Delft, the Netherlands

1 Context: Human joint impedances

The neuromuscular system continuously regulates the properties of the human joints according to the environmental conditions and the task to perform. The result is a change of the joint impedance, a mechanical description of the dynamic behavior of the joints. When the variation of the lower limbs' joint impedance is abnormal, for example after a stroke, cerebral palsy or limb amputation, the execution of motor tasks is affected. Disabilities can be alleviated by prostheses (in the case of amputations) or orthoses (for external support to a limb), termed bionic devices. The ultimate goal of bionic devices is to replicate the dynamic behavior of the joints in concert with the human's intention, such that the device is perceived as a natural extension of the human body. A model of the changes of the joint impedance during daily tasks is required, and system identification can be used as a tool to obtain such a model [1].

2 Time-varying joint impedance identification

The joint impedance can be represented by a linear time-invariant (LTI) model if, in the measuring process, small amplitude perturbations are applied around a fixed operating point [2]. However, during most motor tasks the operating point continuously changes and LTI models are no longer valid: linear time-varying (LTV) models should be employed instead.

Joint impedance identification is currently being applied to bionic devices; yet LTI techniques are primarily utilized, leading to incomplete and inaccurate models of the joint dynamics. The objective of this research¹ is to tackle the identification of the LTV joint impedance for the application to bionic devices from both a fundamental and practical point of view. In the fundamental approach, a method for the identification of the LTV joint impedance will be developed and tested for different experimental conditions. In the practical approach, the gained knowledge will be applied to monitor the performance of orthotic rehabilitation and to refine variable impedance controllers in orthoses.

3 Preliminary Results

When a multisine input (a signal composed of the sum of sinusoids with different frequencies) is applied to a time-varying system, the output spectrum presents power at both the excited and the non-excited frequencies. The power at the non-excited frequencies is due to the time variation in the system, and typically assumes the shape of *Skirts*. The information on the time variation can be extracted using a nonparametric system identification method, referred to as *Skirt Decomposition* (SKD) method.

The SKD method has been applied to the identification of the impedance of the human wrist joint [3]. An experiment was performed, during which small amplitude rotational perturbations were applied to the wrist of the subjects via the handle of a robotic manipulator attached to their right palm. The subjects were requested to vary the voluntary torque applied to the handle to follow an onscreen sinusoidal trajectory, ranging from 5% to 20% of the maximum voluntary torque. The SKD method was applied to the measured rotation (input) and torque (output). The identification results indicate that the joint impedance varied sinusoidally, according to the changes in the voluntary torque. The results show that the method was able to retrieve a plausible time variation of the joint impedance, in which the voluntary torque played the role of the changing operating point.

References

- [1] Perreault, E., Hargrove, L., Ludvig, D., Lee, H. and Sensinger, J., 2014. Considering limb impedance in the design and control of prosthetic devices. In *Neuro-Robotics*, pp. 59-83. Springer Netherlands.
- [2] Van der Helm, F.C., Schouten, A.C., de Vlugt, E. and Brouwn, G.G., 2002. Identification of intrinsic and reflexive components of human arm dynamics during postural control. *Journal of Neuroscience Methods*, 119(1), pp.1-14.
- [3] Van de Ruit, M., Cavallo, G., Lataire, J., van der Helm, F.C.T., Mugge, W., van Wingerden, J.W. and Schouten, A.C., *submitted on Dec. 2017*. Revealing time-varying joint impedance with kernel-based regression and non-parametric decomposition. *IEEE Transactions on Control Systems Technology*.

¹This work is sponsored by FWO-Vlaanderen and the Flemish Government (Methusalem Fund, METH1), and by the ERC, project 4DEEG.

Resilience against Misbehaving Nodes in Asynchronous Networks

Danial Senejohnny^a
d.senejohnny@rug.nl

Shreyas Sundaram^b
sundara2@purdue.edu

Claudio De Persis^a
p.tesi@rug.nl

Pietro Tesi^a
c.de.persis@rug.nl

^a Engineering and Technology Institute, University of Groningen, The Netherlands.

^b School of Electrical and Computer Engineering, University of Purdue, USA.

1 Abstract

Security is one of the challenging issues in dealing with Cyber-Physical Systems (CPSs), systems that integrate computation and communication to accomplish task in physical world. As a matter of fact, a breach in the cyber-domain of such systems can compromise systems in the physical world with safety-critical components, such as power systems and communication networks. One important category of attack to CPSs is deceptive attack. These attacks mainly targets the trustworthiness of data via tampering with the transmitted packets [1].

The prototypical problem to study resilience in the presence of misbehaving nodes is the so-called consensus problem [2], which forms the foundation for distributed computing. In resilient consensus, normal nodes reach a common value despite the presence of misbehaving nodes. The resilient consensus problem has a long history, and it has been investigated first by computer scientists [3], usually under the hypothesis that the network graph is complete.

Most of the research works in this area assume that the network operates in perfect *synchrony*, in the sense that all the nodes, at least the normal ones, update at the same moment in time. Since this condition might be difficult to obtain, a parallel line of research has focused on methods for handling *asynchrony*, which is known to render consensus much more challenging to obtain [3]. Among many notable works, we mention [4] which consider MSR-type algorithms supporting asynchrony. In this work, asynchrony refers to the property that the nodes are equipped with identical clocks, operating synchronously, but can make updates at different steps, that is at different multiples of the clock period.

The objective of this research is to address the problem of resilient consensus in a context where the nodes have their own clocks, possibly operating in an asynchronous way, and can make updates at arbitrary time instants. Besides the practical difficulties in achieving a perfect clock synchronization, one main reason for considering independent clocks is related to developments in the area of networked control systems where, in order to enhance efficiency and flexibility, it is more and more required to have fully au-

tonomous devices, which is the paradigm of event-triggered and self-triggered control. In fact, our approach utilizes a self-triggered control scheme [5]. Each node is equipped with a clock that determines when the next update is scheduled. At the update instant, the node polls its neighbors, collects the data and determines its controls and the next update instant.

The main result of this research establishes approximate consensus under certain conditions on the connectivity of the communication graph and a maximum number of misbehaving nodes, conditions which can be relaxed if misbehavior only occurs in data acquisition or timing. While [6] achieves perfect consensus and require milder connectivity conditions, the present results indicate that the resilient consensus problem can be approached without requiring that the nodes are equipped with identical clocks, even when the graph is not complete, a feature which is very appealing for networked control applications.

References

- [1] F. Pasqualetti, F. Dorfler, and F. Bullo, "Control-theoretic methods for cyberphysical security: Geometric principles for optimal cross-layer resilient control systems." *IEEE Control Systems*, vol. 35, no. 1, pp.
- [2] Y. Cao, W. Yu, W. Ren, and G. Chen, "An overview of recent progress in the study of distributed multi-agent coordination." *IEEE Transactions on Industrial informatics*, vol. 9, no. 1, pp. 427-438, 2013.
- [3] D. Dolev, N. A. Lynch, S. S. Pinter, E. W. Stark, and W. E. Weihl, "Reaching approximate agreement in the presence of faults." *Journal of the ACM*, 1986.
- [4] S. M. Dibaji and H. Ishii, "Resilient consensus of second-order agent networks: Asynchronous update rules with delays." *Automatica*, vol. 81, pp. 123-132, 2017.
- [5] C. De Persis and P. Frasca, "Robust self-triggered coordination with ternary controllers," *IEEE Transactions on Automatic Control*, vol. 58, no. 12, pp. 3024-3038, 2013.
- [6] H. J. LeBlanc, H. Zhang, X. Koutsoukos, and S. Sundaram, "Resilient asymptotic consensus in robust networks." *IEEE Journal on Selected Areas in Communications*, vol. 31, no. 4, pp. 766-781, 2013.

The synchronizing probability function for primitive sets of matrices

Costanza Catalano
 Gran Sasso Science Institute,
 L'Aquila, Italy
 costanza.catalano@gssi.it

Raphaël M. Jungers¹
 ICTEAM Institute, UCLouvain
 Louvain-la-Neuve, Belgium
 raphael.jungers@uclouvain.be

Introduction

The concept of primitivity has recently gained a lot of attention due to its application in stochastic switching systems, consensus theory and automata theory. In particular, it constitutes a promising method to tackle the Černý conjecture, one of the most longstanding open problems on synchronizing automata. A novelty approach to this conjecture, based on a probabilistic game framework, has been proposed lately in [3]. In this work, we adapt that probabilistic framework to primitive sets introducing the *synchronizing probability function for primitive sets of matrices*. Our goal is twofold: on one hand, our formulation makes use of linear programming techniques that enable us to study the primitivity phenomenon, on the other hand, we hope that this approach would help in shedding a light on the Černý conjecture.

1 Primitive sets and synchronizing automata

A set of matrices with nonnegative entries is called *primitive* if there exists a product of these matrices with all positive entries. The length of the shortest positive product is called the *exponent (exp)* of the set. A *synchronizing automaton* is a set of binary row-stochastic matrices that admits a product with a full-ones column. The length of the shortest of these products is called the *reset threshold (rt)* of the automaton. We recall the famous Černý conjecture:

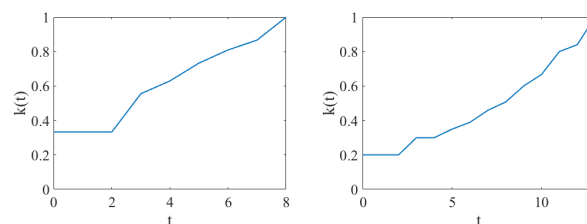
Conjecture 1 ([2]). The reset threshold of an automaton with $n \times n$ matrices cannot exceed $(n-1)^2$.

Blondel et al. [1] showed that the exponent of a primitive set is tightly linked with the reset threshold of an automaton, as illustrated in the following theorem (a matrix is said to be NZ if it has no zero rows and no zero columns):

Theorem 1 (Theorems 16-17 in [1]). For any primitive set M of NZ matrices of size $n \times n$, there exist two synchronizing automata A and A' such that:
 $\max\{rt(A), rt(A')\} \leq exp(M) \leq rt(A) + rt(A') + n - 1$.

It follows that a primitive set with exponent greater than $2(n-1)^2 + n - 1$ would disprove the Černý conjecture; this is also why methods for predicting or approximating

Figure 1: The SPF for set M (left) and for a set with $n = 5$ (right).



the exponent of a set are of interest.

2 The synchronizing probability function

Consider M a NZ set of $n \times n$ matrices and define $M^{\leq t}$ as the set of the products of length smaller than t , for a given $t \in \mathbb{N}$. We introduce the following two-player probabilistic game: Player 2 chooses a vector e_j from the canonical basis, Player 1 chooses a product P in $M^{\leq t}$ and then a vector e_k is chosen uniformly from the canonical basis. Player 1 wins if $e_j^T P \geq e_k^T$, otherwise Player 2 wins. We define the *Synchronizing Probability Function for primitive sets* (SPF) $k_M(t)$ as the probability that Player 1 wins if Player 2 plays optimally; namely, if p is the probability distribution of Player 2 and e is the full-ones vector then:

$$k_M(t) = \min_{p \in \mathbb{R}_+^n, e^T p = 1} \left\{ \max_{P \in M^{\leq t}} p^T P(e/n) \right\}.$$

The SPF is nondecreasing in t and it reaches the value 1 if and only if M is primitive and has exponent smaller than t . The SPF can be reformulated as a linear program; in view of this reformulation, we provide a preliminary analysis of theoretical properties of the SPF and report promising numerical experiments. Fig. 1 shows the SPF for the set

$$M = \left\{ \begin{pmatrix} 0 & 1 & 0 \\ 1 & 0 & 0 \\ 0 & 0 & 1 \end{pmatrix}, \begin{pmatrix} 1 & 0 & 1 \\ 0 & 0 & 1 \\ 0 & 1 & 0 \end{pmatrix} \right\}.$$

References

- [1] V. D. Blondel, R. M. Jungers and A. Olshevsky, On primitivity of sets of matrices, *Automatica*, 61, 80-88, 2015.
- [2] J. Černý, Poznámka k homogénnym eksperimentom s konečnými automatami", *Matematicko-fyzikalny Casopis SAV*, 14, 208-216, 1964.
- [3] R. M. Jungers, The Synchronizing Probability Function of an Automaton, *SIAM Journal on Discrete Mathematics*, 26, 177-192, 2012.

¹R. Jungers is a FNRS Research Associate. He is supported by the French Community of Belgium, the Walloon Region and the Innoviris Foundation.

Asynchronous Proximal Dynamics in Multi-Agent Network Games

Carlo Cenedese

Institute ENTEG
Faculty of Science and Engineering
University of Groningen
9747 AG Groningen, The Netherlands
c.cenedese@rug.nl

Sergio Grammatico

Delft Center for Systems and Control
TU Delft
2628 CD Delft, The Netherlands
s.grammatico@tudelft.nl

Ming Cao

Institute ENTEG
Faculty of Science and Engineering
University of Groningen
9747 AG Groningen, The Netherlands
m.cao@rug.nl

1 Introduction

Research on distributed decision making in multi-agent networks, populated by rational agents, is very active, thanks to its various applications including computer networks [3], power systems, robotic, sensor networks [2] and consumer markets.

In this work we consider a network of noncooperative agents seeking a global equilibrium in an unconstrained network game, based on proximal dynamics, with convex cost functions depending on the neighbor states. The communication in the network is asynchronous, and hence the associated communication graph is time-varying. This is the main difference from [1], where the synchronous case of this problem was introduced. The chosen tool for approaching the problem is functional analysis applied to nonlinear operators in Banach spaces. This choice allows us to analyze the problem under the weakest assumptions. In particular, the property of averaged and nonexpansive nonlinear mapping with respect to their fixed points are used.

2 Problem Formulation

The network is composed by N agents, the state of each agent $i \in [1, N]$ is denoted by $x_i \in \mathcal{X}^i \subseteq \mathbb{R}^n$. The communication is described by a directed graph with adjacency matrix $P := [a_{i,j}]$ where $i, j \in [1 \cdots N]$. The matrix P is assumed to be row stochastic (i.e. $\sum_{j=1}^N a_{i,j} = 1$), hence the elements of the network can update their state asynchronously.

We consider N different local cost functions that share the same basic structure:

$$J^i(y, z^i) = f^i(y) + \frac{1}{2} \|y - z^i\|^2 \quad (1)$$

with $z^i = \sum_{j=1}^N a_{i,j} x^j$ and $i \in [1, N]$. Every function $f^i : \mathbb{R}^n \rightarrow \mathbb{R}$ is assumed to be lower semi-continuous and convex.

The aim of the agents is to reach the *Network Equilibrium* (NE), which is defined as a collective equilibrium state $\bar{\mathbf{x}} = [\bar{x}^1; \bar{x}^2; \cdots; \bar{x}^N]$ such that

$$\bar{x}^i \in \arg \min_{y \in \mathcal{X}^i} J^i \left(y, \sum_{j=1}^N a_{i,j} \bar{x}^j \right) \quad \forall i \in [1, N] \quad (2)$$

3 Operator Theoretic Perspective

The minimization of J^i can be described through the proximal operator with the cost function f^i and argument z^i , i.e. $\arg \min_{y \in \mathcal{X}^i} J^i(y, z^i) = \text{prox}_{f^i}(z^i)$. Grouping together N proximity operators leads to $\mathbf{prox}_f : \mathbb{R}^{nN} \rightarrow (\mathcal{X}_1, \cdots, \mathcal{X}_N) \subset \mathbb{R}^{nN}$, defined as $\mathbf{prox}_f := \text{diag}(\text{prox}_{f^1}, \cdots, \text{prox}_{f^N})$. In order to obtain the sought argument for each operator, \mathbf{prox}_f has to be composed with the $(nN) \times (nN)$ matrix $\mathbf{A} := P \otimes I_n$. The new mapping $\mathbf{T} := \mathbf{prox}_f \circ \mathbf{A}$ completely describes the problem. Indeed from the definition of NE in Eq. 2, it follows directly that a vector $\bar{\mathbf{x}}$ is an NE if and only if it is a fixed point of the mapping \mathbf{T} , i.e. $\bar{\mathbf{x}} \in \text{fix}(\mathbf{T})$.

The focus of our work is studying the convergence of a sequence $\{\mathbf{x}_m\}_{m \in \mathbb{N}}$ generated through the update rule $\mathbf{x}(k+1) = \mathbf{T}\mathbf{x}(k)$. The asynchronous nature of the communication forces the analysis into the Banach spaces, and in particular we consider finite dimensional Banach spaces, since they provide reflexivity. The most interesting characteristics for the convergence of \mathbf{T} is the nonexpansiveness.

The partial result obtained proves that, in the framework of finite dimensional Banach spaces, every nonexpansive mapping that also has the asymptotic regularity property (i.e. $\lim_{n \rightarrow \infty} x_n - Tx_n = 0$) converges to one of its fixed points.

4 Further Work

In order to completely solve the problem, further studies about the properties of the proximity map in finite dimensional Banach spaces are required.

References

- [1] S. Grammatico. Proximal dynamics in multi-agent network games. *IEEE Transactions on Control of Network Systems*, PP(99):1–1, 2017.
- [2] M. S. Stanković, K. H. Johansson, and D. M. Stipanović. Distributed Seeking of Nash Equilibria With Applications to Mobile Sensor Networks. *IEEE Transactions on Automatic Control*, 57(4):904–919, 2012.
- [3] John N. Tsitsiklis, Dimitri P. Bertsekas, and Michael Athans. Distributed asynchronous deterministic and stochastic gradient optimization algorithms. *IEEE Transaction on Automatic Control*, AC-31(9):803–812, 1986.

Smart Detection and Real-time Learning in Water Distribution: an Integrated Data-Model Approach

CVC Geelen^{1,2}, D Yntema², J Molenaar¹, KJ Keesman^{1,2}

¹Biobased Chemicals & Technology, Wageningen University & Research, Bornse Weilanden 9, 6708WG Wageningen, the Netherlands

²Wetsus, European Center of Excellence for Sustainable Water Technology, Oostergoweg 9, 8911 MA Leeuwarden, the Netherlands

E-mail: karel.keesman@wur.nl

1. Introduction

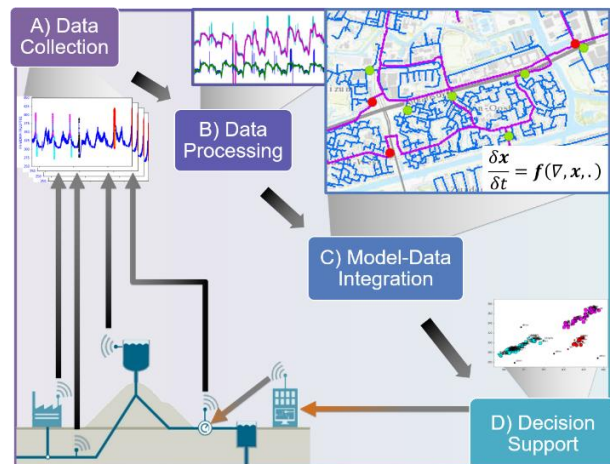
Although Dutch drinking water is of high quality and only 5% of clean drinking water is lost per year [1], the actual behavior of flows within the distribution network and current state of the pipes remain largely unknown. Due to the unknown state and continuous degradation of pipes, water companies yearly spend millions in renewing water mains, without a detailed strategy to target most likely degraded pipes.

Although increasing amount of water sensor placements in water mains yields big & fast data streams, analysis of this data is currently limited to a reactive approach of real-time leak detection [2].

However, in order to enable for robust performance, adequate detection of upcoming degradation or even failure and hence avoiding leakages, a more proactive approach is required. Since increased sensor placement and pipe inspection are costly, the abundance of currently collected sensor data can be deeper analyzed to facilitate cost-effective monitoring and management of the water supply grid.

2. Technological challenges

By processing and integrating the currently available sensor data, more information can be obtained compared to individual sensor monitoring. Data integration and reconciliation of these data streams with flow dynamics from prior (physical) knowledge, will facilitate improved decision support for cost-effective monitoring and management of the water distribution network. Emphasis is put the development of real-time, fault detection & isolation and early warning algorithms.



3. Approach

With the help of Dutch drinking water companies, currently available data streams are investigated (Fig. 1A) and integrated using data science (Fig. 1B) to develop early warning systems for prevention of e.g. leakages and pump failures. Next, the processed data streams are combined with GIS maps and mathematical models of the water distribution grids in order to reconcile flow dynamics with discovered data relationships (Fig 1C). These insights into the state of the network assets are used to develop real-time decision support (Fig 1D). In the current study only steps A and B will be demonstrated.

4. Conclusions

Currently collected sensor data can be further processed to predict faults and failures with corresponding probabilities in an early stage. Combining water flow models with data science allows more insight in the state of the water grid asset

5. References

- [1] "Drinking Water Fact Sheet 2016" VEWIN (2016).
- [2] Gelazanskas, Linas, and Kelum AA Gamage. "Demand side management in smart grid: A review and proposals for future direction." *Sustainable Cities and Society* 11 (2014): 22-30.

Evolutionary game dynamics for two interacting populations under environmental feedback

Lulu Gong, Ming Cao

Discrete Technology & Production Automation, University of Groningen

Nijenborgh 4, 9747 AG, Groningen, The Netherlands

Email: {l.gong@rug.nl, m.cao@rug.nl}

1 Introduction

Recently, there have been studies on the coevolutionary game dynamics with environmental feedback in a single population of players [1]. The corresponding dynamics exhibit interesting oscillating behavior when the game is characterized by the payoff matrix of the prisoner dilemma. We further study more general game dynamics when two populations interact, each characterized by a different payoff structure..

This research investigates whether convergence will take place for the coevolutionary dynamics of the two populations of players and the environment, in particular identifying the scenarios where oscillations offer the best predictions of long-run behavior.

2 Integrated model

The model is based on the existing replicator equation of bimatrix game [2]:

$$\begin{aligned} \dot{x}_i &= x_i[(Ay)_i - xAy], \quad i = 1, \dots, n \\ \dot{y}_j &= y_j[(Bx)_j - yBx], \quad j = 1, \dots, m, \end{aligned} \quad (1)$$

where x_i and y_j are the proportions of individuals in the corresponding population with strategy i and j , respectively; A and B are the payoff matrices for the first and second types of players, respectively.

In some practical situations, however, the environmental factor also plays a critical role because it can not only be affected by the behaviors of individuals but also act back on the strategic choices of the populations by influencing the transient payoff matrix. For this reason, the dynamic payoff matrix is utilized to indicate the influence of the environment factor. In addition, the state of the environment factor is modified by the actions as

$$\dot{r} = r(1-r)h(x,y). \quad (2)$$

Assume the individuals have two strategies and combine Eqs. (1) and (2), we obtain the combined system

$$\begin{aligned} \dot{x} &= x(1-x)f(y,r) \\ \dot{y} &= y(1-y)g(x,r) \\ \dot{r} &= r(1-r)[(1+\theta_1)x + (1+\theta_2)y - 2], \end{aligned} \quad (3)$$

where θ represents the ratio of the enhancement rate over degradation rate of cooperators and defectors, respectively.

3 Main results

Case I: When the dynamic payoff matrices lead to a dominating strategy, e.g.,

$$A(r) = \begin{bmatrix} 0.5r & 1 \\ 0 & 0.5 \end{bmatrix}, \quad B(r) = \begin{bmatrix} 0.5 & 0 \\ 1 & 0.5r \end{bmatrix},$$

the coevolutionary dynamics will converge to some fixed points;

Case II: When the payoff matrices are cyclic, e.g.,

$$A(r) = B(r) = (1-r) \begin{bmatrix} T & P \\ R & S \end{bmatrix} + r \begin{bmatrix} R & S \\ T & P \end{bmatrix},$$

the dynamics tend to exhibit oscillating behavior;

Case III: Theoretically more complicated dynamics, e.g., chaos, can happen when the dynamic payoff matrices are set with specific combinations of parameters.

References

- [1] Joshua S. Weitz, Ceyhan Eksin, Keith Paarporn, Sam P. Brown and William C. Ratcliff. An oscillating tragedy of the commons in replicator dynamics with game-environment feedback. PNAS. 2016, 113(47), pp:E7518-E7525.
- [2] William H. Sandholm. Population Games and Evolutionary Dynamics. 2010. Cambridge, US: The MIT Press.
- [3] Chaitanya S. Gokhale and Christoph Hauert. Eco-evolutionary dynamics of social dilemmas. Theoretical Population Biology. 2016, 111, pp:28-42.
- [4] Yuzuru Sato, Eizo Akiyama and J. Doyne Farmer. Chaos in learning a simple two-person game. PNAS. 2002, 99(7), pp:4748-4751.

The Indefinite Soft-Constrained Differential Game Revisited

Jacob Engwerda, Tilburg University, The Netherlands, P.O. Box 90153, 5000 LE Tilburg
engwerda@uvt.nl

1 Abstract

In this note we reconsider the worst-case design linear quadratic control problem if the system is disturbed by deterministic noise. Başar and Bernhard used in [1] the soft-constrained linear-quadratic dynamic game framework to solve the disturbance attenuation problem and the closely related H^∞ control problem. For that purpose one can assume that the state weighing matrix in the corresponding cost function is positive semi-definite, since the cost function models the L_2 -norm of the output of the system.

In this note we follow this soft-constrained approach to design a worst-case controller for the general indefinite linear-quadratic control problem. As is well-known, these kind of control problems are often used to model problems in, e.g., economic and environmental science. Both in a single and multi-player context.

We assume that the evolution of the state, $x(t)$, over time is described by the differential equation

$$\dot{x}(t) = Ax(t) + Bu(t) + Ew(t), \quad x(0) = x_0 \in \mathbb{R}^n, \quad (1)$$

where the control designer chooses $u(t) = Fx(t)$, such that $(A + BF, E)$ is controllable and

$$F \in \mathcal{F} := \{F \mid \sigma(A + BF) \subset \mathbb{C}^-\},$$

where \mathbb{C}^- are all complex numbers which real part is strictly smaller than zero; and $w(t) \in \mathbb{R}^q$ is some unknown noise with $w(\cdot) \in L_2^q$, the set of square integrable functions on $[0, \infty)$.

It is assumed that in the noise-free case the objective of the control designer is to determine F , such that for any initial state x_0 , $J(F, x_0)$ below is minimized

$$J(F, x_0) := \int_0^\infty \{x^T(t)(Q + F^T R F)x(t)\} dt, \quad R > 0. \quad (2)$$

Note, we don't make definiteness assumptions concerning matrix Q .

In case noise may enter the system, we assume the above cost function (2) is adapted (with $V > 0$) as follows:

$$J(F, w, x_0) := \int_0^\infty \{x^T(t)(Q + F^T R F)x(t) - w^T(t)Vw(t)\} dt. \quad (3)$$

One way to interpret this adapted cost criterion (3) is that at any point in time disturbances have a negative impact on the performance, measured by $w^T(t)Vw(t)$. Assuming the control designer is risk averse, we assume that he likes to determine F in such a way that it minimizes the worst-case cost over all admissible $F \in \mathcal{F}$. In this setting matrix V may also be used as a design "parameter", set by the control designer, expressing to which extent he likes to take into account potentially disrupting noise. If he is "risk seeking" he might choose a \bar{V} larger than V that seems to be the realistic value, and vice-versa.

On the other hand this adapted criterion is closely related to the system being internally stabilizable or, even, having a bounded L_2 -gain, where the bound is implied by matrix V . Assuming that $\min_{F \in \mathcal{F}} \max_{w \in L_2^q} J(F, w, x_0)$ has a solution for a given matrix V and is attained at (F^*, w^*) it follows that $J(F^*, w) \leq J(F^*, w^*) =: J^*$. We will show that, in case the problem has a solution, $J^* = x_0^T K x_0$ for some matrix K that depends on V . This implies, there exists a control $u(t) = F^* x(t)$ such that for every disturbance vector $w(t) \in L_2^q$

$$\int_0^\infty \{\tilde{x}^T(t)(Q + F^{*T} R F^*)\tilde{x}(t) - w^T(t)Vw(t)\} dt \leq J^*, \text{ or}$$

$$\int_0^\infty \tilde{x}^T(t)(Q + F^{*T} R F^*)\tilde{x}(t) dt \leq \int_0^\infty w^T(t)Vw(t) dt + x_0^T K x_0.$$

So, if $Q + F^{*T} R F^* > 0$ it follows that in such cases with this choice of input the system is internally stable, that is there exists a constant β such that, $\|x\| \leq \beta \max\{\|x_0\|, \|w\|\}$ for every $w \in L_2^q$. In case $Q + F^{*T} R F^*$ is not positive definite, still this inequality can be interpreted as that there exists an input such that the performance of the system has the property that it degrades at most with $\beta\|w\|$, whatever $w \in L_2^q$ occurs.

In this presentation we will primarily focus on the one-player case. For the scalar case both necessary and sufficient conditions are derived for solving the problem. These results are partly extended for the multi-variable case.

Keywords: Linear quadratic differential games; linear feedback Nash equilibria; coupled algebraic Riccati equations, deterministic uncertainty.

References

- [1] Başar T. and Bernhard P., 1995. *H_∞ -Optimal Control and Related Minimax Design Problems*. Birkhäuser, Boston.

Inferential control of a wafer stage using disturbance observers

Noud Mooren^{1,*}, Nic Dirx², Robbert Voorhoeve¹, Tom Oomen¹

¹Eindhoven University of Technology, Dept. of Mechanical Engineering, Control Systems Technology, The Netherlands

²ASML Research Mechatronics, Veldhoven, The Netherlands. *Email: n.f.m.mooren@tue.nl

1 Background and problem definition

In high-precision motion systems it is often not possible to directly measure at the location where performance is required. Therefore, performance variables need to be inferred from non-collocated sensor measurements. If flexible behavior is negligible, a static sensor transformation is used to find a rigid-body (RB) approximation of the performance variable. However, for next-generation motion systems positioning accuracy is ever-increasing, leading to a situation where flexible dynamics are not negligible. As a result, traditional single degree-of-freedom (DOF) controllers are inadequate [1]. The aim of this research is to control the unmeasured performance variable while taking flexible behavior into account, through 2-DOF controller structures and disturbance observers.

2 Approach

An explicit distinction is made between measured variables, denoted with y_p , and performance variables denoted with z_p [1]. The control goal is stated as; *track a reference r_z in the unmeasured performance variable z_p , while taking structural deformations into account.* The structural deformation, possibly induced by a (quasi-static) disturbance, causes a RB-estimation of the performance variable to be inaccurate, as in the schematic representation in Fig. 2. The proposed method extends the single DOF controller structure with a disturbance-based observer, as depicted in Fig. 1. The disturbance-observer estimates the disturbance and uses it to create an improved estimate of the performance variable denoted with \hat{z}_p [2]. A feedback controller K_{fb} is designed that minimized the error e_z . Finally, the observer-

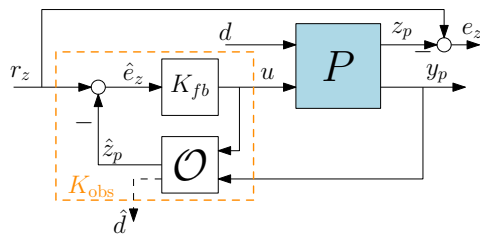


Figure 1: Disturbance observer-based controller structure.

based controller K_{obs} is given by

$$u = S_{\mathcal{O}} \begin{bmatrix} K_{fb} & -K_{fb}\mathcal{O}_2 \end{bmatrix} \begin{bmatrix} r_z \\ y_p \end{bmatrix} \quad (1)$$

with $S_{\mathcal{O}} = (I + K_{fb}\mathcal{O}_1)^{-1}$, $\mathcal{O}_1(s) : u \mapsto \hat{z}_p$ and $\mathcal{O}_2(s) : y_p \mapsto \hat{z}_p$.

3 Experimental results

The proposed observer-based method and the conventional method, i.e., using PID controllers, are applied to a prototype light-weight wafer stage in Fig. 2. A force disturbance and position reference are applied, the resulting positioning error $e_z = r_z - z_p$ for both controllers are depicted in Fig. 3. It can be concluded that the proposed method eliminates the steady-state error which is caused by the deformation, whereas the conventional controller is not capable of dealing with the deformation.

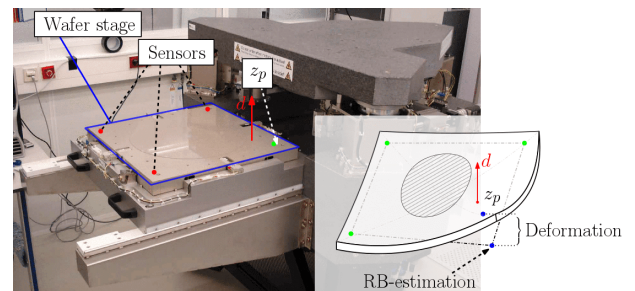


Figure 2: Prototype wafer stage and schematic representation.

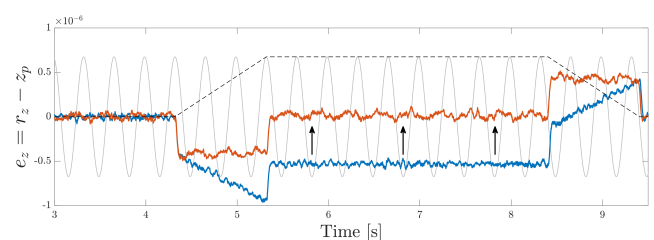


Figure 3: Positioning error e_z obtained with conventional controller (blue) and inferential controller (red), reference (gray) and disturbance (dashed gray).

References

- [1] J.S. Freudenberg, C.V. Hollot, R.H. Middleton: "Fundamental design limitations of the general control configuration", IEEE Transactions on Automatic Control (2003)
- [2] R. Voorhoeve, N. Dirx, T. Melief, W. Aangenent, T. Oomen: "Estimating structural deformations for inferential control: a disturbance observer approach", IFAC Symposium on Mechatronic Systems & 15th Mechatronics Forum International Conference, 642-648 (2016)

Dynamic simulation of ventilated potatoes in large-scale bulk storage facilities

Nik L.M. Grubben

Omnivent Techniek B.V., PO Box 1232, 3890 BA Zeewolde, the Netherlands.
nik.grubben@wur.nl

Karel J. Keesman

Wageningen University, Biobased Chemistry and Technology,
PO Box 17, 6700 AA Wageningen, the Netherlands.
karel.keesman@wur.nl

1 Introduction

To limit storage losses of potatoes in bulk storage, the dynamic interaction between facility climate and product needs to be better understood [1]. A 2D schematic overview of a bulk storage facility is shown in Figure 1. The aim of the study was to improve the storage process for frying potatoes, by making use of CFD simulations.

A CFD model was set up, and calibrated and validated on data from a large-scale potato storage facility. The model contains the convection, diffusion and reaction of heat and mass. To control the climate, two actuators: a moving hatch and a fan, were included in the CFD model. The model supports the re-design of the climate control, preferably in general rules of thumb.

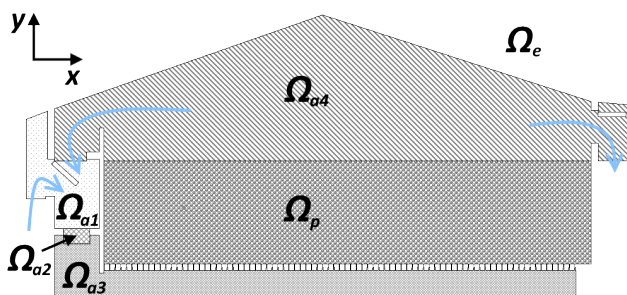


Figure 1: 2D Large-scale bulk-storage facility configuration, with Ω_a the air domain, Ω_p the porous medium domain and Ω_e the environment domain. The climate is controlled by ventilating air into the facility. This ventilation and air mixture is controlled by two actuators: the moving mesh located in Ω_{a1} and the fan Ω_{a2} . In practise the fan ventilates a mixture of air into the air channel Ω_{a3} through the porous medium Ω_p . The air can leave the facility or can be recirculated.

After a CFD modelling procedure a calibration and validation of large-scale storage facility was performed. The work was applied in order to a.o. answer the hypothesis that a 1D CFD model is an appropriate approximation of a real full-

scale storage facility.

2 Material and methods

The CFD model was set up in COMSOL, using a Reynolds averaged Navier-Stokes (RANS) velocity model with a Algebraic yPlus turbulence model. For the climate and product aspects temperature and moisture states were defined in terms of partial differential equations. For the calibration of the model parameter sweeps were performed to obtain an impression of the best fitted parameter estimates. Subsequently, a one point calibration was performed, followed by a validation step using new sampling points.

3 Conclusion

The calibrated CFD model showed significant horizontal gradients in the bulk, when changing the flow. Thus if we want to predict the local conditions in the bulk a 2D CFD model is needed.

Acknowledgements

This work is part of a research project carried out at and financially supported by Omnivent Techniek B.V. in the Netherlands, an international specialist in the storage of fruits and vegetables, such as potatoes, onions, and carrots. This research project will provide Omnivent Techniek B.V. with more information and knowledge on how storage and control strategies influence potato quality and storage losses.

References

- [1] N.L.M. Grubben and K.J. Keesman, "Modelling ventilated bulk storage of agromaterial: A review." *Computers and Electronics in agriculture* 114, 285-295, 2015

Modelling & Control of a Photopolymerization-based Ceramic Additive Manufacturing Process

Thomas Hafkamp¹, Bram de Jager¹, Gregor van Baars², Pascal Etman¹

¹Eindhoven University of Technology, Department of Mechanical Engineering, P.O. Box 513, 5600 MB Eindhoven, The Netherlands

²TNO, Department of Equipment for Additive Manufacturing, P.O. Box 80, 5600 AB Eindhoven, The Netherlands

Email: t.m.hafkamp@tue.nl

1 Introduction

Additive Manufacturing (AM), also known as 3D Printing, currently receives great interest from the manufacturing industry. AM provides for a larger freedom in product design and enables integration of product functionalities. To pursue this promise of AM, the current lack of consistent consistent product quality, productivity and scalability needs to be overcome. To this end, our vision is that AM equipment needs to make the transition from current, mostly open-loop (see Figure 1), control to closed-loop control schemes.

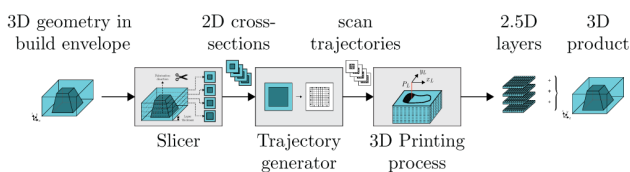


Figure 1: Open-loop control scheme typical for AM.

This work focuses on the modelling and control of a class of AM technologies known as vat photopolymerization or stereolithography of ceramics [1]. Ceramic vat photopolymerization typically consists of (1) depositing a layer of photosensitive slurry, (2) curing the layer by selectively irradiating the product's cross-section, (3) lowering the build platform by one layer thickness and repeating for each layer.

2 Control problem statement

The main objective for the manufacturing process controller at hand is to maximize product quality by minimizing prod-

uction variations despite material and process uncertainties. Two metrics have been identified to be representative for product quality: (1) layer thickness uniformity for the slurry deposition step and (2) degree of conversion homogeneity for the photopolymerization step.

3 First results

Modelling, sensing, actuation and control opportunities are being explored for both the deposition and the photopolymerization step. As a first result, this work presents simulation results of a feedback control scheme that controls the local exposure dose based on a measurement of the layer thickness topography, see Figure 2. This way layer thickness nonuniformity originating from the slurry deposition step, can be compensated for in the photopolymerization step and undercure can be prevented while overcure is minimized. The physical laws of light attenuation, however, limit the controllability of exposure dose with depth into the layer and hence the proposed feedback scheme can only prevent overcure if the layers are not too thick. Future work includes the incorporation of a kinetic model for photopolymerization and the design of a controller that acts on degree of conversion homogeneity rather than exposure.

References

- [1] J. W. Halloran, "Ceramic Stereolithography: Additive Manufacturing for Ceramics by Photopolymerization," *Annual Review of Materials Research*, vol. 46, Aug. 2016.

Acknowledgement: This study was funded by the Netherlands Organisation for Applied Scientific Research (TNO) and was carried out within the AMSYSTEMS Center.

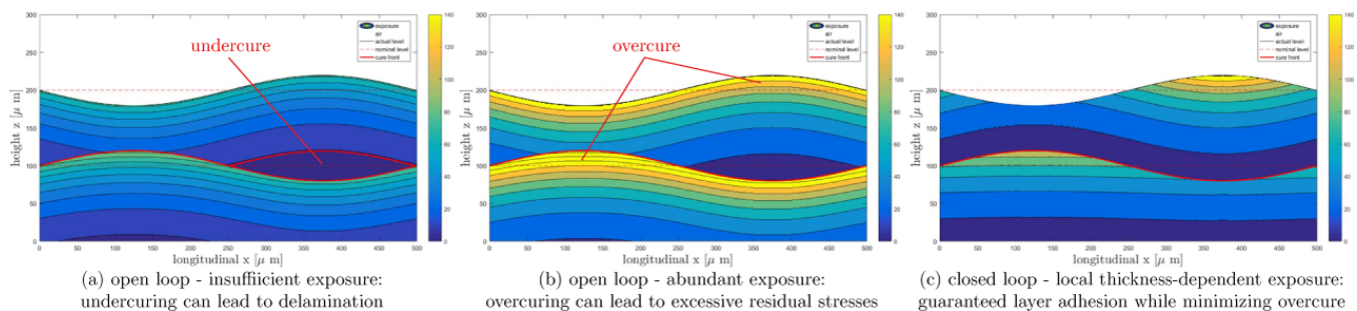


Figure 2: Comparison of simulated exposure for open-loop versus closed-loop control of two uneven photocurable layers.

Modeling non-equilibrium multiphase systems

Aarón Romo-Hernández, Denis Dochain
INMA, ICTEAM

Université catholique de Louvain
1348, Louvain-la-Neuve, Belgium

Email: {aaron.romo, denis.dochain}@uclouvain.be

Nicolas Hudon

Department of Chemical Engineering
Queen's University

Kingston, ON, K7L 3N6, Canada

Email: nicolas.hudon@queensu.ca

Erik Ydstie

Department of Chemical Engineering

Carnegie Mellon University

Pittsburgh, PA 15213, USA

Email: ydstie@cmu.edu

Design and operation of thermodynamic systems in chemical process engineering are challenging tasks. Particularly, dynamic behaviour for multiphase systems is still not completely understood [1]. Looking for an alternative to traditional models, we propose a physics-based modeling framework for liquid-vapor systems based on non-equilibrium thermodynamics. As a first result, a non-linear differential-algebraic system of equations (DAE system) is presented as a tool to simulate open multicomponent liquid-vapor systems far from thermodynamic equilibrium. Results regarding stability properties of the model are discussed through a numerical example using Lyapunov's first method. As a second preliminary result, effects of irreversible phenomena in the system are also considered. We finally discuss entropy production for non-equilibrium models as a tool to analyze multiphase systems within the proposed framework [2].

A liquid-vapor system can be represented as the interconnection of two subsystems, as depicted in Figure 1. For such system, the first law of thermodynamics is expressed as a DAE system:

$$\frac{d}{dt} \begin{bmatrix} z_g \\ z_l \end{bmatrix} = \begin{bmatrix} F_{g,z,\text{in}} \\ F_{l,z,\text{in}} \end{bmatrix} - \begin{bmatrix} F_{g,z,\text{out}}(z_g, z_l) - r_g(z_g, z_l, w) \\ F_{g,z,\text{out}}(z_g, z_l) + r_l(z_g, z_l, w) \end{bmatrix} \quad (1a)$$

$$0 = f(z_g, z_l, w), \quad (1b)$$

where the holdups $z = [U, K, N_1, \dots, N_c]^t$, sub-indexed l for

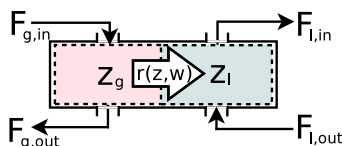


Figure 1: Open liquid-gas thermodynamic System.

the liquid and g for the gas, represent the energy and moles contained in each subsystem; the flow terms (F) account for the rate at which the environment exchanges mass and energy with the system; and, the non-equilibrium internal flow

terms (r) represent exchange rates between phases. The relation between the interface conditions (w) and the bulk-phase holdups (z_l, z_g) is given by the algebraic constraint (1b). Numerical results show that the system (1) linearized around a stationary thermodynamic equilibrium state has unstable eigenvalues. When an isobaric constraint $P_g(z_g) = P_l$ is considered, the system is stable. In the sequel, we would like to understand, from a physical point of view, the stabilizing effect of the isobaric constraint. To do so, we propose to extend the stability analysis through Lyapunov second method.

As a non-conserved property, the entropy (S) satisfies [3]:

$$\frac{dS_g}{dt} + \frac{dS_l}{dt} = F_{S,\text{in}} - F_{S,\text{out}} + \frac{Q}{T_Q} + \sigma, \quad (2a)$$

$$\frac{dS_\alpha}{dt} = \frac{1}{T_\alpha} \frac{dU_\alpha}{dt} + \frac{P_\alpha}{T_\alpha} \frac{dV_\alpha}{dt} - \sum_{j=1}^c \frac{\mu_{\alpha,j}}{T_\alpha} \frac{dN_{\alpha,j}}{dt}, \quad (2b)$$

where the F_S terms represent the entropy convective flows; T_Q is the temperature at which heat transfer rate Q occurs; and T, P and μ stand as temperature, pressure and chemical potential of phase $\alpha \in \{g, l\}$ respectively. The volume is assumed to be a known positive function $V = \phi(t)$. As a positive definite state function, the entropy production (σ) recovered from the coupling (1)-(2) is a Lyapunov function candidate [2]. This open issue is to be considered next in this project.

References

- [1] S. Skogenstad, "Dynamics and control of distillation columns - A critical survey," Modeling, Identification and Control, V18-N3, pages 177-217, 1997.
- [2] J. P. García-Sandoval, V. González-Álvarez, and C. Calderón, "Stability analysis and passivity properties for a class of chemical reactors: Internal entropy production approach", Computers and Chemical Engineering, V75, pages 184-195, 2015.
- [3] S.I. Sandler, "Chemical and Engineering Thermodynamics," Wiley; Third Edition, 1999.

Data-Driven Inverse-Model Feedforward Control using Non-Causal Rational Basis Functions

Lennart Blanken¹, Sjirk Koekebakker², Tom Oomen¹

Eindhoven University of Technology, Dept. of Mechanical Engineering, Control Systems Technology, The Netherlands
Océ Technologies B.V., Venlo, The Netherlands. Email: l.l.g.blanken@tue.nl

Background

Feedforward can compensate for known disturbances before these affect the system, enabling high performance. This is typically achieved by inverting a model of the system. In view of the achievable control performance, the quality of the parametric inverse model is crucial. Especially for lightly damped mechatronic systems such as flatbed printers, see Figure 2, such accurate parametric models can be difficult and expensive to obtain due to, e.g., complex dynamics, and numerical issues. This motivates to directly estimate the inverse model based on measured input/output data, obtained in the same setting as the model is going to be used in, i.e., a feedforward control configuration.

Data-Driven Feedforward: Non-Causal Control

In data-driven feedforward control, measured data is used to iteratively determine a fixed-structure controller $F(\theta)$, such that the tracking error $e = \frac{1}{1+PC}(1-PF(\theta))r$ is minimized when $F(\theta)$ is applied, see Fig. 1. Optimal tracking performance, i.e., $\mathbb{E}e = 0, \forall r$, is achieved if $F(z, \theta) = P^{-1}(z)$. The key difficulty is to choose a compact parametrization for $F(\theta)$, capable to accurately model the *inverse* system P^{-1} .

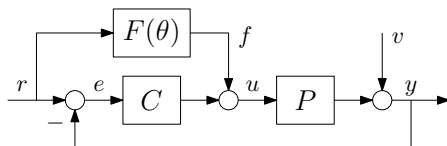


Figure 1: Control configuration for data-driven feedforward: the parameters θ are iteratively optimized based on measured data.

Crucially, if P has non-minimum phase (NMP) zeros, then P^{-1} has poles outside the typical stability region. Interestingly, this can effectively be dealt with in feedforward, where non-causality can be exploited to compensate ‘unstable’ poles. The aim of this research is to enable non-causal control using a suitable parametrization for $F(\theta)$.

The main contribution of the presented research is the development of a compact parametrization for inverse systems, that is suited for inverse-model feedforward control. Crucially, the developed parametrization builds on the use of general *non-causal* rational orthonormal basis functions (ROBFs) in \mathcal{L}_2 [1], to compensate poles outside the usual stability region. As special cases, *causal* ROBFs in \mathcal{H}_2 [2] and finite impulse response (FIR) models are recovered.

Experimental Results: Industrial Flatbed Printer

The developed approach is applied to the Arizona flatbed printer, shown in Fig. 2, which has 3 NMP zeros with input F_L [N] and output x_R [m]. The results in Fig. 3 show that:

- *non-causality*, through basis functions in \mathcal{L}_2 , is crucial to compensate poles outside the typical stability region;
- *rational* functions enable high performance using compact models, in contrast to polynomial (FIR) functions.

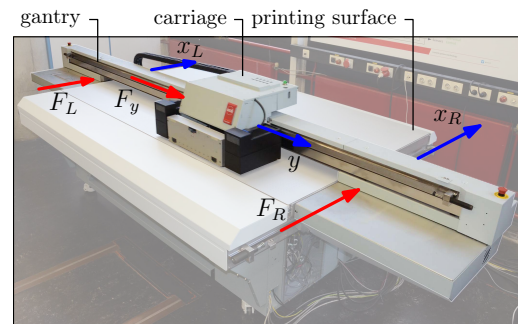


Figure 2: Océ Arizona flatbed printer @TU/e CST Motion Lab.

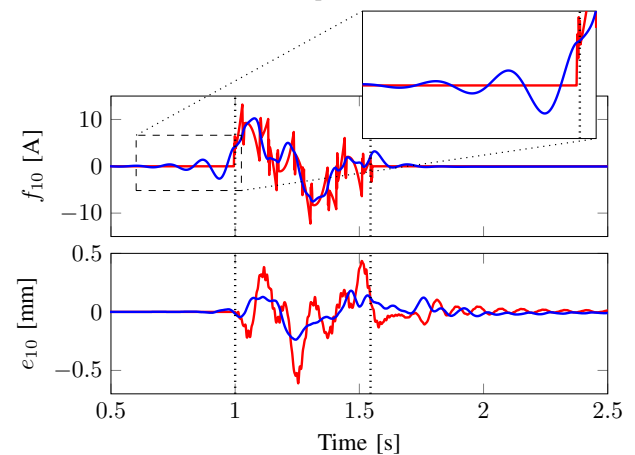


Figure 3: Experimental results: non-causal ROBFs (—) enable infinitely long pre-actuation and post-actuation. Compared to (non-causal) FIR basis functions (—), which enable only a small and finite amount of preview, the error e_{10} is significantly reduced.

References

- [1] L. Blanken, G. Isil, S. Koekebakker, and T. Oomen, “Data-driven feedforward learning using non-causal rational basis functions: Application to an industrial flatbed printer,” In *American Control Conference*, 2018.
- [2] P. Heuberger, P. Van den Hof, and B. Wahlberg. “Modelling and identification with rational orthogonal basis functions,” Springer-Verlag, London, UK, 2005.

A Linear Single Degree of Freedom Model for Acoustophoresis

M. H. Kandemir^{1,2}, R. M. Wagterveld¹, D. Yntema¹, K. J. Keesman^{1,2}

¹Wetsus, European Center of Excellence for Sustainable Water Technology, Oostergoweg 9, 8911 MA Leeuwarden, The Netherlands

²Wageningen University & Research, Bornse Weiland 9, 6708WG Wageningen, The Netherlands
e-mail: karel.keesman@wur.nl

1. Introduction

This paper presents a new modeling method for single node standing wave acoustophoresis. Acoustophoresis exploits the effect of acoustic radiation force on small particles. Particles are exposed to a standing acoustic wave field and they are forced to specific locations called pressure nodes or antinodes. A suspended particle in water, or in any other medium, will converge to such locations sooner or later. Particle properties determine the time required to reach the target location from the initial location, where both locations are known. Behavior of different particles in the same acoustic field enables those particles to be fractionated or separated by acoustic forces.

2. Methodology

Full information for particle behavior can be obtained by solving the differential equation of motion (EOM) [1].

$$\left(\frac{4}{3}\pi r^3 \rho\right)\ddot{z} + (6\mu\pi r)\dot{z} + 4\pi kr^3 \left(\frac{P_0^2}{\rho_0 c_0^2}\right)\Phi(\rho, c) \sin(2kz) = 0 \quad (1)$$

In the above equation r is the particle radius, $\Phi(\rho, c)$ is the acoustic contrast factor, ρ_0 is the density of the medium, c_0 is the speed of sound in the medium, ρ is the particle density, c is the speed of sound in the particle, μ is the viscosity of host medium and P_0 is the amplitude of acoustic pressure. The equation is one dimensional (z) and it is a second order nonlinear differential equation. Nonlinearity in the equation is due to the sinusoidal force profile. It is possible to obtain an analytical solution by ignoring the mass term and reducing the order of the equation by one, thus having a first order nonlinear model [1]. This approach assumes that the particle will asymptotically converge to the pressure node/antinode and it cannot cross the nodal position. In terms of energy, it assumes all the potential and kinetic energy will be dissipated by the viscosity of the medium. However, by ignoring the effect of mass and therefore kinetic energy, this model has no tools to check if the assumption is correct.

Our approach is modifying the EOM by linearizing the acoustic radiation force term. By this method, the particle becomes a linear single degree of freedom (SDOF) mass-spring-damper system. In acoustophoresis applications, the region of interest for a particle is between a starting and a target position. Thus, we only consider the motion of a particle between two predefined locations and linearize the acoustic radiation force between those locations. Details

and methods for linearization can be found in [2]. By linearizing the system, the EOM becomes

$$m\ddot{z} + b\dot{z} + Kz = 0 \quad (2)$$

In equation (2), m is the mass of the particle, b is the damping coefficient and K is the linearized spring coefficient [2]. The parameter that determines whether the particle will cross the nodal line is the damping ratio, expressed as $\zeta = b/(2\sqrt{K/m})$. If ζ is smaller than one, it means all the initial total energy will not be dissipated before the particle crosses the nodal line; the particle will overshoot. This is not a desired behavior of a particle in such systems, and using the SDOF methodology it can now be calculated without solving the differential equation.

Using the linear SDOF model, it is also possible to include the effects of initial velocity. The SDOF model can also be used to calculate the time required to reach the target location from an initial location. Such time calculations yield results within 6% of the nonlinear model.

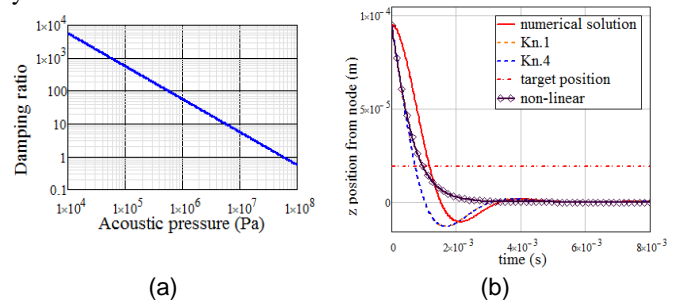


Figure 1 – (a) Damping ratio as a function of acoustic pressure. Parameters adapted from [1]. (b) An overshoot system. For details of Kn.1 and Kn.4, see [2].

3. Conclusions

We presented a linear SDOF model for acoustophoresis applications. The new model can predict the possibility of overshoot of the particle and can further be used to optimize existing or prospective systems.

References

- [1] Bruus, H. (2012). Acoustofluidics 7: The acoustic radiation force on small particles. *Lab on a Chip*, 12(6), 1014–21
- [2] Kandemir, M. H., Wagterveld, R.M., Yntema, D., Keesman, K.J. (2017) Methods to linearize acoustic radiation force for acoustophoresis applications. *Acoustofluidics 2017*, San Diego, California, USA.

Lyapunov stability: Why uniform results are important, and how to obtain them

Erjen Lefeber

Department of Mechanical Engineering, Eindhoven University of Technology

A.A.J.Lefeber@tue.nl

1 Why are uniform results important?

Consider the dynamical system

$$\dot{x}(t) = \begin{cases} -\frac{1}{t+1} \operatorname{sgn}(x) & \text{if } |x| \geq \frac{1}{t+1} \\ -x & \text{if } |x| < \frac{1}{t+1} \end{cases} \quad (1)$$

where

$$\operatorname{sgn}(x) = \begin{cases} -1 & \text{if } x < 0 \\ 0 & \text{if } x = 0 \\ 1 & \text{if } x > 0 \end{cases}$$

Then for each $r > 0$ and $t_0 \geq 0$ there exist constants $k > 0$ and $\gamma > 0$ such that for all $t \geq t_0$ and $|x(t_0)| < r$:

$$|x(t)| \leq k|x(t_0)|e^{-\gamma(t-t_0)} \quad \forall t \geq t_0 \geq 0. \quad (2)$$

However, always a bounded (arbitrarily small) additive perturbation $\delta(t, x)$ and a constant $t_0 \geq 0$ exist such that the trajectories of the perturbed system

$$\dot{x}(t) = \delta(t, x) + \begin{cases} -\frac{1}{t+1} \operatorname{sgn}(x) & \text{if } |x| \geq \frac{1}{t+1} \\ -x & \text{if } |x| < \frac{1}{t+1} \end{cases}$$

are unbounded, see [4].

One of the reasons for this negative result is that in (2) the constants k and γ are allowed to depend on t_0 , i.e., for each value of t_0 different constants k and γ may be chosen. By requiring that those constants are independent of t_0 , we obtain *uniform* asymptotic stability. As shown in [2, Lemma 5.3] uniform asymptotic stability gives rise to some robustness that is not guaranteed by asymptotic stability.

2 How to obtain uniform asymptotic stability

Typically when proving stability of a nonlinear dynamical system, one can find a Lyapunov function candidate of which the time-derivative along solutions is not negative definite, but only negative semi-definite. Often, the Lemma of Barbălat [1] is used to complete the proof and show asymptotic stability.

Though this approach works to show asymptotic stability, it does not yield *uniform* asymptotic stability, which from a robustness point of view is important as mentioned in the previous section. An alternative way to complete the proof is by using Matrosov's Theorem, or one of its generalisations:

Theorem 2.1 (cf. [3, Theorem 1]) Consider the dynamical system

$$\dot{x} = f(t, x) \quad x(t_0) = x_0 \quad (3)$$

with $f(t, 0) = 0$, $f: \mathbb{R}^+ \times \mathbb{R}^n \rightarrow \mathbb{R}^n$ locally bounded, continuous and locally uniformly continuous in t .

If there exist j differentiable functions $V_i: \mathbb{R}^+ \times \mathbb{R}^n \rightarrow \mathbb{R}$, bounded in t , and continuous functions $Y_i: \mathbb{R}^n \rightarrow \mathbb{R}$ for $i \in \{1, 2, \dots, j\}$ such that

- V_1 is positive definite,
- $\dot{V}_i(t, x) \leq Y_i(x)$, for all $i \in \{1, 2, \dots, j\}$,
- $Y_i(x) = 0$ for $i \in \{1, 2, \dots, k-1\}$ implies $Y_k(x) \leq 0$, for all $k \in \{1, 2, \dots, j\}$,
- $Y_i(x) = 0$ for all $i \in \{1, 2, \dots, j\}$ implies $x = 0$,

then the origin $x = 0$ of (3) is uniformly globally asymptotically stable (UGAS).

So in addition to the Lyapunov function V_1 , auxiliary functions V_i need to be found to complete the proof. We will present candidates for the functions V_i that often work to complete a stability proof and show *uniform* asymptotic stability.

References

- [1] I. Barbălat, "Systèmes d'équations différentielles d'oscillations non linéaires," *Revue de mathématiques pures et appliquées*, vol. 4, no. 2, pp. 267–270, 1959.
- [2] H.K. Khalil, *Nonlinear Systems*, Upper Saddle River, NJ, USA: Prentice-Hall, 1996, second ed.
- [3] A. Loría, E. Panteley, and A. Teel, "A nested Matrosov theorem and persistency of excitation for uniform convergence in stable nonautonomous systems," *IEEE Transactions on Automatic Control*, vol. 50, no. 2, pp. 183–198, 2005.
- [4] E. Panteley, A. Loría, and A. Teel, "New tools for UGAS and ULES of nonlinear time-varying systems: a δ -persistency of excitation approach," 1999, lab. d'Automatique de Grenoble, CNRS, Technical Report no. 99–160.

Robust Automatic Generation Control in power systems

M. Cucuzzella*, S. Trip*, J. M. A. Scherpen*, C. De Persis*, A. Ferrara**

* University of Groningen, Nijenborgh 4, 9747 AG Groningen, The Netherlands

** University of Pavia, via Ferrata 5, 27100 Pavia, Italy

Email: m.cucuzzella@rug.nl

Abstract

As a result of power mismatch between generation and load demand, the frequency in a power system can deviate from its nominal value. The frequency is controlled back to its nominal value by the so-called ‘Automatic Generation Control’ (AGC) [1]. This work proposes a decentralized Sliding Mode (SM) control strategy for AGC in power networks, where frequency regulation is achieved, and power flows are controlled towards their desired values. This work considers a power network partitioned into control areas, where each area is modelled by an equivalent generator including second-order turbine-governor dynamics. The network topology is represented by a connected and undirected graph $\mathcal{G} = (\mathcal{V}, \mathcal{E})$, where the nodes $\mathcal{V} = \{1, \dots, n\}$, represent the control areas and the edges $\mathcal{E} \subset \mathcal{V} \times \mathcal{V} = \{1, \dots, m\}$, represent the transmission lines connecting the areas. Let $\mathcal{B} \in \mathbb{R}^{n \times m}$ be the incidence matrix describing the network topology, the power system can be written for all nodes $i \in \mathcal{V}$ as

$$\begin{aligned} \dot{\eta} &= \mathcal{B}^T f \\ T_p K_p^{-1} \dot{f} &= -K_p^{-1} f + P_t - \bar{P}_d - \mathcal{B} \Gamma \sin(\eta) \\ T_t \dot{P}_t &= -P_t + P_g \\ T_g \dot{P}_g &= -R^{-1} f - P_g + u, \end{aligned} \quad (1)$$

where $\eta = \mathcal{B}^T \delta \in \mathbb{R}^m$, $f, P_t, P_g, P_d, u \in \mathbb{R}^n$, $\Gamma = \text{diag}\{\Gamma_1, \dots, \Gamma_m\}$, with $\Gamma_k = \bar{V}_i \bar{V}_j / X_{ij}$, where line k connects areas i and j , $\sin(\eta) = (\sin(\eta_1), \dots, \sin(\eta_m))^T$. Matrices T_p, T_t, T_g, K_p, R are $n \times n$ positive definite diagonal matrices. The meaning of the symbols used in (1) follows straightforwardly from Fig. 1. Now, we make the considered control objectives explicit:

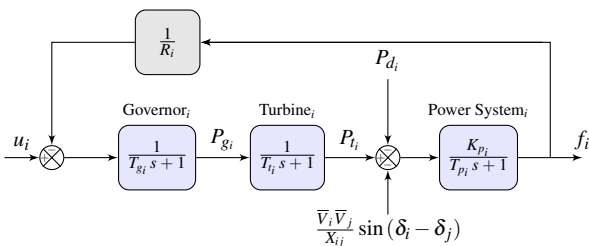


Figure 1: Block diagram of the considered power system, where f denotes the frequency deviation.

Objective 1 (Frequency regulation)

$$\lim_{t \rightarrow \infty} f(t) = \mathbf{0}. \quad (2)$$

Objective 2 (Maintaining scheduled net power flows)

$$\lim_{t \rightarrow \infty} \mathcal{B} \Gamma \sin(\eta(t)) = \mathcal{B} \bar{P}_f, \quad (3)$$

where $\mathcal{B} \bar{P}_f$ is the desired net power flow. In order to achieve Objectives 1 and 2, we first augment system (1) with an additional state variable $\theta \in \mathbb{R}^n$, with dynamics

$$T_\theta \dot{\theta} = -\theta + P_t. \quad (4)$$

Secondly we design the sliding variables vector $\sigma \in \mathbb{R}^n$ as

$$\sigma = M_1 f + M_2 P_t + M_3 P_g + M_4 \theta + M_5 \mathcal{B} (\Gamma \sin(\eta) - \bar{P}_f),$$

where M_1, \dots, M_5 are constant $n \times n$ diagonal matrices, suitable selected. To constrain the state of the system (1) to the manifold $\sigma = \mathbf{0}$, we propose robust controllers of SM type [2]. On the manifold $\sigma = \mathbf{0}$, asymptotic convergence to the desired state is established, and relying on stability considerations made on the basis of an incremental energy (storage) function, the sliding function is designed by choosing $M_1 > 0, M_2 \geq 0, M_3 > 0, M_4 = -(M_2 + M_3)$, and $M_5 = M_1 X$, where X is a diagonal matrix satisfying*

$$\mathbf{0} < T_p K_p^{-1} - X T_p K_p^{-1} \mathcal{B} \Gamma [\cos(\bar{\eta})] \mathcal{B}^T K_p^{-1} T_p X, \quad (5)$$

and

$$\begin{aligned} \mathbf{0} < K_p^{-1} - \frac{1}{4} K_p^{-1} X K_p^{-1} \\ - \frac{1}{2} (T_p K_p^{-1} X \mathcal{B} \Gamma [\cos(\eta)] \mathcal{B}^T + \mathcal{B} \Gamma [\cos(\eta)] \mathcal{B}^T X K_p^{-1} T_p). \end{aligned} \quad (6)$$

References

- [1] D. Apostolopoulou et al., ‘‘An assessment of the impact of uncertainty on automatic generation control systems,’’ *Trans. Power Syst.*, 2016.
- [2] V. I. Utkin, ‘‘Sliding Modes in Control and Optimization,’’ Springer-Verlag, 1992.

*Let $[\cos(\eta)]$ denote the $m \times m$ diagonal matrix $\text{diag}\{\cos(\eta_1), \dots, \cos(\eta_m)\}$.

On guaranteeing tracking performance and stability with LPV control for nonlinear systems¹

Gustavo S. Mazzoccante, Roland Tóth and Siep Weiland
 Control Systems Group, Electrical Engineering, Eindhoven University of Technology
 P.O. Box 513, 5600 MB Eindhoven, The Netherlands
 Email: g.sales.mazzoccante@tue.nl

For the last three decades, systematic design of Nonlinear (NL) and Time-Varying (TV) controllers capable of guaranteeing stability and performance has been in the focus of front-line research. The *Linear Parameter-Varying* (LPV) framework has become a popular choice, since it is based on the extension of the well-understood *Linear Time-Invariant* (LTI) framework and it offers computationally efficient and robust control-synthesis methodologies.

LPV systems are dynamical models capable of describing a NL/TV behavior in terms of a linear structure which depends on a measurable, so-called *scheduling-variable* ρ . Early LPV approaches exploited *Gain-Scheduling* (GS) methods, which basically is the linearization of a NL system model at various operating points, described by ρ , that results in a collection of local LTI models, for which LTI controllers are designed and interpolated to give a “global” control solution to the entire operating region. Due to many successful applications, GS has become part of industrial practice, even though it does not guarantee overall stability of the designed LPV controller, let alone performance.

Later it was realized that it is possible to embed the dynamic behavior of a nonlinear system into a LPV model in which ρ becomes a function of the output, input, or state through the so-called scheduling map. Then, through powerful convex optimization tools involving *Linear Matrix Inequalities* (LMI) constraints, global stability and performance analysis together with control synthesis is possible for this surrogate LPV model. Still, most of the LPV based techniques see controller synthesis confined into the system class itself without considering that the resulting closed-loop control solution is inherently nonlinear and its performance depends on the information structure hidden in ρ .

Indeed, recent studies show that customary \mathcal{L}_2 gain characterization of performance, which is a popular choice in the linear context, fail to ensure the performance specification on the resulting nonlinear performance [3, 4]. In fact, the utter motivation of the LPV control design is the synthesis of an NL/TV controller that can guarantee internal stability and a given bound of worst-case performance on the underlying system compared to the objective of only stabilizing

and optimizing performance with respect to the surrogate LPV model of the plant.

To ensure performance guarantees for the NL controlled system a stronger concept of incremental stability and incremental \mathcal{L}_2 -gain performance has been proposed. A nonlinear system is said to be incrementally bounded on \mathcal{L}_2 if there exists $\eta \geq 0$ such that $\|\Sigma(u_1) - \Sigma(u_2)\|_2 \leq \eta \|u_1 - u_2\|_2$ for all $u_1, u_2 \in \mathcal{L}_2$. Testing incremental properties is, in general, a rather difficult task, hence a more conservative but computationally more attractive notion is introduced: quadratic incremental stability and performance [3]. Also, in order to analyze robust performance the weighted incremental norm seems to be the natural framework [1]. The weighted incremental norm can be also seen as a natural extension of the well-known \mathcal{H}_∞ linear framework concept to the nonlinear context.

Under this motivation, this work is intended to carry on the studies on nonlinear controller design via the LPV framework by focusing on other signal norms such as \mathcal{L}_1 and \mathcal{L}_∞ , so that in the future it will serve as basis to describe the correlation between linear representations and stability and performance guarantees of the NL/TV behaviors using the \mathcal{L}_q -norms. The understanding of this problem would aid a potential breakthrough in understanding and applying LPV control on real-world systems.

References

- [1] V. Fromion, S. Monaco, and D. Normand-Cyrot. The weighted incremental norm approach: from linear to nonlinear \mathcal{H}_∞ control. *Automatica*, 37(10):1585–1592, 2001.
- [2] V. Fromion and G. Scorletti. A theoretical framework for gain scheduling. *Int. J. of Robust and Nonlinear Control*, 13(10):951–982, 2003.
- [3] V. Fromion, G. Scorletti, and G. Ferreres. Nonlinear performance of a PI controlled missile: An explanation. *Int. J. of Robust and Nonlinear Control*, 9(8):485–518, 1999.
- [4] G. Scorletti, V. Fromion, and S. de Hillerin. Toward nonlinear tracking and rejection using LPV control. In *Proc. of the 1st IFAC Workshop on Linear Parameter Varying Systems*, pp. 13–18, Grenoble, France, Oct. 2015.

¹This work has received funding from the European Research Council (ERC) under the European Unions Horizon 2020 research and innovation programme (grant agreement nr. 714663).

Performance Tuning in Extremum Seeking Control via Lie Bracket Approximations

Christophe Labar[†], Jan Feiling[‡] and Christian Ebenbauer[‡]

[†]Department of Control Engineering and System Analysis, ULB, 1050 Brussels, Belgium

[‡]Institute for Systems Theory and Automatic Control, University of Stuttgart, 70569 Stuttgart, Germany
{chlabar@ulb.ac.be,jan.feiling@ist.uni-stuttgart.de,ce@ist.uni-stuttgart.de}

1 Introduction and Problem Statement

Extremum seeking systems based on the Lie bracket formalism typically approximate a simple gradient descent law, namely $\dot{x} = -\rho h'(x)$ with $\rho \in \mathbb{R}_{>0}$ and $h(x)$ the cost to minimize. However, the presence of dithers in extremum seeking systems leads to oscillations on the estimated gradient. Accordingly, considering a gradient descent law in which the gradient is low pass filtered can be a way to improve both the transient and steady state performances. To this end, we consider the system

$$\begin{bmatrix} \dot{x} \\ \dot{y} \end{bmatrix} = \begin{bmatrix} -\rho y \\ -\omega_L(y - h'(x)) \end{bmatrix}, \quad (1)$$

with $x \in \mathbb{R}$, $y \in \mathbb{R}$, $\rho \in \mathbb{R}_{>0}$ and $\omega_L \in \mathbb{R}_{>0}$.

For the sake of simplicity, we consider cost functions $h(x) : \mathbb{R} \rightarrow \mathbb{R}$ of class C^2 such that $\exists x^* \in \mathbb{R} : h'(x)(x - x^*) > 0, \forall x \in \mathbb{R} \setminus \{x^*\}$ (i.e. we optimize a single variable x and $h(x)$ does not have any other stationary point than its minimizer x^*). Exploiting the Lie bracket formalism, we present four extremum seeking systems that approximate (1). The first ensures the boundedness of the update rates. The last three adapt the dither amplitude to enhance the steady state accuracy.

2 Boundedness of the Update Rates

Motivated by [2], we propose the following system that ensures the boundedness of the update rates (i.e. of \dot{x} and \dot{y})

$$\begin{bmatrix} \dot{x} \\ \dot{y} \end{bmatrix} = \begin{bmatrix} -\rho y \\ -\omega_L y \end{bmatrix} + \sqrt{\omega} \begin{bmatrix} \varepsilon \cos(h(x)) & 0 \\ 0 & -2\varepsilon^{-1} \omega_L \sin(h(x)) \end{bmatrix} \begin{bmatrix} \sin(\omega t) \\ \cos(\omega t) \end{bmatrix} \\ + \sqrt{\omega} \begin{bmatrix} \varepsilon \sin(h(x)) & 0 \\ 0 & 2k\varepsilon^{-1} \omega_L \cos(h(x)) \end{bmatrix} \begin{bmatrix} \sin(k\omega t) \\ \cos(k\omega t) \end{bmatrix}, \quad (2)$$

with $\varepsilon \in \mathbb{R}_{>0}$ a small positive parameter adjusting the maximal dither amplitude and $k \neq 1$. In Figure 1, it can be seen that the presence of the low-pass filter in (2) allows to reduce the amplitude of the oscillations compared to [2].

3 Zero Minimal Cost

When the minimal cost is zero, the following extremum seeking system can drastically improve the steady state performances.

$$\begin{bmatrix} \dot{x} \\ \dot{y} \end{bmatrix} = \begin{bmatrix} -\rho y \\ -\omega_L y \end{bmatrix} + \sqrt{\omega} \begin{bmatrix} \frac{\sqrt{h(x)}}{1+\sqrt{h(x)}} & 0 \\ 0 & -2\omega_L(h(x)+2\sqrt{h(x)}) \end{bmatrix} \begin{bmatrix} \sin(\omega t) \\ \cos(\omega t) \end{bmatrix}. \quad (3)$$

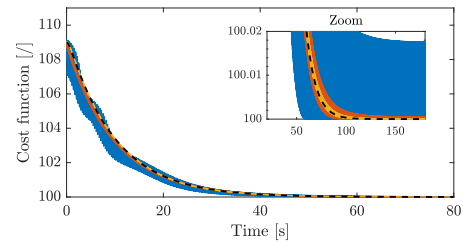


Figure 1: Simulation of (2) for $h(x) = (x-2)^2 + 100$: $\varepsilon = 1$ (—), $\varepsilon = 0.05$ (—); Simulation of the "classical" bounded update rate scheme [2] (---); Filtered Gradient Law (1) (---); $\rho = 0.025$ rad/s, $\omega_L = 2$ rad/s, $k = 1.2$

This system guarantees that the dither amplitude acting on the cost input is always strictly smaller than 1 and tends to zero as the cost approaches its minimum. The simulation result depicted in Figure 2, for $h(x) = (x-2)^2$, suggests that (3) even ensures an asymptotic convergence to the minimum.

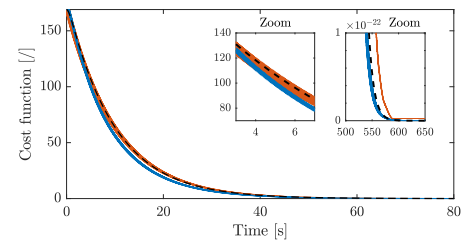


Figure 2: Simulation of (3) (—), Simulation of [3] (—), Lie bracket system (1) (---); $\rho = 0.025$ rad/s, $\omega_L = 2$ rad/s

The two other variable dither amplitude schemes as well as general formulas to approximate (1) can be found in [1].

References

- [1] C. Labar, J. Feiling, and C. Ebenbauer. Gradient-based extremum seeking: Performance tuning via Lie bracket approximations. In *European Control Conference 2018, Accepted*.
- [2] A. Scheinker and M. Krstić. Extremum seeking with bounded update rates. *Systems & Control Letters*, 63:25 – 31, 2014.
- [3] R. Suttner and S. Dashkovskiy. Exponential stability for extremum seeking control systems. In *20th IFAC World Congress, 2017*.

Nonlinear Model Order Reduction For MPD Systems

S. Naderi Lordejani¹, B. Besselink², W. H. A. Schilders³, N. van de Wouw^{1,4}

¹Department of Mechanical Engineering, Eindhoven University of Technology, The Netherlands

²Johann Bernoulli Institute, University of Groningen, The Netherlands

³Department of Mathematics and Computer Science, Eindhoven University of Technology, The Netherlands

⁴Department of Civil, Environmental & Geo-Engineering, University of Minnesota, USA

⁴Delft Center for Systems and Control, Delft University of Technology, The Netherlands

^{1,3,4}{s.naderilordejani, w.h.a.schilders, n.v.d.wouw}@tue.nl, ²b.besselink@rug.nl

1 Introduction

Automated Managed Pressure Drilling (MPD) is a method for fast and accurate pressure control in drilling operations. The performance of automated MPD is limited, firstly, by the control system and, secondly, by the hydraulics model based on which this control system is designed. Thus, an accurate model is needed that, additionally, is simple enough to facilitate the use of high performance control design methods. In this abstract an approach for nonlinear Model Order Reduction (MOR) for MPD systems is presented.

2 Approach

In principle, hydraulics models for MPD systems come in the form of high-fidelity Partial Differential Equations (PDE). From a control perspective, these models are too complex to be used directly for model-based control design and, thus, further simplification/reduction is needed. Complexity-reduction approaches for these systems may be split into three groups: 1) approximating the high-fidelity models by low-order ODE models based on a time-scale separation, 2) model reduction using coarse discretization of the PDE model and 3) model reduction using a combination of a fine discretization and automatic MOR techniques. Models obtained from the first approach have been widely used in practice, but the controllers based on those are incapable of effective rejection of transient and periodic disturbances, due to the fact that wave propagation phenomena key in MPD models are ignored [1]. The second approach provides more effective models especially for the rejection of periodic disturbances, but those still do not provide a full rejection. In the last approach, pursued in this work, the high-fidelity PDE model is discretized using semi-discretization techniques leading to a high-order model in terms of ODEs. This model can be cast into a Lur'e-type form comprising a high order-linear subsystem, Σ_{lin} as in Fig 1, with a low-dimensional nonlinear mapping $h(\cdot, \cdot)$ due to the nonlinear boundary conditions at the actuator and the bit. For this class of systems, a MOR procedure has been developed in [3], where only the linear subsystem is reduced using balanced truncation techniques. This method, unlike many other nonlinear MOR methods, preserve key

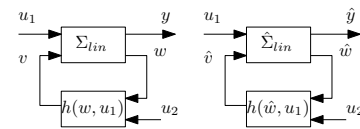


Figure 1: Lur'e-type system form of semi-discretized and reduced-order system models.

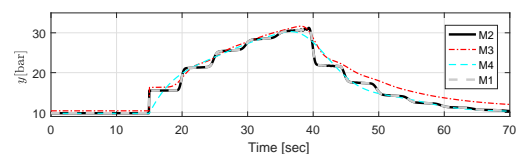


Figure 2: A comparison between the time responses of the high-complexity model and the reduced ones.

system properties (such as stability) and provides a computable bound on the reduction error $y - \hat{y}$. Here, y represents the pressure of the drilling fluid at the surface, which is the measurement typically used for feedback control.

3 An illustrative case study

In Fig 2, a comparison is performed between the original Lur'e-type model (M1), following from semi-discretization of the PDE model, with the low-complexity model M2 (obtained through the proposed approach), model M3 (from approach 2) and M4 (from approach 1). Clearly, M2 gives a far more accurate approximation.

References

- [1] I. S. Landet, A. Pavlov, O. M. Aamo, "Modeling and control of heave-induced pressure fluctuations in managed pressure drilling," *IEEE Trans. Cont. Syst. Tech.*, 21(4): 1340-51, 2013.
- [2] U. J. F. Aarsnes, T. Flåtten, O. Morten Aamo, "Review of two-phase flow models for control and estimation," *Annu. rev. cont.*, 42: 50-62, 2016.
- [3] B. Besselink, N. van de Wouw, H. Nijmeijer, "Model reduction for nonlinear systems with incremental gain or passivity properties," *Automatica*, 49(4): 861-72, 2013.

Construction of PID Passivity-based controllers for port-Hamiltonian systems.

L.P. Borja*, R. Ortega**, J.M.A Scherpen*

*Nijenborgh 4, 9747 AG Groningen, The Netherlands.

l.p.borja.rosales[j.m.a.scherpen]@rug.nl

**3 Rue Joliot-Curie, Plateau du Moulon, 91192 Gif-sur-Yvette, France.

Romeo.Ortega@l2s.centralesupelec.fr

1 Abstract

For almost one century, the Proportional-Integral-Derivative (PID) controllers have been the most popular stabilizers in engineering applications. Whilst these regulators have been shown to be very effective to solve the regulation problem, their construction hinges in the appropriate selection of a set of gains, which are customarily chosen from a linearized approximation of the plant. Nonetheless, when the system is *highly nonlinear*, the procedure to tuning the gains of PID regulators might be a challenging task. A solution to this problem arises when the system under study has passivity properties; in such a case, the PID controller can be designed considering the *passive output* as the feedback signal. These particular PIDs are referred as PID Passivity-based controllers (PID-PBCs) and one appealing feature is that—for stability purposes—the step of tuning the gains is trivialized in this case.

The present work is focused on a particular class of passive systems, namely, the so-called port-Hamiltonian (PH) systems, whose input-state-output representation is given by¹

$$\Sigma: \begin{cases} \dot{x} &= [\mathcal{J}(x) - \mathcal{R}(x)]\nabla H(x) + g(x)u \\ y_{\text{wD}} &= h(x) + [w^\top(x)w(x) + D(x)]u \end{cases} \quad (1)$$

where $x \in \mathbb{R}^n$ is the state vector, $u, y_{\text{wD}} \in \mathbb{R}^m$ are the input and output vectors, respectively, with $n > m$. Furthermore, $H: \mathbb{R}^n \rightarrow \mathbb{R}$ is the Hamiltonian, $\mathcal{J}, \mathcal{R}: \mathbb{R}^n \rightarrow \mathbb{R}^{n \times n}$, with $\mathcal{J}(x) = -\mathcal{J}^\top(x)$ and $\mathcal{R}(x) = \mathcal{R}^\top(x) \geq 0$, are the interconnection and damping matrices, respectively, and $g: \mathbb{R}^n \rightarrow \mathbb{R}^{n \times m}$ is the input matrix, whose rank is equal to m . The mappings $w: \mathbb{R}^n \rightarrow \mathbb{R}^{q \times m}$, $h: \mathbb{R}^n \rightarrow \mathbb{R}^m$, $\phi: \mathbb{R}^n \rightarrow \mathbb{R}^{q \times n}$ and $D: \mathbb{R}^n \rightarrow \mathbb{R}^{m \times m}$ satisfy, for any integer $q \geq \text{rank}\{\mathcal{R}\}$, the following

$$\begin{aligned} \mathcal{R}(x) &= \phi^\top(x)\phi(x), \\ h(x) &:= [g(x) + 2\phi^\top(x)w(x)]^\top \nabla H(x), \\ D(x) &= -D^\top(x). \end{aligned}$$

Moreover, the energy function $H(x)$ satisfies

$$\dot{H} = -|\phi(x)\nabla H(x) + w(x)u|^2 + u^\top y_{\text{wD}}.$$

¹where $\nabla H(x) = [\frac{\partial H(x)}{\partial x_1}, \dots, \frac{\partial H(x)}{\partial x_n}]^\top$.

PH systems have been proved to be suitable to represent many physical systems [1, 3]. On the other hand, in these models the roles of the energy, the dissipation and the interconnection pattern are underscored, which are fundamental ingredients of PBC [2].

The main objectives of this work are:

- To establish the necessary conditions for the construction of a PID-PBC of the form

$$u = -K_P y_{\text{wD}} - K_I [\gamma(x) + \kappa] - K_D \dot{y}_{\text{wD}} \quad (2)$$

where the gains K_P, K_I, K_D are constant, symmetric and positive definite matrices of appropriate dimension, $\kappa \in \mathbb{R}^m$ is a *free* constant vector and $\gamma: \mathbb{R}^n \rightarrow \mathbb{R}^m$ satisfies

$$\dot{\gamma} = y_{\text{wD}}.$$

- To identify under which circumstances the system Σ , given in (1), in closed-loop with the PID-PBC in (2) preserves the passivity property, but with a *new energy function* with an isolated minimum at the desired equilibrium point. Thus, if this former condition holds, the new energy function qualifies as a *Lya-punov function* for the closed-loop system. Finally, a further analysis is carried out to claim *asymptotic stability* of the equilibrium point.

References

- [1] V. Duindam, A. Macchelli, S. Stramigioli, and H. Bruyninckx. *Modeling and Control of Complex Physical Systems: The Port-Hamiltonian Approach*. Springer Science & Business Media, 2009.
- [2] R. Ortega, A. van der Schaft, I. Mareels, and B. Maschke. Putting Energy Back in Control. *Control Systems Magazine, IEEE*, 21(2):18–33, Apr 2001.
- [3] A. van der Schaft. *L₂-Gain and Passivity Techniques in Nonlinear Control*. Springer, Berlin, third edition, 2016.

Robust Greenhouse Climate Control

Wouter Kuijpers^{1,3}, David Katzin², René van de Molengraft¹,
Simon van Mourik² and Eldert van Henten²

¹ Control Systems Technology Group, Eindhoven University of Technology, 5600 MB Eindhoven, The Netherlands

² Farm Technology Group, Wageningen University & Research, 6708 PB Wageningen, The Netherlands

³ Email: w.j.p.kuijpers@tue.nl

1 Introduction

The LED it be 50%-project aims at reducing the energy use in tomato greenhouse horticulture with at least 50%, by the smart use of LED lighting. To optimize the efficiency, amongst other activities within the project, a management support system (MSS) will be designed. The MSS will provide the grower with an optimal strategy for the control of LED lights and the climate management equipment. The provided strategy will aim to maximize the benefits of LED light on crop production. The core of the MSS will consist of a controller, synthesized using optimal control strategies.

2 Greenhouse Climate Control

To control the growth of the crop, growers create setpoint trajectories for relevant climate variables, such as: temperature, humidity and CO_2 concentration. SISO controllers are used to realize the created setpoint trajectories. To cope with the interaction between various climate variables, conditional statements are used. Generating these setpoint trajectories and conditional statements takes a considerable amount of time and requires a lot of knowledge and experience. In literature several methods have been presented which aim at automating this process, e.g.: MPC [1], neural networks, gain scheduling, of which most did not make it to common practice. In [2], van Straten et al. argue that these methods cannot be made understandable for the grower, which is of importance when taking over the control of their crops. In [3], van Beveren et al. mention that the models for the model-based approaches have not matured enough. This research aims at tackling some of these factors, towards automated greenhouse climate control.

3 Crop Modeling

The crops in the greenhouse vary from each other, because of: spatial differences in the greenhouse (e.g. temperature and light distribution) and human disturbances (e.g. harvesting leaves and fruits). Because of interaction between the crops (e.g. shade avoidance syndrome), these variations are even increased. To be able to guarantee performance for the variation in the crops, a model is required which quantifies this variation. In [4], Gary et. al. argue that deterministic crop models, combined with spatially variable climate information have a potential for allowing more precise growing.

4 Greenhouse System

The climate in the greenhouse is mostly influenced by the outdoor climate, to control the climate inside the greenhouse it is important to have predictions of the outdoor climate. Just like the normal weather forecasts these predictions will be uncertain, no perfect models describing the weather exist, yet. Aside from this uncertain forecast also: auction and energy prices play a big role, but also here accurate predictions are still missing.

5 Controller Synthesis

Combining the previous two sections: this research is concerned with the design of robust greenhouse climate control system, which is able to cope with the variation in greenhouse crops and the uncertain forecasts. To do this, we have selected one of the current state-of-the-art methods: Model Predictive Control, during the synthesis of which, specific care will be taken to ensure robust performance with respect to the crop variation and the uncertain forecasts. Methods such as Economic MPC and Stochastic MPC will be employed to synthesize such a controller.

References

- [1] A. Ramirez-Arias, A. F. Rodriguez, J.L. Guzman, M. Berenguel, Multiobjective hierarchical control architecture for greenhouse crop growth, *Automatica*, 2012.
- [2] G. van Straten, H. Challa and F. Buwalda, Towards user accepted optimal control of greenhouse climate, *Computers and Electronics in Agriculture*, 2000.
- [3] P.J.M. van Beveren, J. Bontsema, G. van Straten and E.J. van Henten, Optimal control of greenhouse climate using minimal energy and grower defined bounds, *Applied Energy*, 2015.
- [4] C. Gary, J.W. Jones, M. Tchamitchian, "Crop modelling in horticulture: state of the art", *Scientia Horticulturae*, 1998.

Flexible bio-hydrogen supply based on model predictive control for balancing an urban hybrid renewable energy system

Yu Jiang^{1,*}, Xun Wang¹, Ekko van Ierland², and Karel Keesman¹

¹Biobased Chemistry and Technology, Wageningen University & Research, PO Box 17, 6700 AA, Wageningen, The Netherlands

*Corresponding author email: yu.jiang@wur.nl

²Environmental Economics and Natural Resources Group, Wageningen University & Research, Hollandseweg 1, 6706 KN, Wageningen, The Netherlands

1 Abstract

A low-carbon urban energy system is characterised by a high share of intermittent renewable energy in the energy mix. The stochastic production from intermittent renewable energy poses challenges to the balance between electricity supply and demand in the urban electricity system. The stability of the urban electricity system needs controllable power generation technologies to provide the flexibility. A demand-driven bio-hydrogen production and storage system has the potential to be both controllable and carbon-neutral [1]. It can contribute to the balance of the urban electricity system that is faced with the challenge of integrating intermittent renewable energy such as wind and solar energy.

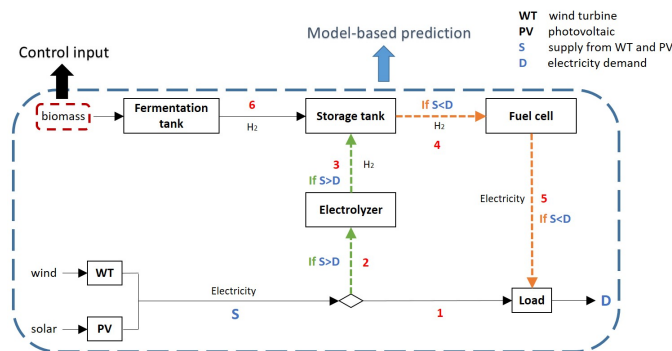


Figure 1: One of the configurations of the biobased hybrid renewable energy system (off-grid design)

The objective of the study was to develop optimal energy management strategies based on model predictive control (MPC) approach for a biobased hybrid renewable energy system (HRES) in an urban environment. We developed three possible configurations of HRES containing micro wind turbines, photovoltaic (PV) cells, a fermentation system, and a hydrogen storage module. As an illustration, we present Figure 1 in this abstract, which shows one of the possible HRES configurations. The electricity system works in an off-grid mode in this configuration. The goal of the model predictive control is to keep the hydrogen storage level in the tank within a safety range while guaranteeing the

stability of the electricity system. The control input is the glucose concentration of the biomass feed-in system. The model output is the storage level of the hydrogen tank. By using an MPC approach [2], the disturbances and system behaviours were studied. A receding horizon optimisation was run for a whole year with a time step of one hour. The control horizon is 4 days, and the prediction horizon is 14 days. The disturbance inputs are wind speed, PV cell temperature, solar irradiation, and the electricity demand. Model predictive controller uses the historical data, weather forecast, and mathematical models to predict system behaviour and to manage energy flows. We illustrated the methodology by conducting a case study in Amsterdam, the Netherlands. Advantages and disadvantages of three different configurations were compared. Furthermore, the biobased HRES was also compared with a natural gas based urban electricity system.

In this study, we demonstrated the usefulness of the MPC approach in managing a bio-based HRES. The model predictive controller was found to be able to keep the hydrogen storage level within the predefined safety range and to balance the electricity system. We found that the required size of the hydrogen storage tank is reduced when applying a model predictive controller. We also found that the biobased HRES is robust when the level of glucose concentration in the biomass feed-in system is between 25 to 28 g/L.

References

- [1] E, Mauky, S, Weinrich, H.F., Jacobi, H.J., Nägele, J, Liebetrau, and M, Nelles, "Demand-driven biogas production by flexible feeding in full-scale—Process stability and flexibility potentials", *Anaerobe*, vol. 46, pp. 86-95, 2017
- [2] J, Rawlings and D, Mayne, "Model predictive control: theory and design", *Nob Hill Pub*, 2009.

Model learning predictive control with applications to batch processes

Marco A.C. Loonen M. Bahadır Saltık Alejandro Marquez-Ruiz Leyla Özkan
Control Systems Group

Eindhoven University of Technology

M.A.C.Loonen@student.tue.nl, {M.B.Saltik,A.Marquez.Ruiz,L.Ozkan}@tue.nl

1 Introduction

The aim of this work is to utilize iterative learning algorithms to improve the parameter accuracy of a linear parameter varying (LPV) model that can be used in model-based control applications for batch processes. In order to improve the model predictions, and hence control performance, the varying parameters are re-estimated in between batches, such that changes in the plant are taken into consideration. With the updated parameters, the reference tracking performance via model predictive controllers (MPC) is desired to be improved.

2 Research problem formulation

In various industrial applications, batch processes are generally used for producing specialized products in smaller quantities. Models of these processes can be derived by using the first principle laws for utilizing the model in a greater range of operating points. These models provide accurate predictions, yet, they are generally complex and non-linear. To use these models for control purposes, it has been shown in [1] that the extent transformation casts these complex models in the LPV setting.

Using LPV models usually is problematic because the parameter identification is an expensive task. For repetitive batch processes, the parameters can be estimated in between batches by using the inputs-outputs. By repeating this estimation between the batches, the parameter can be learned more accurate over time, while still being able to adjust for the changes in the plant/physical parameters such as installation/vessel degradation.

For the control of the temperature and MPC controller is used that penalizes the predicted reference tracking error for a specific output temperature profile. This MPC controller includes the process input and output constraints within multivariate control problems.

3 A case study

In this case study, the temperature control of a nonlinear chemical batch reactor is considered, described by the following dynamics:

$$\frac{dT}{dt} = -\underbrace{\frac{UA}{MC_p}}_{\theta} \underbrace{(T - T_j)}_x - \underbrace{\frac{\Delta H V}{MC_p} k_0 e^{E/RT} C_A^2}_r$$

$$\frac{dC_A}{dt} = -k_0 e^{E/RT} C_A^2$$

Which is transformed in the parameterized model Eq. (1) for use in the MPC.

$$\begin{aligned} \dot{x} &= -\theta x + \theta u + r \\ y &= Cx \end{aligned} \quad (1)$$

The input and output data show the reference tracking improvement of the MPC controller after the updating the parameter θ in between batches.

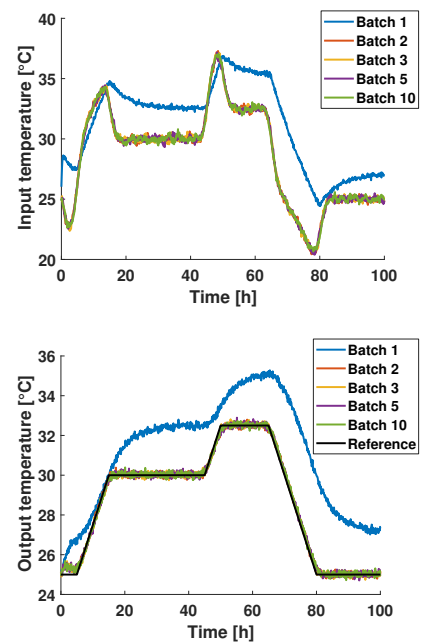


Table 1: Estimated parameter θ

Batch	1	2	3	5	10
θ	3.0000	0.1096	0.1131	0.1133	0.1135

References

- [1] Carlos S. Méndez Blanco. Control of Reactive Batch Distillation Columns via Extents Transformation. Masters thesis, Delft University of Technology, 2017.

A model based scenario study for balanced crop irrigation

Francisco Mondaca Duarte, Simon van Mourik, Eldert van Henten
 Farm Technology Group. Wageningen University
 P.O. Box 16, 6700 AH Wageningen. The Netherlands
 Email: francisco.mondacaduarte@wur.nl

1 Introduction

Efficient water use is one of the main issues within agriculture. To prevent the crop from water stress, many growers tend to over-irrigate as a form of risk aversion. This may lead to drainage, which in turn may transport harmful pesticides and fertilizer into the groundwater. Hence the irrigation strategies currently followed by growers are usually not optimally water efficient, and promote pollution.

From a Systems and Control perspective, an optimal control approach is the most straightforward way to achieve the objective of minimizing drainage without crop stress. However, this will likely result in continuous irrigation which might be unhealthy for soil ecology. Furthermore, a grower will likely not accept a strategy that differs too much from what he is used to.

To circumvent these barriers, we look for irrigation strategies using a model based scenario study. This will serve as a first step towards practical optimal irrigation that balances between crop stress and drainage.

2 Approach

Three simulated strategies were compared. The first strategy was observed from a regular grower. The second strategy used the same amount of water as strategy 1, and consisted of equal water dosages applied every three days. The third strategy was similar to strategy 2, but used 25 percent less water. The performances of all three strategies were compared with respect to crop stress events, and drainage.

The modelled water transport system consisted of crop stress, soil moisture content, and weather. Water transport through soil and crop was described by an integrated model combining Richard's equation for water flow in the soil [1], and the Penman Monteith equation for evapotranspiration [2]. The model describes four soil layers, where the first layer represents the top soil, and the bottom layer represents the groundwater. Drainage was defined as the outflow from the third layer to the groundwater. Crop stress was modelled via the FAO adjusted evapotranspiration equation [3].

First, the model was validated using actual greenhouse drainage and weather data from August 2016. Thereafter, the performances of the three strategies were compared.

3 Results

The model showed good prediction accuracy. The predicted total drainage was 250 litres per square meter, against a measured value of 260. The grower strategy did not result in crop stress according to our model, it required 1590 litres, and resulted in 250 litres drained. Strategy 2 did also not result in crop stress, with 217 litres drained. The third strategy resulted in only 164 litres drained, however here crop stress was predicted to occur.

4 Discussion

This study predicts three things. First, the grower's strategy was already quite balanced with respect to crop stress. Second, with respect to drainage a considerable reduction can be obtained. Third, the balance between crop stress and drainage is a delicate one; a modest reduction in water gift will already lead to crop stress.

5 Outlook

Two valuable next steps would be to 1) validate the model predictions in practice, and 2) compare the robustness of the performance outcomes towards unforeseen variations in weather and soil properties. In this way, we will be able to assess the performance of different strategies, as well as the risks of performance loss they bring along under uncertain circumstances.

References

- [1] Richards, L.A., Capillary Conduction Of Liquids Through Porous Mediums. *Journal of Applied Physics*, 1931. 1(5): p. 318-333.
- [2] Allen, R.G., et al., Crop evapotranspiration - Guidelines for computing crop water requirements, in Food and Agriculture Organization of the United Nations, F.I.a.d.p. 56, Editor. 1998: Rome.
- [3] Pereira, L.S., et al., Crop evapotranspiration estimation with FAO56: Past and future. *Agricultural Water Management*, 2015. 147: p. 4-20.

Supervisory Control Synthesis for a Lock-Bridge Combination

F.F.H. Reijnen, J.M. van de Mortel-Fronczak, J.E. Rooda
 Control Systems Technology Group, Department of Mechanical Engineering
 Eindhoven University of Technology
 P.O.Box 513 5600 MB Eindhoven, The Netherlands
 Email: {F.F.H.Reijnen, J.M.v.d.Mortel, J.E.Rooda}@tue.nl

1 Introduction

Cyber-physical systems have become increasingly complex due to an increase in safety requirements and required functionality. As a result, controllers for these systems are getting more complex as well. Formal methods, such as supervisory control theory from [1] can help in overcoming this growing complexity. A model of the uncontrolled system and a model of the control requirements are used to obtain a minimally restrictive supervisor that per construction adheres to the requirements, and is controllable and nonblocking.

Supervisory control theory is an active research topic, yet realistic applications are few in number. The reasons for this are the computational complexity of synthesis procedures and the lack of experience with discrete-event modeling for industrial systems [2]. In this paper, a realistic case study related to modeling and synthesizing a supervisory controller for the Algera Lock and the Algera Bridge is reported on.

2 Case study description

The Algera Complex, located in the Hollandsche IJssel, consists of a bascule bridge, a lock, and two storm surge barriers, see Figure 1.



Figure 1: The Algera Complex [beeldbank.rws.nl].

In case of extremely high sea water, the storm surge barriers are closed to protect the inlands. In such a situation, the adjacent lock is used to transport vessels between the different water heights. Additionally, the lock in combination with

the movable bridge is used as a route for vessels that are too high to pass under the storm surge barriers. In this case study, only the bascule bridge and the lock are considered.

3 Results

The plant model of the Algera Lock and the Algera Bridge are successfully modeled using extended finite state automata. The control requirements imposed on the system are modeled using logic state-based expressions. From these models, a supervisor has been synthesized. Furthermore, a supervisor for the Algera lock-bridge could easily be synthesized from the combined models and some additional requirements. Table 1 shows the number of states in the uncontrolled system, the number of requirements and the number of states remaining in the controlled system.

Table 1: Size of the models.

	Uncontrolled	Req.	Controlled
Lock	4.2×10^{34}	247	3.2×10^{22}
Bridge	1.9×10^{23}	112	9.4×10^{19}
Lock-bridge	7.8×10^{57}	362	3.0×10^{40}

Simulation-based analysis supported by visualization is used to successfully validate the supervisor. This is done by performing test cases on the simulation model.

Acknowledgements

This work is supported by Rijkswaterstaat, part of the Ministry of Infrastructure and Water Management of the Government of The Netherlands. We thank Bart van Willigen for his assistance with the case study.

References

- [1] P.J. Ramadge, and W.M. Wonham, "Supervisory Control of a Class of Discrete Event Processes", in *SIAM Journal on Control and Optimization*, 25(1), pp. 206-230, 1987.
- [2] W.M. Wonham, K. Cai, and K. Rudie, "Supervisory Control of Discrete-Event Systems: a Brief History – 1980-2015", in *Proceeding of the 20th IFAC World Congress*, pp. 1827-1833, 2017.

Prediction-based delay compensation for staged crystallization

Marcella Porru

Dept. of Electrical Engineering, CS
TU/Eindhoven, The Netherlands
Email: M.Porru@tue.nl

Leyla Özkan

Dept. of Electrical Engineering, CS
TU/Eindhoven, The Netherlands
Email: L.Ozkan@tue.nl

1 Introduction

Traditionally, the crystallization of active pharmaceutical ingredients (API) and other chemical specialties has been operated in batch or semi-batch mode under strictly regulated recipes. However, batch operations have disadvantages such as lack of batch to batch reproducibility, long processing times, scale up issues, poor controllability and observability [1]. Continuous operation can overcome these drawbacks, although a higher degree of automation and a more in depth process understanding is required for successful continuous API production. Therefore, recent research efforts are directed towards the design of continuous crystallization processes. Multistage mixed suspension mixed product removal (MSMPR) crystallization might be the most convenient route of transition from batch to continuous operation, since current crystallizers in industry are of the stirred tank type [2]. Majority of the work in this area has studied the steady state properties of these systems whereas only a few works deal with the process dynamics and control of these units. In this work, an advanced control scheme for average crystal dimension control in industrial-scale two stage MSMPR crystallizers is proposed and tested in simulation.

2 Control problem

The particle size distribution (PSD) is an important property of a crystalline product. It can determine the efficiency of the downstream operations, as well as end-use properties, such as bioavailability. The control of the full PSD is not possible in practice. However, some of its attributes (average size, coefficient of variation, fines fraction, etc.) can be controlled. The scope of this work is to achieve the control of the average crystal length d_{43} . To this end, we opted for a control scheme that combines feedback control with process predictions. This is an effective and simple way to upgrade low level PI controllers to the level of advanced process controllers (APCs) that should not require highly skilled personnel for controller commissioning and maintenance [3].

3 Prediction-based time delay compensator

The core of the control scheme is presented in Fig. 1, and consists of a PI controller ($d_{43}C$ block) which manipulates the temperature setpoint in the first crystallizer jacket (T_1^{SP}) such that the average crystal length d_{43} is maintained at the desired specification. Because of the large volumes involved

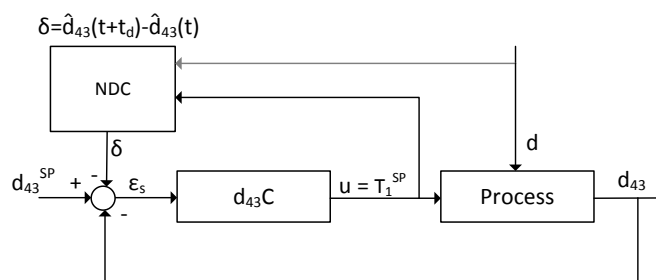


Figure 1: Block diagram of the advanced d_{43} controller. The block $d_{43}C$ is the linear PI controller with modified error signal ϵ_s ; the block NDC is the nonlinear delay compensator which can incorporate exogenous disturbance measurements d .

in the industrial operation, a large time delay t_d between manipulated and controlled variables can exist, resulting in limitations in the performance of this standard PI controller. Hence, a delay compensator is designed to improve closed loop performance by taking into account an additional error signal for future $d_{43}(t+t_d)$ deviations. The delay compensation block (NDC in Fig. 1) for average crystal length prediction consists of the nonlinear dynamic model of the first five PSD moments, solute concentration and temperature in the two crystallizers, with simulation horizon equal to the time delay. Measured disturbances, if available, can be provided to this model-based block for further performance improvements. A good control performance indicator is the ITAE which, in this case, is reduced at least by a factor of 4 by upgrading the PI controller with the NDC.

4 Acknowledgements

This work has been done within the INSPEC project in the Institute for Sustainable Process Technology ISPT.

References

- [1] Porru, M. and Özkan, L. (2017). *Ind. Eng. Chem. Res.*, 56, 9578-9592.
- [2] Power, G., Hou, G., Kamaraju, V.K., Morris, G., Zhao, Y., and Glennon, B. (2015). *Chem. Eng. Sci.*, 133, 125-139.
- [3] Porru, M., Baratti, R., and Alvarez, J. (2014). *IFAC Proceedings Volumes*, 47(3), 1266-1271.

State estimation for nonlinear systems with communication constraints

Quentin Voortman, Alexander Pogromsky, Henk Nijmeijer
Eindhoven University of Technology,
PO Box 513, 5600MB Eindhoven,

Email: {Q.J.T.Voortman, A.Pogromski, H.Nijmeijer}@tue.nl

Introduction

In recent years, a lot of attention has been given to the problem of controlling dynamical systems over channels with limited communication capacity. In this work, we present a communication scheme for the state estimation of nonlinear uncertain systems over channels with limited communication rates. We design a coder/decoder scheme that is robust towards communication losses, in the sense that it is able to function over a one-way communication channel where some losses possibly occur.

Problem statement

We study nonlinear discrete-time time-invariant dynamical systems with an uncertainty in the initial condition. The system is connected to a remote location through a communication channel as depicted in Figure 1. The system has a state vector $x(t)$. The communication channel sends coded messages $e(t)$ through which the decoder reconstructs an estimate of the state $\hat{x}(t)$. The objective is to design a coder/decoder scheme that has the following properties

- The messages $e(t)$ must be part of a finite-size alphabet. The size of the alphabet must be as small as possible in order to limit the resulting communication rate.
- Through the communications, one must be able to obtain estimates that are arbitrarily close to the real state. More precisely, for any given precision, the communication scheme must guarantee the precision of the estimate without exceeding the maximum allowable communication rate.
- The reconstruction of the state at each time step must be based exclusively on the current message and not on the previous estimates. This property ensures that the communication scheme is robust towards communication losses on one-way channels i.e. channels without communication feedback from the decoder to the coder.

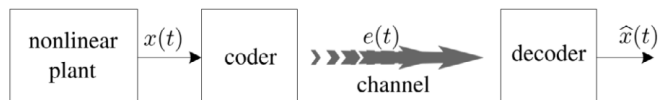


Figure 1: The system and the communication channel.

Solution and simulations

We developed a communication scheme that satisfies the three aforementioned criteria. This communication scheme is based on the upper box dimension [2] of the attractor of the dynamical system. The resulting communication speed involves the upper bound on the largest Lyapunov exponent of the system Λ as well as the upper box dimension of the attractor of the dynamical system d_B . The coder/decoder scheme we developed functions on any channel with rate above $\Lambda d_B/2$. The main result is the usage of the second Lyapunov method in order to obtain analytical bounds on the communication rate.

The communication scheme has been tested through simulations on the smoothed Lozi map [1][3]. Using estimates for the upper box dimension and the largest Lyapunov exponent, we computed the minimum communication rate for the communication scheme. We were able to implement the communication protocol with arbitrary precision on a channel with rates very close to the minimum communication rate.

Acknowledgment

This project has received funding from the European Union's Horizon 2020 research and innovation programme under the Marie Skłodowska-Curie grant agreement No 675080.

References

- [1] Aziz-Alaoui, M. a., Robert, C., and Grebogi, C. (2001) *Dynamics of a Henon-Lozi-type map*. *Chaos Solitons & Fractals*, 12:23232341.
- [2] Falconer, K. (1997) *Fractal Geometry: Mathematical Foundations and Applications*. John Wiley & Sons.
- [3] Lozi, R. (1978) *Un Attracteur Etrange du Type de Henon*. *Journal de Physique Colloques*, 39(C5):C59C510.

Cooperative adaptive cruise control: an observer-based approach to increase robustness over unreliable networks

Francesco Acciani and
Anton A. Stoorvogel
Department of
Applied Mathematics
University of Twente

Enschede, The Netherlands

f.acciani@utwente.nl

a.a.stoorvogel@utwente.nl

Paolo Frasca
Univ. Grenoble Alpes,
CNRS, Inria, GIPSA-lab,
F-38000 Grenoble, France
paolo.frasca@gipsa-lab.fr

Geert Heijenk
Department of
Computer Science
University of Twente
Enschede, The Netherlands
geert.heijenk@utwente.nl

1 Introduction

A promising way to optimise the use of highways, by reducing the distance between vehicles, is the cooperative adaptive cruise control (CACC). Enabled by wireless communication between vehicles, CACC increases highway throughput, safety and comfort, by automatically regulating the acceleration of vehicles in a platoon to achieve a desired speed profile. By allowing the vehicles to share their motion and control information through wireless communication, the minimum allowable inter-vehicular time headway can be decreased [1]. However, the wireless medium that is used to share this information is unreliable. Therefore, the phenomenon of the packet loss should be taken into account for a safe and comfortable behaviour. In this work we present 1) the combination of a local and cooperative controller to achieve stable behaviour for a platoon of vehicles and 2) we explore the use of an observer to reduce the impact of losses on the disturbance rejection among the string.

2 Problem formulation

A way to increase highways throughput is to allow vehicles to drive as close as possible to each other, while keeping the platoon dynamics stable. To do so, a speed dependent time spacing policy is adopted [2]: defining the required distance between vehicle i and its preceding one $i-1$ as

$$d_{r,i}(t) = r_i + hv_i(t)$$

where h is the time gap, $v_i(t)$ is the speed of vehicle i and r_i is the standstill reference distance, we can find a controller to bring the error $d_i(t) - d_{r,i}(t)$ to zero. To achieve such objective, we use a local controller, described by a discrete time transfer function $D(z)$ and a feedforward filter, described as $F(z)$, such that:

$$u_i(z) = D(z)e_i(z) + F(z)u_{i-1}(z)$$

where $e_i(z) = q_{i-1}(z) - q_i(z) - hv_i(z)$ and $u_{i-1}(z)$ is the input of the previous vehicle transmitted over the wireless medium.

3 Losses and observer

When the local and cooperative controller are employed, the performances of the system are satisfactory: the platoon is stable and the disturbances are rejected along the downstream direction of the string. However, if some packets (i.e. some u_{i-1}) are lost, the system is stable but not string stable anymore. When the system is not string stable, disturbances grow bigger over the string: potentially a small disturbance acting on a vehicle at the beginning of the string might lead to a traffic jam at a different position in the string. To prevent this unwanted behaviour, we design an observer to estimate – from locally available measurements – the information transmitted by the preceding vehicles, and we use it when the communication is not available. Using the estimate only when a packet is not received leads to a hybrid observer, which can jump asynchronously when an incoming communication is available.

4 Conclusion

The use of an hybrid observer does increase the robustness performances of the system, reducing the vehicle distance while stabilising the platoon for smaller time headways. However, current work is focussing on a finer model to explicitly take string stability concept into account in the controller and observer design.

References

- [1] J. Ploeg, B. T. M. Scheepers, E. Nunen, N. Van De Wouw, and H. Nijmeijer, "Design and experimental evaluation of cooperative adaptive cruise control," in *IEEE Conference on Intelligent Transportation Systems (ITSC)*, Oct. 2011.
- [2] D. Swaroop, J. Hedrick, C. C. Chien, and P. Ioannou, "A comparison of spacing and headway control laws for automatically controlled vehicles," *Vehicle System Dynamics*, vol. 23, pp. 597–625, 1994.

Real-time plasma state monitoring and supervisory control on the TCV tokamak

T.C. Blanken

Eindhoven University of Technology
Department of Mechanical Engineering
Control Systems Technology
P.O. Box 513, 5600 MB Eindhoven
The Netherlands
Email: t.c.blanken@tue.nl

C. Galperti

École Polytechnique Fédérale de Lausanne
SPC-EPFL, Lausanne, Switzerland

M. Kong

École Polytechnique Fédérale de Lausanne
SPC-EPFL, Lausanne, Switzerland

F. Felici

Eindhoven University of Technology
Department of Mechanical Engineering
Control Systems Technology
P.O. Box 513, 5600 MB Eindhoven
The Netherlands
Email: f.felici@tue.nl

T. Vu

École Polytechnique Fédérale de Lausanne
SPC-EPFL, Lausanne, Switzerland

O. Sauter

École Polytechnique Fédérale de Lausanne
SPC-EPFL, Lausanne, Switzerland

1 Introduction

Controlled nuclear fusion has been considered as an alternative, clean, and sustainable source of energy for several decades. The most developed machine to achieve controlled nuclear fusion is the tokamak, which uses magnetic fields to confine a hot plasma. In a tokamak reactor plasma control system (PCS), a supervisory controller takes decisions about pulse segment scheduling, exception handling, prioritized simultaneous control tasks and actuator sharing [1][2]. Many failure modes of a tokamak are comprised of consecutive events including plasma stability limit violations, deviations from references, and actuator failure [3]. It is key to interrupt sequences that can lead to detrimental plasma disruptions.

2 Main contributions

We implemented a real-time state monitor, supervisory controller and actuator allocator for MIMO feedback controllers with shared actuators on the TCV tokamak [4]. The state monitor provides a finite-state representation of the continuous-valued plant and measurements. A phase locked loop was developed to estimate the frequency of variable-frequency magnetohydrodynamic disturbances. Based on the plasma state, the supervisor takes decisions from user-defined rules about the activation and relative priorities of low-level control tasks.

3 Results

We present first experimental results of several use cases of the state monitor and the supervisor on TCV plasmas. First, we show results of simultaneous control of plasma pressure and magnetohydrodynamic disturbance on TCV. Although the individual feedback controllers are decoupled, they must share a common set of actuators. Here, experimental tests demonstrate satisfactory behaviour of the interconnection of the supervisory controller, an actuator allocator and the feedback controllers [5][6]. Second, we show real-time capable detection and frequency estimation of magnetohydrodynamic disturbances using a phase-locked loop on TCV data.

4 Conclusions

This work provides a first demonstration of centralized state monitoring and supervisory control on TCV. The interconnection of real-time controllers allows more intricate experiments on plasma physics and stability.

References

- [1] D. Humphreys *et al*, Physics of Plasmas 22, (2015).
- [2] N. Eidiētis *et al*, 17th ITPA IOS TGM, (2016).
- [3] P.C. de Vries *et al*, Nucl. Fusion 51 (2011).
- [4] S. Coda *et al*, Nucl. Fusion 57 (2017).
- [5] M. Kong *et al*, 44th EPS Conference on Plasma Physics (2017).
- [6] E. Maljaars *et al*, Nucl. Fusion 57 (2017).

On Experiment Design for Parameter Estimation of Equivalent-Circuit Battery Models¹

H.P.G.J. Beelen H.J. Bergveld M.C.F. Donkers

Department of Electrical Engineering, Control Systems Group

Eindhoven University of Technology, P.O. Box 513, 5600 MB Eindhoven

Email: h.p.g.j.beelen@tue.nl, h.j.bergveld@tue.nl, m.c.f.donkers@tue.nl

1 Introduction

The State-of-Charge (SoC) of a battery cannot be measured directly. Instead, the SoC is typically estimated online using an Equivalent Circuit Model (ECM) combined with e.g., an Extended Kalman Filter (EKF). In [1], it has been shown that the EKF already achieves a close-to-optimal estimation accuracy (i.e., close to the Cramér-Rao lower bound). This suggests that the quality of the state estimates mostly depends on the quality of the ECM used in the estimator.

2 Problem statement

In order to capture the relevant battery dynamics that correspond to a certain application, real application data should be preferred for estimation of the ECM parameters. Surprisingly, a widely used approach to the (offline) parameter estimation of ECMs is to use standard tests, such as a Pulsed-Current Test (PCT), which might not be representative. Therefore, we study the experiment design for estimation of ECM parameters and quantify its impact on the quality of state estimation [2]. To do so, we will use an E-bike experiment where two sets of data were recorded: (1) a PCT on a single battery cell under laboratory conditions and (2) a field test with an E-bike on the entire battery pack with both high-precision sensors as well as production-grade sensors.

3 ECM Modelling and SoC Estimation

The input for the ECM is the battery current I^{batt} , the output is the battery voltage V^{batt} and $V^{\text{EMF}}(\text{SoC})$ denotes the nonlinear EMF-SoC relation. Subsequently, we can write

$$V^{\text{batt}} = V^{\text{op}} + V^{\text{EMF}}(\text{SoC}), \quad (1)$$

where V^{op} denotes the overpotential of the battery. An input-output model of the overpotential V^{op} can be constructed by using an ARX model of the form

$$V_k^{\text{op}} = b_0 I_k^{\text{batt}} + b_1 I_{k-1}^{\text{batt}} - a_1 V_{k-1}^{\text{op}}, \quad (2)$$

where the model parameters b_0 , b_1 and a_1 can be identified for different input-output data, i.e., a PCT or E-bike data. Subsequently, the model can be rewritten to a canonical state-space representation and the SoC dynamics can be added with an additional state. Then, the model can be used in combination with an EKF to perform SoC estimation.

4 Results

Using a PCT for parameter estimation is compared to using field-test data from the E-bike. In Fig. 1, the measured and estimated battery voltages are shown for two second-order models, a PCT-based model and a model based on the E-bike data. The estimated SoC and pseudo-measured SoC are shown in Fig. 2. It can be seen that the model based on the E-bike data yields more accurate estimation results.

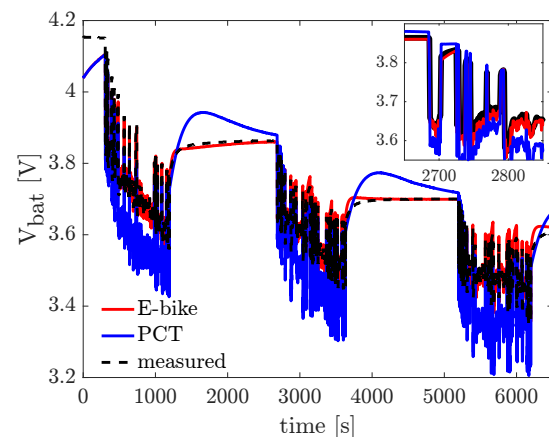


Figure 1: Measured and modelled battery voltage.

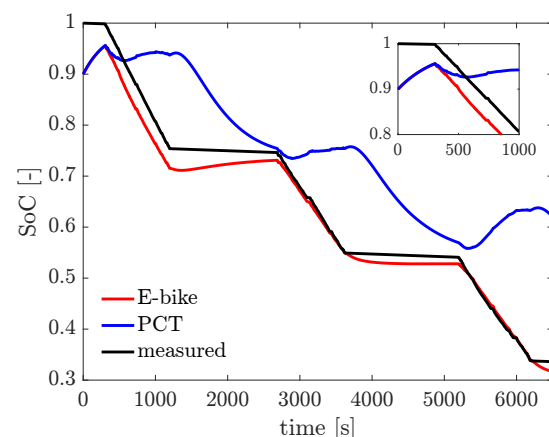


Figure 2: Measured and modelled battery SoC.

References

- [1] A. Klintberg et al., "Theoretical Bounds on the Accuracy of State and Parameter Estimation for Batteries," Proc. ACC 2017.
- [2] H.P.G.J. Beelen et al., "On Experiment Design for Parameter Estimation of Equivalent-Circuit Battery Models," *submitted*.

¹This work has received financial support under the grant 3Ccar.

A Study on Recurrent Deep Learning Methods for State of Charge Estimation in Lithium-Ion Batteries

E. Najafi F.G. Zanjani H.J. Bergveld M.C.F. Donkers

Department of Electrical Engineering
Eindhoven University of Technology, Netherlands

Emails: {e.najafi, f.ghazvinian.zanjani, h.j.bergveld, m.c.f.donkers}@tue.nl

1 Introduction

Lithium-ion (Li-ion) batteries are employed in various applications thanks to their high energy density and long service life. The Li-ion battery models can be broadly classified into two groups: equivalent circuit models and electrochemical models. The circuit models are relatively simple, but do not represent the physical phenomena inside the battery. The electrochemical models explain the internal physical behavior of the battery. For instance, the Doyle-Fuller-Newman model, which is a popular electrochemistry-based Li-ion battery model, represents solid-state and electrolyte diffusion dynamics and accurately predicts the current/voltage response. However, the mathematical structures of the electrochemical models are quite complex for observer design, such as state of charge (SoC) estimation. In this work, we study recurrent neural networks (RNNs), a family of artificial neural models, for SoC estimation in Li-ion batteries. The RNNs are able to capture dynamical behavior of the system by learning from the input-output data.

2 Recurrent Deep Learning Method

Artificial neural networks is a data-driven technique in machine learning that is used widely in several domains of data science as well as for sequential data modeling and analysis of time series signals. Recently, several studies investigated the possibility of applying different architectures of the neural networks for modeling and SoC estimation in Li-ion batteries [1, 2]. In this work, we design a deep recurrent neural network based on long short-term memory (LSTM) modules [3]. An LSTM network is well-suited to classify, process and predict time series given time lags of unknown size and duration between events. Relative insensitivity to gap length gives an advantage to LSTM over alternative RNNs. We investigate different network configurations with respect to the type of inputs-outputs and the impact of inputs length for SoC estimation. Figure 1 illustrates a sample structure of the studied recurrent neural networks with two inputs: current and voltage and one output: state of charge.

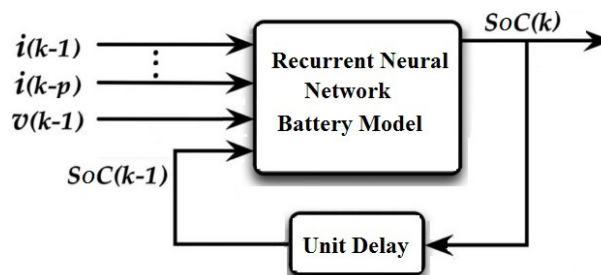


Figure 1: A sample structure of the recurrent neural network for state of charge estimation in the Li-ion batteries

3 Neural Network Implementation

We design an LSTM network with current and voltage as the inputs and SoC as the output. The state of charge equation is described by

$$SoC(k) = f(i(k-1), v(k-1), SoC(k-1)), \quad (1)$$

where f is a nonlinear function, $i(k-1)$, $v(k-1)$, and $SoC(k-1)$ are the current, voltage, and state of charge at time step $k-1$. The main goal of the deep learning network is to learn the nonlinear function f , which represents the relation between the inputs and outputs. However, the type of inputs as well as the length of inputs play an important role on the estimation accuracy. In this network, we study the impact of the current length, hence the battery currents in the last p steps are given as the network input.

References

- [1] S. Park, D. Zhang and S. Moura, "Hybrid electrochemical modeling with recurrent neural networks for Li-ion batteries", in Proceedings of the American Control Conference, Seattle, WA, 2017, pp. 3777-3782.
- [2] G. Capizzi, F. Bonanno and G. M. Tina, "Recurrent neural network-based modeling and simulation of lead-acid batteries charge-discharge", IEEE Transactions on Energy Conversion, vol. 26, no. 2, pp. 435-443, 2011.
- [3] S. Hochreiter and J. Schmidhuber, "Long short-term memory", Neural Computation, vol. 9, no. 8, pp. 1735-1780, 1997.

Similarity-Based Adaptive Complementary Filter for IMU Fusion

Alex Andriën, Duarte Antunes, René van de Molengraft, Maurice Heemels
 Department of Mechanical Engineering, Eindhoven University of Technology
 P.O. Box 513, 5600MB Eindhoven, The Netherlands
 Email: A.R.P.Andrien@tue.nl

1 Introduction

Estimating the attitude of a rigid body, based on sensor data from an Inertial Measurement Unit (IMU), is crucial in many applications and in particular in the context of Unmanned Aerial Vehicles (UAVs). The IMU consists of (three-axes) accelerometers, gyroscopes and magnetometers.

Measurements from the accelerometer and magnetometer can be combined to give an algebraic estimate of the attitude, under the assumptions of negligible body accelerations and magnetic disturbances. This vector estimate contains noise with a mainly high frequency content, caused by motor vibrations. By integrating the gyroscope measurements, another estimate can be derived, containing a low-frequency disturbance component caused by the integration process.

A common technique for attitude estimation is the complementary filter (CF), because it is easily tunable and has a simple form. It consists of low-passing the vector estimate and high-passing the gyroscope estimate with each filter having the same, stationary, break frequency, combining the strengths of both.

However, under high accelerations or magnetic disturbances, a CF with large gain ($\hat{\phi}_L$) will have distortions, whereas a CF with a small gain ($\hat{\phi}_S$) will suffer from the gyroscope bias. This is shown in Figure 2, at 25 and 40 seconds, respectively. Therefore, when using a stationary CF a trade-off has to be made between dynamic distortions or a long term bias.

2 Our Approach

In order to overcome the limitations of a stationary CF, we added a novel adaptation scheme to the filter proposed in [1], which is a stationary, nonlinear complementary filter implemented directly on the special orthogonal group. A linear representation of a CF with adaptation is shown in Figure 1. The adaptation is based on the following observation:

If the angular estimate achieved from integrating the gyroscope measurement is similar to the angular estimate determined from the accelerometer and magnetometer measurements over a time window, then the accelerometer and magnetometer measurements are not distorted.

In order to quantify the similarity between the angle vector and gyroscope measurement, a similarity measure is introduced. We also show convergence of the filter with this adaptive gain.

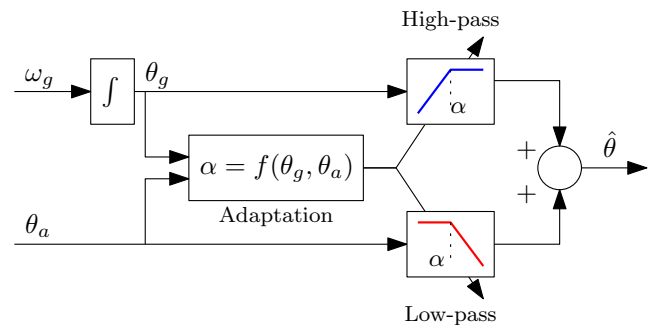


Figure 1: Linear adaptive complementary filter

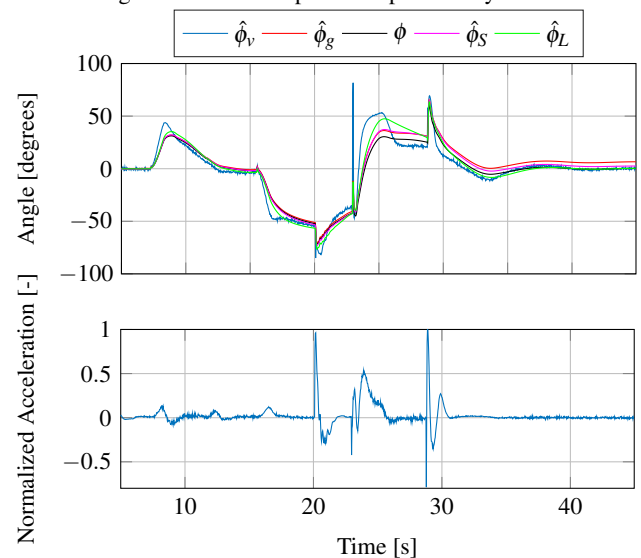


Figure 2: Motivation for adaptive gain strategy using a simulated quadcopter. (top) Typical angle estimates obtained using the vector $\hat{\phi}_v$ and gyroscope $\hat{\phi}_g$ measurements, together with the actual angle ϕ . (bottom) Normalized deviation from normal of acceleration, showing the connection between accelerations and deviations for the vector estimate.

3 Future Work

This work is currently being expanded to incorporate a machine-learning based adaptation scheme, which will use a similar convergence proof.

Acknowledgments

This research has been partially funded by the European Regional Development Fund (ERDF) as part of OPZuid 2014-2020.

References

- [1] R. Mahony, T. Hamel, and J. M. Pflimlin, "Nonlinear complementary filters on the special orthogonal group," *IEEE Transactions on Automatic Control*, vol. 53, no. 5, pp. 1203–1218, June 2008.

Modeling and control of pharmacokinetic models

Pauline Thémans^{*}, Flora T. Musuamba[†], and Joseph J. Winkin^{*}

^{*}Namur Institute for Complex Systems (naXys) and Department of Mathematics
University of Namur, rempart de la Vierge 8, B-5000 Namur, Belgium
Email: pauline.themans@unamur.be, joseph.winkin@unamur.be

[†]U850 INSERM, Faculté de Médecine et de Pharmacie
Université de Limoges, rue du docteur Raymond Marcland, 87025 Limoges Cédex, France
Email: flora.musuamba-tshinanu@unilim.fr

1 Introduction

Pharmacokinetics is a particular field of clinical pharmacology that studies the link between the dose and the (systemic) concentration time course of drugs. In our research, we aim to use control and system theory to develop a method for optimal (i.e. effective) dosing to ensure its applicability in clinical practice. Approaches for individualized drug dosing are suggested. We focus on treatments with repeated administration by intravenous infusion of a fixed dose. Meropenem, a beta-lactam antibiotic used in lung disease, is used as case drug.

2 Population modeling

In a previous work [2], a compartmental pharmacokinetic (PK) model was developed to describe the pharmacokinetic of the drug in patients with severe nosocomial pneumonia. A two-compartment model with an additional compartment for the site of effect (ELF) has provided an adequate fit of the data (consistent with [1]) and was internally and externally validated.

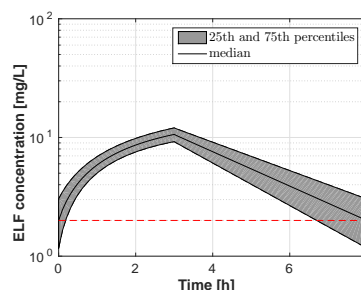
Based on this model, a reduced¹ *physiologically-based pharmacokinetic* (PBPK) model was developed to describe drug concentrations. It is built on physiological and anatomical considerations, and the model parameters include real volumes and blood flows. Such a model is intended to be used to extrapolate drug exposure in other groups of patients. Some of the model parameters will be modified/adapted for the purpose.

The PBPK model was both internally and externally validated with numerical and visual tools, including bootstrap procedures and visual predictive checks. External validation with data from other groups of patients such as neonates is ongoing.

3 Dosing adjustment

The developed models are used as starting point to design control strategies to achieve and maintain concentrations at target levels. The analytical asymptotic response is used

to derive a closed-form formula² designed to compute the dose, given the patient's characteristics and the target minimal concentration.



Meropenem is a time-dependent antibiotic, meaning that the pharmacodynamic parameter corresponds to the time over the MIC (minimal inhibitory concentration). To ensure a bactericidal efficacy, it is required to maintain meropenem concentration above the MIC for at least 40% of the dosing interval [1].

4 Outlook

The first objective of the developed PBPK model is to be used to extrapolate the dosing recommendations in other groups of patients such as children, neonates and pregnant women as well as in other indications. Typically, the main goal is to compute doses for populations for which PK data (i.e. clinical studies) are not available. The impact of the model adaptation on the results will be established.

Acknowledgement

This abstract presents research results of the Belgian Programme on Interuniversity Poles of Attraction, initiated by the Belgian state, the Prime Minister's office for Science, Technology and Culture. The scientific responsibility rests with its authors.

References

- [1] F. Fripiat, F. T. Musuamba, et al. Modelled target attainment after meropenem infusion in patients with severe nosocomial pneumonia: The PROMESSE study. *Journal of Antimicrobial Chemotherapy*, 70(1):207-216, Sep 2015.
- [2] P. Thémans, F. T. Musuamba, and J. Winkin. Modeling, analysis and control of pharmacokinetic systems: application to meropenem. *Submitted*

¹The developed model is made of six compartments.

²It can be easily generalized to a n -compartment model

Control and state estimation for MR-guided HIFU hyperthermia

Daniel Deenen, Bert Maljaars,
Bram de Jager, and Maurice Heemels
Control Systems Technology
Eindhoven University of Technology
P.O. Box 513, 5600 MB Eindhoven,
The Netherlands
Email: D.A.Deenen@tue.nl

Lukas Sebeke, Edwin Heijman*, Holger Gröll
University Clinic of Cologne
Kerpener Strasse 62, 50937 Cologne
*Philips Research Germany
*Philipsstrasse 8, 52068 Aachen
Germany

Introduction

Hyperthermia is an additive therapy that can enhance the effects of radiotherapy and chemotherapy in cancer treatments without increasing toxicity in healthy tissue [1]. Herein, the temperature in the tumor region is raised to 39-45 degrees Celcius for approximately 90 minutes. The target tissue is heated using radio-frequency (RF) or high intensity focused ultrasound (HIFU) applicators. Magnetic resonance thermometry (MRT) can provide on-line non-invasive measurements of the 3D temperature distribution.

In this project, we aim at developing estimation and control tools that enable achieving the desired 3D temperature distribution in the patient, even in the presence of patient- and time-varying tissue properties.

Control

Control over the 3D temperature distribution in the human body is essential to ensure treatment quality and avoid local hotspots in healthy tissue. As spatially distributed tissue properties are patient specific, and even vary in time between and during treatments, an advanced adaptive control approach is required.

A model predictive control (MPC) approach is chosen, due to the presence of critical temperature constraints in the patient's tissues and unilateral actuator constraints. Based on the present temperature state, the MPC controller uses a patient specific thermal model to compute a future actuator input sequence that realizes the desired target temperature while actuator and state constraints are satisfied. Our MPC implementation extends and improves previous work [2, 3].

State estimation

Accurate knowledge of the current temperature distribution is required in the model-based control algorithms developed in this project. Unfortunately, the MRT measurements suffer from significant measurement noise. Therefore, model-based state estimation is desired to reduce the propagation of measurement noise towards the controller. Herein, model predictions are systematically merged with measurements.

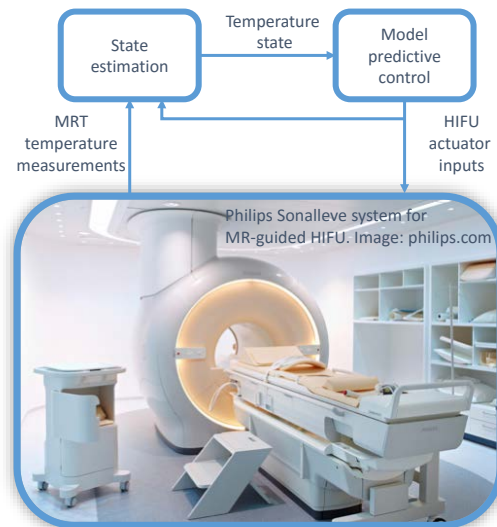


Figure 1: Illustration of state estimation and model predictive control in MR-guided HIFU.

Results and conclusions

The performance of the state estimation and control algorithms is evaluated in extensive simulation studies for MR-guided HIFU. We will also show preliminary experimental results obtained in phantom experiments on a Philips Sonalve system (see Figure 1) at the Uniklinik Köln. These results encourage further development of adaptive models and algorithms as well as more extensive experimental validation.

Acknowledgement

This research has been made possible by the Dutch Cancer Society and the Netherlands Organisation for Scientific Research (NWO) as part of their joint Partnership Programme: 'Technology for Oncology'. This project is partially financed by the PPP Allowance made available by Top Sector Life Sciences & Health.

References

- [1] N.R. Datta *et al.*, *Cancer Treat Rev.* 41(9): 742-53, 2015.
- [2] M. Tillander *et al.*, *Med Phys* 43 (3), 1539-1549. 3, 2016.
- [3] L. Sebeke *et al.*, *5th Int. Symp. on Focused Ultrasound*, North Bethesda, MD, USA, 2016.

Application of Digital Technologies in Proton Therapy Treatment: Fast Calibration

Zheming Wang*

zheming.wang@uclouvain.be

Quentin Flandroy†

Quentin.Flandroy@iba-group.com

Baptiste Herregods†

Baptiste.Herregods@iba-group.com

Raphaël M. Jungers*¹

raphael.jungers@uclouvain.be

*ICTEAM Institute, UCLouvain, Louvain-la-Neuve, Belgium

† IBA, Louvain-la-Neuve, Belgium

Introduction

We introduce the One-click Calibration project within the BiDMed project (application of Big Data digital technologies in the Med-Tech context), which aims to reduce the costs and improve the performance of proton therapy. The BiDMed project includes three work packages associated to the equipment lifecycle. In this project, we aim to improve the equipment installation process by integrating automated machine learning technologies into the beam calibration procedures.

1 Proton Therapy

Proton therapy uses a beam of protons irradiate the diseased tissues. It is an attractive cancer treatment modality for its precision and low overall toxicity as opposed to the conventional X-ray radiotherapy. Recently, a compact proton therapy technology, called Proteus[®]ONE, has been developed by IBA, world leader in proton therapy. Figure 1 shows the configuration of Proteus[®]ONE, which consists of a static and dynamic part. The static part is called the extraction beam line. The dynamic part is a rotating structure with an excursion angle of 220° and is also called the compact gantry. The gantry is equipped with energy selection and beam transport elements.

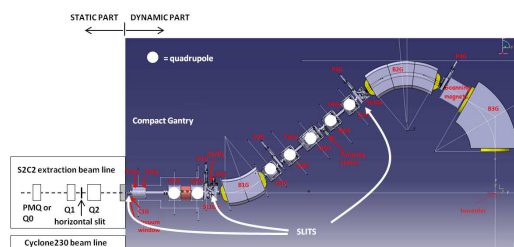


Figure 1: Proteus[®]ONE Configuration

2 Problem Formulation: Beam Line Calibration

The goal of calibration is to tune the parameters of the elements in the beam line in order to produce the proton beam

¹Raphaël M. Jungers is a FNRS Research Associate. He is supported by the French Community of Belgium, the Walloon Region and the Innoviris Foundation.

with desired characteristics. By manipulating the parameters, we aim to steer the beam distribution to some targeted distribution with certain constraints. The main issue is that there is no accurate physical model of the beam line, although the proton trajectory can be described by physical dynamical equations [1].

3 Controlling a Time-Evolving Distribution

To control the beam distribution, one has to solve a multi-input/multi-output problem where the state is a multivariate probability distribution that undergoes several nonlinear transformations. In [2], the behaviour of the beam in a magnetic element is approximately reduced to a process of matrix multiplication. An example of a pair of focusing quadrupoles is given below. The input beam distribution is a truncated gaussian and is given in Figure 2(a)(only the histogram in X-axis is given). By manipulating the currents, the focusing output beam distribution, a narrowed truncated gaussian, can be obtained as shown in Figure 2(b). However, this approximated model may lead to calibration error. To minimize the calibration error, a data-driven calibration procedure should be established to combine physical data and the information from some approximated physical models.

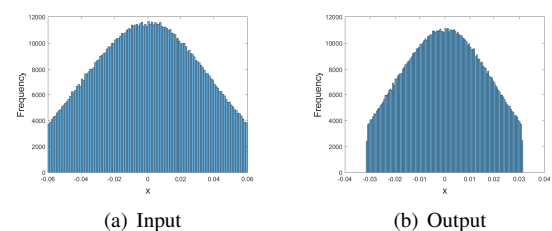


Figure 2: Beam Distributions

References

- [1] M. Reiser. *Theory and design of charged particle beams*. John Wiley & Sons, 2008.
- [2] K. L. Brown, F. Rothacker, D. C. Carey, and F. C. Iselin. TRANSPORT: a computer program for designing charged-particle beam-transport systems. CERN-80-04, 1980.

EEG classification based on inductive means

E. M. Massart¹, S. Chevallier², J. M. Hendrickx¹, P.-A. Absil¹

¹ ICTEAM Institute, Université catholique de Louvain, B-1348 Louvain-la-Neuve, Belgium.

² LISV, Université de Versailles Saint-Quentin, France.

estelle.massart@uclouvain.be

1 Introduction

We propose a set of variants of classification algorithms for EEG signals, an important task for the development of brain computer interfaces (BCI). In our approach, temporal frames of the EEG are represented as covariance matrices, which turns the problem into a classification problem on the manifold of symmetric positive definite (SPD) matrices.

BCI are very promising tools to enable physically disabled people to control a large variety of devices, such as wheelchairs, exoskeletons, and robotic arms. Those interfaces record and analyze brain signals, and translate them into control commands. We consider here interfaces based on EEG signals, which result in non-invasive, wearable, and low-cost systems. However, analyzing and decoding EEG signals is difficult, due to the important noise and the large variability of the signal. The latter can indeed highly vary from hour to hour for a subject, and is highly variable from one subject to another. Consequently, the problem of EEG classification (i.e., determining the intention of the subject based on his EEG) is particularly challenging.

In [1], the EEG, represented by a sequence of covariance matrices, is classified using the minimum distance to mean (MDM) classifier that rely on a definition for the mean of a set of SPD matrices and for the distance between two SPD matrices. We propose to equip this classifier with a family of means, based on the inductive mean, which enables us to produce an incremental learning algorithm for online classification of EEG, to cope with the significant hour-to-hour variability of the signals. This might also allow to reduce calibration time, by classifying the first covariance matrices using a generic classifier (calibrated on a set of typical subjects) and adapting it progressively, to become user-specific.

2 Experimental setup

We consider here a BCI relying on steady-state visual evoked potentials (SSVEP), that is, brain responses to visual stimuli. A subject is looking at a screen, on which there might be a stimulus blinking at some frequency (13Hz, 17 Hz or 21 Hz), or no stimulus at all. The blinking stimulus will elicit the appearance of waves with the same frequency in the EEG. The goal is to detect those waves, to determine at each time instant which frequency has the visual stimulus.

3 The MDM classifier

Let C be a covariance matrix representing a temporal frame

of the EEG. The MDM classifier assigns C to the class k^* , such that

$$k^* = \operatorname{argmin}_{k \in \{1, \dots, n_{cl}\}} \delta(\Sigma_k, C),$$

where n_{cl} is the number of classes (here, equal to four: three frequencies and a resting state), $\delta(A, B)$ is a distance function between A and B , and Σ_k is the mean of the covariance matrices assigned to class k . In [1], several means definitions (and associated distance functions) are considered, e.g., the Euclidean and LogEuclidean means, the Riemannian barycenter with respect to the classical affine-invariant metric, and means based on matrix divergences.

We equip the MDM classifier with the inductive mean, obtained by computing a succession of geodesics. The inductive mean X_N of a set of N SPD matrices A_i , $i = 1, \dots, N$, is obtained by defining $X_1 = A_1$, and $X_i = X_{i-1} \#_{1/i} A_i$, for $i = 2, \dots, N$, where $A \#_t B := A^{1/2} (A^{-1/2} B A^{-1/2})^t A^{1/2}$, with $t \in [0, 1]$, is the geodesic between A and B , evaluated at time t . We also consider the variants of the inductive mean provided in [2]. The distance function $\delta(A, B)$ used in the MDM classifier is the classical affine-invariant distance (see [3] for more information).

Endowing the MDM classifier with the inductive mean provides competitive results with respect to the other means considered, regarding the computation time vs classification accuracy criterion. In the online setting, we trained the classifier on the data of some subjects, and used it then on a new subject, adapting the classifier as new data of the subject considered are available. For some subjects, we observe a progressive improvement of the classification with time, while not for others, which seems to be due to the instability of the adaptation process. We plan to investigate other online adaptation algorithm in the future.

References

- [1] E. Kalunga et al, "From Euclidean to Riemannian Means: Information Geometry for SSVEP Classification", GSI 2015.
- [2] E. M. Massart et al, "Matrix geometric means based on shuffled inductive sequences." Linear Algebra and its Applications, 2017.
- [3] E. M. Massart, S. Chevallier, "Inductive means and sequences applied to online classification of EEG", GSI 2017.

This work was supported by the Fonds de la Recherche Scientifique – FNRS and the Fonds Wetenschappelijk Onderzoek – Vlaanderen under EOS Project no 30468160.

Quench Detection for the Cooling System of a Particle Accelerator for Proton therapy

Boris Dehem*, Nam-Luc Tran[†], François Glineur*

{*UCLouvain/ICTEAM/INMA, [†]IBA group}, B-1348 Louvain-la-Neuve, Belgium

{boris.dehem, francois.glineur}@uclouvain.be, nam-luc.tran@iba-group.com

1 Problem Formulation

Proton therapy is an alternative to radiotherapy where a beam of protons is applied to a tumor instead of X-rays. It has the advantage of subjecting tissue surrounding the target zone to less radiation than radiotherapy, and so causing less severe side effects and being usable near critical organs and on young children.

To create a magnetic field strong enough to accelerate protons, proton therapy machines use a superconducting electromagnetic coil. To remain superconductive, the coil has to stay at very low temperatures (around 4K). A magnet *quench* happens when the coil's temperature rises above the point where it goes from its superconductive to its resistive state. This then causes a large emission of heat as the current in the coil is suddenly pushed through some nonzero electrical resistance. Quenches are quite harmful, as after they happen, the system has to be cooled for approximately 24 hours. Operations programmed during this time must be rescheduled or replaced by conventional radiotherapy, which can have harmful effects.

Quenches can have many causes, such as too low or too high pressure of the cooling liquid, a defective auxiliary cooling system, human error, displacement of the coil's cables, degradation of the cold heads, etc. Our goal is to create a warning system that announces when quenches are likely to happen in the near future, and sends a warning to human operators so that they may undertake any actions necessary to prevent them.

2 Data and Approach

Data signals are available to try to extract trends that would show an upcoming quench. Our data comes from an actual proton therapy center built by IBA, and consists of temperature measurements taken at 8 different physical locations within the machine over one year, with a time resolution of one minute.

We chose a classification approach: we group every temperature measurement over 90 consecutive minutes, and create such an instance starting every 15 minutes. An instance is considered positive if a quench happened in the next 90 minutes after its end, and negative if not. As a result, we have 249 positive and 35674 negative instances.

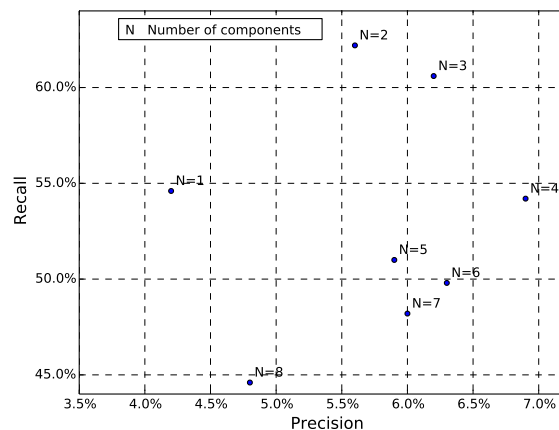


Figure 1: Comparison of classification performance with different numbers of principal components

3 Classification Results

We first report preliminary results for logistic regression. To counteract the fact that the classes are heavily unbalanced, we weigh the classes so that the total weight of each class is constant. We use precision and recall as performance metrics, and obtain a recall of 44.6% and a relatively low precision of 4.8%.

We are able to improve the results by reducing the data's dimensionality with PCA. We find that three components are enough to capture 99.95% of the variance of the 8 temperature signals (this was expected, because six of the temperature sensors are immersed in the cooling liquid). Figure 1 shows that this reduction also significantly improves the results, with a recall of 60.6% and a precision of 6.2% when using 3 principal components.

4 Future Work

We will incorporate electrical current and tension measurements when they become available, as these should allow us to infer the usage state of the system and hopefully improve the prediction. We also plan to introduce an economic model describing the effect of both false and undetected positives, in order to better understand the tradeoff between precision and recall. We also plan to use to apply other structure-exploiting dimensionality reduction techniques.

Acknowledgements This work is supported by the Walloon Region (BiDMed project, BioWin pole).

Composable Skill Programming Framework for Complex Sensor-Based Robot Tasks

Yudha P. Pane, Wilm Decré and Joris De Schutter
 Division PMA, Dept. Mechanical Engineering, KU Leuven ¹
 Celestijnenlaan 300, 3001 Heverlee, Belgium
 Email: yudha.pane@kuleuven.be

1 Introduction

Advancement in control algorithms and sensor technology, in addition to increasing computational power, have enabled robots to perform complex tasks such as force-based assembly. However, programming the skills to execute such tasks is still tedious and requires considerable robotics knowledge. Furthermore, the skills' implementations are typically ad-hoc and do not adhere to a certain framework, thus preventing them from being reusable. This research aims to alleviate this problem by proposing a framework for programming complex robot skills. It enables robot skill programmers to design a new composite skill from existing, proven sub-skills.

In designing the framework, we favor a bottom-up approach starting from existing skills previously developed and tested at KU Leuven Robotics Group. The patterns shared across different skills are analyzed and the common software components/entities are extracted. The description of these components is addressed in Section 2. A motivating example of an assembly task of industrial parts is provided in Section 3.

2 The Skill Pattern

We define composite skill as a coordinated sequence of smaller sub-skills. The smallest granularity, called atomic skill, is a continuous-time task specification implemented as a constrained optimization problem (set of constraints and objective) in eTaSL/eTC libraries [1]. For instance, move joint space or move cartesian space is considered an atomic skill. The framework extends the 5C's composition pattern proposed in [2]. A composite skill comprises the following entities:

- **Sub-skills:** A composite skill consists of multiple smaller sub-skills. For example, an `insert_object` skill may contain `move_cartesian`, `move_guarded` and `insert_with_force` sub-skills.
- **Composer:** The composer deploys and initializes the necessary components for a composite skill to run.

¹The PMA Robotics Research Group is a university core lab of Flanders Make. This work was supported by the Flanders Make ICON FINROP (Fast and Intuitive Robot Programming) project.

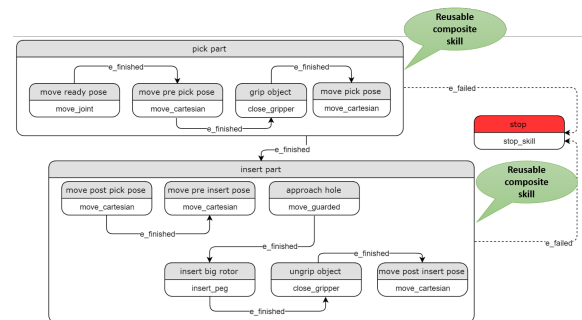


Figure 1: An example sequence of skills used for assembling a part.

For instance, a contour following skill might require a filtering component for state estimation.

- **Scheduler:** The scheduler is an event-based finite state machine (FSM) that regulates the activity of the sub-skills. It manages which skills should be active at a given time.
- **Coordinator:** The coordinator regulates the life cycle of a composite skill. The life cycle is a five-state FSM as described in [2].
- **Configurator:** The configurator provides read and write access to the parameters a skill contains. For instance, `move_cartesian`'s parameters include its speed, acceleration and target pose.

3 Use-Case: Assembly of compressor parts

Figure 1 shows the FSM for assembly of a compressor part. Note that two composite skills `pick part` and `insert part` comprise a number of atomic skills. Furthermore, thanks to the common interface, they can be further reused to compose a more complex skill.

References

- [1] E. Aertbeliën and J. De Schutter, "eTaSL/eTC: A constraint-based Task Specification Language and Robot Controller using Expression Graphs," IROS, 2014.
- [2] D. Vanthienen, M. Klotzbücher and H. Bruyninckx, "The 5C-based architectural Composition Pattern: lessons learned from re-developing the iTaSC framework for constraint-based robot programming," JOSER, 2014.

Modelling and Control of Soft Robot Manipulators

B.J. Caasenbrood, H. Nijmeijer, and A.Y. Pogromsky

Dynamics and Control Group, Department of Mechanical Engineering

Eindhoven University of Technology, P.O. Box 513, 5600 MB Eindhoven, The Netherlands

email: b.j.caasenbrood@tue.nl

1 Introduction

Due to the rigidity that is inherent in traditional robotics, researchers explore the possibility of implementing soft materials in robotics; this branch of robotics is referred to as 'soft robotics.' Soft robots exhibit continuum body motion, large spatial displacements, and they offer high compliance concerning traditional robots. Although the advantage of soft robots is their softness and compliance, the inherent flexibility complicates the development of accurate dynamical models. Moreover, soft robots are highly non-linear systems, and the sensitivity of the hyper-elastic material can easily cause a change in the dynamics of the system. In this work, we present a generalized approach to model and control a soft robot manipulator as shown in Fig 1. We advance the area of soft robotics by exploiting the passivity of soft robotics with the intent of accurate and robust control.

2 Method

We considered a continuum-bodied soft robot manipulator capable of spatial movement in three-dimensional space. Similar to the maneuverability of elephant trunks, the flexible manipulator can vary its length and curvature. The system is described by the generalized coordinate vector as

$$q(t) = [l(t) \quad k_x(t) \quad k_y(t)]^T, \quad (1)$$

where length of the soft robot is denoted as $l(t)$, and the curvatures in $x-z$ plane and $y-z$ plane are denoted respectively as $k_x(t), k_y(t)$. To represent the manipulator's deformation, we introduce a spatial curve (i.e., the backbone curve) passing through the geometric center of the cross-sections. Let $s \in \mathbb{R}_+$ be a point on the backbone curve, such that it satisfies $s = [0, l(t)]$, and let $p(s, t)$ be the mapping of $\mathbb{R}_+ \times \mathbb{R}_+$ into \mathbb{R}^3 , that is,

$$p(s, t) : \mathbb{R}_+ \times \mathbb{R}_+ \mapsto \mathbb{R}^3. \quad (2)$$

Consequently, the set $\{p(s, t) \in \mathbb{R}^3 \mid s \in \mathbb{R}_+\}$ draws a spatial curve at any given time t . An accurate approximation of the flexible hyper-redundant robot can be obtained by discretizing continuous models resulting in multiple slices. Every slice at each point s is linked to individual mass, moment of inertia, and stiffness properties. It shall be clear that the mechanical behavior of hyper-elastic materials plays a crucial role in the development of soft robot models. Thus, finite element methodologies (FEM) are employed to obtain mathematical relations for the non-linear stiffnesses of the system



Figure 1: Elephant-inspired soft robot manipulator made from flexible material. Video: <https://goo.gl/bJJJvu>

imposed by both the hyper-elasticity and geometry. The potential and kinetic energy of the total system can be acquired by summations of each contribution from the slices. From the Euler-Lagrange formalism, the dynamics can be compactly written as

$$D(q)\ddot{q} + C(\dot{q}, q)\dot{q} + N(q) = \tau(t), \quad (3)$$

where $D(q)$, $C(\dot{q}, q)$, and $N(q)$ are nonlinear system matrices. The true values of these of physical parameters can be difficult to obtain due to material impurity, and design imperfection; therefore, only the estimates of the true system $\hat{D}(q)$, $\hat{C}(\dot{q}, q)$, and $\hat{N}(q)$ can be acquired. Passivity-based adaptive control is a control method that exploits the passivity of systems to ensure stability and robustness in the face of parameter uncertainty. Let $\hat{p}(t)$ be the time-varying parameter estimation vector. As proposed by [1], the passivity-based adaptive control approach is synthesized as

$$\tau = \hat{D}(q)\dot{q}_r + \hat{C}(\dot{q}, q)\dot{q}_r + \hat{N}(q) - K_p e - K_d e_r, \quad (4)$$

$$\dot{\hat{p}} = -\Gamma Y^T e_r, \quad (5)$$

where $q_d(t)$ is a smooth trajectory vector, $\dot{q}_r = \dot{q}_d - \Lambda e$ the reference velocity vector, $e_r = \dot{q} - \dot{q}_r$, $e_r(t)$ the reference velocity error, $Y(\cdot)$ the regressor matrix, and $\Lambda, \Gamma, K_p, K_d$ are positive definite matrices.

3 Result and Future Work

Numerical simulations showed that passivity-based control achieves good performance, and future work involves implementation of the control scheme into real systems.

References

- [1] J. J. E. Slotine and L. Weiping, Adaptive manipulator control: A case study, IEEE Trans. Automat. Contr., vol. 33, no. 11, pp. 995-1003, 1988.

Development and implementation of a reconfigurable assembly cell

Maarten Verbandt, Ruben Van Parys, Marcus Kotzé, Jan Swevers, Johan Philips and Goele Pipeleers
 MECO Research Team, Department Mechanical Engineering, KU Leuven
 DMMS lab, Flanders Make, Leuven, Belgium
 maarten.verbandt@kuleuven.be

1 Introduction

As product diversity increases and new designs succeed one another more rapidly than ever before, the value of reconfigurable manufacturing systems (RMSs) cannot be denied. Though the idea of RMSs exists already for a very long time [1], few of such systems have actually been developed. This abstract addresses the development and deployment of such a system, paying special attention to the key aspects of RMSs: modularity, scalability and integrability. The developed RMS, presented in Figure 1, consists of two AGVs collecting orders at the movable work stations. A modular ceiling camera system posts position measurements on the network, allowing the AGVs to plan their path and dock near the right work station. On top of this, a central coordinator gathers tasks and dispatches them to the appropriate agent. The next sections briefly describe the different subsystems.

2 Central coordinator

The central coordinator's responsibility is to dispatch tasks to the different agents within the system. When a new task enters the system, the coordinator splits it in several sub-tasks, e.g. a pick-and-drop task intended for a work station and a move-to task for an AGV. Rather than dispatching tasks based on central intelligence, a bidding system is installed to optimize the overall performance of the system. For instance, when a work piece is to be collected at one of the work stations, a bidding request is sent to all AGVs. All AGVs respond with an actual bid which reflects the estimated required effort for the task. The lowest bid is granted the task. This task dispatching strategy offers two advantages. The dispatching is independent of the number of agents within the system, implying scalability. Moreover different types of AGVs are integrated seamlessly provided they have the same notion of effort (integrability).

3 Transportation

Many production lines rely on a classic conveyer belt whereas more involved transportation systems are based on AGVs following predefined routes. Since these solutions are both restricting the overall flexibility, free motion planning becomes a requirement. The implemented motion planning algorithm is based on the approach of [2]. This method parametrizes the motion as a spline and computes its coefficients to obtain a time-optimal and collision-free path

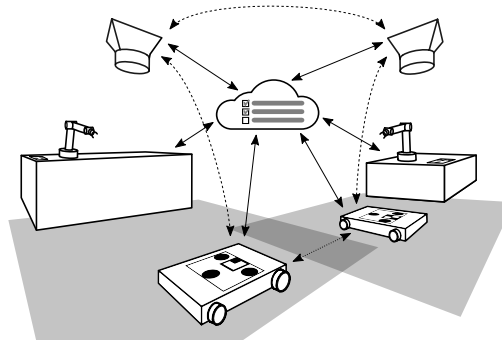


Figure 1: Overview of the developed RMS.

towards the target position. Since multiple AGVs are now sharing the workspace, anti-collision between the different AGVs should also be enforced. This is achieved in a decentralized way by prioritizing vehicles depending on their current motion: AGVs with lower priority actively avoid AGVs with higher priority. This approach ensures the modularity of the system as AGVs can enter or leave the system at will.

4 Vision-based localisation

Within a reconfigurable manufacturing environment, monitoring is a vital aspect. Due to their high information density and low cost, cameras hooked to a small single-board computer, are opted for. A marker which is detected by the smart cameras is installed on all AGVs and work stations. By calibrating all cameras w.r.t. the same world coordinate frame, they form a decentralized localization system in which each agent is capable of providing global position information. The latter again implies modularity and scalability as more cameras are easily added to or removed from the network.

References

- [1] Y. Koren, U. Heisel, F. Jovane, T. Moriwaki, G. Pritschow, G. Ulsoy, and H. Van Brussel. Reconfigurable manufacturing systems. *CIRP Annals - Manufacturing Technology*, 48(2):527–540, 1999.
- [2] R. Van Parys and G. Pipeleers. Distributed model predictive formation control with inter-vehicle collision avoidance. In *Proceedings of the 11th Asian Control Conference*, December 2017.

Acknowledgement. This work has been carried out within the framework of projects Flanders Make SBO ROCSIS: Robust and Optimal Control of Systems of Interacting Subsystems and KU Leuven-BOF PFV/10/002 Centre of Excellence: Optimization in Engineering (OPTEC). This work also benefits from projects G.0915.14 and G0C4515N of the Research Foundation - Flanders (FWO - Flanders) and KUL-C1: KU Leuven Research project C14/15/067: B-spline based certificates of positivity with applications in engineering. Ruben Van Parys is a PhD fellow of FWO-Flanders. Flanders Make is the Flemish strategic research centre for the manufacturing industry.

A Variable Stiffness Joint with Variable Stiffness Springs

R. Carloni
University of Groningen
The Netherlands
Email: r.carloni@rug.nl

V.I. Lapp, A. Cremonese
University of Twente
The Netherlands

J. Belcari, A. Zucchelli
University of Bologna
Italy

1 Introduction

Variable stiffness actuators are a class of actuation systems that embeds tunable physical compliance in the mechanical structure, making them the key enabling technology for robots that physically interact with an unknown dynamic environment or humans [1]. Benefits for using mechanical stiffness over active stiffness on this type of robots are energy efficiency, robustness, and safety.

2 The variable stiffness joint

This work presents a novel rotational variable stiffness joint that relies on one motor and a set of variable stiffness springs, as sketched in Figure 1 and presented in [2]. The variable stiffness springs are leaf springs with a layered design, i.e., an electro-active layer of electrospun aligned nanofibers of poly(vinylidene fluoride-trifluoroethylene-chlorotrifluoroethylene) surrounded by two electrodes of aluminum and held together by inactive material. To achieve a variable stiffness, different voltages and, therefore, different electric fields, are applied to the springs.

3 Electromechanical characterization of the variable stiffness springs

The variable stiffness springs have been electromechanically characterized. More specifically, in the voltage-deflection characterization, different voltage signals are applied to the PVDF-based spring sample and the resulting deflection is measured. This is done to find the relationship between the applied electric field and the developed strain and, thus, to model the sample's dynamic behavior. It was noted that the bending response is not proportional to the voltage level but approximately proportional to the square of the applied electrical field. This quadratic relationship between electric field and strain suggests that the active material can be considered as electrostrictive. Moreover, the samples exhibit creep behavior, which means that the material continues to bend after the voltage has reached a steady level.

In the force-deflection characterization, different displacements are imposed on the PVDF-based spring sample and the resulting force is measured at different voltages. This is done to find the force-deflection curves at different voltages, showing different stiffness characteristics and, therefore, variation of the stiffness. It was noted that the higher

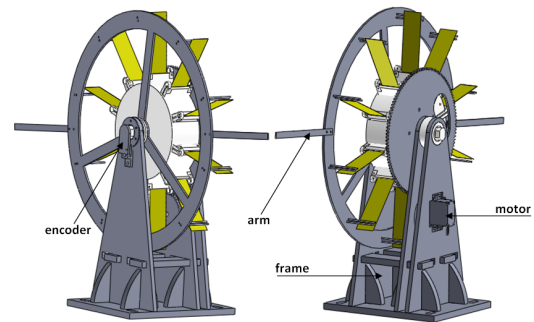


Figure 1: The variable stiffness joint (front and back views).

the applied voltage is, the higher the generative forces are for a certain imposed deflection. This means that the samples get stiffer as the electric field increases.

4 Experiments

Figure 2 shows the torque-deflection curve of the VSJ prototype when different voltages are applied to the samples and when the deflections are limited between 0° and $4^\circ \approx 0.07\text{rad}$. The experimental tests show that, thanks to the variable stiffness springs, the VSJ has increasing output stiffnesses when higher voltages are applied

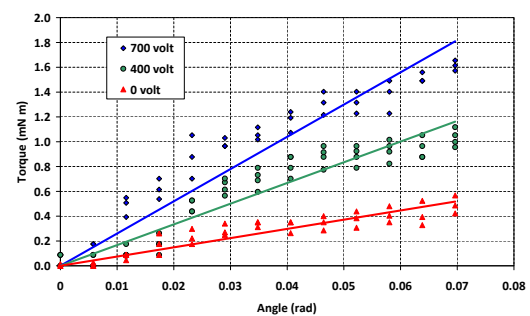


Figure 2: Torque response of the VSJ prototype for different voltages for deflections between 0° and $4^\circ \approx 0.07\text{rad}$.

References

- [1] B. Vanderborcht et al., "Variable impedance actuators: A review," Robotics and Autonomous Systems, Elsevier, 2013.
- [2] R. Carloni et al., "A Variable Stiffness Joint with Electrospun P(VDF-TrFE-CTFE) Variable Stiffness Springs," IEEE Robotics and Automation Letters, 2018.

A Supervisory Control And Data Acquisition (SCADA) system in agriculture and related path planning problems.

Nicolas Bono Rossello, Emanuele Garone
 Department of Control Engineering and System Analysis
 Universite libre de Bruxelles
 50, av. F.D. Roosevelt, CP 165/55
 1050 Bruxelles Belgique
 nbonoros@ulb.ac.be, egarone@ulb.ac.be

Andrea Gasparri, Renzo Carpio
 Department of Engineering
 Roma Tre University
 Via della Vasca Navale, 79
 00146, Roma, Italy
 gasparri@dia.uniroma3.it

1 Introduction

Agriculture has commonly been pioneer in the use of new technologies to improve productivity. This contribution aims at presenting some of the research activities withing the H2020 project PANTHEON. This project is to develop the agricultural equivalent of an industrial Supervisory Control And Data Acquisition (SCADA) system to be used for the precision farming of orchards. By taking advantage of the technological advancements in the fields of control, robotics, remote sensing, and big-data management, our objective is to design an integrated system where a relatively limited number of heterogeneous unmanned robotic components (including terrestrial and aerial robots) move within the orchard to collect data and perform typical farming operations. The information will be collected and stored in a central operative unit that will integrate the data coming from the different robotic (ground and aerial) vehicles to perform automatic feedback actions (e.g. to regulate the irrigation system) and to support the decisions of the agronomists and farmers in charge of the orchard. Figure 1 illustrates the foreseen concept.

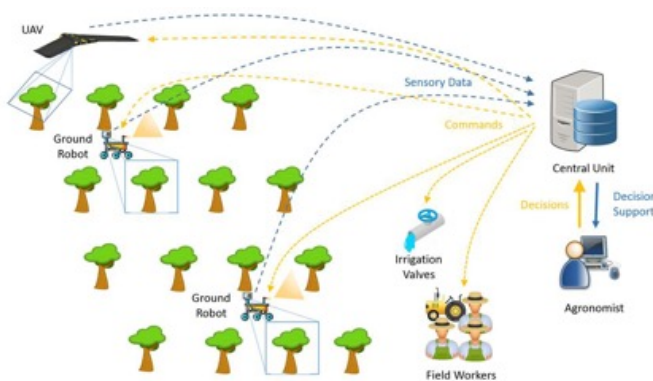


Figure 1: Idea of the SCADA system for agriculture.

We expect that the proposed SCADA system will be able to acquire information at the resolution of the single plant. This will permit to drastically increase the detection of possible limiting factors for each individual plant, such as lack of nutrients or pests and diseases affecting the plant health,

and to react accordingly. Compared to the current state of the art in precision farming, we believe that the proposed SCADA infrastructure represents a relevant step ahead in the context of orchards management and maintenance. In fact, the capability of monitoring the state and the evolution of each single tree will be the enabling-technology to allow more focused interventions. This will result in a better average state of health of the orchard and in an increased effectiveness of Integrated Pest Managements. In conclusion, the proposed architecture has the potential to increase the production of the orchard while, at the same time, being more cost-effective and environmentally-friendly.

2 Optimal trajectory planning

Beside the technology to be developed, several research actions are necessary for the development of a working system. In this talk we will overview some of our research activities concerning path and mission planning for the ground and aerial robots. The main challenge is to determine which are the optimal trajectories[1] to be followed to collect a sufficient amount of data to evaluate the state of each plant.

Acknowledgement

Pantheon project is supported by European Union's Horizon 2020 research and innovation programme under grant agreement no 774571.

References

- [1] Garone, Emanuele, Jean-Francois Determe, and Roberto Naldi. "Generalized traveling salesman problem for carrier-vehicle systems." *AIAA Journal of Guidance, Control, and Dynamics* 37.3 (2014): 766-774.

Projected-Gradient methods for Generalized Equilibrium Seeking in Aggregative Games are Preconditioned Forward-Backward Splitting

Giuseppe Belgioioso
Eindhoven University of Technology
Email: g.belgioioso@tue.nl

Sergio Grammatico
Delft University of Technology
Email: s.grammatico@tudelft.nl

Abstract

We show that projected-gradient methods for the distributed computation of generalized Nash equilibria in aggregative games are preconditioned forward-backward splitting methods applied to the KKT operator of the game. Specifically, we adopt the preconditioned forward-backward design, recently conceived by Yi and Pavel in the manuscript “A distributed primal-dual algorithm for computation of generalized Nash equilibria with shared affine coupling constraints via operator splitting methods” for generalized Nash equilibrium seeking in aggregative games. Consequently, we notice that two projected gradient methods recently proposed in the literature are preconditioned forward-backward methods. More generally, we provide a unifying operator-theoretic ground to design projected-gradient methods for equilibrium seeking in aggregative games.

1 Generalized aggregative games

Aggregative game theory is a mathematical framework to model the interdependent optimal decision making problems for a set of noncooperative agents, or players, whenever the decision of each agent is affected by some aggregate effect of all the agents. This feature emerges in several application areas, such as demand side management in the smart grid, e.g. for electric vehicles and thermostatically controlled loads, demand response in competitive markets and network congestion control.

Existence and uniqueness of Nash equilibria in (aggregative) noncooperative games is well established in the literature. For the computation of a game equilibrium, several algorithms are available, with both distributed protocols and semi-decentralized schemes. Overall, the available methods can ensure global convergence to an equilibrium if the coupling among the cost functions of the agents is “well behaved”, e.g. if the problem data are convex and the so-called pseudo-gradient game mapping is (strictly, strongly) monotone.

2 Projected-Gradient Algorithms

A popular class of algorithms for Nash equilibrium seeking is that of projected-gradient algorithms. Whenever the pseudo-gradient game mapping is strongly monotone, projected-gradient algorithms can ensure fast convergence

to a Nash equilibrium, possibly via distributed computation and information exchange. It follows that projected-gradient methods have the potential to be fast, simple and scalable with respect to the population size. At the same time, in the context of Nash equilibrium seeking, the convergence analyses for the available projected-gradient methods are quite diverse in nature.

3 Operator theory: a unifying framework

In this paper, we aim at a unifying convergence analysis for projected-gradient algorithms that are adopted for the computation of generalized Nash equilibria in aggregative games. Specifically, we adopt a general perspective based on monotone operator theory [1] to show that projected-gradient algorithms with sequential updates belong the class of preconditioned forward-backward splitting methods.

The main technical contribution of the paper is to conceive a design procedure for the preconditioned forward-backward splitting method. Since the convergence characterization of the forward-backward splitting method is well established, the advantage of the proposed design is that global convergence follows provided that some mild monotonicity assumptions on the problem data are satisfied.

Remarkably, we discover that two recent projected-gradient algorithms for Nash equilibrium seeking in aggregative games, [2] and [3], can be equivalently written as preconditioned forward-backward splitting methods with symmetric implementation matrix, despite their algorithmic formulation is “asymmetric”.

References

- [1] H. H. Bauschke and P. L. Combettes, *Convex analysis and monotone operator theory in Hilbert spaces*. Springer, 2011.
- [2] D. Paccagnan, B. Gentile, F. Parise, M. Kamgarpour, and J. Lygeros, “Distributed computation of generalized Nash equilibria in quadratic aggregative games with affine coupling constraints, in *Proc. of the IEEE Conf. on Decision and Control, Las Vegas, USA, 2016*.”
- [3] J. Koshal, A. Nedic, and U. Shanbhag, “Distributed algorithms for aggregative games on graphs, *Operations Research*, vol. 64, no. 3, pp. 680704, 2016.”

Performance comparison of routing strategies for automated guided vehicles

Veronika Mazulina, Alexander Pogromsky, Henk Nijmeijer
 Dept. of Mechanical Engineering
 Eindhoven University of Technology
 The Netherlands

Email: v.mazulina@tue.nl, a.pogromski@tue.nl, h.nijmeijer@tue.nl

Automated guided vehicles (AGVs) are widely employed as a part of material handling system (MHS) for transporting items between workstations in manufacturing systems and warehouses or for transfer of cargo on container terminals. Their main benefits in comparison with manned ones are lower long-term costs and higher operation efficiency.

The chosen routing method has a great impact on the efficiency of the operating system. The goal of our study is to perform a numerical comparison of the fixed-path strategy, which represents a route between key locations as a zones sequence, and free-range routing, when vehicle can choose any possible path between its current position and a target.

As all tasks should be done in a limited time, an applied motion strategy should prevent the deadlocks and collisions of AGVs. Otherwise, all working processes may stall, that could lead to large financial losses. Especially often these problems occur in a dense environment (with a large number of vehicles in a limited space). Moreover, the employed method should provide the better utilization of the workspace and satisfy the scalability condition, i.e. to perform well with increasing number of workstations or vehicles.

The free-range routing guarantees the motion along the shorter path than the fixed strategy. Therefore, it is suitable when vehicles drive over a large area. However, this strategy significantly reduces the vehicles speed in crowded regions. To deal with mentioned drawback the AGVs system requires traffic rules, similar to those imposed in the guided-path method.

To increase the performance of a MHS it is necessary to improve the efficiency of the AGVs. It can be achieved by developing a mixed routing strategy, which will combine the benefits of the above-mentioned approaches and eliminates their disadvantages. For this purpose, it is important to perform the numerical comparison of their performance criteria (throughput, cycle time) [1]. However, such analysis still has not got enough attention in the literature. The authors of [2] performed the similar comparison, but they were concentrated on the scenario when a traffic jam problem occurs only near loading/unloading stations. In fact the congestion situations could happen in any region of the workspace with

increasing the number of workstations and vehicles.

For a case study, we focus on the cargo transshipment tasks on the container terminal. A schematic overview of the working area is presented in Figure 1.

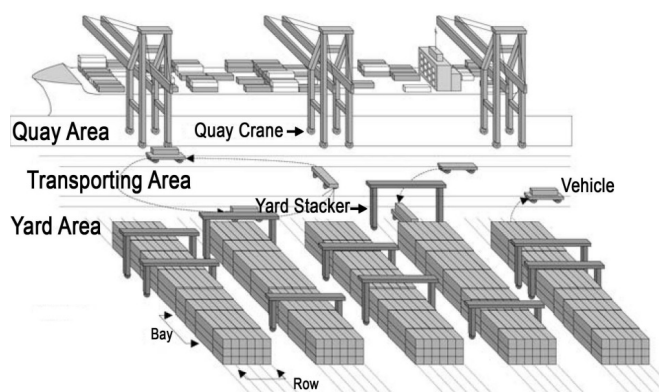


Figure 1: A container terminal layout [3]

The vehicles move within the transport area, which represents a long narrow area with the length of 2000m and width - 40m. On the seaside 20 quay cranes execute discharging and loading operations of vessels. On the opposite side 66 yard stackers store the containers. An assigned task for each vehicle is a sequence of container transportations between quay and yard areas.

In the presentation, a simulation model of routing strategies for the above-mentioned scenario with different number of AGVs will be presented.

References

- [1] S. Adinandra, "Hierarchical Coordination Control of Mobile Robots". PhD thesis, Eindhoven University of Technology, 2012.
- [2] D. Overbeek, "Combining fixed-path and free-range AGV routing on a container terminal". Master's thesis, Delft University of Technology, 2017.
- [3] A. Adriaansen, "An automated guided vehicle system in a container terminal". Master's thesis, Eindhoven University of Technology, 2011.

Exact Potential of Nonlinear Public Good Games on Networks

Alain Govaert and Ming Cao

University of Groningen

The Netherlands

Email: a.govaert@rug.nl, m.cao@rug.nl

1 Introduction

Evolutionary dynamics of (nonlinear) public good games are often used to describe how complex social behavior emerges when groups of selfish agents interact between one another. We show that two typical models admit a potential function that implies (finite time) convergence to a Nash equilibrium for a variety of stochastic and deterministic evolutionary dynamics that may govern these *self-organizing* systems.

2 Exact potential games

Consider a finite number of players given by the set $\mathcal{V} = \{1, 2, \dots, n\}$. Each player $i \in \mathcal{V}$ has a pure strategy set that is denoted by $\mathcal{S}_i = \{1, 2, \dots, m_i\}$, for some integer $m_i \geq 2$. A vector s of pure strategies $s = \{s_1, s_2, \dots, s_n\}$, where $s_i \in \mathcal{S}_i$, is called a *pure strategy profile*. The set of pure strategy profiles denoted by \mathcal{S} is given by the Cartesian product of the players' pure strategy sets. The notation $s^{-i} \in \mathcal{S}^{-i} \triangleq \times_{j \in \mathcal{V} \setminus \{i\}} \mathcal{S}_j$ indicates the pure strategy profile excluding the pure strategy of player i . Each player $i \in \mathcal{V}$ has a payoff function $\pi_i : \mathcal{S} \rightarrow \mathbb{R}$ that maps each pure strategy profile $s \in \mathcal{S}$ to a payoff of player i , i.e., $\pi_i(s)$. We will write $(s_i, s^{-i}) \in \mathcal{S}$ for the strategy profile in which player i plays strategy $s_i \in \mathcal{S}_i$ while the other players play according to the profile $s^{-i} \in \mathcal{S}^{-i}$. Correspondingly, $\pi_i(s_i, s^{-i})$ indicates the payoff of player i for playing strategy $s_i \in \mathcal{S}_i$ against the pure strategy profile $s^{-i} \in \mathcal{S}^{-i}$. We indicate a *game* by the triplet $\Gamma = \{\mathcal{V}, \mathcal{S}, \pi\}$. A function $P : \mathcal{S} \rightarrow \mathbb{R}$ is an exact potential [1] for Γ , if for every $i \in \mathcal{V}$ and for every $s^{-i} \in \mathcal{S}^{-i}$ and every $s_i, s'_i \in \mathcal{S}_i$

$$\pi_i(s_i, s^{-i}) - \pi_i(s'_i, s^{-i}) = P(s_i, s^{-i}) - P(s'_i, s^{-i}) \quad (1)$$

holds. Γ is called an *exact potential game* if it admits a potential.

3 Public goods games on networks

We consider evolutionary games on simple networks. Let $\mathbb{G} = (\mathcal{V}, \mathcal{E})$ be the graph representing the interaction network. The set of nodes $\mathcal{V} = \{1, \dots, n\}$ represent players. We denote by d_i and \mathcal{N}_i the degree and the set of neighbors of agent $i \in \mathcal{V}$, respectively. Corresponding to each agent i , the edge set \mathcal{E} defines a *group* of agents $\mathcal{N}_i^c = \mathcal{N}_i \cup \{i\}$. At each time step t , a subset of these groups play a (nonlinear) Public Good Game (PGG). In this work, two well known

models are considered: the linear PGG and the threshold PGG. In both versions of the PGG, players either defect or cooperate (i.e., $\mathcal{S}_i = \{0, 1\}$, for all $i \in \mathcal{V}$). In the linear PGG, the public good scales linearly with the number of cooperators, resulting in an accumulated payoff function [2]

$$\pi_i(s_i, s^{-i}) = \left(\sum_{j \in \mathcal{N}_i^c} \frac{(n_j^c + s_j)rc}{1 + d_j} \right) - (d_i + 1)cs_i, \quad (2)$$

where n_j^c is the number of cooperators in \mathcal{N}_j , (i.e., $n_j^c = \sum_{l \in \mathcal{N}_j} s_l$). In the threshold PGG, a minimum number of cooperators is required in order for players to obtain a benefit from the game interactions. This results in the nonlinear payoff function

$$\bar{\pi}_i(s_i, s^{-i}) = \left(\sum_{j \in \mathcal{N}_i^c} \frac{(n_j^c + s_j)rc}{1 + d_j} \right) \theta_j(s^{-j}, s_j, \tau_j) - (d_i + 1)cs_i, \quad (3)$$

$$\forall i \in \mathcal{V} : \theta_i(s_i, s^{-i}, \tau_i) = \begin{cases} 1, & \text{if } n_i^c + s_i \geq \tau_i \\ 0, & \text{otherwise} \end{cases}.$$

Here θ_j is a step function depending on n_j^c and $\tau_j \in \mathbb{Z}$ defined to be the required number of cooperators in \mathcal{N}_j^c .

4 Exact potentials

Let Θ, \mathbf{D} be diagonal matrices such that $\Theta_{ii} = \theta_i$, $\mathbf{D}_{ii} = d_i$, for $i = 1 \dots n$. The following Proposition gives the exact potential of the public good games defined on a simple network.

Proposition 1 *Both the linear and the threshold public good games on a simple network \mathbb{G} , with payoff functions (2) and (3) are exact potential games. Moreover, the potential is given by*

$$P(s) = \mathbb{1}_n^\top (rc\Theta(s)(\mathbf{D} + \mathbf{I})^{-1}(\mathbf{A} + \mathbf{I})s - c(\mathbf{A} + \mathbf{I})s),$$

where, for the linear PGG, $\Theta(s)$ is equal to the $n \times n$ identity matrix.

References

- [1] D. Monderer and L. S. Shapley, "Potential games," *Games and economic behavior*, vol. 14, no. 1, pp. 124–143, 1996.
- [2] F. C. Santos, M. D. Santos, and J. M. Pacheco, "Social diversity promotes the emergence of cooperation in public goods games," *Nature*, vol. 454, no. 7201, pp. 213–216, 2008.

Sets of Stochastic Matrices with Converging Products: Bounds and Complexity

Pierre-Yves Chevalier

Vladimir V. Gusev

Raphaël M. Jungers

Julien M. Hendrickx

ICTEAM, Université catholique de Louvain, Belgium

{pierre-yves.chevalier, vladimir.gusev,

raphael.jungers, julien.hendrickx}@uclouvain.be¹

1 Introduction

A stochastic matrix P is an *SIA matrix* (Stochastic¹ Indecomposable Aperiodic) if the limit

$$\lim_{t \rightarrow +\infty} P^t$$

exists and all of its rows are equal, i.e., the limit is a rank-one matrix. These matrices play a fundamental role in the theory of Markov chains as they correspond to chains converging to unique limiting distribution [3]. They also arise in discrete-time *consensus systems*, systems representing groups of agents trying to agree on some value by iterative averaging [4]. Such systems can be modelled by the update equation

$$x(t+1) = P(t)x(t), \quad (1)$$

where $x(t)$ is the vector of the values of the agents at time t and $P(t)$ is a stochastic transition matrix representing how agents compute their new values. Markov chains and consensus systems are often time-inhomogeneous, i.e., the transition matrix $P(t)$ can be different at different steps t , where $P(t)$ typically belongs to a finite set of stochastic matrices $\mathcal{S} = \{A_1, A_2, \dots, A_k\}$. It can be shown that System (1) can be brought to convergence by controlling the switching signal if and only if the corresponding set \mathcal{S} has an SIA product. In this work we study the shortest SIA products of sets of stochastic matrices. We define the SIA-index of a set of stochastic matrices as the length of its shortest SIA product.

2 Results

We show that the largest value of the SIA-index among all SIA sets of $n \times n$ stochastic matrices, $\text{sia}(n)$, is $O(n^3)$. Moreover, we show that $\text{sia}(n)$ grows at least as n . We conjecture that the actual growth rate is closer to the provided lower bound and support this statement by performing an exhaustive search for small values of n on a computer grid. The largest SIA-index for each dimension n is presented in Figure 1.

We show that a SIA set has a scrambling, a Sarymsakov and a positive-column product, and, conversely, a set that has a

¹Raphaël Jungers is an FNRS associate.

¹A matrix is *stochastic* if it is nonnegative and the sum of the elements on each row is 1.

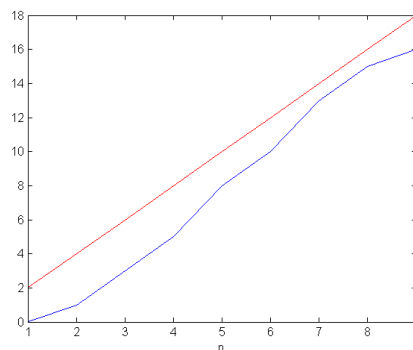


Figure 1: Maximum SIA-index for pairs of matrices (blue) and the curve $y = 2n$ (red).

scrambling, a Sarymsakov or a positive-column product is a SIA set. As a consequence, the same polynomial-time procedure can be used to decide whether a given set of stochastic matrices has any of the aforementioned products. We show the SIA-index is NP-hard to compute, even if all matrices in \mathcal{S} have a positive diagonal. Matrices with positive diagonals appear in consensus applications and many problems are computationally easier for these matrices [1]. We also show the SIA-index is NP-hard to approximate within a factor of $O(\log(n))$.

Finally, we show that the $(n-1)$ st power of any SIA binary stochastic matrix has a positive column and that the $(n^2 - 3n + 3)$ rd power of any SIA matrix has a positive column.

References

- [1] P.-Y. Chevalier, J. M. Hendrickx and R. M. Jungers, *Reachability of Consensus and Synchronizing Automata*, IEEE Conference on Decision and Control, 2015.
- [2] P.-Y. Chevalier, Vladimir V. Gusev J. M. Hendrickx and R. M. Jungers, *Sets of Stochastic Matrices with Converging Products: Bounds and Complexity*, submitted, 2017.
- [3] A. Paz, *Graph-theoretic and algebraic characterizations of some Markov processes*, Israel Journal of Mathematics, 1963.
- [4] V. D. Blondel and A. Olshevsky, *How to decide consensus? A combinatorial necessary and sufficient condition and a proof that consensus is decidable but NP-hard*, SIAM Journal on Control and Optimization, 2014.

Bursty walkers backtrack

M. Gueuning^{*◊}, R. Lambiotte^{*◊}, J.-C. Delvenne^{◊*}

* Naxys, University of Namur, Belgium ◊ ICTEAM Institute, UCLouvain, Belgium

★ CORE, UCLouvain, Belgium ◊ Mathematical Institute, University of Oxford, UK

Email: martin.gueuning@unamur.be

Abstract

We discuss the results of [1] where we consider the problem of diffusion on temporal networks, where edges activate instantaneously and independently. We show that the null-model usually considered as a baseline of comparison present themselves correlations they are supposed to be free of. In particular, we exhibit the tendency of a walker to backtrack (return to the last visited node) at each jump step even though edges are uncorrelated, and the resulting effect on the exploration of the network by the walker.

We consider a standard random walker (RW) taking the first available edge at every step, where the time between two consecutive activations of an edge is random and follows a probability density function $f(t)$.

The waiting time distribution $g(t)$, i.e., the time that the random walker arriving on a node has to wait before a given edge activates is given by:

$$g(t) = \frac{1}{\langle \tau \rangle} \int_t^{+\infty} f(\tau) d\tau \quad (1)$$

where $\langle \tau \rangle \equiv \int_0^{+\infty} \tau f(\tau) d\tau$ is the mean inter-activation time. The observation that $g(t)$ may have larger mean than $f(t)$ is known under the name of bus paradox, or inspection paradox [2].

This paradox applies to every edge on a random walk, with the notorious exception of the edge ij that has just been taken by the walker, for which the time before next activation is given by $f(t)$, see Figure 1.

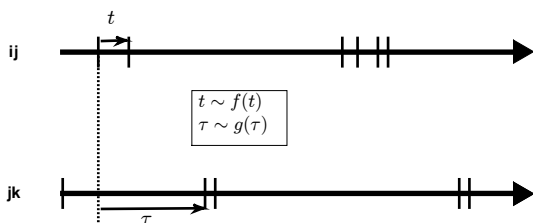


Figure 1: Illustration of the backtracking bias on an edge ij . When the walker arrives on j via ij , the next activation time t of the edge ij is given by the distribution $f(t)$, whereas the next activation time τ of another independent edge jk is given by the distribution associated to the bus paradox $g(t)$.

The waiting-time distribution for j to i is thus the inter-activation distribution $f(t)$, while it is $g(t)$ for other edges, inducing a backtracking bias toward or against a specific edge at each step of the walk, depending on the inter-activation distribution f .

As human interactions distributions tend to be broad, or bursty, the backtracking bias turns out to be positive for random walks on human-related networks. As we show analytically, as well as through empirical data from [3] (see Table 1), non-Markovian dynamics may significantly slow down the diffusion due to this biased backtracking, as exhibited by a reduction of the spectral gap, which controls the number of steps required to reach the stationary distribution.

Data	Spectral Gap of Markovian RW	Spectral Gap of Backtracking RW
Primary	0.4151	0.2738
Work	0.3057	0.0569
Highschool	0.1349	0.0396
Hospital	0.5695	0.2105

Table 1: The reduction of the spectral gap due to the backtracking bias reflects the slow-down of the exploration of the network by the walker.

This work highlights the existence of a neglected, yet important, correlation taking place in a null model actually designed to destroy temporal correlations in temporal networks. The whole concept of 'standard simplest model' on temporal networks with bursty activity is questioned since correlations between events cannot be avoided, either in the jumping or in the activation process.

References

- [1] Gueuning, M.; Lambiotte, R.; Delvenne, J.-C. *Backtracking and mixing rate of diffusion on uncorrelated temporal networks*. *Entropy*, Vol. 19, p. 542 (2017)
- [2] Lambiotte, R.; Tabourier, L.; Delvenne, J.C. *Burstiness and spreading on temporal networks*. *E.P.J. B* (2013)
- [3] Mastrandrea, R.; Fournet, J.; Barrat, A. *Contact Patterns in a High School: A Comparison between Data Collected Using Wearable Sensors, Contact Diaries and Friendship Surveys*. *PLoS ONE* 2015

Torsional vibration- and backlash- compensation in drive-lines using non-linear feedforward control

Cyrano Vaseur, Albert Rosich,
Maarten Witters, Edward Kikken
Flanders Make
P.O. Box 4027, B-3001 Heverlee, Belgium
{cyrano.vaseur, albert.rosich,
maarten.witters, edward.kikken}
@flandersmake.be

Bram de Jager
Control Systems Technology
Eindhoven University of Technology
P.O. Box 513, 5600 MB Eindhoven
The Netherlands
a.g.de.jager@tue.nl

1 Introduction

In order to achieve high position-tracking performance in industrial machines, flexibilities and play in the drive-train are minimized as much as possible. For example, stiff shafts and gearboxes with small play are preferred. However, this might have some negative consequences for the overall design of the machine: i) Stiff components and low play gearboxes are expensive and ii) the connection of these stiffer components can pose difficulties with intercepting alignment errors causing equipment damage and premature fatigue of the components.

To address this problem, a co-design approach of hardware and control is desirable. Advancements in control can recover performance for hardware that is designed with more flexibility and play. Therefore this study focuses on the mitigation of torsional vibrations and backlash of the drivetrain by means of non-linear feed-forward control techniques. The results are validated and demonstrated in a real test rig consisting of a small modular drive-train (SMD).

2 Approach

Models describing the flexible behavior are obtained by means of proper system identification methods. Backlash effects of the components with play are also characterized. Feed-forward control laws are computed from these models. The main challenge here is the detection of the zero-crossings of the load torque, i.e., the instants of backlash gap opening. Therefore, load models are also developed. To track well at non-located/ load side θ_l , quick and smooth gap traversal [1] is applied at the collocated/ motor side θ_m . The proposed control structure can be seen in figure 1.

3 Results and Conclusion

The proposed control technique is applied on the SMD. Here, a motor drives an oscillating disturbance load through a gearbox (with backlash) connected to a flexible drive-shaft, see figure 1. With the load position reference θ_l a simple ramp, the motor position reference θ_m is adjusted with a steep s-curve correction profile θ_b , see the motor position reference. With the applied backlash compensation technique, the maximum tracking error is reduced from 0.11[rad] to 0.035[rad], see the tracking error plot. This however, costs extra torque, i.e., peak torques of 7[Nm] at every zero-crossing, see the motor torque plot. The feed-forward torsional vibration compensation technique also reduces the tracking error significantly. Also here significant torque demand is requested to keep tracking accurately, especially when the shaft is excited at the anti-resonance. The applied techniques do recover performance, but not fully. Nevertheless, the results do illustrate a possible trade-off between high performance and overall machine design.

References

- [1] V. Agrawal, W. J. Peine, B. Yao and S. Choi, "Control of Cable Actuated Devices using Smooth Backlash Inverse," in 2010 IEEE International Conference on Robotics and Automation, May 3-8, 2010, Anchorage, Alaska, USA, 2010.

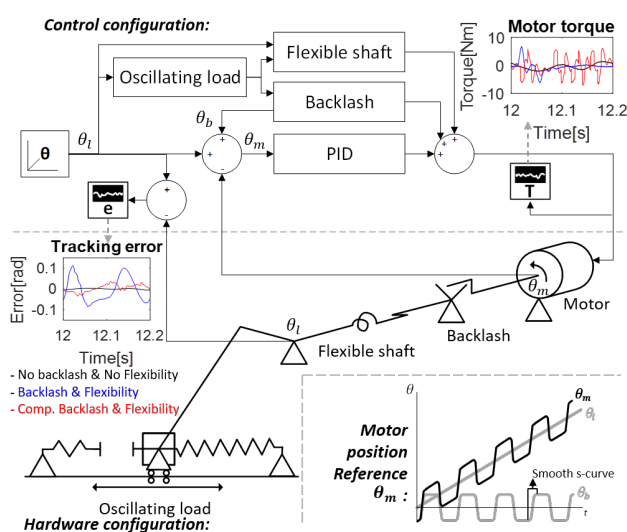


Figure 1: Top: Control configuration; Middle & bottom-left: Hardware configuration; Bottom-right: Motor position reference θ_m .

Identification of the drive train of an electric vehicle

Andreas De Preter^{1,2} (adepreter@octinion.com), Laurens Jacobs^{2,3},
Jan Anthonis¹, Goele Pipeleers^{2,3}, and Jan Swevers^{2,3}

¹ Octinion bvba, Interleuvenlaan 46, 3001 Leuven-Heverlee, Belgium

² MECO Research Team, Department Mechanical Engineering, KU Leuven, Belgium

³ DMMS lab, Flanders Make, Leuven, Belgium

1 Introduction

In this project the characteristics that are relevant for fixed trajectory following are investigated for an electric vehicle designed for logistic operations in greenhouses (Figure 1). All physical and electrical constraints of the system's drive train determine the theoretically achievable performance of a trajectory controller. This work describes the identification of the drive train. The results are twofold: the possible accuracy and bandwidth of the trajectory controller have been quantified and the components that are restrictive for a better performance have been identified.

The trajectory of the vehicle mostly consists of straight lines with a constant forward velocity. Therefore it is particularly interesting to analyze the effects for the rotational (yaw) movement. The identification is performed using two approaches: a theoretical analysis of the setup and an experimental verification of the identified transfer function. A similar approach for a different type of robot is described in [1].

2 Theoretical analysis of the setup

The vehicle is a two-wheel differential drive system. The analysis of the setup occurs in two stages. In the first stage all electrical equipment is investigated. This includes an analysis of the motors and their drives. In the second stage the mechanical properties are characterized. A dynamic model of the movement is derived from the equations of motion, whereof the parameters are calculated from the robot characteristics (mass, dimensions).



Figure 1: Electric vehicle

These two stages are put together to define the complete model of the vehicle. The result is a transfer function that describes the relation between the desired motor velocities, which are the setpoints for the motor drives, and the rotational (yaw) velocity of the vehicle.

3 Experimental validation

From the theoretical analysis the structure of the transfer function is known. This structure is verified by experiments based on black-box system identification methods. The input generation and experiment analysis is carried out with an open source linear control toolbox ('LCToolbox') for MATLAB [2], which is available at www.github.com/meco-group/lc_toolbox. Additional nonlinear effects like time delay are derived from the experimentally estimated transfer function.

4 Use of the results

The results allow us to determine the vehicle's ability of suppressing disturbances when following a trajectory. Because of the insights gained by the theoretical analysis, an overview of components that could be changed for a better performance is provided.

References

- [1] E. Kayacan, E. Kayacan, H. Ramon, W. Saeys, "Towards agrobots: Identification of the yaw dynamics and trajectory tracking of an autonomous tractor," *Computers and Electronics in Agriculture* 115, 2015.
- [2] L. Jacobs, M. Verbandt, A. De Preter, J. Anthonis, J. Swevers, G. Pipeleers "A toolbox for robust control design: an illustrative case study," 15th IEEE International Workshop on Advanced Motion Control, 2018.

Acknowledgement

Grateful thanks to VLAIO (Vlaams Agentschap voor Innoveren en Ondernemen) for the financial support of this doctorate (Baekeland PhD Grant 150712). This work also benefits from KU Leuven-BOF PFV/10/002 Centre of Excellence: Optimization in Engineering (OPTEC).

Constrained Charging of commercial Li-ion batteries

Alejandro Goldar, Raffaele Romagnoli, Luis D. Couto, Emanuele Garone, Michel Kinnaert
 Service d'Automatique et d'Analyse des Systèmes - Université libre de Bruxelles
 Email: agoldard@ulb.ac.be, rromagno@ulb.ac.be, coutome@ulb.ac.be
 egarone@ulb.ac.be, michel.kinnaert@ulb.ac.be

The increasing market of battery-powered devices demands batteries with a longer lifespan and shorter charging times. Most of the charging techniques are based on commonly-used protocols, such as Constant Current (CC), Constant Current-Constant Voltage (CC-CV) or Constant Power (CP). Although, these *ad-hoc* commercial charging algorithms are broadly used, they do not take into account explicitly the State of Charge (SOC) or the impact of the current profiles on battery degradation mechanisms. Thus, these *ad-hoc* strategies can accelerate aging processes and hence the loss of capacity.

Accounting for the SOC and aging processes into the charging mechanism leads to a new control problem. It can be described as *calculating the appropriate amount of current such that the battery can be charged in the shortest time possible avoiding side reactions that cause aging*.

In this study, to model the battery, we used the so-called Equivalent Hydraulic Model (EHM) which is an Electro-Chemical Model (EChM) for lithium-ion batteries deduced from the Single Particle Model (SPM). The main feature of this model with respect to other models is that, although it is just a simple reduced model, the states have a clear physical meaning. This allows stating the operational constraints on the current (I), the State of Charge (SOC⁻) and the Critical Surface Concentration (CSC⁻).

The constrained control charging problem is usually solved by resorting to a classical Model Predictive Control (MPC) scheme. However, due to the high-computational cost of MPC a simpler strategy is the implementation of a Scalar Reference Governor (SRG) scheme, as it has been proposed by [1]. The SRG has the capability of fulfilling operational constraints while avoiding online optimization.

The *goal* of this research is *to validate experimentally* the simulation results of this charging SRG strategy [1] on *real commercial batteries* and *to compare* its performance against CC-CV and MPC strategies.

For this task, **Turnigy 160mAh LCO batteries** were identified within the EHM and the various charging strategies were implemented. The experimental results presented in Table 1. Fig. 1 presents the admissible region of the constrained problem defined by current and CSC limits.

As Table 1 shows, the SRG achieves the same charging time (Charg. time) as the MPC while dramatically lowering the computational time (Comput. avg. time). Although MPC and SRG keep the operating point inside of the admissible re-

Table 1: Experimental results of charging strategies

	Charg. time [min]	Max. I [A]	Max. V [V]	Final V [V]	Max. CSC ⁻	Max. ΔT [°C]	Comput. avg. time[s]
CCCV@1C	58.017	0.160	4.155	4.136	0.694	0.854	0.0010
CCCV@3C	24.917	0.480	4.204	4.165	0.715	1.343	0.0007
MPC	16.050	0.769	4.126	4.033	0.605	1.099	0.4653
SRG	15.983	0.784	4.131	4.028	0.605	1.099	0.0008

gion, these schemes push the charging process with higher currents at low values of CSC in contrast with the first stage of a traditional CC-CV (Fig. 1).

Both MPC and SRG strategies have no temperature constraints. Nevertheless, temperature did not experience relevant increases with respect to the traditional CC-CV at 1C. As it can be observed through the temperature difference between the environment and the surface of the battery (Max. ΔT) in Table 1.

Usually, CC-CV strategies are considered as cautious approaches to maximize the charge of the battery. Nevertheless, Fig.1 also reveals how these techniques violate the side reaction constraints (Max. CSC⁻) possibly accelerating aging processes.

From these experimental results, it can be concluded that the proposed SRG scheme is a simple and effective way to cope with the constrained charge of commercial Li-ion batteries.

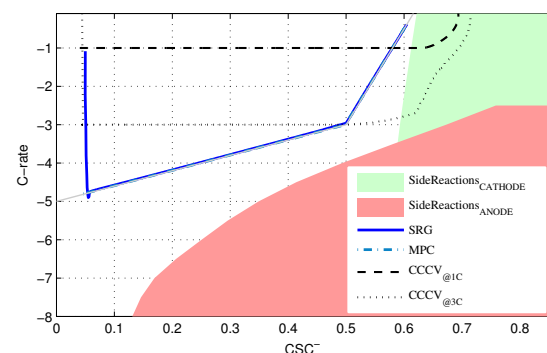


Figure 1: Charging algorithms performance against constraints

References

- [1] R. Romagnoli, L. D. Couto, M. Kinnaert, and E. Garone. Control of the state-of-charge of a li-ion battery cell via reference governor. *IFAC-PapersOnLine*, 50(1):13747–13753, 2017.

On Power Grids with Grounded Capacitors

Mark Jeeninga
 ENTEG / JBI
 University of Groningen
 Email: m.jeeninga@rug.nl

1 Introduction

Electrical networks such as power grids are generally modelled by considering dynamics over a weighted graph. The weights in these graphs correspond to conductances of the lines. In this work we are interested in exploiting the underlying graph structure in the study of such models.

We consider two types of buses in such models: *load buses*, which drain power from the grid, and *generator buses*, which provide power to the grid.

The ratio of the number of lines and buses in benchmark models for power grids typically does not exceed 2:1. However, in the literature we see that power grids are sometimes assumed to be radial (*i.e.* a tree) [1, 2], which roughly corresponds to a 1:1 ratio. This assumption is not only made for the sake of analysis, but also serves the nature of power grids; The underlying graph tends to be sparse.

We assume that the number of cycles among load buses is “not too large”, which means that the lines-to-buses ratio for load buses is close to 1:1.

2 Preliminaries

A spanning tree of a graph is a subgraph which is a tree and contains the same nodes (buses) as the original graph. To each such spanning tree we correspond a weight, which is the product of the weight of the edges (lines) in the tree. The sum over the weights of all spanning trees is known as the *weighted spanning tree number* of the graph, while the number of spanning trees of a graph is the *spanning tree number*.

Let V_L, V_G be the potentials at the load and generator buses respectively, I_G the outgoing current at the generator buses, and $\begin{pmatrix} \mathcal{L}_{LL} & \mathcal{L}_{LG} \\ \mathcal{L}_{GL} & \mathcal{L}_{GG} \end{pmatrix}$ the weighted Laplacian matrix representing the interconnection between buses over the lines. We consider the simple dynamical system described by

$$\dot{V}_L = \mathcal{L}_{LL}V_L + \mathcal{L}_{LG}V_G, \quad I_G = \mathcal{L}_{GL}V_L + \mathcal{L}_{GG}V_G,$$

which models a power grid where grounded capacitors of unit capacitance are connected to the loads.

The transfer function from the potentials at the loads V_G to

the outgoing currents at the loads I_G is given by

$$H_G(s) := \mathcal{L}_{GG} - \mathcal{L}_{GL}(\mathcal{L}_{LL} - sI)^{-1}\mathcal{L}_{LG}.$$

The main issue is the computation of $(\mathcal{L}_{LL} - sI)^{-1}$, which is known as the *resolvent* of the linear operator \mathcal{L}_{LL} . A general method for computing this rational matrix in the variable s is by computing the spectral decomposition of the symmetric matrix \mathcal{L}_{LL} .

3 Contribution

We use a formula which relates the weighted spanning tree numbers of the subgraphs of a graph to a diagonal update of its Laplacian matrix to obtain an expression for $(\mathcal{L}_{LL} - sI)^{-1}$. This formula was derived by the author in a separate paper that is currently being prepared for submission. The described method avoids computing the spectral decomposition of the Laplacian matrix of the graph.

Since the connected components of the graph induced by the load buses has a spanning tree number which is assumed to be “not too large”, the number of subgraphs which should be considered in the formula mentioned above is quite limited.

We ask when this method is computationally feasible compared to the spectral decomposition approach, and how we can incorporate the matrices \mathcal{L}_{LG} and \mathcal{L}_{GL} to improve the computation of $H_G(s)$.

References

- [1] J. W. Simpson-Porco, “A Theory of Solvability for Lossless Power Flow Equations - Part I: Fixed-Point Power Flow,” in IEEE Transactions on Control of Network Systems, vol. PP, no. 99, pp. 1-1.
- [2] J. W. Simpson-Porco, “A Theory of Solvability for Lossless Power Flow Equations - Part II: Conditions for Radial Networks,” in IEEE Transactions on Control of Network Systems, vol. PP, no. 99, pp. 1-1.
- [3] S. Sanchez, R. Ortega, G. Bergna, M. Molinas and R. Grió, “Conditions for existence of equilibrium points of systems with constant power loads,” 52nd IEEE Conference on Decision and Control, Firenze, 2013, pp. 3641-3646.
- [4] C. Godsil, G. Royle, “Algebraic graph theory,” Springer, New York, 2001.

Modelling and control of a nanometer-accurate motion system

Ioannis Proimadis, Tom Bloemers, Roland Tóth and Hans Butler
 Control Systems Group, Electrical Engineering, Eindhoven University of Technology
 Email: i.proimadis@tue.nl

1 Introduction

Modern motion systems are capable of achieving high accelerations while retaining a small positioning error. While these properties are a design trade-off, in high-end industries stringent performance goals render both unequivocally important. For example, in semiconductor industry these goals are realized by accelerations of more than $4g$ and a position error during scanning phase of less than $20nm$ [1].

The current state-of-the-art motion systems are realized by a combination of a long-stroke, moving-coil magnetic levitation system, together with a short-stroke stage. At the Eindhoven University of Technology a one-stage, moving-magnet prototype was designed and realized in the recent years (Fig. 1). The main goal is to investigate the possible benefits and limitations of this setup by deploying a control architecture tailored for this system.



Figure 1: The moving-magnet prototype (NAPAS)

2 Data-driven modelling and control

The developed Nanometer-Accurate Planar Actuation System (NAPAS) can be modelled as an interconnection between an electromagnetic part, that describes the relation between the stationary coils and the moving magnet, together with a mechanical part that describes the motion dynamics of the latter one (Fig. 2). For the decoupling of the relation between the supplied currents and the resulting forces a position-dependent commutation block is added. The position of the magnet is achieved using Laser Interferometers, which are fixed to the metrology frame, leading to a position-dependent relation between the states and the measured output. Through the rigid body position estimation block, the 6 degrees-of-freedom are controlled by means of feedforward and feedback action.

In order to increase the performance an experimental estimation of the frequency response is essential. Especially the spatial deformations due to the position-dependent, asymmetric distribution of forces on the magnetic plate can potentially lead to instability. For this reason, a grid-based FRF

identification was performed.

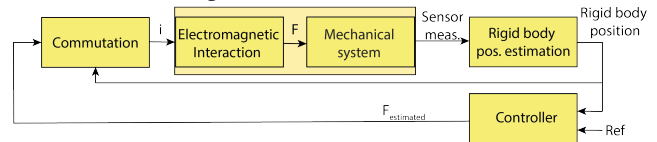


Figure 2: Block diagram of the NAPAS experimental setup. For the control design, the Sequential Loop Closing (SLC) framework is employed since it can directly make use of the non-parametric data. The loop-shaping based design was performed in an iterative manner such that the performance specifications are satisfied with respect to the local FRFs, leading to a $100Hz$ bandwidth controller in x , y and ζ (rotation around z). The performance was validated on the experimental setup and it was compared with the previous, $16Hz$ controller, resulting in approximately $200nm$ error under a $0.2m/s$ speed motion (Fig. 3).

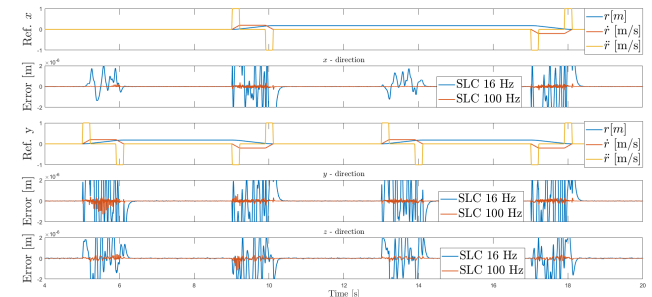


Figure 3: x , y reference profiles and position errors in x , y , z axes for the initial $16Hz$ and the $100Hz$, SLC controller.

Finally, Machine Learning techniques were employed to compensate disturbances through a position dependent feed-forward action. Simulation and experimental results showed that indeed this is a viable way of capturing disturbances.

3 Conclusions

In this paper a non-parametric frequency domain identification was used, followed by an SLC based control approach such that the specified requirements are locally satisfied. Finally, Machine Learning based approaches to compensate disturbances were examined. Next steps include the parametric modelling and LPV embedding of the local FRFs, which will enable an LPV control design approach.

References

- [1] H. Butler, "Position control in lithographic equipment," *IEEE Control Systems Magazine*, vol. 31, no. 5, pp. 28–47, 2011.

Structuring multilevel discrete-event systems modeled with extended finite state automata

M.A. Goorden, M.A. Reniers, J.M. van de Mortel-Fronczak, J.E. Rooda
Control Systems Technology
Eindhoven University of Technology
P.O. Box 513, 5600 MB Eindhoven
The Netherlands

Email: {m.a.goorden, m.a.reniers, j.m.v.d.mortel, j.e.rooda}@tue.nl

1 Introduction

The complexity of high-tech systems has increased due to increasing market demand for verified safety, shorter time-to-market, and better performance. Model-based systems engineering approaches provide advantages for supervisory controller design. We consider discrete-event system (DES) models for which supervisory controllers need to be developed. The supervisory control theory of Ramadge-Wonham provides an approach to synthesize supervisors such that the controlled behavior of the system is restricted to specified behavior [1].

One of the major drawbacks of synthesizing supervisory controllers is the step where the supremal controllable language is calculated. There exist multiple attempts to overcome these computational difficulties. One of them is multilevel supervisory control synthesis [2]. A problem with multilevel synthesis is that the system should be modeled with a tree structure.

Recently, we proposed to use Dependency Structure Matrices (DSMs) to exploit the dependencies within a system to transform it into the tree structure needed for multilevel synthesis [3]. We analyze the relationship between the plant models and requirement models. For finite state automata, there is a relationship between a plant model and a requirement model when they share an event.

2 Result

We propose to enrich the method from [3] to analyze extended finite state automata (EFSAs). In EFSAs, discrete variables can be used and guards on edges can refer to locations in other EFSAs. Furthermore, requirement models can be formulated with state-based expressions.

For EFSAs, there is a relationship between a plant model and a requirement model if they share an event, share a variable, or the requirement refers to a location in the plant model.

We are able to structure DES models of industrial-size systems using EFSAs. An example of such system is a water-

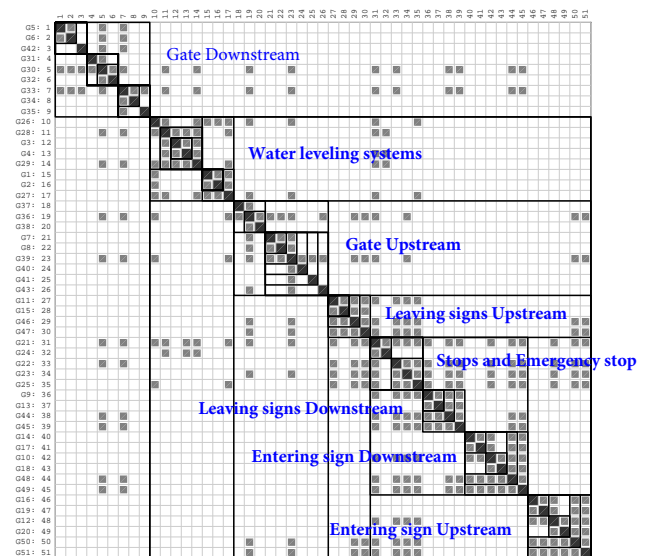


Figure 1: The clustered DSM of a waterway lock

way lock as presented in [4]. Figure 1 shows the clustered DSM of this waterway lock.

By using multilevel synthesis in combination with DSM-based clustering, we can reduce the state-space size. The uncontrolled state-space has 6.0×10^{32} states. The monolithic supervisor for this system has 6.0×10^{24} states. For multilevel synthesis, we can reduce the state-space of the supervisors together to 3.5×10^7 states.

References

- [1] P.J.G. Ramadge and W.M. Wonham, "Supervisory Control of a Class of Discrete Event Processes," *SIAM Journal on Control and Optimization*, Vol. 25, 1, 206–230, 1987.
- [2] J. Komenda, T. Masopust, and J.H. van Schuppen, "Control of an engineering-structured multilevel discrete-event system," *WODES*, 103–108, 2016.
- [3] M.A. Goorden, J.M. van de Mortel-Fronczak, M.A. Reniers, and J.E. Rooda, "Structuring Multilevel Discrete-Event Systems with Dependency Structure Matrices," *CDC*, 558–564, 2017.
- [4] F.F.H. Reijnen, M.A. Goorden, J.M. van de Mortel-Fronczak, and J.E. Rooda, "Supervisory Control Synthesis for a Waterway Lock," *CCTA*, 1562–1568, 2017.

\mathcal{L}_2 -gain Analysis of Periodic Event-triggered Systems with Varying Delays using Lifting Techniques

Nard Strijbosch
Eindhoven University of Technology
Email: n.w.a.strijbosch@tue.nl
P.O. Box 513, 5600 MB Eindhoven
The Netherlands

Geir Dullerud
University of Illinois

Andrew Teel
University of California

Maurice Heemels
Eindhoven University of Technology

1 Introduction

In this paper the stability and \mathcal{L}_2 -gain properties of periodic event-triggered control (PETC) systems including time-varying delays are studied, which summarizes the result of [1]. These PETC systems can be captured in a general framework that encompasses a class of hybrid systems that exhibit linear flow, aperiodic time-triggered jumps (possibly with different deadlines) and arbitrary nonlinear time-varying jump maps. Interestingly, the class of hybrid systems captured by this framework is a generalization and unification of those found in [2, 3]. Inspired by ideas from lifting, it is shown that the internal stability and contractivity in \mathcal{L}_2 -sense of a continuous-time hybrid system in the framework is equivalent to the stability and contractivity in ℓ_2 -sense of an appropriate time-varying discrete-time nonlinear system.

2 PETC systems with varying delays

The PETC setup of Figure 1, with continuous-time linear plant P and controller C , is considered. The event-triggering mechanism decides each sample based on $y(t)$ and $\hat{y}(t)$ if the new measurement output is updated to the controller or not. In particular, $\hat{y}(t)$ is given for $t \in (t_k + \tau_k, t_{k+1} + \tau_{k+1}]$, $k \in \mathbb{N}$, by

$$\hat{y}(t) = \begin{cases} y(t_k), & \text{when } \zeta(t_k)^\top \hat{Q} \zeta(t_k) > 0, \\ \hat{y}(t_k), & \text{when } \zeta(t_k)^\top \hat{Q} \zeta(t_k) \leq 0, \end{cases} \quad (1)$$

where $\zeta := [y^\top \ \hat{y}^\top]^\top$ is the information available at the event-triggering mechanism (ETM) and $t_k, m \in \mathbb{N}$, are the sampling times, which are periodic in the sense that

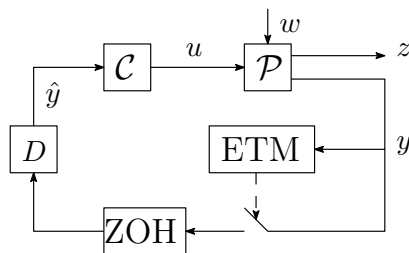


Figure 1: Schematic representation of an event-triggered control setup with communication delay (block D).

$t_k = kh, k \in \mathbb{N}$, with h the sampling period. Although the system has a constant sampling period h , the delay causes unequal inter-jump times (related to a transmission on t_k and an update on $t_k + \tau_k$). Due to this it is not possible to capture this PETC systems in the class of hybrid systems discussed in [2]. The delay varies such that $\tau_k \in \{d_1, d_2, \dots, d_{n_d}\}$, $k \in \mathbb{N}$. All possible delays, $d_j \in \mathbb{R}_{\geq 0}$, $j \in \{1, 2, \dots, n_d\}$ satisfy the small delay assumption $d_j \leq h$, $i \in \{1, 2, \dots, n_d\}$.

3 Lifting based approach exploited for PETC systems with varying delays

By using lifting techniques it can be shown that the internal stability and contractivity of the original continuous-time system is equivalent to the internal stability and contractivity of a discrete-time switched PWL system of the form

$$\chi_{k+1} = \begin{cases} A_{1l_k} \chi_k + B_{l_k} w_k & \text{when } \chi_k^\top Q \chi_k > 0 \\ A_{2l_k} \chi_k + B_{l_k} w_k & \text{when } \chi_k^\top Q \chi_k \leq 0 \end{cases} \quad (2a)$$

$$z_k = \begin{cases} C_{1l_k} \chi_k + D_{l_k} w_k & \text{when } \chi_k^\top Q \chi_k > 0 \\ C_{2l_k} \chi_k + D_{l_k} w_k & \text{when } \chi_k^\top Q \chi_k \leq 0, \end{cases} \quad (2b)$$

$l_k \in \{1, 2, \dots, n_d\}$, $k \in \mathbb{N}$, (note that l_k switches arbitrarily). It is possible to analyse the internal stability and contractivity of (2), by exploiting versatile piecewise quadratic Lyapunov/storage functions. Hence, the lifted discrete-time version of a continuous-time PETC system with varying delays can be analysed to conclude on the internal stability and contractivity properties of the original system.

References

- [1] N.W.A. Strijbosch, G.E. Dullerud, A.R. Teel, and W.P.M.H. Heemels. \mathcal{L}_2 -gain analysis of periodic event-triggered systems with varying delays using lifting techniques. In *IEEE Conf. on Decision and Control*, 2017.
- [2] W.P.M.H. Heemels, G.E. Dullerud, and A.R. Teel. \mathcal{L}_2 -gain analysis for a class of hybrid systems with applications to reset and event-triggered control: A lifting approach. *IEEE Transactions on Automatic Control*, 61:2766–2781, 2016.
- [3] G.E. Dullerud and S. Lall. Asynchronous hybrid systems with jumps - analysis and synthesis methods. *Systems and Control Letters*, 37(2):61–69, 1999.

Systems and Control in Precision Farming: prospects and challenges

Simon van Mourik, Peter Groot Koerkamp, Eldert van Henten
 Farm Technology Group, Wageningen University
 P.O. Box 16 6700 AH Wageningen, The Netherlands
 simon.vanmourik@wur.nl

1 Introduction

The demand for high quality, and affordable food production in high quantities is putting tremendous pressure on our agricultural production system as well as on our environment. Precision Farming (PF) offers a solution to this problem by means of precise management in time and space - ranging from field or barn level to individual crops and animals.

The systems and control paradigm offers some strong concepts and algorithms (such as input-state-output modelling, performance criteria, open loop and feedback control, data assimilation, and model identification) that are useful to PF research, as well as practical implementation.

Current model based algorithms deal well with dynamic and nonlinear system response. However, the difficulty lies in disturbance factors such as weather, diseases, spatial and biological variation, sensor noise, and model errors. These disturbances may undermine algorithm performance [1, 2]. Usually, their influence is ignored or oversimplified in research studies. Yet, they form an integral part of any farming system. Underestimating their roles can easily lead to miscalculations and mismanagement in practice, or even obstruct development of new farming systems [3].

2 Approach

We present a case study of signal filtering to improve climate monitoring inside a greenhouse. Spatiotemporal climate variations combined with sensor noise cause erroneous sensor readings. With the aim to filter out these errors, we tested three filters - an extended Kalman filter, an unscented Kalman filter, and a moving average filter. The filters were tested with in total one and a half year of five minute temperature and humidity data from sensor grids inside two greenhouses. The model based filters were supported with a state of the art greenhouse climate model [4].

3 Results

None of the filters filtered out the signal errors consistently. Moreover, the overall accuracy of all three filters was worse compared to when no filtering was applied. Moving average filtering performed worst overall, due to the erroneous assumption that signal errors and system dynamics have separate frequency bands. The Kalman filters did not perform

well because 1) the signal errors were strongly autocorrelated, which violates the assumptions the filter algorithms are based upon, and 2) the model errors were far larger than the sensor errors. We predict that a Kalman filter can reduce a signal error by 50 per cent, only if the climate model is improved such that the state error covariance is reduced by a factor 10. Furthermore, the nature of the errors needs to be explicitly modelled such that the remaining model and sensing errors are not autocorrelated. In other words, an enormous model improvement is required.

4 Discussion

The question arises whether it is possible to create a filtering algorithm to deal with autocorrelated noise reliably, or that the model should be improved. This example illustrates the possibility of applying systems and control methodology to improve farming systems, but also reveals challenges: How to deal with error structures our algorithms are not designed for? How to deal with multiple errors interacting and propagating through the sensing and control loop?

5 Conclusion

The combination of nonlinearity, dynamics, and unexplained or uncertain disturbances encountered in hi-tech farming systems opens up new prospects and challenges for the field of Systems and Control. A new set of methods is needed that combines the existing nonlinear dynamic systems approach with a probabilistic perspective to enable systematic precision farming research.

References

- [1] M. Mul et al., Development of a model forecasting *Dermanyssus gallinae* population dynamics for advancing Integrated Pest Management in laying hen facilities, *Veterinary parasitology* 245, 128-140, 2017.
- [2] F. Sanderink et al., Automatic detection of oestrus cows via breath sampling with an electronic nose: A pilot study, *Biosystems Engineering* 156, 1-6, 2017.
- [3] S. van Mourik et al., Predicting hairline fractures in eggs of mature hens, *Poultry Science*, 96 (6), 1956-1962, 2017.
- [4] P. van Beveren et al., Minimal heating and cooling in a modern rose greenhouse, *Applied Energy*, 137, 97-109, 2015.

LCToolbox – A MATLAB toolbox for robust control design

Laurens Jacobs, Maarten Verbandt, Jan Swevers and Goele Pipeleers
 MECO Research Team, Dept. of Mechanical Engineering, KU Leuven, BE-3001 Heverlee
 DMMS lab, Flanders Make, BE-3001 Heverlee
 laurens.jacobs@kuleuven.be

1 Introduction

The control engineering opportunities of robust linear controller synthesis based on \mathcal{H}_∞ performance criteria have been thoroughly explored over the past decades. As a result, a mature theoretical understanding and efficient solution algorithms are available by now. Not only have promising (experimental) results appeared in literature, recent research has also shown that different classes of time-varying and nonlinear systems could be dealt with using a similar problem formulation. Nevertheless, these modern approaches seem not to get adopted by control engineers in industry.

Attempting to make the \mathcal{H}_∞ paradigm more attractive, some software packages, both commercial and open-source, provide implementations of the required solution algorithms. A well-known example is the so-called Robust Control Toolbox that is integrated in The Mathworks' MATLAB. Although these tools are very useful for users who are familiar with the advanced mathematical background of modern controller synthesis, control engineers in industry are still left with tedious pre- and postprocessing steps. Furthermore, linear parameter-varying (LPV) models currently only have limited support, while the design procedure is almost identical (for the end user). Some effort has already been made to develop a bridging interface that makes the design procedure more intuitive, unifies the syntax for different algorithms, and shields the user from pre- and postprocessing as much as possible [1].

In this work, we present 'LCToolbox', a linear control toolbox for MATLAB, which is based on the work presented at the 36th Benelux Meeting on Systems and Control [2]. In addition to facilitating the issues mentioned earlier, this new toolbox version also aims at supporting the control engineer throughout the entire design procedure from identification up to verification of the results. This is conceptually illustrated in Figure 1 and will be presented through a mechatronic case study. The support for LPV models has been further improved as well.

2 Features of LCToolbox

2.1 Identification

Since an accurate model is required for \mathcal{H}_∞ controller synthesis to reach its full potential, the linear control toolbox interfaces several algorithms helping the user to obtain an LTI or LPV model with the desired accuracy. At this point, the software mainly focuses on frequency domain identification methods. Apart from a model, these methods usually also allow to estimate the uncertainty on the model, which can be exploited in the robust control problem formulation.

2.2 Controller design

In order to define the control topology, the user can simply define signals, connect systems to each other and define performance channels as an input-output relation between signals. The control problem formulation is then easily formulated as a set of objectives and constraints on these (weighted) channels. The toolbox constructs the generalized plant and automatically selects an appropriate (third-party) solver for the problem.

2.3 Simulation

The toolbox environment also supports the user to close a feedback loop with, for example, a nonlinear model or a linear nonparametric (measured) model. As such, it is possible to verify the performance of the controller both in the time domain and in the frequency domain with a more accurate model than the design model.

References

- [1] M. Verbandt, J. Swevers, and G. Pipeleers. "An LTI control toolbox – Simplifying optimal feedback controller design." European Control Conference (ECC) 2016, June 2016, Aalborg, Denmark.
- [2] M. Verbandt, J. Swevers, and G. Pipeleers. "A Linear Control Toolbox - towards simple LPV control." 36th Benelux Meeting on Systems and Control, March 2017, Spa, Belgium.

Acknowledgement This research is partially supported by Flanders Make: SBO ROCSIS: Robust and Optimal Control of Systems of Interacting Subsystems. This work also benefits from KU Leuven-BOF PFV/10/002 Center-of-Excellence Optimization in Engineering (OPTeC), KU Leuven-C14/15/067: B-spline based certificates of positivity with applications in engineering, and the project FWO-G.0915.14 of the Research Foundation Flanders (FWO).

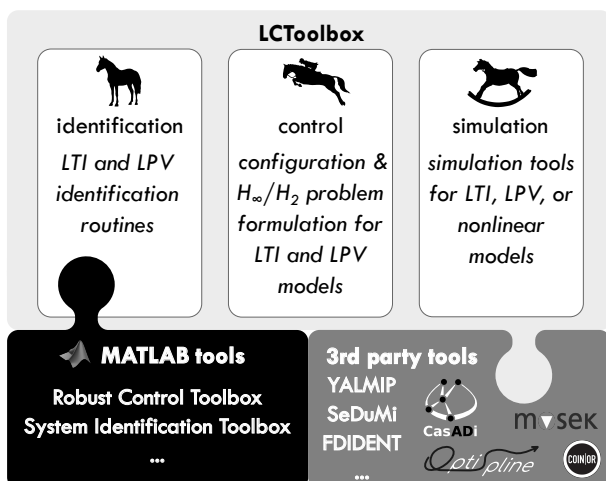


Figure 1: Conceptual overview of the capabilities of LCToolbox and its interface to existing software packages.

Effortless NLP modeling with CasADi's Opti stack

Joris Gillis

MECO Research Team, Department Mechanical Engineering, KU Leuven
DMMS lab, Flanders Make, Leuven, Belgium
joris.gillis@kuleuven.be

1 Introduction

CasADi [1] is an open-source symbolic framework for algorithmic differentiation and numerical optimization, available in C++, Python, MATLAB and Octave. Its scalability, flexibility and efficiency make it an attractive tool for numerically solving nonlinear Optimal Control Problems (OCP).

The software has been used successfully in academia and industry for (a) prototyping formulations [2], (b) building black-box solvers on top of it [3], and (c) teaching [4].

In CasADi, some modeling steps are left to the user so as to offer design freedom that suits use case (b). In this abstract, we present an abstraction layer added in CasADi 3.3 that makes the software easier for use cases (a) and (c).

2 Formulation and solution of an NLP in CasADi

The standard form used for NLP solvers in CasADi reads:¹

$$\begin{aligned} & \underset{x}{\text{minimize}} && f(x, p), \\ & \text{subject to} && \underline{g} \leq g(x, p) \leq \bar{g}, \end{aligned} \quad (1)$$

with decision variables $x \in \mathbb{R}^n$, parameters $p \in \mathbb{R}^q$, objective function $f: \mathbb{R}^n \times \mathbb{R}^q \mapsto \mathbb{R}$ and constraint function $g: \mathbb{R}^n \times \mathbb{R}^q \mapsto \mathbb{R}^m$.

After constructing symbolic primitives, the user declares the vector expressions $x, p, f(x, p), g(x, p), \underline{g}, \bar{g}$, and retrieves a solution vector x^* as numerical vector (a CasADi numeric data-type in fact).

The proposed *Opti stack* abstraction layer offers an alternative that (a) allows natural syntax for constraints, (b) hides the task of indexing/bookkeeping of decision variables, and (c) returns the numerical data-type of the host language.

As a demonstration, we provide a MATLAB implementation of a hanging chain problem, consisting of $N = 25$ point masses on a 2D plane, connected with rigid links of length L , suspended at coordinates $(-2, 1)$ and $(2, 2)$, with an impenetrable curve at the bottom:

```
opti = casadi.Opti()
x = opti.variable(N)
y = opti.variable(N)
```

¹Simple bounds on decision variables omitted for brevity.

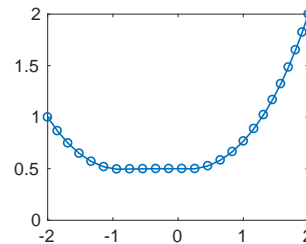


Fig. 1. Hanging chain solution

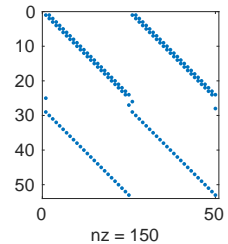


Fig. 2. Sparsity of $\frac{\partial g}{\partial x}$

```
opti.minimize(sum(g*m*y))
opti.subject_to((x(1:N-1)-x(2:N)).^2+...
                (y(1:N-1)-y(2:N)).^2...
                ==L^2)
opti.subject_to([x(1);y(1)]==[-2;1])
opti.subject_to([x(end);y(end)]==[2;2])
opti.subject_to(y>=cos(0.1*x)-0.5)
```

Figure 1 shows the numerical solution, produced with

```
opti.solver('ipopt')
sol = opti.solve()
plot(sol.value(x), sol.value(y), '-o')
```

Introspection of the underlying standard form is possible: Figure 2 shows the sparsity of the constraint Jacobian, produced with

```
spy(sol.value(jacobian(opti.g, opti.x)))
```

Further details can be obtained from opti.casadi.org.


References

- [1] Joel Andersson. *A General-Purpose Software Framework for Dynamic Optimization*. PhD thesis, Arenberg Doctoral School, KU Leuven, Department of Electrical Engineering (ESAT/SCD) and Optimization in Engineering Center, Kasteelpark Arenberg 10, 3001-Heverlee, Belgium, October 2013.
- [2] Sergio Lucia, Joel A E Andersson, Heiko Brandt, Moritz Diehl, and Sebastian Engell. Handling uncertainty in economic nonlinear model predictive control: A comparative case study. *Journal of Process Control*, 24(8):1247–1259, 2014.
- [3] Fredrik Magnusson and Johan Åkesson. Dynamic optimization in jmodelica.org. *Processes*, 3(2):471–496, 2015.
- [4] James B Rawlings, David Q. Mayne, and Moritz M. Diehl. *Model Predictive Control: Theory, Computation and Design*. Nob Hill Publishing, Madison, Wisconsin, 2nd edition, 2017.

Acknowledgement. This work has been carried out within the framework of projects Flanders Make SBO ROCSIS: Robust and Optimal Control of Systems of Interacting Subsystems, Flanders Make ICON: Physical and control co-design of electromechanical drivetrains for machines and vehicles, and KU Leuven-BOF PFV/10/002 Centre of Excellence: Optimization in Engineering (OPTEC). This work also benefits from KUL-C1: KU Leuven Research project C14/15/067: B-spline based certificates of positivity with applications in engineering.

Part 3

Plenary Lectures



Benelux Meeting 2018

NETWORKS OF DISSIPATIVE SYSTEMS

Compositional Certification of Stability, Performance, and Safety

Murat Arcak

Electrical Engineering and Computer Sciences, UC Berkeley

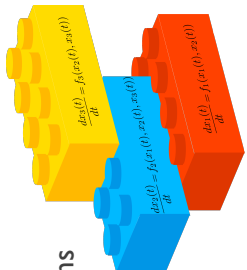
Goal: Design and analysis of networked dynamical systems.

Compositional approach that exploits:

- Dissipativity properties of subsystems
- Special interconnection structures

Outline:

1. Dissipativity for network stability, performance, and safety analysis
2. Searching over dissipativity properties via ADMM
3. Equilibrium-independent dissipativity and case studies
4. Dynamic supply rates and connection to IQC theory



Dissipativity: Basic Definition

The system $u \rightarrow \begin{matrix} \dot{x} = f(x, u) \\ y = h(x, u) \end{matrix} \rightarrow y$ is dissipative with supply rate $s(u, y)$ if there is a storage function $V : \mathcal{X} \rightarrow \mathbb{R}_{\geq 0}$ s.t.

$$V(0) = 0, \quad \nabla V(x)^T f(x, u) \leq s(u, y) \quad \forall x \in \mathcal{X}, u \in \mathcal{U}$$

Examples of quadratic supply rates: $s(u, y) = \begin{bmatrix} u \\ y \end{bmatrix}^T X \begin{bmatrix} u \\ y \end{bmatrix}$

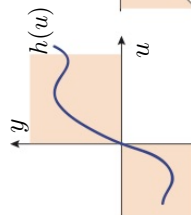
Passivity: $X = \frac{1}{2} \begin{bmatrix} 0 & I \\ I & -\varepsilon I \end{bmatrix} \Rightarrow s(u, y) = u^T y - \varepsilon \|y\|^2, \quad \varepsilon \geq 0$

L₂ gain: $X = \begin{bmatrix} \gamma^2 I & 0 \\ 0 & -I \end{bmatrix} \Rightarrow s(u, y) = \gamma^2 \|u\|^2 - \|y\|^2$

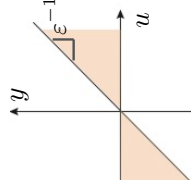
Dissipativity: Basic Definition

A static system $y = h(u)$ is dissipative with supply rate $s(u, y)$ if $s(u, h(u)) \geq 0 \quad \forall u.$

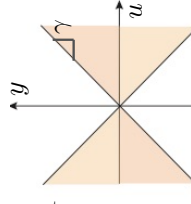
A quadratic supply rate restricts $y = h(u)$ to the conic sector



$$X = \begin{bmatrix} 0 & 1 \\ 1 & 0 \end{bmatrix}$$

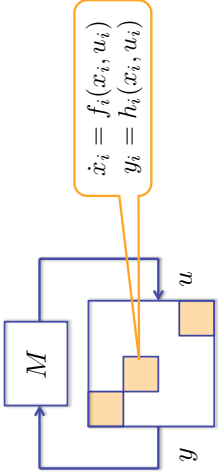


$$X = \begin{bmatrix} 0 & 1 \\ 1 & -\varepsilon \end{bmatrix}$$



$$X = \begin{bmatrix} \gamma^2 & 0 \\ 0 & -1 \end{bmatrix}$$

Verifying Network Stability from Subsystem Dissipativity



If the subsystems are dissipative w/ supply rate $\begin{bmatrix} u_i \\ y_i \end{bmatrix}^T X_i \begin{bmatrix} u_i \\ y_i \end{bmatrix}$ and positive definite V_i , then $\sum_{i=1}^N p_i V_i$ is a Lyapunov function provided $p_i > 0, i = 1, \dots, N, \begin{bmatrix} M \\ I \end{bmatrix}^T S^T \begin{bmatrix} p_1 X_1 \dots p_N X_N \end{bmatrix} S \begin{bmatrix} M \\ I \end{bmatrix} \leq 0$ where S is s.t. $S \begin{bmatrix} u_1 \dots u_N \\ y_1 \dots y_N \end{bmatrix}^T = \begin{bmatrix} u_1 \\ y_1 \end{bmatrix} \dots \begin{bmatrix} u_N \\ y_N \end{bmatrix}^T$.

Proof:

$$\begin{aligned}
 V(x) &= \sum_{i=1}^N p_i V_i(x_i) \\
 \dot{V}(x) &\leq \sum_{i=1}^N \begin{bmatrix} u_i \\ y_i \end{bmatrix}^T p_i X_i \begin{bmatrix} u_i \\ y_i \end{bmatrix} \\
 &= \begin{bmatrix} u_1 \\ y_1 \\ \vdots \\ u_N \\ y_N \end{bmatrix}^T \begin{bmatrix} p_1 X_1 & & & \\ & \ddots & & \\ & & p_N X_N & \\ & & & S \end{bmatrix} \begin{bmatrix} u \\ y \end{bmatrix} \\
 &= y^T \begin{bmatrix} M \\ I \end{bmatrix}^T S^T \begin{bmatrix} p_1 X_1 & & & \\ & \ddots & & \\ & & p_N X_N & \\ & & & S \end{bmatrix} \begin{bmatrix} M \\ I \end{bmatrix} y \leq 0
 \end{aligned}$$

Special Cases

Small-gain: Suppose each subsystem is dissipative with respect to the L_2 gain supply rate

$$X_i = \begin{bmatrix} \gamma_i^2 I & 0 \\ 0 & -I \end{bmatrix}$$

Then $\begin{bmatrix} M \\ I \end{bmatrix}^T S^T \begin{bmatrix} p_1 X_1 & & & \\ & \ddots & & \\ & & p_N X_N & \\ & & & S \end{bmatrix} S \begin{bmatrix} M \\ I \end{bmatrix} \leq 0$

can be rewritten as

$$(\Gamma M)^T P(\Gamma M) - P \leq 0$$

where $\Gamma = \text{diag}(\gamma_1, \dots, \gamma_N), P = \text{diag}(p_1, \dots, p_N)$.

Example: for a feedback interconnection of two subsystems

$$M = \begin{bmatrix} 0 & \pm 1 \\ 1 & 0 \end{bmatrix} \exists p_1, p_2 > 0 \text{ satisfying the above iff } \gamma_1 \gamma_2 \leq 1$$

Special Cases

Passivity: Suppose each subsystem is dissipative with respect to

$$X_i = \frac{1}{2} \begin{bmatrix} 0 & I \\ I & -\varepsilon_i I \end{bmatrix}, \varepsilon_i \geq 0$$

Then $\begin{bmatrix} M \\ I \end{bmatrix}^T S^T \begin{bmatrix} p_1 X_1 & & & \\ & \ddots & & \\ & & p_N X_N & \\ & & & S \end{bmatrix} S \begin{bmatrix} M \\ I \end{bmatrix} \leq 0$

can be rewritten as

$$P(M - E) + (M - E)^T P \leq 0$$

where $E = \text{diag}(\varepsilon_1, \dots, \varepsilon_N), P = \text{diag}(p_1, \dots, p_N)$.

Note: this inequality is satisfied with $P = I$ if $M + M^T = 0$

e.g., the negative feedback interconnection $M = \begin{bmatrix} 0 & -1 \\ 1 & 0 \end{bmatrix}$

Application to Internet Congestion Control

Decentralized resource allocation via passivity (Wen-Arcak, 2004)

User Control

Link Control

Routing Matrix: $R_{li} = \begin{cases} 1 & \text{if } i \text{ uses } l \\ 0 & \text{otherwise} \end{cases}$

$M = \begin{bmatrix} 0 & -R^T \\ R & 0 \end{bmatrix}$

Application to Multi-Agent Robotic Systems

Main Idea: Passivity is intrinsic to Euler-Lagrange systems. We exploit this property for coordinating teams of such systems.

$M = \begin{bmatrix} 0 & -E \\ E^T & 0 \end{bmatrix} \Rightarrow M + M^T = 0$

Application to Multi-Agent Robotic Systems

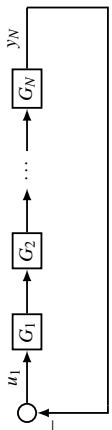
This idea enabled systematic robust and adaptive designs that exploit passivity for motion coordination problems.

UAVs cooperatively carrying a suspended load – collaborative project with Center for Autonomous Marine Operations and Systems (AMOS), Norwegian Univ. of Science and Tech.

Application to Multi-Agent Robotic Systems

Courtesy of Kristian Klausen, Autonomous Marine Operations and Systems (AMOS), Norwegian Univ. of Science and Tech.

Cyclic Interconnection Structure



$$M = \begin{bmatrix} 0 & \dots & 0 & \delta_1 \\ \delta_2 & 0 & \dots & 0 \\ \vdots & \ddots & \ddots & \vdots \\ 0 & \dots & \delta_N & 0 \end{bmatrix} \quad \prod_{i=1}^N \delta_i = -1$$

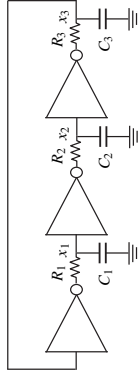
Arcak and Sontag, 2006:

There exists $P = \text{diag}(p_1, \dots, p_N) > 0$ satisfying

$$P(M - E) + (M - E)^T P \leq 0$$

if and only if $(\epsilon_1 \dots \epsilon_N)^{-1} \leq \sec(\pi/N)^N$ (Secant Criterion)

Example: Three-stage Ring Oscillator



Decompose into subsystems:

$$\begin{aligned} \tau_1 \frac{dx_1(t)}{dt} &= -x_1(t) - h_3(x_3(t)) \\ \tau_2 \frac{dx_2(t)}{dt} &= -x_2(t) - h_1(x_1(t)) \\ \tau_3 \frac{dx_3(t)}{dt} &= -x_3(t) - h_2(x_2(t)) \\ \tau_i &= R_i C_i, h_i(x) = \alpha_i \tanh(\beta_i x) \end{aligned}$$

$$\begin{aligned} \frac{dx_i(t)}{dt} &= -x_i(t) + u_i \\ y_i(t) &= h_i(x_i(t)) \end{aligned}$$

$i = 1, 2, 3$, interconnected via:

$$\begin{bmatrix} u_1 \\ u_2 \\ u_3 \end{bmatrix} = \begin{bmatrix} 0 & 0 & -1 \\ -1 & 0 & 0 \\ 0 & -1 & 0 \end{bmatrix} \begin{bmatrix} y_1 \\ y_2 \\ y_3 \end{bmatrix}$$

Each subsystem is passive with $\epsilon_i^{-1} = \alpha_i \beta_i$ and storage function

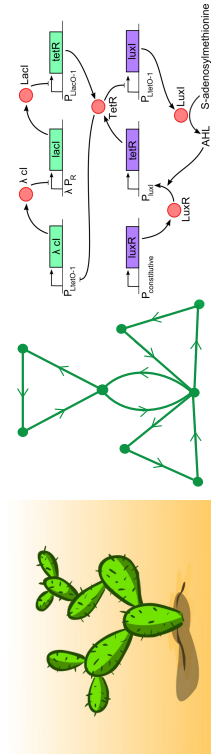
$$\int_0^{x_i} h_i(x) dx.$$

If $\alpha_1 \beta_1 \alpha_2 \beta_2 \alpha_3 \beta_3 \leq \sec(\pi/3)^3 = 8$ then $\exists p_i > 0, i = 1, 2, 3$ s.t.

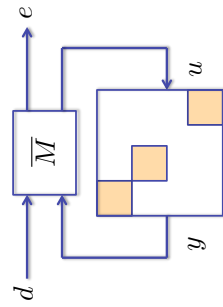
$$V(x_1, x_2, x_3) = \sum_{i=1}^3 p_i \int_0^{x_i} h_i(x) dx$$

is a Lyapunov function that certifies global stability of the origin.

Secant Condition extended to "Cactus Graphs" in (Arcak, 2011)



From Stability to Performance Certification



Verify dissipativity with respect to

$$s(d, e) = \begin{bmatrix} d \\ e \end{bmatrix}^T W \begin{bmatrix} d \\ e \end{bmatrix}$$

where W specifies a performance objective, e.g. L_2 gain from d to e .

Modify the stability test as:

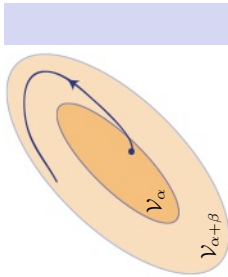
$$\begin{bmatrix} M \\ I \end{bmatrix}^T \bar{S}^T \begin{bmatrix} -W \\ I \end{bmatrix} p_1 X_1 \dots p_N X_N \bar{S} \begin{bmatrix} M \\ I \end{bmatrix} \leq 0$$

where \bar{S} is s.t. $\bar{S} [e u_1 \dots u_N d y_1 \dots y_N]^T = [d e u_1 y_1 \dots u_N y_N]^T$.

Then $\sum_i p_i V_i$ is a storage function for the interconnection.

Safety under Finite Energy Disturbances

If we can verify dissipativity w/ $s(d, e) = |d|^2$ and $\|d\|_2^2 \leq \beta$, then $\frac{d}{dt} V(x(t)) \leq |d(t)|^2 \Rightarrow V(x(T)) - V(x(0)) \leq \beta \forall T \geq 0$. Thus, $x(t)$ starting in $\mathcal{V}_\alpha = \{x : V(x) \leq \alpha\}$ remains in $\mathcal{V}_{\alpha+\beta}$.



Meissen, Arcak, Packard, 2016:

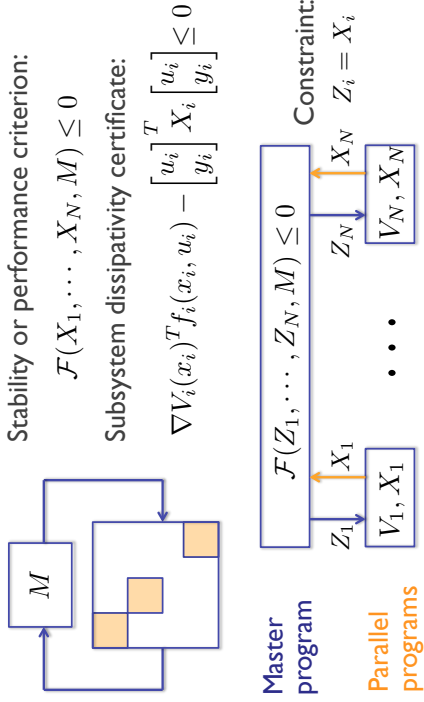
For a polynomial storage function and unsafe set \mathcal{U} described by polynomial inequalities, the disjunction of \mathcal{U} and $\mathcal{V}_{\alpha+\beta}$ can be checked with a sum-of-squares program.

\mathcal{U} : unsafe set

Coogan & Arcak, 2015: $\|d\|_\infty$ bound

Search for Compatible Dissipativity Properties

(Meissen, Lessard, Arcak, Packard, 2015)



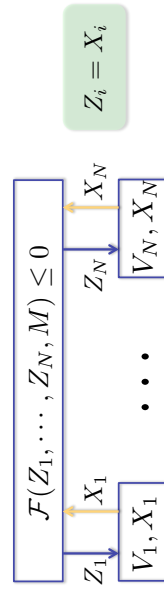
Distributed Optimization Formulation

$$\min_{x,z} d(x) + g(z)$$

$$s.t. Ax + Bz = c$$

$$z = (Z_1, \dots, Z_N)$$

$$g(z) = \begin{cases} 0 & \text{if } \mathcal{F}(Z_1, \dots, Z_N, M) \leq 0 \\ \infty & \text{otherwise} \end{cases}$$



$$d(x) = d_1(x_1) + \dots + d_N(x_N) \quad x = (V_1, X_1, \dots, V_N, X_N)$$

$$d_i(x_i) = \begin{cases} 0 & \text{if } \nabla V_i(x_i)^T f_i(x_i, u_i) - \begin{bmatrix} u_i \\ X_i \end{bmatrix}^T \begin{bmatrix} u_i \\ y_i \end{bmatrix} \leq 0 \\ \infty & \text{otherwise} \end{cases}$$

ADMM Algorithm

$$\min_{x,z} d(x) + g(z)$$

$$s.t. Ax + Bz = c$$

$$x^{k+1} = \arg \min_x d(x) + \rho \|Ax + Bz^k - c + u^k\|^2$$

$$z^{k+1} = \arg \min_z g(z) + \rho \|Ax^{k+1} + Bz - c + u^k\|^2$$

$$u^{k+1} = Ax^{k+1} + Bz^{k+1} - c + u^k$$

Adapting to our problem:

$$X_i^{k+1} = \arg \min_{\{X: d_i(X)=0\}} \|X - Z_i^k + U_i^k\|_F^2$$

$$Z_{1:N}^{k+1} = \arg \min_{\{Z_{1:N}: g(Z)=0\}} \sum_i \|X_i^{k+1} - Z_i + U_i^k\|_F^2$$

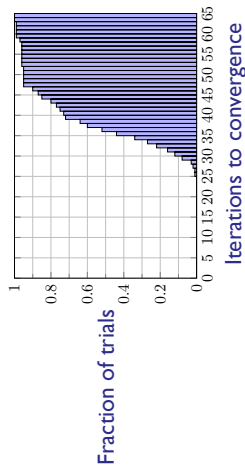
$$U_i^{k+1} = X_i^{k+1} - Z_i^{k+1} + U_i^k$$

Example: Randomly generated 100 interconnection matrices s.t. $M + M^T = 0$ for 50 subsystems

$$\dot{x}_i = \begin{bmatrix} -\epsilon_i & 1 \\ -1 & -\epsilon_i \end{bmatrix} x_i + \begin{bmatrix} 0 \\ 1 \end{bmatrix} u_i \quad i = 1, \dots, 50$$

$$y_i = \begin{bmatrix} 0 & 1 \end{bmatrix} x_i$$

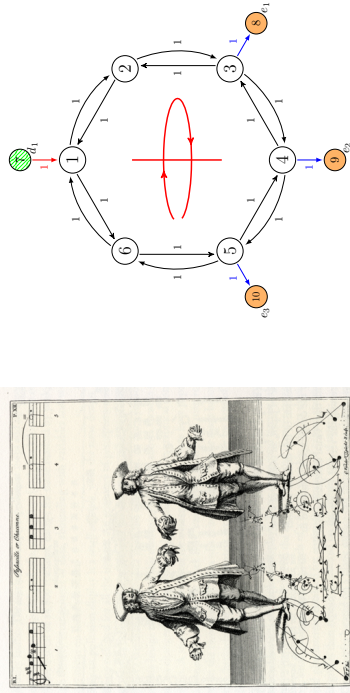
ADMM found $X_i = \begin{bmatrix} 0 & 1 \\ 1 & 0 \end{bmatrix}$ (passivity) as a feasible solution:



Symmetry Reduction

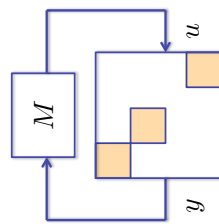
(Ferreira, Meissen, Arcak, Packard, 2018)

Exploit interconnection symmetries to reduce the dimension of stability and performance verification problems.



K. Tomlinson, *The Art of Dancing*, 1735

Symmetry Reduction for Stability Analysis



If R is a permutation matrix such that $RM = MR$ then permuting the subsystems wrto R does not change the interconnection:

$$\tilde{u} = Ru, \tilde{y} = Ry \Rightarrow \tilde{u} = M\tilde{y}$$

The set of all such permutations partitions the subsystems into equivalence classes. If the linear matrix inequality for stability:

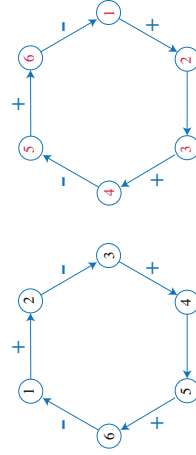
$$\begin{bmatrix} M \\ I \end{bmatrix}^T \Pi^T \begin{bmatrix} X_1 & & \\ & \ddots & \\ & & X_N \end{bmatrix} \Pi \begin{bmatrix} M \\ I \end{bmatrix} \leq 0$$

is feasible, then it is also feasible with identical X_i in each class.

Symmetry Reduction for Stability Analysis

This suggests searching for one common supply rate for subsystems in the same equivalence class, thus reducing the problem dimension.

Example:

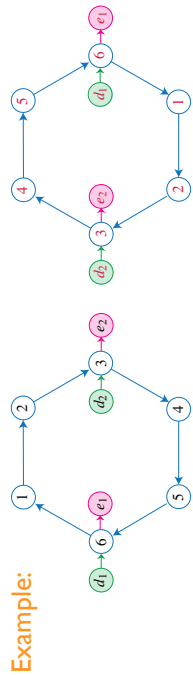


Interconnection unchanged when indices rotated by two nodes. Therefore nodes $\{1, 3, 5\}$ and $\{2, 4, 6\}$ form equivalence classes.

Symmetry Reduction for Performance Analysis

Look for simultaneous permutations (R, R_d, R_e) of nodes, disturbance inputs, and performance outputs, s.t.

$$\bar{M} \begin{bmatrix} R & 0 \\ 0 & R_d \end{bmatrix} = \begin{bmatrix} R & 0 \\ 0 & R_e \end{bmatrix} \bar{M}$$



Interconnection unchanged when nodes rotated by three while, simultaneously, inputs d_1, d_2 and outputs e_1, e_2 are swapped.

Symmetry Reduction for Performance Analysis

The set of all such permutations R partitions the subsystems into equivalence classes, e.g. $\{1,4\}, \{2,5\}, \{3,6\}$ in previous example.

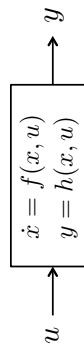
If the performance supply rate $\begin{bmatrix} d \\ e \end{bmatrix}^T W \begin{bmatrix} d \\ e \end{bmatrix}$ is invariant under (R_d, R_e) , e.g., $\gamma_1^2 d_1^2 + \gamma_2^2 d_2^2 - e_1^2 - e_2^2$, $\gamma_1 = \gamma_2$ in the example, and the matrix inequality for performance

$$\begin{bmatrix} \bar{M} \\ I \end{bmatrix}^T \bar{S}^T \begin{bmatrix} -W & \\ & X_1 \dots X_N \end{bmatrix} \bar{S} \begin{bmatrix} \bar{M} \\ I \end{bmatrix} \leq 0$$

is feasible, then it is also feasible with identical X_i in each class. Thus, we may reduce the decision variables to one per class rather than one per each subsystem.

Equilibrium Independent Dissipativity (EID)

Dissipativity with respect to any point \bar{x} that has the potential to become an equilibrium in an interconnection, rather than a specific equilibrium x^* .



Suppose, for all $\bar{x} \in \bar{\mathcal{X}} \subset \mathcal{X}$ there is unique \bar{u} s.t. $f(\bar{x}, \bar{u}) = 0$. We call the system EID if a storage function $V : \mathcal{X} \times \bar{\mathcal{X}} \mapsto \mathbb{R}_{\geq 0}$ can be found such that, for all $x \in \mathcal{X}, \bar{x} \in \bar{\mathcal{X}}, u \in \mathcal{U}$,

$$V(\bar{x}, \bar{x}) = 0, \quad \nabla_x V(x, \bar{x})^T f(x, u) \leq s(u - \bar{u}, y - \bar{y}).$$

Equilibrium Independent Dissipativity (EID)

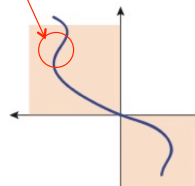
A static system $y = h(u)$ is EID with supply rate $s(u, y)$ if

$$s(u - \bar{u}, h(u) - h(\bar{u})) \geq 0 \quad \forall u, \bar{u}$$

e.g., equilibrium independent passivity (EIP) means that $h(\cdot)$ is increasing:

$$(u - \bar{u})(h(u) - h(\bar{u})) \geq 0 \quad \forall u, \bar{u}.$$

Example: static system below is passive but not EIP



Equilibrium Independent Dissipativity (EID)

Example: $\dot{x} = u, y = x, x \in \mathcal{X} = \mathbb{R}^n$ is EIP.

For every $\bar{x} \in \bar{\mathcal{X}} = \mathbb{R}^n, \bar{u} = 0$ is unique solution to $f(\bar{x}, \bar{u}) = 0$

$$V(x, \bar{x}) = \frac{1}{2} \|x - \bar{x}\|^2 \Rightarrow \nabla_x V(x, \bar{x})^T u \leq (y - \bar{y})^T (u - \bar{u})$$

Example: $\dot{x} = u, y = h(x), x \in \mathcal{X} = \mathbb{R}$ is EIP when $h(\cdot)$ is increasing. To see this let

$$V(x, \bar{x}) = \int_{\bar{x}}^x (h(s) - h(\bar{x})) ds$$

and note that

$$\begin{aligned} \nabla_x V(x, \bar{x}) f(x, u) &= (h(x) - h(\bar{x}))u \\ &= (y - \bar{y})u \\ &= (y - \bar{y})(u - \bar{u}) \end{aligned}$$

Equilibrium Independent Dissipativity (EID)

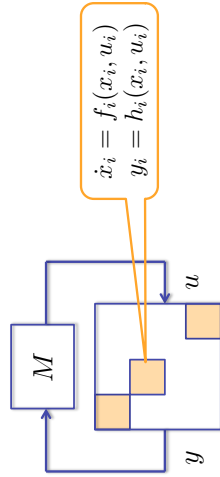
Example: $\dot{x} = f(x) + g(x)u, y = h(x), x \in \mathcal{X} = \mathbb{R}$ is EIP if

- 1) $g(x) > 0 \quad \forall x$
- 2) h is increasing
- 3) $\phi := \frac{f}{g} + \varepsilon h$ is decreasing.

Proof:
$$V(x, \bar{x}) = \int_{\bar{x}}^x \frac{h(s) - h(\bar{x})}{g(s)} ds$$

$$\begin{aligned} \nabla_x V(x, \bar{x}) f(x, u) &= \frac{h(x) - h(\bar{x})}{g(x)} (f(x) + g(x)u) \\ &= (y - \bar{y}) \left(\frac{f(x)}{g(x)} + u - \frac{f(\bar{x})}{g(\bar{x})} - \bar{u} \right) \\ &= \underbrace{(y - \bar{y}) (\phi(x) - \phi(\bar{x}))}_{\leq 0 \text{ by 2,3}} + u - \bar{u} - \varepsilon(y - \bar{y}) \end{aligned}$$

Equilibrium Independent Stability Test



Suppose the interconnection admits an equilibrium x^* and each subsystem is EID with quadratic supply rate defined by X_i and storage function $V_i(x_i, \bar{x}_i) > 0, \forall x_i \neq \bar{x}_i$. The interconnection is stable with Lyapunov function $V = \sum p_i V_i(x_i, x_i^*)$ if $p_i > 0$ and

$$\begin{bmatrix} M \\ I \end{bmatrix}^T \Pi^T \begin{bmatrix} p_1 X_1 & & \\ & \ddots & \\ & & p_N X_N \end{bmatrix} \Pi \begin{bmatrix} M \\ I \end{bmatrix} \leq 0$$

Case Study I: Population Dynamics

Lotka-Volterra-type model for interacting species $i = 1, 2, \dots, N$

$$\dot{x}_i(t) = \left(\lambda_i - \gamma_i x_i(t) + \underbrace{\sum_{j \neq i} m_{ij} x_j(t)}_{=: u_i} \right) x_i(t)$$

- 1) $g_i(x_i) = x_i > 0$ in the positive orthant
- 2) $y_i = h_i(x_i) = x_i$ is increasing
- 3) $f_i(x_i) = (\lambda_i - \gamma_i x_i)x_i, \gamma_i > 0$, therefore $\phi_i(x_i) = \frac{f_i(x_i)}{g_i(x_i)} + \varepsilon h_i(x_i) = \lambda_i - \gamma_i x_i + \varepsilon_i x_i$ is decreasing up to $\varepsilon_i = \gamma_i$.

Case Study 1: Population Dynamics

Therefore, subsystems are EIP with $\varepsilon_i = \gamma_i$ and storage function

$$\begin{aligned} V_i(x_i, \bar{x}_i) &= \int_{\bar{x}_i}^{x_i} \frac{h_i(s) - h_i(\bar{x}_i)}{g_i(s)} ds = \int_{\bar{x}_i}^{x_i} \frac{s - \bar{x}_i}{s} ds \\ &= x_i - \bar{x}_i - \bar{x}_i \ln \left(\frac{x_i}{\bar{x}_i} \right) \end{aligned}$$

If an equilibrium x^* exists and $\exists p_i > 0, i = 1, \dots, N$ such that

$$P(M - E) + (M - E)^T P \leq 0$$

where $E = \text{diag}(\varepsilon_1, \dots, \varepsilon_N), P = \text{diag}(p_1, \dots, p_N)$ then stability is guaranteed with Lyapunov function:

$$V(x) = \sum_{i=1}^N p_i \left\{ x_i - x_i^* - x_i^* \ln \left(\frac{x_i}{x_i^*} \right) \right\}.$$

Case Study 1: Population Dynamics

Example: $m_{12}m_{21} < 0$ (predator-prey)

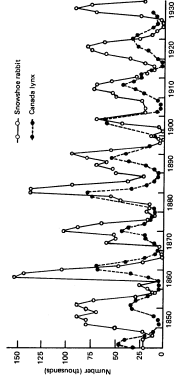
$$P = \begin{bmatrix} |m_{21}| & 0 \\ 0 & |m_{12}| \end{bmatrix} \text{ satisfies } P(M - E) + (M - E)^T P \leq 0$$

In the classical predator-prey model $\gamma_i = 0, i = 1, 2 \Rightarrow E = 0$

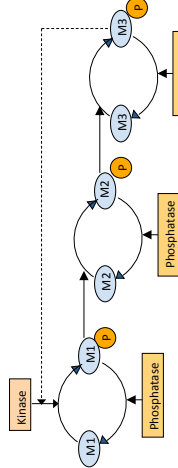
$$P(M - E) + (M - E)^T P = 0$$

and contours of V below define periodic orbits:

$$V(x) = \sum_{i=1}^2 p_i \left\{ x_i - x_i^* - x_i^* \ln \left(\frac{x_i}{x_i^*} \right) \right\}$$



Case Study 2: Cyclic Reaction Network



$$\begin{aligned} \frac{dx_1(t)}{dt} &= -\frac{b_1 x_1(t)}{c_1 + x_1(t)} + \frac{d_1(1 - x_1(t))}{e_1 + (1 - x_1(t))} - \frac{\mu}{1 + kx_3(t)} \\ \frac{dx_2(t)}{dt} &= \frac{b_2 x_2(t)}{c_2 + x_2(t)} - \frac{d_2(1 - x_2(t))}{e_2 + (1 - x_2(t))} - x_1(t) \\ \frac{dx_3(t)}{dt} &= -\frac{b_3 x_3(t)}{c_3 + x_3(t)} + \frac{d_3(1 - x_3(t))}{e_3 + (1 - x_3(t))} - x_2(t) \end{aligned}$$

$x_i \in [0, 1]$: concentration of phosphorylated signaling protein

$1 - x_i$: concentration of inactive form, total normalized to 1

Case Study 2: Cyclic Reaction Network

Subsystems: $\dot{x}_i(t) = f_i(x_i(t)) + g_i(x_i(t))u_i(t), y_i(t) = h_i(x_i(t))$

$$f_i(x_i) = -\frac{b_i x_i}{c_i + x_i} \quad g_i(x_i) = \frac{d_i(1 - x_i)}{e_i + (1 - x_i)}$$

$$h_i(x_i) = x_i \quad i = 1, 2, \quad h_3(x_3) = -\frac{\mu}{1 + kx_3}$$

Estimate the largest $\varepsilon_i > 0$ such that $\phi_i := \frac{f_i}{g_i} + \varepsilon_i h_i$ is decreasing and recall from the secant criterion that

$$P(M - E) + (M - E)^T P \leq 0$$

is feasible with diagonal $P > 0$ iff $(\varepsilon_1 \dots \varepsilon_N)^{-1} \leq 8$. Then,

$$V(x) = p_1 \int_{x_1^*}^{x_1} \frac{s - x_1^*}{g_1(s)} ds + p_2 \int_{x_2^*}^{x_2} \frac{s - x_2^*}{g_2(s)} ds + p_3 \int_{x_3^*}^{x_3} \frac{h_3(s) - h_3(x_3^*)}{g_3(s)} ds$$

Case Study 3: Vehicle Platoon

Velocities and positions of vehicles $i = 1, \dots, N$ governed by:

$$\begin{aligned} \dot{v}_i(t) &= -v_i(t) + v_i^0 + u_i(t) \\ \dot{x}_i(t) &= v_i(t) \end{aligned}$$

Introduce undirected graph s.t. vertices i and j are connected with an edge if i and j have access to relative position $x_i - x_j$. Select one end of edge to be head, the other to be the tail, and define the *incidence matrix*:

$$D_{il} = \begin{cases} 1 & \text{if vertex } i \text{ is the head of edge } l \\ -1 & \text{if vertex } i \text{ is the tail of edge } l \\ 0 & \text{otherwise} \end{cases}$$

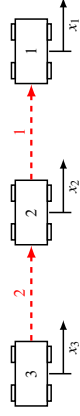
Then the vector of relative positions is given by $z = D^T x$

Case Study 3: Vehicle Platoon

Coordination feedback: $u = -D \begin{bmatrix} h_1(z_1) \\ \vdots \\ h_L(z_L) \end{bmatrix}$ $L : \# \text{ of edges}$

$h_\ell : \mathbb{R} \mapsto \mathbb{R}, \ell = 1, \dots, L$ onto and increasing functions (virtual spring forces)

Example:



$$D = \begin{bmatrix} 1 & 0 \\ -1 & 1 \\ 0 & -1 \end{bmatrix} \Rightarrow \begin{bmatrix} z_1 \\ z_2 \end{bmatrix} = D^T x = \begin{bmatrix} x_1 - x_2 \\ x_2 - x_3 \end{bmatrix}$$

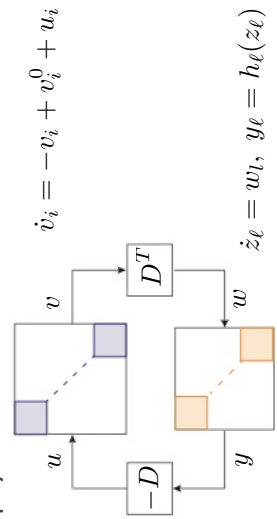
$$u_1 = -h_1(z_1) \quad u_2 = h_1(z_1) - h_2(z_2) \quad u_3 = h_2(z_2)$$

Case Study 3: Vehicle Platoon

Relative position subsystems $\ell = 1, \dots, L$ with inputs w_ℓ and outputs y_ℓ defined as:

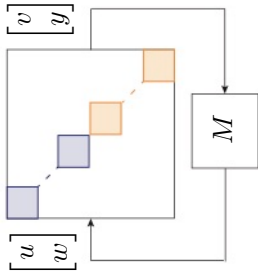
$$\dot{z}(t) = D^T v(t) =: w(t) \quad y(t) := \begin{bmatrix} h_1(z_1(t)) \\ \vdots \\ h_L(z_L(t)) \end{bmatrix}$$

Then the closed loop system is:



Case Study 3: Vehicle Platoon

or, equivalently:



where $M = \begin{bmatrix} 0 & -D \\ D^T & 0 \end{bmatrix}$ is skew symmetric.

Thus, if an equilibrium (v^*, z^*) exists, its stability follows from the equilibrium independent passivity (EIP) of the subsystems:

$$\begin{aligned} \dot{v}_i &= -v_i + v_i^0 + u_i, \quad i = 1, \dots, N \\ \dot{z}_\ell &= w_\ell, \quad y_\ell = h_\ell(z_\ell), \quad \ell = 1, \dots, L \end{aligned}$$

Case Study 3: Vehicle Platoon

Recall: $\dot{x} = f(x) + g(x)u, y = h(x), x \in \mathcal{X} = \mathbb{R}$ is EIP if

- 1) $g(x) > 0 \quad \forall x$
 - 2) h is increasing
 - 3) $\phi := \frac{f}{g} + \varepsilon h$ is decreasing.
- Thus, $\dot{v}_i = -v_i + v_i^0 + u_i, i = 1, \dots, N$ EIP with $\varepsilon_i = 1$
 $\dot{z}_\ell = w_\ell, y_\ell = h_\ell(z_\ell), \ell = 1, \dots, L$ EIP with $\varepsilon_\ell = 0$

$E \geq 0$ and skew-symmetry of M imply the following with $P = I$

$$P(M - E) + (M - E)^T P \leq 0$$

Lyapunov function:

$$V = \frac{1}{2} \sum_i v_i^2 + \sum_\ell \int_{z_\ell^*}^{z_\ell} (h_\ell(s) - h_\ell(z_\ell^*)) ds$$

Case Study 3: Vehicle Platoon

Existence of equilibrium:

$$0 = -v^* + v^0 - D \begin{bmatrix} h_1(z_1^*) \\ \vdots \\ h_L(z_L^*) \end{bmatrix} \tag{1}$$

$$0 = D^T v^* \tag{2}$$

For a connected graph $D^T v^* = 0 \Rightarrow v^* = \alpha \mathbf{1}$
 Substitute in (1) and multiply from the left by $\mathbf{1}^T$:

$$-\alpha \mathbf{1}^T \mathbf{1} + \mathbf{1}^T v^0 = -\alpha N + \sum_i v_i^0 = 0 \Rightarrow \alpha = \frac{1}{N} \sum_i v_i^0$$

Then (1) becomes:

$$-\frac{1}{N} \sum_i v_i^0 + v_i^0 - \sum_{\ell=1}^L D_{i\ell} h_\ell(z_\ell^*) = 0, i = 1, \dots, N$$

from which one can solve for $h_\ell(z_\ell^*)$, and thus for z_ℓ^* .

Case Study 3: Vehicle Platoon

Recall: $\dot{x} = f(x) + g(x)u, y = h(x), x \in \mathcal{X} = \mathbb{R}$ is EIP if

- 1) $g(x) > 0 \quad \forall x$
 - 2) h is increasing
 - 3) $\phi := \frac{f}{g} + \varepsilon h$ is decreasing.
- Thus, $\dot{v}_i = -v_i + v_i^0 + u_i, i = 1, \dots, N$ EIP with $\varepsilon_i = 1$
 $\dot{z}_\ell = w_\ell, y_\ell = h_\ell(z_\ell), \ell = 1, \dots, L$ EIP with $\varepsilon_\ell = 0$

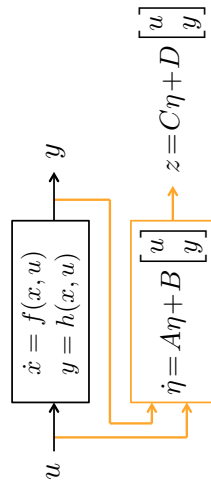
$E \geq 0$ and skew-symmetry of M imply the following with $P = I$

$$P(M - E) + (M - E)^T P \leq 0$$

Lyapunov function:

$$V = \frac{1}{2} \sum_i v_i^2 + \sum_\ell \int_{z_\ell^*}^{z_\ell} (h_\ell(s) - h_\ell(z_\ell^*)) ds$$

Dissipativity with Dynamic Supply Rates



Modify the dissipation inequality as:

$$\nabla_x V(x, \eta)^T f(x, u) + \nabla_\eta V(x, \eta)^T (A\eta + B \begin{bmatrix} u \\ y \end{bmatrix}) \leq z^T X z$$

Static supply rates recovered as special case with $C = 0, D = I$.

Dynamic supply rates capture more detailed I/O information.

Example:

$$\dot{x}_1(t) = x_2(t)$$

$$\dot{x}_2(t) = -x_1(t) - kx_2(t) + u(t)$$

$$y(t) = x_1(t) + x_2(t)$$

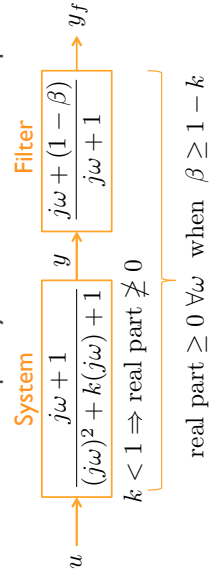
Not passive when $k < 1$. Augmenting the system with "filter"

$$\dot{\eta}(t) = -\eta(t) + y(t)$$

$$y_f(t) = -\beta\eta(t) + y(t)$$

we can show passivity from u to y_f for $\beta \geq 1 - k$.

Choice of filter via frequency domain condition for passivity:



real part $\geq 0 \quad \forall \omega$ when $\beta \geq 1 - k$

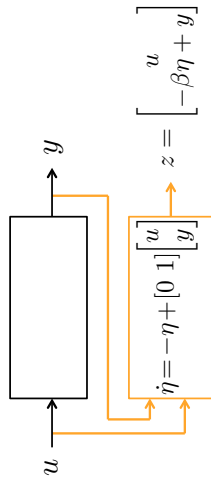
Thus, we conclude dissipativity of the system

$$\begin{aligned} \dot{x}_1(t) &= x_2(t) \\ \dot{x}_2(t) &= -x_1(t) - kx_2(t) + u(t) \\ y(t) &= x_1(t) + x_2(t) \end{aligned}$$

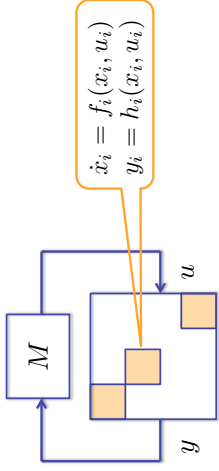
with the dynamic supply rate

$$z^T \begin{bmatrix} 0 & 1/2 \\ 1/2 & 0 \end{bmatrix} z$$

where z is as below and $\beta \geq 1 - k$



Network Stability Test



Suppose each subsystem is dissipative with positive definite storage function $V_i(\cdot, \cdot)$ and dynamic supply rate $z_i^T X_i z_i$.

Search for $p_i > 0, Q \geq 0$ in the candidate Lyapunov function

$$V(x, \eta) = p_1 V_1(x_1, \eta_1) + \dots + p_N V_N(x_N, \eta_N) + \eta^T Q \eta$$

where η is the concatenation of the filter states η_i .

Network Stability Test

$$\begin{aligned} \dot{\eta}(t) &= A\eta(t) + BS \begin{bmatrix} u(t) \\ y(t) \end{bmatrix} = A\eta(t) + BS \begin{bmatrix} M \\ I \end{bmatrix} y(t) \\ z(t) &= C\eta(t) + DS \begin{bmatrix} u(t) \\ y(t) \end{bmatrix} = C\eta(t) + DS \begin{bmatrix} M \\ I \end{bmatrix} y(t) \end{aligned}$$

where S is a permutation matrix defined by:

$$S[u_1 \dots u_N \ y_1 \dots y_N]^T = [u_1 \ y_1 \dots u_N \ y_N]^T$$

The derivative of

$$V(x, \eta) = p_1 V_1(x_1, \eta_1) + \dots + p_N V_N(x_N, \eta_N) + \eta^T Q \eta$$

along system trajectories bounded by

$$\begin{bmatrix} z_1 \\ \vdots \\ z_N \end{bmatrix}^T \begin{bmatrix} p_1 X_1 & & & \\ & \ddots & & \\ & & p_N X_N & \\ & & & 0 \end{bmatrix} \begin{bmatrix} z_1 \\ \vdots \\ z_N \end{bmatrix} + \begin{bmatrix} \eta \\ y \end{bmatrix}^T \begin{bmatrix} A^T Q + QA & QBS \\ [M]^T & [I] \end{bmatrix} \begin{bmatrix} \eta \\ y \end{bmatrix}$$

Network Stability Test

$$\text{Substitute } z = C\eta + DS \begin{bmatrix} M \\ I \end{bmatrix} y$$

$$\begin{bmatrix} z_1 \\ \vdots \\ z_N \end{bmatrix}^T \begin{bmatrix} p_1 X_1 & & & \\ & \ddots & & \\ & & p_N X_N & \\ & & & 0 \end{bmatrix} \begin{bmatrix} z_1 \\ \vdots \\ z_N \end{bmatrix} + \begin{bmatrix} \eta \\ y \end{bmatrix}^T \begin{bmatrix} A^T Q + QA & QBS \\ [M]^T & [I] \end{bmatrix} \begin{bmatrix} \eta \\ y \end{bmatrix}$$

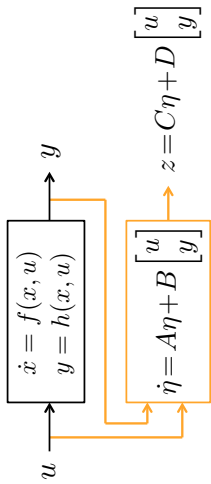
Stability Test: If there exist $p_i > 0, Q \geq 0$ such that

$$\begin{bmatrix} A^T Q + QA & QBS \\ [M]^T & [I] \end{bmatrix}^T \begin{bmatrix} p_1 X_1 & & & \\ & \ddots & & \\ & & p_N X_N & \\ & & & 0 \end{bmatrix} \begin{bmatrix} C & DS \\ [M] & [I] \end{bmatrix} \leq 0 \quad (\text{LMI})$$

then network stability guaranteed with the Lyapunov function

$$V(x, \eta) = p_1 V_1(x_1, \eta_1) + \dots + p_N V_N(x_N, \eta_N) + \eta^T Q \eta$$

Frequency Domain Implications of Dissipativity



The dissipation inequality

$$\nabla_x V(x, \eta)^T f(x, u) + \nabla_\eta V(x, \eta)^T (A\eta + B \begin{bmatrix} u \\ y \end{bmatrix}) \leq z^T X z$$

implies $V(x(T), \eta(T)) \leq V(x(0), \eta(0)) + \int_0^T z^T X z(t) dt$.

Thus, for $x(0) = 0, \eta(0) = 0$,

$$\int_0^T z^T(t) X z(t) dt \geq 0$$

Frequency Domain Implications of Dissipativity

Then, from Parseval's Theorem,

$$\int_{-\infty}^{\infty} \hat{z}^*(\omega) X \hat{z}(\omega) d\omega \geq 0$$

where $\hat{z}(\omega)$ is the Fourier Transform of $z(t)$. Substitute

$$\hat{z}(\omega) = \begin{bmatrix} D + C(j\omega I - A)^{-1} B \\ \Psi(\omega) \end{bmatrix} \begin{bmatrix} \hat{u}(\omega) \\ \hat{y}(\omega) \end{bmatrix}$$

$$=: \Psi(\omega)$$

and rewrite inequality above as

$$\int_{-\infty}^{\infty} \begin{bmatrix} \hat{u}(\omega) \\ \hat{y}(\omega) \end{bmatrix}^* \underbrace{\Psi(\omega)^* X \Psi(\omega)}_{=: \Pi(\omega)} \begin{bmatrix} \hat{u}(\omega) \\ \hat{y}(\omega) \end{bmatrix} d\omega \geq 0$$

This is a frequency domain *integral quadratic inequality (IQC)* as defined by Megretski and Rantzer (1997).

Example:

$$\dot{x}_1(t) = x_2(t)$$

$$\dot{x}_2(t) = -x_1(t) - kx_2(t) + u(t)$$

$$y(t) = x_1(t) + x_2(t)$$

is dissipative with the dynamic supply rate

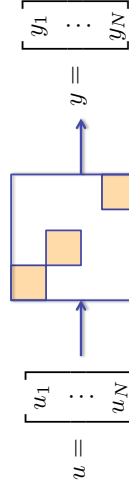
$$z^T \begin{bmatrix} 0 & 1/2 \\ 1/2 & 0 \end{bmatrix} z$$

where $\hat{z}(\omega) = \begin{bmatrix} \hat{u}(\omega) \\ \hat{y}_f(\omega) \end{bmatrix} = \begin{bmatrix} 1 & 0 \\ 0 & \frac{j\omega+(1-\beta)}{j\omega+1} \end{bmatrix} \begin{bmatrix} \hat{u}(\omega) \\ \hat{y}(\omega) \end{bmatrix}$, $\beta \geq 1 - k$.

Therefore, the system satisfies the IQC defined by

$$\begin{aligned} \Pi(\omega) &= \begin{bmatrix} 1 & 0 \\ 0 & \frac{-j\omega+(1-\beta)}{-j\omega+1} \end{bmatrix} \begin{bmatrix} 0 & 1/2 \\ 1/2 & 0 \end{bmatrix} \begin{bmatrix} 1 & 0 \\ 0 & \frac{j\omega+(1-\beta)}{j\omega+1} \end{bmatrix} \\ &= \frac{1}{2} \begin{bmatrix} 0 & \frac{j\omega+(1-\beta)}{j\omega+1} \\ \frac{j\omega+(1-\beta)}{-j\omega+1} & 0 \end{bmatrix} \end{aligned}$$

Frequency Domain Implications of Dissipativity



If each subsystem satisfies an IQC

$$\int_{-\infty}^{\infty} \begin{bmatrix} \hat{u}_i(\omega) \\ \hat{y}_i(\omega) \end{bmatrix}^* \Pi_i(\omega) \begin{bmatrix} \hat{u}_i(\omega) \\ \hat{y}_i(\omega) \end{bmatrix} d\omega \geq 0$$

then their concatenation satisfies the composite IQC

$$\begin{aligned} &\sum_i p_i \int_{-\infty}^{\infty} \begin{bmatrix} \hat{u}_i(\omega) \\ \hat{y}_i(\omega) \end{bmatrix}^* \Pi_i(\omega) \begin{bmatrix} \hat{u}_i(\omega) \\ \hat{y}_i(\omega) \end{bmatrix} d\omega \\ &= \int_{-\infty}^{\infty} \begin{bmatrix} \hat{u}(\omega) \\ \hat{y}(\omega) \end{bmatrix}^* S^T \begin{bmatrix} p_1 \Pi_1(\omega) & & \\ & \ddots & \\ & & p_N \Pi_N(\omega) \end{bmatrix} S \begin{bmatrix} \hat{u}(\omega) \\ \hat{y}(\omega) \end{bmatrix} d\omega \geq 0 \end{aligned}$$

for any $p_i \geq 0, i = 1, \dots, N$.

Back to Network Stability

IQC Stability Theorem adapted to this interconnection:
 Suppose each G_i is a bounded, causal operator mapping $L_2^{n_i}$ to $L_2^{p_i}$, and for every $\kappa \in [0, 1]$, the interconnection of κG_i above is well posed and κG_i satisfies the IQC defined by Π_i . If $\exists p_i \geq 0, \mu > 0$ s.t.

$$\begin{bmatrix} M \\ I \end{bmatrix}^T S^T \begin{bmatrix} p_1 \Pi_1(\omega) \\ p_N \Pi_N(\omega) \end{bmatrix} S \begin{bmatrix} M \\ I \end{bmatrix} \leq -\mu I \quad \forall \omega$$

then the interconnection for $\kappa = 1$ is L_2 stable.

Back to Network Stability

IQC Stability Test:

$$\begin{bmatrix} M \\ I \end{bmatrix}^T S^T \begin{bmatrix} p_1 \Pi_1(\omega) \\ p_N \Pi_N(\omega) \end{bmatrix} S \begin{bmatrix} M \\ I \end{bmatrix} \leq -\mu I \quad \forall \omega$$

Dissipativity-based Stability Test:

$$\begin{bmatrix} A^T Q + Q A & Q B S \\ [M \\ I]^T S^T B^T Q & 0 \end{bmatrix} \begin{bmatrix} M \\ I \end{bmatrix} + \begin{bmatrix} C & D S \\ p_N X_N \end{bmatrix} \begin{bmatrix} p_1 X_1 \\ \dots \\ p_N X_N \end{bmatrix} \begin{bmatrix} C & D S \\ p_N X_N \end{bmatrix} \leq 0 \quad (\text{LMI})$$

This matrix inequality is equivalent, by the KYP Lemma, to:

$$\begin{bmatrix} M \\ I \end{bmatrix}^T S^T \begin{bmatrix} p_1 \Pi_1(\omega) \\ p_N \Pi_N(\omega) \end{bmatrix} S \begin{bmatrix} M \\ I \end{bmatrix} \leq 0 \quad \forall \omega$$

which is less restrictive than the IQC Stability Test (only ≤ 0), but doesn't account for disturbances (only Lyapunov stability).

Delay Robustness of Interconnected Dissipative Systems

- When the interconnection includes time delays, a meaningful stability criterion should restrict the amount of delays relative to the system time constants.
- However, dissipativity with static supply rates does not capture time scale information: if $\dot{x} = f(x, u), y = h(x, u)$ is dissipative with a static supply rate, so is $\tau \dot{x} = f(x, u), y = h(x, u) \forall \tau > 0$

Roll-off IQC to capture time scale information:

$$\int_{-\infty}^{\infty} \begin{bmatrix} \hat{u}(\omega) \\ \hat{y}(\omega) \end{bmatrix}^* \begin{bmatrix} \gamma^2 & 0 \\ 0 & -1 - \left(\frac{\omega}{\omega_c}\right)^2 \end{bmatrix} \begin{bmatrix} \hat{u}(\omega) \\ \hat{y}(\omega) \end{bmatrix} d\omega \geq 0$$

e.g., linear system with Bode plot below shaded region:

Example: Combining passivity with the roll-off IQC

(Summers, Arcak, Packard, 2013)

Interconnection matrix $M(\omega)$ includes delay elements $e^{-j\omega T}$

Subsystems $i = 1, \dots, N$ satisfy passivity and roll-off IQCs:

$$\Pi_i^1(\omega) = \begin{bmatrix} 0 & 1/2 \\ 1/2 & -\gamma_i^{-1} \end{bmatrix} \quad \Pi_i^2(\omega) = \begin{bmatrix} \gamma_i^2 & 0 \\ 0 & -1 - \left(\frac{\omega}{\omega_c}\right)^2 \end{bmatrix}$$

Form composite IQC $p_i^1 \Pi_i^1 + p_i^2 \Pi_i^2, p_i^1, p_i^2 \geq 0$ and apply...

IQC stability test: $\exists p_i^1, p_i^2 \geq 0, \mu > 0$ such that

$$\begin{bmatrix} M(\omega) \\ I \end{bmatrix}^* S^T \begin{bmatrix} p_1^1 \Pi_1^1(\omega) \cdots p_N^1 \Pi_N^1(\omega) \\ p_1^2 \Pi_1^2(\omega) \cdots p_N^2 \Pi_N^2(\omega) \end{bmatrix} S \begin{bmatrix} M(\omega) \\ I \end{bmatrix} \leq -\mu I$$

Special case: **Cyclic interconnection with delay**

$$M(\omega) = \begin{bmatrix} 0 & \cdots & 0 & \delta_1(\omega) \\ \delta_2(\omega) & 0 & \cdots & 0 \\ \vdots & \ddots & \ddots & \vdots \\ 0 & \cdots & \delta_N(\omega) & 0 \end{bmatrix} \quad \delta_1(\omega) \cdots \delta_N(\omega) = -e^{-j\omega T}$$

The IQC stability test above is satisfied if and only if

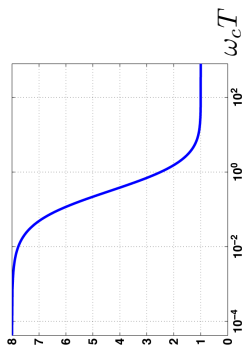
$$\omega_c T < \frac{\pi - N \tan^{-1}(\sqrt{(\gamma_1 \cdots \gamma_N)^{2/N}})}{\sqrt{(\gamma_1 \cdots \gamma_N)^{2/N} - 1}}$$

This formula recovers the secant condition as $\omega_c T \rightarrow 0$, and the small-gain condition $\gamma_1 \cdots \gamma_N < 1$ as $\omega_c T \rightarrow \infty$.

Example: Combining passivity with the roll-off IQC

(Summers, Arcak, Packard, 2013)

e.g., for $N = 3$, stability is guaranteed when $\gamma_1 \gamma_2 \gamma_3$ is under the bound below that decreases with $\omega_c T$:



An Open Problem:

Can one compose Lyapunov-Krasovskii functionals from storage functions verifying passivity and roll-off IQC for the subsystems?

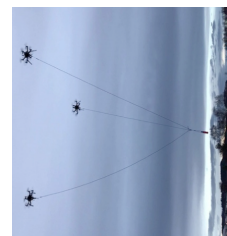
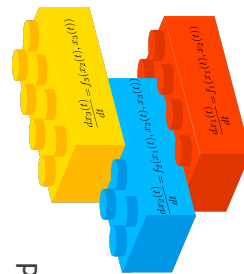
Conclusion

Compositional approach to networked dynamical systems that exploits:

- Dissipativity properties
- Special interconnection structures
- Distributed optimization methods

Contributions to Dissipativity Theory:

- Advancing applicability to networks
- Computational tools
- Various applications



Publications Discussed in the Talk (and some that weren't)



- Robustness to time delay (Summers, Arcak, Packard, 2013)
- Stochastic systems (Ferreira, Arcak, Sontag, 2012)
- Synchronization (Scardovi, Arcak, Sontag, 2010)
- Submanifold stabilization (Montenbruck, Arcak, Allgöwer, 2017)
- Approximate abstractions (Zamani and Arcak, 2018)

Distributed Stochastic Model Predictive Control for Large-Scale Smart Energy Systems

Tamás Keviczky

March 28, 2018



Benelux Meeting on Systems and Control



[Bertsimas, 2018], [den Hertog & Postek, 2016]

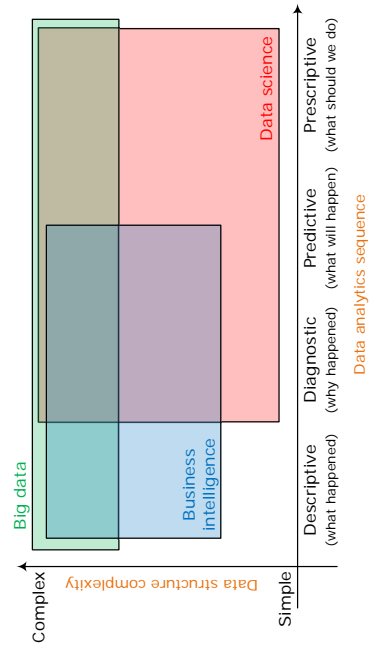
2/84

Data, Models, Large-Scale Optimization

Machine generated data increases at growing rates.

Data, Models, Large-Scale Optimization

Machine generated data increases at growing rates.

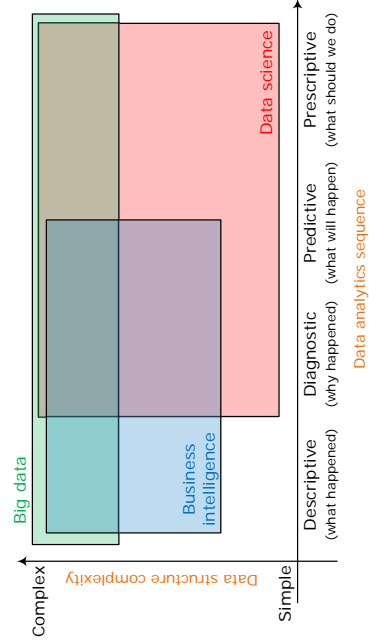


[Bertsimas, 2018], [den Hertog & Postek, 2016]

2/84

Data, Models, Large-Scale Optimization

Machine generated data increases at growing rates.

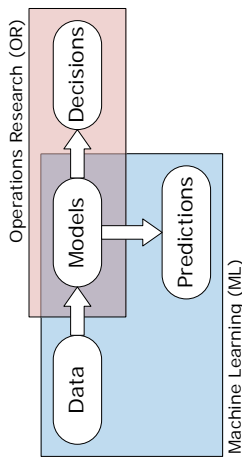


Main question for us is how to use data-driven prediction models (ML) for decision-making (OR).

[Bertsimas, 2018], [den Hertog & Postek, 2016]

2/84

Data, Models, Large-Scale Optimization



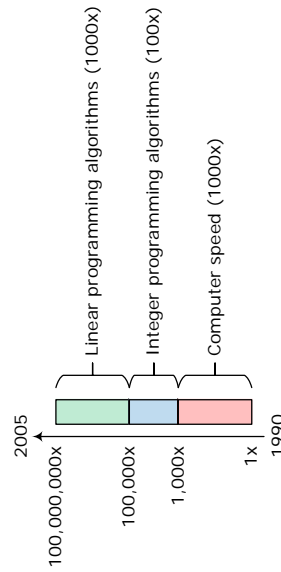
- Primary paradigm for ML: use data to make predictions/models
- Primary paradigm for OR: substitute the world with model (probability theory + optimization)
- Necessary progress: predictive \Rightarrow prescriptive analytics
- De-emphasize models, emphasize data (with interpretability)

[Bertsimas, 2018]. [den Hertog & Postek, 2016]

3/84

3/84

Data, Models, Large-Scale Optimization



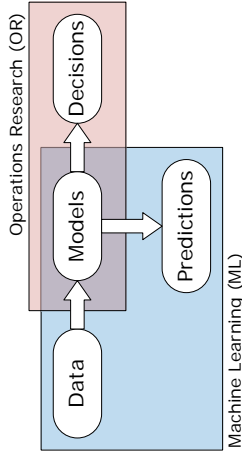
- Software and hardware improvements have accelerated mixed-integer optimization solvers 100 million times in 15 years (1990-2005)
- Requires us to rethink what is tractable...

[Bertsimas, 2018]. [Bixby et al., 2004]

4/84

5/84

Data, Models, Large-Scale Optimization



- Primary paradigm for ML: use data to make predictions/models
- Primary paradigm for OR: substitute the world with model (probability theory + optimization)
- Necessary progress: predictive \Rightarrow prescriptive analytics
- De-emphasize models, emphasize data (with interpretability)

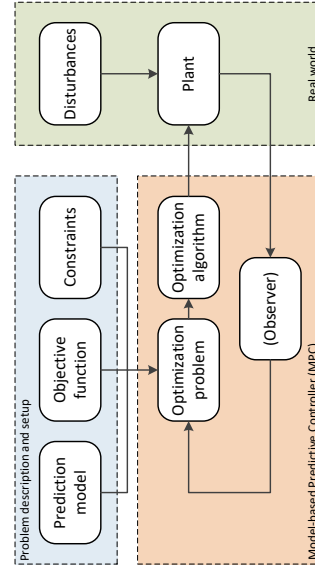
“All models are wrong, but some are useful.”

[Bertsimas, 2018]. [den Hertog & Postek, 2016]

3/84

3/84

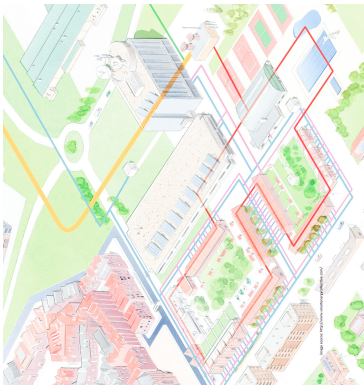
Model Predictive Control



- We use OR for planning and dynamic optimization within MPC approaches.
- Necessary evolution: data-driven distributed optimization

Large-Scale Smart Energy Systems

Complex energy systems with several agents (decision makers) and shared resources.



Energy transition, societal trends:

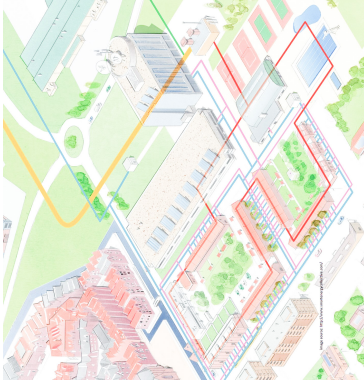
- De-carbonization
- Electrification of all sectors
- Digitization
- Societal awareness

[Scherpen, EJC 2015], [De Persis et al. 2018]

6/84

Large-Scale Smart Energy Systems

Complex energy systems with several agents (decision makers) and shared resources.



Changing assumptions:

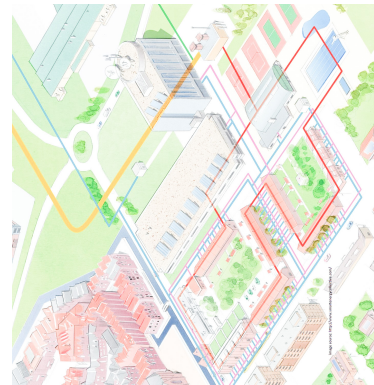
- Load side is not passive
- Generation based on agile power-electronics
- Bottom-up energy markets
- Self-organizing cells (physical, digital, organizational levels)

[Scherpen, EJC 2015], [De Persis et al. 2018]

7/84

Large-Scale Smart Energy Systems

Things get networked and integrated. Interplay between energy carriers, algorithms & data, business mechanisms.



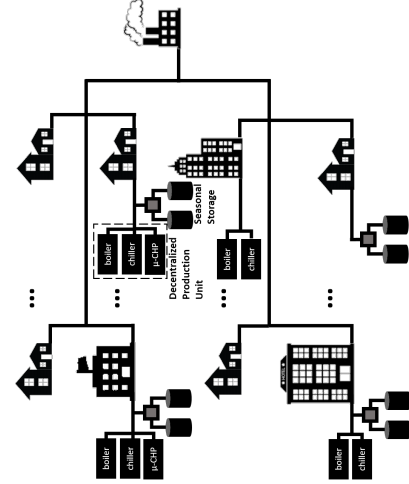
We seek methods that:

- Increase efficiency, sustainability
- Manage inherent uncertainty
- Make use of data, predictions, and models
- Scalable, flexible, reliable

[Scherpen, EJC 2015], [De Persis et al. 2018]

8/84

Smart Thermal Grids

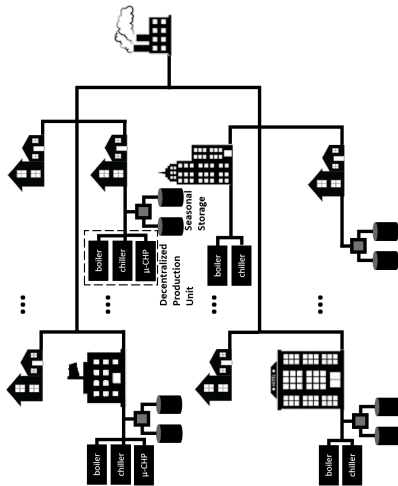


• In The Netherlands, the most energy is within thermal systems / networks, and not the power grid.

- One-third of energy is consumed within the built environment.

9/84

Smart Thermal Grids



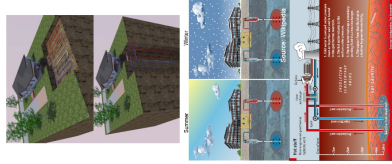
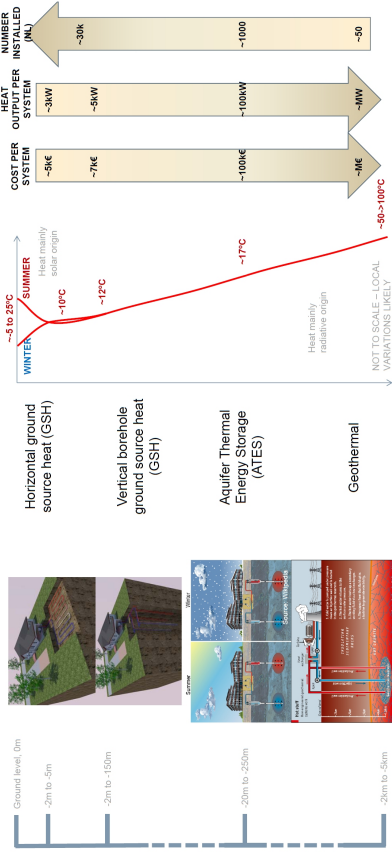
- Thermal networks will become even more important as we aim to replace the gas grid.
- This implies increased attention to exchange of heat/cold and storage

10/84

[Vardon, 2015]

11/84

Ground Source Heat Landscape



Aquifer Thermal Energy Storage (ATES)

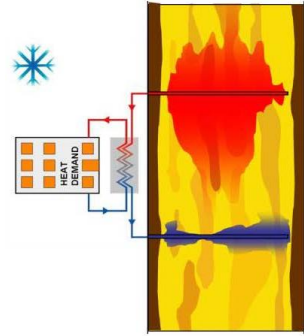
- A large-scale natural subsurface storage for thermal energy
- An innovative method for thermal energy balance in smart grids
- Serves as a **common pool** resource in dense urban environments

[Rostampour et al., JEP, 2016]

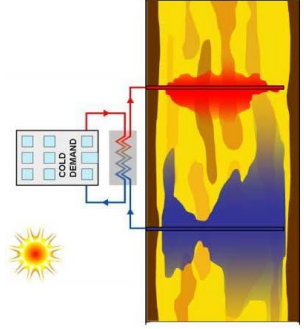
Aquifer Thermal Energy Storage (ATES)

- A large-scale natural subsurface storage for thermal energy
- An innovative method for thermal energy balance in smart grids
- Serves as a **common pool** resource in dense urban environments

[Rostampour et al., JEP, 2016]



- Cold season:**
- The building requests thermal energy for the heating purpose
 - Water is injected into **cold well** and is taken from **warm well**
 - The stored water contains **cold** thermal energy for next season



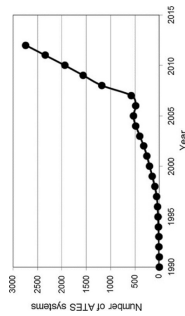
- Warm season:**
- The building requests thermal energy for the cooling purpose
 - Water is injected into **warm well** and is taken from **cold well**
 - The stored water contains **warm** thermal energy for next season

12/84

13/84

Benefits of ATES

- ATES provides sustainable heating and cooling as seasonal energy storage buffers
- Stores large amounts of low quality thermal energy (typical capacities: few 100 kW per well)
- Can reduce energy use (and GHG emissions) by 50% for large buildings
 - 60-80% energy saving for cooling (80-90% electrical peak reduction)
 - 20-30% energy saving for heating.
- Around 3000 systems are in use in NL, rapid growth over the past 10 years



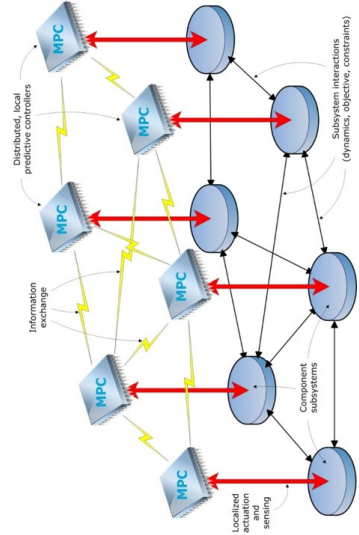
ATES Systems in Smart Thermal Grids

Challenges for Urban ATES Systems in Smart Thermal Grids

- How to manage this technology at a larger scale?
- We need more ATES systems to meet GHG emission reduction goals
- ATES systems accumulate in urban areas
- Current policies are too strict for optimal use of subsurface (artificial scarcity)
 - Static permits to avoid thermal interference
 - Unclear trade-off between individual and overall energy savings
 - Coordination is required to prevent negative interaction

Approach

- ATES systems self-organize subsurface space use to increase efficiency.
- Facilitate communication and negotiation
- Use distributed stochastic cooperative control to take account of uncertainties and variations in (future) energy demand



Uncertainty Drives Cooperation

The most efficient way to reduce uncertainty is to communicate / cooperate between neighboring systems.

Challenge: Optimizing the performance of a network

1. **Computation:** Problem size can be prohibitive
2. **Communication:** Communication bandwidth limitation
3. **Information Privacy:** Agents may not want to share information
4. **Stochastic Nature:**
 - **Private uncertainty source** (local); weather and usage driven uncertain thermal energy demand of a single building
 - **Common uncertainty source** (shared); uncertain common resource pool, e.g., ATEs systems

18/84

* [Rostampour et. al., CDC, 2017], † [Rostampour & Keviczky, IEEE TSG, 2018]

19/84

Why Distributed?

Scalable Methodology

- **Communication:** Only between neighbors
- **Computation:** Local, done in parallel for all agents

Preserving Privacy

- Agents do not reveal information about their preferences (encoded by objective and constraint functions) to each other

* [Rostampour et. al., CDC, 2017], † [Rostampour & Keviczky, IEEE TSG, 2018]

18/84

19/84

Why Distributed?

Scalable Methodology

- **Communication:** Only between neighbors
- **Computation:** Local, done in parallel for all agents

Why Distributed?

Scalable Methodology

- **Communication:** Only between neighbors
- **Computation:** Local, done in parallel for all agents

Preserving Privacy

- Agents do not reveal information about their preferences (encoded by objective and constraint functions) to each other

Numerous Applications

- Wireless Networks
- Electric Vehicle Charging Control
- Optimal Power Flow with Reserve Scheduling *
- Energy Management in STGs with ATEs Systems †

* [Rostampour et. al., CDC, 2017], † [Rostampour & Keviczky, IEEE TSG, 2018]

18/84

19/84

Stochastic robustness

Uncertainty plays a fundamental role in large-scale energy systems.

20/84

Stochastic robustness

Uncertainty plays a fundamental role in large-scale energy systems.

Deterministic, worst-case approaches:

- Guarantee performance for all possible uncertainty outcomes.
- Conservatism – small robustness margin, computational complexity
- Uncertain parameters often enter into the system in a nonlinear/nonconvex fashion
- Relaxation techniques are used to e.g., replace the original nonlinear uncertainty set with a larger affine one

20/84

20/84

Stochastic robustness

Uncertainty plays a fundamental role in large-scale energy systems.

20/84

Deterministic, worst-case approaches:

- Guarantee performance for all possible uncertainty outcomes.
- Conservatism – small robustness margin, computational complexity
- Uncertain parameters often enter into the system in a nonlinear/nonconvex fashion
- Relaxation techniques are used to e.g., replace the original nonlinear uncertainty set with a larger affine one

A probabilistic approach to robustness:

- Based on randomization in uncertainty space
- Guarantee performance for all but very unfortunate uncertainty scenarios.

20/84

21/84

Performance Level Estimation Example

Given small $\varepsilon \in (0, 1)$, estimate a performance level γ such that

$$h_i(\delta) \leq \gamma, \quad \delta \in \Delta$$

holds with probability of at least $1 - \varepsilon$. That is, find γ such that

$$\mathbb{P}(h(\delta) \leq \gamma) \geq 1 - \varepsilon.$$

Performance Level Estimation Algorithm

1. Extract N iid samples $\delta^{(1)}, \dots, \delta^{(N)}$ from Δ according to the probability measure \mathbb{P} .
2. Compute the empirical performance level $\hat{\gamma}_N = \max_{i=1, \dots, N} h(\delta^{(i)})$

If we set a priori $\varepsilon \in (0, 1)$, $\beta \in (0, 1)$, and take

$$N \geq \frac{\log \frac{1}{\beta}}{\log \frac{1}{1-\varepsilon}}$$

then

$$\mathbb{P}(h(\delta) \leq \hat{\gamma}_N) \geq 1 - \varepsilon.$$

holds with probability larger than $1 - \beta$.

[Tempo et al., 1996]

22/84

[Chamanbaz, 2013]

23/84

Probabilistic Robustness Analysis

- Sample size bounds are **independent of the dimension** of the uncertainty vector δ .
- **Bounds depend weakly on β** : in practice, β can be set to a very small value (e.g., $\beta = 10^{-9}$).
- Successful implementation requires the availability of efficient algorithms for generation of random samples according to the distribution \mathbb{P} .
- Randomized algorithms are **inherently parallel**.

Centralized Deterministic Program

$$\begin{aligned} \min_x \quad & \sum_i f_i(x) & \longrightarrow & f_i(\cdot) : \text{convex objective function of agent } i \\ \text{s.t.} \quad & x \in \mathcal{X}_i, \text{ for all } i & \longrightarrow & \mathcal{X}_i : \text{convex constraint set of agent } i \end{aligned}$$

Centralized Deterministic Program

$$\begin{aligned} \min_x \quad & \sum_i f_i(x) & \longrightarrow & f_i(\cdot) : \text{convex objective function of agent } i \\ \text{s.t.} \quad & x \in \bigcap_i \mathcal{X}_i, & \longrightarrow & \mathcal{X}_i : \text{convex constraint set of agent } i \end{aligned}$$

24/84

25/84

Centralized Deterministic Program

$$\begin{aligned} \min_x \quad & \sum_i f_i(x) & \longrightarrow & f_i(\cdot) : \text{convex objective function of agent } i \\ \text{s.t. } \quad & x \in \bigcap_i \mathcal{X}_i, & \longrightarrow & \mathcal{X}_i : \text{convex constraint set of agent } i \end{aligned}$$

How can we deal with uncertain $\mathcal{X}_i(\delta)$?

25/84

[Margellos & Prandini, ECC 2016]

26/84

Centralized Robust Program

$$\begin{aligned} \min_x \quad & \sum_i f_i(x) \\ \text{s.t. } \quad & x \in \bigcap_i \mathcal{X}_i(\delta), \text{ for all } \delta \in \Delta \end{aligned}$$

Centralized Robust Program

$$\begin{aligned} \min_x \quad & \sum_i f_i(x) \\ \text{s.t. } \quad & x \in \bigcap_i \mathcal{X}_i(\delta), \text{ for all } \delta \in \Delta \end{aligned}$$

Stochastic Setting:

- δ : Uncertain parameter $\delta \sim \mathbb{P}$
- Δ : Possibly unknown distribution and unbounded set
- Semi-infinite optimization program

[Margellos & Prandini, ECC 2016]

26/84

Centralized Robust Program

$$\begin{aligned} \min_x \quad & \sum_i f_i(x) \\ \text{s.t. } \quad & x \in \bigcap_{\delta \in \Delta} \mathcal{X}_i(\delta) \end{aligned}$$

Stochastic Setting:

- δ : Uncertain parameter $\delta \sim \mathbb{P}$
- Δ : Possibly unknown distribution and unbounded set
- Semi-infinite optimization program

[Margellos & Prandini, ECC 2016]

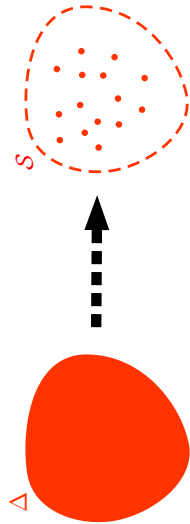
27/84

Scenario Based Approximation

Centralized **Scenario** Program

$$\begin{aligned} \min_x & \sum_i f_i(x) \\ \text{s.t.} & x \in \bigcap_{\delta \in \Delta} \mathcal{X}_i(\delta) \end{aligned}$$

Replace Δ with \mathcal{S} :



28/84

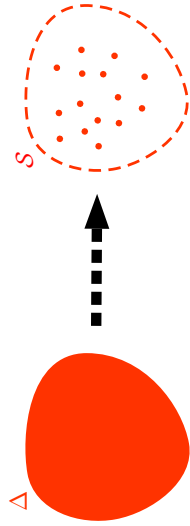
29/84

Scenario Based Approximation

Centralized **Scenario** Program

$$\begin{aligned} \min_x & \sum_i f_i(x) \\ \text{s.t.} & x \in \bigcap_{\delta \in \mathcal{S}} \mathcal{X}_i(\delta) \end{aligned}$$

Replace Δ with \mathcal{S} :



28/84

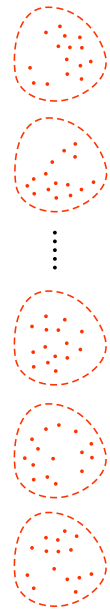
29/84

Probabilistic Feasibility Certificate

Centralized **Scenario** Program \mathcal{P}_S

$$\begin{aligned} \min_x & \sum_i f_i(x) \\ \text{s.t.} & x \in \bigcap_{\delta \in \mathcal{S}} \mathcal{X}_i(\delta) \end{aligned}$$

- Is $x_S^* \models \mathcal{P}_S$ feasible for \mathcal{P}_Δ ?
- Is this true for any \mathcal{S} ?



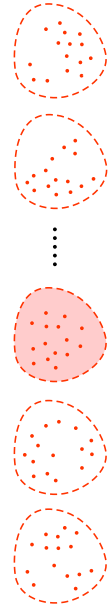
30/84

Probabilistic Feasibility Certificate

Centralized **Scenario** Program \mathcal{P}_S

$$\begin{aligned} \min_x & \sum_i f_i(x) \\ \text{s.t.} & x \in \bigcap_{\delta \in \mathcal{S}} \mathcal{X}_i(\delta) \end{aligned}$$

- Is $x_S^* \models \mathcal{P}_S$ feasible for \mathcal{P}_Δ ?
- Is this true for any \mathcal{S} ?



30/84

Centralized **Stochastic** Program \mathcal{P}_Δ

$$\begin{aligned} \min_x & \sum_i f_i(x) \\ \text{s.t.} & \mathbb{P}(\delta \in \Delta : x \notin \mathcal{X}_i(\delta)) \leq \epsilon \end{aligned}$$

31/84

Probabilistic Feasibility Certificate

Centralized **Scenario** Program \mathcal{P}_S Centralized **Stochastic** Program \mathcal{P}_Δ

$$\begin{aligned} \min_x \quad & \sum_i f_i(x) \\ \text{s.t.} \quad & x \in \bigcap_{i \in \mathcal{S}} \mathcal{X}_i(\delta) \end{aligned} \quad \begin{aligned} \min_x \quad & \sum_i f_i(x) \\ \text{s.t.} \quad & \mathbb{P}(\delta \in \Delta : x \notin \bigcap_i \mathcal{X}_i(\delta)) \leq \varepsilon \end{aligned}$$

Fix $\beta \in (0, 1)$ and \mathcal{S} , then

$$\mathbb{P}^{|\mathcal{S}|} \left(\mathcal{S} \in \Delta^{|\mathcal{S}|} : \mathbb{P}(\delta \in \Delta : x_S^* \notin \bigcap_i \mathcal{X}_i(\delta)) \leq \varepsilon \right) \geq 1 - \beta$$

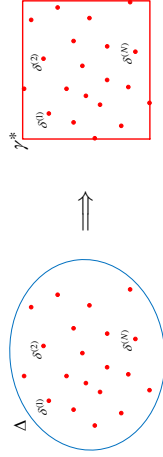
[Calafiore & Campi, TAC 2006]

Robust Randomized Optimization

Two-step approach (instead of nonconvex randomized approximation).

- Determining a bounded set that contains $1 - \varepsilon$ portion of Δ :

$$\begin{cases} \min_{\gamma} \sum_{k=0}^{M-1} \bar{\gamma}_k - \underline{\gamma}_k \\ \text{s.t.} \quad \mathbb{P}(\delta_{i,k} \in [\underline{\gamma}_k, \bar{\gamma}_k], \forall k) \geq 1 - \varepsilon \end{cases} \quad \begin{cases} \min_{\gamma} \sum_{k=0}^{M-1} \bar{\gamma}_k - \underline{\gamma}_k \\ \text{s.t.} \quad \delta_{i,k}^j \in [\underline{\gamma}_k, \bar{\gamma}_k], \forall k, \forall j \end{cases}$$



- Solving the robust counterpart of the problem w.r.t. the bounded set γ^* .

[Margellos, Rostampour, et al., ECC, 2013]

Probabilistic Feasibility Certificate

Fix $\beta \in (0, 1)$ and \mathcal{S} , then

$$\mathbb{P}^{|\mathcal{S}|} \left(\mathcal{S} \in \Delta^{|\mathcal{S}|} : \mathbb{P}(\delta \in \Delta : x_S^* \notin \bigcap_i \mathcal{X}_i(\delta)) \leq \varepsilon \right) \geq 1 - \beta$$

Complexity of ε : $\varepsilon = \frac{2}{|\mathcal{S}|} \left(d + \ln \frac{1}{\beta} \right)$

- Logarithmic in β** : β can be set close to “zero”, implying high confidence even for low violation probability
- Linear in $|\mathcal{S}|^{-1}$** : the more data the smaller the violation probability
- Linear in d** : minimum number of samples in \mathcal{S} that “support” the solution, i.e. active constraints characterizing optimal solution (often equal to # decision variables)

[Calafiore & Campi, TAC 2006]

Uncertainty Types

- Private (local) uncertainty source**: uncertain thermal energy demand of a single building climate comfort

$$x_i \in \mathcal{X}_i(\delta_i), \text{ for all } \delta_i \in \Delta_i \text{ and for all agents } i$$

- Common uncertainty source**: uncertain common resource pool between neighboring agents

$$g_i(x_i, \delta_{c_k}) + \sum_{j \in \mathcal{N}_i} g_j(x_j, \delta_{c_k}) \leq 0, \text{ for all } \delta_{c_k} \in \Delta_{c_k} \text{ and for all agents } i$$

Private Uncertainty Source

Multi Agent Problem

$$\min_x \sum_i f_i(x_i)$$

$$\text{s.t. } x \in \bigcap_{\delta \in \mathcal{S}} \prod_i \mathcal{X}_i(\delta_i)$$

Decomposable Problem

$$\min_x \sum_i f_i(x_i)$$

$$\text{s.t. } x \in \prod_{\delta_i \in \mathcal{S}_i} \mathcal{X}_i(\delta_i)$$

215

36/84

36/84

Private Uncertainty Source

Multi Agent Problem

$$\min_x \sum_i f_i(x_i)$$

$$\text{s.t. } x \in \bigcap_{\delta \in \mathcal{S}} \prod_i \mathcal{X}_i(\delta_i)$$

Decomposable Problem

$$\min_x \sum_i f_i(x_i)$$

$$\text{s.t. } x \in \prod_{\delta_i \in \mathcal{S}_i} \mathcal{X}_i(\delta_i)$$

- Decomposable uncertainty source required:

$$\delta := [\delta_1, \dots, \delta_n] \quad \text{and} \quad \mathcal{S} := \prod_i \mathcal{S}_i$$

Private Uncertainty Source

Single Agent Problem

$$\min_{x_i} f_i(x_i)$$

$$\text{s.t. } x_i \in \bigcap_{\delta_i \in \mathcal{S}_i} \mathcal{X}_i(\delta_i)$$

Probabilistic Feasibility for Single Agent Problem

Fix $\varepsilon_i \in (0, 1)$, $\beta_i \in (0, 1)$ and \mathcal{S}_i , then

$$\mathbb{P}^{|\mathcal{S}_i|} \left(\mathcal{S}_i \in \Delta_i^{|\mathcal{S}_i|} : \mathbb{P} \left(\delta_i \in \Delta_i : x_{\mathcal{S}_i}^* \notin \mathcal{X}_i(\delta_i) \right) \leq \varepsilon_i \right) \geq 1 - \beta_i$$

[Calafiore & Campi, TAC 2006]

37/84

[Rostampour & Keviczky, ACC, 2018]

38/84

Private Uncertainty Source

Multi Agent Problem

$$\min_x \sum_i f_i(x_i)$$

$$\text{s.t. } x \in \bigcap_{\delta \in \mathcal{S}} \prod_i \mathcal{X}_i(\delta_i)$$

Probabilistic Feasibility for Multi Agent Problem
(i.e., the whole network)

If $\varepsilon = \sum_i \varepsilon_i \in (0, 1)$, $\beta = \sum_i \beta_i \in (0, 1)$ and given \mathcal{S} , then

$$\mathbb{P}^{|\mathcal{S}|} \left(\mathcal{S} \in \Delta^{|\mathcal{S}|} : \mathbb{P} \left(\delta \in \Delta : x_{\mathcal{S}}^* \notin \prod_i \mathcal{X}_i(\delta_i) \right) \leq \varepsilon \right) \geq 1 - \beta$$

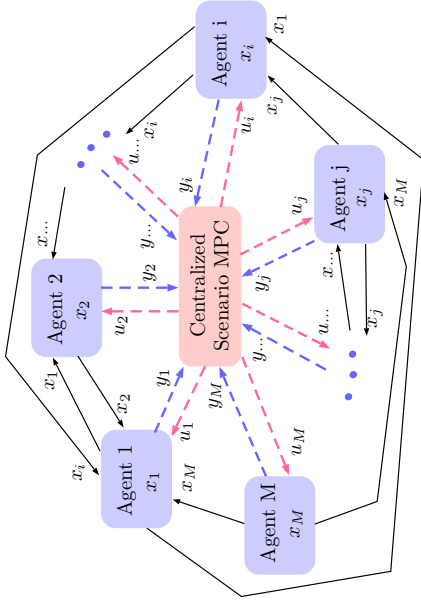
[Rostampour & Keviczky, ACC, 2018]

37/84

38/84

Dynamically Coupled Systems

With private or common uncertainty, but without coupling constraints.



39/84

40/84

Centralized Scenario Program

$$\begin{aligned} & \min_{\{u_i\}_{i \in \mathcal{N}}} \sum_{i \in \mathcal{N}} f_i(x_{i,k}, u_{i,k}) \\ \text{s.t.} \quad & x_{i,k+1}^{(i)} = A_{ii}x_{i,k}^{(i)} + B_i u_{i,k} + C_i \delta_{i,k}^{(i)} + \sum_{j \in \mathcal{N}_i} A_{ij} x_{j,k}^{(i)}, \quad x_{i,k}^{(i)} = x_{i,0} \\ & x_{i,k+\ell}^{(i)} \in \mathcal{X}_i, \quad \forall \ell \in \mathbb{N}_+, \quad \forall \delta_{i,k}^{(i)} \in \mathcal{S}_{\delta_i} \\ & u_{i,k} \in \mathcal{U}_i, \quad \forall k \in \mathcal{T}, \quad \forall i \in \mathcal{N} \end{aligned}$$

39/84

40/84

Centralized Scenario Program

$$\begin{aligned} & \min_{\{u_i\}_{i \in \mathcal{N}}} \sum_{i \in \mathcal{N}} f_i(x_{i,k}, u_{i,k}) \\ \text{s.t.} \quad & x_{i,k+1}^{(i)} = A_{ii}x_{i,k}^{(i)} + B_i u_{i,k} + C_i \delta_{i,k}^{(i)} + \sum_{j \in \mathcal{N}_i} A_{ij} x_{j,k}^{(i)}, \quad x_{i,k}^{(i)} = x_{i,0} \\ & x_{i,k+\ell}^{(i)} \in \mathcal{X}_i, \quad \forall \ell \in \mathbb{N}_+, \quad \forall \delta_{i,k}^{(i)} \in \mathcal{S}_{\delta_i} \\ & u_{i,k} \in \mathcal{U}_i, \quad \forall k \in \mathcal{T}, \quad \forall i \in \mathcal{N} \end{aligned}$$

41/84

42/84

Distributed Scenario Program

Consider effect of neighbor as disturbance, communicate local samples:

$$\begin{aligned} & \min_{\{u_{i,k}\}_{k \in \mathcal{T}}} f_i(x_{i,k}, u_{i,k}) \\ \text{s.t.} \quad & x_{i,k+1}^{(i)} = A_{ii}x_{i,k}^{(i)} + B_i u_{i,k} + q_{i,k}^{(i)}, \quad x_{i,k}^{(i)} = x_{i,0} \\ & x_{i,k+\ell}^{(i)} \in \mathcal{X}_i, \quad \forall \ell \in \mathbb{N}_+, \quad \forall q_{i,k}^{(i)} \in \mathcal{S}_{q_i} \\ & u_{i,k} \in \mathcal{U}_i, \quad \forall k \in \mathcal{T} \end{aligned}$$

41/84

42/84

Distributed Scenario Program

Consider effect of neighbor as disturbance, communicate local samples:

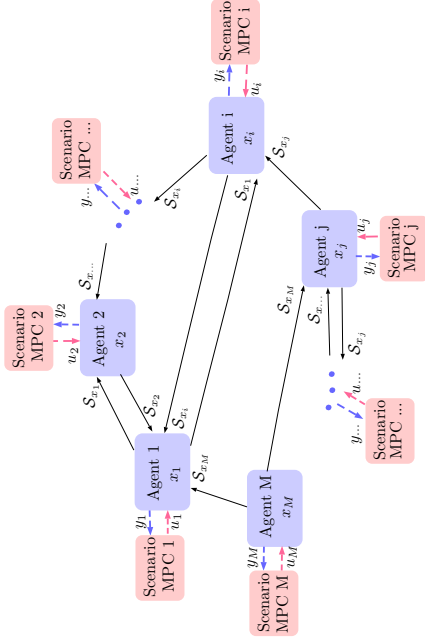
$$\begin{aligned} & \min_{\{u_{i,k} \mid \forall k \in \mathcal{T}\}} f_i(x_{i,k}, u_{i,k}) \\ & \text{s.t.} \quad x_{i,k+1}^{(i)} = A_{ii}x_{i,k}^{(i)} + B_{ii}u_{i,k} + q_{i,k}^{(i)}, \quad x_{i,k}^{(i)} = x_{i,0} \\ & \quad \quad x_{i,k+\ell}^{(i)} \in \mathcal{X}_i, \quad \forall \ell \in \mathbb{N}_+, \quad \forall q_{i,k}^{(i)} \in \mathcal{S}_{q_i} \\ & \quad \quad u_{i,k} \in \mathcal{U}_i, \quad \forall k \in \mathcal{T} \end{aligned}$$

Requirements:

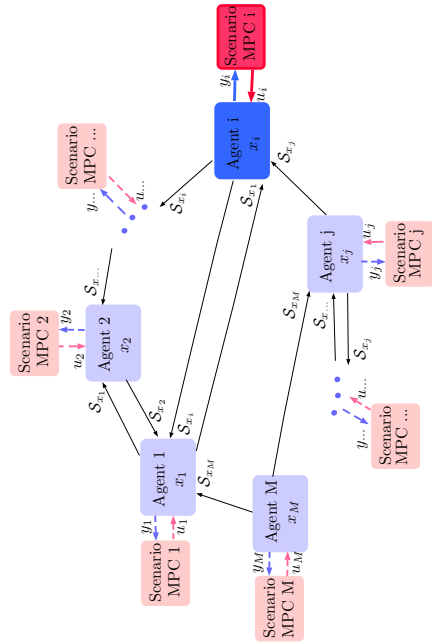
$$\mathcal{S}_{q_i} = \left\{ q_{i,k}^{(i)} : q_{i,k}^{(i)} = C_i \delta_{i,k}^{(i)} + \sum_{j \in \mathcal{N}_i} A_{ij} x_{j,k}^{(i)}, \forall \delta_{i,k}^{(i)} \in \mathcal{S}_{\delta_i}, \forall x_{j,k}^{(i)} \in \mathcal{S}_{x_j} \right\}$$

$$|\mathcal{S}_{x_j}| = N_{s_i}$$

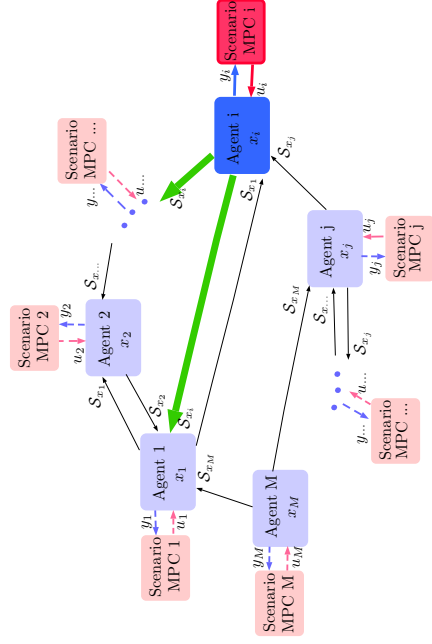
Proposed Distributed Implementation



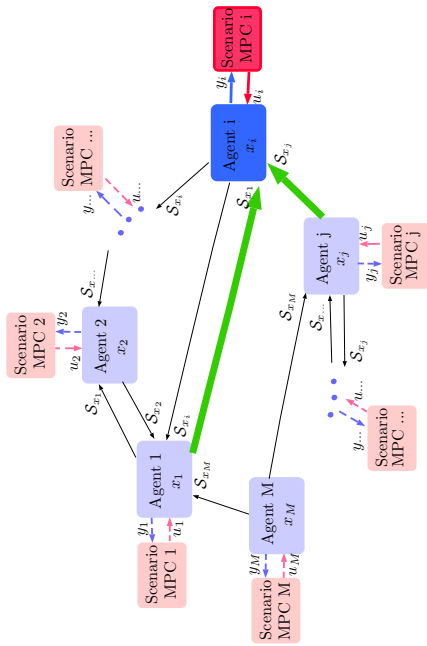
Proposed Distributed Implementation



Proposed Distributed Implementation



Proposed Distributed Implementation



46/84

47/84

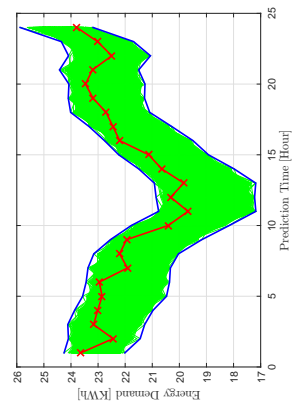
Practical challenges

- How to generate random samples of the uncertainty efficiently?
- How to communicate samples efficiently?

Sample generation

We use historical data (not random, deterministic) to build a Markov Chain model (Markov Chain Monte Carlo method, MCMC).

Provides a good model to represent uncertainty about future predictions, based on the difference between past forecasts and actual realizations.

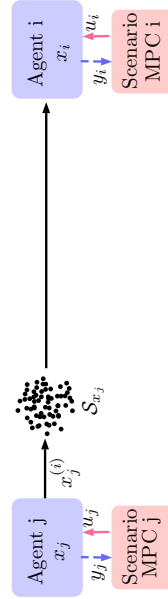


[Papafthymiou & Kikl, IEEE TEC, 2008]

48/84

Hard Communication Scheme

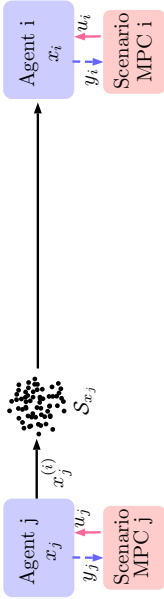
Agent j has to send the complete set S_{x_j} with cardinality N_{s_j} as it is requested by agent i



49/84

Soft Communication Scheme

Agent j sends a parametrized set $\tilde{\mathcal{B}}_j$ with its desired level of reliability $\tilde{\alpha}_j$ to agent i



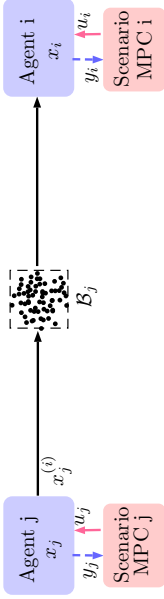
The number of scenarios \tilde{N}_{s_i} is now decided by agent j , instead of requested by agent i (more flexible scheme).

50/84

51/84

Soft Communication Scheme

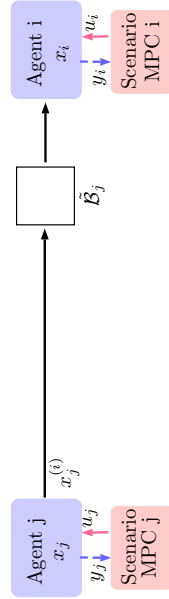
Agent j sends a parametrized set $\tilde{\mathcal{B}}_j$ with its desired level of reliability $\tilde{\alpha}_j$ to agent i



The number of scenarios \tilde{N}_{s_i} is now decided by agent j , instead of requested by agent i (more flexible scheme).

Soft Communication Scheme

Agent j sends a parametrized set $\tilde{\mathcal{B}}_j$ with its desired level of reliability $\tilde{\alpha}_j$ to agent i

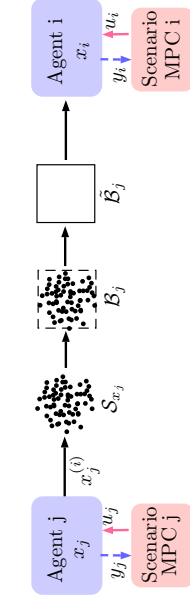


The number of scenarios \tilde{N}_{s_i} is now decided by agent j , instead of requested by agent i (more flexible scheme).

52/84

53/84

Soft Communication Scheme



A set $\tilde{\mathcal{B}}_j \subseteq \mathbb{R}^{m_j}$ is $\tilde{\alpha}_j$ -reliable if

$$\mathbb{P} \left(x_j \in \mathcal{X}_j : x_j \notin \tilde{\mathcal{B}}_j \right) \leq 1 - \tilde{\alpha}_j,$$

and we refer to $\tilde{\alpha}_j$ as the level of reliability of the set $\tilde{\mathcal{B}}_j$.

$\tilde{\mathcal{B}}_j$ (e.g., a hyper-rectangle) can be computed using a convex program.

Soft Communication Scheme

A set $\tilde{\mathcal{B}}_j \subseteq \mathbb{R}^{m_j}$ is $\tilde{\alpha}_j$ -reliable if

$$\mathbb{P} \left(\mathbf{x}_j \in \mathcal{X}_j : \mathbf{x}_j \notin \tilde{\mathcal{B}}_j \right) \leq 1 - \tilde{\alpha}_j,$$

and we refer to $\tilde{\alpha}_j$ as the level of reliability of the set $\tilde{\mathcal{B}}_j$.

How can we determine $\tilde{\alpha}_j$?

Fix $\tilde{\beta}_j \in (0, 1)$, \tilde{N}_{s_j} and let

$$\tilde{\alpha}_j = \sqrt[\tilde{N}_{s_j} - m_j]{\frac{\tilde{\beta}_j}{\binom{\tilde{N}_{s_j}}{m_j}}}.$$

Then $\mathbb{P} \left(\mathbf{x}_j \in \mathcal{X}_j : \mathbf{x}_j \notin \tilde{\mathcal{B}}_j \right) \leq 1 - \tilde{\alpha}_j$, with prob. $1 - \tilde{\beta}_j$.

[Rostampour et al., ACC, 2017]

54/84

[Rostampour et al., ACC, 2017]

55/84

Soft Communication Scheme

The communicated information is reliable with certain level of probability. How one can **accommodate such a probabilistically reliable information** in the **probabilistic feasibility certificate** of the local agent?

Given $\tilde{\alpha}_j \in (0, 1)$ and a fixed $\alpha_i \in (0, 1)$, the state trajectory of a generic agent i is probabilistically $\tilde{\alpha}_i$ -feasible for all $\delta_i \in \Delta_i$, i.e.,

$$\mathbb{P} \left(x_{i,k+\ell} \in \mathcal{X}_i, \ell \in \mathbb{N}_+ \right) \geq \tilde{\alpha}_i,$$

where $\tilde{\alpha}_i = 1 - \frac{1-\alpha_i}{\tilde{\alpha}_i}$ such that $\tilde{\alpha}_i = \prod_{j \in \mathcal{M}_i} (\tilde{\alpha}_j)$.

• If $\tilde{\alpha}_j \rightarrow 1$, i.e., sending a reliable sample set, then we recover $\tilde{\alpha}_i = \alpha_i = 1 - \varepsilon_j$.

• If $\tilde{\alpha}_j$ is small, i.e., sending an unreliable sample set, then we get no practically useful upper bound for local feasibility violation.

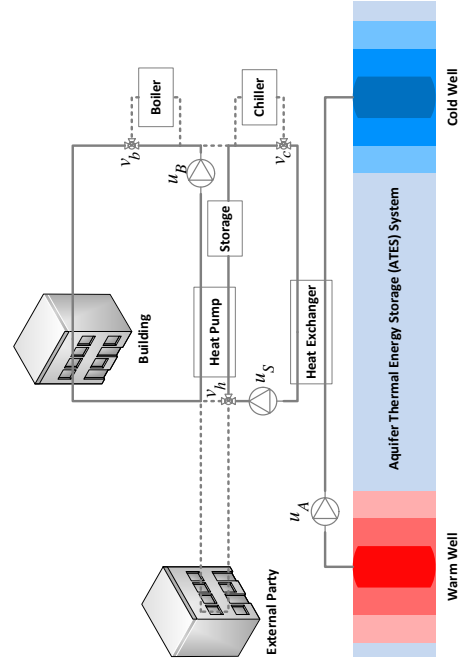
[Rostampour et al., ACC, 2017]

54/84

[Rostampour et al., ACC, 2017]

55/84

Single Building with ATES System



[Rostampour et al., ECC, 2016], [Rostampour et al., HPC, 2017]

56/84

[Rostampour et al., ECC, 2016], [Rostampour et al., HPC, 2017]

57/84

Single Building with ATES System

- A complete model of building thermal system integrated with ATES
- Long prediction horizons needed (more than a month)
- **Nonconvex problem formulation**
- **Computationally intractable for network of ATES systems**

This implies a need for

- Control-oriented building + ATES model development
- Model predictive control formulation for
 - Tracking desired building energy demand profile for comfort
 - Minimizing building operational cost
 - Minimizing thermal imbalance over long time-scales
 - Switching between modes of operation

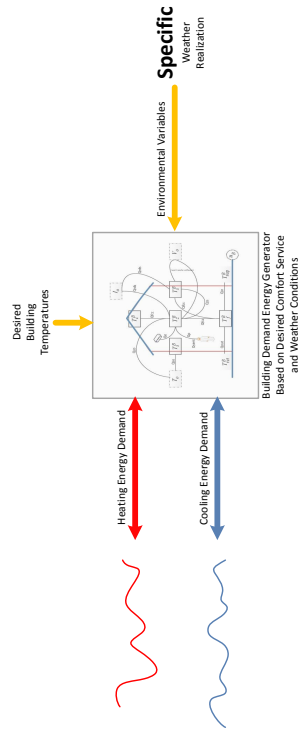
[Rostampour et al., ECC, 2016], [Rostampour et al., HPC, 2017]

57/84

[Rostampour & Keviczky, ECC, 2016]

58/84

Single Building Thermal Energy Demand



Thermal Demand Profile:

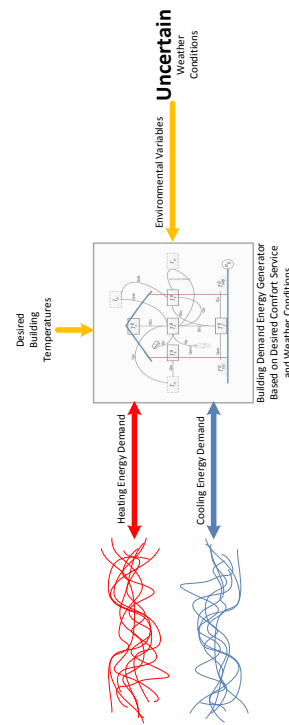
- Complete and detailed building dynamical model
- Energy demands are mapped to desired building temperatures (local controller unit) assuming steady-state conditions

[Rostampour & Keviczky, ECC, 2016]

57/84

58/84

Single Building Thermal Energy Demand



Thermal Demand Profile:

- **Due to uncertain weather conditions, uncertain demand profiles are generated**

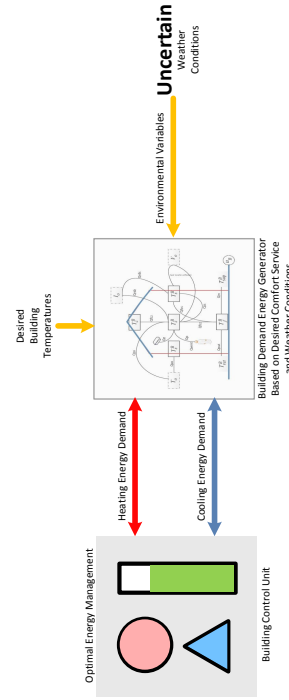
[Rostampour & Keviczky, ECC, 2016]

59/84

[Rostampour & Keviczky, ECC, 2016]

60/84

Single Building Climate Comfort System



Building Control Unit:

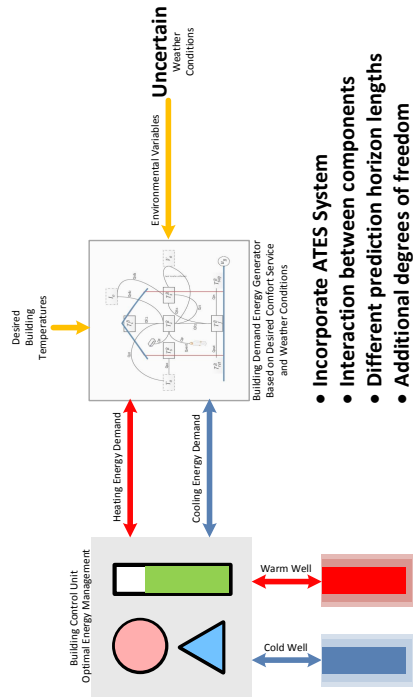
- Main components: Boiler, HP, HE, micro-CHP, Storage Tank
- ON/OFF status together with production schedule as decisions
- Control Objective: thermal energy balance for the overall systems

[Rostampour & Keviczky, ECC, 2016]

59/84

60/84

Building Climate Comfort with ATES Systems



[Rostampour & Keviczky, IFAC, 2017]

61/84

62/84

Urban Energy Management Problem Example

- min thermal energy imbalance error + cost of equipment operation
 s.t. 1) equipment limits
 2) imbalance error dynamics
 3) ATES system dynamics + local thermal energy balance
 4) coupling constraint on the thermal radius between agents

$$\begin{aligned}
 \min_{x_i} \quad & \sum_i f_i(x_i) \longrightarrow f_i(\cdot) : \text{objective function of agent } i \\
 \text{s.t.} \quad & x_i \in \mathcal{X}_i(\delta_{\ell_i}), \forall i \longrightarrow \mathcal{X}_i : \text{constraint set of agent } i \\
 & g_i(x_i, \delta_{c_k}) + \sum_{j \in \mathcal{N}_i} g_j(x_j, \delta_{c_k}) \leq 0 \longrightarrow \text{coupling constraints}
 \end{aligned}$$

[Rostampour & Keviczky, IFAC, 2017]

62/84

Urban Energy Management Problem Example

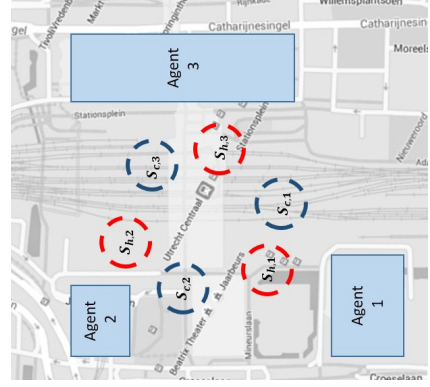
- min thermal energy imbalance error + cost of equipment operation
 s.t. 1) equipment limits
 2) imbalance error dynamics
 3) ATES system dynamics + local thermal energy balance
 4) coupling constraint on the thermal radius between agents

[Rostampour & Keviczky, IFAC, 2017]

62/84

Smart Thermal Grid with ATES Systems

- Three buildings in Utrecht city with real parameters
- Real weather condition data from 2010 to 2012

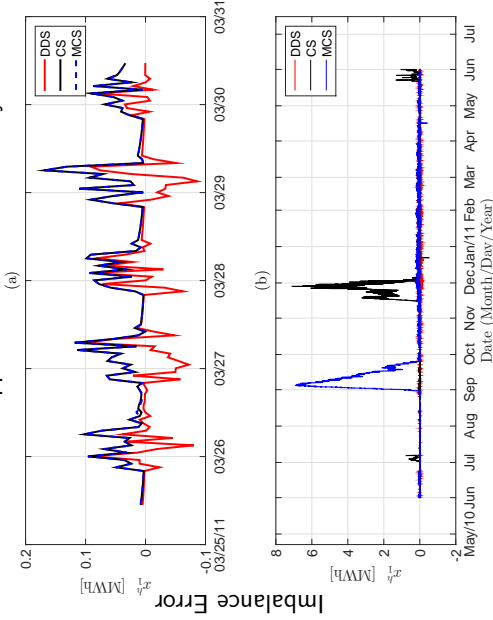


[Rostampour & Keviczky, IFAC, 2017]

63/84

Implementation on Geohydrological Model (MODFLOW)

Uses nonconvex problem formulation with detailed building model/equipment, and set-based approximation of uncertainty.

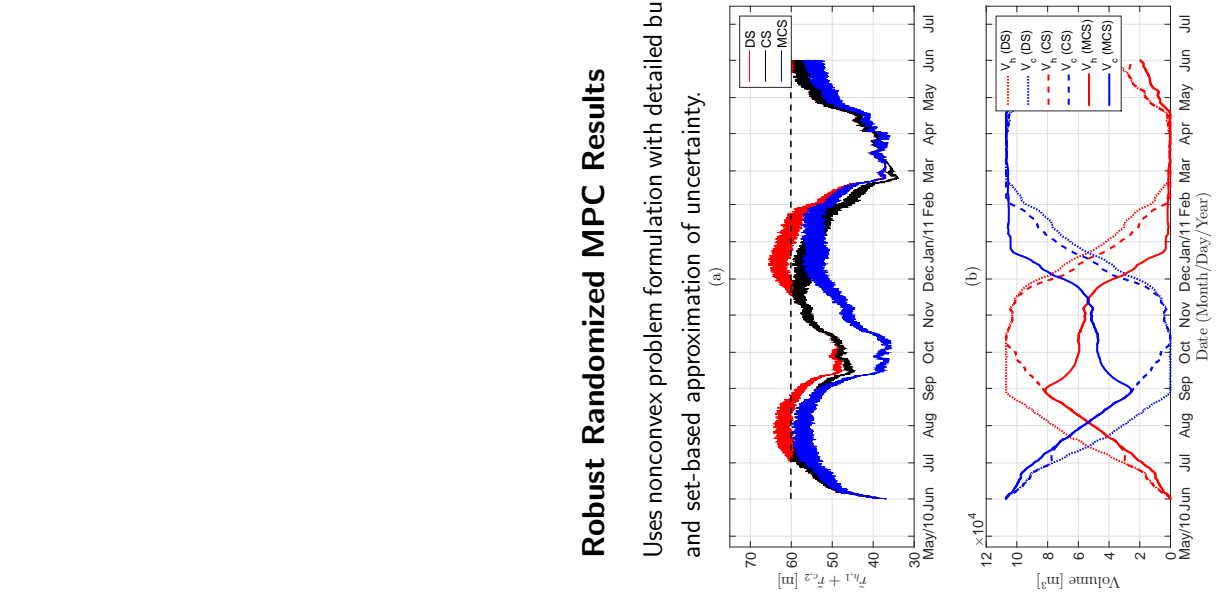


- **Deterministic**
- **Decoupled MPC**
- **Centralized SMPC**
- **Move-Blocking**
- **Centralized SMPC**

65/84

Robust Randomized MPC Results

Uses nonconvex problem formulation with detailed building model/equipment, and set-based approximation of uncertainty.

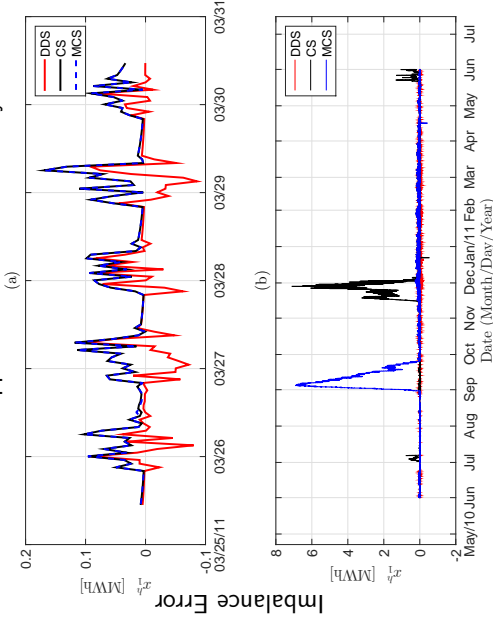


- **Deterministic**
- **Decoupled MPC**
- **Centralized SMPC**
- **Move-Blocking**
- **Centralized SMPC**

66/84

Robust Randomized MPC Results

Uses nonconvex problem formulation with detailed building model/equipment, and set-based approximation of uncertainty.

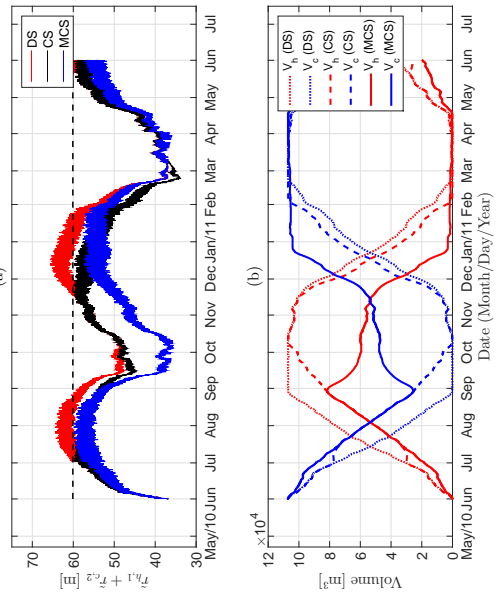


- **Deterministic**
- **Decoupled MPC**
- **Centralized SMPC**
- **Move-Blocking**
- **Centralized SMPC**

65/84

Robust Randomized MPC Results

Uses nonconvex problem formulation with detailed building model/equipment, and set-based approximation of uncertainty.



- **Deterministic**
- **Decoupled MPC**
- **Centralized SMPC**
- **Move-Blocking**
- **Centralized SMPC**

66/84

Hierarchical MPC Scheme

Upper layer: energy-based planning

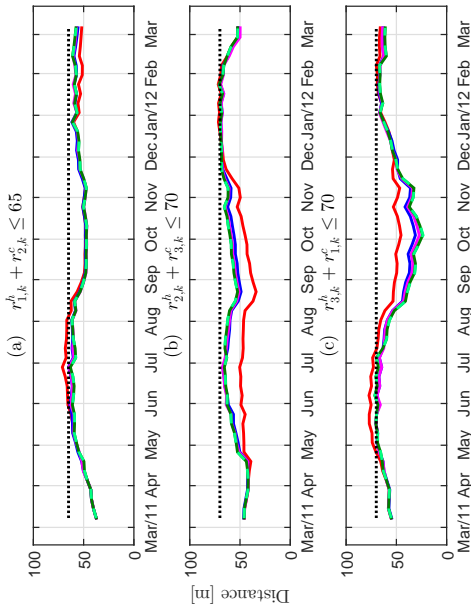
- Slower time-scale (3-month-ahead, weekly)
- Handles the coupling constraints
- Provides flow rate upper bound based on planned ATEs usage
- Convex optimization (no integer variables)
- Distributed computation

Lower layer: local building control

- Faster time-scale (day-ahead, hourly)
- Decoupled mixed-integer optimization
- Provides set points for production units and ATEs

67/84

Smart Thermal Grid with ATEs Systems



- Decoupled SMPC
- Centralized SMPC
- Distributed SMPC
- DSMPC—0.85
- DSMPC—0.50

68/84

Coupling Constraints - ADMM

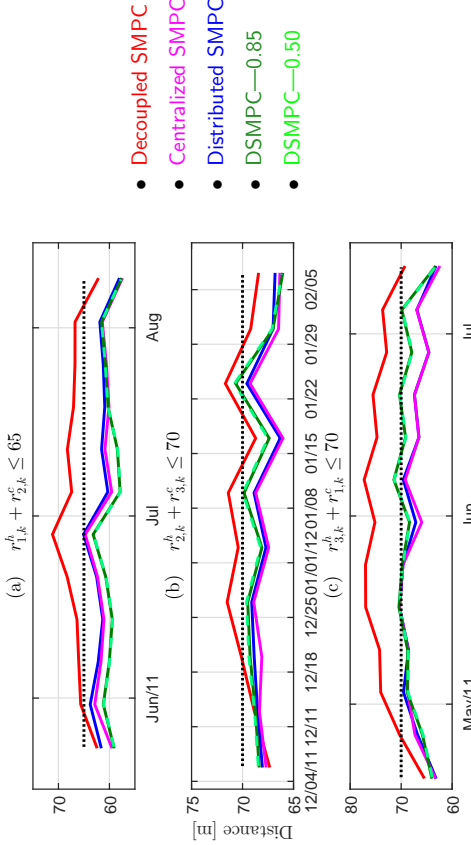
1. Coupling constraints can be handled by drawing local samples that are then shared with all neighbors.
2. The obtained deterministic constraints are then dualized, and e.g., ADMM can be used to solve the resulting problem in a distributed way.

Alternating Direction Method of Multipliers

- Good robustness of method of multipliers
- Supports decomposition
- Can be considered as either "robust dual decomposition" or "decomposable method of multipliers"

70/84

Smart Thermal Grid with ATEs Systems



- Decoupled SMPC
- Centralized SMPC
- Distributed SMPC
- DSMPC—0.85
- DSMPC—0.50

69/84

Alternating Direction Method of Multipliers

Assume two sets of variables with a separable objective function where f and g are convex:

$$\begin{aligned} & \text{minimize} && f(x) + g(z) \\ & \text{subject to} && Ax + Bz = c \end{aligned}$$

and the following augmented Lagrangian

$$L_\rho(x, z, y) = f(x) + g(z) + y^T(Ax + Bz - c) + \frac{\rho}{2} \|Ax + Bz - c\|_2^2.$$

71/84

Alternating Direction Method of Multipliers

Assume two sets of variables with a separable objective function where f and g are convex:

$$\begin{array}{l} \text{minimize} \quad f(x) + g(z) \\ \text{subject to} \quad Ax + Bz = c \end{array}$$

and the following augmented Lagrangian

$$L_\rho(x, z, y) = f(x) + g(z) + y^T(Ax + Bz - c) + \frac{\rho}{2} \|Ax + Bz - c\|_2^2.$$

Then the ADMM method consists of the following steps:

$x^{k+1} := \arg \min_x L_\rho(x, z^k, y^k)$	x -minimization
$z^{k+1} := \arg \min_z L_\rho(x^{k+1}, z, y^k)$	z -minimization
$y^{k+1} := y^k + \rho(Ax^{k+1} + Bz^{k+1} - c)$	dual update

71/84

Alternating Direction Method of Multipliers

ADMM performs a Gauss-Seidel iteration over the two variables. The method reduces to the method of multipliers if we minimized over x and z jointly. Since we minimize over x with z fixed (and vice versa) the problem is split into two.

72/84

Alternating Direction Method of Multipliers

ADMM performs a Gauss-Seidel iteration over the two variables. The method reduces to the method of multipliers if we minimized over x and z jointly. Since we minimize over x with z fixed (and vice versa) the problem is split into two.

Recall:

$$\begin{array}{l} \text{(Jacobi)} \quad x_i^{k+1} = \arg \min_{x_i} f(x_1^k, \dots, x_{i-1}^k, x_i, x_{i+1}^k, \dots, x_N^k) \\ \text{(Gauss-Seidel)} \quad x_i^{k+1} = \arg \min_{x_i} f(x_1^k, \dots, x_{i-1}^{k+1}, x_i, x_{i+1}^k, \dots, x_N^k) \end{array}$$

72/84

Alternating Direction Method of Multipliers

ADMM performs a Gauss-Seidel iteration over the two variables. The method reduces to the method of multipliers if we minimized over x and z jointly. Since we minimize over x with z fixed (and vice versa) the problem is split into two.

Recall:

$$\begin{array}{l} \text{(Jacobi)} \quad x_i^{k+1} = \arg \min_{x_i} f(x_1^k, \dots, x_{i-1}^k, x_i, x_{i+1}^k, \dots, x_N^k) \\ \text{(Gauss-Seidel)} \quad x_i^{k+1} = \arg \min_{x_i} f(x_1^{k+1}, \dots, x_{i-1}^{k+1}, x_i, x_{i+1}^k, \dots, x_N^k) \end{array}$$

Recent extension to asynchronous setting using randomized Gauss-Seidel of Douglas-Rachford splitting (CDC'13).

72/84

ADMM for Consensus Optimization

The problem to be solved contains N objective terms:

$$\text{minimize } \sum_{i=1}^N f_i(x)$$

This can be expressed in ADMM form as:

$$\begin{aligned} &\text{minimize } \sum_{i=1}^N f_i(x_i) \\ &\text{subject to } x_i - z = 0 \end{aligned}$$

where

- the x_i are local variables
- z is the global variable
- $x_i - z = 0$ are consistency or consensus constraints
- we can add regularization using an extra $g(z)$ term

73/84

ADMM for Consensus Optimization

The augmented Lagrangian becomes:

$$L_\rho(x, z, y) = \sum_{i=1}^N \left(f_i(x_i) + y_i^T (x_i - z) + \frac{\rho}{2} \|x_i - z\|_2^2 \right)$$

and the ADMM algorithm can be written as

$$\begin{aligned} x_i^{k+1} &:= \operatorname{argmin}_{x_i} \left(f_i(x_i) + y_i^{kT} (x_i - z^k) + \frac{\rho}{2} \|x_i - z^k\|_2^2 \right) \\ z^{k+1} &:= \frac{1}{N} \sum_{i=1}^N \left(x_i^{k+1} + \frac{1}{\rho} y_i^k \right) \\ y_i^{k+1} &:= y_i^k + \rho (x_i^{k+1} - z^{k+1}) \end{aligned}$$

74/84

ADMM for Consensus Optimization

The problem to be solved contains N objective terms:

$$\text{minimize } \sum_{i=1}^N f_i(x)$$

This can be expressed in ADMM form as:

$$\begin{aligned} &\text{minimize } \sum_{i=1}^N f_i(x_i) \\ &\text{subject to } x_i - z = 0 \end{aligned}$$

where

- the x_i are local variables
- z is the global variable
- $x_i - z = 0$ are consistency or consensus constraints
- we can add regularization using an extra $g(z)$ term

73/84

ADMM for Consensus Optimization

The augmented Lagrangian becomes:

$$L_\rho(x, z, y) = \sum_{i=1}^N \left(f_i(x_i) + y_i^T (x_i - z) + \frac{\rho}{2} \|x_i - z\|_2^2 \right)$$

and the ADMM algorithm can be written as

$$\begin{aligned} x_i^{k+1} &:= \operatorname{argmin}_{x_i} \left(f_i(x_i) + y_i^{kT} (x_i - z^k) + \frac{\rho}{2} \|x_i - z^k\|_2^2 \right) \\ z^{k+1} &:= \frac{1}{N} \sum_{i=1}^N \left(x_i^{k+1} + \frac{1}{\rho} y_i^k \right) \\ y_i^{k+1} &:= y_i^k + \rho (x_i^{k+1} - z^{k+1}) \end{aligned}$$

When regularization is used, the averaging in the z -update is followed by $\operatorname{prox}_{y,\rho}$.

74/84

ADMM for Consensus Optimization

This algorithm can be simplified further. By averaging the y -updates and substituting the result to the z -update, we can write the ADMM as

$$\begin{aligned} x_i^{k+1} &:= \arg \min_{x_i} \left(f_i(x_i) + y_i^{kT} (x_i - \bar{x}^k) + \frac{\rho}{2} \|x_i - \bar{x}^k\|_2^2 \right) \\ y_i^{k+1} &:= y_i^k + \rho(x_i^{k+1} - \bar{x}^{k+1}) \end{aligned}$$

where $\bar{x}^k = \frac{1}{N} \sum_{i=1}^N x_i^k$.

227

75/84

ADMM for Consensus Optimization

This algorithm can be simplified further. By averaging the y -updates and substituting the result to the z -update, we can write the ADMM as

$$\begin{aligned} x_i^{k+1} &:= \arg \min_{x_i} \left(f_i(x_i) + y_i^{kT} (x_i - \bar{x}^k) + \frac{\rho}{2} \|x_i - \bar{x}^k\|_2^2 \right) \\ y_i^{k+1} &:= y_i^k + \rho(x_i^{k+1} - \bar{x}^{k+1}) \end{aligned}$$

where $\bar{x}^k = \frac{1}{N} \sum_{i=1}^N x_i^k$. The dual variables are separately updated to drive the variables into consensus, and quadratic regularization helps pull the variables toward their average value while still attempting to minimize each local f_i .

75/84

ADMM for Consensus Optimization

This algorithm can be simplified further. By averaging the y -updates and substituting the result to the z -update, we can write the ADMM as

$$\begin{aligned} x_i^{k+1} &:= \arg \min_{x_i} \left(f_i(x_i) + y_i^{kT} (x_i - \bar{x}^k) + \frac{\rho}{2} \|x_i - \bar{x}^k\|_2^2 \right) \\ y_i^{k+1} &:= y_i^k + \rho(x_i^{k+1} - \bar{x}^{k+1}) \end{aligned}$$

where $\bar{x}^k = \frac{1}{N} \sum_{i=1}^N x_i^k$.

75/84

ADMM for Consensus Optimization

This algorithm can be simplified further. By averaging the y -updates and substituting the result to the z -update, we can write the ADMM as

$$\begin{aligned} x_i^{k+1} &:= \arg \min_{x_i} \left(f_i(x_i) + y_i^{kT} (x_i - \bar{x}^k) + \frac{\rho}{2} \|x_i - \bar{x}^k\|_2^2 \right) \\ y_i^{k+1} &:= y_i^k + \rho(x_i^{k+1} - \bar{x}^{k+1}) \end{aligned}$$

where $\bar{x}^k = \frac{1}{N} \sum_{i=1}^N x_i^k$. The dual variables are separately updated to drive the variables into consensus, and quadratic regularization helps pull the variables toward their average value while still attempting to minimize each local f_i .

We can interpret consensus ADMM as a method for solving problems where objective and constraints are distributed across multiple processors. Each one has to handle its own objective and constraint term, plus a quadratic term (updated in each iteration). The linear parts of the quadratic terms are updated in such a way that the variables converge to a common value (the solution of the full problem).

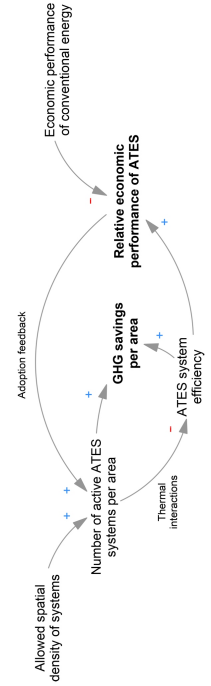
75/84

Socio-Technical Embedding

Critical practical aspects for any development in smart grids:

- embedding in market structure
- new technology vs business case
- governance issues

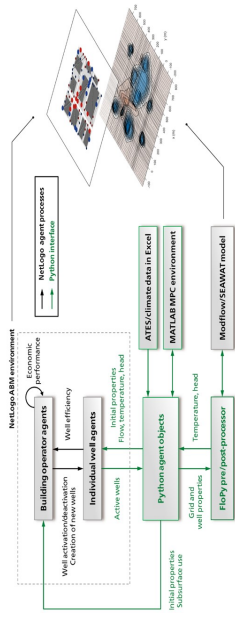
ATES in dense urban environments is a socio-technical system with complex adoption dynamics:



75/84

Policy Analysis Results

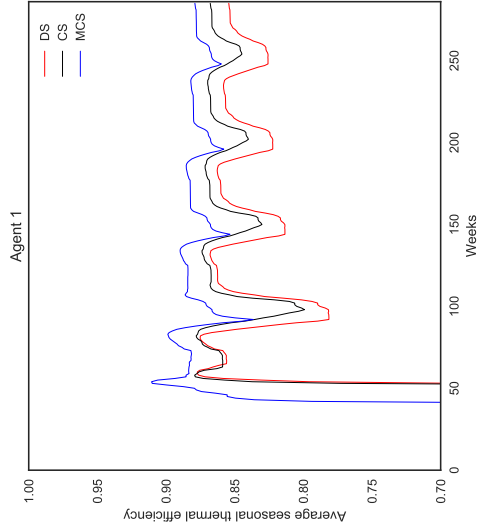
- Agent based modeling of socio-technical interactions
- Geohydrological modeling of subsurface conditions



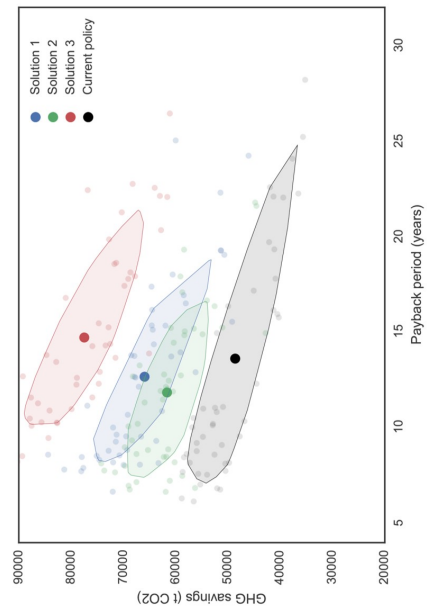
- Clear trade-off between individual costs and GHG savings as function of well distance
- Remains present even under uncertainty
- Improper spatial planning could lead to a “tragedy of the commons”

Policy Analysis Results

Impact of control scheme on average thermal efficiency

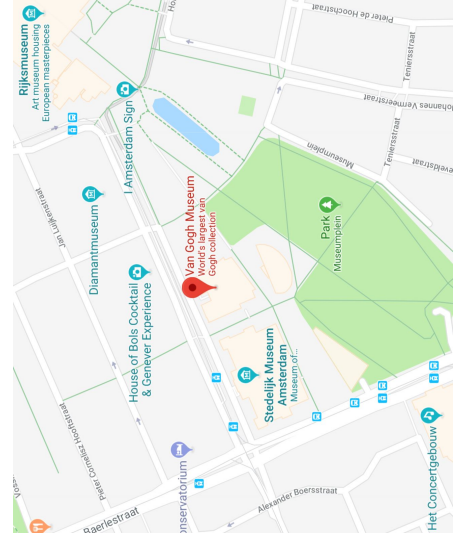


Policy Analysis Results



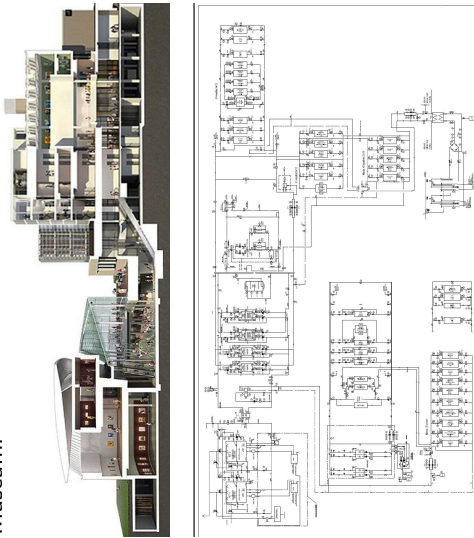
Next Steps

Pilot study: several large buildings near the Museumplein in Amsterdam.



Next Steps

Modeling and implementation over integrated low-level controllers in Van Gogh Museum.



81/84

Conclusions

- Distributed randomized optimization to deal with private or common uncertainty source over
 - a network of dynamically coupled systems
 - a network of systems with coupling constraints
- Soft communication scheme with an extension of probabilistic feasibility guarantee
- Application to energy management of smart thermal grids (STGs) with aquifer thermal energy storage (ATES) system using three different model complexities.

82/84

Open Problems

- Stability analysis and guarantees
- Recursive feasibility analysis
- More data efficient sample generation
- Distributionally robust optimization

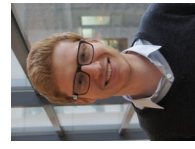
Acknowledgements



Vahab Rostampour



Wayan Wicak Ananduta



Marc Jaxa-Rozen



Martin Bloemendal



Netherlands Organisation
for Scientific Research

83/84

84/84

**Distributed Stochastic Model Predictive Control for
Large-Scale Smart Energy Systems**

Tamás Keviczky

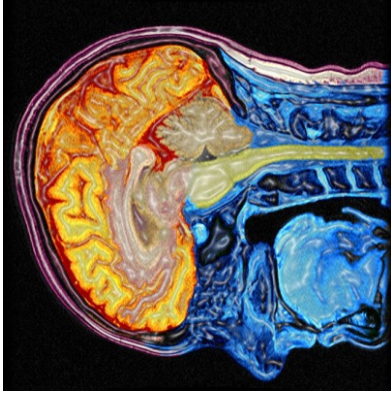
March 28, 2018



Benelux Meeting on Systems and Control



Why do Humans and Animals have Brains?

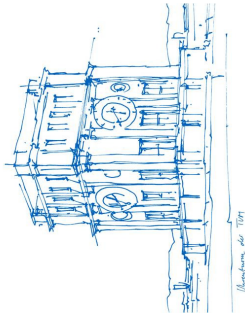


In order to make adaptable and complex movements
[Daniel Wolpert]

2

Robot Learning
through Physical Interaction and Human Guidance

Dongheui Lee



Human-centered Assistive Robotics
Technical University of Munich (TUM)



Institute of Robotics and Mechatronics
German Aerospace Center (DLR)



www.hcr.ei.tum.de



Have Sponges Lost Brains?



3

Programming by Demonstration (PbD)

Programming by Demonstration (PbD)

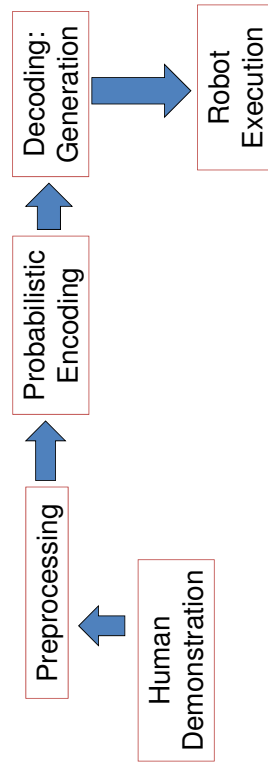
- **What is Programming by Demonstrations (PbD)?**
 - The process used to transfer new skills to a machine by relying on demonstrations from a user.
 - It is inspired by the imitation capability developed by humans and animals to acquire new skills.
 - Synonyms: Learning from Demonstrations (LFD), Imitation Learning
- **Why is it used?**
 - PbD aims at making programming accessible to novice users by providing them with an intuitive interface they are familiar with.
 - Direct: Learn from human
 - Simple: Programming skills are not necessary

Imitation Learning

- Developmental Learning
- Neuroscience
- Optimal Control
- Psychology

6

General Frame of Learning from Demonstrations



7

Imitation Learning in Robotics: Generation vs. Generalization

A different intermediate goal

Reaching to a different goal [Schaal et al]

Grasping a different size ball [Schmidts, Peer & Lee]

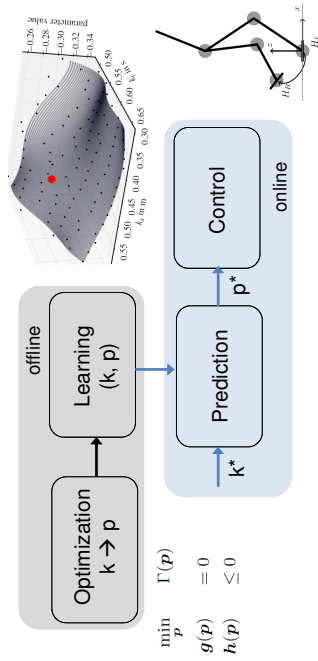
[Pervez, Lee, 2017]

Knot Tying [Abbeel et al]

8

Optimal Motion Trajectories for Bipedal Walking

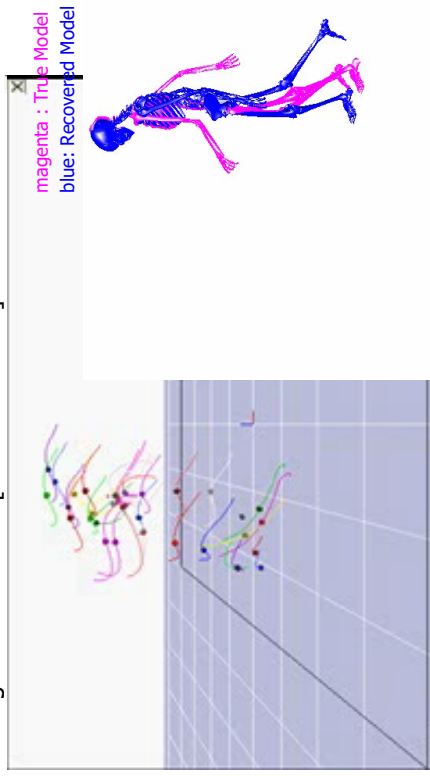
- Task parameter k : step length, step time
- Robot motion p : parameterized with b-splines
- Can generate sub-optimal motion online



[Werner et al, IROS 2015]

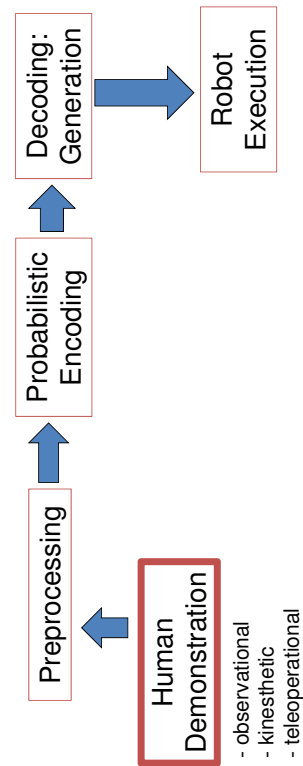
Deal with Incomplete Observations?

- Motion Reconstruction from Monocular Optical Flows
- Biological movements [Johansson 1975]

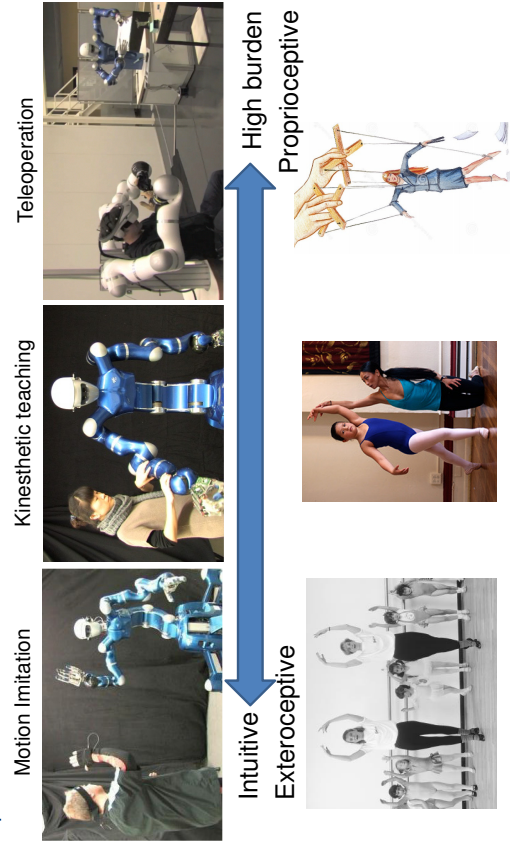


[ICRA 2007, IROS 2008, RAS 2014]

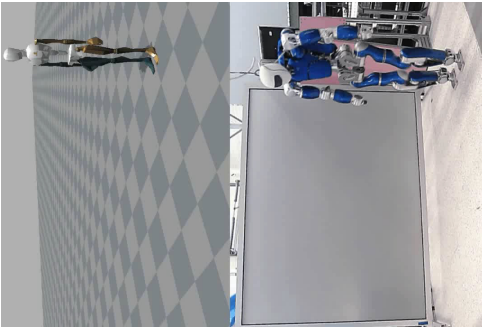
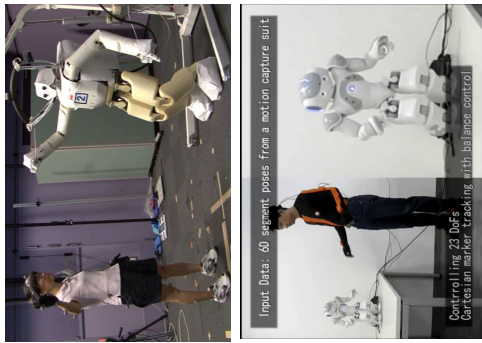
General Frame of Learning from Demonstrations



Teaching modalities



Exteroceptive Teaching



[Humanoids 2008, SYROCO2012, AT 2012, ICRA2014]

13

Motion Imitation by Marker Control



Dynamics of the humanoid's upper body on a base link (floating-base dynamics without gravity):

$$M(q) \begin{pmatrix} \ddot{\phi} \\ \ddot{x} \end{pmatrix} + C(q, \dot{\phi}, \dot{x}) \begin{pmatrix} \dot{\phi} \\ \dot{x} \end{pmatrix} = \begin{pmatrix} \tau \\ f \end{pmatrix}$$

Basic idea: Connect the robot motion to marker trajectories via virtual springs

Implementation via potentials Measured marker position

$$V_i(q, x) = \frac{1}{2} k_i \|r_{d,i} - r_i(q, x)\|^2$$

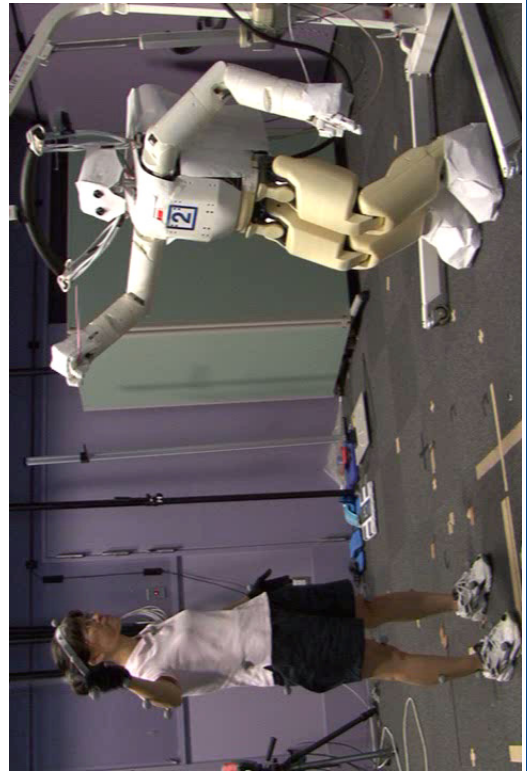
Marker pos. of the simulation

$$\begin{pmatrix} \tau \\ f \end{pmatrix} = -D(q) \begin{pmatrix} \dot{\phi} \\ \dot{x} \end{pmatrix} + \sum_{i \in \text{VEM}} k_i J_i^T(q) (r_{d,i} - r_i(q, x))$$

[Humanoids 2008]

14

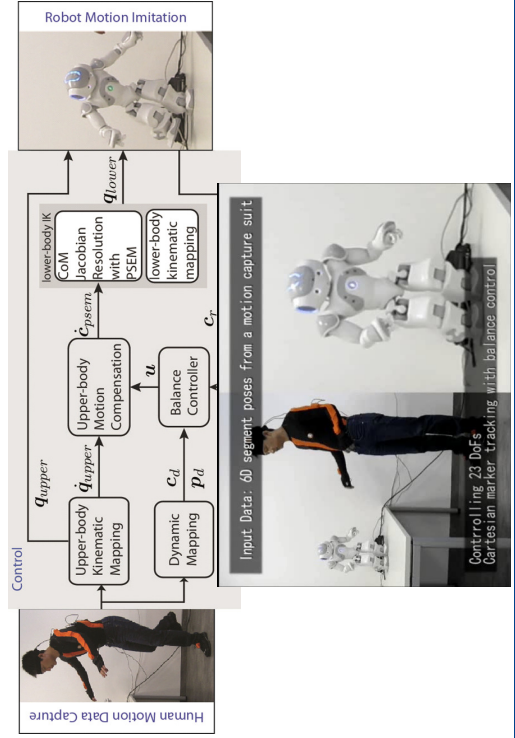
Real-time Whole Body Imitation



[Humanoids 2008]

15

Online Whole-body Human Motion Imitation

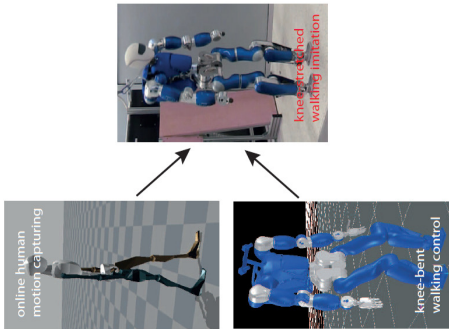


[SYROCO2012][AT 2012]

16

Online Walking Imitation in Task and Joint Space

- ZMP-based walking control
 - Walking pattern generation
 - Stabilization around the pattern
 → knee-bent biped walking
- Human walking
 - Stretched knee
 - Heel strike, toe off
 - Hip not fixed
- Walking imitation
 - Human-like knee-stretched walking
 - Vertical hip motion



[ICRA 2014]

Online Walking Imitation in Joint and Task Space

- Walking Control base on Quadratic Programming

$$\arg \min_{\dot{q}} f(\dot{q}) = \omega_1 f_1 + \omega_2 f_2 + \omega_3 f_3$$

$$f_1 = \|\dot{x}_{leg,xz} - J_{leg,xz}\dot{q}\|^2$$

$$f_2 = \|\dot{x}_{body,ori} - J_{body,ori}\dot{q}\|^2$$

$$f_3 = \|\dot{q}_{knee} - \dot{q}_{knee,human}\|^2$$

subject to $J_{com,xy}\dot{q} = \dot{x}_{com,xy}$ Human Motion

$$J_{leg,y,ori}\dot{q} = \dot{x}_{leg,y,ori}$$

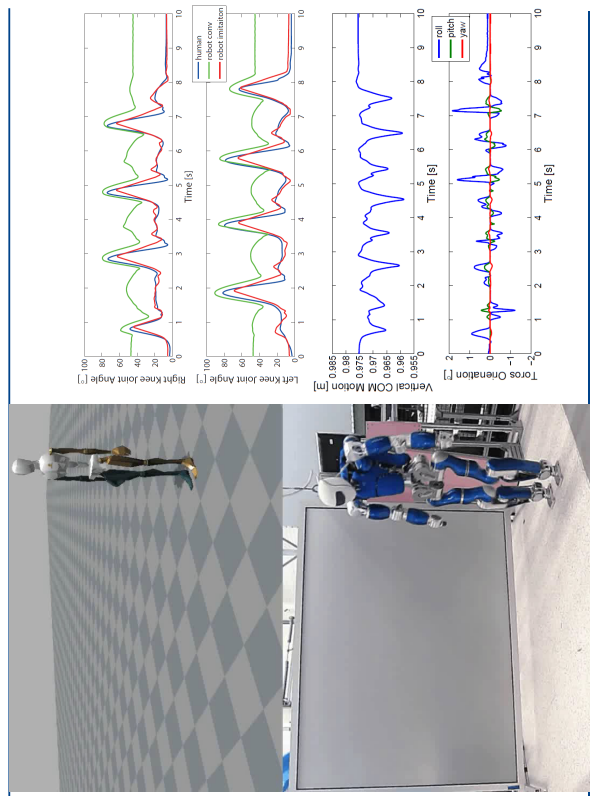
$$J_{leg,xz}\dot{q} = \dot{x}_{leg,xz}$$

$$A_{knee}\dot{q} \leq b_{knee}$$

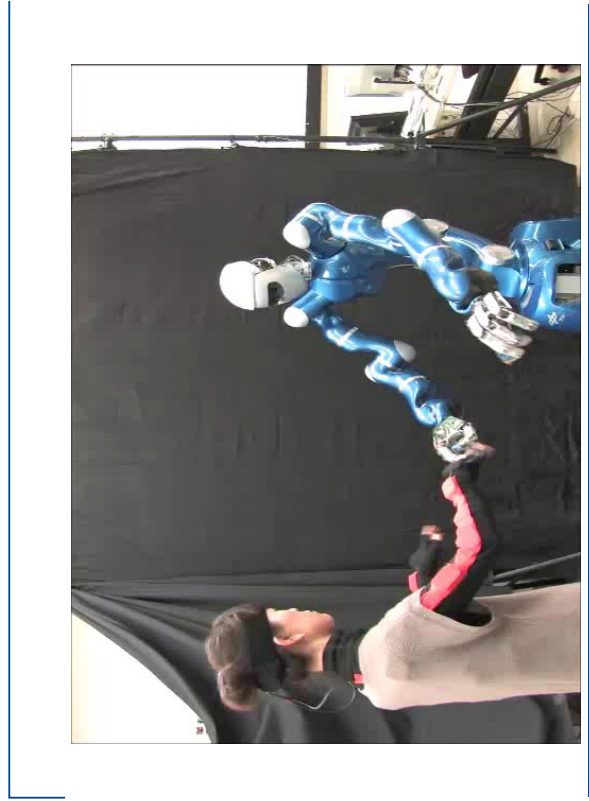
$$A_{com,z}\dot{q} \leq b_{com,z}$$

$$\dot{q}_{min} \leq \dot{q} \leq \dot{q}_{max}$$

[ICRA 2014]



[ICRA 2014]



[Collaboration with Ott at DLR]

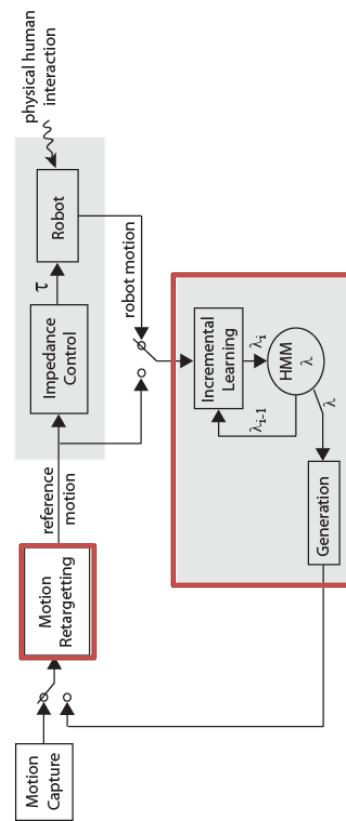
Transfer from one to another is not always straightforward.



Different Teaching Modalities of Skill Learning



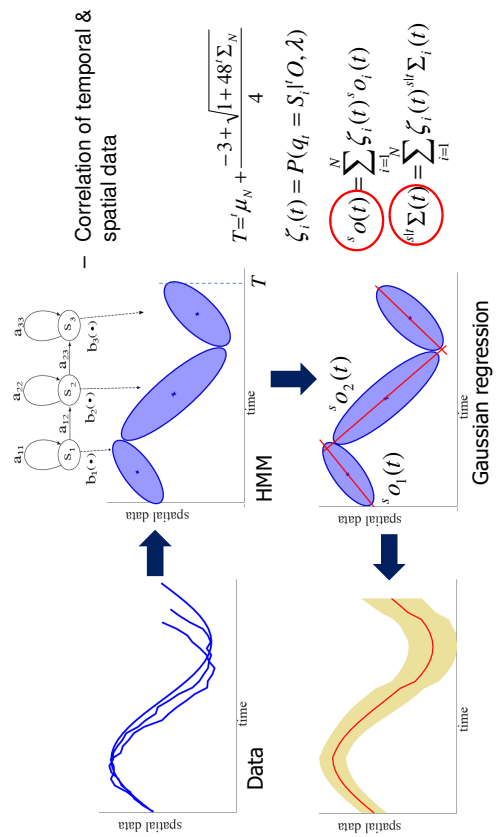
Can we achieve benefits of both observational and kinesthetic demonstrations?



Modified EM for multiple observations (reproduced & observed) with weighting factor

[Autonomous Robots 2011, IFROS 2010]

Primitive Learning & Reproduction



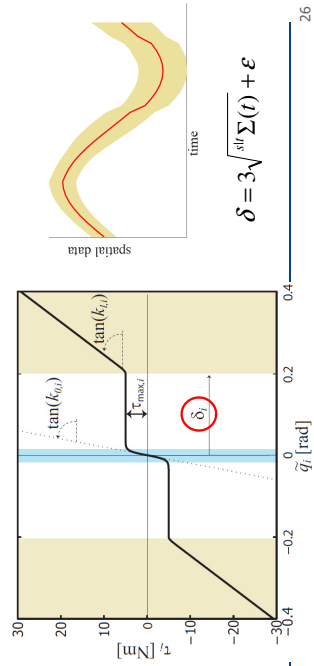
Compliant Control

Requirements

1. Precise tracking in free motion for motion primitive generation
2. Compliant interaction with low stiffness during teaching
3. Refinement tube: Limit the allowed deviation from the motion primitive

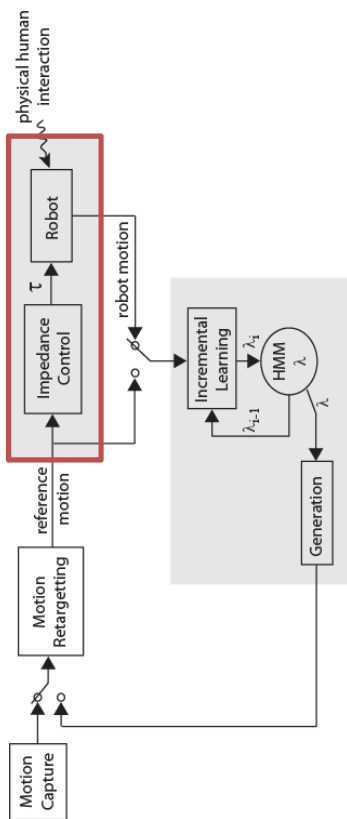
Integration into customized impedance controller

$$\tau = g(q) + M(q)\ddot{q}_d + C(q, \dot{q})\dot{q}_d - D\dot{q} - s(\ddot{q})$$



$$\delta = 3\sqrt{\text{tr}(\Sigma(t))} + \epsilon$$

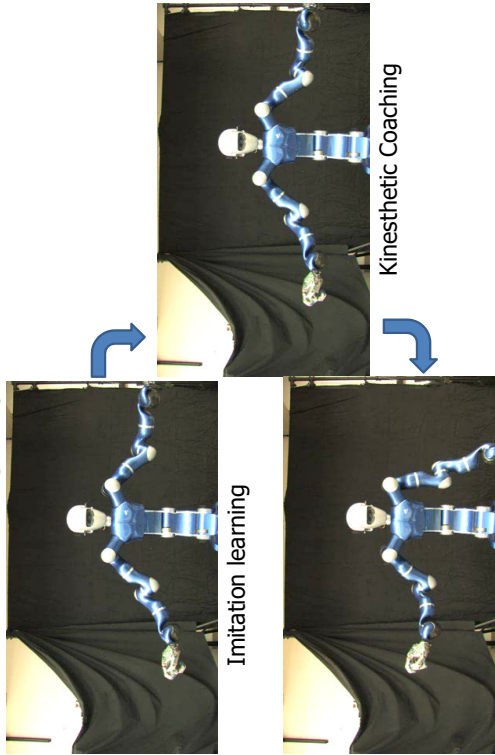
25



I taught a robot
the Pulp Fiction dance.

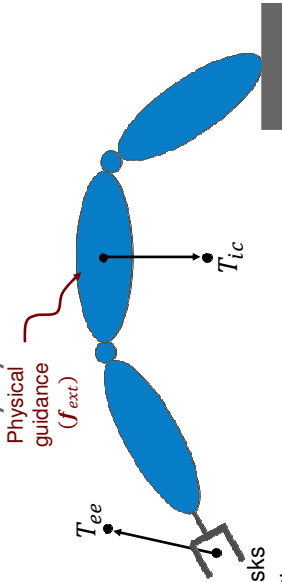


Incremental Learning Steps



[Autonomous Robots 2011, IROS 2010]

Teaching multiple tasks only by kinesthetic demos

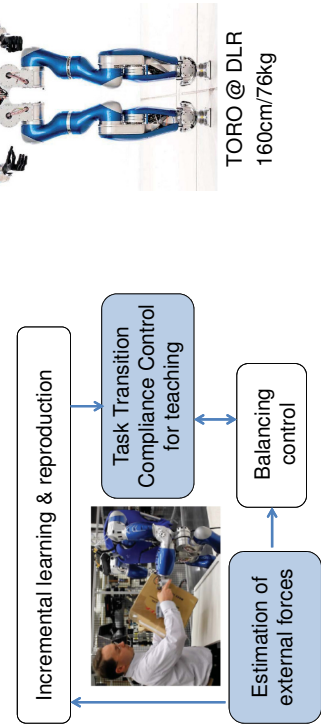


- 3 sets of prioritized tasks
 - $T^1 = T_{ee}$ no intervention
 - $T^2 = [T_{ee}, T_{ic}]$ weak intervention
 - $T^3 = [T_{ic}, T_{ee}]$ strong intervention
- Inverse kinematic solution \dot{q}^i for each T^i
- Transition among prioritized task definitions
 - $\dot{q} = \sum_{i=1}^3 w^i \dot{q}^i, \sum_{i=1}^3 w^i = 1$

[Saveriano et al, ICRA 2015] [An & Lee, ICRA 2015]

How about Kinesthetic teaching of a bipedal robot?

- External forces are detected by disturbance observer
- Teaching forces are integrated into predictive balancing controller



Collaboration with Henze, Ott at DLR [IROS 2013]

Kinesthetic Teaching



Task demonstration (1/5)

Learned Movement



Autonomous task execution

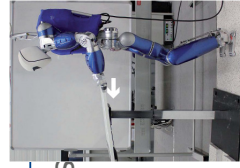
End-Effector



Null Space

Kinesthetic teaching leaving the end-effector task unchanged

Predictive Balancing using Interaction Forces



- Model (COM-ZMP) Effective torque acting around COM

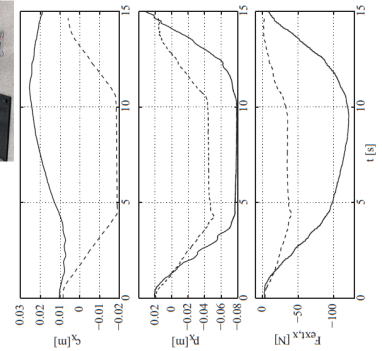
$$\ddot{c} = \omega^2 (c - p) + \frac{1}{m \cdot c_z} \begin{bmatrix} 0 & 1 \\ -1 & 0 \end{bmatrix} \tau^{LIP}$$

COM ZMP

- Model Predictive Control using ZMP input combined with simple disturbance model
Optimization function:

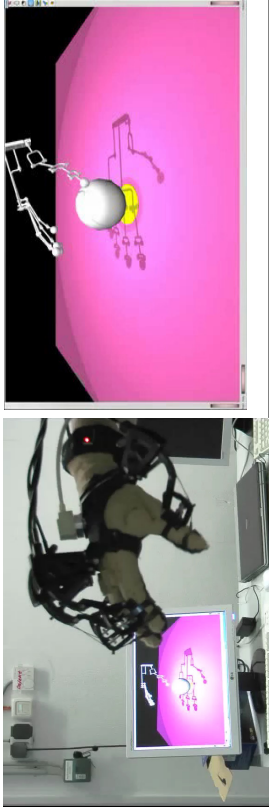
$$J = \frac{1}{2} \dot{z}^T R \dot{z} + \frac{1}{2} p^T Q p + \frac{1}{2} (B \dot{p}_k + \dot{E} \dot{\tau}_k^T)^T P (B \dot{p}_k + \dot{E} \dot{\tau}_k^T)$$

Soft constraint, aims at compensating external forces via ZMP with little COM deviation



[IROS 2013]

Grasping Skill Learning from Motion & Force Data



Teleoperation using Cyberglove, Flock of Birds, & Cybergrasp (Haptic Feedback)

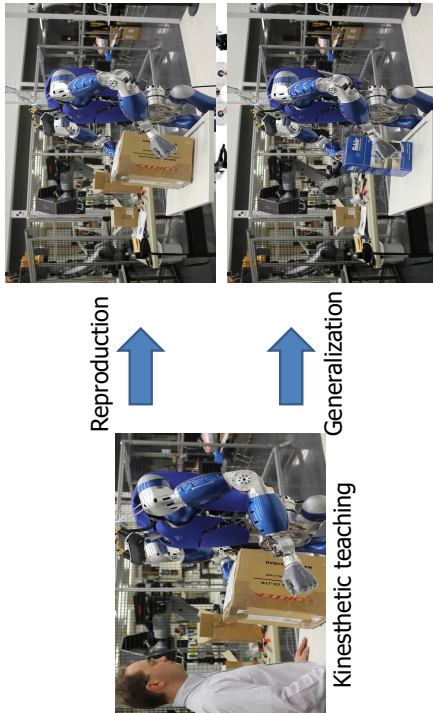
r_i [cm]	$\max(f^{(i)})$ [N]	$\bar{f}^{(i)}$ [N]	ΔT [ms]
3.6	3.21	3.20	28
4.0	5.41	3.20	11
4.8	3.21	7.12	209
5.6	3.21	3.20	7.04
6.0	3.21	12.92	39
Force control	ON	OFF	3.20
	OFF	ON	12.84
	ON	OFF	88
	OFF	ON	531
	ON	OFF	106
	OFF	ON	OFF
	ON	OFF	OFF

* unsuccessful grasping attempt

[Schmidts, Lee and Peer, IROS 2011]

Kinesthetic teaching of a bipedal humanoid robot?

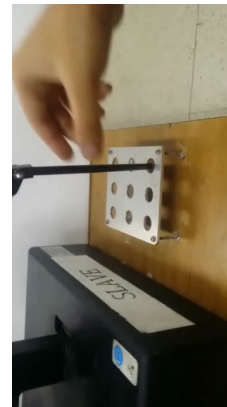
Teaching forces are detected by disturbance observer and integrated into predictive balancing controller



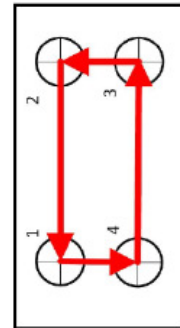
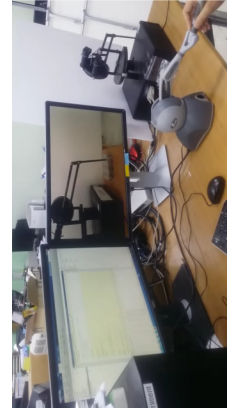
[IROS 2013] [ICRA 2015]

Challenges in Teaching by Teleoperation

Kinesthetic



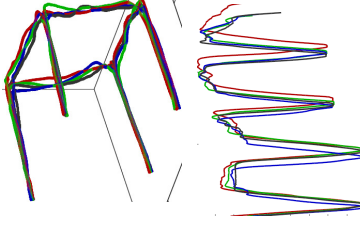
Teleoperation



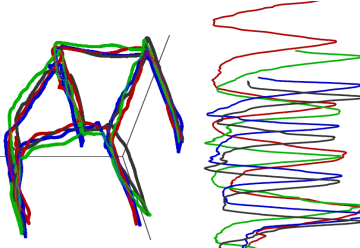
Collaboration with Prof. Ryu, Korea University of Technology and Education

Challenges in Teaching by Teleoperation

Kinesthetic



Teleoperation



- High level of spatial-temporal variations.
- High cost for demonstration

Learning Repetitive Teleoperation Tasks

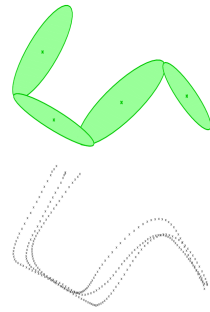
- Rhythmic DMP learning with a GMM

Canonical System $\dot{s} = \tau\omega$

Dynamic Movement Primitive (DMP)

$$\dot{v} = \tau\alpha_x(\beta_x(g-x) - v) + \tau a\mathcal{F}(s)$$

GMM Encoding



[WHC 2017]

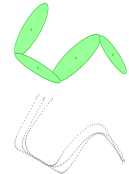
37

Learning Repetitive Teleoperation Tasks with DMP/GMM

Canonical System $\dot{s} = \tau\omega$

DMP $\dot{v} = \tau\alpha_x(\beta_x(g-x) - v) + \tau a\mathcal{F}(s)$

GMM Encoding



Dynamic Time

$$\begin{bmatrix} \mathcal{F}_1(s_0) \\ \vdots \\ \mathcal{F}_1(s_n) \end{bmatrix}$$

time

$$\begin{bmatrix} \mathcal{F}_1(s_0) & x_{1,0} \\ \vdots & \vdots \\ \mathcal{F}_1(s_n) & x_{1,n} \end{bmatrix}$$

unknown

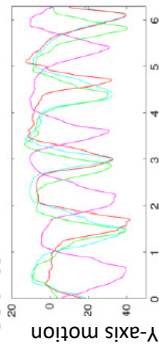
EM
GMM Update

EM
GMM Update
s Update

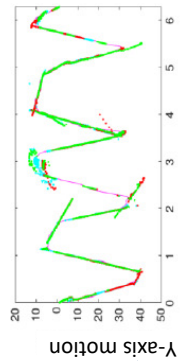
[WHC 2017]

38

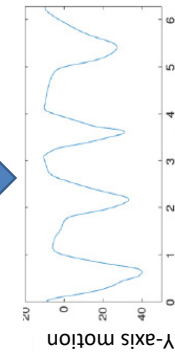
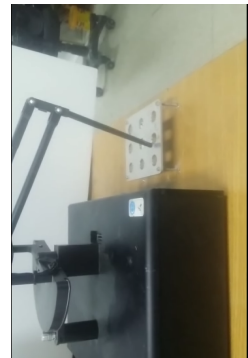
Results



Asynchronous trajectories



Synchronized data

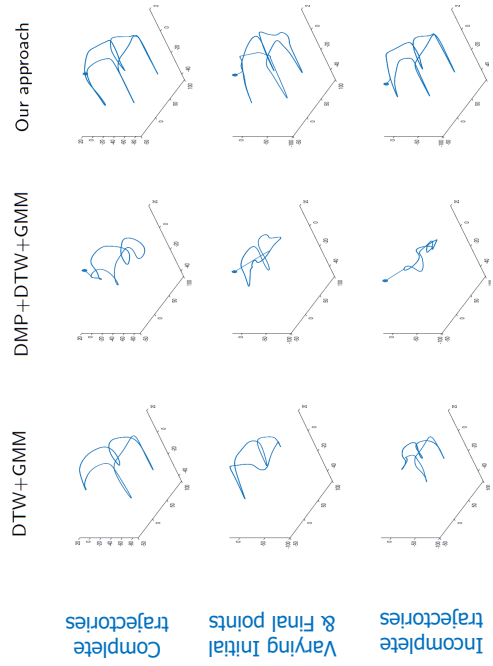


Reproduced trajectory

[WHC 2017]

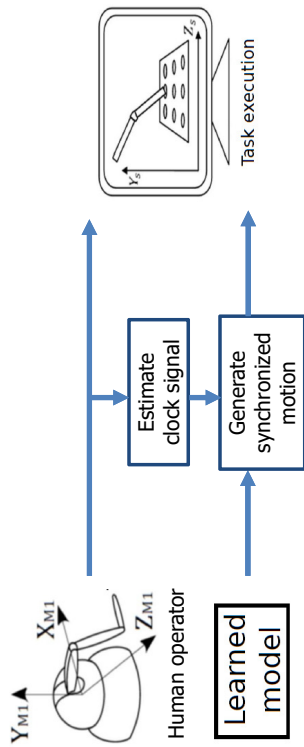
39

Comparison Results



40

Shared Control



[submitted to TIH]

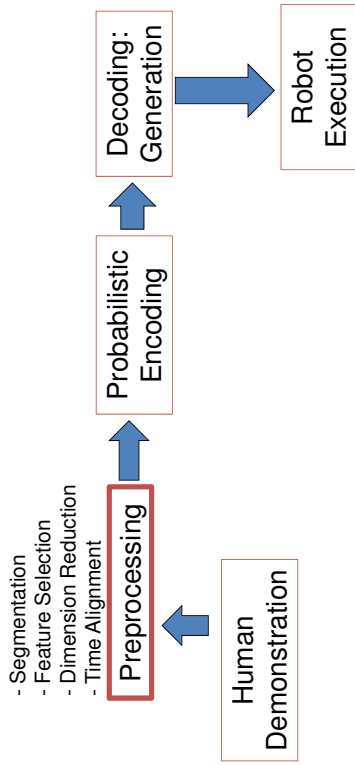
41

Feature Selection

- Desired Properties of Movement Primitives Descriptor
 - Robust to noise
 - Cross-subject motion recognition
 - Reconstruction
- Descriptor 1: CODE (Coordination-based action Descriptor)
- Descriptor 2: Invariant representation (SaLe)
- Descriptor 3: Bidirectional Invariant representation (SoSaLe)

43

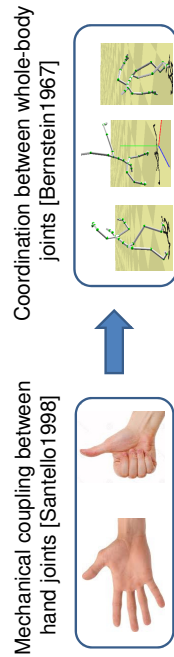
General Frame of Learning from Demonstrations



42

Feature Selection

- Properties of Movement Primitives Descriptor
 - Robust to noise
 - Cross-subject motion recognition
 - Reconstruction
- Descriptor 1: CODE (Coordination-based action Descriptor)

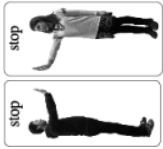


[Falco et al, RAL 2017]

44

Feature Selection

- Properties of Movement Primitives Descriptor
 - ✓ Robust to noise
 - ✓ Cross-subject motion recognition
 - ✓ Reconstruction
- Descriptor 2: Invariant representation (SaLe)
 - Rigid body motion → Extend to Articulated body motion
 - Invariant to translation, rotation, and scale factors



$$\gamma(t) = \frac{\|\dot{r}(t) \times \ddot{r}(t)\|}{\|\dot{r}(t)\|^2}$$

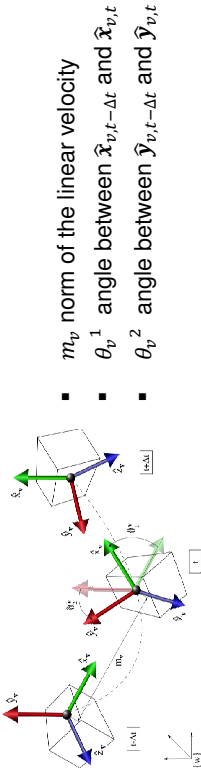
$$\xi(t) = \frac{\|\omega(t) \times \dot{\omega}(t)\|}{\|\omega(t)\|^2}$$

[ICRA 2015, Autonomous Robots 2017]

45

Feature Selection

- Properties of Movement Primitives Descriptor
 - ✓ Robust to noise
 - ✓ Cross-subject motion recognition
 - ✓ Reconstruction
- Descriptor 3: Bidirectional Invariant representation (SoSale)
 - m_v norm of the linear velocity
 - θ_v^1 angle between $\hat{x}_{v,t-\Delta t}$ and $\hat{x}_{v,t}$
 - θ_v^2 angle between $\hat{y}_{v,t-\Delta t}$ and $\hat{y}_{v,t}$

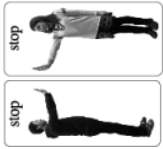


[Falco et al, RAL 2017]

46

Feature Selection

- Properties of Movement Primitives Descriptor
 - ✓ Robust to noise
 - ✓ Cross-subject motion recognition
 - ✓ Reconstruction
- Descriptor 2: Invariant representation (SaLe)
 - Rigid body motion → Extend to Articulated body motion
 - Invariant to translation, rotation, and scale factors



$$\gamma(t) = \frac{\|\dot{r}(t) \times \ddot{r}(t)\|}{\|\dot{r}(t)\|^2}$$

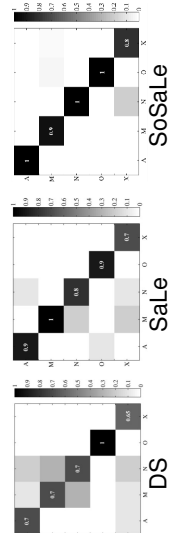
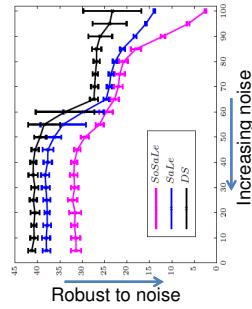
$$\xi(t) = \frac{\|\omega(t) \times \dot{\omega}(t)\|}{\|\omega(t)\|^2}$$

[ICRA 2015, Autonomous Robots 2017]

45

Bidirectional Invariant Representation Results

- Reconstruction Error
 - Without noise
 - DS (0.15 m/s) vs. SoSale (10⁻¹⁴ m/s)
- Robust to noise
- Recognition performance
 - Alphabet drawing using RGB-D



Preprocessing 1: Reduction of dimensionality

- Data presents redundancies $\dot{X}_s = A \xi_s$
- A Principal Component Analysis (PCA) technique is used to reduce the dimensionality of the data set
 - data space $X_s \in \{\theta_s, x_s, y_s\}$
 - latent space $\xi_s \in \{\xi_s^\theta, \xi_s^x, \xi_s^y\}$.
 - $\dot{X}_s = A \xi_s$

[Falco et al, RAL 2017]

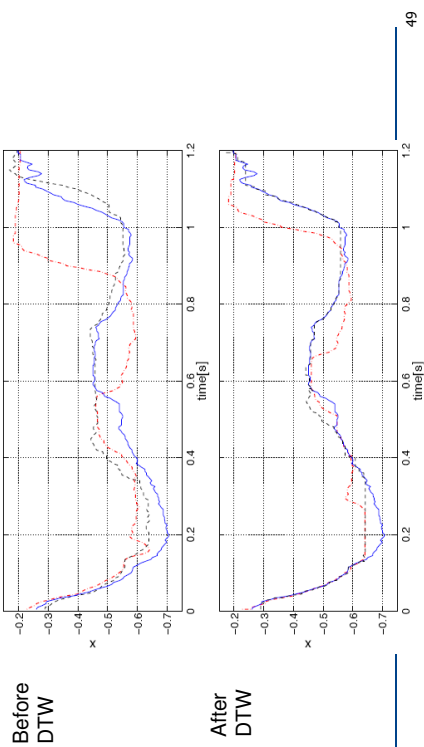
46

47

48

Preprocessing 2: Dynamic Time Warping

- Temporal alignment of the signals
- Performed in Latent space
- constraints: boundary condition, monotonicity, continuity



49

Segmentation

- Segmentation algorithm is an important enabler towards Autonomous Online Incremental Unsupervised Learning
- Velocity-based approach
 - Zero velocity crossing [Fod+ 2002]
- Probabilistic approach
 - focuses on the probabilistic changes [Kulic+ 2012]
- Classification-based approach [Lin+ 2014]
- Object relation based approach.
 - contact changes between objects and end-effectors [Aksoy+2011]

50

Part 1 Summary

- Learning from Demonstrations
 - Different teaching/demonstration modalities are used.
 - Interaction controllers for kinesthetic teaching are proposed for compliant human interaction, Teaching multi-tasks with varying task priorities, and a bipedal humanoid.
 - Preprocessing steps (e.g., feature selection, segmentation, alignment) are usually needed.

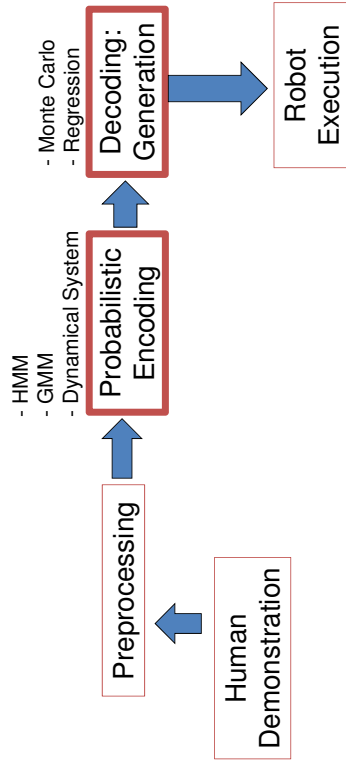


- Correspondence problem
- High dimensional motion
- Accidental disturbances
- Less consistent demonstrations

51

Part 2. Skill Representation in LfD and recent developments in LfD

General Frame of Learning from Demonstrations



53

Dynamical Movement Primitive (DMP)

- What to learn
 - Discrete movement: goal-directed
 - Rhythmic movement: specific amplitude and period
- How to learn
 - By training a system of 2nd order nonlinear differential equations
 - Modulation of spring-damper dynamics by a nonlinear function
 - Learning the nonlinear function based on a kinematic plan

ljspeert, Nakanishi, Schaal, Movement Imitation with Nonlinear Dynamical Systems in Humanoid Robots, ICRA, 2002

54

Dynamical Movement Primitive (DMP)

- a system of **internal states**
- Nonlinear acceleration modulation

$$\dot{s} = -\alpha s$$

$$\ddot{x} = k^p (\mu_T - x) - k^v \dot{x} + \underline{f}(s),$$

Nonlinear forcing term

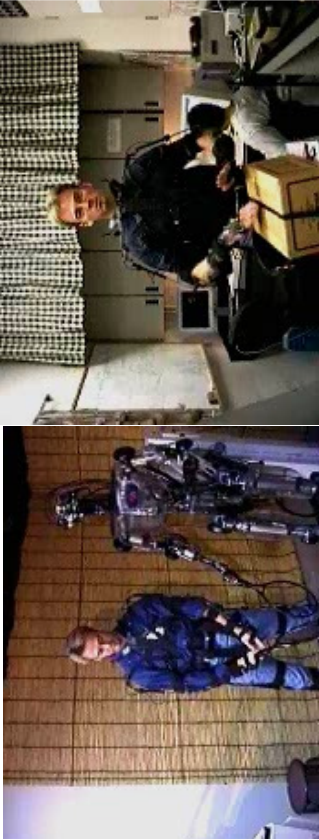
$$\text{with } \underline{f}(s) = \sum_{k=1}^K \phi_k(s) s \mathbf{F}_k.$$

Gaussian basis function

- Train by Locally Weighted Regression (LWR)
- The dynamical system asymptotically converges to the attractor point.

55

Dynamical Movement Primitive (DMP)



Discrete DMP

Rhythmic DMP

56

Gaussian Mixture Model / Gaussian Mixture Regression

- Then, it computes the regression function from the learning joint density model.
- In Gaussian Mixture Regression (GMR), both input and output variables can be multidimensional.

$$x_t = \begin{bmatrix} x_t^I \\ x_t^O \end{bmatrix}, \quad \mu_i = \begin{bmatrix} \mu_i^I \\ \mu_i^O \end{bmatrix}, \quad \Sigma_i = \begin{bmatrix} \Sigma_i^I & \Sigma_i^{IO} \\ \Sigma_i^{OI} & \Sigma_i^O \end{bmatrix}$$

$$\mathcal{P}(x_t^O | x_t^I) \sim \sum_{i=1}^K h_i(x_t^I) \mathcal{N}(\hat{\mu}_i^O(x_t^I), \hat{\Sigma}_i^O)$$

with $\hat{\mu}_i^O(x_t^I) = \mu_i^O + \Sigma_i^{OI} \Sigma_i^I{}^{-1} (x_t^I - \mu_i^I)$,

$$\hat{\Sigma}_i^O = \Sigma_i^O - \Sigma_i^{OI} \Sigma_i^I{}^{-1} \Sigma_i^{IO}$$

and $h_i(x_t^I) = \frac{\pi_i \mathcal{N}(x_t^I | \mu_i^I, \Sigma_i^I)}{\sum_k^K \pi_k \mathcal{N}(x_t^I | \mu_k^I, \Sigma_k^I)}$,

59

Gaussian Mixture Model / Gaussian Mixture Regression

- First, it models the joint probability density of the data in the form of a Gaussian Mixture Model (GMM), which is estimated by the EM procedure.

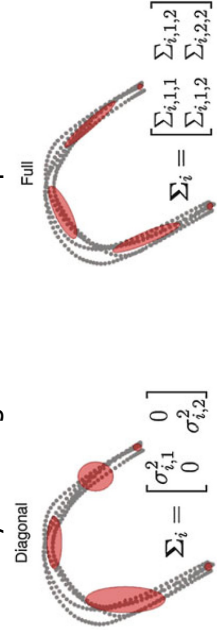
$$p(\xi_j) = \sum_{k=1}^K p(k) p(\xi_j | k) = \sum_{k=1}^K p(k) \mathcal{N}(\xi_j; \mu_k, \Sigma_k)$$

a mixture of K Gaussians

58

Comparison between DMP and GMM/GMR

- A standard DMP corresponds to a GMM with diagonal covariance.
- GMM/GMR extends DMP
 - Encoding of local correlation between the motion variables by full covariances
 - Estimating the parameters of the Radial Basis Functions, similar to a GMM fitting problem
 - Significantly reducing the number of required RBFs



60

Hidden Markov Model (HMM)

• **A Hidden Markov Model is characterized by the following**

- N, the number of states in the model $S=\{S_1, S_2, \dots, S_N\}$
- M, the number of discrete observation symbols $V=\{v_1, v_2, \dots, v_M\}$
- A= $\{a_{ij}\}$, the state transition probability

$$a_{ij} = P(q_{t+1} = S_j | q_t = S_i) \quad \sum_j a_{ij} = 1, \forall i$$

-B= $\{b_j(k)\}$, the observation probability distribution

$$b_j(k) = P(o_t = v_k | q_t = S_j) \quad \sum_k b_j(k) = 1, \forall j$$

- π , the initial state distribution

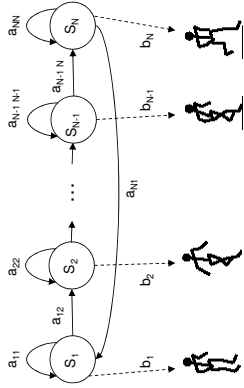
$$\pi_j = P(q_1 = S_j) \quad \sum_j \pi_j = 1$$

• **Therefore, an HMM is specified by two scalars (N and M) and three probability distributions (A, B and π)**

- In what follows, we will represent an HMM by the compact notation

$$\lambda = (A, B, \pi)$$

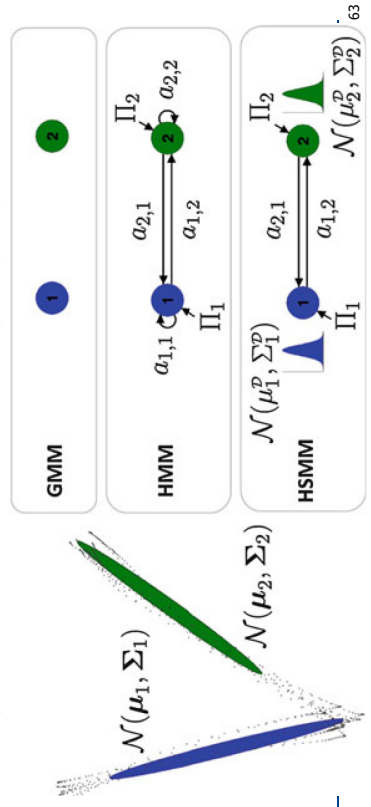
Hidden Markov Model (HMM)



- Stochastic model capturing both spatial and temporal variability
- Model Training by the EM algorithm (Baum-Welch)
- Recognition
- Generation (stochastic or deterministic)

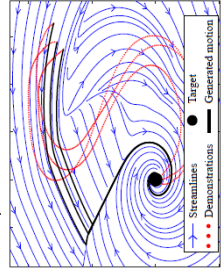
GMM vs. HMM vs. HSMM

- HMM
 - A GMM with latent variables changing over time
 - Not very accurate to model duration information
- HSMM (Hidden Semi-Markov Model)
 - Explicit model of the state duration using a single lognormal distribution



Autonomous Dynamical Systems

- Time-invariant autonomous dynamical systems encode the entire attractor landscape in the state-space of the observed data.
- GMR can be employed to retrieve an autonomous system from the joint distribution encoded in a GMM.
- Stable Estimator of Dynamical Systems (SEDS) [Khansari-Zadeh+ 2011]
 - GMM parameter estimation: instead of EM, a constrained optimization procedure
 - Global asymptotic stability guarantee
 - May distort the original paths



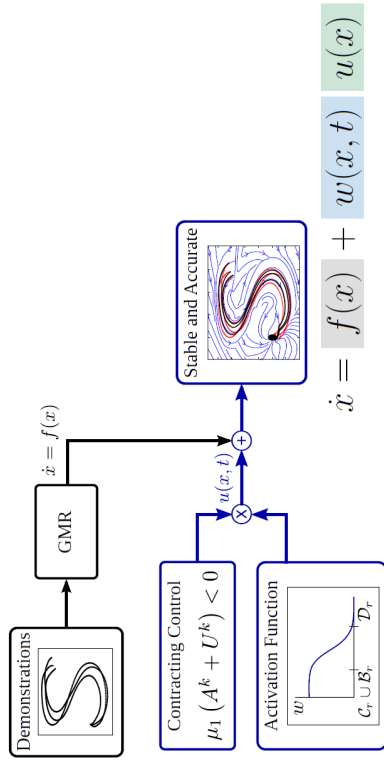
Approaches for Autonomous Dynamical Systems

- Stable Estimator of Dynamical Systems (SEDS) [Khansari-Zadeh+ 2011]
 - **May distort the original paths**
- 2-step Learning approaches
 - Control Lyapunov Function based Dynamic Movements (CLFDM) [Khansari-Zadeh+ 2014]
 - Geometrical diffeomorphic transformation [Perrin+ 2016]
 - Contraction Metric based approach [Ravichandar+ 2015]
 - + **Stability and Accuracy**
 - **Training Time**
- Contracting Gaussian Mixture Regression (C-GMR) [Blocher+ 2017]

65

Can we prove Stability of learned skills?

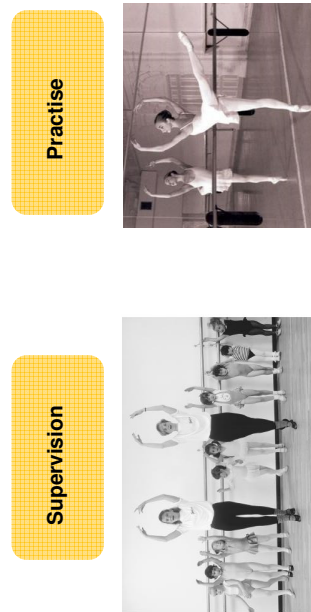
Contracting Gaussian Mixture Regression (C-GMR)



[Blocher+, URA117, Outstanding Paper Award]

66

Behavior Learning Steps

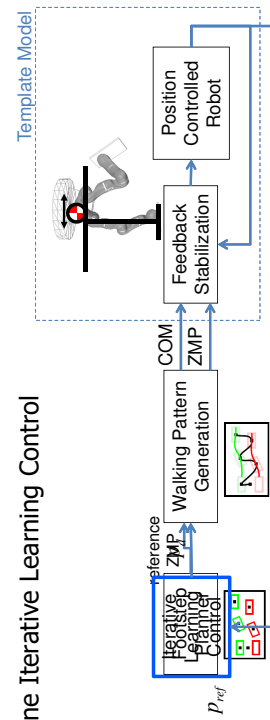
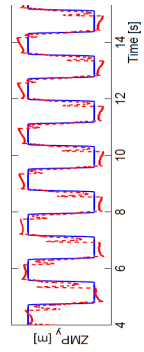


Reinforcement Learning in movement and compliance of manipulation tasks [IROS 2008, IROS 2009, HFR 2014, HFR 2015, IROS 2015, IROS 2017, RAL2017 submitted]

67

Learning Control for Bipedal Walking

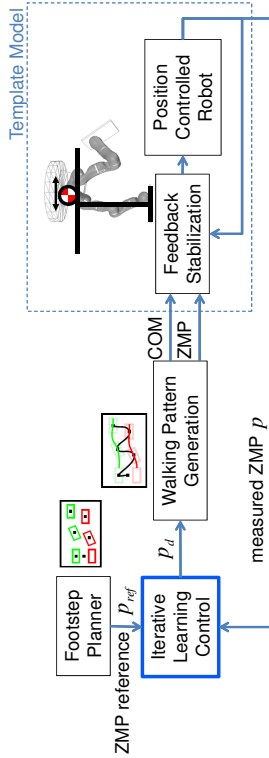
- **Conventional ZMP Based Walking**
 - Feedback stabilization → tracking template model behavior
 - Dynamically consistent walking pattern generation
 - Existing ZMP tracking error
- **Online Iterative Learning Control**



Collaboration with Ott, DLR [ICRA 2015] [TRO 2016]

68

Framework of Online ILC of ZMP



ZMP-OILC update law: P-type ILC with forgetting factor

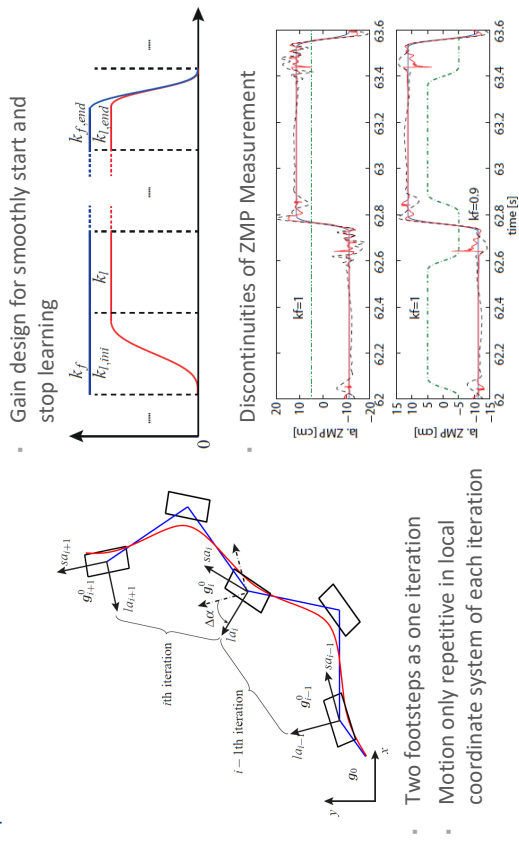
$$p_d(i) = p_{ref}(i) + k_f R(p_d(i-1) - p_{ref}(i-1)) - k_f R(p(i-1) - p_{ref}(i-1))$$

ZMP reference for current step learned ZMP so far ZMP error from last step

[ICRA 2015]

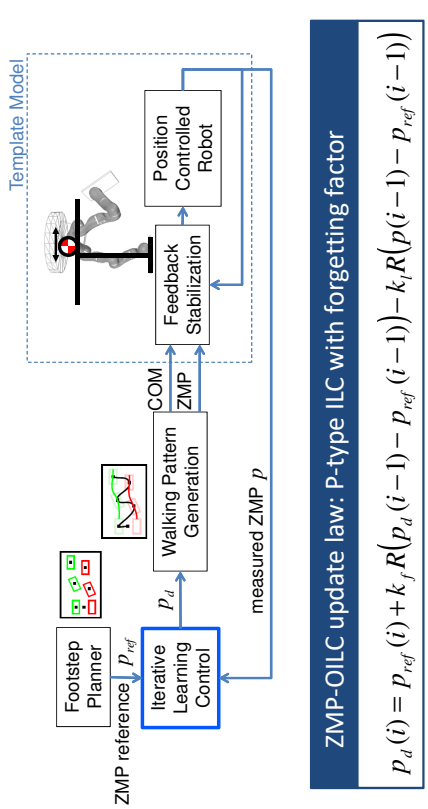
69

Implement of ZMP-OILC



70

Convergence and ZMP Error



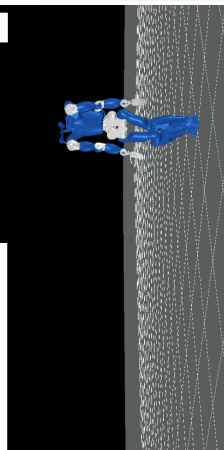
ZMP tracking error decreases fast in the first 3 to 5 iterations.

ZMP-OILC converges slower due to non-repetitive disturbances.

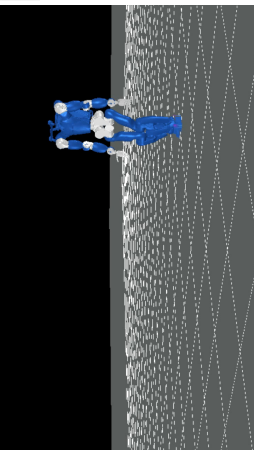
[ICRA 2015]

71

With Online Learning



Without Online Learning



Forward walking
step length 15cm
step time 0.8s
External force at waist joint
Magnitude 65N, Duration 0.5s
In sagittal direction

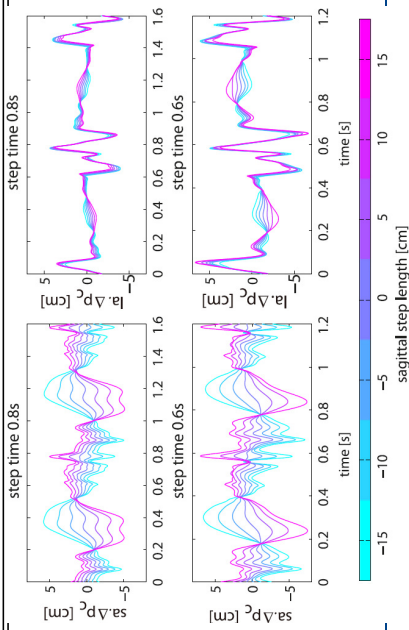
[ICRA 2015] [TRO 2016]

72

Learning Dataset of Compensative ZMP Term

Sagittal Straight Walking (SSW) Lateral Straight Walking (LSW) Circle Walking

$d_{sa} = \{-15, -10, -5, 0, 5, 10, 15\}$ cm $d_{sa} = 0$ cm $r = \{0.5, 0.75, 1\}$ m
 $d_{la} = 0$ cm $d_{la} = \{-7.5, -5, -2.5, 0, 2.5, 5, 7.5\}$ cm $\Delta\alpha = \{10, 20\}^\circ$
 $T_s = \{0.6, 0.8, 1.0\}$ s $T_s = \{0.6, 0.8, 1.0\}$ s $T_s = \{0.6, 0.8, 1.0\}$ s



73

Behavior Learning Steps

- Supervision
- Practise
- Scalability

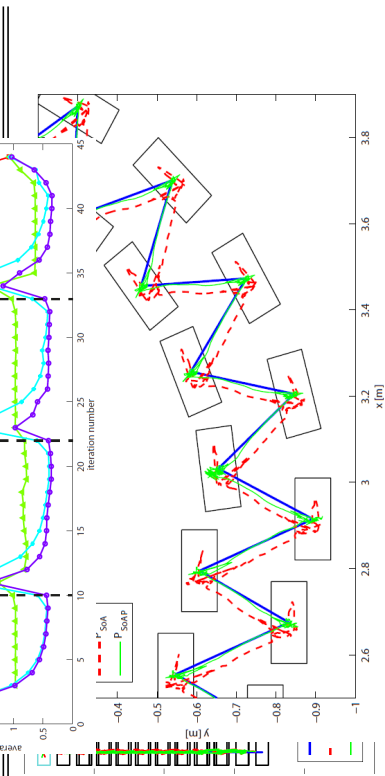


75

Learning Dataset of Compensative Term

Sagittal Su Motion 1 Motion 2 Motion 3 Motion 4 e Walking

$d_{sa} = \{0.5, 0.75, 1\}$ m
 $d_{la} = 0$ cm $\Delta\alpha = \{10, 20\}^\circ$
 $T_s = \{0.6, 0.8, 1.0\}$ s



74

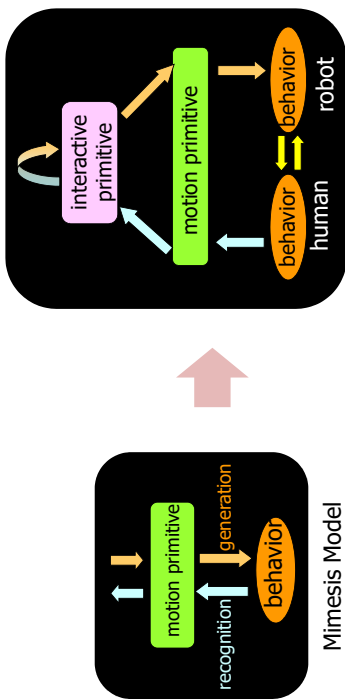
Motion → Interaction



- Human motion imitation
- Learn/Recognize/Generate Motion Primitives
- Learn/Recognize/Generate Interaction Rules
- Contact transition

76

Motion Learning



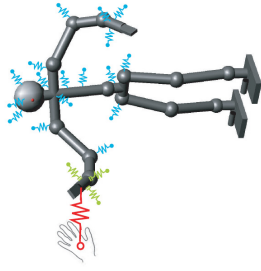
Mimetic Communication Model

- How to react to human's action
- Contact location & timing

[ICRA 2009] [IJRR 2010] [ICRA KUKA Service Robotics Best Paper Award Finalist] 77

Online Adaptation for Physical Contact Establishment

- Additional spring (red) connected to the desired contact point.
- Project the forces of the hand's marker springs (green) into a subspace related to the hand orientation.



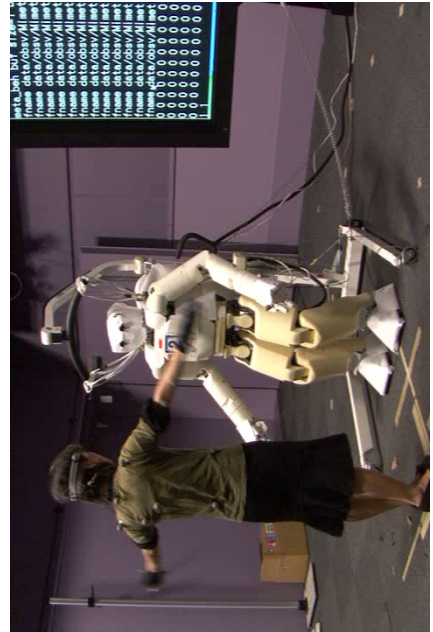
$$\begin{pmatrix} \tau \\ f \end{pmatrix} = -D(q) \begin{pmatrix} \dot{q} \\ \ddot{q} \end{pmatrix} + \sum_{v \in \text{MH}} k_v J_v^T(q) (r_{v,i} - r_i(q, x)) + \sum_{k=R,L} J_{h,k}^T(q) \left(\delta_k F_{v,k} + (q - \delta_k) F_{v,k} \right) T_{v,k}$$

Distance information
→ smooth transition
contact/non-contact

[ICRA 2009] [IJRR 2010] [ICRA KUKA Service Robotics Best Paper Award Finalist] 78

Experiments

- 12 motion primitives and 8 interaction primitives
- Implementation to humanoid robot (38DOF), 30DOF is controlled.
- Position based Impedance Control to the upper body



[ICRA 2009] [IJRR 2010] [ICRA KUKA Service Robotics Best Paper Award Finalist] 79

Cognition enabled physical human robot cooperation

Boost task performance by task knowledge gained over time by

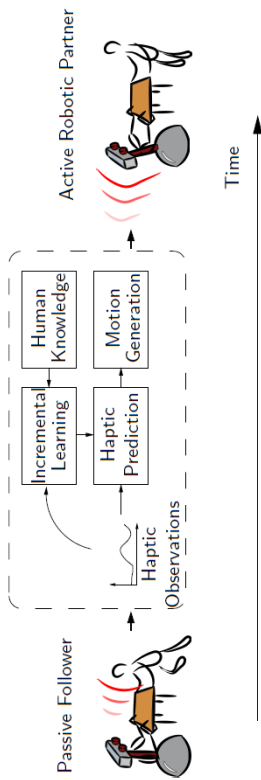
- Observation and statistical analysis of human task execution patterns.
- Online learning and prediction of human motion and force profiles.



Collaboration with Kulic, Nakamura, Hirche
[IJRR 2011, IROS2011, ICRA 2012, IROS 2012]

80

Framework Overview



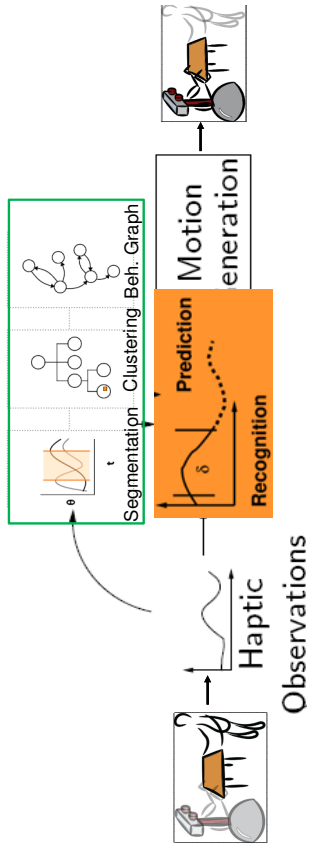
Proposed Method

Combine incremental learning techniques with feedback control

81

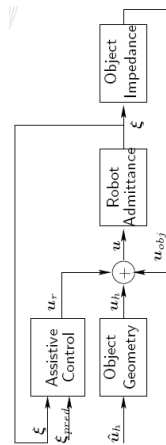
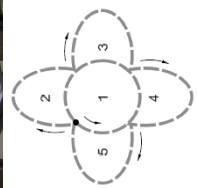
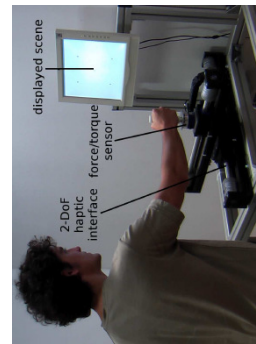
251

Experience-Driven Robotic Assistant



82

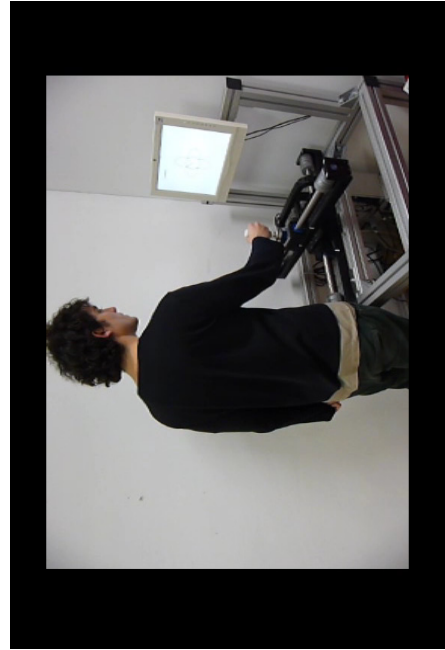
Experiment in 2D Virtual Scenario



- 2D virtual scenario
- No initial knowledge
- As learning proceeds, prediction starts
- Robot behavior is changed from "passive follower" to "load sharing"

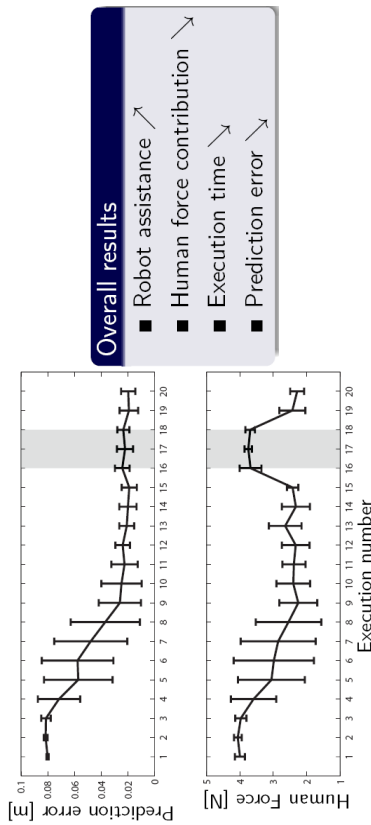
84

Experience-Driven Robotic Assistant



Experiment in 2D Virtual Scenario

- Robot learning, predicting and assisting during execution
- Repetitions 16 to 18 without assistance

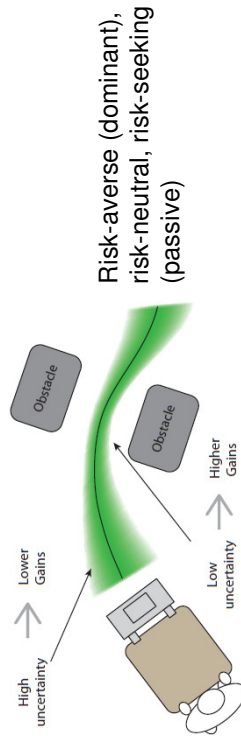


[IJRR 2011, IROS2011, ICRA 2012, IROS 2012]

Risk-sensitive Optimal Feedback Control

- Assistive behavior
 $u = K(\xi - \hat{\xi})$
- Uncertainty model for desired trajectory and exerted force
 $\hat{\xi} = \{\hat{\mu}_\xi, \hat{\Sigma}_\xi\}$, $\hat{a} = \{\hat{\mu}_u, \hat{\Sigma}_u\}$, with $\xi = (x \ \dot{x})^T$
- Risk sensitive stochastic optimal control

$$J = \sum_{k=1}^T ((\xi_k - \hat{\mu}_\xi)^T \hat{\Sigma}_{\xi,k}^{-\frac{1}{2}} Q \hat{\Sigma}_{\xi,k}^{-\frac{1}{2}} (\xi_k - \hat{\mu}_\xi) + u_{r,k}^T R u_{r,k})$$

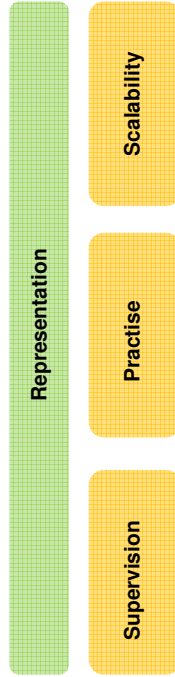


[ICRA2012, IROS2012]

Part 2 Summary

- Various representation forms are used for Movement Primitive Encoding and decoding
 - GMM/GMR, HMM/HMM, DMP, Autonomous Dynamical Systems, GP
- Learning from Demonstration approaches can be combined with Learning through Practice, e.g. iterative learning control, reinforcement learning.
- Recent advances in LfD allows robots to learn not only movements but also human robot interaction and cooperation.
 - With the hierarchical structure of movement primitives and interaction primitives, it can learn interaction patterns.
 - A robotic assistant behavior can be learned and improved for human robot haptic cooperative tasks during interaction, supported by unsupervised continuous learning.

Motor Skill Learning for Autonomous Robots

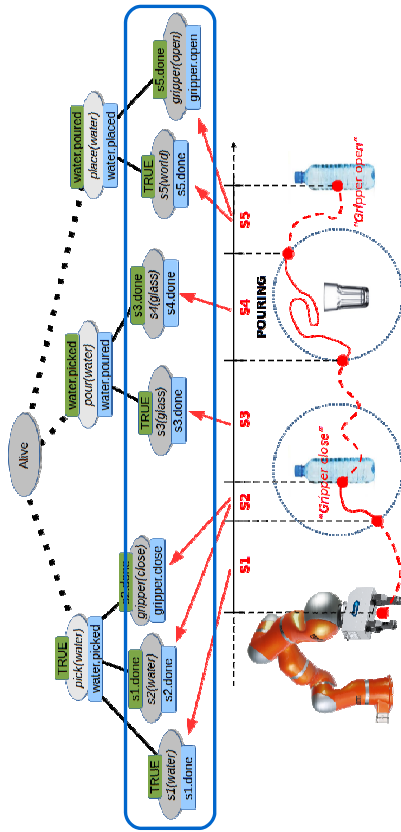


What's next?

- Bridging the Gap between Symbolic and Continuous Knowledge.
 - Current LFD approaches are tightly linked to low-level control capabilities. High-level learning approaches can provide the level of abstraction required to perform (context aware) cognitive tasks.
 - Learning the structure of models

89

Learning Structured Tasks from demonstrations



- Framework that integrates imitation learning, automatic segmentation, attentional supervision, and cognitive control to learn and flexibly execute structured tasks

[Caccavale+ AURO 2018]

90

What's next?

- Learning Control Representation for Wide-Ranging Data
 - A robot can collect a large amount of information from a large variety of sensors.
 - On the other hand, it is limited by the number of experiences or demonstrations that the user can provide.
 - Simulator helps, but often do not reflect reality in a sufficient level of details.
- Social Interaction in Robot Learning Control
 - Existing LFD approaches do not account for the way in which data are collected.
 - Iterative interaction with the users can be exploited to influence the quality and nature of the collected data.
 - How should robots request feedback from the user, either explicitly or implicitly?
 - Linked with active learning with multimodal social interaction aspect.

91

References

1. Calinon and Lee, Learning Control. In: Humanoid Robotics: A Reference. Springer, 2017
2. Ijspeert A.J., Nakanishi J., Schaal S., Learning attractor landscapes for learning motor primitives, *Advances in Neural Information Processing Systems* 15 (NIPS), 2003, pp 1547-1554.
3. Calinon S, Guenter F, Billard A (2007) On learning, representing and generalizing a task in a humanoid robot. *IEEE Transactions on Systems, Man and Cybernetics, Part B, Special issue on robot learning by observation, demonstration and imitation* 37(2):286–298
4. Lee D, Ott C (2011) Incremental Kinesthetic Teaching of Motion Primitives Using the Motion Refinement Tube, *Autonomous Robots (AURO)*, 31(2):115-131, 2011.
5. Lee D, Ott C, Nakamura Y (2010) Mimetic Communication Model with Compliant Physical Contact in Human-Humanoid Interaction, *The International Journal of Robotics Research (IJRR)*, 29(13):1684-1704
6. Caccavale R, Saveriano M, Finzi A and Lee D (2018) Kinesthetic Teaching and Attentional Supervision of Structured Tasks in Human-Robot Interaction, *Autonomous Robots (AURO)*

Thank you

for your attention

Thanks to Collaborators :

- Matteo Saveriano
- Affan Pervez
- Kai Hu
- Sangik An
- Jose Medina
- Angelika Peer
- Alexander Schmidts
- Sandra Hirche
- Joachim Hermsdörfer
- Yoshihiko Nakamura
- Dana Kulic
- Jee-Hwan Ryu
- Christian Ott
- Sami Haddadin
- Roberto Lampariello
- Alexander Werner
- Bern Henze

Part 4

List of Participants

Atte Aalto
University of Luxembourg
Luxembourg
atte.aalto@uni.lu

Francesco Acciani
University of Twente
The Netherlands
f.acciani@utwente.nl

Mahya Adibi
Delft University of Technology
The Netherlands
m.adibi@tudelft.nl

Muhammad Z. Almuzakki
University of Groningen
The Netherlands
m.z.almuzakki@rug.nl

Javier Alonso Mora
Delft University of Technology
The Netherlands
j.alonsomora@tudelft.nl

Hussein Altartouri
Université Libre de Bruxelles
Belgium
hussein.altartouri@ulb.ac.be

Alex R.P. Andrien
Eindhoven University of Technology
The Netherlands
a.r.p.andrien@tue.nl

Murat Arcak
University of California Berkeley
USA
arcak@berkeley.edu

Sajad Azizi
Université Libre de Bruxelles
Belgium
sajad.azizi@ulb.ac.be

Mohammadhadi Balaghiinaloo
Eindhoven University of Technology
The Netherlands
m.balaghiinaloo@tue.nl

Harshit Bansal
Eindhoven University of Technology
The Netherlands
h.bansal@tue.nl

Henrik P.G.J. Beelen
Eindhoven University of Technology
The Netherlands
h.p.g.j.beelen@tue.nl

Ruud Beerens
Eindhoven University of Technology
The Netherlands
r.beerens@tue.nl

Giuseppe Belgioioso
Eindhoven University of Technology
The Netherlands
g.belgioioso@tue.nl

Guillaume Berger
Université Catholique de Louvain
Belgium
guillaume.berger@uclouvain.be

Bart Besselink
University of Groningen
The Netherlands
b.besselink@rug.nl

Georgios Birpoutsoukis
Université Catholique de Louvain
Belgium
georgios.birpoutsoukis@uclouvain.be

Lennart L.G. Blanken
Eindhoven University of Technology
The Netherlands
l.l.g.blanken@tue.nl

Thomas C. Blanken
Eindhoven University of Technology
The Netherlands
t.c.blanken@tue.nl

Nicolas Bono Rossello
Université Libre de Bruxelles
Belgium
nicolas.bono.rossello@ulb.ac.be

Luis P. Borja Rosales
University of Groningen
The Netherlands
l.p.borja.rosales@rug.nl

Giulio Bottegal
Eindhoven University of Technology
The Netherlands
g.bottegal@tue.nl

Dennis Bruijnen
Philips Innovation Services
The Netherlands
dennis.bruijnen@philips.com

Brandon J. Caasenbrood
Eindhoven University of Technology
The Netherlands
b.j.caasenbrood@tue.nl

Ricardo A. Cajo Diaz
Ghent University
Belgium
ricardoalfredo.cajodiaz@ugent.be

Federico Califano
University of Bologna
Italy
federico.califano2@unibo.it

Raffaella Carloni
University of Groningen
The Netherlands
r.carloni@rug.nl

Costanza Catalano
Gran Sasso Science Institute
Italy
costanza.catalano@gssi.it

Gaia Cavallo
Vrije Universiteit Brussel
Belgium
gaia.cavallo@vub.be

Carlo Cenedese
University of Groningen
The Netherlands
c.cenedese@rug.nl

Nelson P.K. Chan
University of Groningen
The Netherlands
n.p.k.chan@rug.nl

Liangming M. Chen
University of Groningen
The Netherlands
l.m.chen@rug.nl

Xiaodong Cheng
University of Groningen
The Netherlands
x.cheng@rug.nl

Pierre-Yves Chevalier
Université Catholique de Louvain
Belgium
pierre-yves.chevalier@uclouvain.be

Benjamin Chiem
Université Catholique de Louvain
Belgium
benjamin.chiem@uclouvain.be

Pieter Collins
Maastricht University
The Netherlands
pieter.collins@maastrichtuniversity.nl

Andrés Cotorruelo Jimenez
Université Libre de Bruxelles
Belgium
andres.cotorruelo.jimenez@ulb.ac.be

Pepijn B. Cox
Eindhoven University of Technology
The Netherlands
p.b.cox@tue.nl

Michele Cucuzzella
University of Groningen
The Netherlands
m.cucuzzella@rug.nl

Jose R. Dominguez Frejo
Delft University of Technology
The Netherlands
j.r.dominguezfrejo@tudelft.nl

Amritam Das
Eindhoven University of Technology
The Netherlands
am.das@tue.nl

Kobe De Becker
Katholieke Universiteit Leuven
Belgium
kobe.debecker@kuleuven.be

Jeroen De Geeter
Vrije Universiteit Brussel
Belgium
jeroen.de.geeter@vub.be

Bram de Jager
Eindhoven University of Technology
The Netherlands
a.g.de.jager@tue.nl

Massimo De Mauri
Katholieke Universiteit Leuven
Belgium
massimo.demauro@kuleuven.be

Andreas De Preter
Katholieke Universiteit Leuven
Belgium
adepreter@octinion.com

Wilm Decré
Katholieke Universiteit Leuven
Belgium
wilm.decre@kuleuven.be

Jan Decuyper
Vrije Universiteit Brussel
Belgium
jan.decuyper@vub.be

Daniel A. Deenen
Eindhoven University of Technology
The Netherlands
d.a.deenen@tue.nl

Boris Dehem
Université Catholique de Louvain
Belgium
boris.dehem@uclouvain.be

Marzieh Dolatabadi Farahani
Eindhoven University of Technology
The Netherlands
m.dolatabadi.farahani@tue.nl

Yanick G.M. Douven
Eindhoven University of Technology
The Netherlands
y.g.m.douven@tue.nl

Jaap Eising
University of Groningen
The Netherlands
j.eising@rug.nl

Jacob C. Engwerda
Tilburg University
The Netherlands
engwerda@uvt.nl

Enzo Evers
Eindhoven University of Technology
The Netherlands
e.evers@tue.nl

Chyannie A. Fahdzyana
Eindhoven University of Technology
The Netherlands
c.a.fahdzyana@tue.nl

Marc A. Favier
Technical University Kaiserslautern
Germany
marc-alexandre.favier@mv.uni-kl.de

Jeroen E. Fransman
Delft University of Technology
The Netherlands
j.e.fransman@tudelft.nl

Caspar Geelen
Wageningen University and Research
The Netherlands
caspar.geelen@wur.nl

Joris Gillis
Katholieke Universiteit Leuven
Belgium
joris.gillis@kuleuven.be

Alejandro Goldar Davila
Université Libre de Bruxelles
Belgium
agoldar@ulb.ac.be

Lulu Gong
University of Groningen
The Netherlands
l.gong@rug.nl

François Gonze
Université Catholique de Louvain
Belgium
francois.gonze@uclouvain.be

Martijn A. Goorden
Eindhoven University of Technology
The Netherlands
m.a.goorden@tue.nl

Alain Govaert
University of Groningen
The Netherlands
a.govaert@rug.nl

Nik L.M. Grubben
Wageningen University
The Netherlands
nik.grubben@wur.nl

Martin Gueuning
University of Namur
Belgium
martin.gueuning@unamur.be

Marvyn Gulina
University of Namur
Belgium
marvyn.gulina@unamur.be

M. Guo
University of Groningen
The Netherlands
m.guo@rug.nl

T.M. Hafkamp
Eindhoven University of Technology
The Netherlands
t.m.hafkamp@tue.nl

Wouter Hakvoort
University of Twente
The Netherlands
wouter.hakvoort@utwente.nl

Jurre Hanema
Eindhoven University of Technology
The Netherlands
j.hanema@tue.nl

Ramy A.M. Hashem
University of Twente
The Netherlands
r.a.m.rashadhashem@utwente.nl

Anthony Hastir
University of Namur
Belgium
anthony.hastir@student.unamur.be

Maurice Heemels
Eindhoven University of Technology
The Netherlands
w.p.m.h.heemels@tue.nl

Hanif Heidari
Damghan University
Iran
hanif.heidari@gmail.com

Hans Hellendoorn
Delft University of Technology
The Netherlands
j.hellendoorn@tudelft.nl

Julien Hendrickx
Université Catholique de Louvain
Belgium
julien.hendrickx@uclouvain.be

Domagoj Herceg
IMT School for Advanced Studies Lucca
Italy
domagoj.herceg@imtlucca.it

Ben Hermans
Katholieke Universiteit Leuven
Belgium
ben.hermans2@kuleuven.be

Laurens Jacobs
Katholieke Universiteit Leuven
Belgium
laurens.jacobs@kuleuven.be

Niloofar Jahanshahi
Delft University of Technology
The Netherlands
n.jahanshahi@tudelft.nl

Bayu Jayawardhana
University of Groningen
The Netherlands
b.jayawardhana@rug.nl

Guillaume Jeanne
Centrale Supelec
France
guillaume.jeanne@centralesupelec.fr

Mark Jeeninga
University of Groningen
The Netherlands
m.jeeninga@rug.nl

Jiajia Jia
University of Groningen
The Netherlands
j.jia@rug.nl

Yu Jiang
Wageningen University and Research
The Netherlands
yu.jiang@wur.nl

Junjie Jiao
University of Groningen
The Netherlands
j.jiao@rug.nl

M. Hakan Kandemir
Wageningen University and Research
The Netherlands
hakan.kandemir@wur.nl

Yuri Kapitanyuk
University of Groningen
The Netherlands
yura.kapitanyuk@gmail.com

Karel Keesman
Wageningen University and Research
The Netherlands
karel.keesman@wur.nl

Tamas Keviczky
Delft University of Technology
The Netherlands
t.keviczky@tudelft.nl

Zuan Khalik
Eindhoven University of Technology
The Netherlands
z.khalik@tue.nl

Dhruv Khandelwal
Eindhoven University of Technology
The Netherlands
d.khandelwal@tue.nl

Lizan Kivits
Eindhoven University of Technology
The Netherlands
e.m.m.kivits@tue.nl

Wouter Kuijpers
Eindhoven University of Technology
The Netherlands
w.j.p.kuijpers@tue.nl

Armin Kuper
Katholieke Universiteit Leuven
Belgium
armin.kuper@gmail.com

Christophe Labar
Université Libre de Bruxelles
Belgium
christophe.labar@ulb.ac.be

Francois Lamoline
University of Namur
Belgium
francois.lamoline@unamur.be

John Lataire
Vrije Universiteit Brussel
Belgium
jlataire@vub.ac.be

Oliver Lauwers
Katholieke Universiteit Leuven
Belgium
oliver.lauwers@esat.kuleuven.be

Mircea Lazar
Eindhoven University of Technology
The Netherlands
m.lazar@tue.nl

Dongheui Lee
Technical University of Munich
Germany
dhlee@tum.de

Erjen Lefeber
Eindhoven University of Technology
The Netherlands
A.A.J.Lefeber@tue.nl

Benoit Legat
Université Catholique de Louvain
Belgium
benoit.legat@uclouvain.be

Johnny Leung
Université Libre de Bruxelles
Belgium
johnny.leung@ulb.ac.be

Daming Lou
Eindhoven University of Technology
The Netherlands
d.lou@tue.nl

Alessandro Luppi
University of Groningen
The Netherlands
a.luppi@rug.nl

Bert Maljaars
Eindhoven University of Technology
The Netherlands
e.maljaars@tue.nl

Alejandro Marquez Ruiz
Eindhoven University of Technology
The Netherlands
a.marquez.ruiz@tue.nl

Estelle Massart
Université Catholique de Louvain
Belgium
estelle.massart@uclouvain.be

Alexandre Mauroy
University of Namur
Belgium
alexandre.mauroy@unamur.be

Veronika Mazulina
Eindhoven University of Technology
The Netherlands
v.mazulina@tue.nl

Carlos S. Mendez Blanco
Eindhoven University of Technology
The Netherlands
c.s.mendez.blanco@tue.nl

Ruben W.H. Merks
Eindhoven University of Technology
The Netherlands
r.w.h.merks@tue.nl

Merouane Abadli
Centrale Supélec / Mons University
France / Belgium
abadlimerouane@live.com

Danial Mohammadi Senejohnny
University of Groningen
The Netherlands
d.senejohnny@gmail.com

Rishi Mohan
Eindhoven University of Technology
The Netherlands
r.mohan@tue.nl

Francisco Mondaca Duarte
Wageningen University
The Netherlands
francisco.mondacaduarte@wur.nl

Pooya Monshizadeh
University of Groningen
The Netherlands
monshizadeh.p@gmail.com

Nima Monshizadeh
University of Groningen
The Netherlands
n.monshizadeh@rug.nl

Noud F.M. Mooren
Eindhoven University of Technology
The Netherlands
n.f.m.mooren@tue.nl

Sajad Naderilordejani
Eindhoven University of Technology
The Netherlands
s.naderilordejani@tue.nl

Esmail Najafi
Eindhoven University of Technology
The Netherlands
e.najafi@tue.nl

Satoshi Nakano
Université Libre de Bruxelles
Belgium
pascale.lathouwers@ulb.ac.be

Tam Nguyen
Université Libre de Bruxelles
Belgium
tanguyen@ulb.ac.be

Henk Nijmeijer
Eindhoven University of Technology
The Netherlands
h.nijmeijer@tue.nl

Brice Njinwoua
Mons University
Belgium
brice.njinwoua@umons.ac.be

Hengameh Noshahri
University of Twente
The Netherlands
h.noshahri@utwente.nl

Michiel E.E. Oom
Eindhoven University of Technology
The Netherlands
m.e.e.oom@tue.nl

Leyla Ozkan
Eindhoven University of Technology
The Netherlands
l.ozkan@tue.nl

Giovanny P. Padilla Cazar
Eindhoven University of Technology
The Netherlands
g.p.padilla.cazar@tue.nl

Yudha P. Pane
Katholieke Universiteit Leuven
Belgium
yudha.pane@kuleuven.be

Goele Pipeleers
Katholieke Universiteit Leuven
Belgium
goele.pipeleers@kuleuven.be

Tomas M. Pippia
Delft University of Technology
The Netherlands
t.m.pippia@tudelft.nl

Marcella Porru
Eindhoven University of Technology
The Netherlands
m.porru@tue.nl

Suraj Prakash
Eindhoven University of Technology
The Netherlands
s.prakash@tue.nl

Mohamad A. Prawira Negara
University of Groningen
The Netherlands
m.a.prawira.negara@rug.nl

Ioannis Proimadis
Eindhoven University of Technology
The Netherlands
i.proimadis@tue.nl

Yuzhen Z. Qin
University of Groningen
The Netherlands
y.z.qin@rug.nl

Karthik R. Ramaswamy
Eindhoven University of Technology
The Netherlands
k.r.ramaswamy@tue.nl

Timo Ravensbergen
Eindhoven University of Technology
The Netherlands
t.ravensbergen@tue.nl

Ferdie F.H. Reijnen
Eindhoven University of Technology
The Netherlands
f.f.h.reijnen@tue.nl

Joey M.F. Reinders
Eindhoven University of Technology
The Netherlands
j.m.f.reinders@tue.nl

Rodolfo Reyes-Baez
University of Groningen
The Netherlands
r.reyes-baez@rug.nl

Kirill Rogov
Eindhoven University of Technology
The Netherlands
k.rogov@tue.nl

Alberto Romero
Université Libre de Bruxelles
Belgium
alberto.romero@ulb.ac.be

Aaron Romo
Université Catholique de Louvain
Belgium
aaron.romo@uclouvain.be

Monica Rotulo
University of Groningen
The Netherlands
m.rotulo@rug.nl

Alessandro Saccon
Eindhoven University of Technology
The Netherlands
a.saccon@tue.nl

Gustavo Sales Mazzoccante
Eindhoven University of Technology
The Netherlands
g.sales.mazzoccante@tue.nl

Jacquelin M.A. Scherpen
University of Groningen
The Netherlands
j.m.a.scherpen@rug.nl

Wouter S. Schinkel
Eindhoven University of Technology
The Netherlands
w.s.schinkel@tue.nl

Maarten Schoukens
Eindhoven University of Technology
The Netherlands
m.schoukens@tue.nl

Johan Schoukens
Vrije Universiteit Brussel
Belgium
johan.schoukens@vub.be

Fahim Shakib
Eindhoven University of Technology
The Netherlands
m.f.shakib@tue.nl

Shengling Shi
Eindhoven University of Technology
The Netherlands
s.shi@tue.nl

Taranjitsingh Singh
Katholieke Universiteit Leuven
Belgium
taranjitsingh.singh@kuleuven.be

Tom R.V. Steentjes
Eindhoven University of Technology
The Netherlands
t.r.v.steentjes@tue.nl

Tjerk W. Stegink
University of Groningen
The Netherlands
t.w.stegink@rug.nl

Maarten Steinbuch
Eindhoven University of Technology
The Netherlands
m.steinbuch@tue.nl

Armin Steinhauser
Katholieke Universiteit Leuven
Belgium
armin.steinhauser@kuleuven.be

Erik Steur
Delft University of Technology
The Netherlands
e.steur@tudelft.nl

Nard W.A. Strijbosch
Eindhoven University of Technology
The Netherlands
n.w.a.strijbosch@tue.nl

Jan Swevers
Katholieke Universiteit Leuven
Belgium
jan.swevers@kuleuven.be

Pauline Themans
University of Namur
Belgium
pauline.themans@unamur.be

Johan Thunberg
University of Luxembourg
Luxembourg
thunberg.johan@gmail.com

Tim Mercy
Katholieke Universiteit Leuven
Belgium
tim.mercy@kuleuven.be

Stephan Trenn
University of Groningen
The Netherlands
s.trenn@rug.nl

Dora Turk
Katholieke Universiteit Leuven
Belgium
dora.turk@kuleuven.be

Laurens Valk
Delft University of Technology
The Netherlands
laurensvalk@gmail.com

Tobias van Damme
University of Groningen
The Netherlands
t.van.damme@rug.nl

Ton J.J. van den Boom
Delft University of Technology
The Netherlands
a.j.j.vandenboom@tudelft.nl

Sebastiaan J.A.M. van den Eijnden
Eindhoven University of Technology
The Netherlands
s.j.a.m.v.d.eijnden@tue.nl

Paul M.J. Van den Hof
Eindhoven University of Technology
The Netherlands
p.m.j.vandenhof@tue.nl

David P.M. van den Hurk
Eindhoven University of Technology
The Netherlands
d.p.m.v.d.hurk@tue.nl

Arjan van der Schaft
University of Groningen
The Netherlands
a.j.van.der.schaft@rug.nl

Robert van der Weijst
Eindhoven University of Technology
The Netherlands
r.v.d.weijst@tue.nl

Niels van Duijkeren
Katholieke Universiteit Leuven
Belgium
niels.vanduijkeren@kuleuven.be

Robbin B.A. van Hoek
Eindhoven University of Technology
The Netherlands
r.b.a.v.hoek@tue.nl

Simon van Mourik
Wageningen University
The Netherlands
simon.vanmourik@wur.nl

Ruben van Parys
Katholieke Universiteit Leuven
Belgium
ruben.vanparys@kuleuven.be

Henk J. van Waarde
University of Groningen
The Netherlands
h.j.van.waarde@rug.nl

Sandra Vasquez
Université Libre de Bruxelles
Belgium
savasque@vub.ac.be

Marco A. Vasquez Beltran
University of Groningen
The Netherlands
m.a.vasquez.beltran@rug.nl

Daniel W.M. Veldman
Eindhoven University of Technology
The Netherlands
d.w.m.veldman@tue.nl

Maarten Verbandt
Katholieke Universiteit Leuven
Belgium
maarten.verbandt@hotmail.com

Frans J.R. Verbruggen
Eindhoven University of Technology
The Netherlands
f.j.r.verbruggen@tue.nl

Cees F. Verdier
Delft University of Technology
The Netherlands
c.f.verdier@tudelft.nl

Bob Vergauwen
Katholieke Universiteit Leuven
Belgium
bob.vergauwen@esat.kuleuven.be

Christof Vermeersch
Katholieke Universiteit Leuven
Belgium
christof.vermeersch@esat.kuleuven.be

Benjamin Vincent
Université Catholique de Louvain
Belgium
benjamin.vincent@uclouvain.be

Quentin J.T. Voortman
Eindhoven University of Technology
The Netherlands
q.j.t.voortman@tue.nl

Steffen Waldherr
Katholieke Universiteit Leuven
Belgium
steffen.waldherr@kuleuven.be

Zheming Wang
Université Catholique de Louvain
Belgium
zheming.wang@uclouvain.be

Harm H.M. Weerts
Eindhoven University of Technology
The Netherlands
h.h.m.weerts@tue.nl

Wengang Yan
Eindhoven University of Technology
The Netherlands
w.yan@tue.nl

Jeroen Willems
Flanders Make
Belgium
jeroen.willems@flandersmake.be

Joseph Winkin
University of Namur
Belgium
joseph.winkin@unamur.be

Chengshuai Wu
University of Groningen
The Netherlands
cwu@zju.edu.cn

Lu Xia
Eindhoven University of Technology
The Netherlands
l.xia1@tue.nl

Qingkai K. Yang
University of Groningen
The Netherlands
q.k.yang@rug.nl

Weijia Yao
University of Groningen
The Netherlands
w.yao@rug.nl

Shiquan Zhao
Ghent University
Belgium
shiquan.zhao@ugent.be

Hans Zwart
University of Twente
The Netherlands
h.j.zwart@utwente.nl

Part 5

Organizational Comments

Welcome

The Organizing Committee has the pleasure of welcoming you to the *37th Benelux Meeting on Systems and Control*, at Kontakt der Kontinenten in Soesterberg, The Netherlands.

Aim

The aim of the Benelux Meeting is to promote research activities and to enhance cooperation between researchers in Systems and Control. This is the thirty-seventh in a series of annual conferences that are held alternately in Belgium and The Netherlands.

Scientific Program Overview

1. Mini course by *Murat Arcaç* (University of California, Berkeley, USA) on **Networks of dissipative Systems: Compositional certification of stability, performance, and safety**.
2. Plenary lectures by *Tamas Keviczky* (Delft University of Technology, The Netherlands) on **Distributed stochastic model predictive control for large-scale smart energy systems**.
3. Plenary lectures by *Dongheui Lee* (Technical University of Munich, Germany) on: **Robot learning through physical interaction and human guidance**.
4. Contributed short lectures. See the list of sessions for the titles and authors of these lectures.

Directions for speakers

For a contributed lecture, the available time is 25 minutes. Please leave a few minutes for discussion and room changes, and adhere to the indicated schedule. In each room LCD projectors are available, as well as VGA and HDMI cables. *When using a projector, you have to provide a notebook yourself.*

Registration

The Benelux Meeting registration desk, located in the foyer, will be open on Tuesday, March 27, from 10:00 to 14:00. Late registrations can be made at the Benelux Meeting registration desk, when space is still available. The on-site fee schedule is:

Arrangement	Price
only meals (no dinners)	€375
one day (no dinner)	€275

The registration fee includes:

- Admission to all sessions.
- A copy of the Book of Abstracts.
- Coffee and tea during the breaks.
- In the case of *accommodation* arrangement: lunch and dinner on Tuesday; breakfast, lunch, dinner on Wednesday; breakfast and lunch on Thursday.
- In the case of *only meals (no dinner)* arrangement: lunch on Tuesday, Wednesday, Thursday.
- In the case of *one day (no dinner)* arrangement: lunch on Tuesday, or Wednesday, or Thursday.
- Free use of a wireless Internet connection (WiFi).

The registration fee does *not* include:

- Cost of phone calls.
- Special ordered drinks during lunch, dinner, in the evening, etc.

Organization

The meeting has been organized by Raffaella Carloni (University of Groningen), Bayu Jayawardhana (University of Groningen), and Mircea Lazar (Eindhoven University of Technology).

The Organizing Committee of the 37th Benelux Meeting consists of

Ming Cao
University of Groningen
E-mail: m.cao@rug.nl

Raffaella Carloni
University of Groningen
E-mail: r.carloni@rug.nl

Sergio Grammatico
Eindhoven University of Technology
E-mail: s.grammatico@tue.nl

Maurice Heemels
Eindhoven University of Technology
E-mail: m.heemels@tue.nl

Julien Hendrickx
Universite' Catholique de Louvain
E-mail: julien.hendrickx@uclouvain.be

Bayu Jayawardhana
University of Groningen
E-mail: b.jayawardhana@rug.nl

Tamas Keviczky
Delft University of Technology
E-mail: t.keviczky@tudelft.nl

Mircea Lazar
Eindhoven University of Technology
E-mail: m.lazar@tue.nl

Manuel Mazo Jr.
Delft University of Technology
E-mail: m.mazo@tudelft.nl

Sarthak Misra
University of Twente
E-mail: s.misra@utwente.nl

Henk Nijmeijer
Eindhoven University of Technology
E-mail: h.nijmeijer@tue.nl

Tom A.E. Oomen
Eindhoven University of Technology
E-mail: t.a.e.oomen@tue.nl

Arjan J. van der Schaft
University of Groningen
E-mail: a.j.van.der.schaft@math.rug.nl

Jacquelien M.A. Scherpen
University of Groningen
E-mail: j.m.a.scherpen@rug.nl

Bart de Schutter
Delft University of Technology
E-mail: b.deschutter@tudelft.nl

Hans Stigter
University of Wageningen
E-mail: hans.stigter@wur.nl

Paul M.J. Van den Hof
Eindhoven University of Technology
E-mail: p.m.j.vandenhof@tue.nl

Steffen Waldherr
Katholieke Universiteit Leuven
E-mail: steffen.waldherr@kuleuven.be

Nathan van de Wouw
Eindhoven University of Technology
E-mail: n.v.d.wouw@tue.nl

Hans J. Zwart
University of Twente
E-mail: h.j.zwart@utwente.nl

Sponsor

The meeting is supported by the following organizations:

- Dutch Institute for Systems and Control (DISC).
- Netherlands Organization for Scientific Research (NWO).

Conference location

The lecture rooms of Kontakt der Kontinenten are situated on the ground and first floors. Consult the map at the end of this booklet to locate rooms. During the breaks, coffee and tea will be served in the St. Janzaal in the ground floor. Announcements and personal messages will be posted near the main conference room. Accommodation is provided in the conference center. Breakfast will be served between 6:30 and 9:30 AM. Room keys can be picked up at the reception from Tuesday at 12:30, and need to be returned before 9:30 on the day of departure. Parking is free of charge.

The address of Kontakt der Kontinenten is

Amersfoortsestraat 20
3769 AS Soesterberg
The Netherlands

Best junior presentation award

Continuing a tradition that started in 1996, the 37th Benelux Meeting will close with the announcement of the winner of the Best Junior Presentation Award. This award is given for the best presentation, given by a junior researcher, and it consists of a trophy that may be kept for one year and a certificate. The award is specifically given for quality of presentation rather than quality of research, which is judged in a different way. At the meeting, the chairs of sessions will ask three volunteers in the audience to fill out an evaluation form. After the session, the evaluation forms will be collected by the Prize Commissioners who will then compute a ranking. The winner will be announced on Thursday, March 29, in room **Steyl**, 13:10-13:25. The evaluation forms of each presentation will be returned to the junior researcher who gave the presentation. The Prize Commissioners are Bart Besselink (University of Groningen), Alessandro Saccon (Technical University of Eindhoven), and Johan Schoukens (Vrije Universiteit Brussel). The organizing committee counts on the cooperation of the participants to make this contest a success.

Website

An *electronic version* of the Book of Abstracts can be downloaded from the Benelux Meeting [web site](#).

Meetings

The following meetings are scheduled:

- Board DISC on Tuesday, March 27, 19:30 – 21:00 (during dinner).
- Management Team DISC on Tuesday, March 27, room Angola, 21:00 – 22:30.

DISC certificates and best thesis award

The ceremony for the distribution of the DISC certificates and for the Best Thesis Award will be held on Thursday, March 29, room **Steyl**, 12:50–13:10. The jury of the Best Thesis Award is formed by Hans Zwart (University of Twente), Manuel Mazo (Delft University of Technology), and Dennis Schipper (CEO Demcon).

Tuesday March 27, 2018

11:25 – 11:30	P0 – Steyl <i>Welcome and Opening</i>									
11:30 – 12:30	P1 – Steyl Murat Arcaç – <i>Networks of dissipative Systems: Compositional certification of stability, performance, and safety</i>									
12:30 – 13:40	Lunch									
13:40 – 14:40	P2 – Steyl Murat Arcaç – <i>Networks of dissipative Systems: Compositional certification of stability, performance, and safety</i>									
14:40 – 15:10	Coffee Break									
Room TuA	Steyl TuA01 <i>System Identification A</i>	Angola TuA02 <i>Optimal Control A</i>	Argentiñië TuA03 <i>Aerospace and Automotive Applications A</i>	Bolivia TuA04 <i>Distributed Control and Estimation A</i>	Botswana TuA05 <i>Model Reduction</i>	Congo TuA06 <i>Nonlinear Control A</i>	Mozambique TuA07 <i>Distributed Parameter Systems</i>	Kenia TuA08 <i>System Theory</i>		
15:10 – 15:35	Cox	Jiao	Nijnwoua	Ravensbergen	Bansal	Azizi	Lamoline	Kivitis		
15:35 – 16:00	Vasquez	Khalik	Creyf	Valk	Leung	Mounshizadeh	Califano	Pippia		
16:00 – 16:25	Evers	Jeltsema	Nguyen	Thunberg	Xia	Adibi	Zwart	Jia		
16:25 – 16:50	Vergauwen	Mercy	Nakano	Cucuzzella	Cheng	Stegink	Das	Rogov		
16:50 – 17:15	Birpoutsoukis	Van Damme	Rashad	Cajo	Merks	v/d Eijnden	Küper	Heidari		
17:15 – 17:40	Yan	Padilla	Oom	Cotorruelo	Lou	Verdier	Benjamin	Lauwers		
17:40 – 18:00	Break									
18:00 – 19:00	Reception									
19:30 – 21:00	Dinner									
19:30 – 21:00	Board DISC									
21:00 – 22:30	Management Team DISC (room Angola)									

Wednesday March 28, 2018

9:15 – 10:15	Murat Arcaak – <i>Networks of dissipative Systems: Compositional certification of stability, performance, and safety</i>									
10:15 – 10:40	P3 – Steyl Coffee break									
10:40 – 11:40	P4 – Steyl Tamas Keviczky – <i>Distributed stochastic model predictive control for large-scale smart energy systems</i>									
11:40 – 12:00	Break									
12:00 – 13:10	Lunch									
Room WeM	Steyl WeM01 <i>System Identification B</i>	Angola WeM02 <i>Optimal Control B</i>	Argentiinië WeM03 <i>Aerospace and Automotive Applications B</i>	Bolivia WeM04 <i>Distributed Control and Estimation B</i>	Botswana WeM05 <i>Mechanical Engineering A</i>	Congo WeM06 <i>Nonlinear Control B</i>	Mozambique WeM07 <i>Model-based Control A</i>	Kenia WeM08 <i>System Biology</i>		
13:10 – 13:35	Decuyper	Hermans	Schinkel	Zhao	Almuzakki	Steinhauser	van den Hurk	Qin		
13:35 – 14:00	Schoukens	Van Parys	van Hoek	Chen	van der Weijst	Willems	de Baar	Jeanne		
14:00 – 14:25	Khandelwal	Singh	Reinders	Chan	Beerens	Borja-Rosales	Mendez-Blanco	Aalto		
14:25 – 14:50	Csurcsia	Mohan	Fahdzyana	Fransman	Gillis	Baez	Hanema	Meroutane		
14:50 – 15:15	Steenjtes	Herceg	Verbruggen	Balaghiinaloo	Shakib	Berger	Veldman	De Becker		
15:15 – 15:40	van Berkel	Eising	Frejo	Jahanshahi	Prakash	Wu	Dresscher	-		
15:40 – 16:00	Break									
Room WeA	Steyl WeA01 <i>System Identification C</i>	Angola WeA02 <i>Optimization</i>	Argentiinië WeA03 <i>Robotics A</i>	Bolivia WeA04 <i>Games and Agent-Based Models A</i>	Botswana WeA05 <i>Mechanical Engineering B</i>	Congo WeA06 <i>Nonlinear Control C</i>	Mozambique WeA07 <i>Model-based Control B</i>	Kenia WeA08 <i>State Observer and Estimation</i>		
16:00 – 16:25	Shi	Legat	Dolatabadi	Senejohnny	Mooren	Lefeber	Kuijpers	Voortman		
16:25 – 16:50	van Waarde	De Geeter	Altartouri	Catalano	Grubben	Cucuzzella	Jiang	Acciani		
16:50 – 17:15	Hendrickx	Vermeersch	van Duijkeren	Cenedese	Halfkamp	Sales Mazzoccante	Loonen	Blanken		
17:15 – 17:40	Weerts	Gillis	Douven	Geelen	Romo-Hernandez	Labar	Mondaca-Duarte	Beelen		
17:40 – 18:05	Turk	De Mauri	Yao	Gong	Blanken	Naderilordejani	Reijnen	Najafi		
18:05 – 18:30	Ramaswamy	Gillis	Cavallo	Engwerda	Hakan Kan-demir	Borja-Rosales	Porru	Andrian		
18:30 – 20:00	Dinner									

Thursday March 29, 2018

8:30 – 9:30	P5 – Steyl Dongheui Lee – <i>Robot learning through physical interaction and human guidance</i>									
9:30 – 9:45	Coffee break									
9:45 – 10:45	P6 – Steyl Dongheui Lee – <i>Robot learning through physical interaction and human guidance</i>									
Room ThM	Steyl -	Angola ThM01 <i>Medical Applications</i>	Argentinië ThM02 <i>Robotics B</i>	Bolivia ThM03 <i>Games and Agent-Based Models B</i>	Botswana ThM04 <i>Electro-Mechanical Engineering</i>	Congo ThM05 <i>Model-based Control C</i>	Mozambique -	Kenia -		
10:45 – 11:10	-	Themans	Pane	Belgioioso	Vaseur	Goorden	-	-		
11:10 – 11:35	-	Deenen	Caasenbrood	Mazulina	De Preter	Strijbosch	-	-		
11:35 – 12:00	-	Wang	Verbandt	Govaert	Goldar	van Mourik	-	-		
12:00 – 12:25	-	Massart	Carlomi	Chevalier	Jeeninga	Jacobs	-	-		
12:25 – 12:50	-	Dehem	Bono Rossello	Gueuning	Proimadis	Gillis	-	-		
12:50 – 13:10	E1 – Steyl DISC Certificates & Best Thesis Award Ceremony									
13:10 – 13:25	E2 – Steyl <i>Best Junior Presentation Award Ceremony</i>									
13:25 – 13:30	P7 – Steyl <i>Closure of the 37th Benelux Meeting</i>									
13:30 – 14:30	<i>Lunch</i>									

